PHY

VOLUME

THE PHYSICAL REVIEW

A journal of experimental and theoretical physics established by E. L. Nichols in 1893

Published by the American Institute of Physics for the

AMERICAN PHYSICAL SOCIETY

Officers

President

C. C. LAURITSEN
California Institute of Technology
Pasadena, California

Vice-President

J. H. VAN VLECK
Harvard University
Cambridge, Massachusetts

Secretary

K. K. DARROW
Bell Telephone Laboratories
Office:
Columbia University
New York 27, New York

Treasurer

G. B. PEGRAM
Columbia University
New York 27, New York

Local Secretary for the Pacific Coast

J. KAPLAN
University of California at Los Angeles
Los Angeles, California

Managing Editor

S. A. GOUDSMIT
Brookhaven National Laboratory
Upton, Long Island
New York

The Physical Review

Entered as second-class matter at Prince and Lemon streets, Lancaster, Pennsylvania.

Acceptance for mailing at special rate of postage provided for in paragraph (d-2), section 34.40, P. L. & R. of 1948, authorized January 31, 1947, at the Post Office at Lancaster, Pennsylvania, under the Act of March 3, 1879.

BOARD OF EDITORS

Editor

S. A. GOUDSMIT

Assistant Editor

S. FLUGGE

Associate Editors

J. BARDEEN	HARVEY BROOKS	M. GOLDHABER
F. BLOCH	R. F. CHRISTY	E. HUTCHISSON
S. G. BRUSH	C. L. CRITCHFIELD	A. W. LAWSON
W. E. LAMB, JR.	M. DEUTSCH	A. PAIS
L. J. F. SIMPSON	T. H. JOHNSON	R. SMOLUCHOWSKI
W. E. STEPHENS	BRUNO ROSSI	C. P. TOWNES

Manuscripts for publication should be submitted to S. A. Goudsmit, Brookhaven National Laboratory, Upton, Long Island, New York. Authors' institutions are requested to pay a publication charge of $[illegible] per page, which, if honored, entitles them to 100 free reprints. Instructions will be sent with galley proofs.

Proof and all correspondence concerning papers in the process of publication should be addressed to the Publication Manager, American Institute of Physics, 57 East 55 Street, New York 22, New York.

Subscription Price

United States and Canada $25.00
Elsewhere $27.00

Back Numbers[1]

Yearly back number rate when complete year is available:
Prior to 1949: $20.00
Thereafter: $27.00

Single copies: $2.00 each, prior to July, 1929;
$1.00 each, July, 1929–December, 1941;
$2.00 each, January, 1942–December, 1946;
$3.00 each, January, 1947–December, 1948;
$3.25 each, thereafter.

General index, 1893–1920: $4.00.

Subscriptions, renewals, and orders for back numbers should be addressed to the American Institute of Physics, 57 East 55 Street, New York 22, New York.

Changes of address in the case of members of the American Physical Society should be addressed to the Treasurer; in the case of other subscribers to the American Institute of Physics.

[1] For Series I (Reports of Physics Department, Cornell University, Ithaca, New York)

THE
PHYSICAL REVIEW

A journal of experimental and theoretical physics established by E. L. Nichols in 1893

SECOND SERIES, VOL. 84, NO. 6 DECEMBER 15, 1951

Gamma-Rays and Nuclear Levels Associated with Radioisotopes of Europium, Erbium, and Cerium*

H. B. KELLER† AND J. M. CORK
Argonne National Laboratory, Chicago, Illinois, and University of Michigan, Ann Arbor, Michigan

(Received June 25, 1951)

The energies of the conversion electrons associated with the decay of 8 radioisotopes were measured using permanent magnet-type photographic beta-spectrometers. The energies of the gamma-rays associated with the various activities are as follows: europium 152 (9.2-hr) 121.9, 344.1 kev; erbium 171 (7.5-hr) 112.8, 117.9, 125.5, 176.4, 294.5, 307.5, 419.7 kev; cerium 137 (36-hr) 253.4 kev; cerium 139 (140-day) 166.0, 275.2 kev; cerium 141 (28-day) 145.7 kev; cerium 143 (33-hr) 57.5, 290.6, 348.4 kev; cerium 144 (300-day) 34.0, 41.3, 46.8, 53.7, 80.9, 95.0, 100.5, 134.5 kev; and praseodymium 144 (17.5-min) 61.0 kev. Energy level schemes are proposed for each product nucleus.

THE evaluation of the energies of gamma-rays associated with short-lived radioactivities can best be carried out close to the source of the activation. For those radioactive isotopes arising from neutron capture, proximity to a pile is an advantage. Through the participating programs sponsored by the National Regional Laboratories, the heavy-water pile at Argonne was kindly made available for the present investigation.

APPARATUS AND METHOD

Spectrometers of the permanent-magnet-type, as previously described,[1] were located a few feet from the pile, so that a pneumatic tube could quickly transfer the irradiated specimens. Two magnets were employed and each was set at a different field value, such as 200 and 600 gauss, and each magnet accommodated two cameras. The camera box, as shown in Fig. 1, was provided with an auxiliary side tube portrayed in Fig. 2 which enabled the rapid injection of the activated specimen with no loss of vacuum. The action of the vacuum gate is as follows: (a) the specimen is placed in the source holder while the gate cover plate is removed, (b) the cover plate is put in position, and the forechamber rapidly evacuated, (c) when the forechamber is evacuated, the gate entrance to the camera is automatically opened by spring action, and (d) the specimen is pushed forward into its exact position within the

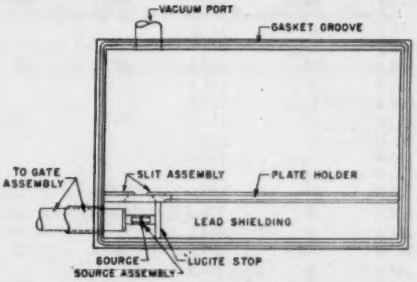

FIG. 1. The camera: a plan section drawing.

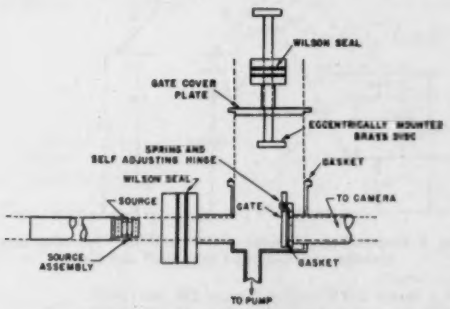

FIG. 2. Sectional sketch of vacuum gate.

* This project was aided by the joint support of the AEC and the ONR.

† Phoenix Project Fellow; now at Radiation Laboratory, University of California, Berkeley, California.

[1] J. Cork, Phys. Rev. **72**, 581 (1947).

TABLE I. The electron energies from Eu^{152}.

Electron energy	Proposed interpretation	Energy sum (kev)	Gamma-ray (kev)	Approx. K/L conversion ratio
75.0	K	121.9		
114.2	L_{I}	122.0		
114.6	L_{II}	121.9		
115.1	L_{III}	121.9		
120.3	M	122.0		
121.5	N	121.9	121.9	4
293.7	K	344.1		
336.2	L_{II}	344.2	344.1	10

camera. If necessary, repeated exposures may be made with no loss in line sharpness. Activities with half-life as short as 19 seconds have been successfully studied with this apparatus.

The magnetic fields were calibrated by the known energies of the electron lines in the radioactive decay of iodine 131, and at higher energies by the electron lines from a radium source. The enriched isotopes of cerium to be studied were supplied by the Oak Ridge National Laboratory. The powdered specimen, usually as an oxide, was made into a line source as massless as compatible with the required activity. Each line source was supported on a frame of very pure graphite, chosen because of its low neutron capture cross section in the pile. Eastman Kodak Type NTB photographic plates were used in the cameras. In addition to the various enriched isotopes of cerium, specimens of ordinary europium and erbium of high purity have been examined for their shorter-lived activities.

RESULTS

Europium 152

March and Sugden[2] were the first to report a 9.2-hour radioactivity in europium. Pool and Quill[3] using fast neutrons from the Michigan cyclotron concluded that the activity was in the isotope of mass 152. Tyler,[4] using a magnetic spectrometer, found the maximum beta-energy to be 1.9 Mev and three gamma-rays to

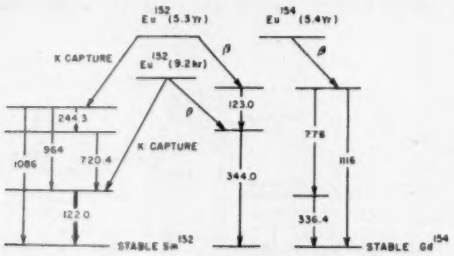

FIG. 3. Proposed level scheme of Gd^{154} and Sm^{152} following beta-emission and K-capture from Eu^{152} and Eu^{154}.

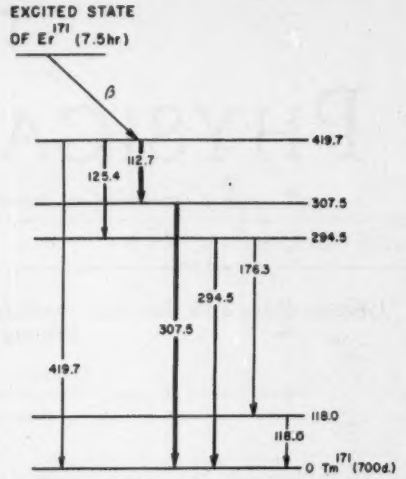

FIG. 4. Proposed level scheme of Tm^{171} following beta-emission from Er^{171}.

have energies 123, 163, and 725 kev. Muehlhause[5] showed that the K-capture process competes with beta-emission in the radioactive decay.

The europium used in the present investigation was brought from Munich by Dr. K. Fajans and is believed to be of very high purity. Two gamma-rays are found, one with an energy of 122.0 kev in samarium 152 following K-capture and another of 344 kev in gadolinium 152 following beta-emission. The electron energies together with their interpretation are shown in Table I. It had been shown[6] by mass spectrometer studies that a 5.3-year radioactivity exists in both Eu^{152} and Eu^{154}, and

TABLE II. Electron energies from Er^{171}.

Electron energy	Proposed interpretation	Energy sum (kev)	Gamma-ray (kev)	Approx. K/L conversion ratio
53.2	K	112.7		
103.1	$L_{I,II}$	112.7		
110.5	M	112.8	112.8	10
58.2	K	117.7		
108.3	$L_{I,II}$	117.9		
115.6	M	117.9	117.9	0.5
66.0	K	125.5		
116.0	$L_{I,II}$	125.6		
123.2	M	125.5		
125.0	N	125.5	125.5	2
116.9	K	176.4	176.4	...
234.8	K	294.3		
285.0	$L_{I,II}$	294.6	294.6	10
248.0	K	307.5		
298.2	$L_{I,II}$	307.8	307.5	10
360.2	K	419.7	419.7	...

[2] J. Marsh and S. Sugden, Nature **136**, 102 (1935).
[3] M. Pool and L. Quill, Phys. Rev. **53**, 437 (1938).
[4] A. Tyler, Phys. Rev. **56**, 125 (1939).
[5] C. Muehlhause, Plutonium Project Report CP-3750, 46 (1947), unpublished.
[6] Hayden, Reynolds, and Inghram, Phys. Rev. **75**, 1500 (1949).

TABLE III. Relative abundance of the cerium isotopes.

Isotope	Normal	Ce^{136}	Ce^{138}	Ce^{140}	Ce^{142}
136	0.19%	8.94%	0.10%	0.02%	0.02%
138	0.26	0.81	4.42	0.02	0.06
140	88.47	84.98	92.00	99.25	16.51
142	11.08	5.27	3.48	0.71	83.42

hence one of these is isomeric with the 9.2-hour activity. A decay scheme had been previously proposed,[7] which, without separated isotopes, could not be established conclusively. An interchange of the gamma-spectra assigned to Eu^{152} and Eu^{154} now appears justified, as shown in Fig. 3.

Erbium 171

The erbium used in this investigation is a portion of the high purity material obtained by Dr. M. Goldhaber from the Oak Ridge Laboratory. An analysis showed no impurities present in amounts beyond the sensitivity limit of the spectrographic method.

The hypothesis of Ketelle and Peacock[8] that erbium 169 decays with a 9.4-hour half-life by beta-emission without gamma-radiation, is confirmed. Erbium 171 decays with a half-life of 7.5 hours. Only two of the previously reported three gamma-rays were found. The third, a high energy gamma-ray (805 kev), was not observed. In addition, five previously unreported gamma-rays were detected. The complete data are given in Table II. A proposed decay scheme is presented in Fig. 4.

TABLE IV. The electron energies from Ce^{137}.

Electron energy	Proposed interpretation	Energy sum (kev)	Gamma-energy (kev)	Approx. K/L conversion ratio
214.5	K ($Z=57$)	253.2		
247.6	L	253.4		
252.0	M	253.5	253.4	10

A Survey of the Radioisotopes of Cerium

Cerium has four stable isotopes, all of even mass numbers. It is thus possible that neutron capture in each will result in a radioactive isotope of odd mass number. In order to facilitate a comprehensive study of the element, stable enriched isotopes of each mass were procured from Oak Ridge. The relative abundance of the isotopes as they occur naturally, and in each of the enriched masses is shown in Table III.

1. Cerium 137

The existence of an activity in cerium with a 36-hour half-life was first reported by Chubbuck and Perlman[9] as the result of a $(d, 4n)$ reaction by the bombardment of lanthanum with forty-Mev deuterons in the Berkeley 184-inch cyclotron. By absorption of electrons in beryllium they reported a conversion electron peak at 230 kev. They found no evidence for positron activity but did report finding x-rays characteristic of lanthanum, and therefore assumed the decay to be by K-electron capture. Absorption of the electromagnetic radiations in lead yielded gamma-rays of energies 280 and 750 kev.

A spectrogram of the 36-hour period of cerium 137 showed three electron lines due to a single gamma-ray of energy 253.4 kev. The sample used was the separated isotope of cerium 136. In normal cerium it occurs with an abundance of 0.2 percent; in the separated isotope it was 8.94 percent abundant, an increase by a factor of 45.

TABLE V. Electron energies from Ce^{139}.

Electron energy	Proposed interpretation	Energy sum (kev)	Gamma-energy (kev)	Approx. K/L conversion ratio
127.4	K ($Z=57$)	166.1		
160.1	L	166.0	166.0	10
236.5	K	275.2	275.2	···

TABLE VI. Electron energies from Ce^{141}.

Electron energy	Proposed interpretation	Energy sum (kev)	Gamma-energy (kev)	Approx. K/L conversion ratio
103.7	K ($Z=59$)	145.7		
138.8	L	145.6		
144.2	M	145.7	145.7	>1

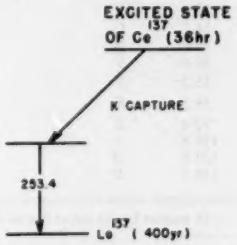

FIG. 5. Proposed level scheme for La^{137} following K-capture from Ce^{137}.

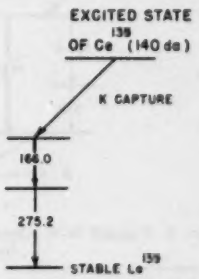

FIG. 6. Proposed level scheme for La^{139} following K-capture from Ce^{139}.

[7] Cork, Keller, Rutledge, and Stoddard, Phys. Rev. **77**, 848 (1950).

[8] B. Ketelle and W. Peacock, Phys. Rev. **73**, 1269 (1948).

[9] J. Chubbuck and I. Perlman, Phys. Rev. **74**, 982 (1948).

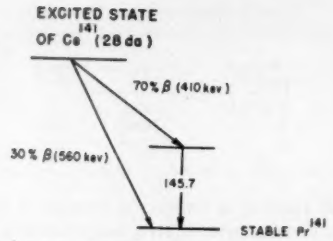

FIG. 7. Proposed level scheme for Pr^{141} following beta-emission from Ce^{141}.

Table IV gives the energies of the electron lines as they were observed, along with their interpretation. The proposed decay scheme is given in Fig. 5.

2. *Cerium 139*

Matthews and Pool[10] were the first to assign the 140-day activity in cerium to the isotope 139. They produced the activity by a (d, n) reaction on lanthanum and established K-electron capture by photographing the x-ray spectrum of the activity and finding the $K\alpha$ line of lanthanum. Further investigations of the activity were carried out by Pool and Krisberg.[11] They found spectrographic evidence for a gamma-ray of about 175 kev and on the basis of lead absorption curves reported a gamma-ray of about 800 kev.

Spectrograms of this activity, derived from the slow neutron bombardment of the separated isotope cerium 138, yielded conversion lines indicative of two gamma-rays of energies 166.0 and 275.2 kev. In Table V are given the energies and interpretations of the lines. A simple decay scheme is proposed in Fig. 6.

3. *Cerium 141*

Of the activities in cerium it is probably cerium 141 with a half-life of about 30 days that has most often been investigated. Ter-Pogossian, *et al.*,[12] investigated the photoelectric as well as the conversion spectrum and reported gamma-rays of 146 and 315 kev. They indicated that the beta-spectrum is complex but did not attempt an evaluation of the components. Shepherd[13] expressed the beta-components as 0.41 and 0.56 Mev, and a single gamma-ray of 141 kev. A survey[14] was conducted especially to verify the existence of the previously reported unconverted gamma-ray at 315 kev, with negative results. The instrument used for this survey was a sodium iodide proportional scintillation counter and a 20-channel pulse discriminator. A summary of the electron line spectrum is presented in Table VI, and the proposed simple-level scheme is portrayed in Fig. 7.

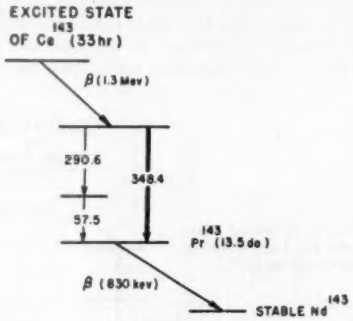

FIG. 8. Proposed level scheme for Pr^{143} following beta-emission from Ce^{143}.

[10] D. Matthews and M. Pool, Phys. Rev. **72**, 163 (1947).
[11] M. Pool and N. Krisberg, Phys. Rev. **73**, 1035 (1948).

TABLE VII. Electron energies from Ce^{143}.

Electron energy	Proposed interpretation	Energy sum (kev)	Gamma-energy (kev)	Approx. K/L conversion ratio
15.6	K ($Z=59$)	57.6		
50.7	L	57.5		
55.9	M	57.4	57.5	<1
248.5	K	290.5		
284.2	L	290.7	290.6	10
306.4	K	348.4	348.4	...

4. *Cerium 143*

A 33-hour activity was first produced by bombarding normal cerium with either deuterons or neutrons[9] and assigned to mass 143. Various investigators,[10] using absorption techniques, report a 1.3-Mev beta-ray and a 550-kev gamma-ray.

An enriched isotope of cerium 142 (83.4 percent) was

TABLE VIII. Electron energies from Ce^{144}.

Electron energy	Proposed interpretation	Energy sum (kev)	Gamma-energy (kev)	Approx. K/L conversion ratio
27.2	L_1 ($Z=59$)	34.0		
32.5	M	34.0	34.0	...
34.5	L_1	41.3	41.3[a]	...
40.0	L_1	46.8	46.8	...
11.7	K	53.7		
47.0	L_1	53.8	53.7	<1
38.8	K	80.8		
74.1	L_1	80.9		
79.4	M	80.9		
80.6	N	80.9	80.9	5
53.0	K	95.0	95.0	...
58.5	K	100.5	100.5	...
92.4	K	134.4		
127.8	L_1	134.6		
133.0	M	134.5		
134.1	N	134.4	134.5	10

[a] M masked by the heavy line at 40.0 kev.

[12] Ter-Pogossian, Cook, Goddard, and Robinson, Phys. Rev. **76**, 909 (1949).
[13] L. R. Shepherd, Research (London) **1**, 671 (1948).
[14] B. Hamermesh (private communication).

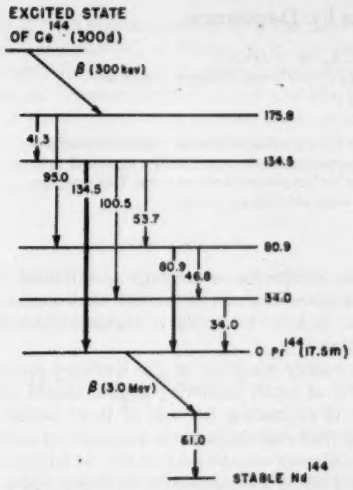

FIG. 9. Proposed level scheme for Pr^{144} and Nd^{144} following beta-decay from Ce^{144}.

irradiated in the reactor and observed. Three gamma-rays were found, none of which approximated the previously reported value of 550 kev. The electron energies and their interpretation are given in Table VII. Figure 8 is a proposed level scheme showing the decay to excited Pr^{143} which in turn decays by beta-emission to stable Nd^{143}.

5. *Cerium 144*

An activity in cerium derived from the fission of uranium has been reported[15] by several investigators to have a half-life of about 300 days. It is beta-active with an end point of about 300 kev, but no gamma-rays had been found in the radiation. The source used in the present study was a fission product obtained from Oak Ridge and was carrier-free, with a very high specific activity. The sources were prepared from an active solution and mounted as thin-etch lines on conducting films. Many conversion electron lines were observed and their energies together with their interpretations are assembled in Table VIII. The eight observed gamma-rays fit remarkably well the nuclear level scheme presented in Fig. 9.

TABLE IX. Electron energies from Pr^{144}.

Electron energy	Proposed interpretation	Energy sum (kev)	Gamma-ray (kev)	Approx. K/L conversion ratio
17.3	K ($Z=60$)	60.9		
53.8	L_I	61.0		<1
59.4	M	61.0	61.0	

6. *Praseodymium 144*

Praseodymium 144 is[16] the 17.5-minute half-lived daughter of cerium 144. It decays[17] by the emission of a 3-Mev beta-particle to an excited state of stable neodymium 144. The excited state then transforms to the stable element with the emission of a 61.0-kev gamma-ray. This value does not agree with that found by the absorption methods of other investigators. The experimental data for the electron conversion lines appear in Table IX. The proposed decay appears along with that of cerium 144 in Fig. 9.

The authors are deeply indebted to Drs. L. A. Turner, J. C. Boyce, C. O. Muehlhause, S. B. Burson, and others of the Argonne staff for their kind and helpful interest in this work.

[15] H. Born and W. Seelmann, Eggebert, Naturwiss. 31, 201 (1943); V. Nedsel and M. Sampson, Plutonium Project Report CC-2283, 1944, and others.

[16] O. Hahn and F. Strassmann, Naturwiss. 31, 499 (1943), and others.

[17] Peacock, Jones, and Overman, Plutonium Project Report, Mon. N. 432 (1947).

The Scattering of π-Mesons by Deuterons

S. FERNBACH,* T. A. GREEN,† AND K. M. WATSON‡
Radiation Laboratory, Department of Physics, University of California, Berkeley, California
(Received September 10, 1951)

A study is made of the expected properties of the cross section for scattering π-mesons by deuterons on the basis of the impulse approximation. The cross section for high energy mesons can then be expressed in a simple manner in terms of the cross sections for meson scattering by free protons and neutrons. This provides a means of deducing the latter when the deuteron and proton cross sections are known.

I. INTRODUCTION

THE interactions of π-mesons with nucleons have been observed to include those which lead to scatterings and those which lead to absorptions. Such interactions can be conveniently classified as of two types: (1) those of mesons with free nucleons and (2) those with nucleons bound in nuclei. The latter types of processes have been observed in several experiments[1–4] and indicate that here both scattering and absorption play an important role. Some implications of these experiments have been discussed previously.[5,6] Processes (1) involve meson interactions with free protons and free neutrons, of which only the former are directly amenable to experimental study.[1,7] Presumably, the free neutron-π cross section must be deduced indirectly from scatterings of type (2).

In this connection there arises, however, the question as to how adequately the free particle scattering cross section can describe the scattering in nuclear matter—i.e., as to the importance of many-body interactions. To obtain information concerning this point as well as the free neutron-π cross section, the scattering of mesons by deuterons would appear to offer the most promise. As a starting point in such an analysis, we shall calculate the properties of the π-deuteron scattering cross section by means of the impulse approximation[8] on the assumption that the meson-nucleon scattering interaction is not modified by the presence of the other nucleon. Granting this assumption, Chew's[8] conditions for the validity of the impulse approximation should be well satisfied, since we are interested in meson velocities much greater than the nucleon velocity in the deuteron and since the expected scattering cross sections are probably less than the nucleon-nucleon cross sections.

The impulse approximation permits us to calculate the ratio of elastic to inelastic scattering as well as the angular distribution and energy spectrum of the scattered mesons in terms of the free nucleon-meson cross sections (subject to certain restrictions to be discussed in Section II).

The energy spectrum of the scattered mesons, particularly at small scattering angles, should provide a means of estimating the role of three particle effects (i.e., of the break down of the assumptions under which the impulse approximation is valid). At larger scattering angles it would appear possible to deduce the π-neutron cross section when these results are combined with the free proton-meson scattering cross section.

A study of meson-deuteron scattering on the basis of weak coupling meson theory has been made by Ferretti and Gallone[9] and by Blair.[10] Blair's results indicate that for scattering angles which are not too small and for meson energies which are not too low, the impulse approximation gives satisfactory results, the exact details depending on the nature of the theory. However, in view of the questionable reliability of meson theories, there seems to be reason for pursuing a phenomenological analysis.

II. THE FORMULATION OF THE SCATTERING PROBLEM IN TERMS OF THE IMPULSE APPROXIMATION

We shall ignore the charge exchange scattering and restrict ourselves to angles sufficiently large that coulomb scattering can be neglected. We shall also not specify whether the scattered meson is positive or negative, since in the impulse approximation any differences will arise through the free nucleon scattering characteristics, which are left arbitrary.

We introduce the scattering matrices,[11] R_P and R_N, referring respectively to scattering on free protons and neutrons. Considering for the moment R_P, we suppose the initial and final meson momenta to be, respectively, $\mathbf{q}_0$ and $\mathbf{q}$, while those for the proton are $\mathbf{p}_0$ and $\mathbf{p}$. We then write R_P in terms of relative momenta as (we use as units $\hbar=c=1$)

$$R_P=[(M+E)^{-1}(M\mathbf{q}-E\mathbf{p})|r_P|(M+E)^{-1}(M\mathbf{q}_0-E\mathbf{p}_0)] \times\delta(\mathbf{q}+\mathbf{p}-\mathbf{q}_0-\mathbf{p}_0), \quad (1)$$

* Now at Stanford University, Stanford, California.
† Now at Columbia University, New York, New York.
‡ Now at Indiana University, Bloomington, Indiana.
[1] Panofsky, Aamodt, and Hadley, Phys. Rev. **81**, 565 (1951).
[2] Camac, Corson, Littauer, Shapiro, Silverman, Wilson, and Woodward, Phys. Rev. **82**, 745 (1951).
[3] H. Bradner and S. Rankin, Phys. Rev. **80**, 916 (1950).
[4] Bernandini, Booth, Lederman, and Tinlot, Phys. Rev. **82**, 105 (1951).
[5] H. A. Bethe and R. R. Wilson, Phys. Rev. **83**, 690 (1951).
[6] Brueckner, Serber, and Watson, Phys. Rev. **84**, 258 (1951).
[7] Chedester, Isaacs, Sachs, and Steinberger, Phys. Rev. **82**, 959 (1951).
[8] G. F. Chew, Phys. Rev. **80**, 196 (1950).
[9] B. Ferretti and S. Gallone, Phys. Rev. **77**, 153 (1950).
[10] J. S. Blair, Ph.D. thesis, University of Illinois (1951). We are indebted to Dr. Blair for sending us a copy of his thesis.
[11] C. Møller, Kgl. Danske Videnskab. Selskab, Mat.-fys. Medd., Vid. **23**, No. 1 (1945).

where M is the nucleon mass and E is the total energy (rest mass plus kinetic) of the meson in the center-of-mass system. In Eq. (1) it is assumed that the proton velocities are nonrelativistic and remain so when transformed to the center-of-mass system. R_N is given by a similar expression in terms of a function r_N of the relative momenta. We write an arbitrary spin dependence for r_P and r_N as

$$r_P = r_P^1 + \sigma^P \cdot r_P^2, \qquad r_N = r_N^1 + \sigma^N \cdot r_N^2, \tag{2}$$

where σ^P and σ^N are the respective spin operators of the proton and neutron. Then the cross section for scattering by a free proton is

$$d\sigma_P/d\Omega = [(2\pi)^4/v_\pi] \int_{E_f} q^2 dq \delta(E_f - E_0) \times [|r_P^1|^2 + |r_P^2|^2], \tag{3}$$

with a similar expression for $d\sigma_N/d\Omega$, the cross section for scattering by a free neutron. Here v_π is the initial meson velocity, E_f and E_0 are the final and initial energies, respectively, of the system, and the integration is taken over final energies. For future reference, we define

$$J_0 \equiv \int_{E_f} q^2 dq \delta(E_f - E_0). \tag{4}$$

For the scattering by a deuteron, we assign the neutron respective initial and final momentum variables $\mathbf{n}_0$ and $\mathbf{n}$. Let the deuteron wave function be (we neglect the admixture of D-state)

$$\psi_D = \chi^t \phi_D(\tfrac{1}{2}(\mathbf{p}_0 - \mathbf{n}_0)) \delta(\mathbf{p}_0 + \mathbf{n}_0),$$

and that for the final state of the neutron and proton be

$$\psi_F = \chi^F \phi_F(\tfrac{1}{2}(\mathbf{p} - \mathbf{n})) \delta(\mathbf{p} + \mathbf{n} - \mathbf{K}),$$

where $\mathbf{K}$ is the recoil momentum and the χ's are spin wave functions. We must distinguish three types of final states F: singlet and triplet states for which the neutron and proton are not bound (inelastic scattering), and triplet deuteron states (elastic scattering). We suppose the relative final momentum of the two nucleons to be $\mathbf{k}$ for the inelastic scattering.

The transition amplitude for the scattering is

$$H_{FA} = (\psi_F, (R_P + R_N)\psi_D) \equiv \delta(\mathbf{q} + \mathbf{K} - \mathbf{q}_0) h_{FA}. \tag{5}$$

The differential cross section for the final triplet state inelastic scattering is

$$d\sigma^t = [(2\pi)^4/v_\pi] \int_{E_F} d^3q d^3k \delta(E_F - E_0) \textstyle\sum_S |h_{FA}^t|^2, \tag{6}$$

where $\sum_S$ means the appropriate sum and average over spin substates. E_F and E_0 are the final and initial energies of the system, the integration being taken over the former. A similar expression holds for $d\sigma^s$, the scattering to a final singlet state. For the elastic scattering, we have

$$d\sigma^d = [(2\pi)^4/v_\pi] \int_{F'} d^3q \delta(E_{F'} - E_0) \textstyle\sum_S |h_{FA}^d|^2, \tag{7}$$

where the integration is taken over the appropriate $E_{F'}$.

Referring to expressions (1) and (5), we can express h_{FA} as

$$\begin{aligned} h_{FA} = \int d^3l \chi^{*F} \Big\{ & \phi_F^*(\mathbf{l} - \tfrac{1}{2}(\mathbf{q} - \mathbf{q}_0)) \\ & \times \Big[\frac{M}{M+E} \Big(\mathbf{q} + \frac{E}{M}(\mathbf{q} - \mathbf{q}_0) - \frac{E}{M}\mathbf{l} \Big) \\ & \times |r_P| \frac{M}{M+E} \Big(\mathbf{q}_0 - \frac{E}{M}\mathbf{l} \Big) \Big] \\ & + \phi_F^*(\mathbf{l} + \tfrac{1}{2}(\mathbf{q} - \mathbf{q}_0)) \\ & \times \Big[\frac{M}{M+E} \Big(\mathbf{q} + \frac{E}{M}(\mathbf{q} - \mathbf{q}_0) + \frac{E}{M}\mathbf{l} \Big) \\ & \times |r_N| \frac{M}{M+E} \Big(\mathbf{q}_0 + \frac{E}{M}\mathbf{l} \Big) \Big] \Big\} \chi^t \phi_D(\mathbf{l}). \end{aligned} \tag{8}$$

To evaluate this integral it is necessary to remove r_P and r_N from the integrand. This can be done rigorously in any one of four limiting cases: (1) ψ_F represents a plane wave; (2) the deuteron binding energy is negligible compared to the recoil energies; (3) the ratio E/M goes to zero; (4) r_P and r_N depend only on the difference of their arguments, as is true in the Born approximation for potential scattering. For large momentum transfers conditions (1) and (2) are valid. For small momentum transfers and elastic scattering we rely largely on condition (3). The validity of condition (4) is doubtful in the present case.

We thus set $l = 0$ in r_P and r_N in Eq. (8) and remove them from the integrand. This leads to expressions of the form

$$h_{FA}^s = (s|r_P|t) I_1^s + (s|r_N|t) I_2^s, \tag{9}$$

where the notation $(s|r_P|t)$ means the matrix element of r_P for a transition from a triplet to a singlet state of the neutron-proton system, etc., and

$$\begin{aligned} I_1^s &= \int \phi_F^{*s}(r) \exp[-i\tfrac{1}{2}(\mathbf{q} - \mathbf{q}_0) \cdot \mathbf{r}] \phi_D(r) d^3r, \\ I_2^s &= \int \phi_F^{*s}(r) \exp[i\tfrac{1}{2}(\mathbf{q} - \mathbf{q}_0) \cdot \mathbf{r}] \phi_D(r) d^3r. \end{aligned} \tag{10}$$

Here $\phi_D(r)$ and $\phi_F^s(r)$ are the coordinate representations of the deuteron and final singlet wave functions of the neutron-proton system. For the elastic and final

triplet state inelastic scattering, we have corresponding expressions $h_{FA}{}^d$ and $h_{FA}{}^t$ with the appropriate wave functions $\phi_F(r)$ in the integrals (10).

As the spread in energy of the scattered meson will in most cases be small, we shall be particularly interested in just its angular distribution. In this case we integrate the differential cross section [Eq. (6)] over the energy spectrum of the scattered particles. To do this we again make use of the smallness of E/M and the loose binding of the deuteron and remove the quantities r_N and r_P from the integrand. This should not lead to significant errors, except perhaps for small angle scatterings (for which we can expect only qualitative information in any case).

Referring to the decomposition of r_P and r_N given by Eq. (2), we define

$$\begin{aligned} L_P{}^t &= |r_P{}^1|^2+\tfrac{2}{3}|r_P{}^2|^2, \\ L_P{}^s &= \tfrac{1}{3}|r_P{}^2|^2, \\ M^t &= R_e\{r_P{}^{1*}r_N{}^1+\tfrac{2}{3}\mathbf{r}_P{}^{*2}\cdot\mathbf{r}_N{}^2\}, \\ M^s &= -R_e\{\tfrac{1}{3}\mathbf{r}_P{}^{*2}\cdot\mathbf{r}_N{}^2\}, \end{aligned} \tag{11}$$

with similar quantities $L_N{}^t$ and $L_N{}^s$. "$R_e\{\cdots\}$" means "the real part of . . . ." The quantities, L, represent incoherent contributions to the cross section while the quantities, M, represent the effects of interference of meson waves scattered from the neutron and proton.

Integration over the energy spectra leads to the following differential cross sections for scattering into an angle θ:

$$\begin{aligned} d\sigma^s/d\Omega &= [(2\pi)^4/v_\tau] \\ &\quad\times J_0[(L_P{}^s+L_N{}^s)H_1{}^s(\theta)+2M^sH_2{}^s(\theta)], \\ d\sigma^t/d\Omega &= [(2\pi)^4/v_\tau] \\ &\quad\times J_0[(L_P{}^t+L_N{}^t)H_1{}^t(\theta)+2M^tH_2{}^t(\theta)], \\ d\sigma^d/d\Omega &= [(2\pi)^4/v_\tau]J_0[(L_P{}^t+L_N{}^t)+2M^t]H^d(\theta), \end{aligned} \tag{12}$$

where

$$\begin{aligned} H_1{}^s(\theta) &= (1/J_0)\int q^2dqd^3k\delta(E_F-E_0)|I_1{}^s|^2, \\ H_2{}^s(\theta) &= (1/J_0)\int q^2dqd^3k\delta(E_F-E_0)|I_2{}^{*s}I_1{}^s|. \end{aligned} \tag{13}$$

J_0 is given by Eq. (4) and $I_1{}^s$, $I_2{}^s$ are given by Eqs. (10). The triplet quantities, $H_1{}^t$ and $H_2{}^t$, are obtained by using the triplet state wave functions, $\phi_F{}^t$ in Eqs. (10). From Eq. (7) we have

$$H^d(\theta) = (1/J_0)|I_1{}^d|^2\int_{EF'} q^2dq\delta(E_F{}'-E_0), \tag{14}$$

where $I_1{}^d$ is obtained from Eq. (10) by replacing $\phi_F{}^{*s}(r)$ by $\phi_D{}^*(r)$.

For the total cross section, we add the three cross sections (12). Reference to Eqs. (11) shows that at least two-thirds of the final states are triplet, which suggests a simplification in the writing of the cross section. We define

$$\begin{aligned} H_1 &= H^d+H_1{}^t, \\ H_2 &= H^d+H_2{}^t. \end{aligned} \tag{15}$$

Then the sum of the three cross sections (12) can be written as

$$\begin{aligned} \frac{d\sigma}{d\Omega} &= \left[\frac{d\sigma_P}{d\Omega}+\frac{d\sigma_N}{d\Omega}\right]H_1+2\cos\omega\left[\frac{d\sigma_P}{d\Omega}\frac{d\sigma_N}{d\Omega}\right]^{\frac{1}{2}}H_2+\frac{(2\pi)^4}{v_\tau}J_0 \\ &\quad\times\{(L_P{}^s+L_N{}^s)(H_1{}^s-H_1)+2M^s(H_2{}^s-H_2)\}. \end{aligned} \tag{16}$$

$d\sigma_P/d\Omega$ and $d\sigma_N/d\Omega$ are defined by Eq. (3). The term proportional to $\cos\omega$ represents an interference effect between waves scattered from the proton and neutron. $\cos\omega$ can, of course, be expressed in terms of the quantities (11). As will be seen below, the last term represents only a small correction to the cross section. We have thus expressed the scattering cross section from deuterium in terms of the cross section from free protons and neutrons.

III. NUMERICAL EVALUATION

We now discuss the dependence of the functions H on the meson energy and scattering angle. We begin with two approximate evaluations, the first of which is the closure approximation.

The closure approximation implies the neglect of the energy of relative motion of the nucleons in the final state on the over-all energy conservation. The meson is assumed to have the energy characteristic of a free particle collision. The completeness relation of the final states then gives [see Eq. (13)]

$$\int d^3k|I_1{}^s|^2=1,$$

$$\int d^3k|I_2{}^{*s}I_1{}^s| = \int \exp[-i(\mathbf{q}-\mathbf{q}_0)\cdot\mathbf{r}]\phi_D{}^2(r)d^3r,$$

etc., so we obtain

$$\begin{aligned} H_1{}^s &= H_1=1, \\ H_2{}^s &= H_2=\int \exp[-i(\mathbf{q}-\mathbf{q}_0)\cdot\mathbf{r}]\phi_D{}^2(r)d^3r. \end{aligned} \tag{17}$$

The last term in Eq. (16) therefore vanishes and we obtain a very simple expression for $d\sigma/d\Omega$ which is expected to be valid for high meson energies (a further discussion is given below).

The second approximation to the total cross section involves the use of plane waves for the final state, with $H^d(\theta)=0$ [Eq. (14)]. That this is not an unreasonable approximation follows from arguments of Gluckstern and Bethe.[12] Again, the last term in Eq. (16) vanishes

[12] R. L. Gluckstern and H. A. Bethe, Phys. Rev. 81, 761 (1951).

since the plane wave approximation does not distinguish between singlet and triplet states, and we are left with just the terms involving H_1 and H_2. A numerical discussion is given in the next section.

The plane wave approximation fails for those final states in which the neutron and proton have a small energy of relative motion. For such energies only the S-wave is sufficiently distorted to necessitate correction, the waves of higher angular momentum being well represented by plane waves. Thus we can calculate the quantities H by correcting the plane wave approximation for S-waves only.

For the deuteron wave function we use the Chew-Goldberger[13] expression:

$$\phi_D(r)=(N/r)[e^{-\alpha r}-e^{-\beta r}], \tag{18}$$

where N is the appropriate factor of normalization and

$$\alpha=45.5 \text{ Mev}, \quad \beta=7\alpha.$$

For the S-wave phase shifts as a first approximation we can use the asymptotic wave functions.[14]

$$\begin{aligned}\phi_k{}^t&=\exp(-i\delta^t)\sin(kr+\delta^t)/kr,\\ \phi_k{}^s&=\exp(-i\delta^s)\sin(kr+\delta^s)/kr,\end{aligned} \tag{19}$$

where δ^s and δ^t are the appropriate singlet and triplet phase shifts.[15] A correction for the finite range of the singlet $n-p$ potential can be given in terms of the effective ranges according to the arguments of Bethe and Longmire.[16] A correction in the triplet case is obtained by replacing

$$\exp[\pm i(\mathbf{q}-\mathbf{q}_0)\cdot\mathbf{r}]$$

by

$$\{\exp[\pm i(\mathbf{q}-\mathbf{q}_0)\cdot\mathbf{r}]-1\}$$

in Eqs. (10), since the correct $\phi_k{}^t$ must be orthogonal to ϕ_D. The latter expression is small for small r, so we shall not make a further correction for small distances.

The integrals (10) can now be done analytically. With the exception of H^d, the H's must be evaluated numerically. The results are given in the next section.

IV. RESULTS AND DISCUSSION

The values of the quantities $H_1(\theta)$ and $H_2(\theta)$ [Eq. (15)] are plotted in Fig. 1 for several meson energies. The corresponding values of $H_1{}^s(\theta)$ and $H_2{}^s(\theta)$ [Eq. (13)] are plotted in Fig. 2.

We wish first of all to show that to a good approximation one may neglect the second term in Eq. (16). Reference to Figs. 1 and 2 shows that $H_1(\theta)$ and $H_1{}^s(\theta)$ differ at most by about 10 percent. For scattering angles less than 45 degrees, $H_2(\theta)$ and $H_2{}^s(\theta)$ differ at most by

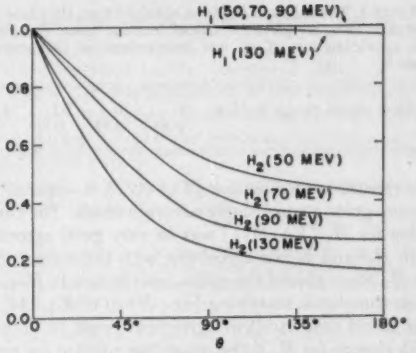

FIG. 1. Values of the functions $H_1(\theta)$ and $H_2(\theta)$ [Eq. (15)] for several incident meson energies. $H_1(\theta)$ was found to be unity at the lower energies, but dropped to about 0.97 at 180° for 130 Mev-mesons.

15 percent; at large angles where the difference is larger, the functions themselves are small compared to $H_1(\theta)$ and their difference is less than 10 percent of $H_1(\theta)$. In addition, reference to Eq. (11) shows that the coefficient of $[H_1{}^s(\theta)-H_1(\theta)]$ in Eq. (16) cannot be greater than one-third the coefficient of H_1. It follows, then, that the correction to $d\sigma/d\Omega$ arising from the second term of Eq. (16) cannot be greater than about 4 percent, except for small-angle scatterings—and so may be neglected. We therefore have

$$\frac{d\sigma}{d\Omega}=\left[\frac{d\sigma_P}{d\Omega}+\frac{d\sigma_N}{d\Omega}\right]H_1+2\cos\omega\left[\frac{d\sigma_P}{d\Omega}\frac{d\sigma_N}{d\Omega}\right]^{\frac{1}{2}}H_2, \tag{16'}$$

to a good approximation.

Reference to Fig. 1 shows that $H_1(\theta)=1$ to within about one percent for the energy range investigated (except for 130-Mev mesons, for which H_1 fell to about 0.97 at 180°). Since this is just the value obtained from

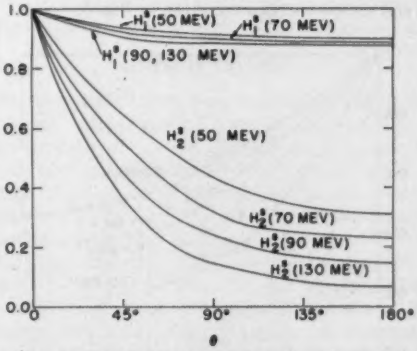

FIG. 2. Values of the functions $H_1{}^s(\theta)$ and $H_2{}^s(\theta)$ [Eq. (13)] for several incident mesons energies. The 90-Mev and 130-Mev curves very nearly coincide.

[13] G. F. Chew and M. L. Goldberger, Phys. Rev. **77**, 470 (1950).
[14] See, for instance, Watson and Stuart, Phys. Rev. **82**, 738 (1951), where the same integrals are discussed.
[15] The familiar expressions for the phase shifts in terms of the effective ranges and scattering lengths were used (see, for instance, Blatt and Jackson, Phys. Rev. **76**, 18 (1949) and H. A. Bethe, Phys. Rev. **76**, 38 (1949)).
[16] H. A. Bethe and C. Longmire, Phys. Rev. **77**, 647 (1950).

TABLE I. The values of $H_1(\theta)$, as obtained from the plane wave approximation, are given for several incident meson energies. In this approximation, $H_1(\theta)$ was independent of the scattering angle θ.

Incident meson energy in Mev	50	70	90	130
H_1	0.80	0.84	0.86	0.90

the closure approximation [Eq. (17)], it appears that closure gives a surprisingly accurate result. The closure value for H_2 [Eq. (17)] was in very good agreement with H_2' and in fair agreement with the correct value for H_2. Since almost the entire contribution to H_2 comes from the elastic scattering [i.e., $H^d(\theta)$ of Eq. (14)], it was found that excellent agreement could be obtained with closure for H_2 if the phase space factor for elastic scattering were used. This means multiplying the value for H_2 given by Eq. (17) by the factor

$$(1/J_0)\int_{EF'} q^2 dq \delta(E_F'-E_0), \qquad (20)$$

[compare Eq. (14)].

Thus, it appears that $d\sigma/d\Omega$ can be given by the closure approximation [with H_2 corrected by the factor (20)] to an accuracy which is probably about as good as the model obtained from the impulse approximation. This is fortunate, as the closure values may be easily calculated from Eq. (17).

In contrast to this, the values of H_1 and H_2 obtained from the plane wave approximation require a lengthy numerical calculation and are in general less accurate than the closure values. The quantities H_1, as obtained from the plane wave approximation, were independent of the angle of scattering (to within the estimated computational accuracy of about one percent) and are given in Table I for those meson energies included in Figs. 1 and 2.

The magnitude of the elastic scattering is described by $H^d(\theta)$ [Eqs. (12) and (14)]. Values of $H^d(\theta)$ for several meson energies are given in Fig. 3.

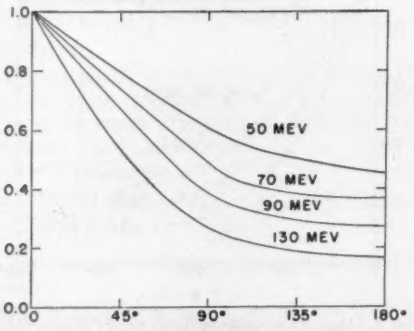

FIG. 3. Plot of the function $H^d(\theta)$ [Eq. (14)] for several incident meson energies.

For the energy spectrum of the scattered mesons, one cannot use an approximation which neglects the final neutron-proton interaction. The mesons scattered elastically have, of course, a fixed energy. Several characteristic energy spectra for the inelastic scattering are given in Fig. 4. These spectra were obtained from H_1^s and H_1^t by not performing the integrations over dq in Eqs. (13).

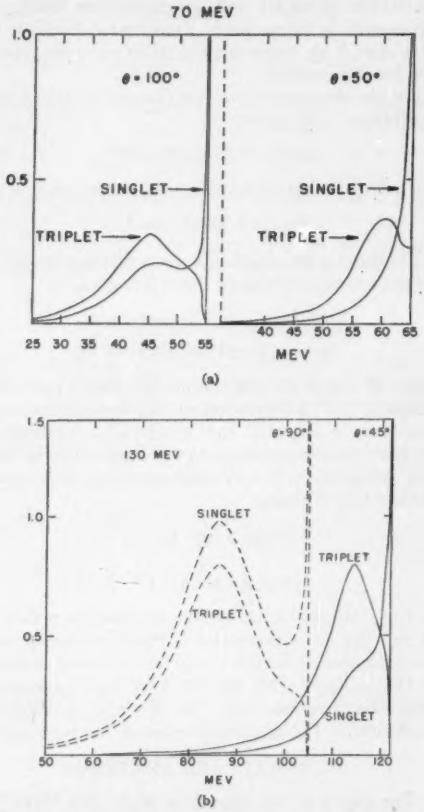

FIG. 4. Meson energy spectrum (in arbitrary units) for inelastic scattering with final singlet and triplet nucleon states. In (a) the spectra are given for an incident energy of 70 Mev and for scattering angles, θ, of 50° and 100°. In 4(b) the incident energy is 130 Mev and the scattering angles are 45° and 90°. The tendency for the curves to peak at the energy corresponding to a free particle collision should be noted.

The use of H_1 only is justified, since the spectra arising from H_2 are nearly the same when the latter is not negligibly small. The energy spectra are of importance, since they should provide a test of the degree of validity of the impulse approximation. It would seem likely that hypothetical three-body interactions should cause considerably larger energy losses for the meson than are predicted on the basis of the present model. As is seen

from Fig. 4, the energy loss of the meson on the basis of the present model tends on the average to be slightly less than that for a collision with a free nucleon.

V. CONCLUSIONS

The use of Eq. (16′) should provide a direct means of deducing the values of $d\sigma_N/d\Omega$ (that is, the cross section for scattering mesons on free neutrons) from experiments on the scattering by deuterons and protons for momentum transfers large enough that H_2 is small. Comparison of the scattering from deuterium at large and small angles should provide information about the relative phase of waves scattered from neutrons and protons.[17] This phase is described by the factor $\cos\omega$ in Eq. (16′), which may, of course, be a function of the scattering angle.

[17] H. A. Bethe and R. R. Wilson, reference 5, have shown that this is of importance in describing the scattering of mesons in complex nuclei.

For these purposes the readily applied closure approximation is satisfactory.

We are indebted to Mr. Richard I. Mitchell, Mr. Glen Culler, Mr. Burns Macdonald, and other members of the computing group at the Radiation Laboratory for performing most of the numerical calculations described in this paper.

This work was performed under the auspices of the Atomic Energy Commission.

Note added in proof:—Since many meson scattering experiments are being done by attenuation methods, it is desirable to know the cross section for charge exchange scattering. This can be calculated simply from the theory above, using the closure approximation. If we let $d\sigma_p^{exch}/d\Omega$ be the exchange cross section for π^- on protons, we obtain for the exchange cross section for π^- on deuterons:

$$\frac{d\sigma_{\pi^- D}^{exch}}{d\Omega}=\frac{d\sigma_p^{exch}}{d\Omega}[1-fH_2],$$

where H_2 is given by Eq. (17) and f is a fraction depending upon the amount of spin flip.

PHYSICAL REVIEW VOLUME 84, NUMBER 6 DECEMBER 15, 1951

Term Values in the $3d^54s$ Configuration of Fe III

R. E. TREES
University of Pennsylvania, Philadelphia, Pennsylvania
(Received August 8, 1951)

The theoretical formulas for d^5s are compared with the experimental data of Fe III. The mean deviation between theory and experiment is found to be ± 852 cm^{-1}.

We compared the values of the parameters B and G_2 which are required to give correctly the observed separations between certain pairs of terms. Adding to the theory a correction term proportional to $L(L+1)$ leads to consistent values of all the radial integral parameters. The mean deviation between the theory corrected in this manner and experiment is reduced to 105 cm^{-1}.

I. INTRODUCTION

IN conjunction with the results of two previous papers,[1,2] this study completes the analysis of the term values of the $3d^54s$ and $3d^6$ configurations in Fe III and Mn II.

A second purpose of this study is to show that the errors between theory and experiment are simply related to the orbital quantum number. Since 23* of the 32 possible terms of the $3d^54s$ configuration of Fe III are known, there is a large amount of experimental data to verify this conclusion. In addition, the term values are not appreciably affected by interactions with nearby configurations, so that the relationship of the errors to the orbital quantum number represents a polarization effect. If this effect is assumed similar in the same configurations of different atoms, one can predict more accurately the positions of terms for the experimentalist. We have tentatively made such an application of the results of this paper in a previous paper and have also used the results to verify the experimental assignments of terms to their configurations.[2]

[1] R. E. Trees, Phys. Rev. **82**, 683 (1951).
[2] R. E. Trees, Phys. Rev. **83**, 756 (1951).
* *Note added in proof:*—There are 26 known term values; the 3 highest levels were inadvertently overlooked. The values for these levels are included in Table I. The failure to include them in the least squares calculation has no effect on the conclusions.

II. TERM VALUES

The experimental term values are taken from Edlen and Swing.[3] The theoretical formulas are the same as those used for d^5s in our previous calculations[2] for Mn II, and the parameters were evaluated by least squares. The results of the calculation are given in column one of Table I; the mean deviation between theory and experiment is 852 cm^{-1}.

The theoretical formulas for all terms observed in $3d^54s$ of Fe III are rational with the exception of the two terms based on the ^3D parent. Partly as a matter of convenience, these two terms were not included in the calculation. However, our subsequent results (Table II) will indicate that the $(^3D)^1D$ term observed at

[3] B. Edlen and P. Swings, Astrophys. J. **95**, 532 (1942).

TABLE I. Term values of the $3d^44s$ configuration of Fe III (cm^{-1}). (1) No correction; (2) With $L(L+1)$−correction.

Term	Obs.	(1) Calc.	Diff.	(2) Calc.	Diff
$(^6S)^7S$	30088	30159	71	29991	−97
$(^6S)^5S$	40999	41143	144	40887	−112
$(^4G)^5G$	63465	62822	−643	63512	47
$(^4P)^5P$	66509	67948	1439	66686	177
$(^4D)^5D$	69776	70030	254	69791	15
$(^4G)^3G$	70713	70145	−568	70776	63
$(^4P)^3P$	73790	75270	1480	73951	161
$(^4D)^3D$	77028	77353	325	77054	26
$(^3I)^3I$	79847	78004	−1843	79867	20
$(^3D)^3D$	82413	(84167)	(1754)	(82855)	(442)
$(^4F)^5F$	83238	83393	155	83370	132
$(^3I)^1I$	83429	81666	−1763	83499	70
$(^3F)^3F$	84380	85189	809	84189	−191
$(^3D)^1D$	86846	(87829)	(983)	(86487)	(−359)
$(^3F)^1F$	87901	88850	949	87821	−80
$(^3H)^3H$	88775	88278	−497	88818	43
$(^3G)^3G$	89811	89330	−481	89733	78
$(^4F)^3F$	90464	90715	251	90633	169
$(^3H)^1H$	92523	91939	−584	92450	−73
$(^3F')^3F$	93395	93449	54	93320	−75
$(^3G)^1G$	93512	92992	−520	93365	−147
$(^3F'')^1F$	97040	97110	+70	96952	−88
$(^4S)^5S$		99627		98701	
$(^3S)^1S$		103288		102333	
$(^3D')^3D$	105914	106812	898	105930	16
$(^3D')^1D$	109570	110473	903	109562	−8
$(^3G')^3G$	114336	114019	−317	114469	133
$(^3G')^1G$	117950	117681	−269	118101	151
$(^3P)^3P$		131524		131008	
$(^3P)^1P$		135185		134640	
$(^3D'')^3D$		139729		138924	
$(^3D'')^1D$		143389		142556	
A		75350.75		76113.95	
B		1029.66		1058.36	
C		4107.18		3901.33	
G_2		1830.70		1816.00	
		...		80.74	
Mean deviation		852 cm^{-1}		105 cm^{-1}	

86,846 cm^{-1} may be disturbed by configuration interaction with the $^1D'$ term of the $3d^6$ configuration which is not known experimentally but which we have predicted at 76,137 cm^{-1}.[1] Interactions with other terms of the $3d^6$ configuration should produce negligible effects (i.e., less than 100 cm^{-1}), since the interacting terms are 45,000 cm^{-1} or more apart in all cases. It is likely that interactions with the $3d^44s^2$ configuration are also small, but since no terms of this configuration are known experimentally we cannot be sure that this is so.

III. CONSISTENCY OF THE PARAMETER G_2

It has been pointed out[4] that the errors between theory and experiment in fitting the $3d^44s$ configuration of VI are similar in magnitude and sign to the errors in fitting the $3d^4$ parent term in VII. The fact that the error is mainly in the parent term seems generally true, and has been pointed out in connection with the comparison of $3d^24p$ of Ti II and the $3d^2$ parent term in Ti III.[5] The addition of a $4s$ electron to the $3d^5$ parent introduces an additional parameter G_2 into the calculations. We conclude that this parameter must be definable with an accuracy that is better than the over-all accuracy of the theory, i.e., the mean deviation of our result, as the error of the parent term would otherwise not dominate.

We have checked this conclusion by subtracting the experimental values for the two possible terms that result when the $4s$ electron is added to the $3d^5$ parent. The results are given in Table II. We see that the separations of the two terms based on the ^6S and of the four pairs of terms based on the quartets of d^5 lead to G_2 values that are included in the limits $G_2=1813\pm7$. As was already pointed out, the separation of terms based on the ^2D may be in error owing to interaction with the d^6 configuration. Even excluding this value, however, the G_2 values are much less consistent for terms based on doublet parents, being included in the limits $G_2=1815\pm59$. We find that the mean deviation in explaining the ten separations of terms based on the same parents with a single parameter $G_2=1815$ cm^{-1} will be about 55 cm^{-1}, which is consistent with the conclusion that the errors are determined chiefly by the parent term.

Part of the inconsistency in G_2 values is due to neglect of nondiagonal spin orbit effects. Our calculation of these effects in the d^6 configuration of Fe III shows that the mean square value of the level shift is about 45 cm^{-1}. We have already pointed out that the effects of configuration interaction are small, but these effects would not be negligible in this calculation, and they would also require consideration. In view of our neglect of these effects, we cannot determine more exactly how consistently the value of the parameter G_2 is defined by subtracting terms based on the same parent; it also seems likely that the close agreement of G_2 values for terms based on the sextet and quartet parents is partly accidental.

TABLE II. Consistency of G_2 from subtraction of terms based on the same parent.

Parent	Separation	G_2
^6S	10911	1818
^4G	7248	1812
^4P	7281	1820
^4D	7252	1813
^4F	7226	1806
^2I	3582	1791
^2D	(4433)	(2216)
^2F	3521	1760
^2H	3748	1874
^2G	3701	1850
$^2F'$	3645	1822
Limiting values of		G_2
Sextet parent		1818
Quartet parents		1813±7
Doublet parents		1815±59

[4] A. A. Schweizer, Phys. Rev. **80**, 1080 (1950).
[5] G. Racah, Phys. Rev. **62**, 438 (1942).

IV. THE DIFFERENCES BETWEEN THEORY AND EXPERIMENT

Inspection of column 1 of Table I will show that the differences are positive for S, P, D, and F terms and are negative for G, H, and I terms. This same conclusion holds for the d^5s configuration[5] in Mn II. We note a general tendency in d^n, d^ns, and d^ns^2 configurations for the difference to decrease as the orbital quantum number increases.[1,4,6] The fact that in d^2 and d^3 the ^3P and ^1D differences are positive and the ^3F and ^1G differences are negative has been pointed out by Racah.[5]

Consideration of polarization effects would lead one to expect a dependence on spin, which is here not evident; it is hard to see a reason for the dependence on orbital quantum number.[7] This dependence of the errors on L may be considered not adequately demonstrated by the qualitative considerations of the previous paragraph, but the fact that we can find a simple formula for the L dependence of the errors that accounts quantitatively for the major part of the errors in the d^5s configuration of Fe III is a more convincing demonstration. The use of least squares in evaluating our parameters leads to a difference between the observed and calculated values that is not a very clear indication of the error in the theory which we are using, as the parameters are able to adjust themselves to compensate for the polarization effects. We propose showing that a somewhat different choice of parameters will not greatly increase the mean deviation, but that with this choice the errors will show a regular dependence on the orbital quantum number.

We simplify our considerations by making subtractions which cancel all parameters in the theory except B. Six differences were determined in this way, and the comparison with theory is given in Table III. With the least squares value of $B=1000$ cm^{-1}, the mean deviation in explaining these differences is ±1100 cm^{-1}. The average value of these six determinations of B is 1039, but the values range from 896 to 1465.

Most of the inconsistency in the values of this parameter can be removed by adding to each theoretical formula a quantity

$$\Delta E=\alpha L(L+1).$$

Table III. Consistency of B from subtraction of terms that cancel other parameters (cm^{-1}). (1) No correction; (2) With $L(L+1)$−correction.

			(1)		(2)	
Term diff.	Theory	Obs.	Calc.	Diff.	Calc.	Diff.
$(^4D)^5D-(^4G)^5G$	$7B-14\alpha$	6311	7000	689	6172	−139
$(^4F)^5F-(^4P)^5P$	$15B+10\alpha$	16729	15000	−1729	16680	−49
$(^4G)^5G-(^5I)^5I$	$11B-22\alpha$	9964	11000	1036	9856	−108
$(^3H)^3H-(^3F)^3F$	$3B+18\alpha$	4395	3000	−1395	4632	237
$(^3F')^3F-(^3G)^3G$	$4B-8\alpha$	3584	4000	416	3584	0
$(^3D')^3D-(^3H)^3H$	$18B-24\alpha$	17139	18000	861	17100	−39
			B	1000	1058	
			α	...	81	
		Mean deviation		±1100 cm^{-1}	±123 cm^{-1}	

We then find that the six differences of Table III lead to values $B=1058$ and $\alpha=81$, and the mean deviation in explaining the differences is reduced to ±123 cm^{-1}. Using the known values of B, α, and G_2, a few more subtractions can be made to show that this correction also gives consistent values for the parameters C and A.

We have also carried out a least squares calculation after adding this correction to the theory. The results of this calculation are given in column 2 of Table I; the mean deviation between theory and experiment is reduced to ±105 cm^{-1}. Since this is only slightly larger than the deviation that we would expect from neglect of configuration interaction and nondiagonal spin orbit interaction, we conclude that the correction accounts rather fully for the difference between theory and experiment. The mean deviation to which this correction corresponds will be

$$\Delta=\pm\alpha\langle\{L(L+1)-\langle L(L+1)\rangle_{\rm Av}\}^2\rangle_{\rm Av}^{\frac{1}{2}},$$

where the averages are taken over the experimentally observed terms. For our calculation, this expression has a value ±980 cm^{-1}. As would have to be the case, this is not quite as good an over-all agreement as is indicated by the deviation ±852 cm^{-1} in column 1 of Table I. However, the difference is not very great, so that our formula for the error

$$\text{Diff}=1200-81L(L+1)\pm105,$$

when the parameters of column 2 are used, will represent rather closely the trend of the errors when the parameters are evaluated by least squares, as was done in column 1.

I am very grateful to Dr. C. W. Ufford for his continued encouragement and for many helpful discussions.

[5] A. Many, Phys. Rev. **70**, 511 (1946).
[7] E. Wigner, Phys. Rev. **46**, 1002 (1934).

On the Theory of Multiple Scattering, Particularly of Charged Particles*

MING CHEN WANG AND EUGENE GUTH
University of Notre Dame, Notre Dame, Indiana
(Received July 19, 1951)

The general theory of the elastic multiple scattering of particles with a strongly anisotropic scattering function is investigated without making the small-angle approximation. The rigorous transport equation is used and approximations are introduced at a later stage. The paper consists of four parts. In the first part the general formulation of the problem is given. The approximations involved in the existing theories of small-angle forward scattering are discussed in some detail. In the second part the spherical harmonic method is formulated in a manner so as to permit an explicit expression for the general nth approximation. There is an ambiguity both in (a) the way of defining successive approximations and in (b) the way of introducing approximate boundary conditions. We have chosen (b) to give the best approximation to the exact solution of the Schwarzschild-Milne problem. In the third part it is shown that our choice of (a) for the spherical harmonic method leads to the same final formulas as the gaussian quadrature method. The relation of these two methods is discussed in detail. In the fourth part the problem of anisotropic multiple scattering is reduced to a quasi-isotropic one by using a generalized Goudsmit-Saunderson type distribution function (defined also for back scattering) as a first approximation. Three different methods are given for forward scattering (including large angles). The first method is a perturbation treatment. The second method is based on the approximate delta-function character of the scattering function and employs a Fokker-Planck type development for the peaked part of the scattering function. The third method is a Liouville-Neumann type of iteration applied directly to the transport equation. For back scattering the second and third of these methods also apply. In addition a special method is developed, based on the smallness of the back single scattering cross section. The generalized Goudsmit-Saunderson distribution function is developed in powers of the thickness of the scatterer and it is shown that all three methods lead to the same single scattering tail. The three methods can be applied for any single scattering law. The screened Born-Rutherford law is introduced in some cases as an example. The relation of the present work to previous theories is discussed.

I. INTRODUCTION

THE theory of multiple scattering has been developed in the past primarily for three groups of problems, namely, (1) radiative transfer, (2) multiple scattering of neutrons, and (3) multiple scattering of charged particles, in particular of electrons. In any problem of multiple scattering we have two steps to consider (a) the law of single scattering, (b) the statistical problem of obtaining the spatial and angular distribution of the multiply scattered light or particles, which is properly governed by a Boltzmann integro-differential equation.

We shall be concerned with the case of axial symmetry in the single scattering law and multiple scattering in a plane-parallel stratified medium. Then the distribution function will depend only on two variables: a cartesian and a polar coordinate describing the spatial and angular behavior respectively. The difficulties inherent in the statistical problem of multiple scattering are well illustrated by the fact that a closed expression for the angular and spatial distribution was obtained only for the simplest problem in multiple scattering.

A method of expanding the distribution function into Legendre polynomials[1] (spherical harmonic method, called SH in the sequel) has been applied by Gratton[2] and Chandrasekhar[3] to the isotropic problem, unfortunately using an inconvenient way of defining successive approximations. This prohibited the general formulation of the method, and made it look inferior to the method of gaussian quadrature (called GQ in the sequel). Wick[4] replaced the integral in the Boltzmann equation by a sum employing gaussian quadrature.[5] Guided by the nth approximation in the GQ method, Chandrasekhar[6] obtained exact expressions for the angular distribution for semi-infinite and finite media.

The SH method was used by several authors, notably Marshak,[7] Mark, Glauber, and Rarita from 1944 on for a variety of neutron diffusion problems. To the authors' knowledge, however, no general expressions were obtained for the nth approximation for the general anisotropic problem, nor was the relation to the GQ method treated in a general manner. The general form of the SH method as developed in this paper will be the principal method we employ. There is an ambiguity in the way of defining (a) successive approximations and (b) approximate boundary conditions in both the SH and the GQ method. This ambiguity does not seem to have been recognized in the literature. The usual procedure for (a) and (b) in the GQ method was chosen for its analytical simplicity. We shall show that for the SH method (a) can be chosen in a natural way so that the GQ and the SH methods give exactly the same

* Supported in part by ONR.

[1] Such methods have, of course, been applied to a great extent to even more complicated Boltzmann equations; see for instance, E. Guth and J. Mayerhofer, Phys. Rev. **57**, 908 (1940).

[2] L. Gratton, Soc. Astron. Ital. **10**, 309 (1937).

[3] S. Chandrasekhar, Astrophys. J. **99**, 180 (1944).

[4] G. C. Wick, Z. Physik **121**, 702 (1943).

[5] The GQ method has been applied to integral equations earlier by Nystrom, Acta Math. **54**, 185 (1930).

[6] S. Chandrasekhar, *Radiative Transfer* (Clarendon Press, Oxford, 1950).

[7] R. E. Marshak, Phys. Rev. **71**, 443 (1947).

solution. Thus GQ and SH methods differ only in analytical details, which do not affect the final form of the solution. (This is not the case when, for the SH method, Gratton or Chandrasekhar's (a) is chosen.) For the SH method our (b) differs from that used in the GQ method. Our (b) was chosen among other reasonable choices to give the best approximation to the exact solution for the isotropic case. This approximation is better than the one obtained by (b) of the GQ method. In the limit $n\to\infty$, both the GQ (b), and our (b), lead to the same exact solution. Although the GQ method and our formulation of the SH method lead to the same final result, there is some analytical advantage to the use of GQ for isotropic or quasi-isotropic problems, while SH is simpler to apply to anisotropic cases. For strongly anisotropic problems exact solutions involving Chandrasekhar's H and X, Y-functions are not practicable, since very many of these functions would have to be tabulated. For quasi-isotropic problems, on the other hand, one needs only a few of these functions.

Placzek[8] has shown that a simple iteration procedure using integral properties of the known exact solution leads to a more accurate solution than polynomial approximations using approximate boundary conditions. For the anisotropic problem, unfortunately, Placzek's procedure cannot be used, because the exact solution is not known.

The simpler features of the multiple scattering of charged particles have been described in a very instructive manner in a recent paper by Bohr.[9] For this reason we shall restrict ourselves to a brief summary of the attempts toward a more rigorous theory. Bothe[10] started with the correct Boltzmann integro-differential equation, but did not state the exact boundary conditions. From the Boltzmann equation he derived a Fokker-Planck type of differential equation. Though the transition "from Boltzmann to Fokker-Planck" assumes the "small-angle approximation," Bothe retained in the latter a factor ($\cos\vartheta$) which goes to unity in that approximation. He then tried to solve this Fokker-Planck type equation with an inexact boundary condition. Bethe, Rose, and Smith[11] have tried to obtain a solution of the same differential equation with the exact boundary conditions. We shall show later [see Sec. II(C)], however, that it seems doubtful whether such a solution does exist. Bethe, Rose, and Smith also derived a diffusion equation for back scattering from thick foils by a procedure similar to the "age" theory of neutron diffusion. Williams[12] developed a consistent theory in the small-angle approximation based on the Fokker-Planck equation, putting the factor mentioned ($\cos\vartheta$) equal to unity and using an approximate boundary condition neglecting the "back scattering." In this approximation the problem is very similar to rotatory Brownian motion, i.e., diffusion on a sphere. Goudsmit and Saunderson[13] developed a more accurate theory, which can be formulated as follows: one applies the small-angle approximation (putting $\cos\vartheta=1$) to the Boltzmann equation (instead of the Fokker-Planck equation of Williams), and uses the same approximate boundary condition as Williams does neglecting "back scattering." Goudsmit and Saunderson point out that a parameter in their theory can be considered either as the thickness of the medium or as path length, and that their solution is an exact one for the somewhat unrealistic problem of equal path lengths. Molière[14] uses an older theory of Wentzel[15] to derive an expression which is just that of Goudsmit and Saunderson if one replaces a series by an integral, and evaluates the integral. Snyder and Scott[16] derive essentially the same integral form from equations equivalent to the approximate Boltzmann equation which lead to the Goudsmit-Saunderson theory. These authors give the most extensive numerical evaluation of their formulas. For thin scatterers both Moliere and Snyder-Scott show how the multiple scattering approaches the single scattering tail. A different approach by Butler[17] leads for thin scatterers also to a separation of the gaussian multiple scattering and the single scattering tail in the small angle approximation. Butler's procedure was generalized to larger angles, still neglecting back scattering, by Teichmann.[18] Lewis[19] treats multiple scattering in an infinite medium using the path-length as a variable. He re-derives the Goudsmit-Saunderson solution and shows the transition to the Snyder-Scott integral form. One may solve the problem by getting a functional relation between path length and actual thickness of the foil, but, of course, this is just as complicated as the original problem. Rose,[20] in a note, gives an approximate expression for the path length-thickness ratio.

As is seen from this brief summary, no treatment of the exact Boltzmann equation with the exact boundary condition seems to exist in the literature. Since all consistent approximative treatments neglect back-scattering, no reliable theory of this phenomenon is available in the literature either. (Bothe[21] has recently given elementary considerations on backscattering.)

It would be very cumbersome to apply in a straightforward manner the SH (or GQ) method to the case of

[8] G. Placzek, *The Neutron Density near a Plane Surface*, National Research Council of Canada, Division of Atomic Energy MT-16.
[9] N. Bohr, Kgl. Danske Videnskab. Selskab, Mat.-fys. Medd. XVIII, 8 (1948).
[10] W. Bothe, Z. Physik **54**, 161 (1929).
[11] Bethe, Rose, and Smith, Proc. Am. Phil. Soc. **78**, 573 (1938).
[12] E. J. Williams, Proc. Roy. Soc. (London) **169**, 531 (1939).
[13] S. Goudsmit and J. L. Saunderson, Phys. Rev. **57**, 24 (1940).
[14] G. Molière, Z. Naturforsch. **3a**, 78 (1948).
[15] G. Wentzel, Ann. Physik **69**, 335 (1922).
[16] H. S. Snyder and W. T. Scott, Phys. Rev. **76**, 220 (1949).
[17] S. T. Butler, Proc. Phys. Soc. (London) **A63**, 599 (1950).
[18] T. Teichmann, *Multiple Scattering of High Energy Charged Particles in Thin Foils*, Palmer Physical Laboratory, Princeton University, Princeton, New Jersey, unpublished.
[19] H. W. Lewis, Phys. Rev. **78**, 526 (1950).
[20] M. E. Rose, Phys. Rev. **58**, 90 (1940).
[21] W. Bothe, Ann. Physik **6**, 44 (1949).

a strongly anisotropic single scattering, like Rutherford scattering. We shall show, however, how the anisotropic problem can be reduced to a quasi-isotropic one. Most of our solutions use the Goudsmit-Saunderson solution as a first approximation. However, we always start from the exact Boltzmann equation with the exact boundary conditions and make approximations at a later stage.

Section II introduces (A) the single scattering function, (B) the exact Boltzmann equation with the exact boundary condition, and (C) the different kinds of approximation for forward scattering. Section III brings the development of the SH method for the isotropic problem without incident current. Section IV contains the application of the SH method (A) to the approximate Boltzmann equation neglecting back scattering (equivalent to Goudsmit-Saunderson theory), and (B) to the exact Boltzmann equation of II(B). Section V makes a comparison of the SH and GQ methods for the case of (A) isotropic scattering and (B) anisotropic scattering, in which we also give the GQ procedure of solving the problem in IV(A). The identity of our SH and the customary GQ method is shown explicitly, apart from the boundary conditions. For the case of the isotropic problem of III, a numerical comparison of the exact, SH and GQ methods is presented. Section VI presents our theory of multiple scattering of charged particles, particularly of electrons, by reducing the anisotropic problem to a quasi-isotropic one. The sub-section (A) on forward scattering consists of: (1) a perturbation treatment using the Goudsmit-Saunderson solution as a first approximation, (2) a simple improvement of the Goudsmit-Saunderson solution based on the δ-function character of the single Rutherford scattering, and (3) an iteration procedure starting again with the Goudsmit-Saunderson solution. The subsection (B) on back scattering consists of (1) a procedure of solving the exact Boltzmann equation based on the smallness of the "backward" single scattering cross section, (2) an approximate solution similar to (A2), and (3) an iteration method similar to (A3). In subsection (C) it is shown that as the thickness of the scatterer approaches zero all three methods lead to the same single scattering tail. This is exhibited both for forward and for back scattering, using a straightforward expansion of the distribution function in powers of the thickness.

II. GENERAL FORMULATION

(A) Law of Elastic Single Scattering for Axially Asymmetric Scattering Potential

Let α be the angle between the incident velocity and the scattered velocity, and $\Phi(\cos\alpha)$ be the single scattering law. The total scattering cross section σ is given by

$$\sigma=\int_0^{2\pi}d\phi\int_0^{\pi}\Phi(\cos\alpha)\sin\alpha d\alpha,$$

where ϕ is the azimuth angle. Then we define our scattering function by

$$p(\cos\alpha)=(4\pi/\sigma)\Phi(\cos\alpha), \tag{1}$$

so that when we develop $p(\cos\alpha)$ in Legendre polynomials

$$p(\cos\alpha)=\sum_{r=0}^{\infty}\omega_r P_r(\cos\alpha), \tag{2}$$

we have $\omega_0=1$. $\Phi(\cos\alpha)$ is related to the amplitude of the scattered wave $f(\cos\alpha)$ by

$$\Phi(\cos\alpha)=|f(\cos\alpha)|^2 =|(1/2ik)\textstyle\sum_r(2r+1)(e^{2i\delta_r}-1)P_r(\cos\alpha)|^2, \tag{3}$$

where the δ_r's are the phases. The relation between the ω_r's and the δ_r's can be obtained by using the formula for the integration of the product of three Legendre polynomials given by Rose *et al.*[22]

Now with reference to an arbitrary spherical coordinate system, the directions of the incident velocity and the scattered velocity can be specified by the angles θ, ϕ and θ', ϕ' respectively. These angles are related to the angle α by the equation

$$\cos\alpha=\mu\mu'+[(1-\mu^2)(1-\mu'^2)]^{\frac{1}{2}}\cos(\phi-\phi') \tag{4}$$

where $\mu=\cos\theta$ and $\mu'=\cos\theta'$. Equation (2) then becomes

$$p(\mu,\phi,\mu',\phi') =\sum_{r=0}^{\infty}\omega_r P_r\{\mu\mu'+[(1-\mu^2)(1-\mu'^2)]^{\frac{1}{2}}\cos(\phi-\phi')\}.$$

Expanding the Legendre polynomials by the addition theorem and integrating over the variable ϕ, we get

$$p(\mu,\mu')=\frac{1}{2\pi}\int_0^{2\pi}p(\mu,\phi,\mu',\phi')d\phi =\sum_{r=0}^{\infty}\omega_r P_r(\mu)P_r(\mu'). \tag{5}$$

Practically, one does not have to take the whole infinite series (2). There is always a maximum term at which one can terminate the series with no appreciable error.

(B) Boltzmann Equation

An axially symmetric beam of particles is incident on a plane slab of scattering material with two of its dimensions infinite. Let the axis parallel to the finite dimension be the x-axis, which is also the axis of symmetry of the incident beam. The beam is incident on the surface $x=0$, and the other surface is $x=a>0$. The steady-state distribution function of the scattered

[22] Rose, Goertzel, Spinrad, Harr, and Strong, Phys. Rev. **83**, 79 (1951), Eq. (11a).

particles obeys the well-known Boltzmann equation

$$\mu(\partial f/\partial\tau)+f=\tfrac{1}{2}\int_{-1}^{1}f(\tau,\mu')p(\mu,\mu')d\mu', \qquad (6)$$

where μ is the cosine of the angle between the velocity of the particle and the x axis, $\tau=N\sigma x$, and N is the number of scattering centers per unit volume. σ and $p(\mu,\mu')$ are defined above. The problem is to solve Eq. (6) with the boundary conditions

$$f(0,\mu)=\pi F\delta(\mu-\mu_0), \quad \mu>0, \qquad (7a)$$

$$f(t,\mu)=0, \quad \mu<0, \qquad (7b)$$

where $t=N\sigma a$, and $\mu_0>0$. For simplicity here we have used a δ-function as the incident beam. Since the integral equation is linear, the solution for any arbitrary axially symmetric incident beam is just a superposition of such fundamental solutions. The integral of the δ-function over the whole solid angle is normalized to unity, while the strength of the incident beam is governed by the constant F.

If we define the integral in Eq. (6) by the function $J(\tau,\mu)$, i.e.,

$$J(\tau,\mu)=\tfrac{1}{2}\int_{-1}^{1}f(\tau,\mu')p(\mu,\mu')d\mu', \qquad (8)$$

Eq. (6) becomes

$$\mu(\partial f/\partial\tau)+f=J(\tau,\mu). \qquad (9)$$

The formal solution of Eq. (9), satisfying the boundary conditions (7), is clearly

$$f(\tau,+\mu)=e^{-\tau/\mu}\int_0^{\tau}J(\tau,\mu)e^{\tau/\mu}(d\tau/\mu) +\pi Fe^{-\tau/\mu}\delta(\mu-\mu_0), \qquad (10a)$$

$$f(\tau,-\mu)=e^{\tau/\mu}\int_{\tau}^{t}J(\tau,-\mu)e^{-\tau/\mu}d\tau/\mu. \qquad (10b)$$

Here μ is in absolute value. The expressions (10a) and (10b) correspond to the range $\mu>0$ and $\mu<0$ respectively. If one substitutes Eq. (10) into Eq. (8), one gets an integral equation for $J(\tau,\mu)$. That is

$$J(\tau,\mu)=\tfrac{1}{4}Fp(\mu,\mu_0)e^{-\tau/\mu_0} +\tfrac{1}{2}\left[\int_0^{\tau}d\tau'\int_0^{1}d\mu'-\int_{\tau}^{t}d\tau'\int_{-1}^{0}d\mu'\right]HJ(\tau',\mu'),$$

where $H=(1/\mu')p(\mu,\mu')e^{(\tau'-\tau)/\mu'}$. The function $J(\tau,\mu)$ determines the solution completely by Eqs. (10). Thus one may obtain the solution of the problem by solving the integral equation for J instead of the original integro-differential equation. For the simple case of semi-infinite, plane-parallel, isotropically scattering material without incident current, the last integral equation for $J(\tau,\mu)$ reduces to

$$J(\tau)=\int_0^{\infty}H(|\tau-\tau'|)J(\tau')d\tau',$$

with

$$H(x)=\tfrac{1}{2}\int_1^{\infty}e^{-xs}ds/s.$$

This is the Schwarzschild-Milne integral equation.

(C) Approximations for Forward Scattering

If the single scattering is mainly in the forward direction, a reasonable approximation is to replace the factor μ in the first term of Eq. (6) by μ_0 and neglect back scattering in the boundary condition. If we take $\mu_0=1$ for simplicity, the problem now becomes

$$(\partial f/\partial\tau)+f=\tfrac{1}{2}\int_{-1}^{1}f(\tau,\mu')p(\mu,\mu')d\mu', \qquad (11)$$

with the boundary condition

$$f(0,\mu)=\pi F\delta(\mu-1), \quad -1\leq\mu\leq 1. \qquad (12)$$

The exact solution of this approximate problem is

$$f(\tau,\mu)=\frac{F}{4}\sum_{r=0}^{\infty}(2r+1)P_r(\mu)e^{-k_r\tau}, \qquad (13)$$

where $k_r=[1-\omega_r/(2r+1)]$, with ω_r given by Eq. (2). This series was first derived by Goudsmit and Saunderson without explicit use of the Boltzmann equation. Their assumptions are thus equivalent to Eqs. (11) and (12).

Another kind of small-angle approximation is to replace the exact integral equation (6) by a differential equation of Fokker-Planck type. Using the definition of the function $p(\mu,\mu')$, we can rewrite Eq. (6) into the form

$$\mu\frac{\partial f}{\partial\tau}=\frac{1}{4\pi}\int_{-1}^{1}d\mu'\int_0^{2\pi}d\phi\,p(\cos\alpha)[f(\tau,\mu')-f(\tau,\mu)]. \qquad (14)$$

The three angles α, $\theta=\cos^{-1}\mu$, and $\theta'=\cos^{-1}\mu'$ form a spherical triangle as shown by Eq. (4). Now let us use the edge opposite the angle θ' as the polar axis, then we have a relation similar to (4),

$$\cos\theta'=\cos\theta\cos\alpha+\sin\theta\sin\alpha\cos\beta, \qquad (15)$$

where β is the azimuth angle in this case. Then one develops $f(\tau,\mu')$ into a Taylor series around μ, keeping terms up to α^2, and gets

$$f(\tau,\mu')=f(\tau,\mu)+\frac{\partial f}{\partial\mu}\left[\{(1-\mu^2)\}^{\frac{1}{2}}\alpha\cos\beta-\frac{\mu\alpha^2}{2}\right] +\frac{1}{2}\frac{\partial^2 f}{\partial\mu^2}(1-\mu^2)\alpha^2\cos^2\beta\cdots. \qquad (16)$$

Putting the last expression for $f(\tau, \mu')$ into Eq. (14) and integrating over the angles α and β instead of μ' and ϕ, we get

$$\mu\frac{\partial f}{\partial \tau}=-\frac{1}{\lambda}\frac{\partial}{\partial \mu}(1-\mu^2)\frac{\partial f}{\partial \mu}, \tag{17}$$

where $1/\lambda=\frac{1}{2}\int_0^\pi p(\cos\alpha)\alpha^2\sin\alpha d\alpha$, a constant. Bethe, Rose, and Smith have tried to obtain a solution of (17) with the exact boundary conditions

$$\begin{aligned} &f(0, \mu)=\pi F\delta(\mu-1), && \mu>0,\\ &f(t, \mu)=0, && \mu<0. \end{aligned} \tag{18}$$

It seems doubtful whether such a solution does exist. In fact, we shall show that the Fokker-Planck Eq. (17) and the exact boundary conditions (18) are most likely not compatible with each other.

One can easily show that the two-dimensional analog of Eq. (17) is

$$\cos\theta\partial f/\partial\tau=(1/\lambda)\partial^2 f/\partial\theta^2 \tag{19}$$

and the boundary conditions are

$$\begin{aligned} &f(0, \theta)=\pi F\delta(\theta-\theta_0), && 0\leq\theta<\pi/2,\\ &f(t, \theta)=0, && \pi/2<\theta\leq\pi. \end{aligned} \tag{20}$$

If we put $\cos\theta=1$ in the left-hand member of (19), it becomes precisely the differential equation for heat conduction in one dimension, with f playing the role of the temperature, τ the time, and θ the distance along the one-dimensional bar. Then the boundary condition (20) corresponds to the following heat conduction problem.

A bar of length π is insulated all over the surface. If the initial temperature distribution along one-half of the bar is given and if it is required that the temperature along the other half of the bar should be zero at a given later time, what is the temperature distribution along the whole bar at any time in between? It is a well-known fact in the theory of heat conduction that the temperature distribution along the bar at any later time is always analytic no matter whether the initial temperature distribution is analytic or not. Therefore, it is impossible to have the temperature zero along part of the bar at a certain later time. Now the original Eq. (19) and its corresponding three-dimensional Eq. (17) belong to the same class of parabolic equations as the heat equation, so we should expect that such general analyticity theorem holds true for all of them. How could then Bethe, Rose, and Smith obtain a solution to this seemingly insoluble problem? The answer lies, of course, in the approximations which these authors made in addition to the small-angle development. Their approximate solution implies that backscattering results mostly from such numerous small-angle single deflexions, for which Eq. (16) is a valid approximation.

The above demonstration[22] of the incompatibility of the approximate Fokker-Planck equation and the exact boundary condition indicates that if we approximate the exact integro-differential Eq. (6) by Eq. (17), we must also approximate, to be self consistent, the exact conditions (7). A self-consistent system results if we apply the same "forward" approximations in connection with the Fokker-Planck equation (17) as we did before, i.e., we put $\mu=1$ in Eq. (17) and neglect back scattering in the boundary condition. Then we solve the equation

$$\frac{\partial f}{\partial \tau}=-\frac{1}{\lambda}\frac{\partial}{\partial \mu}(1-\mu^2)\frac{\partial f}{\partial \mu}$$

with the boundary condition (12). The solution,

$$f(\tau, \mu)=\frac{F}{4}\sum_{r=0}^{\infty}(2r+1)P_r(\mu)\exp\left[-\frac{r(r+1)}{\lambda}\tau\right]$$

is, of course, an approximate form of the Goudsmit-Saunderson solution (13). This type of small-angle approximation leads exactly to Williams' theory of multiple scattering.

III. ISOTROPIC SCATTERING

Here we treat the case of a semi-infinite, plane-parallel, isotropically scattering material without incident current. The appropriate integral equation for this problem is, from Eq. (6),

$$\mu(\partial f/\partial\tau)+f=\tfrac{1}{2}\int_{-1}^{1}f(\tau, \mu)d\mu \tag{21}$$

and the boundary conditions are

$$f(0, \mu)=0, \quad \mu>0, \tag{22a}$$

$$f(\tau, \mu)e^{-\tau}\to 0, \quad \tau\to\infty. \tag{22b}$$

To solve this boundary value problem, we first develop the unknown function $f(\tau, \mu)$ in a series of Legendre polynomials in μ with unknown functions of τ as coefficients, i.e., let

$$f(\tau, \mu)=\tfrac{1}{2}\sum_{r=0}^{\infty}(2r+1)f_r(\tau)P_r(\mu). \tag{23}$$

Substituting (23) into Eq. (21) and using both the recursion formula,

$$(2r+1)\mu P_r(\mu)=(r+1)P_{r+1}(\mu)+rP_{r-1}(\mu),$$

and the orthogonality relation of Legendre polynomials, we get

$$\sum_{r=0}^{\infty}\left[r\frac{df_{r-1}}{d\tau}+(r+1)\frac{df_{r+1}}{d\tau}\right]P_r(\mu) = \sum_{r=0}^{\infty}[\delta_{r0}-(2r+1)]f_rP_r(\mu).$$

[22] We are indebted to G. E. Uhlenbeck for suggesting this argument.

Since this is an identity in μ, we can equate coefficients of the $P_r(\mu)$'s and thus obtain the infinite system

$$r\frac{df_{r-1}}{d\tau}+(2r+1-\delta_{r0})f_r+(r+1)\frac{df_{r+1}}{d\tau}=0,$$

$$r=0, 1, 2\cdots, \quad (24)$$

or, in matrix notation,

$$\begin{bmatrix} 0 & D & 0 & 0 & \cdots \\ D & 3 & 2D & 0 & \cdots \\ 0 & 2D & 5 & 3D & \cdots \\ 0 & 0 & 3D & 7 & \cdots \\ \cdot & \cdot & \cdot & \cdot & \cdots \\ \cdot & \cdot & \cdot & \cdot & \cdots \\ \cdot & \cdot & \cdot & \cdot & \cdots \end{bmatrix}\begin{bmatrix} f_0 \\ f_1 \\ f_2 \\ f_3 \\ \cdot \\ \cdot \\ \cdot \end{bmatrix}=\begin{bmatrix} 0 \\ 0 \\ 0 \\ 0 \\ \cdot \\ \cdot \\ \cdot \end{bmatrix}; \text{ or } \mathbf{\Delta f}=0, \quad (25)$$

where $D=d/d\tau$, $\mathbf{\Delta}=\mathbf{\Delta}(D)$, and $\mathbf{f}$ is a column-matrix.

The infinite system of interconnected Eqs. (25) is hardly manageable. We can approximate, however, this infinite system by a finite system which is much easier to handle. Clearly, there is no unique way of defining the successive approximations. The following choice recommends itself by the ease with which the nth approximation can be obtained explicitly. We define the nth approximation as the solution obtained by retaining the left upper corner submatrix of $2n$ rows and $2n$ columns, and putting all the other elements equal to zero. It is then obvious that the nth approximation approaches the exact solution as $n\to\infty$. This finite system of $2n$ linear differential equations with constant coefficients can be easily solved. All the f_r's are solutions of the differential equation

$$\Delta_n(D)f_r=0 \quad r=0, 1, 2\cdots(2n-1), \quad (26)$$

where

$$\Delta_n(D)=\begin{vmatrix} 0 & D & 0 & 0 & \cdots & \cdots \\ D & 3 & 2D & 0 & \cdots & \cdots \\ 0 & 2D & 5 & 3D & \cdots & \cdots \\ 0 & 0 & 3D & 7 & \cdots & \cdots \\ \cdot & \cdot & \cdot & \cdot & \cdots & \cdots \\ \cdot & \cdot & \cdot & \cdot & \cdots & \cdots \\ \cdot & \cdot & \cdot & \cdot & \cdots & \cdots \\ \cdot & \cdot & \cdot & \cdot & \cdots & (4n-1) \end{vmatrix}. \quad (27)$$

Since the determinant $\Delta_n(D)$ has an even number of rows, $\Delta_n(-D)$ is equivalent to $\Delta_n(D)$ with all the diagonal elements negative instead of positive. But it can be easily proved that $\Delta_n(D)$ does not change its value if all the diagonal elements change their signs, because all terms have even number of diagonal elements as factors. Therefore, $\Delta_n(D)=\Delta_n(-D)$, and its roots are in pairs with same absolute value but opposite in sign. One pair of the roots is obviously $D=0$, and let us denote the other $n-1$ pairs of nonvanishing roots by k_α with $k_{-\alpha}=-k_\alpha$ and $\alpha=\pm1, \pm2, \cdots\pm(n-1)$.

Then the general solution of Eq. (26) is

$$f_r=\sum_{\alpha=-(n-1)}^{n-1}A_{r\alpha}\exp(-k_\alpha\tau)+B_r\tau+C_r,$$

$$r=0, 1, 2\cdots(2n-1), \quad (28)$$

where the $A_{r\alpha}$'s B_r's, and C_r's are arbitrary constants, but they are not all independent.

To find the relations among the constants, we substitute Eq. (28) back into Eq. (24), and equate the coefficients of $\exp(-k_\alpha\tau)$, etc., since the resulting equation is an identity in τ. We get from the coefficient of $\exp(-k_\alpha\tau)$

$$k_\alpha rA_{r-1,\alpha}-(2r+1-\delta_{r0})A_{r\alpha}+k_\alpha(r+1)A_{r+1,\alpha}=0, \quad (29a)$$

from the coefficients of τ

$$(2r+1-\delta_{r0})B_r=0, \quad (29b)$$

from the constant term

$$rB_{r-1}+(2r+1-\delta_{r0})C_r+(r+1)B_{r+1}=0. \quad (29c)$$

Equation (29a) is a recursion formula for the $A_{r\alpha}$'s. The $2n$ linear homogeneous equations ($r=0, 1, 2\cdots(2n-1)$) of $2n+1$ unknowns $A_{0\alpha}, A_{1\alpha}\cdots A_{2n,\alpha}$ cannot determine all the unknowns uniquely. But we know that $A_{2n,\alpha}=0$, since for this nth approximation we have put $f_{2n}=0$. There remains one arbitrary unknown, which we shall take to be $A_{0\alpha}$. All the other $A_{r\alpha}$'s will then be proportional to $A_{0\alpha}$, so let us define $\rho_r(k_\alpha)$ by

$$A_{r\alpha}=\rho_r(k_\alpha)A_{0\alpha}. \quad (30)$$

Then Eq. (29a) becomes a recursion formula for ρ_r, that is

$$\rho_{r+1}(k_\alpha)-\frac{2r+1-\delta_{r0}}{k_\alpha(r+1)}\rho_r(k_\alpha)+\frac{r}{r+1}\rho_{r-1}(k_\alpha)=0,$$

$$\rho_0=1. \quad (31a)$$

Equation (29b) shows that

$$B_r=0 \text{ for all } r, \text{ except } B_0 \text{ is arbitrary.} \quad (31b)$$

Equation (29c) becomes, using (31b),

$$rB_{r-1}+(2r+1-\delta_{r0})C_r=0,$$

which gives

$$\left.\begin{array}{ll} r=0, & C_0 \text{ is arbitrary} \\ r=1, & C_1=-B_0/3 \\ r\geq2, & C_r=0 \end{array}\right\}. \quad (31c)$$

Therefore, we have altogether $2n$ independent arbitrary constants, that is

$$A_{0\alpha}, B_0, C_0, \quad \alpha=\pm1, \pm2\cdots\pm(n-1),$$

among which one is the proportionality factor determined by the assigned constant net flux in the material. The remaining $2n-1$ constants will be determined by the boundary conditions (22). The boundary condition

TABLE I. Values of $(2/B_0)f(0,-\mu)$ from Eq. (36b).

		Gaussian quadrature method			Spherical Harmonic method[a]												Chandrasekhar's SH method[b]		
					$r=0,1,2,\cdots n-1$			$r=n,n+1,\cdots 2n-1$			r even			r odd					
μ	Exact	$n=1$	$n=2$	$n=3$	$n=1$	$n=2$	$n=3$	$n=1$	$n=2$	$n=3$	$n=1$	$n=2$	$n=3$	$n=1$	$n=2$	$n=3$	$n=1$	$n=2$	$n=3$
0	0.5774	0.5774	0.5774	0.5774	0.5	0.5620	0.5656	0.6667	0.8452	5.080	0.5	0.5532	0.5632	0.6667	0.6026	0.5918	0.6667	0.5862	0.5920
0.1	0.7202		0.6965	0.7048		0.6896	0.7000		0.9689	5.393		0.6769	0.6949		0.7195	0.7166		0.7091	0.7047
0.2	0.8373		0.8103	0.8219		0.8094	0.8210		1.0858	5.627		0.7938	0.8146		0.8316	0.8322		0.8224	0.8147
0.3	0.9483		0.9207	0.9338		0.9243	0.9351		1.1986	5.820		0.9066	0.9281		0.9407	0.9432		0.9351	0.9231
0.4	1.0561		1.0288	1.0422		1.0359	1.0453		1.3086	5.989		1.0166	1.0380		1.0478	1.0511		1.0456	1.0301
0.5	1.1621		1.1352	1.1493		1.1452	1.1530		1.4165	6.143		1.1245	1.1455		1.1535	1.1573		1.1543	1.1359
0.6	1.2668		1.2405	1.2547		1.2528	1.2590		1.5231	6.285		1.2311	1.2516		1.2582	1.2623		1.2617	1.2410
0.7	1.3706		1.3450	1.3591		1.3591	1.3639		1.6285	6.420		1.3365	1.3565		1.3620	1.3664		1.3681	1.3454
0.8	1.4738		1.4487	1.4627		1.4645	1.4679		1.7332	6.549		1.4412	1.4604		1.4653	1.4697		1.4736	1.4493
0.9	1.5765		1.5519	1.5658		1.5691	1.5712		1.8371	6.673		1.5451	1.5638		1.5682	1.5726		1.5784	1.5527
1.0	1.6788	1.5774	1.6547	1.6684	1.5	1.6731	1.6740	1.6667	1.9405	6.794	1.5	1.6485	1.6667	1.6667	1.6706	1.6751	1.6667	1.6827	1.6557

[a] The different r means the different choice of the n equations among the system (33) of $2n$ equations to determine the arbitrary constants.
[b] The last three columns are from reference 3.

(22b) forces us to discard all terms with $\exp(+k_\alpha\tau)$, so that

$$A_{0\alpha}=0 \quad \text{for} \quad \alpha=-1,-2\cdots-(n-1). \tag{32}$$

Thus, finally, we have n constants left to be determined by the other condition (22a), which cannot be strictly satisfied in this approximation, of course. There are an infinite number of ways to construct the corresponding approximate boundary condition, just as the ways of defining the nth approximation of the solution were not unique. Again, the logical choice should be based upon simplicity and the convergence of the result. The simple approximation of boundary condition (22a) appropriate for this method is

$$\int_0^1 P_r(\mu)f(0,\mu)d\mu=0, \quad r\leq 2n-1. \tag{33}$$

The system (33) has $2n$ equations, which is double the number of unknowns to be determined. Here we choose to take those equations with odd r, because this choice gives the most convergent approximation, as shown in Table I, among other reasonable choices. Thus the n equations are

$$\sum_{m=0}^{2n-1}\frac{2m+1}{2}f_m(0)\int_0^1 P_r(\mu)P_m(\mu)d\mu=0, \qquad r=1,3\cdots(2n-1) \tag{34}$$

in which we have made the substitution

$$f(0,\mu)=\tfrac{1}{2}\sum_{m=0}^{2n-1}(2m+1)P_m(0)P_m(\mu).$$

The function J in the formal solution (10) for this case is

$$J(\tau)=\tfrac{1}{2}\int_{-1}^1 f(\tau,\mu)d\mu$$

which is just $\frac{1}{2}f_0(\tau)$. Therefore, using (28) and (32), we have

$$J(\tau)=\tfrac{1}{2}\left[\sum_{\alpha=1}^{n-1}A_{0\alpha}\exp(-k_\alpha\tau)+B_0\tau+C_0\right]. \tag{35}$$

Substituting this expression into (10) with $F=0$ and $t\to\infty$, we get the final solution for the nth approximation

$$f(\tau,+\mu)=\tfrac{1}{2}\left[\sum_{\alpha=1}^{n-1}A_{0\alpha}\frac{\exp(-k_\alpha\tau)-e^{-\tau/\mu}}{1-k_\alpha\mu}+B_0\tau+(C_0-B_0\mu)(1-e^{-\tau/\mu})\right] \tag{36a}$$

$$f(\tau,-\mu)=\tfrac{1}{2}\left[\sum_{\alpha=1}^{n-1}A_{0\alpha}\frac{\exp(-k_\alpha\tau)}{1+k_\alpha\mu}+B_0\tau+(C_0+B_0\mu)\right]. \tag{36b}$$

Such a simple form for the nth approximation is not easily obtained from another, otherwise quite reasonable, way of defining successive approximations due to Chandrasekhar. He defines the nth approximation as the solution obtained by retaining $2n+1$ rows and columns of the infinite matrix Δ defined by Eq. (25).

The function $f(0,-\mu)$ (known as the law of darkening in astronomy) has its exact closed form worked out by many authors.[24] They present different ways of deriving the same final solution in the form of a complex integral,[25] which can be evaluated by numerical integration for particular cases. Halpern, Lueneberg, and Clark[26] have obtained an exact solution for the function $f(0,-\mu)$ for the case with incident current in the form of a complex integral, and Chandrasekhar[27] got the same solution later by a different method.

IV. ANISOTROPIC SCATTERING

We generalize the simple problem treated in the previous section in two respects. First, we admit a general anisotropic single scattering function as defined

[24] E. Hopf, *Mathematical Problem of Radiative Equilibrium* (Cambridge University Press, London, 1934); E. A. Schuchard and E. A. Uehling, Phys. Rev. **58**, 611 (1940); M. M. Crum, Quart. J. Math. **18**, 244 (1947); and reference 6, Chap. III and V.
[25] G. Placzek and W. Seidel have given a simplified derivation in Phys. Rev. **72**, 550 (1947).
[26] Halpern, Lueneberg, and Clark, Phys. Rev. **53**, 173 (1938).
[27] See reference 6, Chap. III and V.

by Eq. (1); second, we consider the case with an incident current. It is convenient to reformulate the boundary value problem defined by Eqs. (6) and (7). Let

$$f(\tau, \mu)=I(\tau, \mu)+\pi F\delta(\mu-\mu_0)e^{-\tau/\mu_0}. \quad (37)$$

Putting (37) into Eq. (6), we get the integral equation for $I(\tau, \mu)$,

$$\mu\partial I/\partial\tau+I=\tfrac{1}{2}\int_{-1}^{1}I(\tau, \mu')p(\mu, \mu')d\mu' +\tfrac{1}{4}Fp(\mu, \mu_0)e^{-\tau/\mu_0}. \quad (38)$$

The boundary conditions, Eq. (7), become

$$I(0, \mu)=0, \quad \mu>0, \quad (39a)$$

$$I(t, \mu)=0, \quad \mu<0. \quad (39b)$$

Here we define $J(\tau, \mu)$ as

$$J(\tau, \mu)=\tfrac{1}{2}\int_{-1}^{1}I(\tau, \mu')p(\mu, \mu')d\mu'+\tfrac{1}{4}Fp(\mu, \mu_0)e^{-\tau/\mu_0}. \quad (40)$$

Then the formal solution, similar to Eqs. (10), is

$$I(\tau, +\mu)=e^{-\tau/\mu}\int_0^{\tau}J(\tau, \mu)e^{\tau/\mu}d\tau/\mu, \quad (41a)$$

$$I(\tau, -\mu)=e^{\tau/\mu}\int_{\tau}^{t}J(\tau, -\mu)e^{-\tau/\mu}d\tau/\mu. \quad (41b)$$

(A) Approximate Boltzmann Equation

We have made a small-angle approximation for Eqs. (6) and (7) to get Eqs. (11) and (12). Now if we make the same approximation for Eqs. (38) and (39), we get

$$(\partial I/\partial\tau)+I=\tfrac{1}{2}\int_{-1}^{1}I(\tau, \mu')p(\mu, \mu')d\mu'+\tfrac{1}{4}Fp(\mu, 1)e^{-\tau} \quad (42)$$

and

$$I(0, \mu)=0, \quad -1\leq\mu\leq1. \quad (43)$$

Although we know the exact solution of this approximate boundary value problem, yet we shall work out the approximatioxs of this problem by both the SH and the GQ methods, and compare them with the corresponding approximations of the exact problem later.

In the SH method we develop both functions I and p in Eq. (42) in series of Legendre polynomials. The development for I is

$$I(\tau, \mu)=\tfrac{1}{2}\sum_{r=0}^{\infty}(2r+1)I_r(\tau)P_r(\mu), \quad (44)$$

and that for p is given by Eq. (5). Substituting both developments into (42), and equating coefficients of $P_r(\mu)$, we get the infinite system, similar to (24),

$$dI_r/d\tau=-k_rI_r+\tfrac{1}{2}F(1-k_r)e^{-\tau}, \quad r=0, 1, 2\cdots, \quad (45)$$

where $k_r=1-\omega_r/(2r+1)$. The system (45) can be immediately integrated, and, for the nth approximation, we have

$$I_r(\tau)=\tfrac{1}{2}F(C_re^{-k_r\tau}-e^{-\tau}), \quad r=0, 1, 2\cdots(2n-1), \quad (46)$$

where the C_r's are integration constants to be determined by the boundary condition (43). From (44) we have

$$I_r(0)=\int_{-1}^{1}I(0, \mu)P_r(\mu)d\mu,$$

which, in view of (43), gives $I_r(0)=0$. Therefore, $C_r=1$. Putting (5) and (44) with finite upper limit into (40) and using (46), one gets

$$J(\tau, \mu)=\frac{F}{4}\sum_{r=0}^{2n-1}\omega_rP_r(\mu)e^{-k_r\tau}. \quad (47)$$

The same small-angle approximation by the GQ method will be treated in a later section.

The formal solution, corresponding to Eq. (41), in this case is

$$I(\tau, +\mu)=e^{-\tau}\int_0^{\tau}J(\tau, \mu)e^{\tau}d\tau, \quad (48a)$$

$$I(\tau, -\mu)=e^{-\tau}\int_0^{\tau}J(\tau, -\mu)e^{\tau}d\tau. \quad (48b)$$

Putting the expression (47) for $J(\tau, \mu)$ into Eq. (48), and then from Eq. (37) (with $\mu_0=1$) we obtain the final solution,

$$f(\tau, +\mu)=\frac{F}{4}\sum_{r=0}^{2n-1}(2r+1)P_r(\mu)(e^{-k_r\tau}-e^{-\tau}) +\pi F\delta(\mu-1)e^{-\tau}, \quad (49a)$$

$$f(\tau, -\mu)=\frac{F}{4}\sum_{r=0}^{2n-1}(-1)^r(2r+1)P_r(\mu)(e^{-k_r\tau}-e^{-\tau}). \quad (49b)$$

When $n\to\infty$, the two expressions of (49) reduce to the identical form

$$f(\tau, \mu)=\frac{F}{4}\sum_{r=0}^{\infty}(2r+1)P_r(\mu)e^{-k_r\tau}, \quad -1\leq\mu\leq1, \quad (50)$$

which is the exact solution (13).

(B) Exact Boltzmann Equation

In this section we will get the solution of the exact integral equation (38) with boundary condition (39) by the SH approximation. The procedure is the same as in the isotropic case, except here we have an inhomogeneous term in the integral equation, and the scattering function $p(\mu, \mu')$ is a series given by Eq. (5) instead of just the first term, unity. So now if we develop the function $I(\tau, \mu)$ and equate coefficients,

we get the infinite system, corresponding to (24),

$$r(dI_{r-1}/d\tau)+S_rI_r+(r+1)dI_{r+1}/d\tau=\tfrac{1}{2}Fe^{-\tau/\mu_0}\omega_rP_r(\mu_0), \quad r=0, 1, 2\cdots, \quad (51)$$

where

$$S_r=2r+1-\omega_r, \quad S_0=0. \quad (52)$$

Since Eq. (24) is identical with the homogeneous part of Eq. (51) if δ_{r0} is replaced by ω_r, the general solution of the associated homogeneous system of Eq. (51) in the nth approximation must be of the form (28), i.e.,

$$I_r=\sum_{\alpha=-(n-1)}^{n-1}A_{r\alpha}\exp(-k_\alpha\tau)+B_r\tau+C_r, \quad r=0, 1, 2\cdots(2n-1), \quad (53)$$

where the constants are related by

$$A_{r\alpha}=\rho_r(k_\alpha)A_{0\alpha}, \quad A_{0\alpha} \text{ arbitrary}, \quad (54a)$$

$$\rho_{r+1}(k_\alpha)-\frac{2r+1-\omega_r}{k_\alpha(r+1)}\rho_r(k_\alpha)+\frac{r}{r+1}\rho_{r-1}(k_\alpha)=0, \quad \rho_0=1, \quad (54b)$$

$$B_0 \text{ arbitrary}, \quad B_1=B_2=\cdots=B_{2n-1}=0, \quad (54c)$$

$$C_0 \text{ arbitrary}, \quad C_1=-B_0/(3-\omega_1), \quad C_2=C_3=\cdots C_{2n-1}=0, \quad (54d)$$

equations similar to Eqs. (30) to (31c). The k_α's are the nonvanishing roots of the determinant

$$\Delta_n(D)=\begin{vmatrix} 0 & D & 0 & 0 & \cdots & \cdots \\ D & S_1 & 2D & 0 & \cdots & \cdots \\ 0 & 2D & S_2 & 3D & \cdots & \cdots \\ 0 & 0 & 3D & S_3 & \cdots & \cdots \\ \cdot & \cdot & \cdot & \cdot & \cdots & \cdots \\ \cdot & \cdot & \cdot & \cdot & \cdots & \cdots \\ \cdot & \cdot & \cdot & \cdot & \cdots & \cdots \\ \cdot & \cdot & \cdot & \cdot & \cdots & S_{2n-1} \end{vmatrix}. \quad (55)$$

From the form of the nonhomogeneous part of the system (51), it is obvious that the particular integral must be of the form

$$I_r=g_re^{-\tau/\mu_0}, \quad r=0, 1, 2\cdots(2n-1), \quad (56)$$

where the g_r's are constants, but not arbitrary. To determine the g_r's, we substitute (56) into Eq. (51) and get the recursion formula for g_r

$$(r/\mu_0)g_{r-1}-S_rg_r+[(r+1)/\mu_0]g_{r+1}=-\tfrac{1}{2}F\omega_rP_r(\mu_0). \quad (57)$$

We first split the inhomogeneous term as follows

$$\tfrac{1}{2}F\omega_rP_r(\mu_0)=\tfrac{1}{2}(F/\mu_0)[(2r+1)\mu_0P_r(\mu_0)-S_r\mu_0P_r(\mu_0)] =\tfrac{1}{2}F[(r/\mu_0)P_{r-1}(\mu_0)-S_rP_r(\mu_0) +\{(r+1)/\mu_0\}P_{r+1}(\mu_0)].$$

Then Eq. (57) can be put into the form

$$(r/\mu_0)h_{r-1}-S_rh_r+\{(r+1)/\mu_0\}h_{r+1}=0, \quad (58)$$

where

$$h_r=g_r+\tfrac{1}{2}FP_r(\mu_0). \quad (59)$$

Since the recursion formula (29a) (with δ_{r0} replaced by ω_r) reduces to (58) with $k_\alpha=1/\mu_0$, h_r must be connected with h_0 by an equation similar to (30), that is,

$$h_r=\rho_r(1/\mu_0)h_0, \quad (60)$$

where the ρ_r's obey the recursion formula (54b). Now $g_{2n}=0$ in this approximation, so that, by Eq. (59),

$$h_{2n}=\tfrac{1}{2}FP_{2n}(\mu_0). \quad (61)$$

With Eq. (61) the system of Eqs. (58) determines uniquely all the remaining h_r's, but it is necessary only to determine one of them, say h_0, from which all the other h_r's can be obtained by Eq. (60). It is easier to visualize the result which we are going to obtain, if the system of Eq. (58) is written in the matrix form

$$\begin{pmatrix} 0 & 1/\mu_0 & 0 & 0 & \cdots & \cdot \\ 1/\mu_0 & -S_1 & 2/\mu_0 & 0 & \cdots & \cdot \\ 0 & 2/\mu_0 & -S_2 & 3/\mu_0 & \cdots & \cdot \\ 0 & 0 & 3/\mu_0 & -S_3 & \cdots & \cdot \\ \cdot & \cdot & \cdot & \cdot & \cdots & \cdot \\ \cdot & \cdot & \cdot & \cdot & \cdots & \cdot \\ \cdot & \cdot & \cdot & \cdot & \cdots & \cdot \\ \cdot & \cdot & \cdot & \cdot & \cdots & -S_{2n-1} \end{pmatrix} \begin{pmatrix} h_0 \\ h_1 \\ h_2 \\ h_3 \\ \cdot \\ \cdot \\ \cdot \\ h_{2n-1} \end{pmatrix} = \begin{pmatrix} 0 \\ 0 \\ 0 \\ 0 \\ \cdot \\ \cdot \\ \cdot \\ -{}_nFP_{2n}(\mu_0)/u_0 \end{pmatrix}, \quad (62)$$

where we have made use of (61). Solving this inhomogeneous system, it is easy to see that

$$h_0=nFP_{2n}(\mu_0)(2n-1)!/[\mu_0{}^{2n}\Delta_n(1/\mu_0)], \quad (63)$$

where Δ_n is defined by (55). Therefore, combining (60) and (63),

$$h_r=\frac{FP_{2n}(\mu_0)(2n)!}{2\mu_0{}^{2n}\Delta_n(1/\mu_0)}\rho_r(1/\mu_0). \quad (64)$$

The complete solution is the sum of (53) and (56) with g_r given by (59) and (64). Thus we have

$$I_r=\sum_{\alpha=-(n-1)}^{n-1}A_{r\alpha}\exp(-k_\alpha\tau)+B_r\tau+C_r +\frac{F}{2}\left[\frac{P_{2n}(\mu_0)(2n)!}{\mu_0{}^{2n}\Delta_n(1/\mu_0)}\rho_r\left(\frac{1}{\mu_0}\right)-P_r(\mu_0)\right]e^{-\tau/\mu_0}. \quad (65)$$

The constants in the solution obey the conditions (54a) to (54d), which leaves only $2n$ independent arbitrary constants to be determined by the boundary conditions. We shall again approximate the boundary conditions (39) by the $2n$ equations

$$\int_{-1}^{0} P_r(\mu)I(t,\mu)d\mu=0, \qquad r=1,3,\cdots(2n-1),$$

$$\int_{0}^{1} P_r(\mu)I(0,\mu)d\mu=0,$$

or

$$\sum_{k=0}^{2n-1}\beta_{rk}I_k(t)=0, \qquad r=1,3\cdots(2n-1), \tag{66}$$

$$\sum_{k=0}^{2n-1}\epsilon_{rk}I_k(0)=0,$$

where

$$\beta_{rk}=\tfrac{1}{2}(2k+1)\int_{-1}^{0}P_k(\mu)P_r(\mu)d\mu,$$

$$\epsilon_{rk}=\tfrac{1}{2}(2k+1)\int_{0}^{1}P_k(\mu)P_r(\mu)d\mu.$$

The constants β_{rk}'s and ϵ_{rk}'s can be easily calculated. Table II is sufficient for the first three approximations. The system (66) provides $2n$ equations to determine the $2n$ independent arbitrary constants, $A_{0\alpha}$ ($\alpha=\pm1, \pm2\cdots\pm(n-1)$), B_0 and C_0. The function $J(\tau,\mu)$

TABLE II.

Values of β_{rk}							Values of ω_k						
r \ k	0	1	2	3	4	5	r \ k	0	1	2	3	4	5
1	$\frac{-1}{4}$	$\frac{1}{2}$	$\frac{-5}{16}$	0	$\frac{3}{32}$	0	1	$\frac{1}{4}$	$\frac{1}{2}$	$\frac{5}{16}$	0	$\frac{-3}{32}$	0
3	$\frac{1}{16}$	0	$\frac{-5}{16}$	$\frac{1}{2}$	$\frac{-81}{256}$	0	3	$\frac{-1}{16}$	0	$\frac{5}{16}$	$\frac{1}{2}$	$\frac{81}{256}$	0
5	$\frac{-1}{32}$	0	$\frac{25}{256}$	0	$\frac{-81}{256}$	$\frac{1}{2}$	5	$\frac{1}{32}$	0	$\frac{-25}{256}$	0	$\frac{81}{256}$	$\frac{1}{2}$

defined by (40) is, in this approximation,

$$J(\tau,\mu)=\tfrac{1}{2}\sum_{r=0}^{2n-1}\omega_r P_r(\mu)I_r(\tau) + \frac{F}{4}e^{-\tau/\mu_0}\sum_{r=0}^{2n-1}\omega_r P_r(\mu)P_r(\mu_0). \tag{67}$$

Putting the expression (65) for I_r into Eq. (67) and making use of Eqs. (54a), (54b), and (54c), we have

$$J(\tau,\mu)=\tfrac{1}{2}\Bigg[\sum_{\alpha=-(n-1)}^{n-1}A_{0\alpha}\exp(-k_\alpha\tau)\sum_{r=0}^{2n-1}\omega_r\rho_r(k\alpha)P_r(\mu) + B_0\tau+C_0-B_0\frac{\omega_1}{3-\omega_1}\mu+\frac{FP_{2n}(\mu_0)(2n)!}{2\mu_0{}^{2n}\Delta_n(1/\mu_0)}e^{-\tau/\mu_0} \times\sum_{r=0}^{2n-1}\omega_r\rho_r(1/\mu_0)P_r(\mu)\Bigg]. \tag{68}$$

Then we get the final solution by substituting the expression (68) into Eq. (41) and in turn into (37)

$$f(\tau,+\mu)=\tfrac{1}{2}\Bigg[\sum_{\alpha=-(n-1)}^{n-1}\frac{A_{0\alpha}(\exp(-k_\alpha\tau)-e^{-\tau/\mu})}{1-\mu k_\alpha}\sum_{r=0}^{2n-1}\omega_r\rho_r(k_\alpha)P_r(\mu)+B_0\tau+\left(C_0-\frac{3B_0}{3-\omega_1}\mu\right)(1-e^{-\tau/\mu}) + \frac{FP_{2n}(\mu_0)(2n)!}{2\mu_0{}^{2n}\Delta_n(1/\mu_0)}\frac{e^{-\tau/\mu_0}-e^{-\tau/\mu}}{1-\mu/\mu_0}\sum_{r=0}^{2n-1}\omega_r\rho_r(1/\mu_0)P_r(\mu)\Bigg]+\pi F\delta(\mu-\mu_0)e^{-\tau/\mu_0} \tag{69a}$$

$$f(\tau,-\mu)=\tfrac{1}{2}\Bigg[\sum_{\alpha=-(n-1)}^{n-1}\frac{A_{0\alpha}\left[\exp(-k_\alpha\tau)-\exp\left(-k_\alpha t-\frac{t-\tau}{\mu}\right)\right]}{1+\mu k_\alpha}\sum_{r=0}^{2n-1}(-1)^r\omega_r\rho_r(k_\alpha)P_r(\mu) + B_0(\tau-te^{-(t-\tau)/\mu})+\left(C_0+\frac{3B_0}{3-\omega_1}\mu\right)(1-e^{-(t-\tau)/\mu})+\frac{FP_{2n}(\mu_0)(2n)!}{2\mu_0{}^{2n}\Delta_n(1/\mu_0)} \times\frac{\exp\left(-\frac{\tau}{\mu_0}\right)-\exp\left(-\frac{t}{\mu_0}-\frac{t-\tau}{\mu}\right)}{1+\mu/\mu_0}\sum_{r=0}^{2n-1}(-1)^r\omega_r\rho_r(1/\mu_0)P_r(\mu)\Bigg]. \tag{69b}$$

V. COMPARISON WITH GAUSSIAN QUADRATURE METHOD

(A) Isotropic Scattering

Wick and Chandrasekhar have worked out the problem defined by Eqs. (21) and (22) with the GQ method. Chandrasekhar's expression for the function $J(\tau)$[23] is of the same form as (35), and we shall prove that the k_α's are really identical.

First we shall get a relation between our f_r and

[23] Reference 6, Chapter III, Eq. (44).

Chandrasekhar's I_i, which in our notation is $f(\tau, \mu_i)$. In the nth approximation, the development (23) becomes

$$f(\tau, \mu)=\tfrac{1}{2}\sum_{r=0}^{2n-1}(2r+1)f_r P_r(\mu) \tag{70}$$

where $P_r(\mu)$ can certainly be expressed by the Lagrange interpolation formula

$$P_r(\mu)=\sum_{i=-n}^{n} P_r(\mu_i)\frac{P_{2n}(\mu)}{(\mu-\mu_i)P_{2n}'(\mu_i)}. \tag{71}$$

Here the μ_i's are the roots of $P_{2n}(\mu)$. Putting the expression (71) in Eq. (70) and interchanging the sums, we get

$$f(\tau, \mu)=\sum_{i=-n}^{n}\sum_{r=0}^{2n-1}\frac{2r+1}{2}f_r P_r(\mu_i)\frac{P_{2n}(\mu)}{(\mu-\mu_i)P_{2n}'(\mu_i)}. \tag{72}$$

Now in the GQ method, one simply approximates the function $f(\tau, \mu)$ by the interpolation formula

$$f(\tau, \mu)=\sum_{i=-n}^{n} f(\tau, \mu_i)\frac{P_{2n}(\mu)}{(\mu-\mu_i)P_{2n}'(\mu_i)}$$

$$=\sum_{i=-n}^{n} I_i\frac{P_{2n}(\mu)}{(\mu-\mu_i)P_{2n}'(\mu_i)}. \tag{73}$$

Comparing Eqs. (72) and (73) we have the required relation,

$$I_i=\sum_{r=0}^{2n-1}\tfrac{1}{2}(2r+1)f_r P_r(\mu_i), \quad i=\pm 1, \pm 2\cdots\pm n, \tag{74}$$

or, in matrix notation,

$$\mathbf{I}=\mathbf{S}\mathbf{f},$$

where

$$S_{ir}=\tfrac{1}{2}(2r+1)P_r(\mu_i). \tag{75}$$

The inverse transformation

$$\mathbf{f}=\mathbf{S}^{-1}\mathbf{I} \tag{76}$$

has its matrix elements

$$S_{rk}^{-1}=a_k P_r(\mu_k), \tag{77}$$

where the a_k's are the gaussian weights. Using Eqs. (75) and (77), it can be shown that

$$(S^{-1}S)_{ij}=\sum_{k=-n}^{n}\tfrac{1}{2}(2j+1)a_k P_i(\mu_k)P_j(\mu_k)=\delta_{ij}, \tag{78a}$$

$$(SS^{-1})_{ij}=\sum_{r=0}^{2n-1}\tfrac{1}{2}(2r+1)a_j P_r(\mu_i)P_r(\mu_j)=\delta_{ij}. \tag{78b}$$

These are just the orthogonality and the closure relations of Legendre polynomials in finite dimensions.

Now the two sets of linear homogeneous constant coefficient differential equations of this problem for the two methods are related by the same linear transformation. In the GQ method the set of $2n$ equations[39] is

$$\mu_i(\partial I_i/\partial\tau)+I_i=\tfrac{1}{2}\sum_{j=-n}^{n} a_j I_j, \quad i=\pm 1, \pm 2\cdots\pm n,$$

or, in matrix notation,

$$\boldsymbol{\alpha}\mathbf{I}=0, \tag{79}$$

where

$$\alpha_{ij}=(\mu_j D+1)\delta_{ij}-a_j/2, \quad D\equiv\partial/\partial\tau. \tag{80}$$

In the SH method, the set is (24) or

$$\frac{r}{2r+1}\frac{df_{r-1}}{d\tau}+(1-\delta_{r0})f_r+\frac{r+1}{2r+1}\frac{df_{r+1}}{d\tau}=0,$$

$$r=0, 1, 2\cdots(2n-1),$$

which, in matrix notation, can be written as

$$\boldsymbol{\beta}\mathbf{f}=0, \tag{81}$$

with

$$\beta_{rm}=(1-\delta_{r0})\delta_{rm}+\frac{D}{2r+1}[(m+1)\delta_{r,m+1}+m\delta_{r,m-1}]. \tag{82}$$

Using the definitions (75) and (77) of the matrices $\mathbf{S}$ and $\mathbf{S}^{-1}$, and the orthogonality relation (78a), one can easily verify that

$$\mathbf{S}^{-1}\boldsymbol{\alpha}\mathbf{S}=\boldsymbol{\beta}.$$

Therefore, in view of (76), we have

$$\mathbf{S}^{-1}\boldsymbol{\alpha}\mathbf{S}\mathbf{S}^{-1}\mathbf{I}=\boldsymbol{\beta}\mathbf{f}.$$

Thus, the set of equations (79) are transformed to the set (81).

In order to prove that the k_α's given by the two methods are identical, one notices that the vanishing of the determinant $|\alpha|$ leads immediately to the characteristic equation in the GQ method, and the vanishing of the determinant $|\beta|$, which is essentially our Δ_n defined by (27), gives the characteristic equation in the SH method. Now since $\boldsymbol{\alpha}$ and $\boldsymbol{\beta}$ are connected by the transformation $\mathbf{S}$, it is well known that the characteristic roots must be identical. Chandrasekhar[20] has also derived a characteristic equation which does not explicitly involve the a_i's and μ_i's. This is essentially our equation $|\beta|=0$ with only a different constant factor.

The approximate boundary conditions in the two methods are not identical, so the arbitrary constants and the final solutions too, or course, are slightly

[39] The difference in sign between this system of equations and Chandrasekhar's system (reference 6, Chapter III, Eq. (2)) is because he measures angle from the negative instead of the positive x axis. Consequently all his μ's should be replaced by $-\mu$'s before comparison can be made with our results.

[20] Reference 6, Chapter III, Eq. (33).

different. We shall prove now that the difference vanishes when $n\to\infty$ as it should be since both approach the exact solution.

The boundary condition in the GQ method is when $\tau=0$, $I_i=0$ for $i=1, 2\cdots n$. Using Eq. (74), that means

$$\sum_{r=0}^{2n-1} S_{ir}f_r(0)=0, \quad i=1, 2\cdots n, \tag{83}$$

where S_{ir} is defined by (75). The boundary condition in the SH method is given by Eq. (34), i.e.,

$$\sum_{r=0}^{2n-1} R_{kr}f_r(0)=0, \quad k=1, 3, 5\cdots(2n-1), \tag{84}$$

where

$$R_{kr}=\tfrac{1}{2}(2r+1)\int_0^1 P_k(\mu)P_r(\mu)d\mu. \tag{85}$$

Now if we premultiply the coefficient matrix of the system (83) by any nonsingular constant matrix, say **T**, of n rows and n columns to form a new coefficient matrix for the system, nothing is changed essentially. Let the elements of the T-matrix be defined as

$$T_{ki}=b_iP_k(\mu_i), \qquad \begin{matrix} i=1, 2\cdots n, \\ k=1, 3, 5\cdots(2n-1), \end{matrix}$$

where the μ_i's are the positive roots of $P_{2n}(\mu)$, and

$$b_i=\frac{1}{F_n'(\mu_i)}\int_0^1 \frac{F_n(\mu)}{\mu-\mu_i}d\mu, \tag{86}$$

with

$$F_n(\mu)=\prod_{j=1}^{n}(\mu-\mu_j).$$

Then the new coefficient matrix for (83) will have elements

$$Q_{kr}=\sum_{i=1}^{n} T_{ki}S_{ir}=\tfrac{1}{2}(2r+1)\sum_{i=1}^{n} b_iP_k(\mu_i)P_r(\mu_i). \tag{87}$$

We wish to show that $Q_{kr}=R_{kr}$ as $n\to\infty$. With b_i defined by (86) we can construct the quadrature formula

$$\int_0^1 g(\mu)d\mu=\sum_{i=1}^{n} b_ig(\mu_i),$$

which is exact for any function $g(\mu)$ if $n\to\infty$. Thus it follows that the two expressions (85) and (87) are the same as $n\to\infty$. Therefore, Eqs. (83) and (84) are identical in the limit, and so are the final solutions.

Table I gives the exact value and the approximations of the function $f(0, -\mu)$ for this case. Wick has already plotted the first four columns in his paper mentioned above. Among the different choices of the approximate boundary condition for our SH approximation, the odd-r choice gives the best result, and it converges faster to the exact solution than the GQ approximation also, except at the point $\mu=0$, where the GQ method gives the exact result in all approximations. The last three columns are Chandrasekhar's SH approximation, which is different from ours both in the way of defining the nth approximation and in the choice of the equations of the boundary condition. His successive approximations converge slower than the GQ approximations, and, a fortiori, slower than the SH approximations with the odd-r boundary conditions.

An advantage of the GQ boundary conditions is that they permit one to express the nth approximation in a closed form. Thus, heuristically, the transition to an exact solution by means of an H-function is facilitated, though, as we have seen, the odd-r condition leads to faster convergence. For the anisotropic case, the SH procedure is analytically simpler than the GQ procedure.

(B) Anisotropic Scattering

To solve the approximate problem defined by Eqs. (42) and (43) by means of the GQ method, we, following Chandrasekhar, first approximate the integral in Eq. (42) by a sum. For the nth approximation, put

$$\tfrac{1}{2}\int_{-1}^{1} I(\tau, \mu')p(\mu, \mu')d\mu'=\tfrac{1}{2}\sum_{j=-n}^{n} a_jI_jp(\mu, \mu_j), \tag{88}$$

where the symbols have the usual meaning. Substituting (88) into Eq. (42) and using (5), we get the following system of equations:

$$\frac{\partial I_i}{\partial\tau}+I_i=\tfrac{1}{2}\sum_{r=0}^{2n-1}\omega_rP_r(\mu_i)\sum_{j=-n}^{n}a_jI_jP_r(\mu_j)$$

$$+\frac{F}{4}\epsilon^{-\tau}\sum_{r=0}^{2n-1}\omega_rP_r(\mu_i), \quad i=\pm1, \pm2\cdots\pm n. \tag{89}$$

To get the solution of the associated homogeneous system of (89),

$$\frac{\partial I_i}{\partial\tau}+I_i=\tfrac{1}{2}\sum_{r=0}^{2n-1}\omega_rP_r(\mu_i)\sum_{j=-n}^{n}a_jI_jP_r(\mu_j), \tag{90}$$

let

$$I_i=g_i\epsilon^{-k\tau}$$

where g_i and k are constants. From Eq. (90) we have

$$g_i=\frac{1}{1-k}\sum_{r=0}^{2n-1}\omega_rP_r(\mu_i)\rho_r, \tag{91}$$

where

$$\rho_r=\tfrac{1}{2}\sum_{j=-n}^{n}a_jg_jP_r(\mu_j). \tag{92}$$

Eliminating the g_i's from Eqs. (91) and (92), we get

$$\rho_r=\tfrac{1}{2}\sum_{j=-n}^{n} a_j P_r(\mu_j)\frac{1}{1-k}\sum_{\lambda=0}^{2n-1}\omega_\lambda P_\lambda(\mu_j)\rho_\lambda$$

$$=\frac{1}{1-k}\sum_{\lambda=0}^{2n-1}\omega_\lambda\rho_\lambda\frac{\delta_{\lambda r}}{2r+1}=\frac{1}{1-k}\frac{\omega_r\rho_r}{2r+1},$$

or

$$\left(\frac{1}{1-k}\frac{\omega_r}{2r+1}-1\right)\rho_r=0,\quad r=0,1,2\cdots(2n-1).$$

This is the characteristic equation for k, so the roots are

$$k_r=1-\omega_r/(2r+1),\quad r=0,1,2\cdots(2n-1). \tag{93}$$

For a certain root of k, say k_α, the only nonvanishing ρ_r is ρ_α which is arbitrary. Therefore, the corresponding g_i given by (91) reduces to only one term, that is,

$$g_i=(1-k_\alpha)^{-1}\omega_\alpha P_\alpha(\mu_i)\rho_\alpha;$$

and it follows that

$$I_i=(1-k_\alpha)^{-1}\omega_\alpha P_\alpha(\mu_i)\rho_\alpha\exp(-k_\alpha\tau),$$
$$\alpha=0,1,2\cdots(2n-1). \tag{94}$$

The general solution is a linear combination of (94), i.e.,

$$I_i=\sum_{\alpha=0}^{2n-1}\frac{\rho_\alpha}{1-k_\alpha}\omega_\alpha P_\alpha(\mu_i)\exp(-k_\alpha\tau)$$
$$=\sum_{r=0}^{2n-1}\rho_r(2r+1)P_r(\mu_i)e^{-k_r\tau}, \tag{95}$$

where we have made use of Eq. (93).

To get the particular integral of the nonhomogeneous system (89), let

$$I_i=\tfrac{1}{4}Fh_ie^{-\tau}. \tag{96}$$

Then we get for h_i the following system of linear equations:

$$\sum_{i=-n}^{n}h_i\frac{a_i}{2}\sum_{r=0}^{2n-1}\omega_r P_r(\mu_i)P_r(\mu_j)=-\sum_{r=0}^{2n-1}\omega_r P_r(\mu_j),$$
$$j=\pm1,\pm2\cdots\pm n. \tag{97}$$

It can be easily verified that

$$h_i=-\sum_{r=0}^{2n-1}(2r+1)P_r(\mu_i),\quad i=\pm1,\pm2\cdots\pm n, \tag{98}$$

is the solution of the system (97).

Combining (95) and (96), we get the complete solution for Eq. (89):

$$I_i=\sum_{r=0}^{2n-1}\rho_r(2r+1)P_r(\mu_i)e^{-k_r\tau}-\frac{F}{4}e^{-\tau}\sum_{r=0}^{2n-1}(2r+1)P_r(\mu_i),$$
$$i=\pm1,\pm2\cdots\pm n. \tag{99}$$

The $2n$ constants $\rho_0,\ \rho_1\cdots\rho_{2n-1}$ are determined by the boundary condition (43), which in this approximation becomes when

$$\tau=0,\quad I_i=0\quad\text{for}\quad i=\pm1,\pm2\cdots\pm n. \tag{100}$$

With condition (100), Eq. (99) gives

$$\rho_r=\tfrac{1}{4}F,\quad r=0,1,2\cdots(2n-1).$$

Thus finally we have

$$I_i=\frac{F}{4}\sum_{r=0}^{2n-1}(2r+1)P_r(\mu_i)(e^{-k_r\tau}-e^{-\tau}). \tag{101}$$

One then substitutes the expression (101) into (88) and in turn into Eq. (40) with $\mu_0=1$ to get the function $J(\tau,\mu)$ as follows:

$$J(\tau,\mu)=\frac{F}{4}\sum_{r=0}^{2n-1}\omega_r P_r(\mu)e^{-k_r\tau}. \tag{102}$$

This is identical with (47), since the difference in boundary condition in the SH and GQ method does not show up if we neglect back scattering. However, the analytical procedure is, obviously, simpler in the SH than in the GQ method. This is only natural, since also in the GQ method one develops the scattering function into a Legendre series and then it is clearly advantageous to develop $f(\tau,\mu)$ also into a Legendre series.

The GQ approximation of the exact integral equation (38) has been worked out by Chandrasekhar.[31] Using his expression of I_j in (88), one gets from (40) an expression for $J(\tau,\mu)$ which can be shown to be identical with (68). To prove the identity of these two expressions, we have to redefine the arbitrary constants in the following way

$$A_{0\alpha}=\tfrac{1}{2}FL_\alpha,\quad B_0=\tfrac{1}{2}F(1-\tfrac{1}{3}\omega_1)L_0,\quad C_0=\tfrac{1}{2}FL_n$$

and to show that the k_α's are the same and

$$\frac{P_{2n}(\mu_0)(2n)!}{\mu_0^{2n}\Delta_n(1/\mu_0)}=H(\mu_0)H(-\mu_0). \tag{103}$$

The proof for the identity of the k_α's in this case is essentially the same as that given for the case of isotropic scattering, except that here

$$\alpha_{ij}=(\mu_jD+1)\delta_{ij}-\frac{a_j}{2}\sum_{r=0}^{2n-1}\omega_r P_r(\mu_i)P_r(\mu_j)$$

instead of (80), and in the expression (82) for β_{rm} one should replace δ_{r0} by $\omega_r/(2r+1)$, so that

$$\beta_{rm}=\left(1-\frac{\omega_r}{2r+1}\right)\delta_{rm}+\frac{D}{2r+1}[(m+1)\delta_{r,m+1}+m\delta_{r,m-1}].$$

[31] See reference 6, Sec. 48.

Using the same transformation matrix **S**, the rest of the proof goes through exactly the same. Thus we have shown in this general case how one gets a characteristic equation which does not explicitly involve the a_i's and μ_i's. However, it does not mean that the characteristic roots are independent of the particular quadrature used. In fact, the values of the roots are different if one uses different quadrature formula. The identity of the roots for the two methods in the present case in obviously due to the fact that both are developments of the same polynomial, namely the Legendre polynomial.

To prove the identity (103), we need the explicit expression for $H(\mu_0)H(-\mu_0)$ as given by Chandrasekhar, i.e.,

$$H(\mu_0)H(-\mu_0)=(-1)^n\prod_{i=1}^{n-1}\frac{1}{1-k_i^2\mu_0^2}\prod_{i'=1}^{n}\frac{\mu_0^2-\mu_{i'}^2}{\mu_{i'}^2}.$$

Now since the $\mu_{i'}$'s are the $2n$ roots of $P_{2n}(\mu)$, it is clear that

$$\prod_{i=1}^{n}\frac{\mu_0^2-\mu_{i'}^2}{\mu_{i'}^2}=\frac{P_{2n}(\mu_0)}{(-1)^nP_{2n}(0)}=\frac{2\cdot4\cdot6\cdots2n}{1\cdot3\cdot5\cdots(2n-1)}P_{2n}(\mu_0).$$

Since the k_i's are the $2n-2$ roots of $\Delta_n(D)/(-D^2)$,

$$\prod_{i=1}^{n-1}(1-k_i^2\mu_0^2)=(\mu_0^2)^{n-1}\prod_{i=1}^{n-1}\left(\frac{1}{\mu_0^2}-k_i^2\right)$$

$$=\frac{\mu_0^{2n-2}\Delta_n(1/\mu_0)/(-1/\mu_0^2)}{(-1)^{n-1}[3\cdot5\cdot7\cdots(2n-1)]^2},$$

where the denominator is the coefficient of the highest power of D in $-\Delta_n(D)/D^2$. Combining these results we get (103) immediately.

Since we have proved that the GQ approximation of Chandrasekhar gives an expression for $J(\tau, \mu)$ identical in form with our Eq. (68), it follows that the final solution $f(\tau, +\mu)$ and $f(\tau, -\mu)$ also must be identical in form with our Eqs. (69a) and (69b). However, the numerical values of the arbitrary constants are slightly different because of the different ways of approximating the boundary condition in the two methods. Consequently, for any finite approximation, the two methods will give slightly different numerical values for the final solution too. Table III gives the forward scattering in the first three approximations for both methods, and the corresponding approximations for the approximate integral equation.

The parameters used in constructing Table III coincide with the first case of Goudsmit-Saunderson's Table I[32] (i.e., $\log\xi=4$, $\mu=0.0025$).

[32] S. Goudsmit and J. L. Saunderson, Phys. Rev. **58**, 36 (1940).

TABLE III. Values of $(4/F)[f(t,+\mu)-\pi F\delta(\mu-1)e^{-t}]$ from Eq. (69a).[a]

	n=1			n=2			n=3		
μ	GQ	SH	Ap[b]	GQ	SH	Ap[b]	GQ	SH	Ap[b]
0	2.292	2.430	1.0	−3.60	−4.01	−1.26	3.35	3.89	1.29
0.1				−4.39	−4.65	−1.76	4.13	4.47	1.86
0.2				−4.85	−4.95	−2.04	4.05	4.20	1.82
0.3				−4.86	−4.83	−2.01	2.99	3.01	1.05
0.4				−4.31	−4.17	−1.59	1.08	1.07	−0.34
0.5				−3.07	−2.85	−0.67	−1.24	−1.17	−1.97
0.6				−1.03	−0.79	0.81	−3.09	−2.84	−3.09
0.7				1.93	2.13	2.96	−3.11	−2.62	−2.55
0.8				5.94	6.02	5.85	0.67	1.33	1.30
0.9				11.10	10.98	9.58	10.87	11.49	10.69
1.0	6.256	6.075	3.9	17.54	17.11	14.23	30.90	31.04	28.47

[a] Parameters: $\omega_1=2.9941$, $\omega_2=4.9741$, $\omega_3=6.9343$, $\omega_4=8.8702$, $\omega_5=10.778$, $t=19.46$.
[b] The values in these three columns are from the solution of the approximate integral equation (Eq. (49a) instead of Eq. (69a)).

VI. REDUCTION OF THE ANISOTROPIC PROBLEM TO A QUASI-ISOTROPIC ONE

(A) Forward Scattering

(1) Theoretically the expression (69a) gives the forward scattering to any degree of accuracy one wants. But if the single scattering function is extremely forward, one has to carry the approximation to a large n in order to get some sensible result. This means a tremendous amount of numerical work, so it is not too desirable in practice.

Now, since the Goudsmit-Saunderson solution (50) gives a pretty good approximation for forward scattering, we can consider this as the first approximation of a perturbation treatment. First we rewrite the integral equation (6) as follows:

$$(\partial f/\partial\tau)+f=\tfrac{1}{2}\int_{-1}^{1}f(\tau,\mu')p(\mu,\mu')d\mu'+\epsilon(1-\mu)\partial f/\partial\tau. \quad (104)$$

The parameter ϵ, which is inserted here to indicate that the term is small, will be set equal to unity eventually. Let

$$f=f_1+\epsilon f_2.$$

Putting this into (104), we get one equation with terms free from ϵ

$$(\partial f_1/\partial\tau)+f_1=\tfrac{1}{2}\int_{-1}^{1}f_1(\tau,\mu')p(\mu,\mu')d\mu', \quad (105)$$

and another one involving ϵ (with ϵ put equal to unity)

$$\mu(\partial f_2/\partial\tau)+f_2=\tfrac{1}{2}\int_{-1}^{1}f_2(\tau,\mu')p(\mu,\mu')d\mu'+(1-\mu)\partial f_1/\partial\tau. \quad (106)$$

If f_1 and f_2 satisfy the boundary conditions,

$$f_1(0,\mu)=\pi F\delta(\mu-1), \quad -1\leq\mu\leq1, \quad (107a)$$

$$f_2(0,\mu)=0, \quad \mu>0, \quad (107b)$$

$$f_2(t,\mu)=-f_1(t,\mu), \quad \mu<0, \quad (107c)$$

TABLE IV. Forward scattering.[a]

θ	Goudsmit-Saunderson solution[b]	Correction term[c]
0°	120.9	2.57
6°	72.6	2.45
12°	26.3	2.08
18°	8.3	1.55
24°	2.7	0.97
30°	1.1	0.44
45°	0.1	−0.08

[a] Parameters have same values as in Table III.
[b] Values from reference 32.
[c] Difference of last two columns in Table III.

f will satisfy the original boundary condition (7) with $\mu_0=1$. Up to this point everything is still exact. Equations (105), (106), and (107) are just another way of defining the original problem (6) and (7).

The solution of Eq. (105) with boundary condition (107a) is just the Goudsmit-Saunderson solution (50). With f_1 given, one then wishes to find the correction term f_2 satisfying (106), (107b), and (107c). Here we will make the approximation by taking the finite series solution (49) for f_1 instead of (50) in Eq. (106), and then solve the problem to the same SH approximation with the corresponding approximation in boundary condition. This approximate solution for f_2 is simply the difference of the two series solutions, (69a)−(49a) with $\mu_0=1$ and $\tau=t$. Thus we have for forward scattering

$$f(t,\mu)=\text{Goudsmit-Saunderson solution (50)}+[(69a)-(49a)]. \quad (108)$$

Table IV gives both the Goudsmit-Saunderson value (or f_1) and the correction (or f_2) for the special case which is treated in Table III. In calculating f_2, one does not need to carry the approximation to a large n as in the case of calculating the original f, because the extremely anisotropic part has been taken care of by the first approximation f_1. Here the correction term is calculated with $n=3$, which is, of course, just the difference of the last two columns of Table III. One notices from Table III that in the region with positive values (the negative values in the table are meaningless), the percentage difference between the solutions for the exact and the approximate integral equations decreases steadily with the increase of approximation, and for the third approximation it is only about 8 percent for $\mu=1$. Therefore, the Goudsmit-Saunderson value there probably would not be more than 8 percent off from the exact value. Our correction in Table IV is about 2 percent at $\mu=1$ or $\theta=0°$.

(2) Another simple approximation for f_2 is to make use of the fact that the single scattering function is extremely forward, which means the function $p(\mu,\mu')$ has a sharp peak at $\mu'=\mu$ approximately.[33] So we develop the function f_2 under the integral of Eq. (106) in a Taylor series around $\mu'=\mu$, that is

$$f_2(\tau,\mu')=f_2(\tau,\mu)+[\partial f_2(\tau,\mu)/\partial\mu](\mu'-\mu)\cdots. \quad (109)$$

Then we get

$$\frac{1}{2}\int_{-1}^{1} f_2(\tau,\mu')p(\mu,\mu')d\mu'$$

$$=f_2(\tau,\mu)+\frac{1}{2}\frac{\partial f_2}{\partial\mu}\sum_{r=0}^{\infty}\omega_r P_r(\mu)\int_{-1}^{1}P_r(\mu')(\mu'-\mu)d\mu'\cdots$$

$$=f_2(\tau,\mu)-\mu k_1\frac{\partial f_2}{\partial\mu}\cdots, \quad (110)$$

where $k_1=(1-\frac{1}{2}\omega_1)$. Using (110), Eq. (106) becomes

$$\mu(\partial f_2/\partial\tau)+\mu k_1(\partial f_2/\partial\mu)=(1-\mu)(\partial f_1/\partial\tau). \quad (111)$$

For first approximation, we omit the second term of Eq. (111), since $k_1\ll 1$. Then the solution which satisfies the boundary conditions (107b) and (107c) is

$$f_2(\tau,\mu)=\begin{cases}[(1-\mu)/\mu]f_1(\tau,\mu), & \mu>0;\\ [(1-\mu)/\mu]f_1(\tau,\mu)-(1/\mu)f_1(t,\mu), & \mu<0.\end{cases}$$

For second approximation, we let

$$f_2=g_1+g_2, \quad (112)$$

where $g_1\gg g_2$. Putting Eq. (112) into Eq. (111), but omitting g_2 in the second term, we get the first- and second-order equations

$$\partial g_1/\partial\tau=[(1-\mu)/\mu]\partial f_1/\partial\tau, \quad (113a)$$

and

$$\partial g_2/\partial\tau=-k_1(\partial g_1/\partial\mu), \quad (113b)$$

respectively. The solutions of Eqs. (113a) and (113b) are

$$g_1=[(1-\mu)/\mu]f_1+A(\mu), \quad (114a)$$

$$g_2=-k_1\int_0^{\tau}(\partial g_1/\partial\mu)d\tau+B(\mu)-A(\mu), \quad (114b)$$

where $A(\mu)$ and $B(\mu)$ are arbitrary functions. To satisfy the boundary conditions (107b) and (107c), we find that

$A(\mu)=0$ and $B(\mu)$

$$=\begin{cases}0, & \mu>0;\\ k_1\int_0^{t}(\partial g_1/\partial\mu)d\tau-(1/\mu)f_1(t,\mu), & \mu<0.\end{cases} \quad (115)$$

Combining Eqs. (112), (114), and (115), we have, for

[33] The peak is usually not at $\mu'=\mu$, but a little distance off. For example, in the case we used for constructing Table III, $\mu'=1.000082\mu$ for values of μ^2 not too near unity.

the second approximation,

$$f_2(\tau,\mu)=\begin{cases}\dfrac{1-\mu}{\mu}f_1(\tau,\mu)-k_1\displaystyle\int_0^\tau\left(\frac{1-\mu}{\mu}\frac{\partial f_1}{\partial\mu}-\frac{f_1}{\mu^2}\right)d\tau, & \mu>0;\\ \dfrac{1-\mu}{\mu}f_1(\tau,\mu)-\dfrac{1}{\mu}f_1(t,\mu)-k_1\left[\displaystyle\int_0^\tau-\int_0^t\right]\left(\frac{1-\mu}{\mu}\frac{\partial f_1}{\partial\mu}-\frac{f_1}{\mu^2}\right)d\tau, & \mu<0.\end{cases}$$

Then we have the final solution

$$f(\tau,\mu)=f_1+f_2=\begin{cases}\dfrac{f_1(\tau,\mu)}{\mu}-k_1\displaystyle\int_0^\tau\left(\frac{1-\mu}{\mu}\frac{\partial f_1}{\partial\mu}-\frac{f_1}{\mu^2}\right)d\tau, & \mu>0; \qquad (116a)\\ \dfrac{f_1(\tau,\mu)-f_1(t,\mu)}{\mu}-k_1\left[\displaystyle\int_0^\tau-\int_0^t\right]\left(\frac{1-\mu}{\mu}\frac{\partial f_1}{\partial\mu}-\frac{f_1}{\mu^2}\right)d\tau, & \mu<0, \qquad (116b)\end{cases}$$

where f_1 is the solution (50). The forward scattering is given by (116a) with $\tau=t$, i.e.,

$$f(t,\mu)=\frac{f_1(t,\mu)}{\mu}-k_1\int_0^t\left(\frac{1-\mu}{\mu}\frac{\partial f_1}{\partial\mu}-\frac{f_1}{\mu^2}\right)d\tau,\ \mu>0. \quad (117)$$

The result given by (116) diverges for $\mu=0$. Since, as $\mu\to0$, the terms neglected in (111) might be larger than the ones retained, the whole approximation breaks down. But away from $\mu=0$, the solution (116) might give a reasonable approximation. Of course, it is not allowable to make the same kind of development (109) in the original equation (104), since the function $f(\tau,\mu')$ is a highly peaked function too. In fact such a development applied to $f(\tau,\mu')$ would lead just to a Fokker-Planck differential equation [see Eq. (14)-(17)], which is valid only for small angles. On the other hand, $f_2(\tau,\mu')$ in Eq. (106) is a much more smooth function, so we think it is justified to make such a development.

(3) A third way of getting an approximate expression for f_2 is by an iteration method. To illustrate how one gets an exact solution by iteration, we will use the problem defined by Eqs. (11) and (12), whose exact solution is known to be the series (13). The solution of (11) and (12) is equivalent to that of the integral equation

$$f(\tau,\mu)=e^{-\tau}\int_0^\tau J(\tau,\mu)e^{\tau}d\tau+e^{-\tau}\delta(\mu-1),$$

where

$$J(\tau,\mu)=\tfrac{1}{2}\int_{-1}^{1}f(\tau,\mu')p(\mu,\mu')d\mu'.$$

Now suppose we start with Williams' approximate solution (given at the end of Sec. II) of this problem as a trial solution in the last integral equation defining the function $J(\tau,\mu)$, and then substitute in turn into the integral in $f(\tau,\mu)$, we get

$$f^{(1)}(\tau,\mu)=f^{(0)}(\tau,\mu)+\frac{F}{4}\sum_{r=0}^{\infty}(2r+1)P_r(\mu)(g_r-1)\times\left[e^{-r(r+1)\tau/\lambda}-e^{-\tau}\right],$$

where

$$g_r=\frac{1-k_r}{1-r(r+1)/\lambda}$$

and $f^{(0)}(\tau,\mu)$ is the Williams' solution we start with. If we start with $f^{(1)}(\tau,\mu)$ and iterate once more, we get

$$f^{(2)}=f^{(1)}+\frac{F}{4}\sum_{r=0}^{\infty}(2r+1)P_r(\mu)g_r(g_r-1)\times\left\{\exp\left[-\frac{r(r+1)\tau}{\lambda}\right]-e^{-\tau}-\left[1-\frac{r(r+1)}{\lambda}\right]\tau e^{-\tau}\right\}.$$

One can go on and get the series

$$f^{(\infty)}(\tau,\mu)=\frac{F}{4}\sum_{r=0}^{\infty}(2r+1)P_r(\mu)\left\{\exp\left[-\frac{r(r+1)}{\lambda}\tau\right]+(g_r-1)\sum_{n=0}^{\infty}g_r^n\left[\exp\left[-\frac{r(r+1)}{\lambda}\tau\right]-e^{-\tau}\sum_{s=0}^{n}\frac{\left(1-r\frac{r+1}{\lambda}\right)^s\tau^s}{s!}\right]\right\},$$

which can be easily shown to be identical with Eq. (13).

For the present case we first calculate the function $J(\tau,\mu)$ from Eq. (8) by using f_1 as the approximation for f under the integral; then we obtain $f(t,+\mu)$ by (10a) with $\mu_0=1$. The result is

$$f(t,+\mu)=f_1(t,+\mu)-\frac{F}{4}\sum_{r=0}^{\infty}(2r+1)k_rP_r(\mu)\times\frac{1-\mu}{1-\mu k_r}(e^{-k_rt}-e^{-t/\mu}). \quad (118)$$

(B) Back Scattering

(1) The expression (69b) gives the back scattering, but here again it is unpractical for cases with very anisotropic single scattering function. The perturbation treatment that we are going to give for this case is based upon the extremely small cross section of the back scattering.

First we make a Taylor development of the scattering function $p(\cos\alpha)$ defined by Eq. (1) around any backward direction, say $\cos\alpha=\cos\alpha_0$ with $\alpha_0>\pi/2$; i.e.,

$$p(\cos\alpha)=p(\cos\alpha_0)+p'(\cos\alpha_0)(\cos\alpha-\cos\alpha_0)\cdots. \quad (119)$$

Rearrange the terms to make a series of Legendre polynomials,

$$p(\cos\alpha)=\epsilon_n\sum_{r=0}^{n}\omega_r^*P_r(\cos\alpha), \quad (120)$$

where $\omega_0^*=1$. Though the function $p(\cos\alpha)$ is extremely forward, it is much more isotropic in back scattering. Therefore, we need only a few terms of the development (119) or (120); i.e., n will be small. The factor ϵ_n depends upon n and α_0, and it is small for small n. From (120) we get a development for $p(\mu,\mu')$ similar to (5):

$$p(\mu,\mu')=\epsilon_n\sum_{r=0}^{n}\omega_r^*P_r(\mu)P_r(\mu'). \quad (121)$$

Putting Eq. (121) into Eq. (38), we have (setting $\mu_0=1$)

$$\mu\frac{\partial I}{\partial\tau}+I=\frac{F}{4}p(\mu,1)e^{-\tau}+\frac{\epsilon_n}{2}\sum_{r=0}^{n}\omega_r^*P_r(\mu)\int_{-1}^{1}I(\tau,\mu')P_r(\mu')d\mu'. \quad (122)$$

Now multiply (122) by $\exp(-s\tau)d\tau$ and integrate τ from 0 to t. Also let

$$\varphi(s,\mu)=\int_0^t d\tau e^{-s\tau}I(\tau,\mu).$$

Then Eq. (122) becomes

$$\mu[I(t,\mu)e^{-st}-I(0,\mu)]+s\mu\varphi(s,\mu)+\varphi(s,\mu)=\frac{F}{4}p(\mu,1)\frac{1-e^{-(1+s)t}}{1+s}+\frac{\epsilon_n}{2}\sum_{r=0}^{n}\omega_r^*P_r(\mu)\int_{-1}^{1}\varphi(s,\mu')P_r(\mu')d\mu'. \quad (123)$$

In first approximation we will omit the sum in (123). Then we put $s=-1/\mu$, and introduce the proper boundary condition (39) for $I(\tau,\mu)$. Thus we get

$$I(0,\mu)=0,$$

$$I^{(1)}(t,\mu)=-\frac{F}{4}p(\mu,1)\frac{1-e^{(1-\mu)t/\mu}}{1-\mu}e^{-t/\mu}, \quad \mu>0, \quad (124a)$$

$$I(t,\mu)=0,$$

$$I^{(1)}(0,\mu)=\frac{F}{4}p(\mu,1)\frac{1-e^{(1-\mu)t/\mu}}{1-\mu}, \quad \mu<0. \quad (124b)$$

$I^{(1)}(0,\mu)$ is, of course, the first approximation for back scattering.

In order to get the second approximation for $I(\tau,\mu)$, we have to get the first approximation of $\varphi(s,\mu)$. One just substitutes the two expressions (124a) and (124b) into (123), still omitting the sum, and gets

$$\varphi^{(1)}(s,\mu)=\frac{F}{4}\frac{p(\mu,1)}{1+s\mu}\left[\frac{1-e^{-(1+s)t}}{1+s}+\begin{cases}\dfrac{1-e^{t(1-\mu)/\mu}}{(1-\mu)/\mu}e^{-t/\mu-st} & \mu>0\\[2ex] \dfrac{1-e^{t(1-\mu)/\mu}}{(1-\mu)/\mu} & \mu<0.\end{cases}\right] \quad (125)$$

Putting (125) into the integral in Eq. (123), and carrying out the integration in μ', we get the second approximation by again setting $s=-1/\mu$ and using boundary condition for $I(\tau,\mu)$:

$$I^{(2)}(0,\mu)=I^{(1)}(0,\mu)-\frac{\epsilon_n}{2\mu}\sum_{r=0}^{n}\omega_r^*P_r(\mu)\times\left[\int_{-1}^{1}\varphi^{(1)}(s,\mu')P_r(\mu')d\mu'\right]_{s=-1/\mu}, \quad \mu<0. \quad (126)$$

One can go to higher approximations in a similar manner.[34]

For a semi-infinite medium, $t\to\infty$, the first approximation of back scattering becomes obviously

$$I^{(1)}(0,\mu)=\tfrac{1}{4}Fp(\mu,1)/(1-\mu), \quad \mu<0. \quad (127)$$

Now if we make the development (119) around the direction where we wish to calculate the back scattering,

[34] A similar technique was used by L. V. Spencer, "Penetration and diffusion of x-rays," Natl. Bur. Standards (U. S.) Memo Rept. We are indebted to U. Fano for a copy of this report.

that is, to put $\cos\alpha_0=\mu$, then, in view of Eqs. (119), (120), and (121), we have

$$p(\mu, 1)=p(\mu) \tag{128}$$

exactly. Thus we get finally

$$I^{(1)}(0, \mu)=\tfrac{1}{4}Fp(\mu)/(1-\mu), \quad \mu<0. \tag{129}$$

If the development is made around a direction different from the one where we calculate the back scattering, then $p(\mu, 1)$ is simply the finite series

$$p(\mu, 1)=\sum_{r=0}^{n}\frac{1}{r!}p^{(r)}(\cos\alpha_0)(\mu-\cos\alpha_0)^r, \tag{130}$$

where the r in parenthesis means the rth derivative with respect to the argument. In (128) the value of $p(\mu, 1)$, for a fixed μ, does not change with the number of terms taken in the development (119), but in (130) it does. Since (130) is a series in $(\mu-\cos\alpha_0)$, it requires a larger n to approach (128) for μ further away from $\cos\alpha_0$. With $t\to\infty$, the expression (125) reduces to

$$\varphi^{(1)}(s, \mu)=\frac{F}{4}\frac{p(\mu, 1)}{1+s\mu}\left[\frac{1}{1+s}+\begin{cases}0 & \mu>0,\\ \mu/(1-\mu) & \mu<0,\end{cases}\right]$$

from which one can calculate $I^{(2)}(0, \mu)$ by (126).

To give some idea about the order of magnitude of the first approximation and the convergence of the method, we have calculated a few values for the semi-infinite case with the Rutherford scattering function

$$p(\cos\alpha)=4\beta(1+\beta)/(1+2\beta-\cos\alpha)^2, \tag{131}$$

which is normalized according to the definition (1). β is the screening constant, usually much smaller than unity. Using (131), we get the first approximation immediately from (129):

$$I^{(1)}(0, \mu)=F\beta(1+\beta)/(1+2\beta-\mu)^2(1-\mu) \simeq F\beta/(1-\mu)^2, \quad \mu<0. \tag{132}$$

If the second approximation is written in the form

$$I^{(2)}(0, \mu)=I^{(1)}(0, \mu)(1+k_n\beta), \tag{133}$$

the constant k_n, which determines the convergence, changes with n, the number of terms taken in the development (119) besides the first constant term. Table V gives the values of k_n for $n\leq 4$ at $\mu=-1$ and $\cos\alpha_0=-1$ too. The last two columns, giving the difference between and the ratio of consecutive k_n's, show that the k_n probably would not diverge as n increases.

The calculation for finite t is a little longer, but there is no essential difficulty, but some of the integrals involved must be understood in the sense of cauchy principal value. We have calculated the first and second approximation only for $n=0$ and $\mu=-1$. We get

TABLE V. k_n of Eq. (126).

n	k_n	$k_{n+1}-k_n$	k_{n+1}/k_n
0	0.69	1.89	3.72
1	2.58	2.31	1.89
2	4.89	2.26	1.46
3	7.15	2.06	1.29
4	9.21		

$$I^{(1)}(0, -1)=\tfrac{1}{8}F\beta(1-e^{-2t}),$$

$$I^{(2)}(0, -1)=I^{(1)}(0, -1)\left\{1+\frac{\beta}{1-e^{-2t}}[\ln 2+E_1(2t) -2E_1(t)e^{-t}-(\gamma+\ln t)e^{-2t}]\right\}, \tag{134}$$

where γ is the euler constant and

$$E_1(x)=\int_x^\infty e^{-u}du/u.$$

For the case we treated in constructing Tables III and IV, t is of the order 20. Then Eq. (134) gives practically the same result as the case of infinite t.

From a physical point of view one would expect that such a development is good only for thin foils. However, the results of Table V seem to show that this development may be useful for thicker foils too. Further numerical work would be necessary, however, to make this conclusion safe. Physically, this conclusion would mean that in back scattering a large number of small angle deflections is less probable than a small number of large deflections.

(2) Equation (116b) gives another approximation for backscattering, i.e.,

$$f(0, \mu)=-\frac{f_1(t, \mu)}{\mu}+k_1\int_0^t\left(\frac{1-\mu}{\mu}\frac{\partial f_1}{\partial\mu}-\frac{f_1}{\mu^2}\right)d\tau, \quad \mu<0. \tag{135}$$

The function $f_1(t, \mu)$ in the form of the infinite series (50) is not too practical for numerical calculation, since for an extremely forward single scattering function one has to take a tremendous number of terms. For the case of small t, several authors[14, 16, and 17] have made developments of this function which are more suitable for numerical calculation than the series. However, they all made the small-angle approximation, so their developments are not suitable for $\mu<0$ as required by (135). We shall give another development here which approximates better for smaller μ.

The function $f_1(\tau, \mu)$ is a solution of (105) and (107a).

We first develop $f_1(\tau, \mu)$ in a Taylor series of τ, i.e.,

$$f_1(\tau, \mu)=\pi F\delta(\mu-1)+\tau(\partial f_1/\partial\tau)_{\tau=0}+\tfrac{1}{2}\tau^2(\partial^2 f_1/\partial\tau^2)_{\tau=0}\cdots, \quad (136)$$

in which we have made use of the boundary condition (107a). Putting (136) into (105) and equating coefficients of different powers of τ, we get

$$(\partial f_1/\partial\tau)_{\tau=0}=\tfrac{1}{4}Fp(\mu)-\pi F\delta(\mu-1), \quad (137)$$

$$(\partial^2 f_1/\partial\tau^2)_{\tau=0}=\tfrac{1}{4}F\left\{\tfrac{1}{2}\int_{-1}^{1}p(\mu,\mu')p(\mu')d\mu'-2p(\mu)\right\}+\pi F\delta(\mu-1),$$

where $p(\mu)$, which is written for $p(\mu, 1)$, is just the single scattering function defined by (1). Combining (136) and (137), we get

$$f_1(t, \mu)=(1-t+\tfrac{1}{2}t^2)\pi F\delta(\mu-1)+\tfrac{1}{4}F\left\{tp(\mu)+\tfrac{1}{2}t^2\left[\tfrac{1}{2}\int_{-1}^{1}p(\mu,\mu')p(\mu')d\mu'-2p(\mu)\right]\right\}. \quad (138)$$

One gets, of course, exactly the same series if one develops the solution $f_1(t, \mu)$, as given by (50), into power series of t, only not immediately in this form. In the form of (138), one notices that, besides the singular function at $\mu=1$, the coefficient of t contains only a single-collision term, and that of t^2 contains both single and double-collision terms. The t^3 term will have single-, and double-, and triple-collision terms, and so on.

The first term inside the curly brackets of (138) is the well-known single scattering tail for a thin foil. To evaluate the integral, we notice that the integrand is the product of two extremely peaked functions with one peak at $\mu'=\mu$ and the other at $\mu'=1$. So we break the integral at $\mu'=(1+\mu)/2$, and develop the slowly varying function in both intervals into Taylor series around the peak of the other function. Using the single scattering function (131), and keeping terms of first power of β, we get, combining with other terms of (138),

$$f_1(t, \mu)=(1-t+\tfrac{1}{2}t^2)\pi F\delta(\mu-1)+\tfrac{1}{4}Ftp(\mu)\times\left\{1+\frac{\beta t}{1-\mu}\left[2(3+\mu)\ln\frac{1}{2\beta}-(3+\mu)\ln\frac{2}{1-\mu}-\frac{27\mu^3-15\mu^2-27\mu+47}{4(1-\mu)^2}\right]\right\}. \quad (139)$$

In calculating (139) we have taken the Taylor series up to terms with third derivative. The above result is, of course, incorrect if $\beta/(1-\mu)$ is not small. The deviation from single scattering, given by the term with square brackets, reduces to

$$2\beta t(\ln 1/\beta-\ln 2-1/2) \quad (140)$$

for $\mu=-1$ in our approximate expression (139). For this special value of μ, the integral in (138) can be evaluated exactly. We found the exact value for the deviation up to first power of β to be

$$2\beta t(\ln 1/\beta-1)$$

instead of (140).

If we apply the development (136) to the exact Boltzmann equation (6), we get, instead of (138),

$$f(t, \mu)=\left(1-t+\frac{t^2}{2}\right)\pi F\delta(\mu-1)+\frac{F}{4}\left\{\frac{tp(\mu)}{\mu}+\frac{t^2}{2\mu}\left[\frac{1}{2}\int_{-1}^{1}\frac{p(\mu,\mu')p(\mu')d\mu'}{\mu'}-\frac{1+\mu}{\mu}p(\mu)\right]\right\}.$$

(3) We can get an expression for back scattering similar to (118) for forward scattering by iteration. The only difference in calculation is that here we use (10b) instead of (10a). Thus, we get

$$(0, -\mu)=\frac{F}{4}\sum_{r=0}^{\infty}(-1)^r\omega_r P_r(\mu)\frac{1-e^{-(1+\mu k_r)t/\mu}}{1+\mu k_r}, \quad \mu>0. \quad (141)$$

(C) Final Remark

Making use of the development (138), one can show, in the case of forward scattering, that for small t

$$f(t, \mu)\simeq[1-t(1-k_1)]\pi F\delta(\mu-1)+Ftp(\mu)/4\mu\cdots \quad (142)$$

in the solution (117), and

$$f(t, \mu)\simeq(1-t)\pi F\delta(\mu-1)+Ftp(\mu)/4\mu\cdots \quad (143)$$

in the solution (118). The two expressions (142) and (143) are approximately the same, since $k_1\ll 1$. In the case of back scattering, the three kinds of approximation lead to the solutions (124b), (135), and (141). They represent the same quantity, the angular distribution of back scattering, since $I(0, \mu)$ and $f(0, \mu)$ are identical for $\mu<0$ by definition (37). Now one can also prove that for small t the three solutions approach the same expression

$$f(0, \mu)=-Ftp(\mu)/4\mu, \quad \mu<0.$$

All our approximations described in this Sec. VI, except the one in subsection (B1), are based upon the Goudsmit-Saunderson solution (50) as a first approximation. Therefore, if we want to have some numerical results, it is necessary to tabulate the solution (50) first. For small t, there are some developments in the literature[28] suitable for numerical calculation in the range θ not too large, and we have given the development (139) for large θ. For arbitrary t and θ very small, one can replace the sum (50) by an integral, as done by Moliere and Snyder and Scott[14,16] and get some approximate

values. But when θ is not very small, in fact very large as in the case of backscattering, we are not able to convert the sum to any form more suitable for numerical calculation, except for small t.

In calculating the series (50), one major job is to compute the k_r's, which involves some elementary integrations. For the scattering function (131), we have calculated the first seven k_r's and found, by inspection, the general rule

$$(1-k_r)=\frac{1}{2^r A_0}\sum_{i=0}^{m}(-1)^i\frac{(2r-2i)!}{i!(r-i)!(r-2i)!}A_{r-2i}, \quad (144)$$

where $m=\frac{1}{2}r$ or $\frac{1}{2}(r-1)$ for r even or odd, and

$$A_n=\frac{nx^{n-1}}{2}\ln\frac{x-1}{x+1}+\frac{x^n}{x^2-1}+\frac{n-1}{1}x^{n-2}$$
$$+\frac{n-3}{3}x^{n-4}+\frac{n-5}{5}x^{n-6}\cdots \quad (145)$$

with $x=1+2\beta$. In using the series (145), all terms, after the second, with negative powers of x have to be discarded. Snyder and Scott, and Lewis[16,19] have given some approximate expressions for k_r.

PHYSICAL REVIEW VOLUME 84, NUMBER 6 DECEMBER 15, 1951

The Primeval Lead Isotopic Abundances and the Age of the Earth's Crust*

RALPH A. ALPHER AND ROBERT C. HERMAN
Applied Physics Laboratory, The Johns Hopkins University, Silver Spring, Maryland
(Received September 13, 1951)

Nier's determinations of lead isotopic abundances in common lead ores have been the subject of considerable study in connection with attempts to calculate the age of the earth. The importance of the age of the earth in fixing the age of the elements has led us to remark on the very high precision frequently attributed to the former age determinations. A calculation is presented which yields a rough maximum age of the earth, namely, $t(\max)=5.3$ billion years. The primeval lead isotopic abundances have been estimated and briefly discussed in the light of nuclear systematics.

INTRODUCTION

IN several recent papers dealing with the subject of the age of the elements, use has been made of the important value for the age of the earth's crust due to Holmes,[1] namely, 3.350×10^9 yr. In view of the rather unreasonably high accuracy assigned to this value by many authors[2] and the great interest in such ages for cosmological and cosmogonical problems, it seems pertinent to discuss briefly the analyses leading to such ages, and to point out that, at the present time, the limit of speculations on this subject due to the nature of the data may be a rough estimate of the maximum age of the earth's crust, and of the primeval lead isotopic abundances.

Katcoff, Schaeffer, and Hastings[3] have recently calculated the time between element formation and formation of the earth's atmosphere to be $\Delta t=0.27\times10^9$ yr. Their calculation was based on the addition of Xe^{129} to the atmosphere by the decay of I^{129}, as suggested earlier by Suess.[4] More recently Suess and Brown[5] have pointed out that this calculation actually leads to an approximate lower limit for the value of the time interval Δt. They find a value of $\Delta t\cong0.4\times10^9$ yr. The age of the elements is then given by the sum of this time and the age of the earth's crust, assuming that the time between formation of the crust and of the atmosphere, and between formation of the earth as an entity and its crust, may be neglected. These suggested values of Δt are sufficiently small that, if they are correct even only as to order of magnitude, then the important calculation, in so far as the age of the elements is concerned, is that yielding the age of the earth's crust. However, the determination of Δt is otherwise of great interest in connection with the early history of the universe.

FORMULATION

The determinations of the age of the earth's crust by various investigators are all based on a set of data due to Nier.[6] These data are accurate mass spectro-

* This work was supported by the U. S. Navy, Bureau of Ordnance.

[1] A. Holmes, Nature **157**, 680 (1946); **159**, 127 (1947); **163**, 453 (1949); Endeavour **6**, 99 (1947). See also H. Jeffreys, Nature **162**, 822 (1948); **164**, 1046 (1949), as well as E. C. Bullard and J. P. Stanley, Suomen Geodeetisen Laitoksen Julkaisuja, Veröffentlichungen des Finnischen Geodatischen Institutes, No. 36, 33 (1949). The latter authors obtains 3.29×10^9 yr using the same data as Holmes but employing a least squares analysis.

[2] For example, Fleming, Ghiorso, and Cunningham, Phys. Rev. **82**, 967 (1951), suggest that their new value of the decay constant for U^{235} will alter Holmes' value for the age of the crust, *viz.*, 3.350×10^9 yr, by three percent. It is very difficult to understand how this small change in the crustal age was estimated, in light of the involved nature of Holmes' analysis leading to this age, and its concomitant approximate nature.

[3] Katcoff, Schaeffer, and Hastings, Phys. Rev. **82**, 688 (1951).

[4] H. E. Suess, Z. Physik **125**, 386 (1948); Experientia **5**, 376 (1949).

[5] H. E. Suess and H. Brown, Phys. Rev. **83**, 1254 (1951).

[6] A. O. Nier, J. Am. Chem. Soc. **60**, 1571 (1938); Nier, Thompson, and Murphey, Phys. Rev. **60**, 112 (1941). Of the twenty-five

graphic analyses of the isotopic constitution of the lead in common lead ores, ores containing essentially no uranium or thorium contaminant and consequently unchanged in composition since their deposition as an ore from a magma. Let x_m, y_m, and z_m be the observed number of atoms of Pb^{206}, Pb^{207}, and Pb^{208} relative to the nonradiogenic Pb^{204} in a lead sample m, and let t_m be the time of deposition of this sample (there being no further change in lead abundances from t_m to the present). Then the relative abundances during a period t_0 to t_m are given by the following well-known relations:

$$x_m = x_0 + \alpha V_m e^{\lambda_{238} t_0}[1 - e^{-\lambda_{238}(t_0 - t_m)}], \quad (1a)$$

$$y_m = y_0 + V_m e^{\lambda_{235} t_0}[1 - e^{-\lambda_{235}(t_0 - t_m)}], \quad (1b)$$

and

$$z_m = z_0 + W_m e^{\lambda_{232} t_0}[1 - e^{-\lambda_{232}(t_0 - t_m)}]. \quad (1c)$$

The quantities V_m and W_m are the number of atoms of U^{235} and Th^{232}, relative to Pb^{204}, which would be found in the source magma for the particular sample m at the present time, the present abundance of U^{238} relative to U^{235} is $\alpha = 139$, t_0 is the time at which radiogenic deposition of the various leads initiated in the source material, and x_0, y_0, and z_0 are the initial relative abundances for the three lead isotopes (primeval with respect to the period t_0 to t_m). The λ are the respective U and Th decay constants as noted.[7] In fitting Eqs. (1) to the Nier data, the assumption must be made that there were no changes in the ratios of uranium and thorium to lead other than those due to the decay of these species, since the source materials were established during crustal formation. Otherwise, a determinate analysis is possible only if one has a detailed knowledge of the subsequent changes in these ratios for each sample. Such changes are presumably associated with later orogenic processes in the earth's crust. Inasmuch as the relative amounts of U and Th are not known with sufficient accuracy, the basic procedure of investigators in determining the age of the crust has been to use only the uranium-lead data, involving Eqs. (1a) and (1b), to eliminate V_m between them, and to find, graphically or by least squares, values of the parameters x_0, y_0, and t_0 defining a unique point from which there originates a family of radioactive growth curves. To each such curve in the family there corresponds a V_m associated with a particular sample.[8]

In the least squares analysis, statistical difficulties force the burden of error to be placed on the x_m and y_m values, which are individually determined with good accuracy (~0.5 percent according to Nier). Consequently, probable errors computed for x_0, y_0, and t_0 are misleadingly small. Actually, the stratigraphic determination of the ages of the ore samples, t_m, is at best a crude procedure. It might be that the chronological sequence of the samples discussed by Nier is in error.[9] If the burden of error in the analysis could somehow be put on the t_m values, treating the x_m, y_m, and z_m values as exact, it would appear from the data scatter (Fig. 1) that the probable errors to be assigned to the parameters might be considerably higher. Thus far it has not proved possible to do the least squares analysis in this more desirable way.

MAXIMUM AGE

Since geological evidence favors the existence of multiple orogenies in the histories of the lead ores, and also suggests considerable uncertainty in the stratigraphically determined ages of the samples, it appears reasonable to attempt little more with the present data than an estimate of some kind of upper limit to the age of the earth's crust. One such estimate might be based on a remark of Holmes[1] that any multiple orogenies in the histories of the Nier samples may have involved only small changes in the ratios of uranium and thorium to lead, and that increases or decreases in such ratios may have occurred with equal probability. The main trend of radiogenic deposition of lead may then be supposed, quite approximately, to be that obtained assuming no orogenies. With all the V_m and W_m in Eqs. (1) constant and independent of the sample, a least squares fit to the Nier data yields no unique set of values of x_0, y_0, z_0, and t_0 unless one of these is arbitrarily chosen. In order to determine a rough "maximum" age of the earth's crust, t_0(max), it seems

Nier samples, two were not used for lack of dating, while the three Joplin samples were averaged, in concordance with the practice in other analyses of these data. This averaging is essentially indefensible, except on the grounds that the presence of three presumably identical geological specimens out of twenty-three datum points unduly weights them in the least squares analysis.

[7] In our work we have used $\lambda_{238} = 0.154$ $(10^9 \text{ yr})^{-1}$, $\lambda_{235} = 0.920$ $(10^9 \text{ yr})^{-1}$, and $\lambda_{232} = 0.0498$ $(10^9 \text{ yr})^{-1}$. The value chosen for U^{235} was based on measurements at Oak Ridge reported to us by Dr. E. C. McCrady in a private communication, while the other values are taken from *Nuclear Data*, Circular 499, Nat. Bur. Standards (1950).

[8] It is worthy of note that if the Nier data are accepted and used as they stand, a least squares analysis leads to an age for the earth's crust, $t_0 \cong 1.88 \times 10^9$ yr, which is of course unacceptable even geologically. Furthermore, the computed lead abundances at the time of crustal formation exceed those measured in some of the samples. Bullard and Stanley (reference 1) have also mentioned this difficulty and find a $t_0 = 3.29 \times 10^9$ yr only by discarding certain of the Nier data and averaging others. The rejection of data is justified only if one knows that the discarded samples have undergone multiple orogeny and the retained samples only one. Furthermore, averaging samples obscures the essential feature in the data, namely, that one must assume each sample has a different set of values V_m and W_m. Without this assumption x_0, y_0, z_0, and t_0 are indeterminate unless an *a priori* value is assigned to one such parameter. The analysis of Jeffreys (reference 1) and F. G. Houtermanns, Z. Naturforsch. **2a**, 322 (1947) are essentially equivalent to that stated in the text. All of the methods suffer from the paucity of data as well as the gross extrapolations involved. In addition, Holmes' analysis, a more cumbersome method not employing least squares, appears to weight unduly samples which give points of origin in a physically reasonable domain.

[9] Dr. E. C. McCrady, of the Oak Ridge National Laboratory, has suggested, in a private communication, that the samples be put in chronological order according to the relative magnitudes of their lead isotopic abundances. Such an ordering procedure would appear to presume a knowledge of the effect of orogenies in the history of each sample, since multiple orogenies could well shift the order of samples so dated several times during their histories of contact with uranium and thorium.

reasonable to find, by least squares, a time such that one of the primeval lead abundances x_0, y_0, or z_0 was zero, with the others being still positive. The uranium-lead data were accordingly examined with normal equations derived from Eqs. (1a) and (1b), on the assumption that $x_0=0$ at the time t_0(max) to be determined. The least squares solution yielded a t_0(max) $\cong 5.3\times 10^9$ yr, with $y_0\cong 1.7$ and $V_\infty\cong 0.11$. A least squares solution obtained with $y_0=0$ yields a t_0(max) with $x_0<0$. Since this is inadmissible one may use Eqs. (1) to calculate the t_0(max) when $x_0=0$. This yields a solution for t_0(max) and y_0 identical to that obtained above. With the t_0(max) so determined, the thorium-lead data were fitted with Eq. (1c), yielding, by least squares, $z_0\cong 22$ and $W_\infty\cong 55$.[10] The least squares growth curves corresponding to Eqs. (1) for this solution are shown in Fig. 1.[11] Probable errors for x_0, y_0, z_0, and t_0 are readily computed, but since no error was assigned to t_m, they are misleadingly small.[12] However, it would appear that the specific values of t_m are not important in this way of looking at the problem. For example in an earlier calculation of a "maximum" age, Koczy[13] suggested lumping together all of Nier's data into a single set of points, implying that the times t_m are sufficiently recent compared to a maximum age of the crust as to be negligible. He computed graphically a maximum age on the assumption that all of the observed lead is of radiogenic origin, and that there were no orogenies changing the uranium-to-lead ratios. In this way Koczy obtained a t_0(max)$\cong 5.3\times 10^9$ yr. The fact that his result is consistent with ours is merely a reflection of the small values of x_0 and y_0, since otherwise his analysis would not determine a maximum. It is quite evident from Fig. 1 that calculations of the type described involve a rather extensive extrapolation.

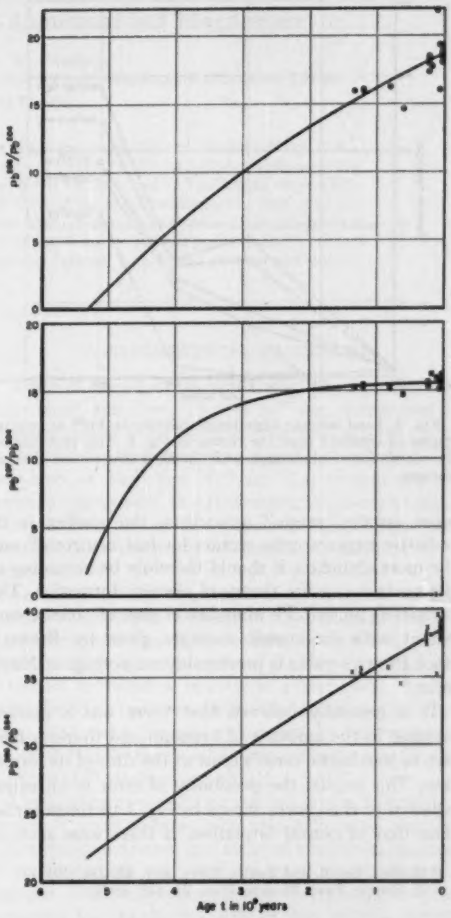

FIG. 1. Lead isotopic abundances relative to Pb^{204} *versus* time. These growth curves were obtained by a least squares analysis of Nier's lead isotopic abundance data (see reference 6).

LEAD ABUNDANCES

Behr[14] has recently reanalyzed the nebular recession data of Hubble, and finds that the start of the expansion, according to his corrections, should be taken at $\sim 3.8\times 10^9$ yr ago. If this be taken as the age of the elements, then the primeval relative lead isotopic abundances which have been estimated by the above maximum age determination are interesting in the light of the magic number properties of the lead isotopes. These abundances may have been as suggested in Fig. 2, where abundances at various epochs consistent with the authors' maximum age analysis are shown. The rise in abundance from Pb^{204} to Pb^{208} is perhaps significant with regard to a suggested mode of element formation, *viz.*, the neutron capture theory.[15] Lead has a magic number of protons, while Pb^{204}, Pb^{206}, Pb^{207}, and Pb^{208} are progressively more nearly magic in neutron content (Pb^{208} is doubly magic). It is to be expected that the

[10] Dr. E. C. McCrady has also been working on this problem, however, employing chronological reordering of the samples according to relative isotopic abundances. We understand that his work is in press.

[11] If one takes the unique point determined by Bullard and Stanley (see reference 1), $x_0'=11.86$, $y_0'=13.86$ and $t_0'=3.29\times 10^9$ yr to define an average curve in the sense of the present analysis one obtains t_0(max)$\cong 5.6\times 10^9$ yr, $x_0\cong 5.3$, $y_0\cong 0$. This result differs in part due to the choice of λ_{238}. The fact that $x_0>0$ when $y_0=0$ does not alter the discussion given later about the connection between the relative isotopic abundances of lead and nuclear systematics at $t\cong 3.8\times 10^9$ yr.

[12] For example, the probable error computed for t_0 is $\sim 0.2\times 10^9$ yr.

[13] F. F. Koczy, Nature **151**, 24 (1943). See also E. K. Gerling, Compt. Rend. URSS **34**, 259 (1942), who did a similar calculation on certain of Nier's samples having minimum lead isotopic contents, relative to Pb^{204} and, therefore, presumably most nearly primeval lead.

[14] A. Behr, Astr. Nachr. **279**, 97 (1951).

[15] R. A. Alpher and R. C. Herman, Revs. Modern Phys. **22**, 153 (1950).

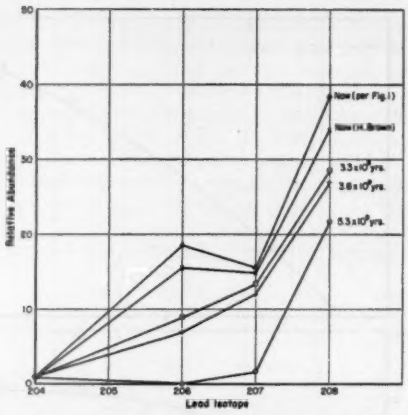

FIG. 2. Lead isotopic abundances relative to Pb^{204} at selected epochs as obtained from the curves in Fig. 1. This plot exhibits the correlation of abundance with the shell structure of the lead isotopes.

more nearly "magic" a nucleus, the smaller is its radiative capture cross section for fast neutrons,[16] and the more abundant it should therefore be according to the neutron-capture theory of element formation. The computed present Pb abundances are, of course, consistent with the cosmic averages given by Brown,[17] since Brown's value is presumably an average of Nier's data.

It is generally believed that there was a marked increase in the amounts of uranium and thorium relative to lead in the earth's crust at the time of its formation. This implies the possibility of error in an extrapolation of the curves shown in Fig. 1 to times earlier than that of crustal formation. If there were such an increase the maximum effect would be that associated with a growth curve which was flat prior to this increase. If 3.3×10^9 yr is the time of crustal formation and 3.8×10^9 yr is the age of the elements, then one would correct for this maximum increase by taking the primeval abundances from the 3.3×10^9 yr curve in Fig. 2 to be the abundances at 3.8×10^9 yr. This change is not large as can be seen from Fig. 2.

CONCLUSION

With regard to the age of the elements, it may be remarked that, if Behr's value for the age of the universe and the time between element formation and formation of the earth's atmosphere discussed earlier are both reliable, then one would infer that Holmes' result of 3.3×10^9 yr is probably reasonable, even though the data and the method of analysis on which it is based cast doubt on its precision. As is abundantly clear to all who have attempted to determine the age of the earth's crust from Nier's data, there is an essential need for a great deal more of such data together with more precise dating of samples. It would appear necessary to develop criteria for deciding whether a given sample has undergone changes in constitution only by radiogenic deposition between the time of formation of the earth's crust and the time of its deposition as an ore. Otherwise detailed study of the cycles of orogeny and their geochemical affects is required.[18]

The kind of analysis attempted in this paper is of interest in connection with theories of element formation, providing that one may obtain detailed knowledge of the fast neutron capture cross sections of the lead, uranium, and thorium isotopes, together with fast neutron fission cross sections. It is this type of information that might eventually lead to an understanding of the detailed variations in the universal relative abundance data of nuclear species.

[16] Hughes, Garth, and Eggler, Phys. Rev. **83**, 234 (1951).
[17] H. Brown, Revs. Modern Phys. **21**, 625 (1949).
[18] Dr. L. R. Stieff, U. S. Geological Survey, is at present carrying on this type of analysis.

Photonuclear Cross Sections in Aluminum and Magnesium

L. KATZ AND A. G. W. CAMERON
Betatron Group, Department of Physics, University of Saskatchewan, Saskatoon, Saskatchewan, Canada
(Received August 8, 1951)

Cross-section curves have been measured as functions of photon energy for the reactions $Al^{27}(\gamma, n)Al^{26}$, $Mg^{24}(\gamma, n)Mg^{23}$, $Mg^{25}(\gamma, p)Na^{24}$, and $Mg^{26}(\gamma, p)Na^{25}$. These curves exhibit the peaked shape characteristic of photonuclear reactions, the maximum cross sections being 8.1, 9.8, 14.8, and 19.3 millibarns respectively. The (γ, p) peak positions occur about 2 Mev higher than those of the (γ, n) reactions, and their cross sections as indicated above are considerably larger. It is shown that these peaked shapes result from a peaking of the photonuclear absorption cross sections. The larger values of the (γ, p) peak positions and cross sections may be explained as resulting from a direct interaction between high energy photons and nuclear protons.

I. INTRODUCTION

IN 1947 Hirzel and Waffler[1] reported that the ratio of (γ, p) to (γ, n) reaction cross sections in medium heavy nuclei was much larger than would be predicted by the statistical theory of Weisskopf.[2,3] Their experiments were performed with γ-rays from the $Li^7(p, \gamma)Be^8$ reaction, having energies of 14.4 and 17.6 Mev; these photon energies are lower than those at which the maximum (γ, p) cross sections occur.[4] Schiff attempted to explain this anomaly by assuming that only a selected set of nuclear levels become populated in photonuclear reactions.[5] Such "regular" level densities lead to disagreement with experimental photoproton energy distributions.[6,7] Recently Courant[8] has proposed a theory of direct photoelectric excitation of nucleons which gives fair agreement with the Hirzel and Waffler ratios of (γ, p) to (γ, n) cross sections.

Aluminum and magnesium are light elements which have low potential barriers against proton emission. On the other hand they are sufficiently heavy that one might expect to predict the qualitative if not the quantitative features of the (γ, p) and (γ, n) yields from statistical theory. Halpern and Mann[4] have measured the cross-section curve for the reaction $Al^{27}(\gamma, p)Mg^{26}$ as a function of photon energy, and Diven and Almy[6] have investigated the photoproton energy distribution from this reaction. Toms and Stephens[9] have measured the same quantities for the reaction $Mg^{25}(\gamma, p)Na^{24}$ and also the photoproton energy distribution from natural magnesium. In the present work we have measured cross-section curves for the reactions $Al^{27}(\gamma, n)Al^{26}$, $Mg^{24}(\gamma, n)Mg^{23}$, $Mg^{25}(\gamma, p)Na^{24}$, and $Mg^{26}(\gamma, p)Na^{25}$.

[1] O. Hirzel and H. Waffler, Helv. Phys. Acta **20**, 373 (1947).
[2] V. F. Weisskopf and D. H. Ewing, Phys. Rev. **57**, 472 (1940).
[3] J. M. Blatt and V. F. Weisskopf, *The Theory of Nuclear Reactions*, Technical Report No. 42, Laboratory for Nuclear Science and Engineering, Massachusetts Institute of Technology.
[4] J. Halpern and A. K. Mann, Phys. Rev. **83**, 370 (1951).
[5] L. I. Schiff, Phys. Rev. **73**, 1311 (1948).
[6] B. C. Diven and G. M. Almy, Phys. Rev. **80**, 407 (1950).
[7] P. R. Byerly, Jr., and W. E. Stephens, Phys. Rev. **83**, 54 (1951).
[8] E. D. Courant, Phys. Rev. **82**, 703 (1951).
[9] M. E. Toms and W. E. Stephens, Phys. Rev. **82**, 709 (1951).

II. EXPERIMENTAL PROCEDURE

Three of the products of the reactions reported here have short half-lives. That of Al^{26} was determined in this experiment to be 6.49 ± 0.10 seconds, in good agreement with the best previous value of 6.3 seconds.[10] The half lives of Mg^{23} and Na^{25} are 11.6 seconds and 60 seconds respectively. It was therefore necessary to make a rapid transfer of the aluminum and magnesium samples from the betatron irradiation position to a counter.

At first a "swing" apparatus was set up, in which a sample was clamped at the end of a wooden arm in the irradiation position. Upon release at the end of an irradiation, the arm swung down positioning the sample above an end-window counter in a lead castle. At the same time the counter voltage was raised to the operating level and a time-stamping recorder was switched on. With this arrangement the activation curve for the $Al^{27}(\gamma, n)Al^{26}$ reaction was obtained.

The apparatus was then modified into a "dropping" device. A vertical brass tube held cylindrical samples which dropped around a cylindrical counter at the end of an irradiation, the other equipment remaining unchanged. With this arrangement activation curves were measured for the $Mg^{24}(\gamma, n)Mg^{23}$ and $Mg^{26}(\gamma, p)Na^{25}$ reactions.

The fourth reaction, $Mg^{25}(\gamma, p)Na^{24}$, gives a product having a half-life of 15 hours. Such activities were counted with standard equipment after thin magnesium disks had been irradiated and the short-lived activities had decayed.

These activation curves were normalized to the known $Cu^{63}(\gamma, n)Cu^{62}$ activity[11] at 22 Mev by irradiating similar cylindrical samples of aluminum, magnesium, and copper in the dropping apparatus. It was necessary to correct such activities for self-absorption of beta-particles in the samples. The corrections for the Cu^{62} activity have been measured in this laboratory for cylindrical geometry by Mr. R. G. Baker, and those for the Al^{26} activity were measured by the dropping tech-

[10] H. Bradner and J. D. Gow, Phys. Rev. **74**, 1559 (1948).
[11] Johns, Katz, Douglas, and Haslam, Phys. Rev. **80**, 1062 (1950).

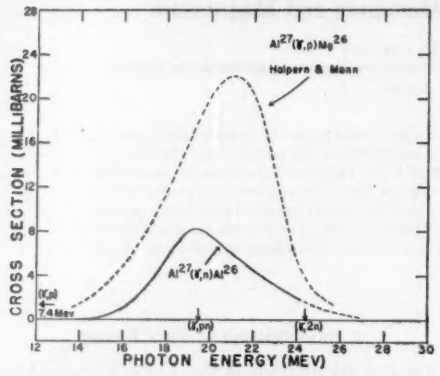

FIG. 1. Cross-section curves for the reactions $Al^{27}(\gamma, n)Al^{26}$ (solid line) and $Al^{27}(\gamma, p)Mg^{26}$ (dotted line, as measured by Halpern and Mann). The arrows indicate thresholds for possible competing reactions.

nique. It was assumed that the self-absorption corrections for the activities produced in magnesium were the same as those for Al^{26}.

The resulting activation curves were analyzed by the photon difference method[12] to obtain the photonuclear cross sections as functions of photon energy. These cross sections are plotted as the solid lines in Figs. 1, 2, 3, and 4.

III. DISCUSSION

In Fig. 1 are plotted the cross-section curves for the reactions $Al^{27}(\gamma, n)Al^{26}$ (solid line) and $Al^{27}(\gamma, p)Mg^{26}$ (dotted line, as measured by Halpern and Mann[4]). This is the only case reported here in which both the (γ, p) and (γ, n) cross-section curves have been measured for the same parent isotope. The curves exhibit the peaked shape characteristic of photonuclear reactions. In the general case such peaks can be thought of as resulting from "cascade" competition, in which a second nucleon can be emitted at higher excitations leaving a different residual nucleus not detected in the experiment, or as resulting from a "resonance" absorption of photons as predicted by Goldhaber and Teller,[13] and by Levinger and Bethe.[14]

These two possibilities are implicit in a general probability equation

$$\sigma(a, b) = \sigma_c(a) G_c(b),$$

in which the cross section for an (a, b) reaction, $\sigma(a, b)$, is set equal to the product of the probabilities for the capture of particle a and the emission of particle b. In statistical theory $\sigma_c(a)$ is the cross section for the formation of a compound nucleus and $G_c(b)$ is the probability that such compound nucleus will decay via the "channel" b. A peaked cross section could therefore result from a peaking of either factor or of some fortuitous combination of the two factors.

The energy thresholds for (γ, pn) and $(\gamma, 2n)$ reactions in Al^{27} are indicated by arrows in Fig. 1. The $(\gamma, 2n)$ threshold is too high to have affected the turnover of the cross-section curves through an influence on G_c. The (γ, pn) threshold occurs at the (γ, n) peak position and below the (γ, p) peak position. Since Halpern and Mann measured proton yields, their cross-section curve is the sum of the cross sections for the reactions $Al^{27}(\gamma, p)Mg^{26}$, and $Al^{27}(\gamma, pn)Mg^{25}$. However the greater part of their curve must have been due to the (γ, p) reaction alone for the following reasons: Diven and Almy found, using 20.8-Mev x-rays, that the aluminum photoproton energy distribution was peaked at 4 Mev. Those (γ, pn) reactions in which a proton is first emitted, followed by neutron emission from the residual nucleus, would therefore have only a small cross section below 23 Mev. The alternative case, in which a neutron is emitted first, followed by proton emission from the residual nucleus, also should have only a small cross section for a few Mev above threshold due to the kinetic energy of the initial neutron. Thus the (γ, pn) reaction would be unimportant where the (γ, p) cross section turns over.

In Table I are listed the energy thresholds for the emission of neutrons, protons, and alpha-particles, both singly and in combination, from the four parent nuclei considered in this paper. The reaction $Al^{27}(\gamma, \alpha)Na^{23}$ has a low threshold and could affect the turn-over of the (γ, n) and (γ, p) cross-section curves, but (γ, α) cross sections are much less than a millibarn in very light elements[15] and are about a millibarn or less in medium heavy elements.[15,16] The (γ, α) cross-sections peak at 18 Mev in carbon and oxygen and at 23 Mev in copper and rubidium.[16] It is therefore probable that (γ, α) reactions

TABLE I. Thresholds (Mev) for competing reactions in magnesium and aluminum. A few values are experimental results; the rest have been computed from mass values (mostly from Bethe[a]).

Reaction	Parent isotope Mg^{24}	Mg^{25}	Mg^{26}	Al^{27}
(γ, n)	16.2[b]	7.1[c]	10.1[c]	14.0[b]
(γ, p)	12.3	11.5[b]	14.0[b]	7.4
(γ, α)	9.5	9.0	11.7	9.5
$(\gamma, 2n)$	29.5	23.3	17.2	24.4
(γ, pn)	22.8	17.9	23.2	19.5
$(\gamma, n\alpha)$	26.3	16.6	21.2	21.3
$(\gamma, 2p)$	20.6	22.1	23.6	21.4
$(\gamma, p\alpha)$	22.4	21.8	27.2	19.1
$(\gamma, 2\alpha)$	14.2	17.2	21.3	20.8

[a] H. A. Bethe, *Elementary Nuclear Theory* (John Wiley and Sons, Inc., New York, 1947).
[b] McElhinney, Hanson, Becker, Duffield, and Diven, Phys. Rev. **75**, 542 (1949).
[c] Sher, Halpern, and Stephens, Phys. Rev. **81**, 155 (1951).

[12] A. G. W. Cameron and L. Katz, Phys. Rev. **83**, 883 (1951); Can. J. Phys., November, 1951 (to be published).

[13] M. Goldhaber and E. Teller, Phys. Rev. **74**, 1046 (1948).
[14] J. S. Levinger and H. A. Bethe, Phys. Rev. **78**, 115 (1950).
[15] C. H. Millar and A. G. W. Cameron (to be published).
[16] R. N. H. Haslam and H. M. Skarsgard, Phys. Rev. **81**, 479 (1951); Haslam, Smith, and Taylor, Phys. Rev. Nov. 15 (in press).

have a negligible effect on the (γ, p) and (γ, n) cross section maxima.

Other possible reactions, $(\gamma, n\alpha)$, $(\gamma, 2p)$, $(\gamma, p\alpha)$, and $(\gamma, 2\alpha)$, which might offer "cascade" competition to the (γ, n) and (γ, p) reactions, have energy thresholds near the cross-section maxima in Fig. 1. The cross sections for such reactions should be very small for a few Mev above threshold since the first particle to emerge is likely to have several Mev of kinetic energy. (γ, d) reactions have energy thresholds 2.2 Mev lower than (γ, pn) thresholds. However, the combined (γ, d) and (γ, pn) cross sections in the neighboring nucleus S^{32} are much smaller[17] than the (γ, p) cross sections in Al^{27}.

From the above considerations we conclude that the turn-over of the two cross-section curves in Fig. 1 is due to a peaking of σ_e rather than G_e, in accord with the theories of resonance dipole absorption of photons.[13,14]

It should also be noted in Fig. 1 that the (γ, p) cross section is much greater than the (γ, n) cross section in the neighborhood of 20 Mev. However, in this case,

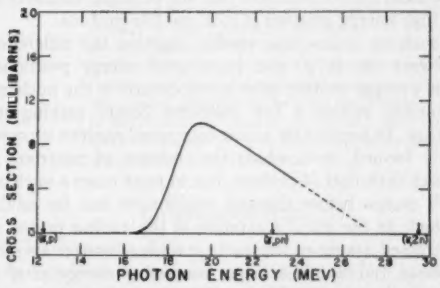

FIG. 2. Cross-section curve for the reaction $Mg^{24}(\gamma, n)Mg^{23}$. The arrows indicate thresholds for possible competing reactions.

the (γ, p) energy threshold is 6.6 Mev below the (γ, n) threshold. The result is therefore consistent with statistical theory.

Figure 2 shows the cross-section curve for the $Mg^{24}(\gamma, n)Mg^{23}$ reaction. The peak cross section is approximately equal to that for the $Al^{27}(\gamma, n)Al^{26}$ reaction. Considerations similar to those above show that the turn-over of this reaction also cannot be explained in terms of competition. It is interesting to note that the curve rises very steeply to the peak due to the high (γ, n) threshold, and that the peak occurs at nearly the same photon energy as does that for the $Al^{27}(\gamma, n)Al^{26}$ reaction. The (γ, p) threshold is in this case also much lower than the (γ, n) threshold, and if the total photonuclear absorption cross section is to be approximately equal to that for aluminum, the (γ, p) cross sections would have to be much larger than the (γ, n) ones in the neighborhood of the peak.

[17] L. Katz and A. S. Penfold, Phys. Rev. **81**, 815 (1951); **83**, 169 (1951); and L. Katz and A. G. W. Cameron, Can. J. Phys., November, 1951 (to be published).

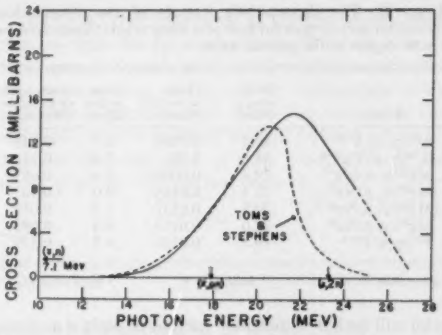

FIG. 3. Cross-section curves for the reaction $Mg^{25}(\gamma, p)Na^{24}$. The dotted line is the determination by Toms and Stephens. The arrows indicate thresholds for possible competing reactions.

In Fig. 3 are plotted two determinations of the cross-section curve for the $Mg^{25}(\gamma, p)Na^{24}$ reaction. The solid line gives the results of the present experiment and the dotted line gives those of Toms and Stephens.[9] The two curves are in good agreement up to 20 Mev, both in relative shape and absolute cross section, but above that energy a serious discrepancy sets in. For Mg^{25} the (γ, n) threshold lies considerably lower than the (γ, p) threshold, yet the (γ, p) peak cross section is only slightly smaller than that for the $Al^{27}(\gamma, p)Mg^{26}$ reaction. The $Mg^{25}(\gamma, n)Mg^{24}$ peak cross section could not be much greater than those of the previously discussed (γ, n) reactions if Mg^{25} is to have the same total photonuclear absorption cross section as Al^{27}.

The threshold for the $Mg^{25}(\gamma, pn)Na^{23}$ reaction is only 17.9 Mev. Since Toms and Stephens found the photoproton energy distribution from both natural magnesium and from Mg^{25} to peak at 4 to 5 Mev, it is evident that for photon energies in the neighborhood of 22 Mev a considerable portion of the (γ, p) residual

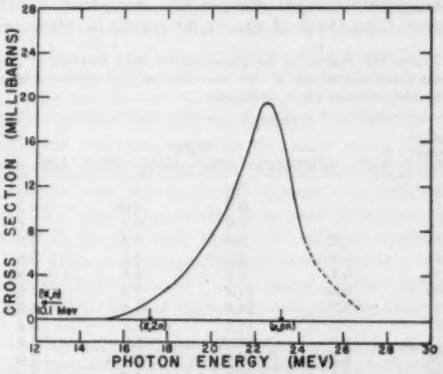

FIG. 4. Cross-section curve for the reaction $Mg^{26}(\gamma, p)Na^{25}$. The arrows indicate thresholds for possible competing reactions.

TABLE II. The characteristic features of the photonuclear cross-section curves reported here plus some others determined for the same region of the periodic table.

Reaction	Peak energy (Mev)	Peak cross section (barns)	Peak width (Mev)	Integrated cross section (Mev-barns)
$Al^{27}(\gamma, n)Al^{26}$	19.2	0.0081	4.7	0.045
$Al^{27}(\gamma, p)Mg^{26}$ [a]	21.2	0.022	5.4	0.12
$Mg^{24}(\gamma, n)Mg^{23}$	19.4	0.0098	5.8	0.057
$Mg^{25}(\gamma, p)Na^{24}$	21.7	0.0148	6.0	0.10
$Mg^{25}(\gamma, p)Na^{24}$ [b]	20.5	0.0137	3.9	0.056
$Mg^{26}(\gamma, p)Na^{25}$	22.6	0.0193	3.3	0.085
$P^{31}(\gamma, n)P^{30}$ [c]	19.5	0.0167	6.5	0.129

[a] Reference 4. [b] Reference 9. [c] Reference 17.

nuclei will be left sufficiently excited to emit a neutron, thus removing such nuclei from detectability in the experiment. It is probable that much of the "reduction" in the (γ, p) maximum cross section is due to this cascade competition of the (γ, pn) reaction.

Figure 4 shows the cross-section curve for the $Mg^{26}(\gamma, p)Na^{25}$ reaction. The maximum cross section is nearly equal to that for the $Al^{27}(\gamma, p)Mg^{26}$ reaction, even though the (γ, n) threshold is 3.9 Mev lower than the (γ, p) threshold. The only multiple reaction with a threshold low enough to offer competition to the (γ, p) reaction near the peak is $Mg^{26}(\gamma, 2n)Mg^{24}$. It is likely that this reaction would be mainly effective in lowering the (γ, n) cross-section curve, and that it would not have much effect on the (γ, p) cross-section turn-over. The $Mg^{26}(\gamma, n)Mg^{25}$ reaction cross section near the peak is again probably not very different from those of the previous cases.

The characteristics of the above cross-section curves are listed in Table II, together with those for the $P^{31}(\gamma, n)P^{30}$ reaction.[17] Values of the photonuclear cross sections for the four new curves reported here are given at one-Mev intervals of photon energy in Table III.

It may be seen in Table II that the (γ, n) cross-section maxima occur at nearly equal photon energies, and that the (γ, p) cross-section maxima are also at approximately equal energies but are about 2 Mev higher than those of the (γ, n) reactions. Moreover, the (γ, p) maximum cross sections are nearly all higher than the (γ, n) maximum cross sections. The lowest (γ, p) peak cross section, for the reaction $Mg^{25}(\gamma, p)Na^{24}$, is slightly less than the highest (γ, n) peak cross section, for the reaction $P^{31}(\gamma, n)P^{30}$. However, the latter reaction occurs in a slightly heavier element where the potential barrier for protons is higher than in magnesium and aluminum and where the total photonuclear absorption cross section is expected to be larger,[13,14] and it has been shown above that the former reaction has its peak cross section reduced by competition with the (γ, pn) reaction.

TABLE III. Values of the photonuclear cross sections in magnesium and aluminum at one-Mev intervals of photon energy. The cross sections are in millibarns.

Photon energy (Mev)	Reaction $Mg^{24}(\gamma, n)Mg^{23}$	$Mg^{25}(\gamma, p)Na^{24}$	$Mg^{26}(\gamma, p)Na^{25}$	$Al^{27}(\gamma, n)Al^{26}$
14	—	0.2	—	—
15	—	0.7	0.05	0.2
16	—	1.9	0.5	1.1
17	0.4	3.9	1.4	2.8
18	4.3	6.5	2.8	5.6
19	9.4	9.1	4.8	8.0
20	9.6	11.8	7.5	7.6
21	8.5	14.1	11.6	6.0
22	7.2	14.5	17.8	4.4
23	5.9	12.2	18.2	3.1
24	4.6	9.4	9.1	2.0
25	3.3	6.6	4.3	1.1
26	1.9	3.6	2.3	0.5

The (γ, p) maximum cross sections are remarkably independent of wide variations in photonuclear thresholds and of the odd-odd, odd-even, and even-even characteristics of the residual nuclei. This is contrary to the predictions of the statistical theory and therefore indicates that photonuclear excitation does not usually produce true compound nuclei. Furthermore, the fact that the emission of protons is the predominant mode of nuclear de-excitation despite the presence of the potential barrier indicates that the principal interaction of high energy photons is with nuclear protons.

Such an interaction readily explains the difference between the (γ, p) and (γ, n) peak energy positions. The average proton, after being excited in the nucleus, probably suffers a few collisions before making its escape. In some cases a true compound nucleus is probably formed, from which the emission of neutrons is easier than that of protons, but in most cases a nucleon will escape before thermal equilibrium can be established. As the initial excitation of the nuclear proton is increased, its mean free path in nuclear matter also increases and it has a larger remaining energy after a given number of collisions. The percentage of protons which escape before the formation of a compound nucleus therefore increases with the energy of excitation. Hence the (γ, n) cross-section curve will turn over below the peak of the total photonuclear absorption cross-section curve (which is also the peak of the (γ, p) cross-section curve).

Courant[8] has proposed that individual nucleons may be excited by a dipole absorption of high energy photons. In this process the nuclear protons are assigned an effective charge eN/A and the nuclear neutrons one of $-eZ/A$. This would give both protons and neutrons nearly the same probability for excitation. While such a process leads to larger (γ, p) to (γ, n) cross-section ratios than would be predicted by statistical theory, the (γ, p) maximum cross sections should still be smaller than those of the (γ, n) reactions. We therefore conclude that the excitation probability for nuclear neutrons is much less than is assumed in this theory.

IV. CONCLUSIONS

Cross-section curves as functions of photon energy have been measured for the reactions $Al^{27}(\gamma, n)Al^{26}$, $Mg^{24}(\gamma, n)Mg^{23}$, $Mg^{25}(\gamma, p)Na^{24}$, and $Mg^{26}(\gamma, p)Na^{25}$.

These curves are plotted in Figs. 1 to 4 and numerical values are listed in Tables II and III.

The curves have the peaked shape characteristic of photonuclear reactions. In three of the four cases such cross-section turn-overs cannot be explained as resulting from a cascade competition with other photonuclear reactions but must be due to a peaking of the photonuclear absorption cross section.

The (γ, p) reactions peak at slightly higher photon energies than the (γ, n) reactions and their cross sections near the peak are considerably greater. These large cross sections are remarkably independent of wide variations in photonuclear thresholds and of the characteristics of the residual nuclei. These facts can be explained in terms of a primary interaction of high energy photons with nuclear protons.

PHYSICAL REVIEW VOLUME 84, NUMBER 6 DECEMBER 15, 1951

Radiation Reaction in Relativistic Motion of a Particle in a Wave Field

E. GORA
Providence College, Providence, Rhode Island
(Received May 7, 1951)

An approximate solution of the equations of motion of Dirac's classical theory f pointlike particles is obtained for a particle in the field of a plane wave, under the assumption that the radiation reaction terms in these equations can be considered as small. The appearance of runaway terms in this solution is avoided by letting the interaction set in gradually. Considerable simplification is achieved by restriction to the domain of high relativistic energies where the transfer of energy and momentum from the wave to the particle appears to be mainly due to radiation reaction. A quantitative discussion of the conditions of applicability of the formulas obtained is made possible by the assumption that there is correspondence between a photon and a classical wave train of finite length. This assumption leads to the conclusion that the classical formulas can be valid for arbitrarily high energies. An estimate of a lower limit for the duration of the interaction between particle and wave train yields an expression which resembles formulas for lifetimes of unstable particles both in its dependence upon fundamental constants and in its increase with the energy involved in the process.

I. INTRODUCTION

THE transfer of linear momentum from a wave to a particle is usually considered as a typical quantum effect, particularly in the E.R.[1] domain. It is the primary purpose of this paper to show that in classical theory such momentum transfers can be accounted for as radiation reaction effects, and that correspondence can be established between relevant results of classical and quantum theory. The equations of motion of Dirac's classical theory of charged, pointlike particles in an electromagnetic[2] field are used as starting point and transformed in a way which simplifies the treatment of the motion of a particle under the influence of a plane wave (Sec. II). A solution of the transformed equations is worked out explicitly in a first approximation, under the assumption that the radiation reaction terms can be considered as small. Runaway terms in this solution are made to disappear by the device of letting the interaction set in gradually, but no attempt is made to prove the consistency of this procedure (Sec. III). Restriction to the E.R. domain leads to simple formulas which are not likely to depend upon any particular assumptions (Sec. IV).

A quantitative discussion of the conditions of applicability of the first approximation is made possible by the assumption that the particle absorbs the energy of a photon while interacting with a wave train of finite length. This leads to the conclusion that the first approximation is likely to be valid for arbitrarily high energies. At first sight such a conclusion seems surprising, since in the N.R. domain the relative order of magnitude of the radiation reaction terms is given by the expression $\frac{2}{3}e^2\omega/mc^3$ (ω angular frequency) which becomes larger than unity for photon energies $\hbar\omega > 205mc^2$. But radiation reaction makes the particle recede in the direction of incidence of the wave. This effect, though small, is cumulative, and can account for large momentum transfers in the E.R. domain. It leads to such a reduction of the frequency of the wave relative to the particle that, on the average, the ratio of the radiation reaction terms to the main terms in the equations of motion does not exceed the order of magnitude of the fine structure constant, $e^2/\hbar c \cong 1/137$ (Sec. V). Analogous results have been previously obtained in the quantum theory of radiation damping.[3]

The same assumptions lead to an estimate of a lower limit for the duration of the interaction between particle and wave train. The expression obtained for this limit

[1] E.R. for extreme relativistic, N.R. for nonrelativistic.
[2] P. A. M. Dirac, Proc. Roy. Soc. (London) **A167**, 148 (1938).
[3] For scattering of photons by charged, spinless particles, the case corresponding to the proposed semiclassical treatment, see E. Gora, Z. Physik **120**, 121 (1943). The present paper originated from an attempt to find a classical analog to the results obtained there.

increases with the energy of the incident photon in a way analogous to the relativistic increase of the lifetime of unstable particles, and resembles the formulas for meson lifetimes in its dependence upon fundamental constants. This result suggests that one may have to distinguish between interaction times and lifetimes in interpreting meson processes (Sec. VI).

II. TRANSFORMATION OF THE EQUATIONS OF MOTION

Dirac[2] has shown that the equations

$$\dot{v}_\mu - b\ddot{v}_\mu - b\dot{\mathbf{v}}^2 v_\mu = (e/m)v_\nu F_\mu{}^\nu{}_{\text{in}} \tag{1}$$

represent the correct equations of motion for a charged, pointlike particle in an electromagnetic field. v_μ is the velocity four-vector (v_0, v_1, v_2, v_3), $\dot{\mathbf{v}}^2 = \dot{v}_0^2 - \dot{v}_1^2 - \dot{v}_2^2 - \dot{v}_3^2$, and $b = \frac{2}{3}e^2/mc^3$ is a constant characteristic for the radiation reaction terms. Dots denote differentiation with respect to the proper time of the particle in Eq. (1), but from now on they will be used to denote differentiation with respect to normal time. $F_\mu{}^\nu{}_{\text{in}}$ is the field tensor of the incident field. The units used will in general be such that the velocity of light $c=1$.

In treating the motion of a particle under the influence of a plane wave we use the coordinate system $x=x_1$, $y=x_2$, $z=x_3$, $t=x_0$, and choose the z axis as direction of incidence of the wave which we represent in the usual way by $E_x=B_y$, $E_y=-B_x$, $E_z=B_z=0$. In conformity with this notation we write

$$\eta = (1-v^2)^{-\frac{1}{2}} = v_0, \quad \pi_x = \eta\dot{x} = v_1, \quad \text{etc.}; \tag{2}$$

$m(\eta, \boldsymbol{\pi})$ is the energy-momentum four-vector of the particle.

Considerable simplification is achieved by introducing the new variable $s=(t-z)$ together with the auxiliary function

$$f = \eta - \pi_z = \eta(1-\dot{z}) = \eta\dot{s}. \tag{3}$$

From these definitions one can easily derive the relations

$$d_t = (1-\dot{z})d_s, \quad \eta d_t = f d_s, \quad dt/ds = \eta/f \tag{4}$$

($d_t = d/dt$, $d_s = d/ds$), which will be used repeatedly.

With these definitions subtraction of the last two equations of (1) leads to

$$d_s(f - bff') + bR = 0, \tag{5a}$$

while the first two assume the form

$$d_s(\pi_x - bf\pi_x') + b\pi_x R/f = (e/m)E_x, \tag{5b}$$

$$d_s(\pi_y - bf\pi_y') + b\pi_y R/f = (e/m)E_y. \tag{5c}$$

The accents denote differentiation with respect to s, and

$$R = -\dot{\mathbf{v}}^2 = \eta^2(\dot{\boldsymbol{\pi}}^2 - \dot{\eta}^2) = f^2(\boldsymbol{\pi}'^2 - \eta'^2). \tag{6}$$

Equations (5) contain no other unknown functions but f, π_x, π_y, and their derivatives. The functions π_z and η are linked up with f, π_x, π_y by Eq. (3) and by the four-vector relation $\eta^2 = 1+\boldsymbol{\pi}^2$. Combining these two relations, we obtain

$$\pi_z = (1 - f^2 + \pi_x^2 + \pi_y^2)/2f, \tag{7a}$$

$$\eta = (1 + f^2 + \pi_x^2 + \pi_y^2)/2f. \tag{7b}$$

Using these expressions in Eq. (6), we find

$$R = f^2(\pi_x'^2 + \pi_y'^2) - 2ff'(\pi_x\pi_x' + \pi_y\pi_y') + f'^2(1 + \pi_x^2 + \pi_y^2). \tag{7c}$$

The system of differential Eqs. (5), supplemented by Eq. (7c), can be solved by the method of successive approximations with b as expansion parameter, provided that this procedure is convergent.

III. SOLUTION OF THE TRANSFORMED EQUATIONS

For the sake of simplicity we assume that the incident wave is circularly polarized, for instance,

$$(e/m)E_x = F\sin\omega s, \quad (e/m)E_y = F\cos\omega s. \tag{8}$$

The appearance of multiples of ω in the radiation reaction terms is thus avoided.

In general, the influence of radiation reaction is likely to be small, and we might expect to obtain a satisfactory approximation by retaining in Eqs. (5) only linear terms in b:

$$f' + bf^2F^2 = 0, \tag{9a}$$

$$\pi_x' - b(\pi_x'' - \pi_x F^2)f = F\sin\omega s, \tag{9b}$$

$$\pi_y' - b(\pi_y'' - \pi_y F^2)f = F\cos\omega s. \tag{9c}$$

The expression $R=f^2F^2$, which has been used here, follows from Eqs. (7c) and (5b, c) with Eqs. (8) if radiation reaction is neglected. The term $bd_s(ff')$ in Eq. (5a) turns out to be of third order in b and is of no influence in this approximation.

With initial conditions of the usual type, for instance, $\boldsymbol{\pi} = \boldsymbol{\pi}' = 0$ for $s=0$ (particle initially at rest), a solution of Eqs. (9) is fully determined; but it contains rapidly increasing, and physically meaningless, radiation reaction terms. It is well known that Dirac's Eqs. (1) lead to such runaway solutions.[4] Probably this difficulty can be avoided in theories where the particle is no longer considered as pointlike, but such theories are necessarily complicated and have not yet been tested.[5]

The appearance of the runaway terms is connected with the use of initial conditions according to which the interaction sets in with full strength at the space-time point of the particle. These terms disappear, at least to any desired order in b, if a suitable starting function is introduced in Eqs. (8) to let the interaction set in gradually. It does not seem likely that such a procedure could be made to fit consistently into the framework of Dirac's classical theory of pointlike particles. Our main

[4] A comprehensive survey of the problems involved has been given by C. J. Eliezer, Revs. Modern Phys. **19**, 147 (1947).

[5] See, for instance, R. E. Peierls and H. McManus, Phys. Rev. **70**, 795 (1946); H. McManus, Proc. Roy. Soc. (London) **A195**, 323 (1949).

reason for using it is that it enables us to derive results which look interesting and new. We do not go beyond the formalism of customary classical theory in using this procedure, but we hope that it might represent a first tentative step towards a formalism of a theory of extended particles and that the results obtained might be confirmed by such a theory.

A function of the type required is $[1-\exp(-n\alpha s)]^n$; it vanishes together with its $(n-1)$st derivatives for $s=0$, and approaches unity for $\alpha s \gtrsim 1$. We multiply the expressions (8) by this function and derive equations corresponding to the linear approximation (9) in b, where now $R=f^2F^2[1-\exp(-n\alpha s)]^{2n}$. The solution of these equations is comparatively simple if it is permissible to omit not only terms of higher than first order in b, but also in $(\alpha n/\omega)$. It does not contain any runaway terms if $n \geqslant 2$. For $\alpha s \gg 1$ this solution reduces to

$$f=A/(1+Bs), \tag{10a}$$

$$\pi_x=(F/\omega)[-\cos\omega s+b\omega f \sin\omega s(1+F^2/\omega^2)], \tag{10b}$$

$$\pi_y=(F/\omega)[\sin\omega s+b\omega f \cos\omega s(1+F^2/\omega^2)], \tag{10c}$$

where

$$A=1/(1-K_n e^2F^2/m\alpha), \quad B=bAF^2. \tag{11}$$

Here we have $K_1=1$, $K_2=25/36$, $K_3=49/90$, $K_4=761/1680$, etc. Using Eqs. (10) in Eq. (7), we obtain

$$\pi_x=(1-f^2+F^2/\omega^2)/2f, \tag{12a}$$

$$\eta=(1+f^2+F^2/\omega^2)/2f, \tag{12b}$$

$$R=f^2F^2. \tag{12c}$$

In these expressions all the linear terms in b cancel out.

Apart from the factor A in f which should not affect the order of magnitude, Eqs. (10) represent just the forced solution of Eqs. (9). Thus, the use of a starting function makes it possible to leave aside the free solution of Eqs. (9) which contains the runaway terms.

We have still to consider whether the procedure is consistent apart from the more fundamental difficulties involved. It seems reasonable to expect that the influence of the starting function should not be considerable, or that $A \sim 1$. According to Eq. (11), this will be the case if $K_n e^2F^2/m < \alpha$. Further, since we have omitted terms of order $(\alpha n/\omega)^2$ in Eq. (10), $(\alpha n/\omega)$ should be small. We obtain thus lower and upper limits for α:

$$K_n e^2F^2/m < \alpha \ll \omega/n. \tag{13}$$

Such a condition can obviously only be fulfilled if $e^2F^2/m \ll \omega$. A similar condition (see Eq. (21) below) is obtained for the validity of the linear approximation in b.

IV. ENERGY AND MOMENTUM RELATIONS

To interpret our formulas, we need a few energy and momentum relations. With the help of Eqs. (2), (3), and (10) we calculate the energy and the momentum which the particle absorbs:

$$E_{\text{abs}}=P_{\text{abs}}=m\int^{t_1}(\dot{x}F\sin\omega s+\dot{y}F\cos\omega s)dt$$
$$=mbF^2(1+F^2/\omega^2)s_1; \tag{14}$$

here t_1 is the value of t which corresponds to the length s_1 of the incident wave train. To determine the energy and the momentum which the particle emits, we use Eqs. (10a), (12a, c), and (14):

$$E_{\text{em}}=m\int^{t_1} bR dt=\tfrac{1}{2}(E_{\text{abs}}+mf_1Bs_1), \tag{15a}$$

$$P_{\text{em}}=m\int^{t_1} bR\dot{z}dt=\tfrac{1}{2}(E_{\text{abs}}-mf_1Bs_1). \tag{15b}$$

The energy and the momentum which the particle retains should be given by the difference between the absorbed and the reemitted energies and momenta. One can easily verify that

$$m(\eta_1-\eta_0)=E_{\text{abs}}-E_{\text{em}}, \tag{16a}$$

$$m(\pi_{x1}-\pi_{x0})=P_{\text{abs}}-P_{\text{em}}; \tag{16b}$$

but, since the formulas used here are valid only for $s \gg 1/\alpha$, η_0 and π_{x0} represent the expressions obtained from Eqs. (12a, b) with $s=0$, and not the correct values for a particle initially at rest. This inconsistency is of little importance in the E.R. domain, where a satisfactory approximation is obtained by substituting 1, 0 for η_0, π_{x0} in our formulas; but, in general, such a simplification is not permissible.

To verify this statement, we consider first that our formulas describe a particle moving both in the direction of incidence of the wave and around this direction. In the N.R. case, where $\eta \cong 1$, $F \ll \omega$, $A \cong 1$, and $f \cong 1$, the kinetic energy of the particle, $m(\eta-1) \cong \tfrac{1}{2}m(\pi_x^2+\pi_y^2) \cong \tfrac{1}{2}mF^2/\omega^2$, is mainly due to an approximately circular motion in the (x, y) plane under the direct influence of the incident wave and Eqs. (12a, b) reduce to $\pi_x=\tfrac{1}{2}(F^2/\omega^2)+bF^2s$, $\eta=1+\tfrac{1}{2}(F^2/\omega^2)$. The final value of the radiation reaction term in π_x is not likely to exceed the order of magnitude of the direct interaction term, F^2/ω^2, since it seems plausible to consider the classical coherence length $1/b\omega^2$ as an upper limit for s_1 and with this expression $bF^2s_1=F^2/\omega^2$. A term of this order is of negligible influence upon the kinetic energy. Thus, we have $(\eta_0-1)<(\eta_1-1)$, and $\pi_{x0} \sim \pi_{x1}$. From these relations, it is evident that formulas like Eq. (16) do not apply to the N.R. case.

In the E.R. domain, we find $\eta_1 \gg 1$; and, according to Eqs. (3), (10), and (12), provided that $F \lesssim \omega$ (see Sec. VI), we have $f_1 \cong 1/bF^2s_1 \cong \tfrac{1}{2}/2\eta_1$, and $\eta_1 \cong \pi_{x1} \cong \tfrac{1}{2}bF^2s_1$. These relations show that in the E.R. domain the influence of radiation reaction predominates. From Eqs. (12a, b) it follows further that $\pi_{x0} \sim 1 \ll \pi_{x1}$, $(\eta_0-1) \sim 1$

$\ll\eta_1$. Obviously, it is permissible to substitute 1, 0 for η_0, π_{s0} in the approximation where terms of relative order $1/\eta_1$ are omitted. The contribution of the particle's motion in the (x, y) plane to its total energy, $\sim(m/2\eta_1)(F^2/\omega^2)$, is also negligible in this case. The approximate validity of our formulas in the E.R. domain is thus demonstrated. To derive formulas valid for all energies, one would have to take into account explicitly both the starting process and a final stage where the particle reemits the energy of its motion in the (x, y) plane. Since this would lead to considerable complications, we prefer to restrict our considerations to the E.R. case.

V. COMPARISON WITH QUANTUM THEORY

In comparing our classical formulas with quantum theory, we have to use the corresponding formulas for scattering of photons by spinless particles which can be derived from expressions given by Pauli.[6] In the E.R. case, where the ratio of the photon energy to the rest energy of the particle $\gamma=\hbar\omega/mc^2\gg1$, the total scattering cross section is

$$\Phi\cong\pi r_0^2/\gamma \quad (r_0=e^2/mc^2). \tag{17}$$

Terms of relative order of magnitude $1/\gamma$ have been omitted. The average energy of the secondary photons and their average momentum in the direction of incidence of the primary photon follow from

$$(E_{\rm em})_{\rm av}=m\left(\int\gamma' d\Phi\right)\Big/\Phi,$$

$$(P_{\rm em})_{\rm av}=m\left(\int\gamma'\cos\vartheta d\Phi\right)\Big/\Phi,$$

where $\gamma'=\gamma/[1+\gamma(1-\cos\vartheta)]$ refers to the secondary photon which is scattered in the direction ϑ. Evaluating these integrals and using Eq. (17), we obtain the E.R. relations:

$$(E_{\rm em})_{\rm av}\cong(P_{\rm em})_{\rm av}\cong\tfrac{1}{2}m\gamma. \tag{18}$$

Since m is the energy initially absorbed by the particle, we see that $(E_{\rm em})_{\rm av}/E_{\rm abs}\cong\frac{1}{2}$. The same result follows from the classical formulas (14), (15), since $mf_1Bs_1\sim m\ll E_{\rm abs}$ in the E.R. domain. Thus both classical and quantum theory lead to the result that in the E.R. case about one-half of the energy which scattering spinless particles initially absorb is retained by them and the other half is emitted in form of secondary radiation.

The classical expressions (15) become identical with the quantum-theoretical expressions (18) if it is assumed that the particle absorbs the energy of a photon, $E_{\rm abs}=\hbar\omega$, or

$$E_{\rm abs}/m=bF^2(1+F^2/\omega^2)s_1=\gamma. \tag{19}$$

We propose to use this relation to supplement our classical formulas. It appears that such a procedure may contribute to a better understanding of why customary quantum-theoretical methods can lead to correct results for high energy photon-electron processes. In fact, the expression for the interaction is still taken over from classical theory there, and it is by no means obvious that classical concepts can be valid for arbitrarily high energies.

Let us consider the conditions of applicability of our classical formulas. It is evident from Eqs. (9) or (10), and it can be confirmed by working out higher approximations, that radiation reaction terms which do not contain s explicitly will, in general, be small if

$$b\omega f\ll1, \tag{20}$$

$$bf(F^2/\omega)\ll1. \tag{21}$$

Since for particles initially at rest $f\leqslant1$, these conditions are certainly fulfilled if they are fulfilled for $f=1$.

If $f\cong1$, it follows from Eq. (20) that $\hbar\omega\ll h/b\cong205\ mc^2$. Obviously, for high energies and $f\cong1$, the use of our classical formulas is not permissible. But if high relativistic energies are transferred to the particle during the interaction, it will rapidly recede from the incident wave, and the function f can be expected to decrease considerably during the interaction.

To determine the average E.R. value of f, we make use of Eq. (19). If the particle acquires the energy $\eta_1m\cong\frac{1}{2}\gamma m$ during the interaction, it follows from Eq. (3) that

$$f_1\cong1/2\eta_1\cong1/\gamma. \tag{22}$$

The average value of f can be obtained from the relations

$$(f)_{\rm av}=\left(\int^{t_1}fdt\right)\Big/\left(\int^{t_1}dt\right)$$

$$=\left(\int^{s_1}\eta ds\right)\Big/\left[\int^{s_1}(\eta/f)ds\right],$$

where Eq. (4) has been used to carry out the transformation from t to s; t_1 is the time during which the interaction takes place.

With f and η as given by Eqs. (10a) and (12b), these integrals are easily worked out. Using the E.R. relation $f_1\cong A/Bs_1\ll1$, and omitting terms of relative order $1/Bs_1$, we obtain

$$\int^{s_1}\eta ds\cong\tfrac{1}{4}(1+F^2/\omega^2)Bs_1^2/A, \tag{23}$$

$$t_1=\int^{s_1}(\eta/f)ds\cong\tfrac{1}{6}(1+F^2/\omega^2)B^2s_1^3/A^2. \tag{24}$$

Using these expressions and Eq. (22), we obtain the E.R. formula:

$$(f)_{\rm av}\cong3A/2Bs_1\cong3f_1/2\cong3/2\gamma. \tag{25}$$

[6] W. Pauli, Revs. Modern Phys. **13**, 230 (1941).

With this expression for f, condition (20) assumes the form

$$b\omega(3mc^3/2\hbar\omega)=e^2/\hbar c\ll 1. \qquad (20')$$

Since $e^2/\hbar c\cong 1/137$, it appears that, except during an initial stage of the process when f is relatively large, condition (20) can be fulfilled for arbitrarily high frequencies of the incident photon. It is possible that the influence of this initial stage upon the total process is small and that classical results still apply, in a correspondencelike way, even for $\hbar\omega > 205\ mc^2$. As mentioned already in Sec. I, this somewhat surprising result may prove of some help in understanding the quantum-theoretical result that, for the process considered, radiation reaction corrections do not exceed the relative order of magnitude $e^2/\hbar c$.

VI. ESTIMATES OF LOWER LIMITS FOR s_1 AND t_1

We have still to consider condition (21). Since condition (20) leads to the plausible condition (20'), it would seem desirable that condition (21) should not lead to an additional restriction of the domain of applicability of our formulas. It can be seen immediately that condition (21) will be fulfilled simultaneously with condition (20) if

$$F\lesssim\omega, \quad \text{or} \quad E\lesssim m\omega/e\cong(e/137r_0^2)\gamma. \qquad (26)$$

For $\gamma\sim 1$, this upper limit for E is of the order of magnitude of the critical field intensity in positron theory,[7] $e/137r_0^2$; and for $\gamma > 137$ it is larger than e/r_0^2, the field intensity on the surface of the classical electron model. Certainly, neither classical nor quantum theory will be expected to apply if the field intensities exceed these limits, and so it seems plausible to require that condition (26) be fulfilled.

This requirement leads to interesting conclusions concerning the admissible values of s_1 and t_1. An estimate of a lower limit for s_1 is obtained by substituting ω for F in the expression $s_1=\gamma/bF^3(1+F^2/\omega^2)$ which follows from Eq. (19):

$$s_1\gtrsim\gamma/2b\omega^3=(3\hbar c/8\pi e^2)\lambda, \qquad (27)$$

where λ is the wavelength of the incident radiation. Since s_1 represents an extension of the incident wave-train along its direction of propagation and $(3\hbar c/8\pi e^2)\cong 16.3$, this looks like a reasonable condition.

The corresponding order of magnitude of a lower limit for t_1 is obtained by combining the E.R. expression (24) with (19) and substituting ω for F. This leads to the estimate

$$t_1\gtrsim\tau_0\gamma, \quad \tau_0=\hbar^2/16me^2c. \qquad (28)$$

Since τ_0 is a constant, this lower limit for t_1 increases with the energy of the incident photon in a way analogous to the relativistic increase of the lifetime of unstable particles.

In our classical theory t_1 represents the duration of the interaction between wave and particle. In deriving the condition (28) for t_1, no unusual assumptions have been made, apart from the use of a starting function which may be nothing more but a mathematical device and which does not directly affect our results. It seems thus likely that such lower limits for interaction times really exist. Analogous results for normal Compton scattering would probably lead to the prediction of a lower limit for the delay in the appearance of the secondary particles. Times of the order given by Eq. (28), $\tau_0\cong 10^{-20}$ sec, are, however, far below the present limit of experimental accuracy, around 10^{-8} sec, in attempts to observe such a delay.[8]

Results of this kind might be of some interest in meson theory. Perhaps it is not just coincidence that the expression for τ_0 in condition (28) resembles the formulas for meson lifetimes in its dependence upon fundamental constants. In earlier theories of meson decay where the existence of mesons of different masses has not been taken into account, meson lifetimes of the order of magnitude $\hbar^3/\mu f^2c$ have been obtained; μ is the meson mass, and f is a constant of the dimension of a charge, $\sim(10^{-8}-10^{-7})e$, which determines the interaction between mesons and light particles in the same way as e determines the coupling between the electromagnetic field and charged particles. There is direct analogy between these meson theories and the quantum theory of electromagnetic radiation in all their aspects, including the classical foundations.[9] If our semiclassical results corresponded to physical reality, one might expect analogous results for interaction processes between mesons and light particles, and that would imply lower limits for interaction times which might be of the same order of magnitude as the meson lifetimes. In recent versions of meson theory which distinguish between mesons of different masses, the situation is more involved, but still essentially the same. It seems conceivable that an interaction process between some type of meson and a high energy light particle might last long enough to be observable. At present, such an observation would probably be interpreted as indicating formation and decay of a heavier meson. A possibility of reducing the number of independent elementary particles by taking finite interaction times into account is thus suggested.

It was in particular this possibility which seemed to make the semiclassical treatment of radiation reaction worth pursuing. A quantum-theoretical investigation of relevant problems would seem desirable, but apparently no attempt in this direction has as yet been made.

[7] See, for instance, W. Heisenberg and H. Euler, Z. Physik **98**, 714 (1936).

[8] R. Hofstadter and J. A. McIntyre, Phys. Rev. **78**, 24 (1950); W. G. Cross and N. F. Ramsey, Phys. Rev. **80**, 929 (1950).

[9] See, for instance, H. Yukawa, Proc. Math. Phys. Soc. (Japan) **17**, 48 (1935); H. A. Bethe and L. W. Nordheim, Phys. Rev. **57**, 998 (1940).

Proton Bombardment of the Lithium Isotopes*

S. BASHKIN† AND H. T. RICHARDS
University of Wisconsin, Madison, Wisconsin
(Received August 13, 1951)

Thin targets of ordinary lithium have been bombarded by protons over the energy range 0.4 Mev to 3.6 Mev. Observations of the magnetically analyzed reaction and scattered particles were made at 164° to the incident beam. Differential cross-section curves were obtained for protons scattered elastically and inelastically from Li^7, elastically from Li^6, and for the He^4 and He^3 particles from the $Li^6(p, \alpha)He^3$ reaction. The Li^6 data show an excited state in Be^7 at about 7.2 Mev and also a lower and very broad state. Possible correspondence to levels in the mirror nucleus Li^7 is discussed. The protons scattered inelastically from Li^7 do not show any resonances above $E_p = 1.5$ Mev. The Li^7 elastic scattering cross section has maxima at proton energies of 1.05 Mev, 1.88 Mev, and 2.06 Mev.

INTRODUCTION

WHEN Li^6 is struck by protons, the compound nucleus, Be^7, is formed with an excitation energy of 5.60 Mev$+6E_p/7$, where E_p is the proton energy in laboratory coordinates. The two most probable modes of decay of these virtual states are

$$Li^6+p \rightarrow (Be^7)^* \rightarrow Li^6+p \quad (1)$$

$$\searrow$$

$$He^4+He^3+4.024\pm0.005 \text{ Mev.}^1 \quad (2)$$

In the present experiment, the excitation functions of the above reactions have been studied for incident protons up to 3.6-Mev energy. It was hoped to find the location and character of the states of Be^7 which lie between 6- and 9-Mev excitation energy. In particular, it was hoped to locate the state in Be^7 which should mirror the 7.5-Mev level in Li^7 which was observed by Blair[2] as a resonance in the $Li^6(n, \alpha)H^3$ reaction for 250-kev neutrons. Gove and Harvey[3] have seen this level (7.50 ± 0.17 Mev) in the $Be^9(d, \alpha)Li^7$ reaction and also report a level in Li^7 at 4.77 ± 0.10 Mev.

At the same time that the virtual levels of Be^7 were being investigated, it proved convenient to study the elastic and inelastic scattering of protons by Li^7. These data provide information concerning very highly excited states of the compound nucleus, Be^8.

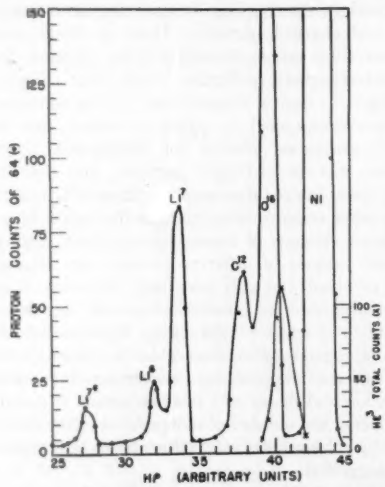

FIG. 1. Momentum spectrum at laboratory angle 164 ± 5 degrees of the protons scattered by the Li target, the 1000A nickel foil backing and by carbon and oxygen contaminants. The group at about 40 Hp units are He^3 reaction products and were separated from the scattered protons by pulse-height discrimination. The incident proton energy was 1.91 Mev.

PROCEDURE

Targets of ordinary lithium metal (92.5 percent Li^7) were prepared by evaporation upon thin nickel foil.[4] These backings were only 500A thick for some of the work. The lithium targets were about 10-kev thick for 2-Mev protons. The targets were placed on a heated support at one focus of a 90° magnetic analyzer[5] and struck by protons monoergic to 0.1 percent. Particles which emerged from the target at an angle of $164\pm5°$ to the incident beam and which had the proper momentum to charge ratio were directed by the analyzer's magnetic field through a conjugate focus and detected by a proportional counter. The counter window prevented detection of protons of energy less than 320 kev. A schematic diagram of a similar experimental arrangement is shown in Fig. 1 of reference 5. The resolution of particle groups of different momentum to charge ratio and of different specific ionization is illustrated in Fig. 1. Pulse-height discrimination in the proportional counter allowed a clean separation of the He^3 particles from protons. The He^4 particles could also have been distinguished by pulse-height analysis, but were actually

* Work supported by the AEC and the Wisconsin Alumni Research Foundation.
† Now at Louisiana State University, Baton Rouge, Louisiana.
[1] Williamson, Browne, Craig, and Donahue, Phys. Rev. 84, 731 (1951).
[2] J. M. Blair, private communication. Older cross-section data are shown in Adair's summary article, Revs. Modern Phys. 22, 249 (1950).
[3] H. E. Gove and J. A. Harvey, Phys. Rev. 82, 658 (1951).
[4] S. Bashkin and G. Goldhaber, Rev. Sci. Instr. 22, 112 (1951).
[5] Shoemaker, Faulkner, Bouricius, Kaufmann, and Mooring, Phys. Rev. 83, 1011 (1951).

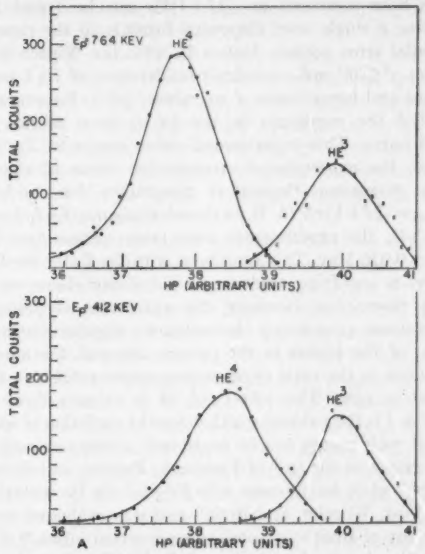

FIG. 2. Typical momentum spectrum of reaction products from $Li^6(p, He^4)He^3$ at low incident proton energies. The rapid variation of He^4/He^3 yield with proton energy is apparent.

studied only in an energy region where the magnetic field separated them from the other particles (see Fig. 2).

The yields of some of the well-resolved particle groups were followed as a function of the bombarding energy. At each energy the magnetic field was varied until the greatest number of counts per incident charge was found. The excitation functions presented in this paper show how those maxima varied with energy. For large enough exit slits to the analyzer, the maxima should be flat-topped and proportional to the total number of particles. For reasonable target thicknesses and for resolution sufficient to separate protons scattered from Li^6 and from Li^7, the flat-topped portion in many cases disappeared. Hence, there is some question concerning the exact proportionality to differential cross section of some of the yield curves here reported. This questionable proportionality was checked over part of the momentum range by comparing the total number of particles entering the analyzer as determined from the maximum yield with the number calculated from $\int N(p)dp/p$, where $N(p)$ is the number of particles observed for a given setting of the magnetic field and dp/p is given by the momentum resolution of the analyzer. The agreement was within 10 percent for the points so checked.

The lithium content of one target was found by measuring the neutron yield from the $Li^7(p, n)Be^7$ reaction. A flat-response long counter,[6] calibrated with a radium-beryllium source of known neutron strength, was used as a detector. Taschek and Hemmendinger's data[7] on the absolute differential cross section of the $Li^7(p, n)Be^7$ reaction were used to compute the lithium content of the target. The uncertainty in the lithium thickness is probably about 15 percent and the uncertainty in the absolute differential cross sections reported in this paper is at least 20 percent.

[6] A. O. Hanson and J. L. McKibben, Phys. Rev. **72**, 673 (1947).

RESULTS AND DISCUSSION

Li^6+p

Figure 3 shows the yield of protons scattered elastically from Li^6 for bombarding energies between 1.2 and 3.1 Mev. The scattering yield above background outside of this energy interval was too small to permit a reliable extension of the curve. The maximum in the curve at 1.75 ± 0.1 Mev indicates a virtual level of Be^7. The He^3 yield curve, Fig. 4, also shows a similar maximum, but at $E_p=1.82\pm0.08$ Mev. This latter energy may be used to locate the resonance energy as (6/7)(1.82) Mev above the dissociation energy of Be^7 or as 7.16 ± 0.08 Mev above the ground state of Be^7.

There are reasons for identifying this state of Be^7 as the mirror level to one observed in Li^7 at 7.46 ± 0.03 Mev.[2,3] The similarity in resonance energy (7.16 *vs* 7.46 Mev) and the paucity of other levels points strongly to this identification. A few hundred kilovolt shift of the mirror levels at this excitation energy is not unexpected. It could presumably result from the combined effects of, (1) a differential reduction in coulomb energies as the radii increase with excitation energies, (2) a difference in electromagnetic spin-orbit interaction for the odd neutron and proton, and (3) a difference in boundary conditions at the nuclear surface for the neutron and proton wave functions. (Table I shows that the difference in level shift probably accounts for ~70 kev of the discrepancy in excitation energy.)

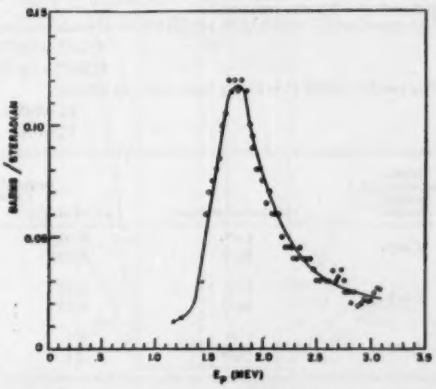

FIG. 3. Differential cross section (barns/steradian) at laboratory angle of 164° for protons scattered elastically from Li^6.

[7] R. F. Taschek and A. Hemmendinger, Phys. Rev. **74**, 373 (1948).

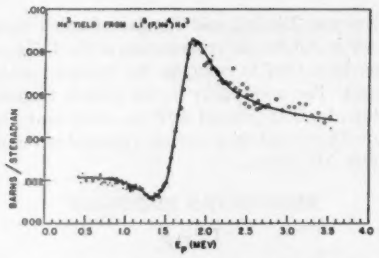

FIG. 4. Differential cross section (barns/steradian) at laboratory angle of 164° for the He^3 particles from $Li^6(p, He^3)He^4$.

Mirror levels should not only have corresponding excitation energies, but also the same J values, parity, and reduced widths. This last condition may be used not only to support the mirror level identification, but also to fix the parity and give limits on the J value of the level. Therefore, in Table I we have calculated the reduced widths of these levels in Li^7 and Be^7 for various assumptions regarding the angular momentum of the neutron or proton incident on Li^6. Six-sevenths of the experimental resonance width at half-maximum gives in each case the total width, Γ, of the level in gravicentric coordinates. The (p, He^3) differential cross section is at resonance only 1/14 that of the elastic scattering (see Figs. 3 and 4). If one neglects effect of angular distribution on the ratio of total cross sections, then the partial width, Γ_α, for alpha-emission is $\sim\Gamma/15=(6/7)(0.5/15)=0.03$ Mev. The proton width, $\Gamma_p=\Gamma-\Gamma_\alpha$, is therefore $\sim$0.40 Mev. Since $\Gamma_\alpha\ll\Gamma_p$, the reduced proton width of Be^7 will be very insensitive to the exact value of Γ_α and hence our neglect of the unknown angular distribution is not serious. In the case of Li^6+n, it is the total (n, α) cross section which has been measured so $(2J+1)\Gamma_\alpha$ can be found by fitting a single level dispersion formula to the experimental cross section. Unless $\Gamma_\alpha\gg\Gamma_n$, the Wigner sum rule, $\gamma^2\leq 3\hbar^2/mR$ excludes consideration of $l\geq 2$ neutrons and hence limits J to values $\leq 5/2$. Experimentally,[7] the maximum in the (n, α) cross section is $\sim$3 barns. This experimental value points to $J=5/2$ since the experimental cross-section value is almost the maximum theoretical absorption for $J=5/2$: $\sigma_{max}=(2J+1)\pi\lambda^2/6$. If we therefore assume $J=5/2$ and $\Gamma_n>\Gamma_\alpha$ the experimental total cross section fixes Γ_α as $\sim$0.036 Mev. This agreement with the Γ_α for the Be^7 level is gratifying evidence of the mirror character of the resonances; however, the agreement is perhaps fortuitous considering the unknown angular distribution of the alphas in the proton case and the uncertainties in the total cross-section measurements in the neutron case. The $\gamma_0^2=\Gamma_\alpha A_l^2/2k$ in column three of Table I is the reduced width when the variation of level shift with energy can be neglected. A_l^2 for neutrons is the same as the $|v|^2$ of Feshbach, Peaslee, and Weisskopf,[8] while for protons $A_l^2=F_l^2+G_l^2$ (in the notation of Yost, Wheeler, and Breit[9]) and was evaluated with the use of Breit's coulomb wave-function tables.[9a] The fourth column, $\gamma^2=\gamma_0^2/(1-\gamma_0^2/R\cdot dg/dE)$ is the reduced width when account is taken of the variation of level shift with energy.[10] R is the reaction radius and $g=d(\ln A_l)/d(\ln kR)$. The fifth column, $\Delta=-\gamma^2(g+l)/R$ gives the actual level shift at resonance and the last column corrects the observed resonance energy (as measured from the ground state of the nucleus) for the level shift Δ.

Inspection of Table I shows that the reduced widths agree satisfactorily only if $l=1$ incident particles are involved in the resonance. Independent confirming evidence for this assignment in the case of the Li^7 level

TABLE I. Possible level parameters of the neutron (or proton) plus Li^6 resonance. An interaction radius $R=0.4\times10^{-12}$ cm (i.e., $\sim\frac{1}{4}(e^2/mc^2)(6^{\frac{1}{3}}+1^{\frac{1}{3}})$ was assumed.

The experimental total widths are (in center-of-mass coordinates)

$\Gamma(Li^{7*})=(6/7)(0.1)$ Mev$=0.086$ Mev

$\Gamma(Be^{7*})=(6/7)(0.5)$ Mev$=0.43$ Mev.

The partial widths $\Gamma_s=\Gamma-\Gamma_\alpha$ were taken as follows:

$\Gamma_n=0.086-0.036=0.05$ Mev

$\Gamma_p=0.43-0.03=0.40$ Mev.

Orbital momentum of incident nucleon	Compound nucleus	Reduced nucleon width ($\times10^{13}$ Mev-cm) $\gamma_0^2=\Gamma_\alpha A_l^2/2k$	$\gamma^2=\gamma_0^2/(1-\gamma_0^2/R\times dg/dE)$	Level shift (Mev) $\Delta=-\gamma^2(g+l)/R$	Energy of level (Mev above ground state) $E_\lambda=E_R-\Delta$
$L=0$	Li^{7*}	0.025	0.025	0	7.46
	Be^{7*}	0.103	0.104	+0.04	7.12
$L=1$	Li^{7*}	0.18	0.24	−0.08	7.54
	Be^{7*}	0.25	0.26	−0.15	7.31
$L=2$	Li^{7*}	9.7	(All values of γ^2 for $L\geq2$ exceed $3\hbar^2/2mR\approx1.8\times10^{-12}$.)		
	Be^{7*}	2.1			

[8] Feshbach, Peaslee, and Weisskopf, Phys. Rev. **71**, 145 (1947).
[9] Yost, Wheeler, and Breit, Phys. Rev. **49**, 174 (1936).
[9a] Bloch, Hull, Broyles, Bouricius, Freeman, and Breit, Revs. Modern Phys. **23**, 147 (1951).
[10] R. G. Thomas, Phys. Rev. **81**, 148 (1951).

comes from the angular distribution[11] of the $Li^6(n, \alpha)H^3$ reaction at the 250-kev resonance.

We thus conclude that correspondence of mirror levels is indicated if $l=1$ neutrons or protons are assumed responsible for the resonances. Further, since Li^6 apparently has even parity, this would fix the parity of the Li^7 level as odd. The magnitude of the (n, α) cross section favors $J=5/2$. This level could therefore be one member of the low-lying F doublet predicted on the quasi-atomic model.[12]

A noteworthy feature of the He^3 yield in both laboratory coordinates (Fig. 4) and in c.m. coordinates (Fig. 5) is the appearance of a broad yield maximum at low proton energies (0.6 to 0.9 Mev). Consideration was given to the possible influence on this maximum of alpha-particles from reactions of protons with the Li^7 isotope. The only Li^7 reaction giving alphas of the proper energy is the (p, γ) reaction in which Be^8 is left in an excited state which decays by alpha-emission. The (p, γ) cross section is apparently so small[14] that alphas from this reaction are difficult to detect. Furthermore, the 2-Mev half-width of the excited Be^8, plus the broadening in alpha-momentum because of the recoil from the preceding 14.5-Mev gamma-ray, would produce about twice the experimental momentum spread observed in the present experiment (Fig. 2). We therefore believe that reactions with the Li^7 isotope did not contribute significantly to the above low energy maximum.

This low energy maximum must then be associated with a very broad level in Be^7. It is tempting to assume that it is the mirror level to the one in Li^7 which must be postulated to account for the high thermal neutron cross section of Li^6. This identification is consistent with the fact that the great breadth of the low energy resonance requires that s-protons be responsible for the resonance. Higher momenta incident particles would give a reduced width exceeding the Wigner limit.

Figure 5 also shows a comparison of the present low energy He^3 and He^4 data with previous work by Rumbaugh, Roberts, and Hafstad,[13] Burcham and Freeman,[14] and Bowersox.[15] All data of Fig. 5 have been converted to cm coordinates and to differential cross sections to make comparisons more meaningful.

Our present data agree qualitatively in shape with the data of Rumbaugh, *et al.*,[13] and also with Burcham and Freeman.[14] The disagreement in absolute cross sections of the various experiments is marked. (The Burcham and Freeman cross section used in Fig. 5 is based on their comparison of the (p, α) yield of Li^6 and B^{10}. Were their other comparison to the (p, α) yield of Be^9 to be used, their cross-section values would be increased by a factor 1.7 and the disagreement would be even more marked.)

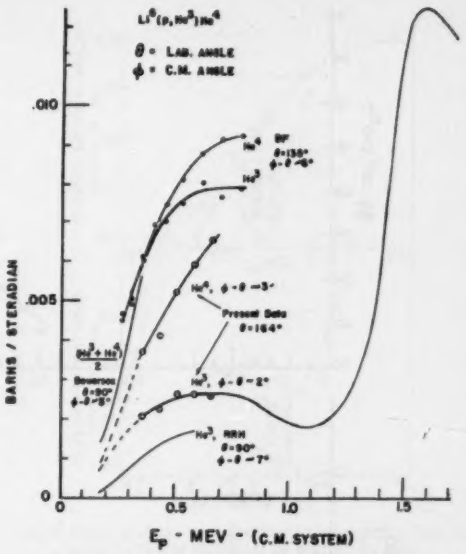

FIG. 5. Comparison (in gravicentric coordinates) with other measurements of the differential cross section of the $Li^6(p, He^4)He^3$ reaction. Note that the measurements have been made at several different angles. BF refers to Burcham and Freeman, reference 14; RRH to Rumbaugh, Roberts, and Hafstad, reference 13. Bowersox's data are from reference 15.

The larger yield of He^4 compared to that of He^3 is noteworthy, both in the 135 degree data of Burcham

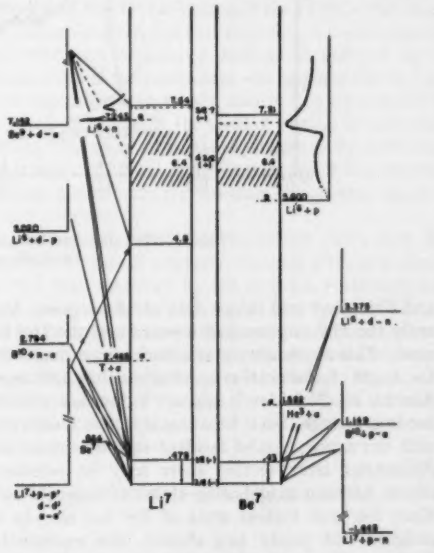

FIG. 6. Comparison of energy levels of the mirror nuclei Li^7 and Be^7.

[11] Roberts, Darlington, and Haugness, Phys. Rev. **82**, 299 (1951).
[12] E. Feenberg and M. Phillips, Phys. Rev. **51**, 597 (1937).
[13] Rumbaugh, Roberts, and Hafstad, Phys. Rev. **54**, 657 (1938).
[14] Burcham and Freeman, Phil. Mag. **41**, 921 (1950).
[15] R. B. Bowersox, Phys. Rev. **55**, 323 (1939).

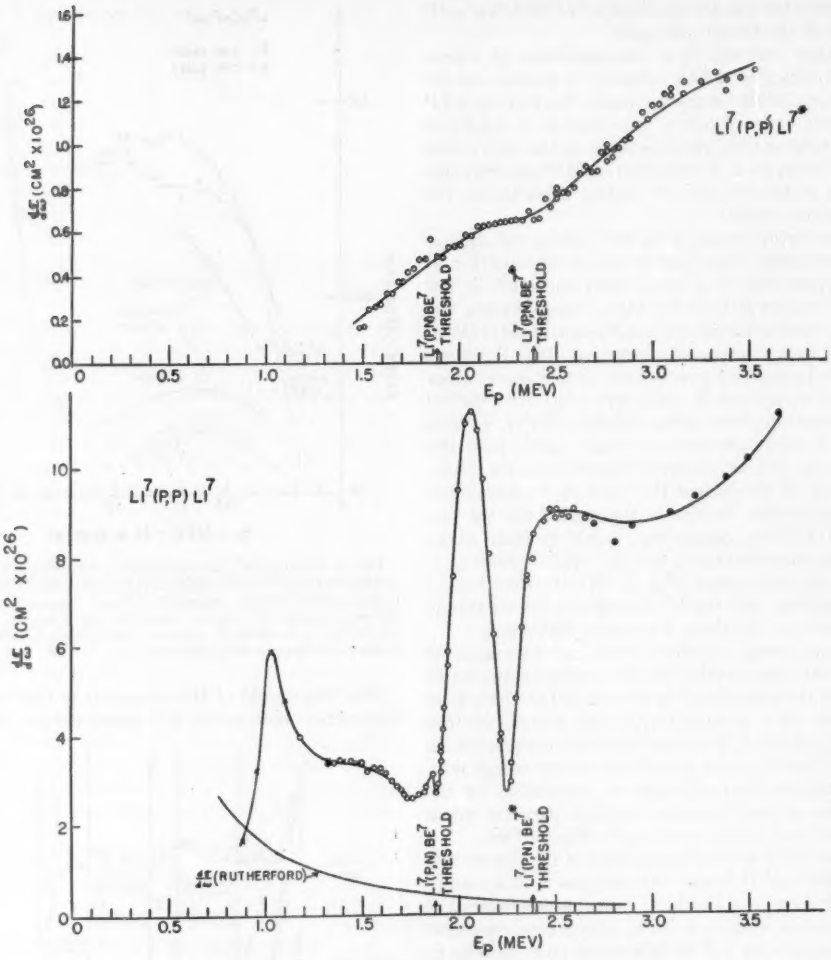

FIG. 7. Differential cross section at laboratory angle 164° for protons scattered elastically and inelastically from Li^7.

and Freeman[14] and in our data at 164 degrees. Apparently the He^3 are bunched forward and the He^4 backward. This asymmetry seems to increase markedly as the angle of observation approaches 0 or 180 degrees. Also for $E_p<0.9$ Mev it appears to increase with bombarding voltage. Such behavior is not in disagreement with our assumption of incident s protons since in the differential cross section there may be interference effects between neighboring states of opposite parity. Since the next highest state of Be^7 has already been assigned odd parity (see above), this asymmetry is further evidence of a lower-lying even parity state in Be^7. Asymmetries have also been observed in the mirror reaction $Li^6(n, \alpha)H^3$ and given a similar interpretation.[11]

The effect on the differential cross section of the interference with the neighboring odd-parity level disappears in the total cross section which may be computed from $\sigma/4\pi=\frac{1}{2}(d\sigma_\alpha/d\Omega+d\sigma_{He^3}/d\Omega)$. Some attempts at fitting such computed total cross-section data with a one-level dispersion formula have been made. However, Γ_p and Δ vary by such large factors over the resonance that such curve fitting is tedious and perhaps not too significant in view of the present experimental uncertainties in the very low energy data. A very rough fit was obtained for $(2J+1)\Gamma_\alpha=0.24$ Mev, $E_\lambda=(0.8+5.6)=6.4$ Mev (above

the ground state of Be^7), and with a reduced proton width $\gamma^2 \sim 0.9 \times 10^{-12}$ Mev-cm. The same interaction radius was used as for Table I. This value of the reduced width is of the order of $\hbar^2/mR$.

The existence of this low energy resonance accounts qualitatively for the observation of Gamow and Critchfield[16] that the difference in penetration factors for s and p wave collisions is a factor 10 too small to account for the cross-section ratio of $Li^6(p\alpha)$ to $Li^7(p\alpha)$ observed by RRH.[13]

If the same parameters are assumed for the level in Li^7 responsible for the high thermal neutrons cross section of Li^6, the observed thermal capture cross section of 910 barns may be used to fix the neutron resonance energy as -0.88 Mev (i.e., ~ 6.4 Mev above the ground state of Li^7). There is perhaps some evidence for such a broad state in Li^7 from the inelastic alpha-scattering data of Gove and Harvey[3] (see in particular Figs. 2 and 3 of their article).

In Fig. 6 we have summarized the data on the energy levels of the mirror nuclei Li^7 and Be^7. Satisfactory correspondence of the energy levels is apparent wherever the corresponding regions of excitation have been carefully investigated.

$Li^7 + p$ REACTIONS

Figure 7 shows the yield curves for the protons scattered elastically and inelastically from Li^7.

The counter window prevented following the elastic and inelastic scattering cross sections to lower proton energies than those shown. The maximum in the elastic scattering at 1.05 Mev corresponds to the $(p, p'\gamma)$ resonance first observed by Hudson, Herb, and Plain.[17] The Cal Tech group[18] has also measured the elastic scattering cross section at this resonance. In the gravicentric system, our peak differential cross section is ~ 0.08 barn/steradian at 166°17′, while the Cal Tech group reports 0.12 barn/steradian at 143°25′ and 0.11 barn/steradian at 90°. It is not clear whether there is an appreciable departure from isotropy at this resonance.

A most interesting feature of the elastic scattering is the small wiggle, entirely reproducible, just at the threshold of the $Li^7(p, n)Be^7$ reaction. Figure 8 shows a more detailed examination of this anomaly. Wigner[19] has predicted that the yield from an extant reaction will exhibit a cusp at the threshold for the emission of S neutrons. Perhaps the observed fluctuation provides verification of the prediction, but this is not certain.

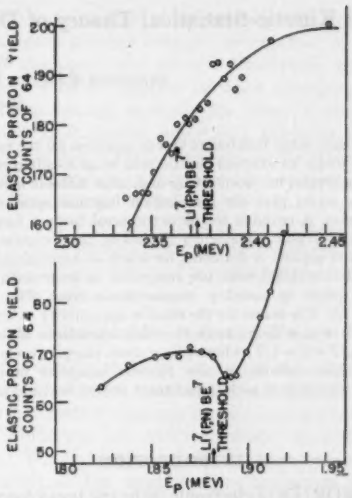

FIG. 8. Study of elastic proton scattering cross section from Li^7 in the vicinity of thresholds for neutron emission.

In an effort to obtain further information about the cusp suggestion, a careful study was made of the elastic scattering in the neighborhood of the threshold for the formation of Be^7 in its first excited state (see Fig. 8). However, the proton yield is changing so rapidly in that region that a small effect could not have been distinguished, and none was found.

Breit and Bloch[20] have studied the $Li^7(p, n)Be^7$ reaction and have concluded that the neutron yield is associated with two odd-parity resonances induced by S protons. One of the resonances was presumed to be just below the neutron threshold, and it may be this which produced the wiggle in the yield of elastically scattered protons. The second resonance suggested by Breit and Bloch was at 2.2 Mev, the energy at which the neutron yield has a maximum and the elastic scattering shows a distinct minimum.

In contrast to the elastic scattering yield, with its large fluctuations in intensity, the only structure above $E_p = 1.5$ Mev exhibited by the inelastic scattering is a slight change in slope between 2.2 Mev and 2.3 Mev.

It is a pleasure to thank the many people who assisted in taking the data in this work. Dr. Gerson Goldhaber was particularly helpful. F. Ajzenberg, Dr. C. P. Browne, D. Craig, D. J. Donahue, Dr. V. R. Johnson, M. J. W. Laubenstein, and D. H. Martin also contributed generous amounts of help.

[16] G. Gamow and C. Critchfield, *Atomic Nucleus and Nuclear Energy Sources* (Oxford Press, London, 1949), p. 255.
[17] Hudson, Herb, and Plain, Phys. Rev. **57**, 587 (1940).
[18] Brown, Snyder, Fowler, and Lauritsen, Phys. Rev. **82**, 159 (1951).
[19] E. P. Wigner, Phys. Rev. **73**, 1002 (1948).
[20] G. Breit and I. Bloch, Phys. Rev. **74**, 397 (1948).

Kinetic-Statistical Theory of Dielectric Breakdown in Nonpolar Crystals*†

WILLIAM R. HELLER‡§
Department of Physics, Washington University, St. Louis, Missouri
(Received May 15, 1951)

The steady-state Boltzmann kinetic equation for the motion of electrons under an external electric field in an idealized nonpolar insulating crystal has been set up and, after suitable approximations, solved to give the distribution function appropriate to strong fields. A criterion for dielectric breakdown is formulated in terms of crystal parameters (including the ionization probability) and applied to diamond, for which an approximate range of 75,000 to 300,000 volts per centimeter is determined by the existing spread of mobility measurements from 4000 to 900 cm²/volt sec. The reason for the relative insensitivity to impurities of this criterion is shown to be the weak dependence of the result on $\langle\beta\rangle N_{tr}(F=0)=1/T$, where $\langle\beta\rangle_{tr}$ = mean trapping cross section of impurities, defects, or any electron acceptors in cm³/sec, $N(F=0)$ = number of such traps vacant at zero field and temperature, and $1/T$ = mean reciprocal trapping time. It is also necessary and almost always true that N_e, the number of electron donors (shallow filled traps) in natural crystals be small relative to the atomic density of the perfect lattice. The new criterion is shown to be more critical than that of Fröhlich or von Hippel, in agreement with the suggestion of Seitz that the fluctuations from mean energy of the electrons govern the breakdown. Since, however, the electron-lattice collision probability decreases with increasing electron energy at energies above $\hbar^2/8m\lambda_{min}^2$, where λ_{min} = shortest lattice vibration wavelength, the ionizing fluctuations governing breakdown are already present in the steady-state solution. Thus the value of the breakdown field is *not* sensitive to the presence of externally produced electrons, as would be true of an ordinary fluctuation phenomenon, even in uniform fields.

I. INTRODUCTION

THEORIES of electronic dielectric breakdown, particularly in polar crystals, have been proposed by von Hippel[1] and further developed by Fröhlich,[2] Seeger, and Teller,[3] Callen,[4] and Seitz.[5] A comprehensive summary of the relevant experiment work has recently been given by von Hippel and Alger.[6] In the present paper, a treatment of dielectric breakdown in nonpolar crystals (numerically, for diamond) is attempted on the basis of the Boltzmann kinetic-statistical equation for the electron distribution function, the electrons being assumed to move in the almost filled lower band and in the almost empty upper band of an idealized insulating crystal. Explicit attention is given to the collisions of the electrons with lattice vibrations, and also to ionization and recombination collisions between the upper and lower band electrons.

The effect of the ionization collisions is to make the distribution function decrease rapidly with increasing energy at energies above ionization threshold (band gap) and to give a maximum at energies close to the bottom of the almost empty upper band. The recombination collisions take place with comparable probability only very near the zero of energy. The result of these facts is to make possible the following program for a simplified calculation:

1. A distribution function is found which is a good approximation under the circumstances that (a) electron energy is greater than a fraction of an electron volt relative to the bottom of the empty band; (b) the field strength is "high" (mean electron energy determined by the field). This function is normalizable, but is the solution of an equation in which the recombination terms do not explicitly appear.

2. The normalization is used to allow for the required number of recombinations per second.

With this approach, a result is obtained that demonstrates clearly the reason that the correct order of magnitude is given by the previous theories (which do not specifically take into account ionization and recombination processes), and permits the formulation of a relatively more rigorous criterion for breakdown. This criterion is then applied to calculate numerically the breakdown field in a reasonably pure diamond crystal as a function of various lattice parameters.

II. PROPERTIES OF THE IDEALIZED INSULATING CRYSTAL

1. Strength of Field and Form of Crystal

We shall concern ourselves with the problem of the behavior of electrons as they move in insulating crystals under electric fields which are uniform in time and space over regions large compared with the periods and characteristic lengths of the electron motion and lattice vibrations, and strong in the sense, later made precise, that the mean electronic energy depends on the field rather than on the lattice temperature. We shall, at first, consider crystals which are ideal in crystalline form and free from impurities.

---

* This work is a condensed version of a manuscript submitted in partial fulfillment of the requirement for the Ph.D. in physics, in June, 1950. A preliminary report was given in a talk at the Chicago meeting of the American Physical Society in November, 1949.

† Partially assisted by the joint program of the ONR and AEC.

‡ AEC Predoctoral Fellow in physics, 1949–1950.

§ Now at the University of Illinois, Urbana, Illinois.

[1] A. von Hippel, Z. Physik **67**, 707 (1931).

[2] H. Fröhlich, Proc. Roy. Soc. (London) **A160**, 230 (1937); **A172**, 94 (1939); **A178**, 493 (1941); **A188**, 521, 532 (1947).

[3] R. J. Seeger and E. Teller, Phys. Rev. **54**, 515 (1938); **56**, 352 (1939).

[4] H. Callen, Phys. Rev. **76**, 1394 (1949).

[5] F. Seitz, Phys. Rev. **76**, 1376 (1949).

[6] A. von Hippel and R. S. Alger, Phys. Rev. **76**, 127 (1949).

2. Connection with Band Structure of Crystalline Solids

The second simplifying assumption is that of spatial isotropy in the electronic motion and among the lattice vibrations. The connection with the ideal anisotropic solid conventional in the theory of solids is as follows:

(a) The electrons are allotted to energy bands which, in wave number space, form regions between concentric spheres of volume appropriate to the crystal being idealized. The gap between the highest filled and the lowest empty bands is taken from experiment. The outer sphere in wave number space limiting the normally (almost) empty conduction band is taken at infinity; this describes, in an approximate way, the actual overlapping of zones of higher wave number which permits electrons to be accelerated in a variety of directions without collision with zone boundaries.

The existence of exciton states between the bands of actual crystals is neglected in this calculation.[7]

(b) The distribution of lattice vibrations in wave number space (σ) is also taken as spherically symmetric; collisions with electrons which involve changes of electrons wave number greater than $|\sigma|_{\max}$ in the first lattice zone correspond to "*Umklappprozesse.*" Since these involve the vectors $\mathbf{g}$ of the reciprocal lattice, such collisions are averaged over all relative orientations of the vector system $\mathbf{k}$, $\mathbf{k}'$, and $2\pi\mathbf{g}$. A distinction is made between the acoustic longitudinal modes and the optical longitudinal modes (whenever the latter are present), the idealization here being the customary assumption of a linear frequency-wave number relation in the first case and a constant frequency-wave number relation in the second. Furthermore, a Debye temperature is used for the first of these two modes and an Einstein temperature for the second, as experiment indicates that these in general give a better fit to the specific heat data than a single Debye temperature.[8]

(c) The wave number of the electron is accepted as a good quantum number even in the presence of strong fields (if electron-lattice vibration collisions, etc., are neglected). This assumption becomes questionable at fields strong enough to make the Zener "tunneling" mechanism[9] of dominant importance. However, for the insulating crystals which correspond to the theory here developed, the energy gap between filled and conduction bands is large enough to eliminate this process. In semiconductors at low temperatures, however, the competition for passage into conducting states between steady-state ionization processes and tunneling transitions may become noticeable.

3. Validity of Perturbation Theory

We also assume that the conventional perturbation theory applies to the electron-lattice collisions,[10] and shall further assume that only longitudinal modes of the lattice vibrations are affected except in *Umklappprozesse.*[11] While the effect of this last assumption may be apparent in the quantitative comparison of the theory with experiment, it should not markedly disturb the predictions as they change with such crystal properties as the separation of zones, characteristic frequencies, and the temperature.

4. Basis of Boltzmann Equation and Fundamental Statistical Method

Finally, we may mention the most basic premise of the discussion, one customary in quantum kinetic-statistical treatments of electronic conduction in metals, and also applicable at the electron energies and concen-

---

[7] The justification for the neglect is as follows: The theory shows that at a critical field, large numbers of electrons will pass from the almost filled lower band into the higher-lying states. Even though a large fraction of these electrons may be associated with their residual holes in the form of excitons, it seems likely that, among other possible mechanisms, subsequent collisions between excitons and conduction electrons uncorrelated with holes in the lower band will (in a time of order 10^{-8} second) dissociate enough of the excitons present to constitute breakdown. The existence of the excitons is then a mere short-lived intermediate step in the transition of electrons into the conducting states of the higher band.

As will be seen later, at breakdown, approximately 10^{10} excitations sec will be effected by each electron. One may assume that about 10^6 electrons/cc are present just below breakdown. Then, in 10^{-8} sec, 10^7/cc excitons will be generated. If we assume plausible values for the quantities involved, the number of excitons dissociated in the same time will be $\approx n_0 W_{ex} \sigma_{ex} v_{el} \approx 10^6 \cdot 10^7 \cdot 10^{-14} \cdot 10^7 \approx 10^6$/cc. That is to say, the electron concentration will roughly double in this interval, indicating that breakdown will proceed. In addition, excitons will be dissociated, leaving mobile holes, upon collision with impurities, thus providing another mechanism which makes exciton production equivalent to charge production. Finally, as has been pointed out by Seitz, excitons in diamond will be dissociated by the electric field.

[8] See, for example, the case of diamond, studied experimentally by A. Magnus and A. Hodler, Ann. Physik **80**, 818 (1926). The present writer has found that a good rough fit of these data is given by taking $C_v = (3/2)NkD(T/\Theta_D) + (3/2)NkE(T/\Theta_E)$, where $\Theta_D \approx 1900°$, $\Theta_E \approx 1400°$. $D(x)$ and $E(x)$ are the Debye and Einstein functions, respectively.

[9] C. M. Zener, Proc. Roy. Soc. (London) **A145**, 523 (1934). A later paper by F. Cernuschi, Proc. Cambridge Phil. Soc. **32**, 256 (1936) makes additional calculations. See also W. V. Houston, Phys. Rev. **57**, 184 (1940), and W. Franz, Physik **113**, 607 (1939). In Phys. Rev. **83**, 650 (1951) Shockley and co-workers report the observation of breakdown by pulse measurements in germanium $n-p$ junctions. While they ascribe this phenomenon to the operation of the Zener mechanism, it may well be that another electron generation mechanism there encountered is the one which appears in the present work as the cause of breakdown. The present formalism however, cannot be directly applied to $n-p$ junctions, as it considers trapping and not diffusion as the major electron removal process. The writer is indebted to Professor Seitz and Dr. Shockley for making available a preprint of Dr. Shockley's paper on high field conduction processes.

[10] The criterion for applicability of the perturbation theory was discussed by Peierls [Z. Physik **88**, 786 (1934)], who showed that a sufficient condition is given by $\tau_{coll}/\hbar/\Delta E > 1$. Here ΔE is the range of energy over which the distribution function for electron energies (in the conducting states) varies appreciably, and τ_{coll} is a suitably defined average time between successive collisions of conducting electrons with lattice vibrations. When ΔE is taken about the same as the mean energy of electrons, this condition is satisfied for nonpolar crystals, since $\tau \sim 1/E$, and it is satisfied at low energies (low fields). See also the article of J. Bardeen and W. Shockley, Phys. Rev. **80**, 69 (1950).

[11] At higher energies (higher wave numbers) the electrons will interact with modes no longer simply describable as longitudinal and transverse, but the variation of collision frequency with energy should not differ greatly from the idealized pattern (see Sec. IV).

trations characteristic of breakdown in insulators. This is the hypothesis that the Boltzmann equation, referring to the distribution function (over energy or wave number in both the lower and upper bands) of a single typical electron, is to be regarded as a satisfactory representation of the equation of motion of the quantum-mechanical density matrix when the trace of the latter is taken successively over all the states of particles in the system other than the particle under consideration.[12–15]

One other point which has arisen in connection with the application of statistical methods to the analysis of electron motion in solids is the question of the role of fluctuations in affecting electronic breakdown. Such fluctuations are automatically given by the distribution function, which describes the probability of finding a typical electron in any state of either the almost empty upper band or the lower, almost filled band. On the other hand, experimental difficulties with the time-dependent formation of space charge, which, of course, have nothing to do with fundamental fluctuation questions, could easily lead to a spread in the observed values of $\Delta V/d$ (for crystals with plane parallel sides) required to produce breakdown.

We now proceed to the actual formulation of the Boltzmann kinetic-statistical equation of our problem which, incidentally, requires further approximations of more mathematical than physical significance to make it tractable.

III. FORMULATION OF THE QUANTUM KINETIC-STATISTICAL EQUATIONS

In what follows we take as a model of the crystal a cubical shape of volume V. The wave number of any of its electrons in the highest filled or lowest empty bands is $k=(2\pi/\lambda)\kappa$, where κ is a unit vector. The function $f(\mathbf{k}, t)$ is the probable number of electrons (with a given spin orientation) occupying at time t a particular elementary cell of phase space (here measured in non-dimensional units, because $\mathbf{k}$ has dimensions of cm^{-1}) specified by the wave number vector $\mathbf{k}$. Hence, we may say that

$$\sum_{\substack{\mathbf{k} \text{ over all cells in} \\ \text{upper band: 1}}} f_1(\mathbf{k}, t)n_{\mathbf{k};1}+\sum_{\substack{\mathbf{k} \text{ over all cells in} \\ \text{lower band: 2}}} f_2(\mathbf{k}, t)n_{\mathbf{k};2}=NV, \quad \text{(III.1)}$$

where $n_{\mathbf{k},1}$ is the number of elementary cells characterized by the wave number $\mathbf{k}$, in ith band ($I=1, 2$ for the upper and lower bands, respectively) and N is the number density of electrons with a given spin orientation in the two bands of the crystal. The Pauli exclusion principle ensures that

$$0\leq f_i(\mathbf{k}, t)\leq 1 \quad \text{for all } i, \mathbf{k}, t,$$

so that $f_i(\mathbf{k}, t)$ may be regarded alternatively as the probability at time t that an electron with a given spin orientation will be found in a cell with wave number $\mathbf{k}$ in the ith band.

The Boltzmann equation then gives for either the upper or the lower band

$$Df_i(\mathbf{k}, t)/Dt=\sum_{\mathbf{k}', \text{ coll}} n_{\mathbf{k};i}f_i(\mathbf{k}, t)W_{\text{coll}}(\mathbf{k}'\rightarrow\mathbf{k}) - \sum_{\mathbf{k}, \text{ coll}} n_{\mathbf{k};i}f_i(\mathbf{k}, t)W_{\text{coll}}(\mathbf{k}\rightarrow\mathbf{k}'), \quad \text{(III.2)}$$

where the large "D" signifies the total derivative and the terms on the right side stand for the increases and decreases of probability per unit time which may come about because of various types of collisions.

The next task is that of examining in more detail the nature of the various W_{coll} which enter into this problem. These will be considered at first without specifying which band is under discussion, and the presence of interaction among the electrons will be recognized to the extent of considering binary collisions and the application of Fermi-Dirac statistics. The expression for the electron energies will be taken as that appropriate to the general band model.

1. Collision with the Lattice

This term has been discussed by numerous authors, the most recent applications of perturbation theory to insulating crystals having been performed by Seitz[16, 16a] and Callen.[4] The calculation required for the purposes of the present work differs somewhat in its treatment of the *Umklappprozesse*, but takes into account both acoustic and optical modes of the lattice vibrations, as is also done by Seitz.

2. Collisions Involving Two Electrons of the Same Band

This term will have the form:

$$\sum_{\mathbf{k}_i'\mathbf{k}_i''\mathbf{k}_i'''} n_i^2 f_i(\mathbf{k}_i')f_i(\mathbf{k}'')\{1-f_i(\mathbf{k}_i''')\} \times\{1-f_i(\mathbf{k}_i)\}W_{\text{coll}}\begin{pmatrix}\mathbf{k}_i'\mathbf{k}_i'' \\ \downarrow \\ \mathbf{k}_i'''\mathbf{k}_i\end{pmatrix} - \sum_{\mathbf{k}_i'''\mathbf{k}_i'\mathbf{k}_i''} n_i^2 f_i(\mathbf{k}_i)f_i(\mathbf{k}_i''')\{1-f_i(\mathbf{k}_i')\}\{1-f_i(\mathbf{k}_i'')\} \times\{1-f_i(\mathbf{k}_i')\}W_{\text{coll}}\begin{pmatrix}\mathbf{k}_i\mathbf{k}_i''' \\ \mathbf{k}_i''\mathbf{k}_i'\end{pmatrix}. \quad \text{(III.3)}$$

The notation used here is that adopted throughout. The subscripts refer to the upper band (1) and lower

[12] M. Born and H. S. Green, Proc. Roy. Soc. (London) **A191**, p. 168 (1947).

[13] See *Convegno Internazionale di Meccanica Statistica*, Suppl., Vol. **VI**, (Nuovo Cimento, 1949), pp. 166–170, especially the remarks of W. Pauli, and pp. 233–239, a talk by Kirkwood.

[14] J. G. Kirkwood, J. Chem. Phys. **14**, 180 (1946); **15**, 72 (1947).

[15] Attempts at giving the transition in the Boltzmann equation, etc., from quantum-mechanical to classical terms in a more exact fashion have been made by D. Blochintzev and P. Nemirovsky, J. Phys. (U.S.S.R.) **3**, 191 (1940); J. E. Moyal, Proc. Cambridge Phil. Soc. **45**, 99 (1949).

[16] F. Seitz, Phys. Rev. **73**, 549 (1948).

[16a] See also J. Bardeen and W. Shockley, Phys. Rev. **80**, 72 (1950).

band (2). The primes signify merely that the primed quantity is to be summed over. The Bloch wave functions of form $e^{i\mathbf{k}\cdot\mathbf{r}}u_{\mathbf{k}}(\mathbf{r})$, where the $u_{\mathbf{k}}$ have the periodicity of the lattice, may be used to calculate the transition probability of the individual collision processes; this corresponds to the Born approximation (plane waves) in the treatment of collisions of free electrons, and should be equally successful here, in a semiquantitative way.

3. Collisions Involving Two Electrons of Different Bands, in Which the Number in Each Band is Conserved

This term will take the form:

$$\sum_{\mathbf{k}_i'\mathbf{k}_j'\mathbf{k}_j''} n_i n_j f_i(\mathbf{k}_i')f_j(\mathbf{k}_j')\{1-f_i(\mathbf{k}_i)\}\times\{1-f_j(\mathbf{k}_j'')\}W_{\text{coll}}\begin{pmatrix}\mathbf{k}_i'\mathbf{k}_j'\\ \downarrow\\ \mathbf{k}_i\mathbf{k}_j''\end{pmatrix} - \sum_{\mathbf{k}_i'\mathbf{k}_j'\mathbf{k}_j''} n_i n_j f_i(\mathbf{k}_i)f_j(\mathbf{k}_j'')\{1-f_i(\mathbf{k}_i')\}\times\{1-f_j(\mathbf{k}_j')\}W_{\text{coll}}\begin{pmatrix}\mathbf{k}_i\mathbf{k}_j''\\ \downarrow\\ \mathbf{k}_i'\mathbf{k}_j'\end{pmatrix}. \tag{III.4}$$

These collisions, of course, include "exchange" collisions with the final state as specified.

4. Collisions Involving the Net Transfer of an Electron from Either Band to the Other

As they apply to the upper band, these correspond to "ionization" and "radiationless (many-body) recombination" of electrons in a gas. Here for the first time we take account of the fact that all transitions cannot be written down with arbitrary indices, applying formally to either band. The reason for this is that collisions which start with the two electrons involved in the upper and lower bands, respectively, will not, in some crystals, result in a radiationless rearrangement in which both electrons are then to be found in the lower band. Such transitions are excluded because of the large ratio (in some actual insulating crystals) of gap between bands to the lower band width, implying that energy would not be conserved in such an encounter.

For the upper band (1), we then write

(a) "ionization,"

$$\sum_{\mathbf{k}_1'\mathbf{k}_2'\mathbf{k}_1''} n_1 n_2 f_1(\mathbf{k}_1')f_2(\mathbf{k}_2')\{1-f_1(\mathbf{k}_1)\}\times\{1-f_1(\mathbf{k}_1'')\}W_{\text{coll}}\begin{pmatrix}\mathbf{k}_1'\mathbf{k}_2'\\ \downarrow\\ \mathbf{k}_1\mathbf{k}_1''\end{pmatrix} - \sum_{\mathbf{k}_1'\mathbf{k}_1''\mathbf{k}_1'} n_1 n_2 f_1(\mathbf{k}_1)f_2(\mathbf{k}_2')\{1-f_1(\mathbf{k}_1')\}\times\{1-f_1(\mathbf{k}_1'')\}W_{\text{coll}}\begin{pmatrix}\mathbf{k}_1\mathbf{k}_2''\\ \downarrow\\ \mathbf{k}_1'\mathbf{k}_1''\end{pmatrix};$$

(b) "recombination,"

$$+\sum_{\mathbf{k}_1'\mathbf{k}_1''\mathbf{k}_1'} n_1^2 f_1(\mathbf{k}_1')f_1(\mathbf{k}_1'')\{1-f_1(\mathbf{k}_1)\}\times\{1-f_2(\mathbf{k}_2')\}W_{\text{coll}}\begin{pmatrix}\mathbf{k}_1'\mathbf{k}_1''\\ \mathbf{k}_1\mathbf{k}_2''\end{pmatrix} - \sum_{\mathbf{k}_1'\mathbf{k}_1''\mathbf{k}_2'} n_1^2 f_1(\mathbf{k}_1)f_1(\mathbf{k}_1')\{1-f_1(\mathbf{k}_1'')\}\times\{1-f_2(\mathbf{k}_2')\}W_{\text{coll}}\begin{pmatrix}\mathbf{k}_1\mathbf{k}_1'\\ \mathbf{k}_1''\mathbf{k}_2\end{pmatrix}.$$

Now for the lower band we write

(a) "ionization,"

$$-\sum_{\mathbf{k}_1'\mathbf{k}_2''\mathbf{k}_1'''} n_1 n_2 f_2(\mathbf{k}_2)f_1(\mathbf{k}_1')\{1-f_1(\mathbf{k}_1'')\}\times\{1-f_1(\mathbf{k}_1''')\}W_{\text{coll}}\begin{pmatrix}\mathbf{k}_1'\mathbf{k}_2\\ \mathbf{k}_1''\mathbf{k}_1'''\end{pmatrix};$$

(b) "recombination,"

$$+\sum_{\mathbf{k}_1'\mathbf{k}_1''\mathbf{k}_1'''} n_1^2 f_1(\mathbf{k}_1')f_1(\mathbf{k}_1'')\{1-f_1(\mathbf{k}_1''')\}\times\{1-f_2(\mathbf{k}_2)\}W_{\text{coll}}\begin{pmatrix}\mathbf{k}_1'\mathbf{k}_1''\\ \mathbf{k}_1'''\mathbf{k}_2\end{pmatrix}.$$

5. Collisions Involving Emission of Radiation or Dissipation of Energy in Lattice Modes, as Well as an Electronic Transition

This term is most difficult of all to discuss, as the processes involved in even an ideal crystal are quite complex. For example, if a quantum of radiation is emitted during a transition from the upper to the lower band, there is a good probability that it will be absorbed and re-emitted several times before it leaves the crystal. This can be seen at once from the absorption curves of Peter,[17] which refer to diamond, and lead to the extrapolated estimate of some 10^6 cm^{-1} for the mean absorption coefficient near resonance for a diamond crystal, the absorption taking place over a band some 900A wide. Such a behavior implies that we must take as the effective cross section for the process of recombination, a number smaller by a sizable factor than what would be estimated from the theory for a single process. This is due to the effective imprisonment of the radiation, which means that radiative recombination is not completely effective in removing electrons from the upper to the lower band during time intervals which are significant for the attainment of the steady state of the kinetic-statistical equation. Strictly speaking, we should also write a Boltzmann equation for the light quanta, as has been done for gases by Holstein,[18] and then con-

[17] F. Peter, Z. Physik **15**, 358 (1923).
[18] T. Holstein, Phys. Rev. **72**, 1212 (1947).

sider the equilibrium of the triple system of upper band electrons, lower band electrons, and quanta, adding a loss term to the kinetic-statistical equation for the quanta to allow for their escape from the crystal.

We should also insert a term giving the probability of radiationless transitions of upper band electrons to the lower band in which the lattice acts as absorber of energy in vibrational modes. Such transitions violate the Franck-Condon principle and are likely to be less probable for this reason, especially because so much energy has to be converted into vibrational motion. A rough idea of the relative importance of this process can be obtained[19] from the behavior of luminescence in certain organic solids at temperatures far below the melting point. Under ultraviolet irradiation, such solids show close to 100 percent quantum yield in luminescence. It is noteworthy, of course, that not all solids behave this way; but those which do are more worthy of attention in making an estimate, because it is less likely that extraneous processes like trapping of electrons are important in the luminescence of such organic crystals.

Since even a rough estimate of the order of magnitude and energy dependence of the two modes of electron removal under discussion in this Sec. 5 is questionable, we shall merely insert a formal probability coefficient into our equations; later, we shall find it possible to estimate the effect of taking different values for it on the breakdown field.

For the upper band, then, we shall have

$$-\sum_{\mathbf{k}_2'} n_1 f_1(\mathbf{k}_1)\{1-f_2(\mathbf{k}_2')\}W_{\text{rec}}\begin{pmatrix}\mathbf{k}_1\\ \downarrow\\ \mathbf{k}_2'\end{pmatrix}, \quad \text{(III.7)}$$

and for the lower band

$$+\sum_{\mathbf{k}_1'} n_1 f_1(\mathbf{k}_1')\{1-f_2(\mathbf{k}_2')\}W_{\text{rec}}\begin{pmatrix}\mathbf{k}_1'\\ \downarrow\\ \mathbf{k}_2\end{pmatrix}. \quad \text{(III.8)}$$

This completes the discussion of the rigorous form of the various contribution, which are now written out symbolically for each band:

$$\frac{\partial f_1}{\partial t}(\mathbf{k}_1,t)=-\left(\frac{e\mathbf{F}}{\hbar}\cdot\frac{\partial f_1}{\partial \mathbf{k}_1}\right)_{\substack{\text{external}\\ \text{field } \mathbf{F}}}+\left(\frac{\partial f_1}{\partial t}\right)_{\substack{\text{lattice}\\ \text{collisions}}}+\left(\frac{\partial f_1}{\partial t}\right)_{\substack{\text{upper band-}\\ \text{upper band}\\ \text{collisions}}}+\left(\frac{\partial f_1}{\partial t}\right)_{\substack{\text{upper-lower}\\ \text{"non-ionizing"}\\ \text{collisions}}}+\left(\frac{\partial f_1}{\partial t}\right)_{\substack{\text{upper-lower}\\ \text{"ionizing"}\\ \text{collisions}}}+\left(\frac{\partial f_1}{\partial t}\right)_{\substack{\text{upper-lower}\\ \text{"recombination"}\\ \text{collisions}}}+\left(\frac{\partial f_1}{\partial t}\right)_{\substack{\text{other}\\ \text{electron-}\\ \text{removing}\\ \text{collisions}}}$$

$$\frac{\partial f_2}{\partial t}(\mathbf{k}_2,t)=-\left(\frac{e\mathbf{F}}{\hbar}\cdot\frac{\partial f_2}{\partial \mathbf{k}_2}\right)_{\substack{\text{external}\\ \text{field, } \mathbf{F}}}+\left(\frac{\partial f_2}{\partial t}\right)_{\substack{\text{lattice}\\ \text{collisions}}}+\left(\frac{\partial f_2}{\partial t}\right)_{\substack{\text{lower band-}\\ \text{lower band}\\ \text{collisions}}}+\left(\frac{\partial f_2}{\partial t}\right)_{\substack{\text{upper-lower}\\ \text{"non-ionizing"}\\ \text{collisions}}}+\left(\frac{\partial f_2}{\partial t}\right)_{\substack{\text{upper-lower}\\ \text{recombination}\\ \text{collisions}}}+\left(\frac{\partial f_2}{\partial t}\right)_{\substack{\text{other}\\ \text{electron-removing}\\ \text{collisions}}}+\left(\frac{\partial f_2}{\partial t}\right)_{\substack{\text{upper-lower}\\ \text{"ionizing"}\\ \text{collisions}}}$$

At this point it becomes possible to consider the generality of the method being outlined. We are neglecting the variation of the distribution function with respect to spatial coordinates, and we may ask what limitations this imposes on the applicability of the results. Clearly the discussion will be inadequate in a situation where sharp spatial discontinuities appear (regions near the electrodes, for example). If spatial diffusion of the electrons is important, this too falls outside the limits of discussion. Finally, if ionic conduction processes are relatively important, we are in no position to account for them.

On the other hand, the present formulation of the problem has a more general application than might be apparent thus far from the title and previous discussion. Whenever we can neglect the effects of non-uniform space charge and of diffusion loss of electrons, we may apply the method developed. This means that when diffusion loss of electrons in gases is not the dominant factor, our equations apply to their motion. The analogy in gases to the lattice vibrations in solids as the collision mechanism for the conduction electrons is, of course, the "elastic" collision of the free electrons with the gas atoms. Ionization and recombination will in gases be supplemented by "attachment" processes.

Also, in liquids in which ionic conduction is not primary, similar considerations should be valid. In fact, for liquids not too far from the freezing point, it may prove fruitful to use the same formalism as for the corresponding solid, with appropriate changes in characteristic temperature Θ, and minimum lattice vibration wavelength $2\pi/|\sigma|_{\max}$, as has been done for the calculation of resistance of liquid metals by Mott.[20]

IV. REDUCTION OF KINETIC-STATISTICAL EQUATIONS TO TRACTABLE FORM

In this section we shall be dealing with the problem of expressing the kinetic-statistical equations in a form suitable for practical calculations. As a consequence, rigor will recede somewhat further into the background. We shall be forced to rely in part on arguments of a

[19] S. Weissman, Washington University (private communication).

[20] N. F. Mott, Proc. Roy. Soc. (London) **A146**, 465 (1934).

more intuitive nature, although they will be conservative from the point of view of demonstrating the existence of a critical breakdown field, and moreover, should not affect our estimate of the order of magnitude of the field. This, of course, will be better seen from the behavior of the solution as subsequently obtained.

1. Lattice Collisions

(a) *Collision Probability for Any Lattice Mode*

In this subsection we write down the expression given by conventional perturbation theory for the probability that the mutually interacting system of electron and vibrating lattice makes a transition resulting in the scattering of the electron and in the emission or absorption of a phonon by the lattice. The formula obtained is combined with the expression for the distribution function $f(\mathbf{k}, t)$ to give the lattice collision term for each band.

In the continuum representation for $\mathbf{k}$ the probability for lattice collisions becomes

$$\int_{\mathbf{k}_i} \frac{V}{8\pi^3} d\mathbf{k}_i f_i(\mathbf{k}_i')\{1-f_i(\mathbf{k}_i)\} W_{\text{coll}}\begin{pmatrix}\mathbf{k}_i' \\ \downarrow \\ \mathbf{k}_i\end{pmatrix} - \int_{\mathbf{k}_i'} \frac{V}{8\pi^3} d\mathbf{k}_i f_i(\mathbf{k}_i)\{1-f_i(\mathbf{k}_i')\} W_{\text{coll}}\begin{pmatrix}\mathbf{k}_i \\ \downarrow \\ \mathbf{k}_i'\end{pmatrix}, \quad \text{(IV.1)}$$

where it should be noticed that in both integrals, the integration variable is $\mathbf{k}_i'$, so that we have to rely on the presence of the density of states hidden in $W_{\text{coll}}(\mathbf{k}_i \to \mathbf{k}_i')$ in the second integral for the possibility of an integration. W_{coll} may be obtained, for nonpolar insulating crystals, by methods analogous to those used in the electron theory of metals for calculating the conduction electron-vibrating lattice collision probability; one finds[21]

$$W_{\text{acoust coll}}\begin{pmatrix}\mathbf{k}_i \\ \downarrow \\ \mathbf{k}_i'\end{pmatrix} = \frac{2\pi}{\hbar}\frac{\hbar}{2NM\omega}\frac{4}{9}C^2\sigma^2\frac{V}{8\pi^3} \times d\mathbf{k}_i' \begin{Bmatrix} n(\boldsymbol{\sigma})+1 \\ n(\boldsymbol{\sigma}) \end{Bmatrix} \delta^*(\mathbf{k}_i-\mathbf{k}_i' \mp \boldsymbol{\sigma}) \times \delta(E(\mathbf{k})-E(\mathbf{k}') \mp \hbar\omega(\boldsymbol{\sigma})), \quad \text{(IV.2)}$$

$$W_{\text{opt coll}}\begin{pmatrix}\mathbf{k}_i \\ \downarrow \\ \mathbf{k}_i'\end{pmatrix} = \frac{2\pi}{\hbar}\frac{\hbar}{2NM\omega}\frac{4}{9}D^2\sigma^2\frac{V}{8\pi^3} \times d\mathbf{k}_i' \begin{Bmatrix} n(\boldsymbol{\sigma})+1 \\ n(\boldsymbol{\sigma}) \end{Bmatrix} \delta^*(\mathbf{k}_i-\mathbf{k}_i' \mp \boldsymbol{\sigma}) \times \delta(E(\mathbf{k})-E(\mathbf{k}') \mp \hbar\omega(\boldsymbol{\sigma})). \quad \text{(IV.3)}$$

These expressions refer to the probability of the electron being scattered from $\mathbf{k}$ into $\mathbf{k}'$ and simultaneously emitting or absorbing a longitudinal phonon, in the case that no *Umklappprozesse* is involved. The mode of oscillation may be either acoustic or optic.

In these equations C is proportional to the matrix element of the electron-lattice vibration interaction energy, assumed roughly independent of $\mathbf{k}$.

$$\int_{\text{unit cell}} u_{\mathbf{k}}^*(\mathbf{r}) u_{\mathbf{k}'}(\mathbf{r})(\xi(\boldsymbol{\sigma})\cdot\nabla)U(\mathbf{r})d\mathbf{r} \approx \tfrac{2}{3} i\sigma\cdot\xi(\boldsymbol{\sigma}) \int_{\text{unit cell}} \frac{1}{2}\frac{\hbar^2}{m} |\operatorname{grad} u_{\mathbf{k}}(\mathbf{r})|^2 d\mathbf{r}. \approx \tfrac{2}{3} i|\boldsymbol{\sigma}|C, \quad \text{where} \quad \mathbf{k}' = \mathbf{k} \mp \boldsymbol{\sigma}$$

(The collision probability for the optical modes is taken to be exactly analogous to that for the acoustic modes. At the time the present work was done, this assumption was made without further physical justification than its conservatism in allowing for all possible electron-lattice collisions. Since then, Shockley (reference 21, page 523) has pointed out that degeneracy in the unperturbed energy band for conduction electrons can give rise to just such a term, whose presence is experimentally detectable in another connection. D is taken $=C$.) The notation used involves $u_{\mathbf{k}}(\mathbf{r})e^{i\mathbf{k}\cdot\mathbf{r}}$, the Bloch wave function of the electron with wave number $\mathbf{k}$; $\boldsymbol{\sigma}$, the wave number of the phonon; $\xi(\boldsymbol{\sigma})$, the polarization unit vector of the $\boldsymbol{\sigma}$-mode; $U(\mathbf{r})$, the time average (static) periodic potential energy of the electron at point $\mathbf{r}$ in the lattice, arising from the electrostatic forces of the nuclei and all the other electrons; N, the number of unit cells in the crystal lattice; M, twice the mass of the vibrating lattice atoms; $n(\boldsymbol{\sigma})$, the number of phonons in the mode $\boldsymbol{\sigma}$, appropriate to thermal equilibrium of the lattice at temperature T; $\omega(\boldsymbol{\sigma})$, the frequency appropriate to $\boldsymbol{\sigma}$, i.e., for optical modes, $\omega(\boldsymbol{\sigma})=\omega_{\text{opt}}$; for acoustic, $\omega(\boldsymbol{\sigma})=v_{\text{ac}}\sigma$, according to the conventional simplifying assumption. The δ^*-function is nondimensional, while the δ-function in energy is the customary one, with dimensions erg^{-1}.

Next we have to treat the terms involving *Umklappprozesse*. These have a form similar to the probabilities just mentioned, with the exception that we have to replace[18] $4C^2|\boldsymbol{\sigma}|^2/9$ by H^2:

$$H = \int_{\text{unit cell}} u_{\mathbf{k}}^*(\mathbf{r}) u_{\mathbf{k}'}(\mathbf{r})(\xi(\boldsymbol{\sigma})\cdot\nabla)U(\mathbf{r}) \exp(\mp i\mathbf{K}\cdot\mathbf{r})d\mathbf{r},$$

where the $\mathbf{K}$ specify the various reciprocal lattice vectors, and $\mathbf{k}' = \mathbf{k} \mp \boldsymbol{\sigma} \mp \mathbf{K}$.

It now remains to formulate the lattice collision terms in the kinetic-statistical equation. This will allow the evaluation of the angular integrations (over $\mathbf{k}$), which in the case of the ordinary collisions afford little difficulty, but which are less simple in the case of the

[21] See, e.g., A. Sommerfeld and H. A. Bethe, Handbuch der Physik **24**, II (Verlag. Julius Springer, Berlin, 1933); and particularly for insulating crystals, F. Seitz, reference 16. We adopt a notation essentially equivalent to that of Seitz. See also W. Shockley, *Electrons and Holes in Semiconductors* (D. Van Nostrand Company, Inc., New York, 1950).

Umklappprozesse, because of the different selection rule, and of the necessity for averaging over all relative orientations of $\mathbf{K}$ and $\mathbf{k}$. This last procedure is, of course, a consequence of the idealization of the actual anisotropic crystal in which $\mathbf{K}$ would represent a fixed direction, relative to the field. As in Eq. (IV.1), we start from

$$\int_{\mathbf{k}'} f_i(\mathbf{k}_i')\{1-f_i(\mathbf{k}_i)\}W_{\text{coll}}\begin{pmatrix}\mathbf{k}_i'\\ \downarrow\\ \mathbf{k}_i\end{pmatrix}d\mathbf{k}_i'\frac{V}{8\pi^3}$$

$$-\int_{\mathbf{k}'} f_i(\mathbf{k}_i)d\mathbf{k}_i\frac{V}{8\pi^3}\{1-f_i(\mathbf{k}_i')\}W_{\text{coll}}\begin{pmatrix}\mathbf{k}_i\\ \downarrow\\ \mathbf{k}_i'\end{pmatrix}.$$

It is then convenient to introduce $\boldsymbol{\sigma}$, instead of $\mathbf{k}'$, as the variable of integration. We can then, since the number of electrons in the conducting states of the upper band is relatively small even at breakdown (see Sec. VI), take $f_1(\mathbf{k}_1)\ll 1$. Also, $\{1-f_2(\mathbf{k}_2)\}\approx 0$, even at breakdown, so that the electron-lattice vibration collisions contribute relatively little to $(\partial/\partial t)f_2(\mathbf{k}_2, t)$. We drop the subscript 1 on $\mathbf{k}_1$ in the electron-lattice collision term for the upper band. The contributions from the various types of vibrational modes and non-*Umklapp* and *Umklapp* scattering, may now be summarized as follows, making use of the wave number selection rule given by δ^*:

$$\int\{W^{(+)}{}_{\text{emiss}}(\mathbf{k}+\boldsymbol{\sigma}_i)f_1{}^{(+)}(\mathbf{k}+\boldsymbol{\sigma}_i)$$

$$+W^{(-)}{}_{\text{abs}}(\mathbf{k}+\boldsymbol{\sigma}_i)f_1{}^{(-)}(\mathbf{k}+\boldsymbol{\sigma}_i)-W^{(-)}{}_{\text{emiss}}(\mathbf{k})f_1{}^{(-)}(\mathbf{k})$$

$$-W^{(+)}{}_{\text{abs}}(\mathbf{k})f_1{}^{(+)}(\mathbf{k})\}d\sigma. \quad \text{(IV.4)}$$

where

$$W^{\mp}{}_{\substack{\text{emiss}\\ \text{abs}}}=L^{(i)}l^{(i)}{}_{\substack{\text{emiss}\\ \text{abs}}}(\boldsymbol{\sigma})\delta(E(\mathbf{k})-E(\mathbf{k}+\boldsymbol{\sigma})\mp\hbar\omega(\boldsymbol{\sigma})).$$

The superscript $-$ or $+$ signs act to distinguish the δ-function required (whether with $\pm\hbar\omega(\boldsymbol{\sigma})$), while the $L^{(i)}$, $l^{(i)}$ are given by

$$L^{(1)}=L^{(1)}{}_{\text{acous}}=\frac{2\pi}{\hbar}\frac{4}{9}\frac{C^2\hbar V}{2NMv_{\text{ac}}\cdot 8\pi^3};$$

$$l^{(1)}{}_{\substack{\text{emiss}\\ \text{abs}}}=|\boldsymbol{\sigma}|\begin{Bmatrix}n(\boldsymbol{\sigma})+1\\ n(\boldsymbol{\sigma})\end{Bmatrix}, \quad \text{(IV.5)}$$

$$L^{(2)}=L^{(2)}{}_{\text{optic}}=\frac{2\pi}{\hbar}\frac{4}{9}\frac{D^2\hbar V}{2NM\omega_{\text{op}}\cdot 8\pi^3};$$

$$l^{(2)}{}_{\substack{\text{emiss}\\ \text{abs}}}=|\boldsymbol{\sigma}|^2\begin{Bmatrix}n(\boldsymbol{\sigma})+1\\ n(\boldsymbol{\sigma})\end{Bmatrix}, \quad \text{(IV.6)}$$

$$L^{(3)}=L^{(3)}{}_{\text{acous }Umklapp}=\frac{2\pi}{\hbar}\frac{H^2\hbar V}{2NMv_{\text{ac}}\cdot 8\pi^3};$$

$$l^{(3)}{}_{\substack{\text{emiss}\\ \text{abs}}}=\frac{1}{|\boldsymbol{\sigma}|}\begin{Bmatrix}n(\boldsymbol{\sigma})+1\\ n(\boldsymbol{\sigma})\end{Bmatrix}, \quad \text{(IV.7)}$$

$$L^{(4)}=L^{(4)}{}_{\text{optic }Umklapp}=\frac{2\pi}{\hbar}\frac{H'^2\hbar V}{2NM\omega_{\text{op}}\cdot 8\pi^3};$$

$$l^{(4)}{}_{\substack{\text{emiss}\\ \text{abs}}}=\begin{Bmatrix}n(\boldsymbol{\sigma})+1\\ n(\boldsymbol{\sigma})\end{Bmatrix}. \quad \text{(IV.8)}$$

(b) Transformation of Integral to Sum of Derivatives

We now introduce the basic assumption that we can represent

$$f_1(\mathbf{k}) \quad \text{by} \quad f_{10}(E(\mathbf{k}))+f_{11}(E(\mathbf{k}))k_z/k+\cdots, \quad \text{(IV.9)}$$

which is an expansion in Legendre polynomials,

$$\mathcal{P}_0(\alpha)=1, \quad \mathcal{P}_1(\alpha)=\cos\alpha=k_z/k, \text{ etc., with } \alpha=\sphericalangle(\mathbf{k}, \mathbf{F}),$$

and that we can neglect in this expansion terms higher than the second because of the strong effect of the lattice collisions in preventing the electron wave number distribution from having too much asymmetry with respect to the axial ($\mathbf{x}$ or $\mathbf{F}$ = field) direction. We shall illustrate the subsequent calculations by giving those for the acoustic modes without *Umklapp*. We then obtain[22]

$$\frac{V}{8\pi^3}d\mathbf{k}\left(\frac{\partial f_1(\mathbf{k}, t)}{\partial t}\right)_{\text{acous coll}}=\frac{V}{8\pi^3}d\mathbf{k}L^{(1)}$$

$$\times 2\pi\int_0^{|\boldsymbol{\sigma}_m|\text{ upper limit}}\sigma^3 d\sigma\int_0^{\pi}\sin\theta d\theta\{R\}$$

$$\times\delta(E(\mathbf{k})-E(\mathbf{k}+\boldsymbol{\sigma})\mp\hbar\omega),$$

[22] Here we neglect the terms arising from those extremely low energy ("cold") electrons with $\hbar k\leq m^*v_{\text{ac}}$, which cannot emit phonons in lattice collisions. Such electrons form a negligibly small fraction of the total number of electrons in conducting states even in thermal equilibrium at low temperatures (but $\geq 1°$K) and *a fortiori*, when strong fields are present. The condition $\hbar k\leq m^*v_{\text{ac}}$ arises from the energy and wave number conservation selection rules, which when combined, give for a phonon emission transition:

$$-2\mathbf{k}\cdot\boldsymbol{\sigma}=\frac{2m^*}{\hbar}v_{\text{ac}}|\boldsymbol{\sigma}|+|\boldsymbol{\sigma}|^2;$$

i.e.,

$$\cos\theta=-\left(\frac{|\boldsymbol{\sigma}|}{2k}+\frac{m^*v_{\text{ac}}}{\hbar k}\right), \text{ and so } \hbar k\geq m^*v_{\text{ac}}.$$

We, furthermore, oversimplify the terms involving collisions with the optic modes, by allowing all angles of collision, and all magnitudes of $|\boldsymbol{\sigma}|$ up to the maximum, even when the selection rules are more restrictive (in a range of energies $\hbar\omega_{\text{op}}<E(\mathbf{k})<\hbar^2\sigma^2/8m^*$). This gives an estimate of breakdown field higher by a factor near one than the true value.

$$\{R\}=\Big[f_{10}^{(+)}(E(\mathbf{k}+\boldsymbol{\sigma}))\{n(\sigma)+1\}$$
$$+f_{10}^{(-)}(E(\mathbf{k}+\boldsymbol{\sigma}))\{n(\sigma)\}-f_{10}^{(+)}(E(\mathbf{k}))\{n(\sigma)+1\}$$
$$-f_{10}^{(+)}(E(\mathbf{k}))\{n(\sigma)\}+f_{11}^{(+)}(E(\mathbf{k}+\boldsymbol{\sigma}))\frac{k_z}{k'}$$
$$\times\left(1+\frac{\sigma\cos\theta}{k}\right)\{n(\sigma)+1\}$$
$$+f_{11}^{(-)}(E(\mathbf{k}+\boldsymbol{\sigma}))\left(1+\frac{\sigma\cos\theta}{k}\right)\{n(\sigma)\}$$
$$-f_{11}^{(-)}(E(\mathbf{k}))\frac{k_z}{k}\{n(\sigma)+1\}$$
$$-f_{11}^{(+)}(E(\mathbf{k}))\{n(\sigma)\}\frac{k_z}{k}\Big]. \quad \text{(IV.10)}$$

Here we have used the relations: $\mathbf{k}'=\mathbf{k}+\boldsymbol{\sigma}$, $|\mathbf{k}'|=|\mathbf{k}|$, $\theta=(\boldsymbol{\sigma},\mathbf{k})$ and

$$\sigma_z=\sigma\cos(\boldsymbol{\sigma},\mathbf{F})=\sigma\cos\theta\frac{k_z}{k}$$
$$+\sin\theta\frac{(k^2-k_z^2)^{\frac{1}{2}}}{k}\cos(\varphi_{\boldsymbol{\sigma}}-\varphi_{\mathbf{F}}). \quad \text{(IV.11)}$$

The aximuthal integration cancels contributions from the second term above, and gives the 2π found in front of the integral. Introducing the variable,

$$Z=E(\mathbf{k})-E(\mathbf{k}+\boldsymbol{\sigma})\mp\hbar v_{ac}\sigma$$
$$=(\hbar^2/2m^*)(k^2-k'^2)\mp\hbar v_{ac}\sigma$$
$$=(-\hbar^2/2m^*)2k\sigma\cos\theta\mp\hbar v_{ac}\sigma-(\hbar^2/2m^*)\sigma^2,$$

so that

$$dZ=(\hbar^2/2m^*)2\sigma k d(-\cos\theta), \quad \text{(IV.12)}$$

we can carry out the θ-integration, the δ-function insuring that contributions come only from

$$\cos\theta=-(\sigma/2k)-(m^*v_{ac}/\hbar k)\approx-\sigma/2k. \quad \text{(IV.13)}$$

The σ-integration remains. Before carrying out the θ-integration, however, we expand the f's in Taylor series about $E(\mathbf{k})$:

$$\left.\begin{aligned} f_{10}^{(\pm)}(E(\mathbf{k}+\boldsymbol{\sigma}))&=f_{10}^{(\pm)}(E(\mathbf{k}))\\ &\quad\pm\hbar v_{ac}\sigma\cdot df_{10}(E(\mathbf{k}))/dE_{\mathbf{k}}\cdots,\\ f_{11}^{(\pm)}(E(\mathbf{k}))&=f_{11}^{(\pm)}(E(\mathbf{k}))+\cdots. \end{aligned}\right\} \quad \text{(IV.14)}$$

The expansion, if expressed in nondimensional units, would properly involve powers of $\hbar v_{ac}\sigma/E(\mathbf{k})$,[22] which is of the order of $10^{-27}10^{6}10^{8}/10^{-12}\sim\frac{1}{10}$ at the most, so that we can neglect the second and higher derivatives of f_{10} and the first and higher derivatives of f_{11}. If the field is not strong, it is necessary to keep the second derivative of f_{10}; and this then gives the maxwell distribution for $f_{10}(E(\mathbf{k}))$, which, of course, could be more easily obtained directly from the original expression for the lattice collision transition probability (in equilibrium). The real reason why we can here neglect the higher derivatives of f with respect to $E(\mathbf{k})$ in the presence of the field is that the total time derivative of f_1 brings in its first derivative with respect to $E(\mathbf{k})$ with a large coefficient depending linearly on $|\mathbf{F}|$. If we wanted to calculate mobilities, for example, in the intermediate region where lattice temperature and field determine (with about equal emphasis) the mean electron energy, it would be necessary to keep the second derivative terms.

Carrying out the indicated operations, we have:

$$\frac{\partial f_1(\mathbf{k},t)}{\partial t}\Big]_{\text{acous coll}}=2\pi\frac{m^*L^{(1)}}{k\hbar^3}\int_0^{\sigma_{\text{upper limit}}}\sigma^2 d\sigma$$
$$\times\Big[\hbar v_{ac}\sigma\frac{df_{10}(E(\mathbf{k}))}{dE(\mathbf{k})}\{n(\sigma)+1\}$$
$$-\hbar v_{ac}\sigma\frac{df_{10}(E(\mathbf{k}))}{dE(\mathbf{k})}\{n(\sigma)\}$$
$$-f_{11}(E(\mathbf{k}))\frac{\sigma^2}{2k^2}\{2n(\sigma)+1\}\cos\alpha\Big].$$

The value of $\sigma_{\text{upper limit}}$ is different for the two situations, $\sigma_{\max}>2k$ and $\sigma_{\max}<2k$; it is $2k$ in the first instance and $\sigma_{\max}$ in the second.

For the present we shall confine ourselves to the problem of low temperatures, so that

$$n_\sigma=1/[\exp(\hbar v_{ac}\sigma/k_0T)-1]\approx0,$$

i.e., $T\ll T_{\text{Debye}}$, and a further reduction and integration give, when $\sigma_{\max}>2k$

$$\left(\frac{\partial f_1(\mathbf{k},t)}{\partial t}\right)_{\text{acous coll}}=a_{10}k^2\frac{df_{10}(E(\mathbf{k}))}{dE(\mathbf{k})}\mathcal{P}_0(\cos\alpha)$$
$$-a_{11}k^2f_{11}(E(\mathbf{k}))\mathcal{P}_1(\cos\alpha),$$

where

$$a_{10}=\frac{4}{9\pi}\frac{m^*}{M}\frac{C^2}{\hbar n_0}, \quad \text{and} \quad a_{11}=\frac{16}{45\pi}\frac{m^*}{M}\frac{C^2}{\hbar^2n_0v_{ac}}, \quad \text{(IV.15)}$$

and $n_0\equiv N/V=$number of unit cells per unit volume in the crystal lattice. Similarly, when $\sigma_{\max}<2k$, one obtains

$$\left(\frac{\partial f_1(\mathbf{k},t)}{\partial t}\right)_{\text{acous coll}}=\frac{c_{10}}{k}\frac{df_{10}(E(\mathbf{k}))}{dE(\mathbf{k})}\mathcal{P}_0(\cos\alpha)$$
$$-\frac{c_{11}}{k^2}f_{11}(E(\mathbf{k}))\mathcal{P}_1(\cos\alpha),$$
$$c_{10}=\frac{m^*}{M}\frac{C^2\sigma_{\max}^4}{\hbar n_0}\frac{1}{36\pi}; \quad c_{11}=\frac{m^*}{M}\frac{C^2\sigma_{\max}^5}{\hbar^2n_0v_{ac}}\frac{1}{90\pi}. \quad \text{(IV.16)}$$

[22] $E(\mathbf{k})$ is an average energy (of the electrons in the conduction band), of the order of several electron volts.

The computations for the other cases are entirely analogous, except for the *Umklappprozesse*. The last mentioned processes prove to give negligible contributions essentially because of the oscillatory character of the integral H.[24] It should be mentioned that for the (non-*Umklapp*) collisions with optical modes, we have different expressions for $(\partial f_i(\mathbf{k}, t)/\partial t)_{\text{optic coll}}$ when when $E(\mathbf{k}) < \hbar\omega_{\text{opt}}$, and, when $E(\mathbf{k}) > \hbar\omega_{\text{opt}}$, since in the former case only phonon absorption can take place in the electron-lattice interaction. If, in addition,

$$T \ll \Theta_{\text{Einstein}} \equiv (\hbar\omega/k_0)_{\text{opt}},$$

no optical phonons are excited and the corresponding contribution to $(\partial f(\mathbf{k}, t)/\partial t)_{\text{optic coll}}$ vanishes.

2. Collisions Involving Two Electrons of the Same Band

Terms of this kind [see Eq. (2) in previous chapter], which are discussed in this and succeeding sections, give a formally complete representation of the situation, as long as the electron-electron collisions can be considered as processes in which only two electrons change their states. The subsequent steps depend on the form we adopt for the transition probabilities, and, in particular, for the electron wave functions. If we adopted for these wave functions the conventional form, $u_{\mathbf{k}}(\mathbf{r})e^{i\mathbf{k}\cdot\mathbf{r}}$, we should have the possibility of writing down wave number and energy conservation laws applying to the two bands considered together as a sort of mixture of gases, in analogy to the kinetic theory of binary gas mixtures.[25] We have then in the continuum approximation:

$$d\mathbf{k}_i\left(\frac{V}{8\pi^3}\right)\left(\frac{\partial f_i}{\partial t}\right)_{\text{coul coll}} = \left(\frac{V}{8\pi^3}\right)^3 \times \int_{\mathbf{k}_i'}\int_{\mathbf{k}_i''}\int_{\mathbf{k}_i'''} f_i(\mathbf{k}_i')f_i(\mathbf{k}_i'')d\mathbf{k}_i'd\mathbf{k}_i''d\mathbf{k}_i''' \times\{1-f_i(\mathbf{k}_i''')\}\{1-f_i(\mathbf{k}_i)\}W_{\text{coll}}\begin{pmatrix}\mathbf{k}_i'\mathbf{k}_i''\\ \downarrow\\ \mathbf{k}_i'''\mathbf{k}_i\end{pmatrix} \quad \text{(IV.17)}$$

$$-d\mathbf{k}_i\left(\frac{V}{8\pi^3}\right)f_i(\mathbf{k}_i)\left(\frac{V}{8\pi^3}\right)^2\int_{\mathbf{k}_i'}\int_{\mathbf{k}_i''}\int_{\mathbf{k}_i'''} f_i(\mathbf{k}_i''')d\mathbf{k}_i''' \times\{1-f_i(\mathbf{k}_i'')\}\{1-f_i(\mathbf{k}_i')\}W_{\text{coll}}\begin{pmatrix}\mathbf{k}_i\mathbf{k}_i'''\\ \downarrow\\ \mathbf{k}_i'\mathbf{k}_i''\end{pmatrix}.$$

The probability expressions, W_{coll} are obviously dependent upon the wave functions and the interaction energy. They involve δ-functions in energy and wave number which leave only the angular integrations in one of the two final states to be performed, and cancel two of the V's in each of the terms on the right-hand side.

Now we estimate the orders of magnitude. We may safely assume that a concentration of upper band electrons of, say, 10^{12}/cc gives evidence of breakdown; but this means that the value of f (in the conducting upper band) is never larger than $10^{12}/10^{23} = 10^{-11} \ll 1$. We obtain this last estimate by considering that there are enough states in either band to accomodate essentially all the electrons. Then, since there are of the order of 10^{23} states (per cc) in the lower almost filled band of an unexcited insulating crystal, we can assume at least this many levels in the idealized upper almost empty band.

The lattice collisions are most important below ionization energies in the upper band, and we may estimate their importance by the magnitude of the mean reciprocal collision time, of order $10^{13}-10^{15}$ sec^{-1}.[26] Now, in estimating the effect of coulomb collisions, we can take

$$(\partial f_i/\partial t)_{\text{coul coll}} \sim 10^{17}\langle f_1^2\rangle_{\text{Av}} \lesssim 10^6\langle f_1\rangle_{\text{Av}},$$

or

$$\tau^{-1}{}_{\text{coul coll}} \sim 10^6 \text{ sec}^{-1} \quad \text{(IV.18)}$$

which, since

$$(\partial f_1/\partial t)_{\text{coul coll}} \sim \sigma_{\text{coul}}\bar{v}_k\frac{4\pi k^3}{3}\langle f_1^2(1-f_1)^2\rangle_{\text{Av}};$$

$$(\partial f_2/\partial t)_{\text{coul coll}} \sim \sigma_{\text{coul}}\bar{v}_k\frac{4\pi k^3}{3}\langle f_2^2(1-f_2)^2\rangle_{\text{Av}}$$

and

$$f_1 \lesssim 10^{-11}, \quad \bar{f}_2 \sim 1, \quad \bar{\sigma}_{\text{coul}} \sim e^2/m^*\bar{v}_k \sim 10^{-15} \text{ cm}^2,$$

$$\bar{v}_k \sim 10^5 \text{ cm/sec}, \quad k \sim 10^{-8} \text{ cm}.$$

Thus, the effect of the coulomb collisions is completely negligible, compared with that of the lattice collisions. At extremely low electron energies, one might think that this conclusion could conceivably be altered; but there recombination collisions (and also, in actual crystals, scattering by imperfections and ionized centers) play a dominant role. The discussion above, or an analogous one, can also be applied with a similar result to collisions of Sec. III, Part 3, and to those of Sec. III, Part 4, which refer to "radiationless recombination" processes. It remains only to discuss the "ionization" collisions of Sec. III, Part 4.

[24] The integral H, evaluated over a unit cell, will give a result dependent on the quantity $|\mathbf{K}|a$, where a is some mean cross-sectional dimension of the unit cell. Because of the imaginary exponential character of the integrand, it is important to notice that $|\mathbf{K}|a$ is, for all crystals, greater than 360°, and thus that the integrand oscillates at least once, even for the smallest $|\mathbf{K}|$. It can be shown by a rough estimate that the integral is at most only a few percent of the corresponding "non-*Umklapp*" integral and that integration over σ-directions further reduces its relative contribution.

[25] S. Chapman and T. G. Cowling, *Mathematical Theory of Non-Uniform Gases* (Cambridge University Press, Cambridge, 1939), Chapter 8.

[26] This estimate follows from the expression for

$$\left(\frac{\partial f_i}{\partial t}\right)_{\text{acous coll}} \sim a_{10}k^3\frac{df_{10}}{dE(\mathbf{k})} \sim \frac{4}{9\pi}\frac{m^*}{M}\frac{C^2k^2}{kn_0}\frac{f_{10}(E(\mathbf{k}))}{\hbar^2k^2/2m^*},$$

so that

$$\tau_{\text{coll}}{}^{-1} \sim \frac{(m^*)^2}{M}\frac{C^2k^-}{\hbar^3n_0} \sim \frac{(10^{-27})^2(10^{-11})^2\cdot 10^8}{10^{-22}(10^{-27})^2\cdot 10^{22}} \sim 10^{14} \text{ sec}^{-1}.$$

3. Ionizing Collision

In order to avoid the necessity of ultimately solving four bilinear integro-differential equations, we shall consider the lower band as a line in energy space. This means neglecting the contribution to the electric current from the lower band, but this is not serious in its effect on the critical field later deduced. It would indeed be serious were one to attempt a calculation of conductivity at very high fields, although even there it should affect only the magnitude and not the field dependence of the current.[27] The question of the location of the monoenergetic line relative to the upper band is next to be considered. This is somewhat arbitrary, but placing the line at a position suggested by the lower band-upper band optical absorption maximum should clearly not be too far from an optimum choice.

In the limit of contracting the lower band to a line, we can take $\sum_2 n_2 = N_2$, where N_2 is the number of electrons per cc with a given spin orientation in the lower band of the unexcited crystal. Next we have to guess at the form of the ionization curve near threshold. It is not true, as an unjustified extrapolation of the Bohr-Bethe-Bloch formula would lead one to suppose, that in gases the cross section rises from threshold with a finite slope. This was first made questionable by the experiments of Tate and co-workers,[28] and definitely contradicted by the later work of Stevenson and Hipple on the rare gases.[29] Their work gives a result fairly well approximated at threshold by an expression containing the factor $(E(\mathbf{k})-E_{\text{ion}})^2$, where E_{ion} is the threshold energy for ionization.

Since there is an approximately linear portion to the curve beginning at some 10 percent of the threshold value above threshold followed by a maximum and a subsequent decrease, one is led to suspect a law of the form (for gases):

$$Q_{\text{tot ion}}(E) \approx Q_{\text{ion}}{}^0 E_{\text{ion}}(E(\mathbf{k})-E_{\text{ion}})^2/(E(\mathbf{k}))^3,$$

where $Q_{\text{tot ion}}(E)$ is the total ionization cross section at energy E and Q_{ion} is a constant. We need also to know, or rather to guess, the angular distribution of the two electrons which result from the ionization process. We can, however, safely assume this as spherical, very near threshold.

But how well can we transpose the above result from gases to solids? One can say qualitatively that the threshold energy dependence of internal "ionization" in solids should not be too different from that in gases. The effect of screening on the wave functions of the outgoing electrons should be to increase the slope or at least the curvature of the ionization cross section at threshold, so that by taking the functional form of the cross section from the ionization in gases, we are being conservative in estimating the ionization probability in solids. Finally, we may test the effect of different assumptions as to magnitude, threshold, and energy dependence of the ionization cross section after we have used the present formulation. As we shall see below, the numerical value of the critical breakdown field is quite insensitive to everything but E_{ion}.[11]

There are, now, two terms in the upper band equation due to ionization, and one term in the lower band, or rather line, which must be considered. According to the discussion given above, a fairly adequate representation of these terms should be given by the following expression:

$$\frac{V}{8\pi^3}\left(\frac{\partial f_1}{\partial t}\right)_{\text{ion is}} d\mathbf{k}_1 = N_2 V \langle f_2\rangle_{\text{Av}} \int_{\mathbf{k}_1'}\int_{\mathbf{k}_1''} f_1(\mathbf{k}_1') \times Q_{\text{ion}}[\mathbf{k}_1' \to \mathbf{k}_1, \mathbf{k}_1'']\left(\frac{V}{8\pi^3}\right)^3 d\mathbf{k}_1 d\mathbf{k}_1' \frac{\hbar k_1'}{m^* V} d\mathbf{k}_1'' - N_2 V \langle f_2\rangle_{\text{Av}} \int_{\mathbf{k}_1'''}\int_{\mathbf{k}_1''} f_1(\mathbf{k}_1)\frac{V}{8\pi^3} d\mathbf{k}_1 \times Q_{\text{ion}}[\mathbf{k}_1 \to \mathbf{k}_1''', \mathbf{k}_1'']\left(\frac{V}{8\pi^3}\right)^2 d\mathbf{k}_1''' d\mathbf{k}_1'' \frac{\hbar k_1}{m^* V}, \quad \text{(IV.19)}$$

where $Q_{\text{ion}}(\mathbf{k}_1' \to \mathbf{k}_1, \mathbf{k}_1'')(V/8\pi^3)^2 d\mathbf{k}_1 d\mathbf{k}_1''$ is the "cross section for internal ionization" by an electron in a conducting state (wave number $\mathbf{k}_1'$) in a collision with any one of the electrons of the lower band (line) with the two electrons present after collision occupying states within $d\mathbf{k}_1$, $d\mathbf{k}_1''$.

We now define the total cross section for "internal ionization" by

$$Q_{\text{tot ion}}(\mathbf{k}_1) = \int_{\mathbf{k}_1'''}\int_{\mathbf{k}_1''} Q_{\text{ion}}(\mathbf{k}_1 \to \mathbf{k}_1''', \mathbf{k}_1'') \times (V/8\pi^3)^2 d\mathbf{k}_1''' d\mathbf{k}_1'', \quad \text{(IV.20)}$$

and $G(\mathbf{k}_1', \mathbf{k}_1)$ by

$$G(\mathbf{k}_1', \mathbf{k}_1) \equiv \frac{1}{Q_{\text{tot ion}}(\mathbf{k}_1')} \times \int_{\mathbf{k}_1''} Q_{\text{ion}}(\mathbf{k}_1' \to \mathbf{k}_1, \mathbf{k}_1'')\frac{V}{8\pi^3} d\mathbf{k}_1'', \quad \text{(IV.21)}$$

[27] We may neglect the contribution of holes to breakdown because they are not usually involved in ionizing collisions, as deduced from the following: (a) If the width of the lower band is less than the band gap, ionizing collisions of this type are energetically impossible. (b) Even if (a) is violated, the exclusion principle practically rules out "upward" transitions by holes, since these are rare in the lower part of the band.

[28] W. Bleakney, Phys. Rev. **35**, 139 (1930); **36**, 1303 (1930); P. T. Smith, Phys. Rev. **38**, 1293 (1930); J. T. Tate and P. T. Smith, Phys. Rev. **39**, 270 (1932).

[29] D. P. Stevenson and J. A. Hipple, Phys. Rev. **62**, 237 (1942).

[11] *Note added in proof:*—T. Holstein (private communication) has informed me of recent experimental work at the Westinghouse Research Laboratory which re-establishes the linear slope near threshold, as predicted by the Born approximation. The work of E. Stueckelberg (Helv. Phys. Acta **5** (1932)), shows that, just at threshold, one expects zero slope but this portion of the curve is unobservable in practice. The assumption sketched here is conservative in estimating breakdown field but has almost no effect on its value.

so that we obtain

$$\frac{V}{8\pi^3}\left(\frac{\partial f_1}{\partial t}\right)_{\text{ion is}} d\mathbf{k}_1 = d\mathbf{k}_1 \frac{V}{8\pi^3} N_2 V \langle f_2\rangle_{Av} \times \int_{\mathbf{k}_1'} f_1(\mathbf{k}_1') \frac{d\mathbf{k}_1'}{8\pi^3} V Q_{\text{tot ion}}(\mathbf{k}_1') \times \frac{\hbar k_1'}{m^* V} G(\mathbf{k}_1', \mathbf{k}_1) - \frac{d\mathbf{k}_1}{8\pi^3} V f_1 N_2 V \langle f_2\rangle_{Av} \times Q_{\text{tot ion}}(\mathbf{k}_1) \frac{\hbar k_1}{m^* V}. \quad \text{(IV.22)}$$

It remains to make an assumption about $G(\mathbf{k}_1', \mathbf{k}_1)$. This quantity is the cross section for production (in an "internal ionization" process) of an electron in $d\mathbf{k}_1$ and the other electron with any $\mathbf{k}_1''$, divided by the cross section for production (in such a process) of two electrons each with any permissible wave number (the original electron having wave number $\mathbf{k}_1'$). A conservative way of estimating $G(\mathbf{k}_1', \mathbf{k}_1)$ is the following:

$$\frac{G(\mathbf{k}_1', \mathbf{k}_1) d\mathbf{k}_1 V}{8\pi^3} \approx \frac{d\mathbf{k}_1 \text{ (total available wave number space volume for other electron)}}{\text{(total available volume of wave number space for both of the two electrons created with any permissible wave number)}}$$

$$\approx \frac{d\mathbf{k}_1 \int_{\mathbf{k}_1''} d\mathbf{k}_1'' \delta(E_{\mathbf{k}_1'} - E_{\text{ion}} - E_{\mathbf{k}_1} - E_{\mathbf{k}_1''})}{\int d\mathbf{k}_1'' \int d\mathbf{k}_1''' \delta(E_{\mathbf{k}_1'} - E_{\text{ion}} - E_{\mathbf{k}_1''} - E_{\mathbf{k}_1'''})}$$

$$\approx d\mathbf{k}_1 \left\{ \frac{4\pi}{3} \frac{(2m^*)^{\frac{3}{2}}}{\hbar^3} [E_{\mathbf{k}_1'} - E_{\text{ion}}]^{\frac{1}{2}} \right\}. \quad \text{(IV.23)}$$

In the lower "band" one has a term

$$\frac{V}{8\pi^3}\frac{\partial f_2}{\partial t} d\mathbf{k}_2 = -\frac{V}{8\pi^3} d\mathbf{k}_2 \langle f_2\rangle_{Av} \times \int_{\mathbf{k}_1'} \int_{\mathbf{k}_1''} \int_{\mathbf{k}_1'''} f_1(\mathbf{k}_1') \frac{d\mathbf{k}_1'}{8\pi^3} V \frac{\hbar k_1'}{m^* V} \times Q(\mathbf{k}_1' \to \mathbf{k}_1'', \mathbf{k}_1''') \left(\frac{V}{8\pi^3}\right)^2 \times d\mathbf{k}_1'' d\mathbf{k}_1'''$$

$$= -\frac{V}{8\pi^3} d\mathbf{k}_2 \langle f_2\rangle_{Av} \int_{\mathbf{k}_1'} f_1(\mathbf{k}_1') d\mathbf{k}_1' \times \frac{V}{8\pi^3} Q_{\text{tot ion}}(\mathbf{k}_1') \frac{\hbar k_1'}{m^* V}. \quad \text{(IV.24)}$$

This represents the loss of electrons due to "internal ionization," it being implied that the contraction of the lower band to a line leaves a small uncertainty in $\mathbf{k}_1$, *viz.*, $d\mathbf{k}_2$.

4. Electron Removal Processes

The physical discussion of these terms has been given previously in Sec. III, Part 4, and there it was concluded that the safest path along which to proceed was to combine the two processes into a single electron removal coefficient, varying inversely with energy, as a fair estimate applying to the situation in actual crystals. We shall then have, for the upper band:

$$\frac{V}{8\pi^3}\left(\frac{\partial f_1}{\partial t}\right)_{\text{rec}} d\mathbf{k}_1 = -\frac{V}{8\pi^3} d\mathbf{k}_1 f_1(\mathbf{k}_1) \times N_2 V (1 - \langle f_2\rangle_{Av}) Q_{\text{rem}} \frac{\hbar k_1}{m^* V}, \quad \text{(IV.25)}$$

and for the lower band:

$$\frac{V}{8\pi^3}\left(\frac{\partial f_2}{\partial t}\right)_{\text{rem}} d\mathbf{k}_2 = \frac{V}{8\pi^3} d\mathbf{k}_2 (1 - \langle f_2\rangle_{Av}) \frac{V}{8\pi^3} \times \int_{\mathbf{k}_1'} f_1(\mathbf{k}_1') Q_{\text{rem}}(\mathbf{k}_1') \frac{\hbar k_1'}{m^* V} d\mathbf{k}_1'. \quad \text{(IV.26)}$$

This completes the discussion of individual terms in the kinetic equation, and we can now collect all the resulting expressions, giving final mathematical form to the problem in question.

V. MATHEMATICAL FORM OF THE FINAL EQUATIONS AND THEIR FORMAL SOLUTION

1. Form of the Equations

The equations applying to the upper band have to be considered in a number of regions, where the functional forms of the collision mechanisms differ in their dependence on the conducting electron energy. In particular, a crystal like diamond with two atoms per unit cell, permits monoenergetic "optical" vibrations of the lattice, thus necessitating the separation of a lower energy region, where the electrons may excite only acoustical modes, from an upper energy region, where both modes are excited, in general.

We shall call "region A" that part of phase space (here, wave number space) between the inner sphere denoting the lower boundary of the upper band, and the sphere whose radius is defined by $\hbar\omega_{\text{opt}} = E(\mathbf{k})$. Region B extends from $\hbar\omega_{\text{opt}}$ up to $\hbar^2\sigma_{\max}^2/8m^*$, where the energy dependence of both the acoustical and the optical lattice collision probabilities changes in form.

Region C extends from $\hbar^2\sigma_{\max}^2/8m^*$ up to E_{ion}, the threshold of ionization, and region D on out to infinity. In the stationary case, one then has upper band equa-

tions from the work of the previous two chapters, in each region, after expanding the field dependent terms in Legendre polynomials.

Upper Band Equations

A: $0 \leq E(\mathbf{k}) \leq \hbar\omega_{\text{opt}}$:

$$\frac{eF}{\hbar}\Big[\mathcal{P}_0(\cos\alpha)\Big\{\frac{1}{k}\frac{d}{dE(\mathbf{k})}(\tfrac{2}{3}E(\mathbf{k})f_{11}(E(\mathbf{k})))\Big\}$$
$$+\mathcal{P}_1(\cos\alpha)\Big\{\frac{df_{10}}{dE(\mathbf{k})}\cdot\frac{\hbar^2 k}{m^*}+\cdots\Big\}+\cdots\Big]$$
$$=a_{10}k^2\frac{df_{10}(E(\mathbf{k}))}{dE(\mathbf{k})}\mathcal{P}_0(\cos\alpha)-a_{11}k^2 f_{11}(E(\mathbf{k}))\mathcal{P}_1(\cos\alpha)$$
$$+N_2\langle f_2\rangle_{\text{Av}}\int_{E(\mathbf{k})+E_{\text{ion}}}^{\infty} f_{10}(E(\mathbf{k}')\cdot Q_{\text{tot ion}}(E(\mathbf{k}'))\frac{\hbar k'}{m^*}$$
$$\times\frac{4\pi k'^2 dk'}{\frac{4\pi}{3}\left(\frac{2m^*}{\hbar^2}\right)^{\frac{3}{2}}(E(\mathbf{k}')-E_{\text{ion}})^{\frac{1}{2}}}$$
$$-N_2\langle 1-f_2\rangle_{\text{Av}}Q_{\text{rec}}(E(\mathbf{k}))\frac{\hbar k}{m^*}\{f_{10}(E(\mathbf{k}))\mathcal{P}_0(\cos\alpha)$$
$$+f_{11}(E(\mathbf{k}))\mathcal{P}_1(\cos\alpha)+\cdots\}. \quad \text{(V.1)}$$

B: $\hbar\omega_{\text{op}} < E(\mathbf{k}) < \hbar^2\sigma_{\max}{}^2/8m^*$:

$$\frac{eF}{\hbar}\Big[\mathcal{P}_0(\cos\alpha)\Big\{\frac{1}{k}\frac{d}{dE(\mathbf{k})}(\tfrac{2}{3}E(\mathbf{k}))f_{11}(E(\mathbf{k}))\Big\}$$
$$+\mathcal{P}_1(\cos\alpha)\Big\{\frac{df_{10}}{dE(\mathbf{k})}\cdot\frac{\hbar^2 k}{m^*}+\cdots\Big\}\Big]$$
$$=2b_{10}k^3\frac{df_{10}}{dE(\mathbf{k})}\mathcal{P}_0(\cos\alpha)$$
$$-(b_{11}k^2+b_{11}{}^*k^2)f_{11}(E(\mathbf{k}))\mathcal{P}_1(\cos\alpha)$$
$$+N_2\langle f_2\rangle_{\text{Av}}\int_{E(\mathbf{k})+E_{\text{ion}}}^{\infty} f_{10}(E(\mathbf{k}'))Q_{\text{tot ion}}(E(\mathbf{k}'))$$
$$\times\frac{\hbar k'}{m^*}\frac{4\pi k'^2 dk'}{\frac{4\pi}{3}\left(\frac{2m^*}{\hbar^2}\right)^{\frac{3}{2}}(E(\mathbf{k}')-E_{\text{ion}})^{\frac{1}{2}}}$$
$$-N_2\langle 1-f_2\rangle_{\text{Av}}Q_{\text{rec}}(E(\mathbf{k}))\frac{\hbar k}{m^*}\{f_{10}(E(\mathbf{k}))\mathcal{P}_0(\cos\alpha)$$
$$+f_{11}(E(\mathbf{k}))\mathcal{P}_1(\cos\alpha)+\cdots\}. \quad \text{(V.2)}$$

C: $\hbar^2\sigma_{\max}{}^2/8m^* < E(\mathbf{k}) < E_{\text{ion}}$:

$$\frac{eF}{\hbar}\Big[\mathcal{P}_0(\cos\alpha)\Big\{\frac{1}{k}\frac{d}{dE(\mathbf{k})}(\tfrac{2}{3}E(\mathbf{k})f_{11}(E(\mathbf{k})))\Big\}$$
$$+\mathcal{P}_1(\cos\alpha)\Big\{\frac{df_{10}(E(\mathbf{k}))}{dE(\mathbf{k})}\cdot\frac{\hbar^2 k}{m^*}+\cdots\Big\}\Big]$$
$$=\frac{2c_{10}}{k}\frac{df_{10}(E(\mathbf{k}))}{dE(\mathbf{k})}\mathcal{P}_0(\cos\alpha)$$
$$-\frac{(c_{1,}+c_{11}{}^*)}{k^2}f_{11}(E(\mathbf{k})\mathcal{P}_1(\cos\alpha)$$
$$+N_2\langle f_2\rangle_{\text{Av}}\int_{E(\mathbf{k})+E_{\text{ion}}}^{\infty} f_{10}(E(\mathbf{k}))Q_{\text{tot ion}}(E(\mathbf{k}'))$$
$$\times\frac{\hbar k'}{m^*}\cdot\frac{4\pi k'^2 dk'}{\frac{4\pi}{3}\left(\frac{2m^*}{\hbar^2}\right)^{\frac{3}{2}}(E(\mathbf{k})-E_{\text{ion}})^{\frac{1}{2}}}$$
$$-N_2\langle 1-f_2\rangle_{\text{Av}}Q_{\text{rec}}(E(\mathbf{k}))\frac{\hbar k}{m^*}\{f_{10}(E(\mathbf{k}))\mathcal{P}_0(\cos\alpha)$$
$$+f_{11}(E(\mathbf{k}))\mathcal{P}_1(\cos\alpha)+\cdots\}. \quad \text{(V.3)}$$

D: $\hbar^2\sigma_{\max}{}^2/8m^* < E(\mathbf{k}) < E_{\text{ion}}$:

$$\frac{eF}{\hbar}\Big[\mathcal{P}_0(\cos\alpha)\Big\{\frac{1}{k}\frac{d}{dE(\mathbf{k})}(\tfrac{2}{3}E(\mathbf{k})f_{11}(E(\mathbf{k})))\Big\}$$
$$+\mathcal{P}_1(\cos\alpha)\Big\{\frac{df_{10}}{dE(\mathbf{k})}\cdot\frac{\hbar^2 k}{m^*}+\cdots\Big\}\Big]$$
$$=2d_{10}\frac{df_{10}(E(\mathbf{k}))}{dE(\mathbf{k})}\mathcal{P}_0(\cos\alpha)$$
$$-\frac{(d_{11}+d_{11}{}^*)}{k^2}f_{11}(E(\mathbf{k}))\mathcal{P}_1(\cos\alpha)$$
$$+N_2\langle f_2\rangle_{\text{Av}}\int_{E(\mathbf{k})+E_{\text{ion}}}^{\infty} f_{10}(E(\mathbf{k}'))Q_{\text{tot ion}}(E(\mathbf{k}))$$
$$\times\frac{\hbar k'}{m^*}\cdot\frac{4\pi k'^2 dk'}{\frac{4\pi}{3}\left(\frac{2m^*}{\hbar^2}\right)^{\frac{3}{2}}(E(\mathbf{k})-E_{\text{ion}})^{\frac{1}{2}}}-N_2\langle 1-f_2\rangle_{\text{Av}}$$
$$\times Q_{\text{rec}}(E(\mathbf{k}))\frac{\hbar k}{m^*}\{f_{10}(E(\mathbf{k}))\mathcal{P}_0(\cos\alpha)$$
$$+f_{11}(E(\mathbf{k}))\mathcal{P}_1(\cos\alpha)+\cdots\}-N_2\langle f_2\rangle_{\text{Av}}Q_{\text{tot ion}}(E(\mathbf{k}))$$
$$\times\frac{\hbar k}{m^*}\{f_{10}(E(\mathbf{k}))\mathcal{P}_0(\cos\alpha)+\cdots\}, \quad \text{(V.4)}$$

where

$$b_{10}=a_{10}=\frac{4}{9\pi}\frac{m^*}{M}\frac{C^2}{\hbar n_0};\quad b_{11}=a_{11}=\frac{16}{45\pi}\frac{m^*}{M}\frac{C^2}{\hbar^2 n_0 v_{ac}};$$

$$b_{11}^*=b_{11}-\frac{5}{3}\frac{v_{ac}}{\omega_{op}};\quad c_{10}=d_{10}=\frac{1}{36\pi}\frac{m^*}{M}\frac{C^2}{\hbar n_0}\sigma_{max}{}^4;$$

$$c_{11}=d_{11}=\frac{1}{90\pi}\frac{m^*}{M}\frac{C^2\sigma_{max}{}^5}{\hbar^2 n_0 v_{ac}};\quad c_{11}^*=d_{11}^*=c_{11}-\frac{5}{6}\frac{v_{ac}\sigma_{max}}{\omega_{op}}.$$

Here the terms in b_{11}^*, c_{11}^*, d_{11}^* represent the contributions to $\partial f_1/\partial t$ due to electron collisions with the optical modes of the lattice vibrations (within the approximation mentioned in footnote 22).

We can also write down the equations of the lower band, or line, as our approximation will consider it. Since we are considering the lower band as closely monoenergetic, we are neglecting its conduction properties, which as noted before should not appreciably affect a breakdown calculation. Thus, the contributions to changes in $\langle f_2(\mathbf{k})\rangle_{Av}$ arising from the field and from the lattice vibrations are neglected in the case of the lower band. A further simplification is achieved by assuming spherical symmetry for the wave number distribution in the lower band, thus leaving the number $\langle f_2\rangle_{Av}$ as the single parameter (aside from the ionization threshold and cross section) characterizing the lower band. The discussion of this paragraph could be revised with ensuing mathematical difficulties, if the opportunity arises to study the contour and electron distribution in the lower band. For the sake of breakdown (and possible pulse conductivity experiments) however, accuracy and theoretical expedients of this sort are not in serious conflict.

Lower Band Equations

$$0=\underset{\text{field}}{0}\quad\underset{\text{lattice vibrations}}{0}\quad-\langle f_2\rangle_{Av}\int f_{10}(E(\mathbf{k}'))\times Q_{\text{tot ion}}(E(\mathbf{k}'))\frac{\hbar k'}{m^*V}d\mathbf{k}'\frac{V}{8\pi^3}+\langle(1-f_2)\rangle_{Av}\times\int f_{10}(E(\mathbf{k}'))Q_{rec}(E(\mathbf{k}'))\frac{\hbar k'}{m^*V}d\mathbf{k}'\frac{V}{8\pi^3},\quad\text{(V.5)}$$

or

$$\langle f_2\rangle_{Av}=\frac{\int f_{10}(E(\mathbf{k}'))Q_{rec}(E(\mathbf{k}'))k'd\mathbf{k}'}{\int f_{10}(E(\mathbf{k}'))[Q_{\text{tot ion}}(E(\mathbf{k}'))+Q_{rec}(E(\mathbf{k}'))]k'd\mathbf{k}'}.$$

Using this last expression, $\langle f_2\rangle_{Av}$ can be formally eliminated from the upper band equation above so that the latter involves explicitly $f_{10}(E(\mathbf{k}))$ and $f_{11}(E(\mathbf{k}))$ only. Such a form however is not necessarily convenient for practical solution to obtain these quantities. In addition, we set down the condition for the conservation of the total number of electrons in the lower and upper bands.

$$\frac{1}{V}\left\{\int_{(1)}\frac{V}{8\pi^3}d\mathbf{k}_1'f_1(\mathbf{k}_1')+\int_{(2)}\frac{V}{8\pi^3}d\mathbf{k}_2'f_2(\mathbf{k}_2')\right\}\equiv N_2=N_1+N_2\langle f_2\rangle_{Av},\quad\text{(V.6)}$$

where N_2 is the number of electrons per cm^3 (with a given spin orientation) in the lower bands of the unexcited (and temporarily assumed perfect) crystal, i.e., near $T=0$, $F=0$. This condition can therefore be written

$$N_1\equiv\int\frac{d\mathbf{k}_1}{8\pi^3}f_1(\mathbf{k}_1)=\int\frac{d\mathbf{k}_1'}{8\pi^3}f_{10}(E(\mathbf{k}_1'))=N_2\langle(1-f_2)\rangle_{Av}$$

$$=N_2\times\frac{\int f_{10}(E(\mathbf{k}'))Q_{\text{tot ion}}(E(\mathbf{k}'))k'd\mathbf{k}'}{\int f_{10}(E(\mathbf{k}'))[Q_{\text{tot ion}}(E(\mathbf{k}'))+Q_{rem}(E(\mathbf{k}'))]k'd\mathbf{k}'}.\quad\text{(V.7)}$$

2. Solution of Equations

The next task is the actual solution of the equations in each region of the upper band. Here, as seen previously, we shall use

$$f_1(\mathbf{k}_1)\approx f_{10}(E(\mathbf{k}_1))\mathcal{P}_0(\cos\alpha)+f_{11}(E(\mathbf{k}_1))\mathcal{P}_1(\cos\alpha)$$

and

$$f_{10}(E(\mathbf{k}_1+\boldsymbol{\sigma}))\approx f_{10}(E(\mathbf{k}))\pm\hbar\omega(\boldsymbol{\sigma})\frac{df_{10}(E(\mathbf{k}))}{dE(\mathbf{k})},\quad\text{(V.8)}$$

$$f_{11}(E(\mathbf{k}_1+\boldsymbol{\sigma}))\approx f_{11}(E(\mathbf{k}_1))$$

in the lattice collision term, although both these approximations (as well as the description of the electron-lattice vibration interaction by means of ordinary phonon emission and absorption as in Sec. IV) are inadequate very near $|\mathbf{k}|\approx 0$. However, since the final quantities of interest are

$$N_1\equiv\int(d\mathbf{k}_1/8\pi^3)f_1(\mathbf{k}_1)=\int(d\mathbf{k}/8\pi^3)f_{10}(E(\mathbf{k})),\quad\text{(V.9)}$$

and

$$\mathbf{J}_1\equiv\int(e\hbar/m^*)\mathbf{k}_1f_1(\mathbf{k}_1)\frac{d\mathbf{k}_1}{8\pi^3}$$

$$=\int(e\hbar/m^*)\mathbf{k}_1f_{11}(E(\mathbf{k}))\mathcal{P}_1(\alpha)d\mathbf{k}/8\pi^3,\quad\text{(V.10)}$$

integrals of f_{10}, f_{11} over wave number space, the error incurred by the failure of the approximations very near $\mathbf{k}_1 \approx 0$ is greatly minimized.

The solution of the equations in (B) and (C) depends through the integral terms on the solution in (D). The only feasible procedure found by the writer to solve these last two equations (for f_{10} and f_{11}) involved the neglect of the integral term over $Q_{\text{tot ion}}$ in region (D), on the physical grounds that the distribution function should fall off with tremendous rapidity in the ionization region (at $E(\mathbf{k}) \geq 2E_{\text{ion}}$) at all fields up to breakdown. This was borne out by numerical calculations which used the solution to the approximate equations (without the integral terms) to test the self-consistency of the procedure. We also neglect in D the terms in $\langle 1-f_2\rangle_{\text{Av}} \cdot Q_{\text{tot}} \cdot f_{10}(E(\mathbf{k}))$ because of the exceeding smallness of $\langle 1-f_2\rangle_{\text{Av}}$. One then obtains, on eliminating f_{11} from these approximate equations, a second-order equation for f_{10} in region D, *viz.*,

$$\frac{d^2 f_{10}}{dE(\mathbf{k})^2} - \frac{df_{10}}{dE(\mathbf{k})}\left\{\frac{d\log m}{dE(\mathbf{k})} - mn\right\} - lmf_{10} = 0. \quad \text{(V.11)}$$

Here one has

$$m = \left[\frac{1}{90\pi}\frac{m^*}{M}\frac{C^2\hbar}{4m^*}\frac{E_{\text{ion}}{}^3\sigma_{\max}{}^5}{n_0 v_{ac}}\left(1+\frac{5}{6}\frac{\sigma_{\max}v_{ac}}{\omega_{op}}\right)\frac{1}{eF}\right]\frac{1}{E(\mathbf{k})^3} + \left[\frac{N_2\langle f_2\rangle_{\text{Av}} Q_{\text{ion}}{}^{(0)} E_{\text{ion}}{}^2}{eF}\right]\frac{(E(\mathbf{k})-E_{\text{ion}})^2}{E(\mathbf{k})^4};$$

$$l = \left[\frac{3N_2\langle f_2\rangle_{\text{Av}} Q_{\text{ion}}{}^{(0)}}{eFE_{\text{ion}}}\right]\frac{(E(\mathbf{k})-E_{\text{ion}})^2}{E(\mathbf{k})^2};$$

$$n = \frac{1}{12\pi}\frac{m^*}{M}\frac{C^2}{n_0}\frac{\sigma_{\max}{}^4}{eFE_{\text{ion}}{}^2}.$$

This equation may be reduced to a form considered by Langer[30] if one makes the following substitutions: let $f_{10} = wv$, where

$$v = \left[\exp\left(-\int_{E_{\text{ion}}}^{E_k} mn dE_k\right)\right](m^{\frac{1}{4}}),$$

and $E(\mathbf{k}) = s \cdot E_{\text{ion}}$. Then one has:

$$(d^2w/ds^2) - \{\lambda(s-1)^2\psi_1(s) + \tau(\lambda, s)\}w = 0, \quad \text{(V.12)}$$

where

$$\lambda = \left(\frac{3}{2}\frac{N_2\langle f_2\rangle_{\text{Av}} Q_{\text{ion}}{}^{(0)} E_{\text{ion}}}{eF}\right)\left[\frac{1}{90\pi}\frac{m^*}{M}\frac{C^2\hbar}{4m^* E_{\text{ion}}} \times \frac{\sigma_{\max}{}^5}{n_0 v_{ac}}\left(1+\frac{5\sigma_{\max}v_{ac}}{6\omega_{op}}\right)\frac{1}{eF}\right]$$

$$\psi_1(s) = \frac{1}{s^5} + \frac{1}{6s^7}\left(\frac{1}{12\pi}\frac{m^*}{M}\frac{C^2\sigma_{\max}{}^4}{n_0 E_{\text{ion}} eF}\right) + \frac{(s-1)^2}{s^6}\left[\frac{2N_2\langle f_2\rangle_{\text{Av}} Q_{\text{ion}}{}^{(0)} E_{\text{ion}}}{\frac{1}{90\pi}\frac{m^*}{M}\frac{C^2\hbar}{2m^* E_{\text{ion}}}\frac{\sigma_{\max}{}^5}{n_0 v_{ac}}\left(1+\frac{5\sigma_{\max}v_{ac}}{6\omega_{op}}\right)}\right] \times\left[1+\frac{1}{3s^3}\left(\frac{1}{12\pi}\frac{m^*}{M}\frac{C^2\sigma_{\max}{}^4}{n_0 E_{\text{ion}} eF}\right)\right],$$

and $\tau(\lambda, s)w$ is a small term which may be regarded as a correction term to the original equation. A necessary condition for Langer's asymptotic approximation is that λ be large, and, under these circumstances, his solution is valid even near the zero of the coefficient at $(s=1;\ E(\mathbf{k}) = E_{\text{ion}})$; that is, his solution is asymptotic in λ and unrestricted for $s \geq 1$. Even, for example, in the neighborhood of breakdown in diamond ($F \leq 1000$ esu) $\lambda \sim 130$,[31] and is inversely proportional to F^2. Hence this method should give good numerical results. The solution, finally, is

$$f_{10}{}^D(E(\mathbf{k})) = C_{1D} m^{\frac{1}{4}} \exp\left(-\int_{E_{\text{ion}}}^{E(\mathbf{k})} mn dE_k\right) \times e^{9\pi i/16}\left[\left(\frac{\Phi}{\varphi}\right)^{\frac{1}{2}}\left(\frac{E(\mathbf{k})}{E_{\text{ion}}}-1\right)^{\frac{1}{4}}\left(\frac{\lambda^{\frac{1}{2}}}{4}\right)^{1/8} e^{i\pi/16}\right] \times H_{1/4}{}^{(1)}\left(\frac{i\lambda^{\frac{1}{2}}\Phi}{8}\right) \quad \text{(V.13)}$$

for $E(\mathbf{k}) \geq E_{\text{ion}}$. Here,

$$\varphi = \left(\frac{E(\mathbf{k})}{E_{\text{ion}}}-1\right)^{\frac{1}{2}}\psi^{\frac{1}{4}}\left(\frac{E(\mathbf{k})}{E_{\text{ion}}}\right)(8)^{\frac{1}{4}},$$

$$\Phi = \frac{1}{E_{\text{ion}}{}^{\frac{1}{2}}}\int_{E_{\text{ion}}}^{E(\mathbf{k})}\frac{\varphi(E(\mathbf{k}))dE(\mathbf{k})}{(E(\mathbf{k})-E_{\text{ion}})^{\frac{1}{2}}},$$

and $H_{1/4}{}^{(1)}$ is the imaginary Hankel function of order $\frac{1}{4}$, chosen because it is the only Bessel function satisfying the equation (in the sense of a solution asymptotic in λ), which falls off when $E(\mathbf{k}) \geq E_{\text{ion}}$ in a way such that $\int f_{10}(E(\mathbf{k}))d\mathbf{k} < \infty$. The constant in front of the square bracket has been adjusted to make the function real; using Heine's integral representation,[32] we can see that the required constant is $e^{i9\pi/16}$, since

$$H_{1/4}{}^{(1)}(ix) = (2/\pi)e^{(-i\pi/2)(1+\frac{1}{2})}\int_0^\infty e^{-x\cosh u}\cosh(u/4)du.$$

[30] R. E. Langer, Trans. Am. Math. Soc. **37**, 397 (1935).

[31] In this estimate we took $Q_{\text{ion}}{}^0 \sim 5\times10^{-16}$ cm^2; $E_{\text{ion}} = 7$ ev, $C = 12.6$ ev, $m^* = m_{\text{free electron}}$, $\sigma_{\max} = 1.73\times10^8$ cm^{-1}; $\omega_{\text{opt}} = 1.83\times10^{14}$ sec^{-1}, the other constants being well known.

[32] W. Magnus and F. Oberhettinger, *Special Functions of Mathematical Physics* (Chelsea Publishing Company, New York, 1949), p. 26.

Thus, one has the multiplicative constant

$$C_{1D}e^{i9\pi/16}e^{+i\pi/16}\cdot e^{-i5\pi/8}=C_{1D},$$

where C_{1D} has to be chosen in accord with continuity across boundaries DC, CB, BA, and with the conservation condition.

If the rigorous integro-differential equation in region D had been solved, we should have had essentially a similar result, since that solution would have to be chosen which gives $\int f_1(\mathbf{k})d\mathbf{k}<\infty$ and each of whose derivatives vanish sufficiently strongly to make higher moments of the distribution function also finite. This requirement would limit the arbitrariness again to a single multiplicative constant. In either situation this constant is essentially determined only by the conservation equation, since the continuity conditions at boundaries AB, BC, CD merely determine the arbitrary constants of the solutions in these lower regions in terms of C_{1D}.

3. Discussion of Solutions

We shall now give some physical discussion of the nature of the solution $f_{10}(E(\mathbf{k}))$ for $E(\mathbf{k})>E_{\text{ion}}$ (region D), obtained upon neglect of the expression

$$N_2\langle f_2\rangle_{\text{Av}}\int_{E(\mathbf{k})+E_{\text{ion}}}^{\infty} f_{10}(E(\mathbf{k}'))Q_{\text{ion}}{}^{(0)}\frac{E_{\text{ion}}(E(\mathbf{k})-E_{\text{ion}})^2}{E(\mathbf{k})^2}$$
$$\times\frac{\hbar k'}{m^*}\cdot\frac{4\pi k'^2dk'}{(4\pi/3)(2m^*/\hbar^2)^{\frac{3}{2}}(E(\mathbf{k}')-E_{\text{ion}})^{\frac{1}{2}}}$$
$$=3N_2f_2Q_{\text{ion}}{}^{(0)}\left(\frac{m^*}{2}\right)^{\frac{3}{2}}E_{\text{ion}}$$
$$\int_{E(\mathbf{k})+E_{\text{ion}}}^{\infty} f_{10}(E(\mathbf{k}))\frac{(E(\mathbf{k})-E_{\text{ion}})^{\frac{1}{2}}}{E(\mathbf{k}')^2}dE(\mathbf{k}'),$$

i.e., upon the assumption that $f_{10}(E(\mathbf{k}))\ll 1$ for $E(\mathbf{k})>2E_{\text{ion}}$ for all $F\lesssim F_{\text{breakdown}}$. As noted above and as discussed further in Sec. VI, this assumption is checked for self-consistency by calculation of $f_{10}(E(\mathbf{k}))$ from formula (V.13). The physical significance of the rapid decrease in the distribution function $[f_{10}(E(\mathbf{k}))]$ with increasing $E(\mathbf{k})(E(\mathbf{k})>E_{\text{ion}})$ is that the mean energy lost by an electron in an "internal ionization" (itself a relatively probable process, compared to lattice collisions) is so large, that tremendous fields (much higher than $F_{\text{breakdown}}$) are required to keep electrons this high in energy, on the average, in a relatively dense medium. It is indeed possible for a small fraction of the total number of electrons to be present just above the ionization threshold at fields $F\approx F_{\text{breakdown}}$. It is interesting and important to note in addition that the behavior of the solution very close to ionization threshold, but above it, (even at fields $F\approx F_{\text{breakdown}}$) is still governed largely by the lattice collision parameters, because the ionization terms have factors $(E(\mathbf{k})-E_{\text{ion}})^p$. This bears out (since the previously mentioned presence of electrons just above threshold is indeed an indication of breakdown) the idea of Fröhlich that only the position in energy of the threshold of ionization and not the actual cross section for the process (as long as it is large) is relevant for the estimate of $F_{\text{breakdown}}$.

The solution f_{10} (and so f_{11}) in region D $(E(\mathbf{k})>E_{\text{ion}})$ being determined, the solutions in the lower regions can be specified by inserting $f_{10}{}^D(E(\mathbf{k}))$ in the equations, solving them, and evaluating the arbitrary constants in terms of C_{1D}, by using the requirements of continuity of the logarithmic derivative at the CD, BC, AB boundaries (appropriate to second-order equations). We drop recombination terms in the lower regions also because $\langle 1-f_2\rangle_{\text{Av}}\approx 0$, even in regions A, B, C except near $\mathbf{k}=0$. Thus, we can expect f_{10}, f_{11} to be quite accurate in form except near $|\mathbf{k}|=0$, where recombination and trapping, in actual crystals, are dominant. Now the single remaining constant, C_{1D}, can be evaluated by the use of the conservation equation for electrons.

Here one point may be emphasized. Since the recombination term has been neglected even in region A for $k\approx 0$, our procedure will not give the correct $f_1(\mathbf{k})$ for very small $|\mathbf{k}|$, and, as a matter of fact, might be expected to give an $f_1(\mathbf{k})$ which for $k\to 0$ has such a strong pole (because of the "piling up" effect of the ionization integral terms degrading electrons from higher k to $k\approx 0$, which effect is not compensated if recombination terms are neglected) that $\int f_1(\mathbf{k})d\mathbf{k}$ required for determination of C_{1D} in terms of N_1 will not exist. However, the approximation made in the representation of the lattice collision terms, owing to the Taylor expansion employed [see Eq. (IV.13)] has the effect of decreasing the order of the pole in $f_1(\mathbf{k})$ as $k\to 0$ so that $\int f_1(\mathbf{k})d\mathbf{k}$ exists and the form for $f_1(\mathbf{k})$ for $k\approx 0$ is still a fair approximation to the rigorous $f_1(\mathbf{k})$ obtained if (a) recombination terms were not neglected and (b) the Taylor expansion were replaced by a more exact mathematical procedure.

Thus, our doubly approximate solution should give a good representation of the form of the solution for $f_1(\mathbf{k})$ (except near $k\approx 0$) if the constant C_{1D} is properly chosen in terms of N_1, the total number of electrons in equilibrium in the upper band. In the next section, by means of an auxiliary physical argument, we formulate the breakdown criterion in terms which do not even require the explicit knowledge of $f_{10}(E(\mathbf{k}))$ in regions A and B, but proceed merely from the assumption of its integrability in those regions. This argument also makes possible taking into account in an approximate way, the effects of traps present in actual crystals, and yields a simpler numerical calculation than the formulation of the present section.

VI. SIMPLIFIED DISCUSSION OF PROBLEM

1.

(a) The distribution function f_{10} in the upper band will be assumed to go to zero for $E(\mathbf{k})$ just greater than

E_{ion}. This is justified by the form of the rigorous solution for f_{10} in region D, as given by Eq. (V.13) of the previous chapter. It turns out that the expression $i\lambda^{\frac{1}{2}}\Phi/8$ which is the argument of the Hankel function, becomes large very rapidly as $E(\mathbf{k})$ increases from E_{ion}. This means that the asymptotic expansion can be used already when $E(\mathbf{k})/E_{\text{ion}}=1.05$; and, when this is done, it is found that $f_{10}^{(D)}$ decreases with extreme rapidity, so that, for example, in diamond at $E(\mathbf{k})/E_{\text{ion}}=1.1$, and $F=300$ esu, $f_{10}^{(D)}$ is already e^{-15} of its value at $E(\mathbf{k})/E_{\text{ion}}=1.$[33]

(b) Another consequence of the very rapid falling-off of $f_{10}^{(D)}$ above ionization threshold is that electrons "ionized into region C" almost all derive from ionizations that take place with the original high energy electron having an $E(\mathbf{k})\approx E_{\text{ion}}+\hbar^2\sigma_{\max}^2/8m^*$. This means that the expression

$$N_2\langle f_2\rangle_{\text{av}}\int_{E(\mathbf{k})+E_{\text{ion}}}^{\infty} f_{10}(E(\mathbf{k}'))Q_{\text{ion}}(E(\mathbf{k}'))\frac{\hbar k'}{m^*}\times\frac{4\pi k'^2dk'}{(4\pi/3)(2m^*/\hbar^2)^{\frac{3}{2}}(E(\mathbf{k})-E_{\text{ion}})^{\frac{1}{2}}}\quad\text{(see Eq. V.3)},$$

which represents the contribution of freshly ionized electrons to the region C of wave number space, is negligible at all fields of interest for breakdown (just as is its companion in region D which has already been omitted above).

2. Final Form of the Equations

The form of the equations in region C for f_{10}, f_{11} is then [see Eq. (V.3)]

$$\frac{1}{(2m^*E(\mathbf{k}))^{\frac{1}{2}}}\frac{d}{dE(\mathbf{k})}\{-\tfrac{2}{3}eFE(\mathbf{k})f_{11}(E(\mathbf{k}))+2c_{10}\hbar f_{10}(E(\mathbf{k}))\}=\frac{\partial f_{10}}{\partial t}=0,\quad\text{(VI.1a)}$$

$$-eF\left(\frac{2E(\mathbf{k})}{m^*}\right)^{\frac{1}{2}}\frac{df_{10}}{dE(\mathbf{k})}=\frac{-(c_{11}+c_{11}^*)}{k^3}f_{11};\qquad\frac{\partial f_{11}}{\partial t}=0.\quad\text{(VI.1b)}$$

If we now multiply Eq. (VI.1) by the differential element of wave number space, we obtain the fundamental result

$$-\int_{\text{region }C}\frac{d}{dE_k}S(E(\mathbf{k}))dE(\mathbf{k})=\frac{\partial}{\partial t}\int f_{10}(E(\mathbf{k}))\frac{d\mathbf{k}}{8\pi^3}=\frac{\partial}{\partial t}\int f_1(\mathbf{k})\frac{d\mathbf{k}}{8\pi^3}=0,\quad\text{(VI.2)}$$

with

$$S(E(\mathbf{k}))\equiv\frac{m^*E_{\text{ion}}}{2\pi^2\hbar^3}\times\left[\tfrac{2}{3}eF\frac{E(\mathbf{k})}{E_{\text{ion}}}f_{11}(E(\mathbf{k}))-\frac{2c_{10}\hbar}{E_{\text{ion}}}f_{10}(E(\mathbf{k}))\right]\quad\text{(VI.3)}$$

a kind of "current in $E(\mathbf{k})$-space." Thus, $S(E(\mathbf{k}))$ is "conserved," being independent of $E(\mathbf{k})$ throughout the region C (including its boundaries). The quantity $S(E(\mathbf{k}))$ which represents the mean number of electrons passing per unit time through the region C (reckoned per unit volume of the crystal) will then be just equal to the mean number of electrons passing per unit time (and per unit volume of the crystal) into the "ionization" region D.

Solving for f_{10} in terms of the constant S, we now obtain

$$f_{10}(E(\mathbf{k}))=-\frac{S}{k_e}+\mathfrak{C}\exp(l_eE_{\text{ion}}^2/2E(\mathbf{k})^2),\quad\text{(VI.4)}$$

$$f_{11}(E(\mathbf{k}))=-\frac{4m^*E(\mathbf{k})^2eF}{\hbar^2(c_{11}+c_{11}^*)}\frac{df_{10}}{dE(\mathbf{k})}=\mathfrak{C}\cdot\left(\frac{4m^*E(\mathbf{k})^2eF}{\hbar^3(c_{11}+c_{11}^*)}\right)\times\frac{\exp(l_eE_{\text{ion}}^2/2E(\mathbf{k})^2)}{E(\mathbf{k})^3}l_eE_{\text{ion}}^2,\quad\text{(VI.5)}$$

where $\mathfrak{C}$ is an integration constant, and

$$l_e=\frac{3}{40}\left(\frac{\hbar\sigma_{\max}}{m^*v_{\text{ac}}}\right)\left(1+\frac{5\sigma_{\max}v_{\text{ac}}}{6\omega_{\text{op}}}\right)\times\left[\frac{1}{18\pi}\cdot\frac{m^*C^2\sigma_{\max}^4}{ME_{\text{ion}}n_0eF}\right]^2;$$

$$k_e=\frac{m^*E_{\text{ion}}}{2\pi^2\hbar^3}\cdot\frac{1}{18\pi}\cdot\frac{m^*}{M}\frac{C^2\sigma_{\max}^4}{E_{\text{ion}}n_0}.\quad\text{(VI.6)}$$

[33] It is unfortunate, but true, that each computation of a single value of the function at a given value of $E(\mathbf{k})/E_{\text{ion}}$ requires several hours work by an efficient computer, largely because Φ is an integral not expressible in terms of elementary functions, and must be numerically calculated with extreme accuracy. This is the case because it appears in the exponent of the function $f_{10}^{(D)}$ when the asymptotic expansion for the latter is used.

At the boundary of regions C, D, we have

$$\left[\frac{d}{dE(\mathbf{k})}\log f_{10}{}^{C}(E(\mathbf{k}))\right]_{E(\mathbf{k})=E_{CD}=E_{\text{ion}}} = \left[\frac{d}{dE(\mathbf{k})}\log f_{10}{}^{D}(E(\mathbf{k}))\right]_{E(\mathbf{k})=E_{CD}=E_{\text{ion}}} = \frac{(-\frac{3}{2}-\frac{1}{2}l_c)}{E_{\text{ion}}}. \quad \text{(VI.7)}$$

The last equality follows from the rigorous solution for $f_{10}{}^{(D)}(E(\mathbf{k}))$ given in the previous section. From Eqs. (VI.4)–(VI.7) we obtain

$$\mathfrak{C}=\frac{3+l_c}{3-l_c}\frac{S}{k_c}\exp\left(-\frac{l_c}{2}\right), \quad \text{(VI.8)}$$

so that $f_{10}{}^{(C)}$, $f_{11}{}^{(C)}$ are uniquely determined via the "current in $E(\mathbf{k})$-space," S, and the boundary value of the logarithmic derivative of $f_{10}{}^{(D)}(E(\mathbf{k}))$, *viz.*,

$$f_{10}{}^{D}(E(\mathbf{k}))=\frac{S}{k_c}\left\{\left(\frac{3+l_c}{3-l_c}\right)\times\exp\left[\frac{l_c}{2}\left(\frac{E_{\text{ion}}{}^2}{E(\mathbf{k})^2}-1\right)\right]-1\right\}, \quad \text{(VI.9)}$$

$$f_{11}(E(\mathbf{k}))=\frac{S}{k_c}\left(\frac{3+l_c}{3-l_c}\right)(l_cE_{\text{ion}}{}^2)\left(\frac{4m^*E(\mathbf{k})^2eF}{\hbar^3(c_{11}+c_{11}{}^*)}\right)\times\frac{\exp\{\frac{1}{2}l_c[(E_{\text{ion}}{}^2/E(\mathbf{k})^2)-1]\}}{E(\mathbf{k})^3}, \quad \text{(VI.10)}$$

which is valid for sufficiently high fields.[34]

We now obtain an expression for S, the mean number density of conduction electrons[35] passing per unit time into the "ionization" region D. This quantity necessarily has, in a stationary state the additional significance of constituting one-half the net mean number density of electrons passing per unit time into regions A, B, of the wave number space (from the "ionization" region D) as a result of the ionizing, energy-degrading collisions (with electrons of the lower band) suffered by conduction electrons immediately upon entering the region D.

Thus, if the number density of electrons in the whole of wave number space of the upper conduction band is to remain constant in time, S electrons per unit time must be "trapped or recombined" in the wave number regions A, B by holes in the lower band, by electron acceptor impurity atoms, etc. Thus, we have

$$S\equiv\alpha(F)\mathfrak{N}_1=\langle\beta\rangle_{Av}\mathfrak{N}_1[N(F)+N_2(1-\bar{f}_2)] = \langle\beta\rangle_{Av}\mathfrak{N}_1(\mathfrak{N}_1+N(0)), \quad \text{(VI.11)}$$

where the total number of electrons in the conduction band deriving from all sources, $\mathfrak{N}_1=N_1+N(F)-N(0)$; $N(F)$ = number of empty trapping centers, i.e., electron acceptor impurity atoms of various kinds at field F; $N(F)\gtrsim N(0)\sim 10^{17}/\text{cm}^3$, since some of the trapping centers will on the average remain ionized at field F,[36] N_1, N_2, $\langle f_2\rangle_{Av}$ as before (i.e., $N_1=N_2(1-\bar{f}_2)_{Av}$, N_2 = number density of lattice atoms); $\alpha(F)=S/\mathfrak{N}_1$ and will be shown below to depend only on the field and the lattice collision parameters, and not on $\mathfrak{N}_1$; and $\langle\beta\rangle_{Av}$ = mean recombination coefficient of the (slow) conduction electrons in region A, $\langle\beta\rangle_{Av}\approx 10^{-8}$ cm^3/sec.

If the temperature is extremely low (strictly if $T=0$) and F is such that $\alpha(F)/\langle\beta\rangle_{Av}<N(0)$, Eq. (VI.11) can be satisfied only for $\mathfrak{N}_1=0$, a mathematical expression of the fact that for these fields the number of available traps is sufficient to swallow any electrons released (e.g., by ionization) into regions A, B. (At higher temperatures, there will, of course, be some electrons present when $F=0$; but a discontinuity will still be present at a critical field almost equal to the one indicated here.) Thus when the field is such that $\alpha(F)/\langle\beta\rangle_{Av}$ exceeds $N(0)$, $\mathfrak{N}_1$ begins to vary proportionately to the rapidly rising $\alpha(F)/\langle\beta\rangle_{Av}$. Thus a reasonable breakdown criterion is

$$\alpha(F)/\langle\beta\rangle_{Av}\approx N(0)\approx 10^{17}\text{ cm}^{-3}$$

or

$$\alpha(F)\approx 10^{17}\langle\beta\rangle_{Av}\text{ sec}^{-1}. \quad \text{(VI.12)}$$

[34] The singularity in $f_{10}(E(\mathbf{k}))$ and $f_{11}(E(\mathbf{k}))$, which occurs as l_c approaches 3 from below (i.e., as F approaches from above the value 750 esu for diamond) arises from the following cause. First of all, we have neglected the small correction term to the Langer approximation for $f_{10}(E(\mathbf{k}))$ in region D. We have neglected $d^2f_{10}/dE(\mathbf{k})^2$, $df_{11}/dE(\mathbf{k})$ in the Taylor expansions (Sec. IV) of $f_{10}(E(\mathbf{k}+\boldsymbol{\sigma}))$, $f_{11}(E(\mathbf{k}+\boldsymbol{\sigma}))$, in terms of $f_{10}(E(\mathbf{k}))$, $f_{11}(E(\mathbf{k}))$. The singularity does not affect the numerical results very appreciably, for $F\approx F_{\text{breakdown}}$, since the exponential dependence is then decisive. Finally, we see from Eqs. (VI.9) and (VI.10) that the expansion of $f_1(\mathbf{k})$ into $\mathcal{P}_0(\alpha)f_{10}(E(\mathbf{k}))+\mathcal{P}_1(\alpha)f_{11}(E(\mathbf{k}))+\cdots$ (Sec. IV) converges properly only if

$$F\gg\frac{1}{6\pi}\frac{m^*}{M}\frac{C^2\sigma_{\max}{}^4}{eE_{\text{ion}}n_0}\frac{1}{(3+l_c)}\sim\frac{1}{54\pi}\frac{m^*}{M}\frac{C^2\sigma_{\max}{}^4}{eE_{\text{ion}}n_0},$$

which again corresponds to sufficiently high fields ($F\gtrsim 500$ esu for diamond). Under those circumstances $f_{11}\ll f_{10}$. If the electron mobility is higher than 900 cm^2 volt sec this condition is correspondingly relaxed.

[35] All the electrons involved in the succeeding discussion are of given spin orientation.

[36] In order to apply the subsequent formulas, some discussion of the properties of crystals must be given. (See a related discussion to the present one, and useful material on ionic crystals, given by Davydov and Shmushkevitch, J. Phys. (U.S.S.R.) **3**, 359–377 (1940). In this paper the current in energy space is used and strong fields are considered, but no attempt is made to find a solution which takes ionization explicitly into account.) Actual crystals seem to show the presence of certain electron "traps" which are only partially filled even at absolute zero. The electrons in these traps can be excited to the conduction band by heating the crystal, and for diamond, use of von Wartenberg's high temperature measurements [see the article by H. von Wartenberg, Physik Z. **13**, 1125 (1912)] gives the number of "electron donors" as of order 10^{18}/cm^3 and the depth in energy below the conduction band as about 0.5 volt. On the other hand, the experiments of McKay [see the paper of K. G. McKay, Phys. Rev. **77**, 816 (1950)] show that there exist ordinarily vacant traps of concentration about 10^{17}/cm^3.

It remains to find the quantity $\alpha(F)=S/\mathfrak{N}_1$. We have

$$\left(\frac{\sqrt{2}(m^*E_{\rm ion})^{\frac{1}{2}}}{2\pi^2\hbar^3}\int_{(E(\mathbf{k}))_{BC}=\hbar^2\sigma_{\max}^2/8m^*}^{(E(\mathbf{k}))_{CD}=E_{\rm ion}} f_{10}(E(\mathbf{k})')(E(\mathbf{k})')^{\frac{1}{2}}\frac{dE(\mathbf{k})'}{E_{\rm ion}^{\frac{1}{2}}}\right)$$

$$=\left(\frac{\mathfrak{N}_1\int_{(E(\mathbf{k}))_{BC}}^{(E(\mathbf{k}))_{CD}} f_{10}(E(\mathbf{k})')E(\mathbf{k})'^{\frac{1}{2}}dE(\mathbf{k})'}{\int_0^{(E(\mathbf{k}))_{BC}} f_{10}(E(\mathbf{k})')E(\mathbf{k})^{\frac{1}{2}}dE(\mathbf{k})'+\int_{(E(\mathbf{k}))_{BC}}^{(E(\mathbf{k}))_{CD}} f_{10}(E(\mathbf{k})')E(\mathbf{k})'^{\frac{1}{2}}dE(\mathbf{k})'}\right)=p\mathfrak{N}_1, \quad \text{(VI.13)}$$

where p is the average fraction of the total number of electrons in region C. Using equations for f_{10}, f_{11} in regions A, B analogous to Eqs. (VI.1) and (VI.2) for f_{10}, f_{11}, and joining the f's and their derivatives continuously at the C, B; B, A boundaries, we have found that $p\gtrsim\frac{1}{10}$ for fields $\gtrsim$1500 esu in diamond. (It is clear that the specification of F and the lattice collision parameters, a_{10}, a_{11}, b_{10}, $\cdots$ gives a unique value of p for a particular insulating crystal.) Substituting Eq. (VI.9) in the left side of (VI.13), we obtain

$$\alpha(F)=\frac{S}{\mathfrak{N}_1}=\frac{1}{18\pi}\frac{m^*}{M}\frac{C^2\sigma_{\max}^4}{n_0E_{\rm ion}}\cdot\frac{1}{(2m^*E_{\rm ion})^{\frac{1}{2}}}\cdot\frac{p}{R}, \quad \text{(VI.14)}$$

where

$$R\equiv\int_{(E(\mathbf{k}))_{BC}}^{(E(\mathbf{k}))_{CD}}\left[\left(\frac{3+l_e}{3-l_e}\right)\exp\left\{\frac{l_e}{2}\left(\frac{E_{\rm ion}^2}{E_{BC}^2}-1\right)\right\}-1\right]\times\frac{E(\mathbf{k})^{\frac{1}{2}}dE(\mathbf{k})}{E_{\rm ion}^{\frac{1}{2}}},$$

and

$$l_e=\frac{3}{40}\left(\frac{\hbar\sigma_{\max}}{m^*v_{\rm ac}}\right)\left(1+\frac{5\sigma_{\max}v_{\rm ac}}{6\omega_{\rm op}}\right)\left(\frac{m^*}{18\pi M}\frac{C^2\sigma_{\max}^4}{E_{\rm ion}n_0eF}\right).$$

The principal dependence on field and lattice parameters lies in the exponent of the integrand of R. In particular, as is also evident on dimensional grounds, we may write

$$F_{\rm br}=F_{\rm crit}\Phi\times\left(\frac{\hbar\omega_{\rm op}}{E_{\rm ion}},\frac{\hbar^2\sigma_{\max}^2}{8m^*E_{\rm ion}},\langle\beta\rangle_{\rm av}N(0)\tau_{\rm latt},\frac{v_{\rm ac}}{v_{\rm ion}}\right), \quad \text{(VI.15)}$$

where

$$F_{\rm crit}=\frac{m^*}{M}\frac{C^2}{e}\left(\frac{m^*}{\hbar^3\omega_{\rm op}}\right)^{\frac{1}{2}};\quad\frac{1}{\tau_{\rm latt}}=\frac{4}{9\pi}\frac{(m^*)^2}{M}\frac{C^2}{\hbar^3n_0}\sigma_{\max};$$

$$v_{\rm ion}=(2E_{\rm ion}/m^*)^{\frac{1}{2}}.$$

In order to give an idea of the relative importance of these parameters, Fig. 1, has been drawn; this figure is based upon a use of the distribution function found in regions A and B, to calculate "p," upon neglect of ionization and recombination effects in those regions. As a result, one may expect that the curves do not have quite the quantitative significance that a more exact distribution function would yield, but the inaccuracy cannot be large, for reasons previously adduced (see Sec. V). No figure to represent the dependence on $v_{\rm ac}/v_{\rm ion}$ has been drawn, since this parameter is certainly small for all actual insulating crystals; and this leads to a negligible dependence on the parameter, as borne out by an examination of our approximate distribution function.

In evaluating the constants required for the numerical estimates (VI.16) (i.e., the C^2, $\omega_{\rm opt}$, $E_{\rm ion}$, etc.), the data of Klick and Maurer[37] may be used. Klick and

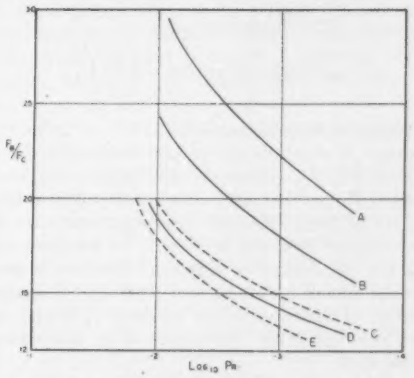

FIG. 1. Breakdown field *vs* probability of removal by trapping (nondimensional units).

Curve	U_{AB}	U_{BC}	
A	0.0081	0.29	$F_c=\frac{m^*}{M}\frac{C^2}{e}\left(\frac{m^*}{\hbar^3\omega_{\rm op}}\right)^{\frac{1}{2}}$
B	0.0121	0.29	$P_B=\langle\beta\rangle_{\rm av}N\left(\frac{F=0}{T=0}\right)\tau_{\rm latt}$
C	0.0173	0.41	$\frac{1}{\tau_{\rm latt}}=\frac{4}{9\pi}\frac{(m^*)^2}{M}\frac{C^2\sigma_{\max}}{\hbar^3n_0}$
D	0.0173	0.29	$u_{AB}=\hbar\omega_{\rm op}/E_{\rm ion}$ $u_{BC}=\hbar^2\sigma_{\max}^2/8m^*E_{\rm ion}$
E	0.0173	0.20	

[37] C. Klick and R. Maurer, Phys. Rev. **81**, 124 (1951). Since these results were obtained, Pearlstein and Sutton, Phys. Rev. **79**, 907 (1950), have used a pulse method to measure μ_{300} in diamond, obtaining a value larger by at least a factor of four. The dis-

Maurer find $\mu_{\text{upper band}}$ in diamond to be 900 (cm/sec)·(cm/volt) at about 300°K. One can use the assumption that Maxwell-Boltzmann statistics prevailed in the measurement (small field) and consequently that the formulas given by Seitz[38] apply. In addition, we assume $m^*=1$ electron mass. Then

$$\mu=\frac{8}{3\pi}\frac{e}{m^*}\frac{\lambda}{\bar{v}},$$

where λ=mean free path at 300°K, $\bar{v}$=mean velocity at 300°K,

$$\mu=\frac{8}{3\pi}\frac{e}{m^*}\left(\frac{2\pi m^*}{k_0T}\right)^{\frac{1}{2}} \times\frac{1}{4}\frac{1}{(4/9\pi)(C^2k_0Tm^{*2}/\hbar^4v_{\text{ac}}^2n_0M)}, \quad \text{(VI.16)}$$

and hence

$$C^2=\tfrac{3}{2}(2\pi)^{\frac{1}{2}}\left[\frac{eMn_0v_{\text{ac}}^2\hbar^4}{(m^*)^{5/2}\mu(k_0T)^{\frac{1}{2}}}\right]=(12.6\text{ ev})^2. \quad \text{(VI.17)}$$

We have used the following numerical values:

$$\rho=3.514\text{ g/cc.}$$

$$v_{\text{ac}}=1.64\times10^6\text{ cm/sec}=\left(\frac{c_{11}}{\rho}\right)^{\frac{1}{2}},$$

in addition to those already quoted.[39]

Further, a word should be said concerning the assumption that 7 ev represents the "internal ionization" potential E_{ion} in diamond. This value is used because the data of Peter[17] show an absorption maximum in a pure diamond specimen at 1700A. It is known, also, from the calculations of Kimball[40] that this is about what one obtains by a theoretical treatment of the band structure of diamond by the methods of Wigner and Seitz, although Seitz[41] has suggested an improvement on this work.

4. Discussion of Results

In an abstract, the author[20] previously gave criteria for breakdown according as the ionization energy of the crystal lay above or below $\hbar^2\sigma_{\max}^2/8m^*$, and also considered "impurity" breakdown. We can see from arguments analogous to those leading to Eq. (VI.12), that such a rise in current (due to ionization of electrons in traps) can take place in such a way as to mask the previously discussed "intrinsic" breakdown, only if both of the following conditions are satisfied: $[N(F)-N(0)]/N(0)\approx1$ for $F\sim F_{\text{intrinsic breakdown}}$, i.e., a large number of full ionizable traps exist without field; and their trap-depth is very small relative to the mean energy of conduction electrons. Since the ordinarily full traps number some 10^{12}/cc and have mean depths of 0.5 volt in diamond, an order of magnitude calculation shows that this crystal, in the pure form ordinarily seen, should not show "impurity" breakdown. Class *C* crystals, in the notation of the abstract,[20] would include the last mentioned group, whereas almost all other crystals would be included under class *B*, for which we now have a definite breakdown criterion [Eq. (VI.12); (14)] rather than a lower limit.

It remains to compare this discussion with the results of Fröhlich and von Hippel, who make semiquantitative use of the idea that energy loss to the lattice vibrations controls breakdown. Although these authors applied their methods only to polar crystals, it is possible to use the criteria given by them also for diamond and other nonpolar crystals. Both use formulas for average gain of energy from the field and loss of energy to the lattice which are derived by use of the transition probabilities for lattice collisions, but which are not averaged over the distribution function, as a more accurate estimate of these quantities demands. In order to apply the formulas of von Hippel and Fröhlich, one calculates the expected rate of energy gain and loss for a single electron in the crystal, using for the energy loss formula

$$(dE/dt)_{\text{loss}}=\textstyle\sum_i W_{\text{coll}}(\mathbf{k}\rightarrow\mathbf{k}'+\boldsymbol{\sigma})\hbar\omega_i, \quad \text{(VI.18)}$$

where the i runs over all types of lattice vibrations. The energy gain formula is derived from a rough statistical treatment of a familiar type, obtaining

$$(dE/dt)_{\text{gain}}=e^2F^2\tau/m^*. \quad \text{(VI.19)}$$

Here τ is taken as the "momentum transport" collision time, $\sum_i W_{\text{coll}}(\overline{\Delta k_z}/k)$; where $\overline{\Delta k_z}/k$ is the fractional loss of momentum in a collision, averaged over angle. Performing these calculations, one obtains

$$\left(\frac{dE}{dt}\right)_{\text{loss}}=\frac{1}{18\pi}\frac{m^*}{M}\frac{C^2}{\hbar^2N_0}\frac{\sigma_{\max}^4}{k} =\frac{2c_{10}}{k}\ \begin{matrix}\text{(the factor 2}\\ \text{because of the}\\ \text{optical vibrations)}\end{matrix} \quad \text{(VI.20)}\cdots\text{(A)}$$

and

$$\left(\frac{dE}{dt}\right)_{\text{gain}}=\frac{e^2F^2}{m^*}\cdot90\pi\frac{M}{m^*}\frac{\hbar^2n_0k^2}{C^2\sigma_{\max}^5} \times\frac{1}{\left(\dfrac{1}{v_{\text{ac}}}+\dfrac{5\sigma_{\max}}{6\omega_{\text{op}}}\right)}. \quad \text{(VI.20)}\cdots\text{(B)}$$

crepancy may be due to experimental difficulties in the measurements, and also in part to a difficulty in theoretical interpretation (private communication from Maurer and Pearlstein).

[38] F. Seitz, Phys. Rev. **73**, 557 (1948), and reference 16.

[39] Bhagavantam and Bhimasenacar, Nature **154** (1944). (c_{11}=cubic elasticity coefficient)=9.4×10^{12} dynes/cm^2.

[40] G. E. Kimball, J. Chem. Phys. **3**, 560 (1935).

[41] F. Seitz, Phys. Rev. **73**, 561 (1948), and reference 16.

Fröhlich argues that when B first exceeds A at the ionization energy, breakdown will take place, so that

$$(dE/dt)_{\text{gain}}=(dE/dt)_{\text{loss}} \quad \text{at} \quad E=E_{\text{ion}}, \quad \text{(VI.21)}$$

gives the required criterion. Von Hippel and Callen stipulate that all electrons must have sufficient energy to overcome the "frictional loss" to the lattice vibrations, and hence that

$$(dE/dt)_{\text{gain}}=(dE/dt)_{\text{loss max}}$$

even at the maximum rate of energy loss, which occurs at $E=E_{BC}=\hbar^2\sigma_m^2/8m^*$ (where the change in wave number of an electron in a collision reaches its maximum, and in our (the usual) approximation, the energy dependence of the lattice collisions changes its form).

To compare these two conceptions with the present treatment (Fig. 2) is shown. For diamond, the criteria give, assuming $\mu_{300^\circ}=900$ cm/sec/volt/cm), $F_{\text{von Hippel}}=12\times10^5$ volts/cm, $F_{\text{Fröhlich}}=4.8\times10^5$ volts/cm, and $F_{\text{Kinetic}}=2.7\times10^5$ volts/cm (if $\langle\beta\rangle_{Av}(N)0)\sim10^9$ sec^{-1}). If one assumes a smaller ionization energy than 7 ev for diamond, the breakdown field remains unchanged according to the von Hippel criterion, increases according to the formulation of Fröhlich, and (in the region where the mathematical approximations are best) decreases according to the kinetic-statistical treatment of the present paper. It is rather implausible, as Fröhlich's theory would predict, that breakdown should require a higher field when a crystal differs from another only by having a smaller internal ionization energy. This may provide a test of the present theory, if two crystals with similar lattice parameters, but distinctly different internal ionization energies, can be tested. Furthermore, the dependence of the breakdown strength on temperature should not be noticeable when $T\ll T_{\text{Debye}}\equiv\Theta$, as in diamond up to room temperatures.

It is appropriate at this point to stress the contrast between the basic arguments of prior theories and those of the present one. None of the previous proposals determine the breakdown in terms of a steady-state criterion; all conceive of the phenomenon as a sign that no steady-state, short of a plasma, is possible. The present approach is to think of the attainment of the critical field strength in terms of a sudden but definite increase in the number of conduction electrons (strictly, in the slope of the number *versus* field curve over an immeasurably small interval), which can theoretically maintain itself in the steady state. The only reason that we instead observe "breakdown" according to the present theory is that the steady-state current which would supposedly flow at breakdown field cannot be maintained with any practically conceivable experimental apparatus, although pulse measurements may be possible. Even near breakdown, moreover, there will be a sufficient number of electrons present in the conduction band so that those time-dependent statistical fluctuations which are not included in the steady-state solution should only cause noticeable effects if observations can

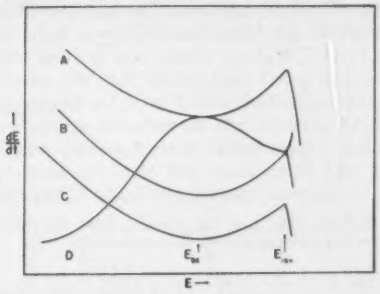

FIG. 2. Energy gain and loss rates for an electron in a nonpolar crystal. *A*. Energy gain curve for breakdown field according to von Hippel's criterion; *B*. Energy gain curve for breakdown field according to Fröhlich's criterion; *C*. Energy gain curve for breakdown field according to present theory; *D*. Loss curve (independent of field); $E_{BC}=\hbar^2/8m\lambda_{\min}$, $\lambda_{\min}$=shortest lattice vibration wavelength.

be made within a time after application of the field $=t\ll t_{\text{trapping}}$. It is conceivable that such measurements could be made, although this may not be experimentally simple. Otherwise, such time dependent effects should cause no more "spread" in the observations of breakdown field than similar fluctuations which would characterize thermodynamic changes of phase involving a number of atoms similar to the number of electrons in our problem. In this sense, the present theory conceives of the breakdown field as a sort of "melting point," although, of course, no cooperative phenomena are involved. Extra electrons introduced by other means (photoeffect or effect of high energy particles) should not affect the breakdown field.

It will be noticed from Fig. 2, and the previous calculations that breakdown will take place at a field lower than the value given by either of the two semiquantitative arguments of Fröhlich and von Hippel. That this is true can be conceived of as being a consequence of the constant "fluctuations" of electrons up to higher energy from their mean energy (which will be of the order of a fraction of a volt) and which are automatically described by the kinetic-statistical treatment using the steady-state distribution functions $f_1(\mathbf{k}_1)$. This is in qualitative agreement with the argument of Seitz that the breakdown field is less than would be given by a straightforward application of the von Hippel criterion, although the fluctuations here treated are different in nature.

The most interesting single result, as demonstrated in Fig. 1, is the relative insensitivity of the breakdown field to changes in $\tilde{\beta}N(0)$, the trapping probability. This, together with the previous discussion of the effect of full traps, makes clear why it is that one can speak, in an approximate way, of the breakdown field as a crystal "constant."

It is, of course, possible to give the theory for higher temperatures but the method is completely analogous,

and this will not be done here. The principal difference is to multiply the breakdown field by a factor of the form $[1+(k_0T/\hbar\langle\omega\rangle_{Av})]$, where $\langle\omega\rangle_{Av}$ is a less strongly varying function of temperature than the numerator. At higher temperatures still ($T>\Theta$), the thermal release of trapped electrons, and the reduction in $\langle\beta\rangle_{Av}$ because of the higher mean energy of electrons may combine to reverse this dependence, and give "impurity breakdown," as has been observed previously.[42] Polar crystals may also be treated, and results will be tabulated in a future publication.

The writer wishes to acknowledge the advice and help of Professor Henry Primakoff, who suggested studying dielectric breakdown in nonpolar crystals, and that of Professor A. L. Hughes in discussions of experimental work. I should like to express my thanks to Dorothy Heller, who performed necessary computations, to Beatrice Broomall for typing assistance, and to the Atomic Energy Commission for a predoctoral fellowship, during the term of which the work was completed.

[42] H. Fröhlich, Proc. Roy. Soc. (London) **A188**, 521 (1947), and references to experimental work there contained.

PHYSICAL REVIEW VOLUME 84, NUMBER 6 DECEMBER 15, 1951

The Reaction $Mn^{55}(p, n)Fe^{55}$

J. J. G. McCUE AND W. M. PRESTON
*Laboratory for Nuclear Science and Engineering, Massachusetts Institute of Technology, Cambridge, Massachusetts**

(Received August 9, 1951)

The neutron spectrum from the reaction $Mn^{55}(p, n)Fe^{55}$ has been examined from the threshold to a proton bombarding energy of 2.85 Mev. The reaction threshold was found to be 1.020±0.010 Mev. Many resonances were found in the neutron yield; these correspond to excited states of Fe^{56}. A limited region was studied with a resolution width of about 2 kev, and an upper limit of 4.5 kev was found for the average observed level spacing.

I. INTRODUCTION

THE yield of neutrons from a (p, n) reaction on a target nucleus ${}_ZX^A$, as a function of proton energy, will show maxima corresponding to excited states of the compound nucleus ${}_{(Z+1)}X^{(A+1)}$ in the range of excitation above the neutron binding energy. This same range may be investigated by measuring the total neutron cross section, as a function of neutron energy. In the latter case, the compound nucleus is ${}_ZX^{(A+1)}$. The nature of the experimental results depends very much on the energy spread, Δ, in the proton (or neutron) beam owing to poor voltage control in the accelerator, finite target thickness, or other causes.

TABLE I. Previously reported work on (p, n) yields.

Target isotope	Proton energy range (Mev)	Resonances reported	Resolution	Reference
T^3	1.02–2.8	0	good	a
Li^7	1.88–3.6	1	good	b
Be^9	2.06–4.0	1	good	c
B^{11}	3.01–4(?)	0	good	c
C^{13}	3.24–3.96	1	good	d
C^{14}	1.00–2.6	9	good	e
O^{18}	2.59–3.70	7	good?	c
K^{41}	1.25–3.50	8	poor?	c
Sc^{45}	2.9 –3.7	9	poor	f
V^{51}	1.5 –3.8	22	poor	f

[a] Jarvis, Hemmendinger, Argo, and Taschek, Phys. Rev. **79**, 929 (1950).
[b] R. Taschek and A. Hemmendinger, Phys. Rev. **74**, 373 (1948). Hanson, Taschek, and Williams, Revs. Modern Phys. **21**, 635 (1949).
[c] Richards, Smith, and Browne, Phys. Rev. **80**, 524 (1950).
[d] Adamson, Buechner, Preston, Goodman, and Van Patter, Phys. Rev. **80**, 985 (1950).
[e] Roseborough, McCue, Preston, and Goodman, Phys. Rev. **83**, 1133 (1951).
[f] Baker, Howell, Goodman, and Preston, Phys. Rev. **81**, 48 (1951). Recent unpublished work in this laboratory (W. A. Schoenfeld and R. W. Duborg) on the reaction $Sc^{45}(p, n)$ shows at least 31 resonances between 2.91 and 3.11 Mev.

* This work was jointly supported by the ONR and the Bureau of Ships.

If $\Delta>D$, where D is the average level spacing at a given excitation energy, the resolution is "poor." The resulting information is an average of the effects of a usually unknown number of neighboring resonances, and it is therefore difficult to interpret. We may define "intermediate resolution" as the experimental situation in which $\Gamma<\Delta<D$, where Γ is the natural resonance width. In this case it becomes possible to estimate the level spacing, D, but not the amplitudes or widths of resonances, which are required before spin assignments can be made. Finally, if $\Delta<\Gamma$, the resolution is "good" and a detailed comparison can be made between experiment and the predictions of the resonance theory of nuclear reactions.

The level width Γ increases and the spacing D decreases with excitation energy, so that eventually resonances overlap. The meager information now available indicates that at least for light and intermediate weight nuclei, Γ remains less than D for the order of one million electron volts above the neutron binding energy. Both Γ and D decrease (in general) with increasing atomic weight A, so that even for $A=50$ the best practical resolution of electrostatic generators at the present time can barely be considered "good." Improvement in resolution is limited largely by lack of intensity, owing to the low efficiency of fast neutron

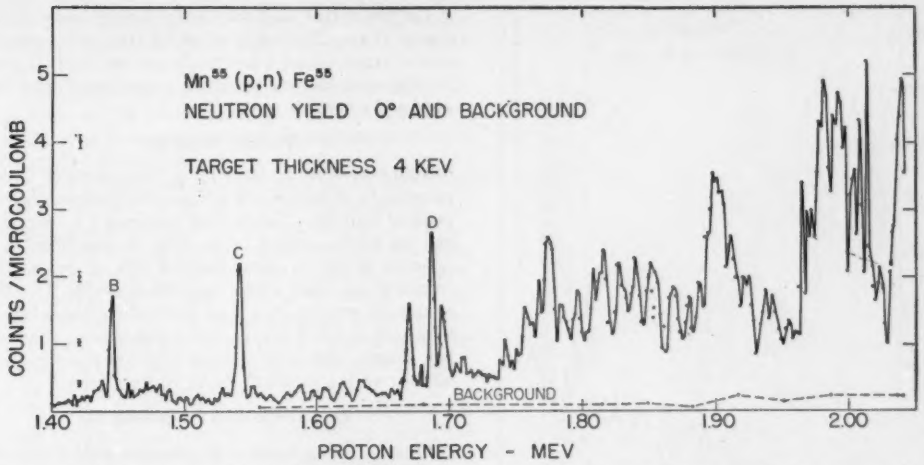

FIG. 1. Neutron yield from $Mn^{55}(p,n)Fe^{55}$; target thickness about 4 kev. Each experimental point represents 500 microcoulombs. The rms errors are shown at the left. The lower curve represents the background.

detectors. In this respect, study of (p,n) reaction yields has some advantage over total cross-section measurements.[1]

A survey of total cross-section measurements is given by Adair.[2] Among the intermediate weight nuclei, only sulfur has been studied with really good resolution. Table I lists recent work on the (p,n) reaction; the estimates of the degree of resolution are our own. It is doubtful that individual levels were resolved in the case of K^{41} and certain that they were not with Sc^{45} and V^{51}. We have selected Mn^{55} for the work described in the present paper because it occurs naturally as a single isotope, it has a low (p,n) threshold, and it may be evaporated readily to form stable targets.

II. EXPERIMENTAL METHOD

The Proton Beam

Protons of energy between 1.0 and 2.8 Mev were obtained from the Rockefeller electrostatic generator.[3] The beam is analyzed by 90-degree deflection in a magnetic field which is stabilized and measured by a proton magnetic moment resonance device; the generator voltage is stabilized by a corona load which is modulated by error signals obtained from that portion of the beam which hits the jaws of the object slit of the analyzer. Currents of 5 to 10 μa can be obtained with object and image slits 1 mm wide, as used throughout the present work. In this case the beam resolution function probably approximates a triangle of width 0.00075 E_p at half-maximum, where E_p is the proton energy.

At energies of 2 Mev, experimental points can readily be taken 0.2 kev apart and reproduced over short intervals of time. All energy measurements are made relative to the $Li^7(p,n)$ threshold, taken as a standard at 1.8822 Mev.[4] Over periods of several days, the voltage calibration has varied over an extreme range of 3 kev. Since the machine was not recalibrated for each run, our energy measurements are in general subject to this error. In addition, for most of the data we used as reference a standard frequency meter which was later found to have systematic errors between calibration points, at the maximum equivalent to 3 kev. For these reasons, we assign an uncertainty of ± 5 kev to most energy measurements, relative to the $Li(p,n)$ threshold. For the threshold measurement and for the run with 2-kev resolution, we used a frequency meter with an accuracy of one part in 10^5.

Targets

The targets were prepared from manganese powder of high purity.[5] The manganese was heated in a tantalum boat and deposited on a clean 10-mil tantalum backing in a standard evaporating unit. The surface oxide on the manganese powder apparently decomposed during evaporation; the targets, when fresh, looked metallic. Interference colors showed that the film was deposited symmetrically about the center of the target.

[1] In the (p,n) reaction we may, if we wish, measure the total neutron yield at all angles. For cross-section measurements, the detected neutrons from the source (e.g., the $Li^7(p,n)$ reaction) must be limited to a very small solid angle in order to obtain good resolution.

[2] R. K. Adair, Revs. Modern Phys. 22, 249 (1950).

[3] W. M. Preston and C. Goodman, Phys. Rev. 82, 316(A) (1951).

[4] Herb, Snowdon, and Sala, Phys. Rev. 75, 246 (1949).

[5] A spectroscopic analysis supplied by the vendors, Johnson, Matthey and Company, London, showed no lines from Al, B, Co, Cr, Cu, Fe, Mo, Ni, Pb, Si, Sn, Ti, V, W, Zn, or Zr. Lines of Mg, Ca, and Na were present, but the (p,n) threshold of Mg, Na, and the abundant isotopes of Ca are higher than the proton energies used in this experiment.

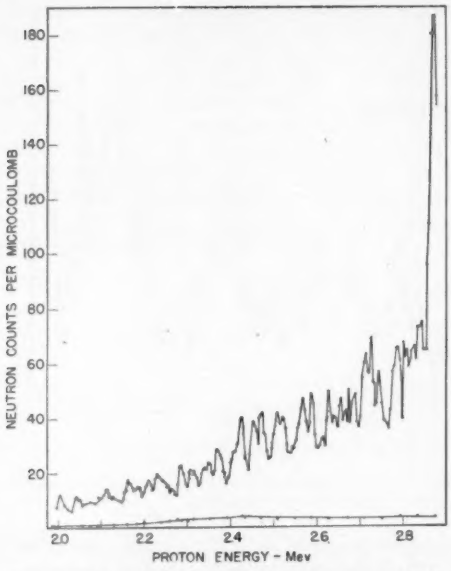

FIG. 2. Neutron yield from $Mn^{55}(p, n)Fe^{55}$; target thickness 15 kev. The rms errors are about 1 percent for all points. The lower curve represents the background.

The tantalum backing was mounted in a conventional rotating target assembly. After prolonged exposure to air, the target film tarnished and thickened. The work reported here was done with targets which had not been exposed to air for more than one hour.

The first target, used for a rough survey, had a thickness of 15 kev. The region below 2.0 Mev was examined with a target about 4 kev thick, and an interval near 1.8 Mev with one <2 kev thick, as estimated from the widths of resonance peaks.

Neutron Detector

Neutrons were detected by a "long counter"[6] surrounded by a cadmium shield to eliminate response to thermal neutrons. The counter tube was 1 in. o.d. and had an active volume 12 in. long. It was filled to a pressure of 55 cm with enriched BF_3. A model 100 amplifier[7] was used with a commercial scaler. The discriminator was set at a level about three times higher than that at which γ-rays were counted from a radium test source. The counter sensitivity was checked periodically with a standard Ra-Be neutron source.

III. EXPERIMENTAL RESULTS

Figure 1 shows a plot of the neutron yield from 1.40 to 2.05 Mev, with a target of about 4 kev stopping power at 1.54 Mev. The most striking features are the isolated peaks, *B* and *C*, that stand out above a background of much smaller resonances. Another strong peak, *D*, is accompanied by large satellites. At a slightly higher energy, the character of the spectrum seems to change; neighboring resonances have more nearly equal amplitudes. The dashed line represents the background counting rate with a carefully cleaned, bare tantalum target. A paraffin shadow cone placed between the latter target and the counter reduced the background by only 20 percent, showing that few, if any, of the neutrons originated in the tantalum; it is likely that

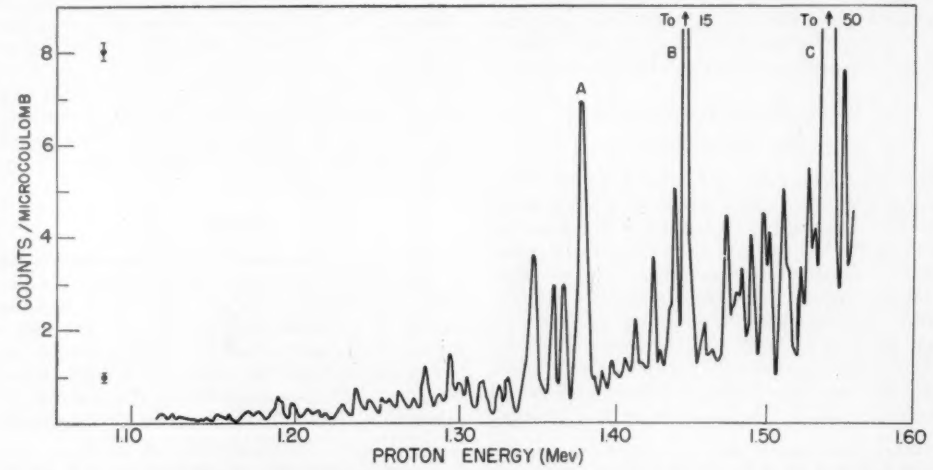

FIG. 3. Neutron yield from $Mn^{55}(p, n)Fe^{55}$; target thickness about 4 kev; long counter close to target and turned broadside to get a high counting rate. The experimental points, not shown, were 1.5 kev apart. The rms errors are shown at the left.

[6] A. O. Hanson and J. L. McKibben, Phys. Rev. **72**, 673 (1947).
[7] W. C. Elmore and M. Sands, *Electronics* (McGraw-Hill Book Company, Inc., New York, 1949).

they came from (d, n) reactions in the analyzing chamber, since deuterium was present in the ion-source hydrogen supply in the normal concentration of 0.016 percent.

Each point in Fig. 1 represents 500 microcoulombs of protons. At the lowest energies, some of the peaks as drawn may be due to statistical fluctuations; above 1.6 Mev, they are certainly nearly all real.

Figure 2 shows the general course of the yield from 2.0 to 2.9 Mev, taken with a 15-kev target. In this region, the levels are so closely spaced that it did not seem worth while to attempt to resolve them. The peaks as drawn probably represent the integrated yield over an interval that includes several resonances. We did not investigate further the surprisingly large peak at 2.86 Mev, which was at the upper limit of operating voltage at that time. We have not been able to assign it to any likely contaminant in the target.

The data for Figs. 1 and 2 were obtained with the long counter 30 cm from the target, on the axis of the beam. Figure 3 shows the yield from 1.10 to 1.55 Mev, but because of the low yield in this region the counter was placed with its axis perpendicular to the beam and its side about 2 cm from the target. The counter then subtended a large angle in the forward direction, but its efficiency can no longer be assumed to be almost independent of energy. The ratio of the height of peak C to that of B is over 3 to 1 in this case, while in Fig. 1 it is nearly unity. This difference may be due to changing efficiency of the counter or to differing angular distributions. Below 1.2 Mev, the yield diminishes gradually towards the background level.

The resonance energies of the peaks A, B, C, and D are 1.375 ± 0.005, 1.443 ± 0.005, 1.539 ± 0.002, and 1.684 ± 0.005 Mev, respectively, relative to a Li(p, n) threshold of 1.8822 Mev. Corrections have been applied for relativity and target thickness.

The threshold for neutron production was measured with a target about 100 kev thick. Figure 4 indicates that the threshold is at 1.020 Mev, to which we assign an uncertainty of ±10 kev. The corresponding Q-value for the $Mn^{55}(p, n)Fe^{55}$ reaction is -1.001 ± 0.010 Mev. This Q-value disagrees with that found by Richards, Smith, and Browne,[8] -1.16 ± 0.01 Mev; it agrees better with the determination of Stelson and Preston, -1.05 ± 0.05 Mev, by a photographic method[9] and -1.006 ± 0.010 Mev by the resonant scatterer method.[10]

Figure 5 shows two runs over the resonance C at 1.539 Mev, taken with the thinnest target used, about two hours apart. The yields at resonance and the experimental half-widths Γ_e are approximately the same, indicating negligible deterioration of the target. The experimental half-widths are 2.0 and 1.8 kev. This means that $(\Gamma^2+\Delta^2)^{\frac{1}{2}}=1.9$ kev, where Γ is the natural resonance half-width and Δ is the resolution width,

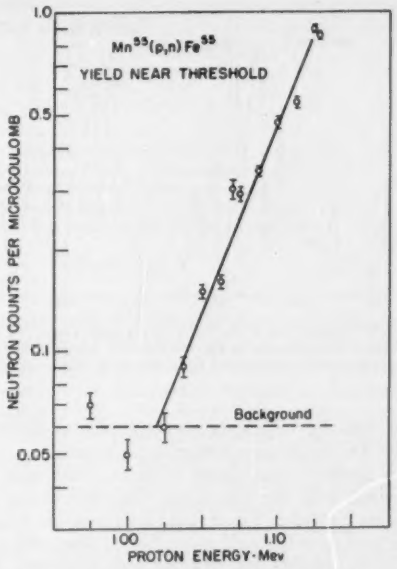

FIG. 4. Neutron yield, near threshold, from a Mn^{55} target >100 kev thick.

including target thickness and spread in the energy of the proton beam. Thus both the target thickness and the natural half-width of the 1.539 resonance are less than 1.9 kev. With thicker targets, as used for Figs. 1, 2, and 3, the target thickness could be taken as equal to the measured half-width of this resonance. The shift of 1.1 kev in the position of the resonance peak may

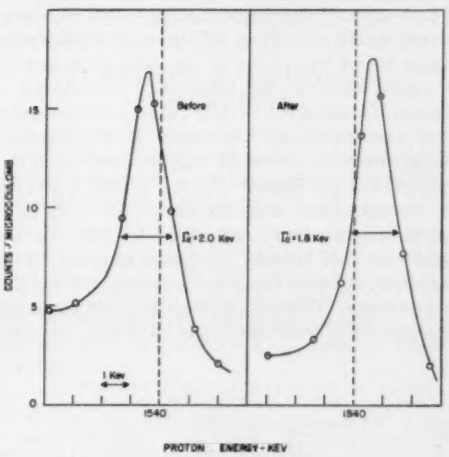

FIG. 5. The resonance at 1.539 Mev, before and after a two-hour run.

[8] Richards, Smith, and Browne, Phys. Rev. **80**, 524 (1950).
[9] P. H. Stelson and W. M. Preston, Phys. Rev. **82**, 655 (1951).
[10] P. H. Stelson and W. M. Preston, Phys. Rev. **83**, 469 (1951).

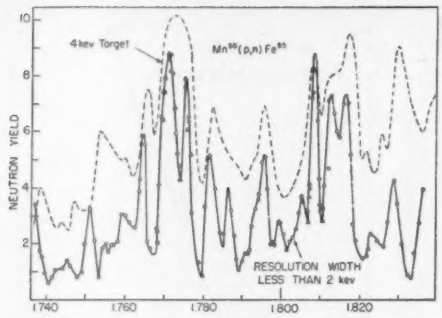

FIG. 6. Comparison of the yield curves with 4-kev and 2-kev resolution. The ordinate scales for the two curves are not the same. The counter subtended different solid angles in the two cases.

have been due to surface contamination of the target during the run or to a change in calibration.

An interval from about 1.740 to 1.835 Mev was examined with the thin target discussed above. The data are plotted in Fig. 6 (solid line) together with the same portion of the yield curve, Fig. 1, taken with 4-kev resolution (dashed line, ordinate scale arbitrary). With the improved resolution, the very broad or unsymmetrical peaks of Fig. 1 split up. The approximately symmetrical character of most of the larger resonances in Fig. 6 and the fact that several of these are appreciably wider than the 1.9-kev limit set on the resolution width indicate that we have approached "good resolution" as defined in the introduction.

It seemed possible that the large observed amplitudes of the resonances B and C, relative to their neighbors, were due to a preferred yield in the forward direction. We accordingly made a run from 1.4 to 2.2 Mev, with a 4-kev target, taking counts simultaneously with long counters on the axis and at 90 degrees. A small Ra-Be neutron source was placed at the point of impact of the proton beam on the target, and this showed a difference in sensitivity of 1.65 between the counters which was applied as a correction to the observed counting rates. A plot of the quantity, yield at 0 degrees/yield at 90 degrees$=Y_0/Y_{90}$, showed a one-to-one correspondence with maxima in the yield at 0 degrees in nearly every case. Near 1.4 Mev, Y_0/Y_{90} varied from 0.35 between resonances to about 1.0 at resonances; at higher energies, the average value of the ratio increased. We are in considerable doubt about the interpretation of these results. In particular, however, the yield at peaks B and C seems to be approximately equal at 0 and 90 degrees.

Stelson and Preston[9] have shown that the first two excited states of Fe^{55} lie 0.42 and 0.94 Mev above the ground state. Transitions to these states can occur at proton bombarding energies above 1.45 ± 0.05 and 1.98 ± 0.05 Mev, respectively. There is no obvious change observed in the character of the spectrum near these energies.

IV. DISCUSSION

In Fig. 6 we can detect about 21 resonances in an energy interval of 95 kev, giving an average level spacing $D=4.5$ kev. The fact that the yield curve taken with the thinnest target at places approaches the background level in this region shows that the resolution width Δ, estimated to be $\lesssim 2$ kev, is considerably less than the spacing of strong levels.[11] However, two peaks will be counted as one if their separation is appreciably less than their observed width, Γ, and peaks of intensity less than 10 percent that of the strongest are generally indistinguishable. Thus it is not easy to define the significance of the above value for D beyond stating that it represents an upper limit for the average spacing between strong levels.

From the reaction equation $Mn^{55}+H^1\rightarrow n+Fe^{55}+Q$, the mass difference $Fe^{55}-Mn^{55}=-Q-(n-H^1)$. Using our value $Q=-1.001\pm0.010$ Mev and $(n-H^1)=0.782\pm0.001$ Mev,[12] the mass difference is 0.219 ± 0.010 Mev. (We have not applied corrections for electronic shielding.)

The binding energy, E_b, of the last neutron in the compound nucleus Fe^{56} may be computed from the following:

$$Fe^{55}+n\rightarrow Fe^{56}+E_b \tag{5a}$$

$$Mn^{55}+n\rightarrow Mn^{55}+7.25 \tag{5b}$$

$$Mn^{56}\rightarrow Fe^{56}+3.63 \tag{5c}$$

$$Fe^{55}-Mn^{55}\rightarrow 0.22. \tag{5d}$$

(The neutron binding energies in Eqs. (5b) and (5c) are taken from Kinsey *et al.*[13] and Mitchell,[14] respectively.) These relations give $E_b=11.10$ Mev, so that our value for the average observed level spacing $D=4.5$ kev refers to a region of total excitation energy of Fe^{56} about $11.10+0.75=11.85$ Mev above the ground state.

[11] Compare the general rise of the yield curve in Fig. 2, where $\Delta=15$ kev.

[13] Tollestrup, Fowler, and Lauritsen, Phys. Rev. **78**, 372 (1950).

[13] Kinsey, Bartholomew, and Walker, Phys. Rev. **78**, 481 (1950).

[14] A. C. G. Mitchell, Revs. Modern Phys. **22**, 36 (1950).

Polarization and Alignment of Nuclei*

A. SIMON, M. E. ROSE, AND J. M. JAUCH†
Oak Ridge National Laboratory, Oak Ridge, Tennessee
(Received September 10, 1951)

Four methods for nuclear polarization and alignment are discussed and compared. In particular, a general theorem regarding the leading term in the expression for nuclear polarization by hfs coupling with external field is obtained. A general method is derived for treating the computation of higher order terms in the expansions of these quantities, as well for use with complicated hamiltonians, and application is made to three cases of interest. It is shown that the higher order terms are very small, in cases of interest, compared to the leading terms.

I. INTRODUCTION

THE first suggestion that nuclei can be polarized experimentally was advanced by Simon[1] in 1939. A thermodynamic argument indicated that the direct coupling of external magnetic fields of 10^6 gauss to the nuclear spins at temperatures of 0.01°K would decrease the entropy of the nuclear spin system by 20 or 30 percent. Since that time, three alternative methods have been proposed. One is the polarization of nuclei by hyperfine coupling, with an external magnetic field polarizing the electrons, which was proposed independently by Rose[2] and Gorter[3] (hereafter referred to as R-G polarization). A second method, due to Pound,[4] utilizes the electric quadrupole splitting in crystals and results in a change in the second moment of the nuclear spins only, i.e., an alignment.

We follow the nomenclature introduced by Bleaney and use the term polarization to indicate a resulting net magnetic moment of the nuclei. Alignment will indicate a condition in which the odd nuclear moments are zero but in which the even moments depart from their values for complete spatial isotropy.

Finally, there is the recent suggestion of Bleaney[5] utilizing the anisotropic hyperfine structure, which sometimes occurs in paramagnetic ions in the solid state, to obtain an alignment. Of the four methods, the requirements with regard to field strength and temperature are most favorable experimentally for the R-G polarization. Next in order of difficulty are the Pound and Bleaney alignments, and finally the direct polarization makes the greatest demands as far as large field strengths and/or low temperatures are concerned.

Nuclear polarization, in conjunction with polarized neutron beams, can be used to determine the spin of the compound state resulting from neutron capture.[6] By simply observing whether the induced activity increases or decreases upon reversal of the neutron polarization, we can determine the compound state angular momentum from the two choices $I\pm\frac{1}{2}$ where I is the spin of the target nucleus. Alternative methods would observe the capture γ-rays or the transmission of the neutron beam. Yet another approach is to observe the deviations from isotropy of the radiations (for example, γ-rays) from polarized (or aligned) nuclei.[7] Here a knowledge of the multipolarity of the emitted radiation is required in order to obtain information on the excited level. This is the only method that can be used for aligned nuclei. Finally Simon[1] has suggested that polarized nuclei can be used in further adiabatic demagnetizations to obtain temperatures of the order of 10^{-6}°K.

It is the purpose of this paper to discuss and compare the various methods of nuclear polarization and alignment with a view to clarifying the underlying assumptions that are made in the predictions of the magnitude of the effects. In Sec. II we will derive expressions for the polarization or alignment resulting from the four methods. In addition a general result regarding the leading (and most important) term in the R-G polarization is derived. Section III will contain a method of calculation which is quite useful for complicated hamiltonians and for higher order terms.

II. LOWEST ORDER POLARIZATION AND ALIGNMENT

The complete expression for the expectation value of an observable, when we are dealing with a statistical ensemble, is obtained by use of the density matrix. This is defined in the usual fashion as

$$\rho_{ij}=\frac{1}{N}\sum_{a=1}^{N} c_{ja}^{*}c_{ia}, \tag{1}$$

where c_{ka} represents the expansion coefficients of a given system of the ensemble, ψ_a, in terms of a basic representation u_k.

$$\psi_a=\sum_k c_{ka}u_k. \tag{2}$$

* This document is based on work performed for the Atomic Energy Project at Oak Ridge.
† Permanent address: Department of Physics, State University of Iowa, Iowa City, Iowa.
[1] F. E. Simon, *Le Magnetisme*, Conférence à Strasbourg, May, 1939.
[2] M. E. Rose, Phys. Rev. **75**, 213 (1949).
[3] C. J. Gorter, Physica **14**, 504 (1948).
[4] R. V. Pound, Phys. Rev. **76**, 1410 (1949).
[5] B. Bleaney, Proc. Phys. Soc. (London) **A64**, 315 (1951); Phil. Mag. **42**, 441 (1951).
[6] M. E. Rose, Phys. Rev. **75**, 213 (1949).
[7] J. A. Spiers, Nature **161**, 807 (1948). As shown by H. A. Tolhoek and S. R. deGroot, Physica **17**, 81 (1951), in the case of $\beta^{\pm}$ emission an anisotropy is observed only if the β-particles are observed with a polarization-sensitive detector. This would require, for example, a scattering of the β particles before they reach the detector.

The sum in (1) is taken over all the systems of the ensemble and the expectation value of an observable O is given by

$$\langle O\rangle = \mathrm{Tr}[O\rho]/\mathrm{Tr}[\rho]. \tag{3}$$

In particular, the density matrix for a system in thermal equilibrium, at a temperature T, is given by[8]

$$\rho = \exp[-\mathcal{H}/kT], \tag{4}$$

where $\mathcal{H}$ is the complete hamiltonian of the system and where we are using a canonical ensemble.

The degree of nuclear polarization of a statistical ensemble having a hamiltonian $\mathcal{H}$ is conveniently defined as

$$f_N = \frac{\mathrm{Tr}\{I_z \exp[-\mathcal{H}/kT]\}}{I\,\mathrm{Tr}\{\exp[-\mathcal{H}/kT]\}}, \tag{5}$$

where I_z is the z-component of the nuclear spin and T is the temperature of the system. The alignment is defined as

$$\Delta = \frac{\mathrm{Tr}\{I_z^2 \exp[-\mathcal{H}/kT]\}}{I^2\,\mathrm{Tr}\{\exp[-\mathcal{H}/kT]\}} - \frac{I+1}{3I}. \tag{6}$$

and represents the excess of the normalized second moment over the isotropic value represented by the second term in (6).

It will be convenient to work in the strong field representation, in which case sums over electronic and nuclear states may be done separately. We will use the notation Tr_E and Tr_N to indicate the partial sums over the electronic or nuclear states, respectively.

Let us consider the various hamiltonians that enter into the four cases of interest. Since all experiments are necessarily done at helium temperatures, or below, the available states of our spin systems are just the lowest degenerate states. In this spin manifold the typical hamiltonian for a paramagnetic salt with complete quenching is given by Abragam and Pryce[9] as

$$\mathcal{H} = \sum_i \{D_i S_i^2 + g_i\beta S_i H_i + A_i S_i I_i + Q_i I_i^2\} - g\beta_N \mathbf{H}\cdot\mathbf{I}. \tag{7}$$

The first term represents the second-order splitting of the electronic spin degeneracy by the combined action of the spin-orbit coupling and other terms. The $Q_i I_i^2$ term describes the nuclear spin splitting due to the interaction of the quadrupole moment of the nucleus with the electrons and the crystalline field. We have chosen coordinates along the principle axis of the crystalline electric field. The usual range of values of the constants are $A\sim 0.1$–10^{-2} cm^{-1}, $D\sim 10^{-1}$–10^{-2} cm^{-1}; $\beta\sim 10^{-4}$ cm^{-1} gauss^{-1}, $Q\sim 10^{-3}$–10^{-4} cm^{-1} and $\beta_N\sim 10^{-7}$ cm^{-1} gauss^{-1}. In addition to these interactions there exist various spin-spin interactions between neighboring ions which we will lump together in the general term $G(S)$ with the understanding that it is a function of the electronic spin and space coordinates only. Direct nucleus-nucleus and nucleus-neighboring ion interactions are small and may be neglected. Finally, it should be noted that the temperatures available at present for practical nuclear polarization work are those resulting from adiabatic demagnetization; *viz.*, of the order of 0.2°K. Thus we see that kT will be large compared with all terms in the hamiltonian except for the term $\beta g_i H_i S_i$ when fields of the order of 10^3 gauss are used, as is customary. Saturation effects are thus of interest only for the direct coupling between electron spin and external field.

(a) Polarization by hfs Coupling (R–G)

We can write the appropriate hamiltonian as

$$\mathcal{H} = g_i\beta S_i H_i + A_i S_i I_i + G'(S), \tag{8}$$

where we have dropped the small quadrupole and direct nuclear coupling terms in Eq. (7) and where we have combined the spin-splitting (D) term and $G(S)$ in the term $G'(S)$. We wish to evaluate the leading term of f_N in an expansion in powers of (A/kT).[10] If we expand the exponential in Eq. (5), we obtain the general term for the numerator

$$[(-1)^n/(kT)^n n!]\,\mathrm{Tr}[I_z\mathcal{H}^n]. \tag{9}$$

This expression has n terms which are linear in A, the prototype term of this set being

$$\sum_i \frac{(-1)^n A_i}{(kT)^n n!}\mathrm{Tr}[I_z\mathcal{H}_e{}^r I_i S_i \mathcal{H}_e{}^{n-r-1}]$$

$$= \frac{I(I+1)(2I+1)A_z(-1)^n}{3(kT)^n n!}\mathrm{Tr}_E[\mathcal{H}_e{}^r S_z \mathcal{H}_e{}^{n-r-1}], \tag{10}$$

since

$$\mathrm{Tr}_N[I_z I_i] = \tfrac{1}{3}I(I+1)(2I+1)\delta_{zi},$$

and where

$$\mathcal{H}_e = \sum_i g_i\beta S_i H_i + G'(S),$$

contains all the purely electronic terms. Making use of the invariance of the trace to cyclic permutations Eq. (10) becomes

$$= \frac{-I(I+1)(2I+1)A_z}{3nkT}\,\frac{(-1)^{n-1}}{(kT)^{n-1}(n-1)!} \times \mathrm{Tr}_E[S_z\mathcal{H}_e{}^{n-1}]. \tag{11}$$

Recombining all our terms we obtain

$$f_N = \frac{-(I+1)A_z}{3kT}\,\frac{\mathrm{Tr}_E\{S_z\exp[-\mathcal{H}_e/kT]\}}{\mathrm{Tr}_E\{\exp[-\mathcal{H}_e/kT]\}}, \tag{12}$$

[8] See R. C. Tolman, *The Principles of Statistical Mechanics* (Oxford University Press, London, 1948), p. 347.

[9] A. Abragam and M. H. L. Pryce, Proc. Roy. Soc. (London) **A205**, 135 (1951).

[10] Since the various terms of our hamiltonian do not commute, we cannot obtain terms of higher order in (A/kT) in closed form by the method of this section. However, a simple result will still hold for the (A/kT) term.

where the result for the denominator follows from noting that the leading term is $(2I+1)\,\mathrm{Tr}_E\{\exp[-3\mathcal{C}_e/kT]\}$ and that the linear term in (A/kT) vanishes. Neglecting the very small effect of the hfs coupling on the degree of electronic polarization we write for the electron polarization

$$f_e=\frac{\mathrm{Tr}_E\{S_z\exp[-3\mathcal{C}_e/kT]\}}{S\,\mathrm{Tr}_E\{\exp[-3\mathcal{C}_e/kT]\}},\tag{13}$$

so that $f_e=1$ corresponds to complete saturation of the electron spins. Therefore,

$$f_N=-[S(I+1)A_z/3kT]f_e,\tag{14}$$

which is the result previously communicated.[2]

The only assumption made in this derivation is that $A/kT\ll 1$. This permits the following general statement: To first order in A/kT the complete effect of all inter-electronic interactions on the R-G polarization is contained in their influence on the electronic susceptibility. Since this quantity is readily measured in an experiment and is usually of order 0.8–0.9, all uncertainties due to these effects can be eliminated. In particular the requirements stated by Bleaney,[5] magnetic dilution and cooling of the salt by contact with a second paramagnetic salt, are seen to be unnecessary. Experiments at this laboratory[11] have amply demonstrated that low temperatures and large electronic polarizations are obtained at quite small magnetic fields. The influence of dipole-dipole coupling on f_e has been thoroughly discussed by Van Vleck.[12]

(b) Alignment by Quadrupole Coupling (Pound)

No external field is necessary here. In fact there is no necessity for the use of a paramagnetic salt. For simplicity let us assume that we have a crystalline field of tetragonal symmetry. Under these circumstances the appropriate hamiltonian is simply

$$3\mathcal{C}=Q[3I_z^2-I(I+1)],\tag{15}$$

where $Q=eq\lambda/[4I(2I-1)]$ and q is the nuclear quadrupole moment, λ is the second derivative of V (the intercrystalline field) at the nucleus, and z is the axis of symmetry of the field. Then,

$$\begin{aligned}\Delta&=-\frac{Q}{I^2kT}\left\{\frac{3}{2I+1}\mathrm{Tr}[I_z^4]-\frac{I^2(I+1)^2}{3}\right\}\\&=-\frac{Q(I+1)}{5IkT}\left[\frac{4}{3}I(I+1)-1\right],\end{aligned}\tag{16}$$

where the result follows immediately from an expansion of the exponential, noting that

$$\mathrm{Tr}_N[I_z^4]=I(I+1)(2I+1)(3I^2+3I-1)/15.$$

The inclusion of a term $A_eS_zI_z$ will not alter this result, since there is no tendency to polarize the electrons without an external field. For fields with less than tetragonal symmetry we must use the general quadrupole term given in Eq. (7). This method requires a single crystal since there is no external field to give a preferred direction in space.

(c) Alignment by Anisotropic hfs (Bleaney)

No external magnetic field is required. If we assume tetragonal symmetry and neglect the quadrupole term in (7), we have

$$3\mathcal{C}=D[S_z^2-S(S+1)/3]+AI_zS_z+B(I_xS_x+I_yS_y).\tag{17}$$

The alignment cannot be calculated as simply as in our previous cases. This is due to the non-commutativity of the purely electronic and hfs terms and to the fact that the leading term is of order $(A/kT)^2$. Instead this case will be treated by the general method of the next section. For the present let us assume that $D=0$. We immediately obtain

$$\Delta=\frac{S(S+1)}{6(kT)^2I^2(2I+1)}\times\left\{\frac{A^2\,\mathrm{Tr}_N[I_z^4]+2B^2\,\mathrm{Tr}_N[I_z^2I_x^2]}{1+\dfrac{S(S+1)I(I+1)}{18(kT)^2}(A^2+2B^2)}\right\}-\tfrac{1}{3}I(I+1),$$

which becomes

$$\Delta=\frac{(A^2-B^2)(I+1)S(S+1)}{90I(kT)^2}\left[\frac{4}{3}I(I+1)-1\right],\tag{18}$$

noting that

$$\mathrm{Tr}[I_z^2I_x^2]=I(I+1)(2I+1)(2I^2+2I+1)/30.$$

This method also requires the use of a single crystal.

(d) Direct Polarization

There is no necessity to use a paramagnetic salt in this case. The only essential term in the hamiltonian is simply $g\beta_N\mathbf{H}\cdot\mathbf{I}$ and the degree of polarization is given exactly by the well-known result

$$f_N=B_I(g\beta_NH/kT),$$

where $B_I(y)$ is the brillouin function. To first order in $1/kT$ this becomes

$$f_N=g\beta_NH(I+1)/3kT,\tag{19}$$

as may be verified by use of Eq. (5).

III. HIGHER ORDER EFFECTS

The direct calculational techniques used up to this point are not very convenient when we wish to obtain the general term of an expansion of the density matrix

[11] J. W. T. Dabbs and L. D. Roberts, Phys. Rev. **83**, 201 (1951).
[12] J. H. Van Vleck, J. Chem. Phys. **5**, 320 (1937).

in terms of only one noncommuting part of the hamiltonian. The straightforward calculation leads to a result which is expressed as an infinite series for each term. This complication can be avoided by the following procedure.

We wish to expand the operator $\rho=\exp[-\mathcal{H}/kT]$, where $\mathcal{H}=\mathcal{H}_0+\mathcal{H}_1$, in powers of $\mathcal{H}_1/kT$. In general $\mathcal{H}_0$ and $\mathcal{H}_1$ do not commute. Let $\tau\equiv-1/kT$. Now if the operator ϕ obeys the "equation of motion,"

$$\mathcal{H}\phi=\partial\phi/\partial\tau; \tag{20}$$

a particular solution is

$$\phi=\exp[\mathcal{H}\tau]=\rho. \tag{21}$$

Let us transform to the "interaction representation"[13] by defining an operator

$$\psi=\exp[-\mathcal{H}_0\tau]\phi, \tag{22}$$

then

$$\partial\psi/\partial\tau=\mathcal{H}_1'(\tau)\psi, \tag{23}$$

where

$$\mathcal{H}_1'(\tau)=\exp[-\mathcal{H}_0\tau]\mathcal{H}_1\exp[\mathcal{H}_0\tau];$$

note that $\psi(0)=\phi(0)=1$ and $\phi=\exp[\mathcal{H}_0\tau]\psi$. Equation (23) can be solved immediately, by an iteration technique, in powers of $\mathcal{H}_1'(\tau)$ as

$$\psi=\sum_{n=0}^{\infty}S_n, \tag{24}$$

where

$$S_n=\int_0^{\tau}\int_0^{\tau_1}\cdots\int_0^{\tau_{n-1}}\mathcal{H}_1'(\tau_1)\cdots\mathcal{H}_1'(\tau_n)d\tau_n\cdots d\tau_1,$$

$$S_0=1.$$

Using Eqs. (21) and (22) we can write the density matrix as

$$\rho=\exp[-\mathcal{H}/kT]=\exp[\mathcal{H}_0\tau]\sum_{n=0}^{\infty}S_n. \tag{25}$$

Thus we have obtained the expansion in powers of $\mathcal{H}_1$. We apply this method to three cases.

(a) Second-Order Term in R–G Polarization

For simplicity we take $\mathcal{H}=\mathcal{H}_0+\mathcal{H}_1$ with

$$\mathcal{H}_0=g\beta\mathbf{S}\cdot\mathbf{H}\equiv\alpha S_z,\quad \mathcal{H}_1=A\mathbf{I}\cdot\mathbf{S}, \tag{26}$$

where we have chosen the z-axis along the direction of the external field and set $\alpha=g\beta H$. We make the usual definitions:

$$S_+=(S_x+iS_y)/\sqrt{2},\quad S_-=(S_x-iS_y)/\sqrt{2},\quad S_0=S_z.$$

Then

$$\mathcal{H}_1'(\tau)=\exp[-\alpha S_0\tau]A(\mathbf{I}\cdot\mathbf{S})\exp[\alpha S_0\tau]$$
$$=AI^m\exp[-\alpha S_0\tau]S_m\exp[\alpha S_0\tau],$$

where m takes on the values $(+,0,-)$, and $Y^m=Y_{-m}$. By use of the commutation rules

$$S_0S_+=S_+(S_0+1),\quad S_0S_-=S_-(S_0-1),$$

we find

$$\mathcal{H}_1'(\tau)=AI^mS_m\exp[-\alpha m\tau]. \tag{27}$$

Then to first order in (A/kT) the density matrix is

$$\rho=\exp[\alpha S_0\tau]+AI^m\exp[\alpha S_0\tau]S_m\int_0^{\tau}\exp[-m\alpha\tau_1]d\tau_1.$$

Taking the trace of the electronic states we have

$$\mathrm{Tr}_E[\rho]=Z-(AI_z/kT)\,\mathrm{Tr}_E\{S_0\exp[\alpha S_0\tau]\},$$

where

$$Z=\mathrm{Tr}_E\{\exp[\alpha S_0\tau]\},$$

and by use of Eq. (5) we obtain the previous result of Eq. (14).

The second order term is

$$\rho_2=A^2I^mI^n\exp[\alpha S_0\tau]S_mS_n$$
$$\times\int_0^{\tau}\exp[-m\alpha\tau_1]\int_0^{\tau_1}\exp[-n\alpha\tau_2]d\tau_2d\tau_1.$$

Only the terms S_+S_-, S_-S_+, and S_0S_0 will contribute to a trace over the electronic states. The integrals are readily evaluated

$$I(+,-)=\int_0^{\tau}\exp[-\alpha\tau_1]\int_0^{\tau_1}\exp[\alpha\tau_2]d\tau_2d\tau_1$$
$$=(\alpha\tau+\exp[-\alpha\tau]-1)/\alpha^2,$$
$$I(-,+)=(-\alpha\tau+\exp[\alpha\tau]-1)/\alpha^2,$$
$$I(0,0)=\tfrac{1}{2}\tau^2.$$

The diagonal elements of S_mS_n are given by use of

$$S_+S_-=\tfrac{1}{2}[\mathbf{S}^2-S_z^2-S_z],$$
$$S_-S_+=\tfrac{1}{2}[\mathbf{S}^2-S_z^2+S_z],$$
$$S_0S_0=S_z^2.$$

Summing over electronic states we have

$$\rho_2=(A/kT)^2Z(a_0+a_1I_z+a_2I_z^2)/\theta^2, \tag{28}$$

where

$$a_0=-\tfrac{1}{2}I(I+1)M_1\theta,$$
$$a_1=M_1[1-(\theta/2)\coth(\theta/2)],$$
$$a_2=\tfrac{1}{2}\theta^2S(S+1)+\tfrac{1}{2}\theta M_1[1+\theta\coth(\theta/2)],$$

and the first moment of the electronic spins is given by

$$M_1\equiv\tfrac{1}{2}[\coth(\theta/2)]-(S+\tfrac{1}{2})\coth(S+\tfrac{1}{2})\theta,$$

noting that

$$Z=[\sinh(S+\tfrac{1}{2})\theta]/\sinh(\theta/2),$$

with

$$\theta=g\beta H/kT.$$

[13] The use of the interaction representation is a convenient and familiar device in quantum electrodynamics. For the definition and use of the interaction representation see, e.g., J. Schwinger, Phys. Rev. 74, 1448 (1948).

These results can be inserted in Eq. (5) to obtain the next correction to f_N, which is

$$\frac{1}{3}\left(\frac{A}{kT}\right)^2(I+1)\frac{a_1}{\theta^2}$$
$$=\frac{1}{3}\left(\frac{A}{kT}\right)^2(I+1)Sf_e\left[\frac{1-(\theta/2)\coth(\theta/2)}{\theta^2}\right]. \quad (29)$$

The function in the brackets has the maximum absolute value $+\frac{1}{12}$ and thus the entire second term represents a correction of less than one percent when $T=0.2°\text{K}$ and $A=0.01\ \text{cm}^{-1}$.

(b) Bleaney Alignment Including the Electronic (D) Term

Here $\mathcal{H}=\mathcal{H}_0+\mathcal{H}_1$ with

$$\mathcal{H}_0=D[S_z^2-\tfrac{1}{3}S(S+1)],$$
$$\mathcal{H}_1=AI_zS_z+B(I_xS_x+I_yS_y).$$

This calculation follows along similar lines. In general,

$$S_m(\tau)=S_m\exp[-Dm(2S_0+m)\tau], \quad (30)$$

and we find that the term in $(1/kT)^2$ (after taking the electronic trace) is

$$\rho_2=\tfrac{1}{2}(A/kT)^2I_z^2M_2Z$$
$$+\tfrac{1}{2}(B/kT)^2[I(I+1)-I_z^2]G(\tau), \quad (31)$$

where

$$G(\tau)=\text{Tr}_E\{\exp[\mathcal{H}_0\tau][S(S+1)-S_z^2-S_z]F(\tau,S_z)\},$$

$$F(\tau,S_z)=\frac{\exp[D(2S_z+1)\tau]-1-D(2S_z+1)\tau}{D^2(2S_z+1)^2\tau^2},$$

$$Z=\text{Tr}_E\{\exp[\mathcal{H}_0\tau]\},$$

and M_2 is the second moment of the electronic spins. We can evaluate the traces by expanding in powers of (D/kT). The zero order term reduces to our previous result of Eq. (18). The linear term in (D/kT) becomes

$$\rho_2'=\frac{D\tau S(S+1)(2S+1)}{60(kT)^2}\left[\frac{4}{3}S(S+1)-1\right]$$
$$\times\{2A^2I_z^2-B^2[I(I+1)-I_z^2]\},$$

and this is easily shown to lead to the following correction term to the Bleaney alignment:

$$\Delta'=\frac{-D[2A^2+B^2]}{900(kT)^2}\frac{(I+1)}{I}S(S+1)$$
$$\times\left[\frac{4}{3}I(I+1)-1\right]\left[\frac{4}{3}S(S+1)-1\right]. \quad (32)$$

At temperatures of 0.1°K this term is of the same order as the leading term which means that the influence of the electronic splitting must be carefully investigated for a given experiment and several terms taken in the expansion. Alternatively, one can choose an ion with $S=\frac{1}{2}$ and then the D term reduces to a constant factor in the hamiltonian and has no effect, as may also be seen by the form of our result.

(c) Spin-Spin Coupling of Two Ions

The general result stated in Sec. II showed that to first order in A/kT the spin-spin coupling between ions only affected f_N by altering the value of f_e. It is of interest to inquire as to the effect of this coupling on the next higher term $(A/kT)^2$. To investigate this we assume the model of a system composed of two ions coupled together by spin-spin coupling. If λ represents the coefficient of the spin-spin coupling, we can expand the $(A/kT)^2$ term in powers of (λ/kT). The zero order term is simply part (a) of this section. The first term of interest is of order $A^2\lambda/(kT)^3$. We take $\mathcal{H}=\mathcal{H}_0+\mathcal{H}_1$ with

$$\mathcal{H}_0=g\beta\mathbf{H}\cdot(\mathbf{S}_1+\mathbf{S}_2)+\lambda\mathbf{S}_1\cdot\mathbf{S}_2,$$
$$\mathcal{H}_1=A\mathbf{I}_1\cdot\mathbf{S}_1+A\mathbf{I}_2\cdot\mathbf{S}_2, \quad (33)$$

where the subscripts refer to a particular ion. Since we have expanded in powers of λ, the new $\mathcal{H}_0$ is just the same as in part (a). Carrying through a similar analysis we find

$$\rho_2'=-[A^2\lambda M_1Z/2(kT)^3](a_0+a_1I_z+a_2I_z^2), \quad (34)$$

where

$$a_0=-[2I(I+1)/\theta^2]\{4M_1[1-(\theta/2)\coth(\theta/2)]$$
$$+M_1\theta[1+\theta\coth(\theta/2)]+S(S+1)\theta^2\},$$

$$a_1=(M_1/\theta^2)[\theta-3\coth^2(\theta/2)+6\coth(\theta/2)]$$
$$+[4S(S+1)/\theta^2][1-(\theta/2)\coth(\theta/2)],$$

$$a_2=-[a_0/I(I+1)]-2S(S+1)\coth(\theta/2)$$
$$-M_1[2S(S+1)-1+3\coth^2(\theta/2)],$$

and M_1, θ, and z are the same as in case (a). The correction term to the R-G polarization is then

$$f_N'=-[A^2\lambda/6(kT)^3]M_1(I+1)a_1$$
$$=-\tfrac{1}{6}(A/kT)^2(\lambda/kT)S(I+1)f_ea_1. \quad (35)$$

The term a_1 is well-behaved and has a maximum absolute value of about $+S(S+1)/3$. Thus this term is still small compared to the linear term in A/kT for $A\sim0.01\ \text{cm}^{-1}$, $T\sim0.2\ °\text{K}$, $\lambda/kT\sim0.1$.

These three cases illustrate the wide applicability of the method.

Coherent Neutron-Proton Scattering by Liquid Mirror Reflection

M. T. BURGY AND G. R. RINGO, *Argonne National Laboratory, Chicago, Illinois*
AND
D. J. HUGHES, *Brookhaven National Laboratory, Upton, Long Island, New York*
(Received August 30, 1951)

A measurement of the coherent neutron-proton scattering amplitude, utilizing total reflection of slow neutrons from a liquid hydrocarbon, was first reported in 1950. As the result $(-3.75\pm0.03)\times10^{-13}$ cm) was significantly different from existing values, the measurements have been continued with a series of liquids in order to investigate systematic errors and to improve the accuracy. Final measurements have now been made utilizing a series of carefully purified hydrocarbon liquids, and a method in which no measurement of neutron wavelength is necessary. The ratio of the amplitude of hydrogen to that of carbon has been determined to 0.3 percent and the final value of the hydrogen amplitude, including the error (0.5 percent) in the carbon amplitude, is $(-3.78\pm0.02)\times10^{-13}$ cm (standard error).

I. INTRODUCTION

THE coherent neutron-proton scattering amplitude is one of the quantities which must be accurately known to fix the constants of low energy neutron-proton interactions. An accurate knowledge of the neutron-proton interactions allows a comparison with the corresponding proton-proton interactions, and this comparison in turn leads to important conclusions concerning charge dependence of nuclear forces. For some years the singlet $n+p$ force range was not determined with sufficient accuracy for comparison with the precisely measured singlet $p-p$ force range. An accurate comparison of $n-p$ and $p-p$ singlet ranges was of fundamental importance to nuclear theory, for inequality of these ranges would imply charge dependence of nuclear forces. In 1948 the $n-p$ singlet range, although of low accuracy, seemed to imply charge dependence.[1] Blatt and Jackson,[2] and Bethe,[3] in their reviews of the low energy scattering data, showed that, of the parameters that fix the singlet range, the one most in need of improved accuracy was the coherent $n-p$ scattering amplitude.

The coherent $n-p$ amplitude is difficult to measure, of course, because it constitutes only about 2 barns of a total bound atom cross section of 80 barns, the remainder representing spin-dependent incoherent scattering. The first measurements of the coherent $n-p$ amplitude were made by a study of interference effects in scattering of slow neutrons from ortho- and para-hydrogen.[4] These measurements showed that the singlet state of the deuteron was virtual, but the value for the coherent amplitude combined with other scattering data implied an approximately zero singlet $n-p$ range. More accurate ortho-para measurements were made in 1947,[5] and these resulted in a coherent amplitude of $(-3.95\pm0.12)\times10^{-13}$ cm. The statistical accuracy of the measurements was reasonably high, but there was a strong possibility of systematic error resulting from the presence of ortho contamination in the para-hydrogen. Because of the high cross section of the ortho-hydrogen relative to that of the para, a small amount of contamination would raise the observed amplitude appreciably. About the same time as the improved ortho-para measurements, the coherent amplitude was determined by Shull *et al.*[6] by the Bragg scattering of slow neutrons from crystals containing hydrogen. This diffraction method is quite straightforward, but suffers from the necessity of a correction for the reduction in observed coherent scattering by thermal vibrations of the crystal (Debye-Waller factor). The result of the crystal measurement was $(-3.96\pm0.20)\times10^{-13}$ cm in agreement with the ortho-para value. It was this value of 3.95 that was used by Blatt[1] in his 1948 calculation of the triplet and singlet force ranges. Blatt concluded that "this result (singlet range) is in direct contradiction to the commonly used hypothesis of the charge-independence of nuclear forces in the singlet state." It was clear that an accurate measurement of the coherent scattering was needed, especially in view of the possible systematic errors in the existing measurements.

II. FIRST EXPERIMENT

When the need for another measurement of the coherent scattering became clear, a repetition of the ortho-para experiment was considered at the Argonne National Laboratory. High intensities of velocity selected thermal neutrons were available, and it was certain that the actual cross-section measurements could be accurately made. It was clear, however, that the primary uncertainty in the experiment would not arise from statistical inaccuracy, but from the presence of ortho-hydrogen, and that there was no simple way of determining the ortho-contamination in the para-hydrogen. About the same time at Argonne, Hughes

[1] J. M. Blatt, Phys. Rev. **74**, 92 (1948).
[2] J. M. Blatt and J. D. Jackson, Phys. Rev. **76**, 18 (1949).
[3] H. A. Bethe, Phys. Rev. **76**, 38 (1949).
[4] Halpern, Estermann, Simpson, and Stern, Phys. Rev. **52**, 142 (1937); Brickwedde, Dunning, Hoge, and Manley, Phys. Rev. **54**, 266 (1938); L. W. Alvarez and K. S. Pitzer, Phys. Rev. **58**, 1003 (1940).
[5] Sutton, Hall, Anderson, Bridge, DeWire, Lavatelli, Long, Snyder, and Williams, Phys. Rev. **72**, 1147 (1947).
[6] Shull, Wollan, Morton, and Davidson, Phys. Rev. **73**, 842 (1948).

and Burgy[7] had shown in a series of mirror experiments that the critical angle for total reflection is related to the coherent scattering in an unambiguous way. For instance, the critical angle for an unmagnetized iron mirror is unaffected by magnetic scattering even though the iron is composed by domains (about 10^{-3} cm in extent) that are completely magnetized. The critical angle is determined by the average coherent scattering amplitude, and the magnetic amplitude, when averaged over the surface of the mirror, becomes zero, leaving only the nuclear amplitude. Because of this averaging property of a mirror, the critical angle could be measured for a mixture of substances (liquid, solid, or gas) and the coherent amplitude obtained would be an accurate average of the amplitudes of the constituents, regardless of their molecular form or crystalline state. The coherent amplitude obtained with a mirror, furthermore, is not affected by temperature vibration of the material, hence there is no Debye-Waller correction to be made, as in the diffraction method. The essential reason for the disappearance of the Debye-Waller correction is that the index of refraction and the critical angle are determined by the scattering in the forward direction.[8]

It was suggested by Hamermesh and Wattenberg[9] that the advantages of the mirror technique would be of great value for the hydrogen scattering, in which the coherent scattering is so much larger than the coherent. Reflection of neutrons from a hydrogen mirror would give the coherent amplitude directly with no interference from the incoherent scattering. However, the required accuracy in the hydrogen amplitude (about 1 percent) could not be obtained by a direct measurement of reflection from hydrogen. Further difficulty would be encountered because the negative scattering amplitude would necessitate internal reflection and a consequent serious loss in intensity. Some months later, however, a method was devised that would overcome the difficulties of reflection from hydrogen itself. The method consists of over-balancing the hydrogen amplitude slightly by adding carbon which has a positive, accurately known amplitude. External reflection is then used for the mixture and, as only the unbalanced amplitude is measured, the required accuracy is greatly reduced.

The results of the first measurements with the balancing method were reported in a Letter to the Editor,[10] and the details will not be repeated here. Neutrons were reflected from a liquid, triethylbenzene, and the limiting wavelength reflected was measured by transmission through gold and by reflection at a beryllium error. The amplitude of the liquid is then given by

$$\theta=\lambda(N\Delta a/\pi)^{\frac{1}{2}}, \qquad (1)$$

where θ is the incident angle, λ the limiting wavelength reflected, and N the number of carbon atoms per cm^3. The amplitude Δa represents the net or unbalanced amplitude per carbon atom and its value gives the hydrogen amplitude in terms of that of carbon. The experiment was not difficult to perform to the planned accuracy of one percent and was free from any uncertainties in interpretation. The result, however, was $-(3.75\pm0.03)\times10^{-13}$ cm which value disagreed with the ortho-para and diffraction results by more than the errors involved.

III. SECOND EXPERIMENT

Although no source of systematic error was known, it was decided to extend the measurements to investigate the possibility of such errors, and to increase the accuracy. The possibility of systematic errors could be investigated by repeating the measurement for various liquids and by using different neutron wavelengths. An increase in the accuracy beyond the one percent already obtained necessitated a change in method to eliminate effects which could be circumvented in the first experiment but which would prevent any significant increase in accuracy. The natural way to increase the accuracy would be to use a liquid in which the hydrogen amplitude was more nearly balanced by the carbon. For such a liquid the limiting wavelength reflected would be longer if the incident angle remained the same as shown by Eq. (1). With thermal neutrons this meant very low intensities since even in the first experiment the wavelengths involved were well below the maximum of the thermal spectrum. The intensities were so low that transmission and second reflection experiments were considered impractical. It was therefore decided to use the intensity itself as a measure of the critical wavelength. On the low velocity side of the maximum of the distribution of thermal neutrons, the reflected intensity depends on the fourth power of the critical wavelength if the distribution is maxwellian. From Eq. 1 it can be seen that at a given angle the intensity depends then on the square of the residual amplitude, and hence is a fairly sensitive measure of it. A plot of the square root of the intensity at a given angle for a number of hydrocarbons *vs* the hydrogen to carbon content ratio should thus cross the zero ordinate at the ratio where the two amplitudes balance. In this method it is assumed that the reflectivity of the liquid surfaces is nearly the same for all liquids for neutrons of greater than critical wavelengths. Measurements on liquids of known amplitude bear out this assumption.

At long wavelengths, however, the neutron distribution is no longer maxwellian, and the method just described becomes increasingly difficult to interpret. As the neutron wavelength increases above about 5A the intensity drops far more rapidly with wavelength than

[7] D. J. Hughes and M. T. Burgy, Phys. Rev. **81**, 498 (1951).

[8] It was suggested recently by D. Kleinman and G. Snow, Phys. Rev. **82**, 952 (1951), that there might be a correction as large as 1 percent in the liquid mirror experiment, arising from virtual inelastic scattering. Further calculation by Kleinman and Snow shows that the correction is probably negligible (private communication).

[9] M. Hamermesh, Phys. Rev. **77**, 140 (1950).

[10] Hughes, Brugy, and Ringo, Phys. Rev. **77**, 291 (1950).

expected for a maxwellian distribution. At 6.6A units the intensity increases discontinuously as the wavelength becomes longer than the largest lattice spacing in the graphite of the pile, and at still longer wavelengths it continues to decrease faster than the maxwellian. Another effect that becomes increasingly important with wavelength is the finite reflectivity for neutrons of wavelength less than the limiting wavelength. This "spill-over" effect becomes so large with wavelength, that for limiting wavelengths in the 10–15A range, approximately as many neutrons with wavelengths shorter than critical are reflected as those of wavelength longer than critical. Because of these effects it was clear that an improvement in the experiment must involve a method that would avoid any dependence on an accurate knowledge of the wavelength distribution of the incident neutrons.

The method of measurement finally adopted in these experiments avoided the dependence on knowledge of the distribution in the following way. Even though the spectrum is not maxwellian, it decreases sharply in intensity with increasing wavelength, so the reflected intensity (which is proportional to the integral from ∞

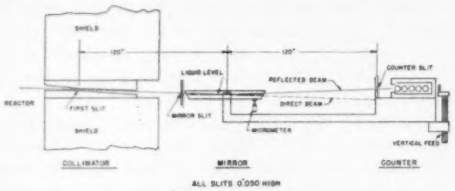

FIG. 1. Apparatus for neutron reflection from liquids.

wavelengths up to the critical wavelength), decreases even faster, and is a very sensitive function of wavelength. Thus a given intensity of reflection means a given critical wavelength. The experiment consists of measurements of those values of the incident angle that give constant intensity (i.e., a constant critical wavelength) in the reflected beam for several liquids of different hydrogen/carbon content ratios. As can be seen from Eq. 1, for a given wavelength the square of the incident angle is proportional to the net amplitude, which in turn is a linear function of the H/C ratio. A plot of θ^2 *vs* H/C content should then be a straight line reaching $\theta^2=0$ at the point when the H/C ratio is the negative inverse of the ratio of the coherent scattering amplitudes of H and C.

This method is very simple to use, involves no measurement of the wavelength, works on any reasonable spectrum shape, and is even valid if the reflection is dominated by spill-over. This last property can be seen from the equation for reflectivity beyond the critical angle:

$$\text{Reflectivity}=\tfrac{1}{16}(\theta_c/\theta)^4 \text{ for } \theta_c/\theta\gg 1.$$

Here θ_c is the largest angle at which a wavelength λ is totally reflected as given by Eq. (1). This result shows that the spill-over intensity decreases rapidly as the critical wavelength increases, so that again the intensity is a sensitive measure of the critical wavelength.

IV. APPARATUS

The experimental arrangement at the thermal column of the Argonne heavy water moderated reactor is shown roughly in Fig. 1. It is quite similar to that of the first experiment with a few exceptions. The second mirror is absent and a considerably longer mirror tray was used, giving a liquid surface 48 in. long. The ends of this tray were tilted 60° from the vertical so that the meniscus would not extend above the surface of the liquid and interfere with the beams. The counter slit and counter were mounted on a steel frame, which was pivoted at a point near the center of the mirror surface so that the beams always traversed the counters at nearly the same place. The mirror tray was made of stainles steel with windows of 0.005 in. stainless steel seam welded in the ends of the tray. The tray was provided with a gasket and a glass cover to minimize evaporation of the mirror liquid. No special precautions were taken to damp out surface waves in the mirror. It was found that the reflected beam was not appreciably wider than the direct beam even when there were distinctly visible waves on the mirror surface with several large fans and pumps running within 50 ft of the mirror.

The mirror and counter slits consisted of machined blocks of cadmium held on an aluminum frame which could be readily adjusted in height and level. The collimator was made of graphite with a cadmium-plated steel lining. It was designed so that fast neutrons would have to pass through at least 2 in. of steel and 1 ft of graphite to go directly from the first slit to the counter. The collimator and the slits were 4 in. wide in the direction perpendicular to the plane of Fig. 1. The counter consisted of a bank of $5B^{10}F_3$ counters which were nearly "black" to neutrons in the energy region of interest in these experiments. A fission counter used as a monitor was placed in the shield at the side of the collimator.

The liquids used in the measurement were triethylbenzene, $C_6H_3(C_2H_5)_3$, cyclohexene, C_6H_{10}, and a mixture of benzene and cyclohexane, C_6H_{12}, designed to give a hydrogen to carbon atomic ratio of 1.700. In the first set of experiments using the present method, it was found that the principal uncertainty in the measurement lay in the ratio of the hydrogen to carbon content of the liquids. The experiments were therefore repeated, taking considerable pains with this point. The best commercial grades of the hydrocarbons were obtained and these were carefully repurified by fractional distillations. As a check, however, quantitative analyses of this material were run by Ralph Bane of the Argonne Chemistry Division. To make the measurements conveniently about 400 cc of each liquid were needed.

V. MEASUREMENTS

A. Angle

The direct beam was first located with the mirror tray removed, then the mirror tray was put into place, the liquid poured in, and the reflected beam located and its intensity measured. An example of such a measurement is shown in Fig. 2. The incident angle is, of course, given by half the difference in the positions of direct and reflected beam, divided by the distance from the counter slit to the point on the mirror surface where the center of the beam is incident.

The most difficult part of the angle measurement is the determination of the incident point on the mirror. It was done by making a series of measurements of the reflected beam intensity as a function of mirror height for a given setting of the mirror slit, i.e., a given angle of incidence. When the incident beam over-shoots the far end of the mirror the intensity drops, similarly when the beam undershoots the near end, the intensity drops. A plot of the reflected intensities (always measured at the peak of the reflected beam) as a function of mirror position is shown in Fig. 3. It was assumed that the center of the beam was incident on the center of the mirror surface when the mirror height was halfway between the two heights where the intensity was half that of the plateau. This was a rather tedious measurement, but fortunately it was only necessary to do it once as all other angles could be determined relative to the measured one by noting the change in the position of the mirror slit, or the direct beam at the counter slit, in going to the new angle. For speed and accuracy the reference angle measurement of Fig. 3 was made using carbon tetrachloride in the mirror as it is a good reflector. In actual practice both the mirror slit position and the direct beam measurement were used to give the change in angle and agreed within the accuracy of each—about 0.1 min. At the end of the measurements the position of the direct beam was always checked by removing the mirror and it was always found in the original position, indicating that the apparatus was sufficiently stable.

B. Intensity

For the intensity measurements on the various liquids it was necessary only that the mirror be in a position on the plateau of Fig. 3 and this was not a critical adjustment. It could in fact be determined simply from the position where the mirror cut off the direct beam. The measurements were, of course, made on the peaks of the reflected beams, and for comparison were reduced to a given number of counts from the monitor counter.

In general, the backgrounds were not obtained by putting cadmium in the beam, but rather by interpolating the intensities on either side of the beam. This procedure was necessary for there was a small background of scattered thermal neutrons, whose intensity decreased fairly rapidly away from the direct beam

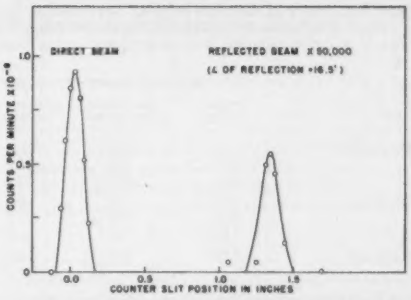

FIG. 2. Direct beam and beam reflected from triethylbenzene mirror. The zero on the position scale is arbitrary.

but was still quite appreciable at the smaller angles of reflection. This small thermal neutron background could not be excluded in spite of careful placing of cadmium slits to define the beam.

In the measurement on the liquids mixed to give a 1.700 H to C content ratio, the possibility of differential evaporation was checked by observing the intensity reflected from the mirror over a period of hours, and no change was observed. For brevity the description of the experiment has omitted the discussion of a number of small corrections. We have, however, made a correction for the density of the mirror liquid, and we have considered and found negligible, corrections for the change in wavelength resolution of the mirror with angle, and the change in position of the neutron path inside the counter with incident angle.

VI. RESULTS

The results of the measurements on the three liquids are given in Table I and the points obtained from these results are shown in Fig. 4. As can be seen from Table I, the incident angles were not set to give precisely equal intensities for the different liquids, and the values of θ^2 in Fig. 4 were adjusted to equal intensities (as well as to equal densities). Figure 4 gives a value of the ratio of the carbon amplitude to the hydrogen amplitude

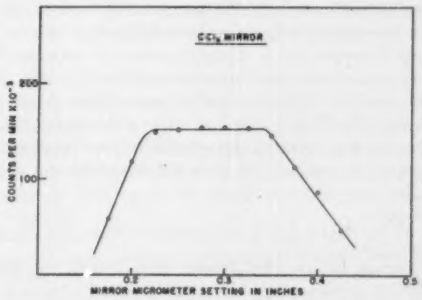

FIG. 3. Reflected intensity as a function of the height of the mirror surface. Thus curve is used to center the beam on the mirror.

TABLE I. Intensity of neutrons reflected from various liquids as a function of incident angle. The limiting wavelength for total reflection is included, although it is not necessary in the analysis (Fig. 4).

Liquid	Angle minutes	Intensity in counts per min*	λ(calculated) angstroms
Triethylbenzene	16.5	130	13.5
	14.6	244	12.3
	12.7	465	10.7
Cyclohexene	9.50	121	14.2
	8.33	185	12.5
	7.02	451	10.5
1.700 mixture	7.02	129	13.6

* Here and in the figure the intensity is normalized to a monitor rate of 17,000 cpm.

(a_C/a_H) of -1.748 ± 0.005. The error is estimated largely from the variation of the ratio deduced from measurements at different intensities, and from the differences between the formulas and analyses for the H/C ratio. Including the results of the first experiment, with appropriate weighting, we obtain finally

$$a_C/a_H=-1.753\pm0.005.$$

To obtain the value of a_H we must know the value of a_C. The transmission measurements on carbon give the total cross section to quite high accuracy $\sigma_C=4.70\pm0.05$[11] from 1 to 500 ev. If there is no incoherent scattering, $a_C=(13/12)(\sigma/4\pi)^{\frac{1}{2}}$. Since the capture cross section is negligible and the spin of C^{12} is zero, the only uncertainty is obtaining a_C from σ_C is the cross section of C^{13}. Recent studies at Brookhaven[12] of thermal incoherent scattering show that the isotopic plus spin-incoherent scattering is less than 0.1 barn. This result in turn shows that the scattering amplitude of C^{13} times its isotopic abundance is not more than 1 percent that of C^{12}. In addition the total absence of any indication of a resonance in the neutron cross section of carbon below 5000 ev makes it quite plausible that C^{13} has a positive scattering amplitude and one within a factor of two that of C^{12}. It then follows that $a_C=6.63(\pm0.03)\times10^{-13}$ cm and $a_H=-3.78(\pm0.02)\times10^{-13}$ cm.

As can be seen from the errors quoted, we now believe this measurement of the ratio of the coherent scattering amplitude of carbon and hydrogen to be more accurate than the current values for the amplitude of carbon. It seems, however, fairly straightforward to improve this last to about the same error as that for the ratio. The fact that the different liquids and different critical wavelengths all give values in quite good agreement, as shown by Fig. 4, encourages the belief that there are no important systematic errors in this measurement of the ratio.

[11] W. W. Havens and L. J. Rainwater, Phys. Rev. **75**, 1296 (1949).
[12] Johnson, Palevsky, and Hughes, Phys. Rev. **82**, 345 (1951).

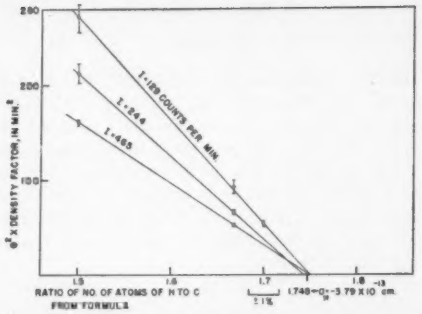

FIG. 4. Graph for determination of balance point of H to C coherent neutron scattering amplitudes.

The value for a_H quoted, $-3.78(\pm0.02)\times10^{-13}$ cm, together with Melkonian's[13] value for the free proton cross section $20.36(\pm0.10)$ barns, gives the triplet and singlet amplitudes:

$$a_T=5.377(\pm0.023)\times10^{-13}\text{ cm}$$

and

$$a_S=-23.69(\pm0.06)\times10^{-13}\text{ cm}.$$

The triplet amplitude plus the Mobley and Laubenstein[14] value for the binding energy of the deuteron, $2.226(\pm0.003)$ Mev, gives the effective range of the triplet well:[15–17]

$$\rho_t=1.704(\pm0.030)\times10^{-13}\text{ cm}.$$

These values do not differ significantly from those used[10] in several papers on the comparison of neutron-proton and proton-proton forces,[16–18] the mass of the π-meson,[19] the binding energy of the triton[20] and the shape of the neutron-proton interaction potential.[21,17] It can be seen from reference 17 that within the limits of error, which now appear to come mainly from the 1- to 5-Mev neutron-proton cross-section measurements, the derived $n-p$ and $p-p$ singlet ranges are consistent with charge independence of nuclear forces.

It is a pleasure to acknowledge the considerable help we received on theory from Dr. Morton Hamermesh and Dr. Hartland Snyder, and on chemistry from Dr. Solomon Wexler.

[13] E. Melkonian, Phys. Rev. **76**, 1744 (1949).
[14] R. C. Mobley and R. A. Laubenstein, Phys. Rev. **80**, 309 (1950).
[15] H. A. Bethe, Phys. Rev. **76**, 38 (1949).
[16] J. Schwinger, Phys. Rev. **78**, 135 (1950).
[17] E. E. Salpeter, Phys. Rev. **82**, 60 (1951).
[18] Lampi, Freier, and Stratton, Phys. Rev. **80**, 853 (1950).
[19] L. Hulthén, Phys. Rev. **79**, 166 (1950).
[20] R. L. Pease and H. Feshbach, Phys. Rev. **81**, 142 (1951).
[21] J. H. Carver and D. H. Wilkinson, Nature **167**, 154 (1951).

The Definition of Moving Coordinate Systems in Relativistic Theories

E. L. HILL
Department of Physics, University of Minnesota, Minneapolis, Minnesota
(Received September 13, 1951)

A kinematic analysis is given of the ambiguities which arise in the definitions of moving reference systems when general transformations are allowed on the space-time variables. It is shown how the classical theory permits an extension to any order of kinematic derivatives. In a relativistic treatment only the step to uniformly accelerated motions is possible in a direct manner. The discussion is limited to one-dimensional motions.

I. INTRODUCTION

IN all branches of mathematical physics one encounters the problem of making transformations to moving reference systems. The definitions to be given for such systems are trivially evident from the point of view of classical physics, but they become highly ambiguous when the methods of tensor analysis and the general theory of relativity are employed. Several special examples are known which are of some importance in the establishment of the relationship between kinematic and gravitational forces, for which the solutions are incomplete on this account. Among these the most important are the uniformly accelerated motions,[1] the clock problem,[2] and uniform rotational motion (rotating disk).[3]

The guiding idea which led to the present work was that of establishing nested sequences of groups of transformations of increasing generality which could be used for the successive reduction of motions of progressive kinematic complexity. For example, in treating the motion of a single particle, one can bring the latter to the origin of coordinates by a translation; it can then be brought to rest instantaneously by a lorentz transformation; and finally, its acceleration can be reduced to zero instantaneously by a conformal transformation. This much has been determined in previous work,[4] and the problem set is to see whether the method can be extended to the reduction of the kinematic derivatives of higher order.

The result at which we arrive is that the possibilities are more restricted than was anticipated at first. In the "classical" case this process can be developed in a step-by-step manner to the reduction of any finite order of the derivatives of the motion, but in the "relativistic" case it breaks off abruptly with the third-order derivatives. In the latter case the conformal group gives a very satisfactory generalization of the lorentz transformations to the treatment of uniformly accelerated motions, but the structure of this group is such that it, in turn, does not permit of a direct extension to motions of fourth and higher order, at least without a considerable alteration in the usual notions relating to the classical limit of relativistic physics.

II. THE GENERAL METHOD

In order to maintain to the fullest the intuitive physical and kinematical elements of our analysis, we state it in terms of the reduction of the motion of a single particle. Let $\mathcal{S}$ be a standard ("laboratory") reference system in which a particle, P, is observed to move. We suppose that associated with P there is a "local" reference system, $\mathcal{P}$, in which P is located permanently at rest at the origin. Our ultimate aim is the establishment of the sense in which $\mathcal{P}$ can be defined, and the coordinate transformation from $\mathcal{S}$ to $\mathcal{P}$ determined. In pursuit of this aim we study various special classes of motions of P, such that types of motion of increasing complexity include those of simpler character. Our method then becomes one of an attempted reduction of the elements of motion of P in successive approximations.

The mathematical basis of the theory is the description of the types of motion of P by means of canonical differential equations, and it is here that we are able to receive major help from the Lie theory of ordinary differential equations. For the most part only the results of the various calculations will be given, since the details require only straightforward applications of known theory.[5]

The discussion will be limited to the case of one-dimensional motion, since this is sufficiently general to indicate the nature of the problem. The kinematic treatment can be extended directly to 3-dimensional motions, but the analysis becomes so tedious as to indicate strongly the need for more powerful mathematical methods.

[1] L. Page, Phys. Rev. **49**, 254 (1936); H. P. Robertson, Phys. Rev. **49**, 755 (1936); J. Haantjes, Proc. Konink. Akad. Wetenschap. Amsterdam **43**, 1288 (1940). The writer regrets that this paper, which was published during the war years, is known to him only by reference; E. L. Hill, Phys. Rev. **67**, 358 (1945); **72**, 143 (1947); J. A. Schouten, Revs. Modern Phys. **21**, 421 (1949).

[2] C. Møller, Kgl. Danske Videnskab. Selskab, Mat.-fys. Medd. **20**, No. 19 (1943); E. L. Hill, Phys. Rev. **72**, 236 (1947); E. A. Milne and G. J. Whitrow, Phil. Mag. (7) **40**, 1244 (1949).

[3] C. W. Berenda, Phys. Rev. **62**, 280 (1942); E. L. Hill, Phys. Rev. **69**, 488 (1946); N. Rosen, Phys. Rev. **71**, 54 (1947); M. G. Trocheris, Phil. Mag. (7) **40**, 1143 (1949).

[4] E. L. Hill, Phys. Rev. **67**, 358 (1945); **72**, 143 (1947).

[5] A. Cohen, *An Introduction to the Lie Theory of One-Parameter Groups* (G. E. Stechert and Company, New York, 1931); L. P. Eisenhart, *Continuous Groups of Transformations* (Princeton University Press, Princeton, New Jersey, 1933); G. Kowalewski, *Integrationsmethoden der Lieschen Theorie* (Edwards Brothers, Inc., Ann Arbor, Michigan, 1944).

It may be well to emphasize explicitly that we are not concerned directly here with the problem of the metric structure of space-time as it is interpreted in the general theory of relativity. We deal rather with the group of transformations on the space-time variables which lies at the basis of the tensor calculus itself. Since kinematical problems in three dimensions become purely geometrical problems when viewed in 4-dimensional space-time, every transformation on the space-time variables carries with it certain kinematic implications. It follows that the analysis of moving reference systems is bound up inextricably with the structure theory of the general group of transformations on space-time. However, this group is not only of great complexity, but in practice its exact nature is only poorly defined,[6] so that no detailed theory of its structure is possible at the present time. Our discussion may be considered, from a purely mathematical point of view, as an attempt at a partial theory of the structure of this group, however incomplete it is in this respect.

The reader will recognize also that the terms in which we have introduced our problem, by means of the motion of a single particle, may seem more restrictive than is actually the case. If we think of the points of the (space) reference system $\mathcal{P}$ as the particles of an imaginary fluid, then the world-lines of these particles will be straight lines parallel to the time-axis of the associated space-time diagram. When a transformation is applied to map $\mathcal{P}$ onto S these world-lines will be mapped into curves of other forms. According to our theory of canonical forms of motion all of the transformed curves will obey the same associated differential equation. The essence of the method is, then, the attempt to resolve the flow pattern of the points of $\mathcal{P}$, when mapped onto the space-time diagram associated with S, into a sequence of canonical forms which can be used as approximations for more general patterns.

III. A PARTICLE AT REST

As our first case we take the seemingly trivial one of a particle at rest at a point on the x-axis[7] of our standard reference system, S. In its kinematical aspects this state of motion is described completely by the differential equation,

$$dx/dt=0. \tag{1}$$

We now inquire what transformations of the space-time variables, x and t, will have the property that in the new reference system the particle will also be at rest; i.e., what transformations leave Eq. (1) invariant. Restricting ourselves to infinitesimal transformations, we have, in general,

$$x'=x+\xi(x,t)\cdot\delta\alpha, \quad t'=t+\eta(x,t)\cdot\delta\alpha, \tag{2}$$

where ξ and η are unspecified functions, and $\delta\alpha$ is an infinitesimal constant. On computing dx'/dt' we have, to first orders in $\delta\alpha$,

$$\frac{dx'}{dt'}=\frac{dx}{dt}+\left[-\frac{\partial\eta}{\partial x}\left(\frac{dx}{dt}\right)^2+\left(\frac{\partial\xi}{\partial x}-\frac{\partial\eta}{\partial t}\right)\frac{dx}{dt}+\frac{\partial\xi}{\partial t}\right]\cdot\delta\alpha. \tag{3}$$

We now see that when Eq. (1) is satisfied, the corresponding equation $dx'/dt'=0$ will be satisfied provided only we have

$$\partial\xi/\partial t=0, \tag{4}$$

so that ξ is a function of x alone. The possible transformations thus are very general, involving the two arbitrary functions $\xi(x)$ and $\eta(x,t)$.

The extreme freedom which we find in this case is associated with the fact that Eq. (1) is of first order, and it exceeds that which is allowable for motions of higher order. We shall therefore restrict it by the observation that on physical grounds the most interesting types of transformation are the translations of the origins of the space and time variables. This yields the 2-parameter translation group generated by the operators

$$\{\partial_x, \partial_t\}, \tag{5}$$

with finite transformations of the form,

$$x'=x-x_0, \quad t'=t-t_0. \tag{5'}$$

IV. MOTION WITH UNIFORM SPEED

If the motion of P in S is one of uniform velocity along the x-axis, the characteristic differential equation is

$$d^2x/dt^2=0. \tag{6}$$

The general Lie group which leaves Eq. (6) invariant is the 8-parameter group with the generating operators[8]

$$\{\partial_x, \partial_t, t\partial_x, x\partial_x, t\partial_t, x\partial_t, x^2\partial_x+xt\partial_t, xt\partial_x+t^2\partial_t\}. \tag{7}$$

Comparison with (5) shows that the translation group in the (x,t)-plane is contained in (7) as a subgroup. Since this subgroup will be present in all of our later considerations, it will not be mentioned explicitly in each case.

So long as Eq. (6) is taken as our sole criterion of uniform motion, the general class of uniformly moving reference systems would have the full flexibility of this 8-parameter group of transformations. However, within this group we can isolate a number of subgroups each of which can be used to give a particular definition of such transformations.

The three operators

$$\{\partial_x, \partial_t, t\partial_x\}, \tag{8}$$

generate the elementary galilean transformation group which is the basis of the classical definition, the corresponding finite transformations being reducible to the form

$$x'=(x-x_0)-v_0(t-t_0), \quad t'=t-t_0. \tag{8'}$$

Alternatively, we can isolate the 3-parameter subgroup with the generators

$$\{\partial_x, \partial_t, t\partial_x+(x/c^2)\partial_t\}, \tag{9}$$

[6] When the discussion of tensor analysis is specifically limited to local properties near a point in space-time, the allowed transformations are usually restricted to those which are *analytic* in the variables. On the other hand, when problems must be treated in the large, this requirement becomes too drastic and transformations of singular character must be admitted. To the writer's knowledge no classification of such allowable types of singularities is feasible.

[7] For the sake of visualization of the problem, we shall speak of the motion as taking place along the x-axis of the space coordinate system. However, we actually treat it as a true one-dimensional motion in that we do not consider the transformations on the other two space variables.

[8] The following theorem is of interest here. Let n be the order of an ordinary differential equation, and let r be the maximum number of parameters in the Lie group which leaves this equation invariant. Then if $n=2$, $0\leqslant r\leqslant 8$; while if $n>2$, we have $0\leqslant r\leqslant n+4$. See Cohen, reference 5, p. 148.

the finite transformations of which can be put in the canonical form,

$$x'=\frac{(x-x_0)-v_0(t-t_0)}{[1-(v_0/c)^2]^{\frac{1}{2}}},$$
$$t'=\frac{(t-t_0)-(v_0/c^2)(t-t_0)}{[1-(v_0/c)^2]^{\frac{1}{2}}}. \tag{10}$$

This is clearly the group of (inhomogeneous) lorentz transformations for one-dimensional motion. We shall designate it as $\mathfrak{L}_2$.

It is clear that neither the galilean nor the lorentz transformations exhaust the kinematic possibilities inherent in the full 8-parameter group generated by the operators (7).

One may also note with interest that both the classical and the relativistic theories employ the same definition of "uniform motion," as specified in Eq. (6). While this is so well known as to be accepted ordinarily as trivial, its peculiarity becomes evident from the observation that the corresponding definitions for the higher-ordered derivatives must necessarily differ.

V. THE (CLASSICAL) GALILEAN SEQUENCE

The result of Sec. IV for the group of transformations of classical physics to uniformly moving (one-dimensional) reference systems can be generalized at once to apply to any desired order. Let $\mathfrak{G}_n$ be the $(n+1)$-parameter group generated by the set of operators

$$\left\{\partial_x,\ \partial_t,\ t\partial_x,\ \frac{t^2}{2}\partial_x,\ \cdots,\ \frac{t^{n-1}}{(n-1)!}\partial_x\right\}. \tag{11}$$

This group leaves invariant the family of motions satisfying the differential equation,

$$d^nx/dt^n=0. \tag{12}$$

It is essential to the classical theory of transformations to moving reference systems that $\mathfrak{G}_n$ can be analyzed into the nested sequence of subgroups defined by the pattern[9]

$$\mathfrak{G}_1\subset\mathfrak{G}_2\subset\mathfrak{G}_3\cdots\subset\mathfrak{G}_{n-1}\subset\mathfrak{G}_n. \tag{13}$$

It is this property which gives one the power to eliminate successively the various orders of the motion without altering the whole structure of the set of transformations at each step.

Since the index n can be allowed to assume any positive integral value, we can proceed to the limit $n\to\infty$. We let $\mathfrak{G}_\infty$ represent the totality of transformations so obtained. This infinite sequence of nested subgroups of $\mathfrak{G}_\infty$ will be referred to as the classical galilean sequence.

[9] From a geometrical point of view the use of the classical galilean sequence corresponds to the ordinary process of curve fitting in the (x, t) plane by means of polynomials of increasing degrees.

VI. THE AUGMENTED GALILEAN SEQUENCE

Although the group $\mathfrak{G}_n$ leaves invariant the motions defined by Eq. (12), it is not the full symmetry group of point transformations of this equation. It is of interest to the present discussion to consider this more general set of transformations, to which we shall refer as the augmented galilean group, $\mathfrak{G}_n^*$.

The generating operators of $\mathfrak{G}_2^*$ have been specified already as the set (7).

The generators of $\mathfrak{G}_3^*$ have been given earlier[4] in the form

$$\{\partial_x,\ \partial_t,\ t\partial_x,\ \tfrac{1}{2}t^2\partial_x,\ x\partial_x+t\partial_t,\ x\partial_x-t\partial_t,\ xt\partial_x+\tfrac{1}{2}t^2\partial_t\}. \tag{14}$$

Being a 7-parameter group, $\mathfrak{G}_3^*$ is of lower order[5] than is $\mathfrak{G}_2^*$.

When $n\geqslant 3$, the generators of $\mathfrak{G}_n^*$ form the set

$$\{\mathfrak{G}_n,\ x\partial_x,\ t\partial_t,\ xt\partial_x+[t^2/(n-1)]\partial_t\}. \tag{15}$$

It is apparent from (15) that $\mathfrak{G}_n^*$ does not contain $\mathfrak{G}_{n-1}^*$ $(n>3)$, the default arising from the circumstance that the operator

$$xt\partial_x+[t^2/(n-1)]\partial_t$$

depends explicitly on the index n. The embedding process thus fails in the case of the augmented galilean groups for all values $n\geqslant 3$.

VII. THE EXTENSION OF THE LORENTZ GROUP TO UNIFORMLY ACCELERATED MOTIONS

The extension of the lorentz group to higher order motions is not so trivial as it is for the classical galilean case. It is illuminating to alter the argument to seek first the various possible extensions to uniformly accelerated motions. We therefore search for the possible third-order differential equations which are invariant under $\mathfrak{L}_2$. Each such equation will give us a definition of uniformly accelerated motion which is acceptable so far as kinematical considerations are concerned, and which is of "relativistic" character.

Let the desired equation be

$$F(x, t, v, a, b)=0, \tag{16}$$

with $v=dx/dt$, $a=dv/dt$, $b=da/dt$. It is convenient to observe at once that, since the translations in the (x, t) plane form a subgroup of $\mathfrak{L}_2$, it follows that F will not depend explicitly on x and t. Furthermore, we shall suppose that an explicit solution has been made for b, so that our differential equation has been brought to the canonical form,

$$F\equiv b+\varphi(v, a)=0. \tag{16'}$$

The infinitesimal transformation associated with (9), extended to third-order derivatives is

$$\delta x=\delta\alpha+t\delta\beta, \qquad \delta t=\delta\gamma+(x/c^2)\delta\beta,$$
$$\delta v=(1-v^2/c^2)\delta\beta, \quad \delta a=-(3va/c^2)\delta\beta, \tag{17}$$
$$\delta b=-[(3a^2+4vb)/c^2]\delta\beta.$$

The condition that the differential Eq. (16′) be invariant under $\mathfrak{L}_2$ is expressed by the equation,

$$\frac{\partial F}{\partial v}\delta v+\frac{\partial F}{\partial a}\delta a+\frac{\partial F}{\partial b}\delta b=0, \tag{18}$$

which yields the differential equation for $\varphi(v, a)$:

$$(c^2-v^2)\partial\varphi/\partial v-3va\partial\varphi/\partial a+4v\varphi-3a^2=0. \tag{18′}$$

One solution of this equation is

$$\varphi_1(v, a)=3va^2/(c^2-v^2), \tag{19}$$

which, on substitution in Eq. (16′), leads to the differential equation for one-dimensional uniformly accelerated motion which has been used in earlier work:[4]

$$b+3va^2/(c^2-v^2)=0. \tag{20}$$

It will now be shown that if we make the requirement that Eq. (16′) is to reduce to the classical form for small values of v, then Eq. (20) is the only acceptable form.

The proof of this statement is as follows. First we observe that, since the difference of any two solutions of Eq. (18′) obeys the homogeneous equation obtained by dropping the last member of Eq. (18′), we can write the general solution of Eq. (18′) in the form,

$$\varphi(v, a)=\varphi_1(v, a)+\theta(v, a), \tag{21}$$

where $\theta(v, a)$ is a solution of the homogeneous equation,

$$(c^2-v^2)\partial\theta/\partial v-3va(\partial\theta/\partial a)+4v\theta=0. \tag{22}$$

If we now assume that θ is an analytic function of v, for small values of v, we find from Eq. (22) that it has the power series expansion

$$\theta(v, a)=\sum_{k=0}^{\infty} u_{2k}(a)\cdot v^{2k}, \tag{22′}$$

with

$$u_{2k+2}=\frac{1}{(2k+2)c^2}\left[3a\frac{du_{2k}}{da}+(2k-4)u_{2k}\right]. \tag{22″}$$

The function $\theta(v, a)$ is thus determined entirely by the arbitrary function $u_0(a)$. On introducing our requirement of reduction to the classical limit for vanishingly small values of v, we have $u_0(a)=0$, so that $\theta(v, a)=0$, identically, which completes the proof.

Since it is known that the symmetry group of point transformations of Eq. (20) is the 6-parameter conformal group, it is now clear that the embedding of the lorentz transformations in the conformal group for the treatment of uniformly accelerated motions is not only reasonable, but it is also unique if we require that it reduce to the ordinary classical limit for vanishingly small velocities.

VIII. THE EXTENSION OF THE CONFORMAL GROUP TO MOTIONS OF HIGHER ORDER

The argument of Sec. VII leads at once to the attempt to extend the relativistic definition of uniformly accelerated (third-order) motions to the fourth and higher orders. To do this we look for those differential equations of order 4 and greater which are invariant under the one-dimensional conformal group (which we here designate as $\mathfrak{L}_3$ to suggest that the lorentz group $\mathfrak{L}_2$ is embedded in it and that it has an invariant differential equation of order 3). The set of generating operators of this group is[4]

$$\{\partial_x,\ \partial_t,\ t\partial_x+(x/c^2)\partial_t,\ x\partial_x+t\partial_t,\ [(c^2t^2+x^2)/2c^2]\partial_x +(xt/c^2)\partial_t,\ xt\partial_x+[(c^2t^2+x^2)/2c^2]\partial_t\}. \tag{23}$$

We observe first that if we take the classical limit ($c\to\infty$) the set (23) reduces to the form,

$$\{\partial_x,\ \partial_t,\ t\partial_x,\ x\partial_x+t\partial_t,\ \tfrac{1}{2}t^2\partial_x,\ xt\partial_x+\tfrac{1}{2}t^2\partial_t\}. \tag{23′}$$

Comparison with the set (14) shows that the group defined by (23′) is a subgroup of $\mathfrak{G}_3^*$, and consequently leaves the differential equation $d^3x/dt^3=0$ invariant. The conformal group, $\mathfrak{L}_3$, thus reduces to the expected classical limit. This is apparent also at once from its invariant differential Eq. (20).

On the other hand, it follows from the discussion of Sec. VI that the group defined by (23′) is not a subgroup of $\mathfrak{G}_n^*$ for $n\geqslant 4$. From this we conclude that $\mathfrak{L}_3$ has no invariant differential equation of order 4 or higher which reduces to the classical form for small velocities.

It can be shown by direct calculation that, in fact, $\mathfrak{L}_3$ has no invariant differential equation of orders 4 or 5 which is independent of Eq. (20). However, the detailed proof does not seem to be of sufficient intrinsic interest to justify its presentation here.

IX. DISCUSSION

The two major points which we have found in this analysis are (a) the uniqueness of the conformal group for the discussion of uniformly accelerated motions when the theory is required to reduce to the classical limit and (b) the failure of the direct extension to motions of higher order. Even though the methods which have been used are not sufficiently powerful to provide a comprehensive theory of the embedment of the conformal group in more extended groups, they do raise a serious question on the nature and feasibility of the process. It seems to the writer that this is not only of purely mathematical interest, but is also of concern if one is to consider seriously any extension of quantum mechanics beyond invariance under the lorentz group. The extension to the conformal group has been studied by Dirac,[10] Bhabha,[11] and others, but beyond this the path is unexplored. The difficulties which stand in the way of an extension of the concept of covariant differentiation to spinor fields[12] suggest that progress in this direction will require a more detailed knowledge of the general theory of the embedment of the lorentz group within larger transformation groups.

[10] P. A. M. Dirac, Ann. Math. (2) **37**, 429 (1936).
[11] H. J. Bhabha, Proc. Cambridge Phil. Soc. **32**, 622 (1936).
[12] É. Cartan, *Leçons sur la théorie des spineurs, II* (Hermann and Cie., Paris, 1938), Chap. 9.

The Uniform Theory of Nuclear Binding Energies*

DAVID H. FRISCH
Physics Department and Laboratory for Nuclear Science and Engineering, Massachusetts Institute of Technology, Cambridge, Massachusetts

(Received August 1, 1951)

Wigner's "uniform" theory of nuclear binding energies is reviewed with the following additions: (1) The potential energy is generalized by using other exchange operators as well as the Majorana operator; (2) a rough calculation of the magnitude of the interaction integrals is made from the central forces between the elementary nucleons, leading to a calculation of the potential energy and a discussion of stability at the observed nuclear radii. The results are that the uniform model cannot be improved appreciably by a reasonable more general central potential operator, and the calculated interaction integrals probably cannot give the observed binding energies and radii simultaneously.

1. INTRODUCTION

THE binding energies of nuclei have been computed[1] by detailed calculation of the nuclear wave function for light nuclei, and by statistical methods for nuclei of mass number $A>$approximately 16. The recent re-emphasis[2] on "magic number" regularities indicates that any statistical model must be supplemented by a study of the dependence of the structure of individual nuclei on orbital and intrinsic spin quantum numbers.

Wigner's "uniform" theory[1,3,4] of nuclei of $A>$ approximately 16 consists of a statistical model in which most details of the space distribution of the nuclear wave function are neglected. Regularities in the binding energy, otherwise difficult to explain, are predicted by assuming a dependence of the interaction operator between pairs of nucleons on the symmetry of the wave function under the interchange of their space coordinates (Majorana force). This assumption gives a periodicity associated with the maximum number (four) of nucleons which can occupy the same space state if there are only two distinguishable nuclear particles with half-integral spin, i.e., neutrons and protons.

The prediction of the binding energies of the ground states of nuclei has been accomplished by Wigner in terms of only two parameters other than the assumed radius $R=A^{\frac{1}{3}}r_0$. These two parameters are average interaction integrals in the expression for the potential energy, and are assumed to be only very slowly varying functions of mass number and of neutron excess.

The uniform model obtains the kinetic and coulomb energies from a statistical model, and describes the potential energy in terms of its symmetry properties and of interaction integrals determined empirically. The sum of these energies is the total energy E, the negative of the binding energy,

$$E=K+C+V. \tag{1}$$

Typical approximate values for these quantities, computed on the uniform model, are illustrated in Fig. 1.

The procedure in predicting nuclear binding energies by the uniform theory may be as follows: one parameter in the potential energy is obtained from the energy ΔE observed released in any one β-transition (or K-capture) between isobars. It is supposedly necessary to know only this one number to predict all other isobaric transitions. Knowing the value of the first parameter, the second may be obtained from the observed total binding energy E of any one nucleus. Alternatively, the total binding energies of two different nuclei would determine both parameters. In practice it is necessary to take the average over many transitions between isobars to get significant values by the first method, and the second method is too insensitive to determine both parameters independently.

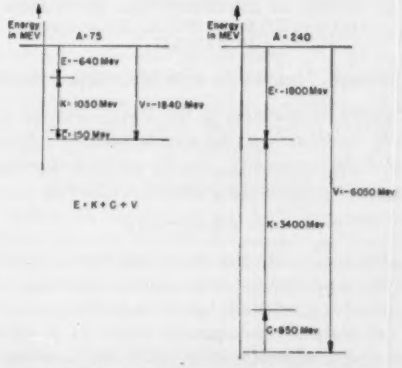

FIG. 1. Binding energy of typical nuclei.

* Much of this material was submitted as a Ph.D. thesis, Massachusetts Institute of Technology, September, 1947. A complete presentation of the present paper, including tables, is available as Massachusetts Institute of Technology LNSE Technical Report No. 43, June, 1950. This work was supported in part by the joint program of the ONR and AEC.

[1] For a comprehensive review see, for example, E. Feenberg and E. Wigner, Reports on Progress in Physics, 1941.

[2] See E. Feenberg and K. C. Hammack, Phys. Rev. **75**, 1877 (1949); L. Nordheim, Phys. Rev. **75**, 1894 (1949).

[3] E. Wigner, (a) Phys. Rev. **51**, 106 (1937); (b) Phys. Rev. **51**, 947 (1937).

[4] E. Wigner, *University of Pennsylvania Bicentennial Conference:* "Nuclear Physics" (University of Pennsylvania Press, Philadelphia, 1941).

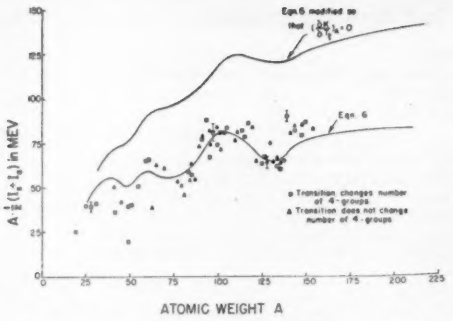
Eqn 6 modified so that $(\frac{\partial E}{\partial T_z})_A = 0$
Eqn. 6
o Transition changes number of 4-groups
Δ Transition does not change number of 4-groups
A $\frac{1}{2}(I_e - I_o)$ in MEV
ATOMIC WEIGHT A

FIG. 2. A times average interaction integral vs A for nuclei with odd A.

The uniform theory, as it stands at present, has been remarkably successful in predicting the isotopic excess and the approximate binding energy of most stable nuclei. However, the following points may merit more discussion:

1. (Sec. II) (a) With more data available on the transition energies between even isobars, the agreement between theory and experiment for middle-weight nuclei is not as good as indicated earlier.[4] (b) The question arose whether a modification of the Majorana force, particularly in the direction of the recently popular $\sigma\cdot\sigma\tau\cdot\tau$ force of symmetric meson theory, would make a consistent improvement in the agreement. (c) Wigner noted some disagreement between the dependence on A of interaction integrals calculated from isobaric transitions and those calculated from total binding energy.

2. (Sec. III) An attempt can be made to compute the magnitude of the interaction integrals from the forces between neutrons and protons observed in $n-p$ and $p-p$ scattering. This will also make possible a discussion of whether in the uniform model a nucleus can be in stable equilibrium at its observed radius and at the same time have the observed binding energy.

II. REVIEW OF EXPERIMENTAL DATA AND CALCULATION OF EFFECT OF $\sigma\cdot\sigma\tau\cdot\tau$ POTENTIAL

a. Isobaric Transitions with Majorana Potential

Wigner's computation of the energy released in an isobaric transition may be accomplished as follows in terms of the numbers N_s, N_a, I_s, and I_a. The potential energy with a Majorana potential operator is

$$V=-N_sI_s+N_aI_a. \tag{2}$$

N_s is the number of pairs of nucleons for each of which pairs the total nuclear wave function is unchanged by the interchange of their space coordinates alone—we will call them space-symmetric pairs. N_a is the corresponding number of pairs for which the wave-function changes sign under interchange of space coordinates—antisymmetric pairs. Their values are

$$N_s=\tfrac{3}{16}A^2+(5/4)A-\tfrac{1}{4}\langle(P''+2)^2+(P'+1)^2+P^2\rangle+5/4, \tag{3}$$

$$N_a=\tfrac{3}{16}A^2-(5/4)A+\tfrac{1}{4}\langle(P''+2)^2+(P'+1)^2+P^2\rangle-5/4. \tag{4}$$

The values of P'', P', and P are chosen from the expectation values of the three operators $\mathbf{T}$, $\mathbf{S}$, and $\mathbf{Y}$,[5] each taken as small as possible[3,4] so as to maximize the number N_s of space-symmetric pairs, subject to the observed isotopic excess $2T_\zeta$, which gives the minimum magnitude $T=T_\zeta$ for the isotopic quantum number $\mathbf{T}$. The observed total spin $\mathbf{I}$ does not fix the intrinsic spin $\mathbf{S}$ in this statistical model.

One of the tentative assumptions of the uniform model is that P'', P', and P will be good quantum numbers. At high A particularly, the effect of the coulomb force and non-central forces will be to prohibit the use of the lowest values, without admixture of higher values, for these numbers. Nevertheless, use of the lowest values still does not make the theory as dependent on detailed 4-group structure as the experimental data, and the assumption probably sets a limit of agreement between theory and experiment.

$-I_s$ is the expectation value $\int\psi_{sij}{}^*V^{ij}\psi_{sij}d(\text{vol})$ of the potential energy operator V^{ij} acting between any pair i and j of space-symmetric nucleons. I_a is the corresponding interaction integral for space-antisymmetric pairs. I_s and I_a are assumed to be the same for all pairs in a nucleus with a given A, independent of the neutron excess. These interaction integrals are assumed also to drop off as $1/A$ for heavy nuclei since the chance of a given pair being within the range of the forces between them drops off as the volume increases, and since we assume constant density the volume is proportional to A. In an electron or positron transition between isobars the total number of pairs of nucleons remains the same, but the numbers of pairs of the two different types may change.

The net change in potential energy is

$$\Delta V=-\Delta N_s\cdot I_s+\Delta N_a\cdot I_a$$
$$=\Delta(N_a-N_s)\cdot\tfrac{1}{2}(I_s+I_a)+\Delta(N_a+N_s)\cdot\tfrac{1}{2}(I_a-I_s) \tag{5}$$

and, since $\Delta(N_a+N_s)$ is zero for an isobaric transition,

[5] The quantum numbers used for the description of the symmetry properties of the nuclear wave functions are the diagonal values of the operators $\mathbf{S}=\frac{1}{2}\sum_i\boldsymbol{\sigma}^i$, $\mathbf{T}=\frac{1}{2}\sum_i\boldsymbol{\tau}^i$, and $\mathbf{Y}=\frac{1}{2}\sum_i\boldsymbol{\sigma}^i\boldsymbol{\tau}^i$. $\mathbf{S}$ is the nuclear intrinsic spin, and its magnitude is half the following number: nucleons with intrinsic spin up minus those with spin down. Note that $\mathbf{S}$ is not necessarily the observed nuclear total spin $\mathbf{I}$. The isotopic spin quantum number $\mathbf{T}$ has no direct physical interpretation, but its projection on the ζ-axis in hypothetical "isotopic-spin space" is $T_\zeta=\frac{1}{2}(N-Z)$ half the neutron excess, i.e., half the following number: nucleons with isotopic spin up minus those with isotopic spin down. The quantum number $\mathbf{Y}$ also has no direct physical interpretation, but Y_ζ is half the following number: (neutrons with spin up plus protons with spin down) minus (neutrons with spin down plus protons with spin up).

the observed ΔV and the computed $\Delta(N_a-N_s)$ give the parameter $\frac{1}{2}(I_s+I_a)$, called L in Wigner's notation.

The difference in numbers of the two types of pairs of nucleons (N_a-N_s), has been plotted in Fig. 2 of reference 3(b), as a function of the neutron excess $2T_{t<}$. Consider a transition between isobars with charges $Z=\frac{1}{2}A-(T_{t<}+1)$ and $Z+1=\frac{1}{2}A-T_{t<}$ (i.e., $T_{t<}$ is half the neutron excess for the member of the pair with lesser $T_{t<}$ and greater Z). For odd nuclei the net change $\Delta(N_a-N_s)$ is $T_{t<}+5/2$ (provided $T_{t<}$ is positive). For even nuclei $\Delta(N_a-N_s)$ is $T_{t<}+1$ or $T_{t<}+4$ depending respectively on whether an odd-multiple-of-two neutron excess is converted to an even-multiple-of-two neutron excess by changing a proton to a neutron, or by changing a neutron to a proton, i.e., whether a three-group or a four-group is broken up by the change. The potential energy change thus goes up with $T_{t<}$, giving the familiar quadratic dependence (smooth for odd nuclei; kinky for even nuclei) of the total potential energy on neutron excess.

The kinetic energy change also goes up to a first approximation linearly with the neutron excess, and has kinks in it for even nuclei only.

The magnitudes of the kinetic and coulomb energies are based on a choice of radius $R=A^{\frac{1}{3}}r_0$ with $r_0=e^2/2mc^2$ $=1.41\times10^{-13}$ cm.

Calculations of the energy differences between ground states of isobaric pairs are given in the LNSE Technical Report previously mentioned.*

Figures 2 and 3(a) give the atomic weight times the average interaction integral per pair of nucleons $A\cdot\frac{1}{2}(I_s+I_a)=\Delta V/\Delta(N_a-N_s)$. This quantity is to be constant for very large nuclei, and a slowly-varying function of A and still inedpendent of $T_{t<}$ for middle-weight nuclei, if the uniform model is literally correct. We hope that it will vary at least smoothly as a function of A and $T_{t<}$ even if the uniform model is not very good. A symbol □ indicates that the transition makes or breaks up a 4-group; a symbol △ indicates that no 4-group is affected.

In addition to studying the individual transitions, Wigner[4] used the correspondence of a certain neutron excess $2T_{tA}$ with each mass number A for the observed stable odd nuclei, smoothing out this correspondence into a relation for which the most stable hypothetical nucleus may have a non-integral neutron excess.[4] This procedure corresponds to averaging over the location of the ground-states of the stable nuclei. The condition for stability then becomes (for $T_{tA}>\frac{1}{2}$),

$$(\partial E/\partial T_t)_A=(T_{tA}+2)\cdot\tfrac{1}{2}(I_s+I_a)-0.6(A-2T_{tA}-1)A^{-\frac{1}{3}}+64T_{tA}A^{-1}-83T_{tA}^2A^{-2}+0.8=0. \quad (6)$$

The first term is the change of potential energy, the second coulomb, the third and fourth kinetic, and the last takes into account the $n-p$ mass difference and the possibility of K-capture. Approximate values of $\frac{1}{2}(I_s+I_a)$ derived from this relation are drawn as a smooth curve in Fig. 2. (See also Table 2, reference 3(c).) A curve with no kinetic energy term is also drawn to show that it contributes a relatively smaller fraction to the potential necessary in isobaric transitions than in the total binding energy. The ups and downs are due to the well-known winding about of the stable valley, and are left unexplained by anything in this whole statistical treatment.

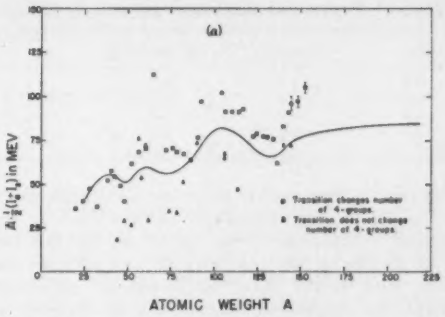

FIG. 3(a). A times average interaction integral *vs* A for nuclei with even A, for Majorana potential.

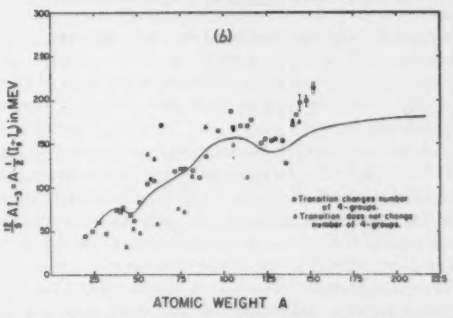

FIG. 3(b). A times average interaction integral *vs* A for nuclei with even A, for $\sigma\cdot\sigma\,\tau\cdot\tau$ potential.

The average interaction integrals $\frac{1}{2}(I_s+I_a)$ computed from isobaric transitions in odd nuclei (Fig. 2) scatter considerably but exhibit no systematic eccentricities except those due to the winding of the valley of stable nuclei. There is no apparent dependence on whether the nuclei have $4k+1$ or $4k+3$ nucleons.

There are, however, systematic eccentricities in the values of $\frac{1}{2}(I_s+I_a)$ computed from transitions between even isobars. As displayed in Fig. 3(a), increasing from an odd to an even number of neutrons (we could use the number of protons equally well for discussion) takes less energy to break bonds and provide the additional kinetic energy than would be predicted by the values of $\frac{1}{2}A(I_s+I_a)$ computed from other transitions. In other words, three-groups are not as bound as they should be or four-groups more than they should be.

* N. Bohr and J. A. Wheeler, Phys. Rev. **56**, 426 (1939).

TABLE I. Simultaneous eigenvalues of potential operators.

$\sigma^i\cdot\sigma^j$	$\tau^i\cdot\tau^j$	$\sigma^i\cdot\sigma^j\tau^i\cdot\tau^j$	P^{ij}
+1	+1	+1	−1
+1	−3	−3	+1
−3	+1	−3	+1
−3	−3	+9	−1

This effect is most marked at low mass numbers, where $\Delta(N_e-N_o)$ is most dependent on the details of the nucleus. Comparison of the transitions for the two types of even nuclei, those with $4k$ total nucleons and those with $4k+2$, shows no systematic differences except the dependence on oddness or evenness of numbers of neutrons.

b. Isobaric Transitions with Other Potentials

Choosing another potential energy operator than Majorana will give steps in the potential energy, on transition between isobars, different from those of Fig. 3(a). We want the steps to show still greater odd-even dependence for even nuclei. An "ordinary" potential, which does not act on the symmetry properties of the wave-function, may be included along with a Majorana potential without changing the form of the expression for the expectation value of the potential energy; all that results is that the symmetric and antisymmetric interaction integrals are made more nearly equal. If, however, a potential which does act on other than the space-symmetry properties of the wave function is added to or replaced entirely a Majorana potential, the expectation value of the potential energy may be changed considerably.

The qualitative success of this theory necessitates that the potential give a greater attraction for space-symmetric than for space antisymmetric states, which the Majorana operator P^{ij} is designed to do. The latter happens to be a rather complicated combination of the few properly invariant combinations of velocity-independent spin and isotopic spin operators that can go with a central force field[7]

$$P^{ij}=-\tfrac{1}{2}(1+\boldsymbol{\sigma}^i\cdot\boldsymbol{\sigma}^j)\times\tfrac{1}{2}(1+\boldsymbol{\tau}^i\cdot\boldsymbol{\tau}^j)$$
$$=-\tfrac{1}{4}-\tfrac{1}{4}\boldsymbol{\sigma}^i\cdot\boldsymbol{\sigma}^j-\tfrac{1}{4}\boldsymbol{\tau}^i\cdot\boldsymbol{\tau}^j-\tfrac{1}{4}\boldsymbol{\sigma}^i\cdot\boldsymbol{\sigma}^j\boldsymbol{\tau}^i\cdot\boldsymbol{\tau}^j. \quad (7)$$

The operator $\boldsymbol{\sigma}^i\cdot\boldsymbol{\sigma}^j\boldsymbol{\tau}^i\cdot\boldsymbol{\tau}^j$ occurs more naturally and displays the same basic properties, except that while it has only one eigenvalue, -3, corresponding to space-symmetry, it has two eigenvalues $+1$ and $+9$, corresponding to space antisymmetry, so that we may have three interaction integrals, rather than two, at our disposal in fitting the data. If there is a $\boldsymbol{\sigma}^i\cdot\boldsymbol{\sigma}^j$ and a $\boldsymbol{\tau}^i\cdot\boldsymbol{\tau}^j$ potential, or both, in addition to a $\boldsymbol{\sigma}^i\cdot\boldsymbol{\sigma}^j\boldsymbol{\tau}^i\cdot\boldsymbol{\tau}^j$ potential, there are four distinct eigenvalues, as shown in Table I, and hence four interaction integrals.

[7] E. Wigner and L. Eisenbud, Proc. Natl. Acad. Sci. **27**, 281 (1941).

We may write for any potential energy operator V^{ij},

$$V=\sum_{\kappa=1}^{\nu}\lambda_\kappa N_\kappa I_\kappa, \quad (8)$$

where the sum is over the ν types of symmetry (in all three spaces) distinguished by the ν eigenvalues λ_κ of the symmetry dependent part of the protential energy operator. Each interaction integral I_κ is the magnitude of the expectation value $|\int\psi_\kappa{}^{ij}V^{ij}\psi_\kappa{}^{ij}d\tau|$ of the potential energy operator V^{ij} acting between any two nucleons i and j such that the total nuclear wave-function has the κth type of symmetry under their interchange. N_κ is the effective number of pairs of nucleons with the κth type symmetry.

While it is possible to evaluate the number of interactions N_κ corresponding to each eigenvalue in terms of the T, S, and Y quantum numbers, Blatt has pointed out[8] that these will be good quantum numbers only for two eigenvalue operators. Thus for $\nu>2$ the N_κ are not constants of the motion since we will evaluate N_κ in terms of T, S, and Y and these are not good quantum numbers. The potential must act on the symmetry properties of the wave function in only one of the space, spin, or isotopic spin subspaces if T, S, and Y are to be good quantum numbers.

It may be possible, nevertheless, to treat sufficiently small spin or isotopic spin-dependent potentials as a perturbation on the Majorana potential. Even though the potential is not small, if the space-symmetric interaction integrals, each multiplied by the appropriate eigenvalue of the interaction operator, are nearly the same they may be treated as the space-symmetric Majorana interaction split by small perturbations. Likewise for the two space antisymmetric interactions. Thus considering the three-eigenvalue $\boldsymbol{\sigma}\cdot\boldsymbol{\sigma}\boldsymbol{\tau}\cdot\boldsymbol{\tau}$ potential alone, although the $+1$ and $+9$ eigenvalues are so different, the $+9$ eigenvalue may have such a small interaction integral (because the two nucleons repel each other so greatly) that the eigenvalues times interaction integrals, $+1\cdot I_1$ and $+9\cdot I_9$, do not differ a great deal, especially if both are small in magnitude compared with $-3I_{-3}$. If $I_{+1}=9I_{+9}$, there is in effect no difference between the $\sigma\cdot\sigma\tau\cdot\tau$ potential and the Majorana potential.

If, however, I_{+1} and I_{+9} do not nearly satisfy this condition, it is incorrect to use the smallest possible T, S, and Y values, as for nucleons arranged in the maximum number of four-groups in Wigner's treatment. If $9I_{+9}>I_{+1}$ as seems reasonable, the configuration will favor having a smaller number of states with antisymmetry in all sub-spaces, and N_{+1} will increase at the expense of N_{+9} and N_{-3}. The actual average quantum

[8] J. Blatt, private communication. G. Racah has also pointed out that if the potential has sufficiently long range so that the whole wave-function is in a constant potential—i.e., not in a force-field—one may have good quantum numbers even with spin or isotopic spin dependent interactions added to a Majorana interaction.

numbers T, S, and Y will be larger than for the close packing in four groups. We will use the T, S, and Y as in the close-packed configuration, and look for a reasonable set of interaction integrals which emphasizes the odd-even neutron number differences in isobaric transitions in even nuclei. Then the actual steps in potential energy will probably be less odd-even dependent than those we compute, so we may have an upper limit to the improvement made.

The evaluation of the numbers of pairs corresponding to the three different eigenvalues of $\boldsymbol{\sigma}\cdot\boldsymbol{\sigma}\boldsymbol{\tau}\cdot\boldsymbol{\tau}$ is carried out in terms of the Majorana N_s and N_a. The results are

$$N_1^{\sigma\cdot\sigma\,\tau\cdot\tau}=\tfrac{1}{8}A(2A-5)+\tfrac{1}{4}(N_a-N_s)+\tfrac{1}{4}S(S+1)+\tfrac{1}{4}T(T+1), \quad (9)$$

$$N_{-3}^{\sigma\cdot\sigma\,\tau\cdot\tau}=N_s=\tfrac{1}{4}A(A-1)-\tfrac{1}{2}(N_a-N_s), \quad (10)$$

$$N_9^{\sigma\cdot\sigma\,\tau\cdot\tau}=\tfrac{3}{8}A+\tfrac{1}{4}(N_a-N_s)-\tfrac{1}{4}S(S+1)-\tfrac{1}{4}T(T+1). \quad (11)$$

It should be remembered that N_a-N_s is a function of A so that for large $AN_9^{\sigma\cdot\sigma\,\tau\cdot\tau}$ goes up quadratically with A as $A^2/32$, and $N_1^{\sigma\cdot\sigma\,\tau\cdot\tau}$ goes as $9A^2/32$.

The potential may now be put in the most general form (*) of a linear combination of ordinary $\boldsymbol{\sigma}\cdot\boldsymbol{\sigma}$, $\boldsymbol{\tau}\cdot\boldsymbol{\tau}$, and $\boldsymbol{\sigma}\cdot\boldsymbol{\sigma}\,\boldsymbol{\tau}\cdot\boldsymbol{\tau}$ potential operators and their respective interaction integrals. We will confine discussion here to a particular example of a pure $\boldsymbol{\sigma}\cdot\boldsymbol{\sigma}\,\boldsymbol{\tau}\cdot\boldsymbol{\tau}$ potential.

It should be pointed out here that the $\boldsymbol{\sigma}\cdot\boldsymbol{\sigma}\ \boldsymbol{\tau}\cdot\boldsymbol{\tau}$ potential just satisfies the "saturation" condition that in a very large nucleus in a collapsed state (i.e., $I_1=I_{-3}=I_9$) the potential energy has no negative (attractive) term in A^2. This may be seen from Eqs. (9), (10), and (11) since N_a-N_s goes as $+A^2/8$ and also would go as $T^2/2$ if T were large. In fact, the most negative potential energy in a large collapsed nucleus is just that of $A/4$ alpha-particles, $V=-(9/2)AI_{-3}$.

It will be shown in Sec. II, in first approximation, that the ratio of any space antisymmetric interaction integral to any space-symmetric interaction integral is roughly 0.37, thus letting $I_1=I_9=0.37I_{-3}$ where I is the interaction integral for $\boldsymbol{\sigma}\cdot\boldsymbol{\sigma}\,\boldsymbol{\tau}\cdot\boldsymbol{\tau}=1$, etc. Note that this is very probably an overestimate for the space-antisymmetric interaction integrals, especially for $I_{9,-3,-3}$, which corresponds to a very strong repulsion ($\lambda=+9$). For odd isobars this gives a potential energy change:

$$\Delta V^{\sigma\cdot\sigma\,\tau\cdot\tau}\doteq 0.94I_{-3}[T_<+4.88]. \quad (12)$$

For even isobars,

$$\Delta V^{\sigma\cdot\sigma\,\tau\cdot\tau}=0.94I_{-3}\begin{Bmatrix}T_<+8.0\\ T_<+1.8\end{Bmatrix}. \quad (13)$$

The upper line in curly brackets holds when a four-group is broken up by the transition, and the lower line when a three-group is broken up. With the same ratio of antisymmetric to symmetric interaction integrals the potential change for the Majorana case is, for odd isobars,

$$\Delta V^M=0.69I_s^M[T_<+5/2]. \quad (14)$$

For even isobars,

$$\Delta V^M+0.69I_s^M\begin{Bmatrix}T_<+4\\ T_<+1\end{Bmatrix}. \quad (15)$$

The $\boldsymbol{\sigma}\cdot\boldsymbol{\sigma}\,\boldsymbol{\tau}\cdot\boldsymbol{\tau}$ symmetry dependence thus increases the odd-even neutron excess dependence and at the same time reduces the magnitude of the step for a given interaction potential, since $3I_{-3}$ is equivalent to I_s^M.

Values of $A\cdot(12/5)I_{-3}=A\cdot\frac{1}{2}(I_s+I_a)$, a weighted average interaction integral computed from transitions between even isobars, using the choice of $\boldsymbol{\sigma}\cdot\boldsymbol{\sigma}\,\boldsymbol{\tau}\cdot\boldsymbol{\tau}$ potential with $I_1=I_9=0.37I_{-3}$, are plotted in Fig. 3(b). It is seen that the plot of $A(12/5)I_{-3}$ *vs* A is somewhat smoother than that of the corresponding $\frac{1}{2}(I_s^M+I_a^M)$ *vs* A, but still far from perfectly smooth. The values of the interaction integrals which we used make as much difference from the Majorana potential as may reasonably be accomplished, since I_9 is greatly emphasized in the example we chose, and N_9 gives the greatest odd-even neutron excess differences.

An admixture of a $-\boldsymbol{\tau}\cdot\boldsymbol{\tau}$ or a $+\boldsymbol{\sigma}\cdot\boldsymbol{\sigma}$ potential gives a trend in the same direction. These signs of the isotopic and ordinary spin interactions are opposite from the sense of the difference between singlet and triplet deuterons. A drastic reduction in the coefficient of the kinetic energy change makes some improvement in the smoothness in the plot of $\frac{1}{2}(I_s+I_a)$ *vs* A, but almost complete removal of the kinetic energy term is needed to improve the situation at high A, and simultaneously hurts the agreement at low A. Space-symmetry dependent terms in the kinetic energy have been shown by Feenberg[9] to be expressible as two-particle operators and thus essentially could be included in the choice of the relative magnitudes of Majorana interaction integrals.

c. Total Binding Energy

The quantity $\frac{1}{2}(I_s+I_a)$ for a Majorana interaction has been evaluated by Wigner[3] from the observed total binding energy of the nuclei by computing the total kinetic and coulomb energies. It is necessary to assume some additional relation between I_s and I_a, which we will take as a fixed ratio I_a/I_s independent of A. For the most stable nucleus of mass A (a hypothetical neutron excess $2\tau_A$), Eq. 1 becomes

$$\begin{aligned}V&=-N_sI_s+N_aI_a\\&=\left[(N_a-N_s)-(N_a+N_s)\frac{(1-I_a/I_s)}{(1+I_a/I_s)}\right]\tfrac{1}{2}(I_s+I_a)\\&=E-0.15A(A-2)A^{-\frac{1}{3}}+6\tau_A(A-\tau_A-1)A^{-1}\\&\qquad-14.1A-32\tau_A^2A^{-1}. \quad (16)\end{aligned}$$

[9] E. Feenberg, Phys. Rev. **70**, 768 (1946).

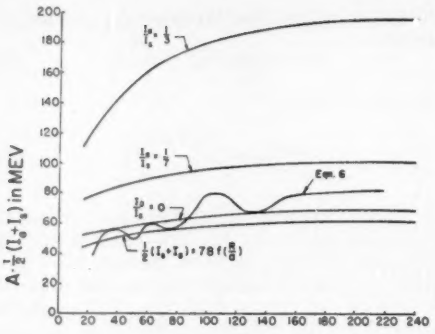

FIG. 4. A times average interaction integral *vs* A for various I_a/I_s, taken from total binding energy.

The predominant term in this expression is the part, $14.1A$, of the kinetic energy increasing linearly with the number of nucleons. The correction $-32\tau_A^2A^{-1}$ (because of the inequality of numbers of neutrons and protons) to the kinetic energy is unimportant. The binding energy E is computed from the packing fraction f by $E=-0.0931A(85.3-10^{-4}f+8\tau_A/A)$ Mev.

The values of $\frac{1}{2}(I_s+I_a)$ thus deduced are plotted for different ratios I_a/I_s as a function of A in Fig. 4. It is seen that the computed value $I_a/I_s=0.37$ requires $\frac{1}{2}A(I_s+I_a)$ to be many times the values calculated from the $p-p$ potential (to be discussed below) or taken from isobaric transitions. As Wigner noted, the ratio I_a/I_s must be $\frac{1}{10}$ or less to give values of $\frac{1}{2}A(I_s+I_a)$ computed from the total binding energy close to the values computed from isobaric transitions, and the slope of $\frac{1}{2}A(I_s+I_a)$ computed from the total binding energy is flatter. With $I_a/I_s=0$, there is the best agreement possible. No appreciable improvement even in the shape of the curve can be made by using a $\sigma\cdot\sigma\,\tau\cdot\tau$ potential no matter what relative magnitudes are assigned the three interaction integrals, so the best agreement for a $\sigma\cdot\sigma\,\tau\cdot\tau$ potential is also with $I_1=I_0=I_a=0$.

Our conclusion is as follows: to give a best fit to both isobaric transitions and total binding energies the best choice of interaction integrals for a $\sigma\cdot\sigma\,\tau\cdot\tau$ potential is indistinguishable from that for a Majorana potential; in both cases the antisymmetric interaction integrals must be very small.

III. CALCULATION OF INTERACTION INTEGRALS AND DISCUSSION OF STABILITY

The interaction integrals, which so far have been introduced as arbitrary parameters, may be estimated from the forces observed in proton-proton and neutron-proton scattering, and from observations of nuclear radii. If the same free particle model is taken as for the kinetic and coulomb energies, no new assumptions need be made.

1. The Wigner-Seitz computation of the first-order perturbation between the plane-wave-functions of Fermi particles in their lowest state in a very large volume Ω is well known;[10,11] the average probability density for a separation r_{ij} between a pair of nucleons is

$$\langle\Psi^*\Psi\rangle_{Av}=\frac{1}{\Omega^2}\left[1\pm9\left\{\frac{\sin k_0r_{ij}-k_0r_{ij}\cos k_0r_{ij}}{(k_0r_{ij})^3}\right\}^2\right]. \quad (17)$$

Here $k_0\cong\frac{3}{2}r_0$ is the maximum magnitude of the propagation vector of any nucleon of the four different types of $A/4$ nucleons each, in a volume $\Omega=(4\pi/3)Ar_0^3$. The upper sign corresponds to a space-symmetric interchange and the lower to antisymmetric. To obtain the average expectation value of the nuclear potential between pairs, the potential must be weighted by $\langle\Psi^*\Psi\rangle_{Av}$ and integrated over $d\Omega_1$ and $d\Omega_2$.

If we take the potential for the space-symmetric interaction as $V_0/(r/a)e^{-r/a}$, the symmetric interaction integral becomes

$$I_s=\frac{3V_0}{A}\left(\frac{a}{r_0}\right)^3\left[1+4\left(\frac{r_0}{a}\right)^2\int_0^\infty\left(\frac{\sin x-x\cos x}{x^3}\right)^2x\times\exp(-2r_0x/3a)dx\right]$$
$$=(3V_0/A)(a/r_0)^3[1+I], \quad (18)$$

where I is defined as the second term in the bracket. The expression for I_a is the same except for a minus sign before I.

If we assume charge independence of nuclear forces and take the singlet $p-p$ strength and range as basic, then $V_0=45.6$ Mev and $a=1.185\times10^{-13}$ cm. The dubious assumptions of this procedure are: (a) The apparent spin-orbit or spin-spin force in the triplet deuteron, evidenced also in magic number phenomena, is assumed to cancel out on the average in the binding energy of complex nuclei; (2) the sign of the potential is assumed to be negative at all distances. The exclusion of a strongly repulsive central region and an attractive tail, or of its inverse, the so-called "mermaid"[12] potential, is of course necessary to not only the following calculation of the potential energy but also the Fermi statistical calculation of the kinetic energy.

We note that the range a does not affect I_s as strongly as r_0 does, because V_0a^2 as derived from proton-proton scattering is approximately constant. The relative size of the symmetry-dependent term is a function of r_0/a

[10] F. Seitz, *Modern Theory of Solids* (McGraw-Hill Book Company, Inc., New York, 1940).

[11] This evaluation of the particle density has been given by Volz (to next-order terms) and is developed in L. Rosenfeld, Nuclear Forces, II (Inter-Science Publications, New York, 1949), p. 255, though it is not applied to the evaluation of the interaction integrals.

[12] Observed by J. R. Zacharias.

alone; for example, a decrease of 10 percent in r_0/a will increase I_a/I_s by about the same percentage.

Putting the singlet $p-p$ constants into Eq. (18), we get

$$AI_s \cong 78[1+0.46] = 114 \text{ Mev}. \quad (19)$$

For a Majorana potential, I_a would be given by the above expression with a minus sign before the second term

$$AI_a^M \cong 78[1-0.46] = 42 \text{ Mev}; \quad I_a^M/I_s^M = 0.37. \quad (20)$$

For a $\boldsymbol{\sigma}\cdot\boldsymbol{\sigma}\,\boldsymbol{\tau}\cdot\boldsymbol{\tau}$ potential [see Sec. II(b)], there are two types of antisymmetric interaction integrals, giving a weighted average of a strength of repulsive forces $\frac{3}{8}$ the magnitude of the V_0 used for the attractive forces, so that $\bar{I}_a^{\sigma\cdot\sigma\,\tau\cdot\tau} = \frac{3}{8} I_a^M$.

$$\begin{aligned} A\bar{I}_a^{\sigma\cdot\sigma\,\tau\cdot\tau} &\cong \tfrac{3}{8}\cdot 78(1-0.46) = 25 \text{ Mev}; \\ \bar{I}_a^{\sigma\cdot\sigma\,\tau\cdot\tau}/I_s^{\sigma\cdot\sigma\,\tau\cdot\tau} &= 0.22. \end{aligned} \quad (21)$$

The shape of the potential (subject to reservation 2 above) is not very important in determining the ratio I_a/I_s if its range and strength have been determined by proton-proton scattering. For example, a gaussian well gives very nearly the same results as a meson well;

$$I_s = (3\pi^{\frac{1}{2}}V_0/4A)(a/r_0)^3[1+0.42]; \quad I_a^M/I_s^M = 0.41. \quad (22)$$

2. We may attempt to correct the above calculation for the finite size of the nuclei. Proper normalization of the wave functions in a finite volume Ω would increase the computed I_a/I_s by the order of 10 percent for the lightest nuclei ($A\sim 20$) we are considering, and less for heavier nuclei.

More important is the effect of the finite size on the magnitude of the interaction integrals due to the contribution of the "tail" of the potential to the integration at distances of the order of a nuclear radius or more. This effect may be computed for a constant probability density (half-symmetric and half-antisymmetric) over a spherical nucleus and zero density outside, with

$$\langle \Psi^*_{\frac{1}{2}(s+a)} \Psi_{\frac{1}{2}(s+a)} \rangle_{Av} = 1/\Omega^2, \quad (23)$$

giving

$$\frac{I_s+I_a}{2} = \int_{r_1\le R}\int_{r_1\le R} \frac{V_0}{(|r_1-r_2|/a)} \times \exp(-|r_1-r_2|/a)\, d\,\mathrm{Vol}_1\, d\,\mathrm{Vol}_2. \quad (24)$$

Carrying out the integrations over the volume of the nucleus of radius $R = A^{\frac{1}{3}}r_0$ as indicated, we get

$$\tfrac{1}{2}(I_s+I_a) = (3V_0/A)(a/r_0)^3 f(R/a), \quad (25)$$

where

$$f\left(\frac{R}{a}\right) = 1 - \frac{3}{(R/a)^3}\left(1+\frac{R}{a}\right)e^{-R/a}\left(\frac{R}{a}\cosh\frac{R}{a} - \sinh\frac{R}{a}\right).$$

This function $f(R/a)$ rises as $\frac{1}{10}(R/a)^2$ from zero at $R/a=0$ and is asymptotic to unity, behaving as

$$f\left(\frac{R}{a}\right) \cong 1 - \frac{3}{2}\frac{(R/a)^2-1}{(R/a)^3}$$

at large R/a, giving the required saturation behavior. This expression for $\frac{1}{2}A(I_s+I_a)$ is plotted in Fig. 4 with the coefficient of $f(R/a)$ taken as 78 Mev as above. The shape of this function will be rather independent of the shape of the potential chosen, if the range a is taken as a fixed constant times $\langle r^2\rangle^{\frac{1}{2}}$ for each potential; e.g., for a meson potential $\langle r^2\rangle^{\frac{1}{2}} = 2.45a$ and for a gaussian $\langle r^2\rangle^{\frac{1}{2}} = 1.22a_G$, so that values of R/a, for a given R, are increased by approximately $(2.45/1.22)(1.185/1.776) = 1.34$ on going from a meson potential with $a_m = 1.185$ to a gaussian with $a_G = 1.776$. The meson potential thus exhibits more tail as far as saturation effects are concerned.

The first-order perturbation calculation of the interaction energy, including the full correction for the finite size of the nucleus, should serve as a lower limit to the magnitude of the potential energy. The approximate potential energy thus calculated is given by the expressions,

$$\begin{aligned} V^M &= N_s I_s + N_a I_a = \tfrac{3}{16}A^2[(-114/A)f(R/a)] \\ &\quad + \tfrac{5}{16}A^2[(+42/A)f(R/a)], \end{aligned} \quad (26)$$

$$V^M/A = -8.3 f(R/a) \text{ Mev}$$

or, for a $\boldsymbol{\sigma}\cdot\boldsymbol{\sigma}\,\boldsymbol{\tau}\cdot\boldsymbol{\tau}$ potential where I_a is the average antisymmetric interaction integral,

$$\begin{aligned} V^{\sigma\cdot\sigma\,\tau\cdot\tau} &= N_s I_s + N_a I_a \cong \tfrac{3}{16}A^2[(-114/A)f(R/a)] \\ &\quad + \tfrac{5}{16}A^2[(25/A)f(R/a)], \end{aligned} \quad (27)$$

$$V^{\sigma\cdot\sigma\,\tau\cdot\tau}/A = -13.6 f(R/a) \text{ Mev}.$$

It should be remembered that the above calculation of the average interaction integral $\frac{1}{2}(I_s+I_a)$ should be considerably better in this approximation than either I_s or I_a.

3. An adequate discussion of higher order terms in the perturbation calculation is difficult. Euler[13] has calculated the binding energy per particle for nucleons in very large volume, starting with plane wave functions, and using a gaussian interaction. His calculation is probably an overestimate of the binding energy, since it computes second-order terms in the perturbation treatment of the binding energy (the calculation of still higher terms would be extremely difficult) without renormalizing the zeroth order wave function to first order.

Furthermore, Euler's calculation was for an infinite fluid and the interaction integrals are therefore overestimated and each should be corrected by the factor $f(R/a)$ computed above. For reasonable values of a the second-order perturbation terms are therefore even

[13] H. Euler, Z. Physik **105**, 553 (1937).

TABLE II. First stability condition for Meson-shape potential.

1	2	3	4	5	6	7
Type	A	$\frac{2K+C}{V_{\text{theor}}}$	$\frac{2K+C}{V_{\text{obs}}}$	$\frac{R}{a}\frac{f'(R/a)}{f(R/a)}$	$g(r_0/a)$	$-3+$Col. 6 $+$Col. 5
$\sigma\cdot\sigma\tau\cdot\tau$	16	−3.6	−1.3	0.5	0.7	−1.8
	200	−2.6	−1.2	0.26	1.0	−1.8
P^{13}	16	−5.8	−1.3	0.5	1.0	−1.5
	200	−4.3	−1.2	0.2	2.9	+0.1

more overestimated than the first-order terms. With a $\sigma\cdot\sigma\,\tau\cdot\tau$ potential Euler's first-order term should vanish entirely in the limit of very large a/r_0. The question of the convergence of the higher terms, which Euler did not consider, was discussed by Wigner and is reviewed in Rosenfeld's recent book.[11]

The binding energy calculated by substituting the values $V_G=31.6$ Mev, $a_G=1.776\times10^{-13}$ in

$$V=\sigma^1\cdot\sigma^2\,\tau^1\cdot\tau^2 V_G\exp(-r_{12}/a_G)$$

into Euler's expression is approximately zero rather than the 10 Mev per nucleon[14] it should be to fit the experimental data. We may conclude that a gaussian or square potential of the strength observed in $p-p$ scattering, with $\sigma\cdot\sigma\,\tau\cdot\tau$ spin and charge dependence, cannot alone account for nuclear binding energies in heavy nuclei. An increase of strength V_G of 60 percent would be necessary to get the observed binding energies by Euler's formula, and correcting for the finite size of the nucleus would require an increase of 100 percent for the heaviest nuclei and more for the lighter ones.

A Majorana exchange nature of the potential would make the total energy positive, and as we saw in Sec. II a $\sigma\cdot\sigma\,\tau\cdot\tau$ exchange nature is the most attractive allowed by the usual saturation requirements.

If no interaction between nucleons in space-antisymmetric states is taken, the binding energy is given adequately by the calculation of paragraph 2. Even admitting $\sigma\cdot\sigma\,\tau\cdot\tau$ interaction between unlike nucleons, but no interaction between like nucleons in space antisymmetric states, would give an adequate binding energy. These choices would, of course, be in violation of the usual saturation requirements.

Since it is so difficult to estimate the effect of higher terms, especially in a nucleus of finite radius with a finite number of particles, it cannot be said definitely whether the potential observed in $p-p$ scattering is insufficient to give the observed binding of heavy nuclei. It should be noted that a continuation to higher terms of the calculation of the interaction between a typical pair of nucleons in a large volume will give no binding even for a space-symmetric wave function, since this is just $p-p$ scattering, for which this potential does not give a bound state. Even four nucleons in the same space state in an infinite volume (the α-particle) have a binding energy of only 8 Mev per nucleon. Nevertheless, it is conceivable that the many-particle wave-function may be distorted in such a way as to give very large attractive interactions between many nucleons and to reduce the magnitude of the more numerous repulsive interactions, and at the same time not increase the kinetic energy as much as the potential is decreased.

4. The interaction integrals calculated in 2 should, if correct, give stability of nuclei at the observed radius $R=A^{\frac{1}{3}}r_0$. Setting the first derivative of the total energy with respect to R, at constant A, equal to zero, we get (using Eqs. 1 and 26 or 27 and defining I as the second term in the square bracket in Eq. 18),

$$\frac{2K+C}{V}=-3+\frac{R}{a}\frac{f'(R/a)}{f(R/a)}+\frac{r_0}{a}\frac{dI}{d(r_0/a)}\left(\frac{1}{1-I^2}\right)\left(\frac{N_eI_e+N_oI_o}{N_eI_e-N_oI_o}-I\right)\equiv-3+\frac{R}{a}\frac{f'(R/a)}{f(R/a)}+g\left(\frac{r_0}{a}\right). \quad (28)$$

In the case of the $\sigma\cdot\sigma\,\tau\cdot\tau$ potential, this stability condition specializes, for large A, to approximately

$$\frac{2K+C}{V}=-3+\frac{R}{a}\frac{f'(R/a)}{f(R/a)}+\frac{(r_0/a)}{I}\cdot\frac{dI}{d(r_0/a)}. \quad (29)$$

In these expressions the term on the left is the negative of the change of kinetic energy with logarithm of radius, $-2K$, plus that of the coulomb energy, $-C$, normalized to the potential energy V. The first term on the right is the fractional change in the potential energy due to a uniform dilation; the second is the correction due to changing surface effects; and the third is the correction due to the changing relative magnitudes of symmetric and antisymmetric interaction integrals on dilation of the wave function.

Values of these three terms are given for Majorana and $\sigma\cdot\sigma\,\tau\cdot\tau$ potentials in Table II for two values of the mass A. $A=16$ is an extreme case where the number of symmetric interaction integrals equals the number of antisymmetric integrals. The case for large A ($A=200$) is much more typical. It is seen that for reasonable values of R/a the surface effects contribute only slightly to the stability, but that the change of the interaction integrals with density gives an appreciable effect. If $(2K+C)/V$ is taken from the previous theoretical expressions for kinetic, coulomb, and potential energies, stability would occur only at much larger radii than observed because of the small magnitude computed for the potential energy. On the other hand, if the ratio $(2K+C)/-V$ is taken from the observed binding energy and from the theoretical expressions for the kinetic and coulomb energies (but not the potential

[14] Euler's expression does not include the coulomb energy, necessitating a binding energy in his expression of ~10 Mev for heavy nuclei instead of ~8 Mev.

energy V) we have used, the computed V is such that $(2K+C)/V$ is not more than 1.3, and for large A the nucleus would have an r_0 of the order of 0.6×10^{-13} for a $\sigma\cdot\sigma\,\tau\cdot\tau$ force and of the order of 1.4×10^{-13} cm for a Majorana force.[15] A gaussian shape potential will improve the situation for the $\sigma\cdot\sigma\,\tau\cdot\tau$ force only slightly.

If no interaction is taken between like nucleons in antisymmetric states, along with $\sigma\cdot\sigma\,\tau\cdot\tau$ interaction or no interaction between unlike nucleons, stability will be achieved only by the finite number of nucleons all coming within approximately one range of force, i.e., $R\sim a$, unless a potential is postulated with no attraction or even a repulsion at distances of the order of a for symmetric states also.

The result is essentially that any potential strong enough to give the observed binding energy, unless it is repulsive at short distances, causes the nucleus to collapse to a much smaller radius than observed[16] whereas a potential which accounts for stability at approximately the observed radius does not give an appreciable binding energy. It is difficult to anticipate that in a large nucleus any reasonable central potential can give even the minimal kinetic energy and coulomb energy and observed binding energy required by the uniform model, and also give the observed radius, and still have the effective range and (especially difficult) the strength given by low-energy singlet $p-p$ scattering.

IV. CONCLUSIONS

1. The uniform model cannot be improved appreciably by the substitution of a more general potential for the Majorana potential. With the Majorana potential the change in binding energy is isobaric transitions for odd nuclei fits in fairly well with the location of the valley of stable nuclei. But for even nuclei—and this is a much more critical test of the uniform theory—there is considerable disagreement between theory and experiment. No reasonable choice of the potentials we have considered appears to subsume completely the trends in binding energies of different homologous groups into a single statistical model. Furthermore, no choice can even minimize the disagreement in isobaric transitions without widening greatly the discrepancy between theory and experiment in the total binding energy. The choice of interaction integrals giving the best fit to almost all experimental data is such that pairs of nucleons with a repulsion between them (space-antisymmetric) must be so far apart that they give only a very small contribution to the potential energy. In this extreme the $\sigma\cdot\sigma\,\tau\cdot\tau$ and Majorana forces approach each other, because no use can be made of the different weights of the two repulsive eigenvalues of the $\sigma\cdot\sigma\,\tau\cdot\tau$ operator.

2. The relative magnitude of space-symmetric and space-antisymmetric interaction integrals, $I_a/I_s\cong0.37$ computed by the Wigner-Seitz method, is not small enough to fit in with the preceding conclusion if the range of forces is taken from low-energy $p-p$ scattering.

The absolute magnitude and the A-dependence of the interaction integrals computed for a diffuse sphere of nuclear matter are in reasonable agreement with the values of the interaction integrals estimated from the total binding energy of nuclei, provided that the space-antisymmetric interaction integrals are negligibly small.

The conditions for stability at the observed radius are satisfied only with appreciable space-antisymmetric interaction integrals (at least in this first-order calculation).

3. The assumptions of this model—especially constant density of nuclear matter; fairly well defined nuclear radius; Fermi kinetic energy; neglect of tensor, velocity dependent, and many-body forces; equality of all interaction integrals of the same symmetry type—are not tested conclusively by the limited qualitative success of the uniform theory.

V. ACKNOWLEDGMENTS

Grateful thanks are due to Professor V. F. Weisskopf, who suggested many of these ideas but is not to be held responsible for their execution; also to Professors J. M. Blatt and E. Feenberg for very helpful discussions, and to Miss I. Goldin for use of her compilation of experimental results on energies released in isobaric transitions.

[15] The condition on the second derivative, $d^2E/dR^2>0$, gives

$$\frac{4K+C}{-V}>12+\frac{R}{a}\frac{F'(R/a)}{F(R/a)}\left[-6+2g\left(\frac{r_0}{a}\right)\right]+\left(\frac{R}{a}\right)^2\frac{F''(R/a)}{F(R/a)}$$
$$-7g(r_0/a)+g^2(r_0/a)+g'(r_0/a),$$

where $g(r_0/a)$ is the last term on the right in Eq. (28) or Eq. (29). If $g(r_0/a)$ were large enough to satisfy the stability condition of Eq. (28) it would also cause the inequality of Eq. (30) to be satisfied.

[16] This is the same conclusion reached by Bethe and Bacher (Revs. Modern Phys. 8, 82 (1936)) using essentially a special case of the same method.

Microwave Spectroscopy in the Region from Two to Three Millimeters, Part II*

CHARLES M. JOHNSON, RALPH TRAMBARULO, AND WALTER GORDY
Department of Physics, Duke University, Durham, North Carolina
(Received July 30, 1951)

Precise frequency measurements on rotational transitions occurring in the wavelength range from 2 to 3 mm for a number of molecules have been made. From these, centrifugal stretching effects have been determined and accurate values of the rotational constants obtained. A table including all frequencies so far measured in this region of the spectrum is given.

INTRODUCTION

THE present work is a continuation of a program[1] which has been underway in this laboratory for the past four years to extend the range of accurate radiofrequency methods of spectroscopy to wavelengths shorter than 5 mm (frequencies above 60,000 Mc/sec). This is the second of the papers to report precision measurements in the region from two to three millimeters. In the first paper, measurements on the rotational line of carbon monoxide at 115,270.56 Mc/sec were reported. The present work extends the measurements to a large number of other molecules and extends the range of precise frequency measurements to 130,000 Mc/sec—a frequency 26,000 times the 5 Mc/sec WWV frequency used as a monitoring standard. An accuracy of 3 parts in 10^6 is maintained in these measurements.

One of the advantages which the high frequency millimeter-wave spectroscopy has over that in the centimeter-wave region is the more accurate determination of centrifugal distortion effects of molecular rotation. For example, the third rotational line of ICN occurring at 1.5 cm wavelength is displaced only 0.095 Mc/sec, by centrifugal distortion, whereas the twentieth line at 2.3 mm wavelength is displaced 28 Mc/sec. The evaluation of these effects in some relatively simple molecules which will allow a critical testing of existing theories of molecular distortions and the establishment of secondary spectrum line frequency standards in this newly explored region are the primary purposes of the present investigation. Furthermore, when the rotational lines of a given molecule which occur in the region from 2 to 3 mm wavelength are accurately fitted to a formula, this formula can then be used to compute the positions of lines at still higher frequencies, even in the far infrared region, with sufficient accuracy for use as secondary frequency standards. For example, the centrifugal stretching constant, D_J, of N_2O is known from the present work to an accuracy of 0.05 kc/sec, and the B_0 value is known to an accuracy of 25 kc/sec. The rotational lines occurring at 100 microns (0.1 mm) wavelength can be computed to an accuracy of one part in 10^4. If microwave measurements were made only in the K-band region (1 cm), the centrifugal stretching effects could not be evaluated, and the rotational lines at 100 microns could be calculated to an accuracy of one part in 10^2 only. At one millimeter wavelength the N_2O rotational lines can be computed to an accuracy of three parts in 10^6, taking into account the centrifugal stretching information, or to one part in 10^4 without this information.

EXPERIMENTAL

Some descriptions of the methods and instruments are given in the earlier reports mentioned.[2] The principal difference in the present work is that fourth and fifth harmonic energy (third and fourth overtones) from silicon crystals driven by K-band klystrons was used almost exclusively, whereas in the previous measurements the second and third harmonics (first and second overtones) were employed. Because of the greater power output of the K-band tubes, approximately the same power in the region from 2 to 3 millimeters can be obtained from a higher harmonic of these tubes as from a lower harmonic of available millimeter wave tubes. Also, the use of K-band tubes as drivers for the multipliers considerably simplifies the problem of frequency measurement, since in the K-band region such strong markers are obtainable from the frequency standard that only a small fraction of the oscillator power need be used to "beat" with the markers. Thus, most of the power is reserved for driving the source multiplier.

RESULTS

Table I lists all spectral lines so far measured in the region from 2 to 3 mm wavelength. All except those for CO and O_2 are new measurements. For the sake of completeness those of the latter molecules are repeated from the previous papers.[1] In the same table are given molecular constants computed from the present data and those of lower transitions measured previously by others.

Linear Molecules

The rotational frequencies for linear molecules in the ground vibrational and ground electronic states are

* The research reported in this paper has been sponsored by the Geophysical Research Directorate of Air Force Cambridge Research Laboratories.

[1] Smith, Gordy, Simmons, and Smith, Phys. Rev. **75**, 260 (1949); Gilliam, Johnson, and Gordy, Phys. Rev. **78**, 140 (1950); Anderson, Johnson, and Gordy, Phys. Rev. **83**, 1061 (1951).

[2] Further details will appear in the Proc. N. Y. Acad. Sci.

given by the theoretical formula,[3]

$$\nu = 2B_0(J+1) - 4D_J(J+1)^3, \quad (1)$$

where $B_0 = h/8\pi^2 I_B{}^0$ and D_J is the constant which depends upon centrifugal stretching. By combining our results with the measurements on N_2O and OCS made at lower frequencies by others, one can check the accuracy of this formula. No higher order terms had to be included for present accuracy and range of frequencies. The values of B_0 and D_J determined from the observed frequencies are given in Table I.

For diatomic molecules or for symmetric, linear, XYZ triatomic molecules, D_J can be computed very accurately from Kratzer's formula[4]

$$D_J = 4B_0{}^3/\omega^2, \quad (2)$$

where ω is the fundamental stretching vibrational frequency. If the linear triatomic molecule is of the form XYZ, there are two fundamental stretching frequencies, ω_1 and ω_3, and Kratzer's formula no longer applies. However, our results indicate that it can still be used to obtain the D_J to a first approximation if the lower of the two fundamental bond-stretching frequencies is used (see also Herzberg and Spinks[5]).

A. H. Nielsen has derived the expression,[6]

$$D_J = 4B_0{}^3(\xi^2{}_1/\omega_1{}^2 + \xi^2{}_3/\omega_3{}^2), \quad (3)$$

which applies explicitly to the linear XYZ molecule, where ω_1 and ω_3 are the two fundamental vibrational frequencies which correspond to stretching of the molecule, and ξ_1 and ξ_3 are constants which weight each stretching frequency. The present experimental evaluation of D_J's with the known vibrational frequencies provides a test of Nielsen's equation. The results are shown in Table II along with values estimated with the simple approximation of Kratzer's formula and only the lower fundamental stretching frequency.

Symmetric-Top Molecules

The rotational frequencies of a symmetric-top molecule in the ground vibrational and the ground electronic state are given by the formula,[7]

$$\nu = 2B_0(J+1) - 2D_{JK}(J+1)K^2 - 4D_J(J+1)^3, \quad (4)$$

where $B_0 = h/8\pi^2 I_B{}^0$ and D_{JK} and D_J are coefficients of distortion for the rotational motions described by the molecule. Like Eq. (1), this formula was found to hold within the accuracy of the measurements. Table I lists the values of the three constants, B_0, D_J, and D_{JK}, as determined from the observed frequencies.

TABLE I. Observed transitions and resulting values of B_0, D_J, and D_{JK} in the region from 2 to 3 mm wavelength.

Molecule and transition	Measured frequency Mc/sec	D_J kc/sec	D_{JK} kc/sec	B_0 Mc/sec	Ref.
O_2					
$J=0\rightarrow1$					
$K=1$	118,745.5 ±0.3				(a)
$C^{13}O^{16}$					
$J=0\rightarrow1$	115,270.56±0.25			57,635.66	(b)
$C^{12}O^{18}$					
$J=0\rightarrow1$	110,201.1 ±0.4			55,100.90	(b)
$O^{16}C^{12}S^{34}$					
$J=7\rightarrow8$	97,301.31±0.20	1.27±0.05		6081.494	
$J=9\rightarrow10$	121,624.79±0.25				
$N_2{}^{14}O^{16}$					
$J=3\rightarrow4$	100,491.76±0.25	5.75±0.05		12,561.66	
$J=4\rightarrow5$	125,613.68±0.30				
$PO^{16}F_3$					
$J=9\rightarrow10$					
$K=0$	91,881.24±0.20				
$K=3$	91,880.95±0.20				
$K=5$	91,880.50±0.40				
$K=6$	91,880.34±0.30				
$K=7$	91,879.96±0.25				
$K=8$	91,879.58±0.30				
$K=9$	91,879.20±0.40				
$PO^{16}F_3$					
$J=10\rightarrow11$					
$K=0$	101,068.35±0.30	1.10±0.05	1.25±0.05	4504.282	
$K=3$	101,068.04±0.20				
$K=5$	101,067.62±0.40				
$K=6$	101,067.33±0.20				
$K=7$	101,066.91±0.20				
$K=8$	101,066.52±0.20				
$K=9$	101,066.06±0.20				
$J=12\rightarrow13$					
unresolved	119,441.32±0.45				
$J=13\rightarrow14$					
unresolved	128,535.60±0.20				
$C^{13}H_3F$					
$J=1\rightarrow2$					
$K=0$	102,142.62±0.20	32.5	443	25,535.91	
$K=1$	102,140.85±0.20				
$C^{13}D_3F$					
$J=2\rightarrow3$					
$K=0$	122,695.50±0.30				
$K=1$	122,694.20±0.30	32.5[c]	228±8	20,449.83[c]	
$K=2$	122,690.02±0.30				
$N^{14}F_3$					
$J=4\rightarrow5$					
$K=0$	106,805.93±0.20				
$K=2$	106,804.54±0.50	14.2	−25.7	10,681.072	
$K=3$	106,803.62±0.20				
$PS^{32}F_3$					
$J=22\rightarrow23$					
$K=0$	122,237.90±0.30				
$K=5$ or 6	122,235.80±0.30				
$K=9$	122,231.30±0.30	0.30±0.05	1.8±0.07	2657.663	
$K=12$	122,225.50±0.30				
$K=15$	122,219.00±0.30				
$C^{12}H_3C^{13}C^{12}H$					
$J=6\rightarrow7$					
$K=0$	119,637.90±0.30				
$K=1$	119,635.95±0.30				
$K=2$	119,628.50±0.50				
$K=3$	119,617.00±0.20	2.12	164±2	8345.87	
$K=4$	119,601.06±0.20				
$K=5$	119,580.50±0.20				
$K=6$	119,555.62±0.20				
PF_3					
$J=7\rightarrow8$					
$K=0$	125,108.89±0.20				
$K=3$	125,105.60±0.20				
$K=4$	125,106.85±0.25	7.5±0.1	−11.7±0.1	7820.01	
$K=5$	125,108.60±0.20				
$K=6$	125,110.64±0.30				

[a] Anderson, Johnson, and Gordy (to be published).
[b] Gilliam, Johnson, and Gordy, Phys. Rev. 78, 140 (1950).
[c] Obtained from these data and the $J=0\rightarrow1$ transition at 40,890.54 mc measured by one of us (R.F.T.).

[3] G. Herzberg, *Infrared and Raman Spectra of Polyatomic Molecules* (D. Van Nostrand Company, Inc., New York, 1945), p. 19.
[4] A. Kratzer, Z. Physik 3, 289 (1920).
[5] G. Herzberg and J. W. T. Spinks, Proc. Roy. Soc. (London) 147, 434 (1934).
[6] A. H. Nielsen, J. Chem. Phys. 11, 160 (1943); H. H. Nielsen, Phys. Rev. 78, 296 (1950).
[7] See reference 2, p. 31.

TABLE II. Centrifugal distortion constants D_J for linear XYZ molecules.

Molecule	D_J (kc/sec) Obs.	Calc.[a] Kratzer's approx.[b]	Nielsen's formula[c]
OCS	1.27±0.05	1.35	1.32
N_2O	5.75±0.05	5.21	4.83
$Br^{79}CN$	0.91±0.09[d]	0.92	0.85
$Br^{81}CN$	0.81±0.09[d]	0.91	0.83

[a] The fundamental frequencies and force constants used in these calculations were taken from G. Herzberg, *Infrared and Raman Spectra of Polyatomic Molecules* (D. Van Nostrand Company, Inc., New York, 1945), p. 174, with the exception of those for N_2O which are given by W. S. Richardson and E. B. Wilson, Jr., J. Chem. Phys. **18**, 694 (1950).
[b] See reference 3.
[c] See reference 5.
[d] J. W. Simmons and W. E. Anderson, Phys. Rev. **80**, 338 (1950).

TABLE III. Comparison of calculated and observed centrifugal distortion constants, D_J for the methyl halides and methyl acetylene.

Molecule	D_J (kc/sec) Obs.	Calc.[a] Kratzer's approx.[b]
CH_3F	32.5	67.0
CH_3Cl	26.4[c]	19.5
CH_3Br	11.1[c]	10.4
CH_3I	7.95[c]	6.6
CH_3CCH	3.12	3.24

[a] The values of the stretching frequencies used for the calculations were taken from G. Herzberg, *Infrared and Raman Spectra of Polyatomic Molecules* (D. Van Nostrand Company, Inc., New York, 1945), pp. 315 and 338.
[b] See reference 3.
[c] J. W. Simmons and W. E. Anderson, Phys. Rev. **80**, 338 (1950).

Pyramidal XY_3 Molecules

Phosphorus trifluoride and nitrogen trifluoride are pyramidal oblate ($I_A > I_B$) symmetric-top molecules. The moment of inertia I_B for an XY_3 pyramidal symmetric top is given by

$$I_B = \frac{3M_Y d_{ZY}^2}{2(1+3M_Y/M_X)}[2-(1-3M_Y/M_X)\sin^2\beta],$$

where M_Y and M_X are the masses of the atoms Y and X and β is the angle between the XY internuclear axis and the figure axis. It is readily seen that I_B increases with an increase in β when $3M_Y/M_X > 1$, and decreases with an increase in β when $3M_Y/M_X < 1$. For both NF_3 and PF_3, I_B increases with an increase in β. An increase in the angular momentum $Kh/2\pi$ about the symmetry axis should increase β and should also stretch the XY bond, both of which would increase I_B. However, as K increases, the component of angular momentum N which is perpendicular to K must decrease for a given J. A decrease in N tends to decrease I_B. The observed lines of a given J transition fall to higher frequency with increasing K. (D_{JK} is negative.) Therefore the net effect of increasing K and decreasing N is to decrease I_B.

X_3YZ Symmetric-Top Molecules

From infrared spectral constants Slawsky and Dennison[8] predict negative values of D_{JK} for the methyl halides. Earlier microwave measurements[9] in this laboratory revealed that D_{JK} is positive in the methyl halides as well as in a large number of molecules such as CH_3F, CD_3F, POF_3, PSF_3, and CH_3CCH investigated here.

By a partial differentiation of the expression for the moment of inertia I_B with respect to β (the acute angle between the bond XY and the symmetry axis), it is seen that I_B decreases as β increases. In the methyl halides both an increase in K and the accompanying decrease in the component of momentum perpendicular to K tend to increase β and hence should decrease I_B. Since the opposite effect is observed, it is apparent that the change in bond lengths must also be considered. The surprising implication is that the stretching of the CH bonds more than compensates for the bond-bending effects. Simmons and Anderson[8] suggest that the unexpected sign of D_{JK} in the methyl halides indicates considerable lengthening of the CH bonds.

In POF_3 the center of gravity if between the plane of the F atoms and the P. In this case, the increase in K tends to increase β as before, but now the associated decrease in N lowers β, and the two effects on I_B are opposed. D_{JK} is small and positive. Hence, the two effects are almost balanced. In PSF_3 the center of gravity is near the central atom P, and again D_{JK} is small and positive.

No very satisfactory theory is available for calculating the stretching constant D_J from the vibrational frequencies of the symmetric-top molecule, as can be done for diatomic or linear triatomic molecules. It was shown by Simmons and Anderson that the D_J's calculated by Slawsky and Dennison for the methyl chloride, bromide, and iodide differ by a factor of about ten from the observed value, although they have the correct sign. The agreement in the value for methyl fluoride is much better but still differs by a factor of about 2.

We have applied the simple Kratzer formula (2) to the methyl halides with ω taken as the normal vibrational frequency ω_1 for which the nuclear displacement most nearly corresponds to those of centrifugal stretching for end-over-end motion. This is the mode which represents essentially the stretching of the C—Hal bond. The results are shown in Table III. The agreement with observation is fairly good except for the fluoride. Also included in this table is CH_3CCH, with ω taken as $\omega_5 = 926$ cm^{-1}, the normal frequency which most nearly approximates the motion for end-over-end centrifugal stretching.

We wish to thank Dr. John Sheridan, who prepared the samples of NF_3, POF_3, and PSF_3 used in these measurements.

[8] Z. I. Slawsky and D. M. Dennison, J. Chem. Phys. **7**, 509 (1939).
[9] Gordy, Simmons, and Smith, Phys. Rev. **74**, 243 (1948); J. Simmons and W. E. Anderson, Phys. Rev. **80**, 338 (1950).

Theoretical Spectra of Luminescent Solids

FERD E. WILLIAMS AND MALCOLM H. HEBB
General Electric Research Laboratory, Schenectady, New York
(Received September 17, 1951)

From the potential energy curves for the ground and excited states of the thallium activator in potassium chloride, the absorption spectrum of this phosphor is calculated by direct evaluation of the matrix elements for electronic transitions between the individual vibrational levels of the initial and final states. Harmonic oscillator wave functions in the initial state and wave functions for a linear potential in the final state are used. The results verify the classical and semiclassical spectra previously reported, and provide a new insight into the application of the Franck-Condon principle to solid-state luminescence.

I. INTRODUCTION

IN a recent publication,[1] a fundamental calculation of the absorption and emission spectra of potassium chloride activated with thallium has been reported. The calculation yields the potential energy curves shown in Fig. 1 for the unexcited and excited Tl^+. The abscissa is the configurational coordinate of the system and is taken as the distance between the Tl^+ ion and its nearest Cl^- neighbors. The energies are calculated with the condition that the remainder of the lattice assumes the configuration of minimum potential energy for each value of the configurational coordinate. The curves are accurately parabolic, and the classical formula for absorption or emission spectrum can be written:

$$P(\epsilon)=(K/2\pi kT)^{\frac{1}{2}}\exp(-Kq^2/2kT)(dq/d\epsilon), \quad (1)$$

where q measures the displacement in coordinate a from the minimum for the initial state, ϵ is the difference between the two potential energy curves at q, and K is the force constant for the initial state. According to the Franck-Condon principle ϵ is the energy absorbed or emitted in the transition. In Eq. (1) the exponential measures the probability of the system having a displacement q in the initial state and the final factor is a Jacobian to take account of the change of variable from q to ϵ. The spectra computed at 80°K and 298°K by Eq. (1) were found to be in satisfactory agreement with experiment.

II. SEMICLASSICAL CALCULATION OF SPECTRA

The spectrum (1) will be in serious error at low temperatures where only a few vibrational levels* of the initial state are occupied. In particular at $T=0$, Eq. (1) narrows to a sharp line, whereas the quantum mechanical zero-point energy will insure a finite breadth. In a subsequent note,[2] therefore, the classical distribution in the initial state was replaced by the quantum-mechanical sum over the vibrational levels:

$$\rho(q)=\sum_i[\psi_i(q)]^2e^{-(2i+1)\theta/T}, \quad (2)$$

where $k\theta=h\nu/2$ is the zero-point energy, and $\psi_i(q)$ is the normalized wave function for the harmonic oscillator in the ith vibrational level at the displacement q and can be expressed in terms of the polynomial proposed by Hermite.[3] To obtain the semiclassical spectrum the exponential factor of (1) is replaced by (2), and a suitable change made in the normalization constant. Owing to the properties of the Slater sum (2) for the harmonic

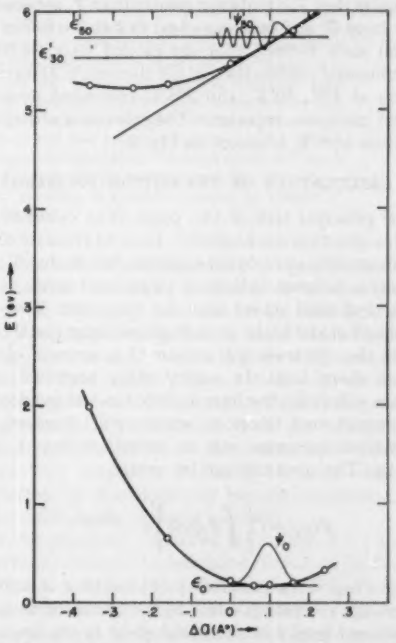

FIG. 1. Potential energy *versus* configuration coordinate plot including representative vibrational wave functions for the thallium-activated potassium chloride phosphor.

[1] F. E. Williams, J. Chem. Phys. 19, 457 (1951).

* *Note added in proof:*—The harmonic oscillator model follows from the assumption that the normal modes of motion which involve appreciable changes in the potential energy of the activator system are approximated by an Einstein distribution of frequency $2k\theta/h$.

[2] F. E. Williams, Phys. Rev. 82, 281 (1951).

[3] Eyring, Walter, and Kimball, *Quantum Chemistry* (John Wiley and Sons, Inc., New York, 1944), p. 75.

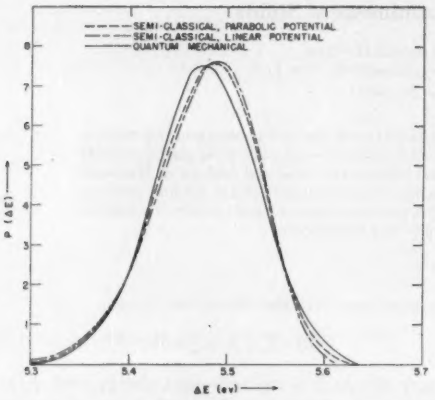

FIG. 2. Theoretical absorption spectrum of thallium-activated potassium chloride.

oscillator[4] this change is equivalent to replacing T in Eq. (1) by an effective temperature:

$$T_{eff}=\theta \coth(\theta/T).$$

One notes that T_{eff} is always greater than T, approaches T for large T, and becomes equal to θ at $T=0$. For the ground state $\theta=96°$K; for the excited state $\theta=60°$K. Experimental confirmation of the theoretical absorption spectra at 4°K, 80°K, and 298°K computed semiclassically[2] have been reported.[5] The calculated absorption spectrum at 0°K is shown on Fig. 2.

III. CALCULATION OF TRANSITION PROBABILITY

The principal task of this paper is to calculate the spectra quantum mechanically. Thus, to evaluate either the absorption or emission spectrum the probability of transition between individual vibrational levels of the initial and final states must be computed. With the simplified model based on a single configurational coordinate the spectrum will consist of a series of closely spaced sharp lines. In reality other neglected coordinates will cause the lines to broaden and overlap. In the present case where no structure is observed, the theoretical spectrum will be smoothed into a continuum. The spectrum can be written:

$$P(\epsilon_{if})=C\left[\int \psi_i\psi_f dq\right]^2 e^{-(2i+1)\theta/T}, \qquad (3)$$

where $P(\epsilon_{if})$ is the probability of absorbing or emitting the energy ϵ_{if} corresponding to the transition from the vibrational level i of the initial state to the level f of the final state. The functions ψ_i and ψ_f are the vibrational wave functions for the initial and final levels. The dependence of the transition probability on the electronic wave functions and on the operator for the electronic transition is the same irrespective of the vibrational quantum numbers i and f and is included in the constant C. The exponential of Eq. (3) weights the spectrum according to the occupation probability of the vibrational levels of the initial state.

A serious problem arises in the evaluation of Eq. (3) because transitions occur to high vibrational levels in the final state. In fact, the most probable final levels are $f=41$ for absorption and $f=67$ for emission. Hermite polynomials of this order are not available in tabulated form and their computation would involve enormous labor. Therefore, a different approach is used: For evaluating Eq. (3) it is sufficient to know ψ_f in the region of configuration where ψ_i is appreciable. This region is clearly near the equilibrium configuration for the initial state since the kinetic energy of the initial state is always small. The parabolic potential energy function for the final state is, therefore, replaced by a linear potential tangent to the parabola at the equilibrium configuration for the initial state. The linear potential for absorption is shown on Fig. 1, and it is evident that the deviation from the parabola is small for a considerable range of a about $q=0$.

As a check on the validity of replacing the parabolic by the linear potential for the final state, the absorption spectrum at $T=0$°K was computed semiclassically using the linear potential. Incidentally, the semiclassical calculation in general is equivalent to substituting δ functions having nonzero values at the classical turning point for ψ_f in Eq. (3). Inspection of Fig. 2 reveals only a small difference in the semiclassical spectrum between the parabola and the tangent.

It is warranted, therefore, to evaluate ψ_f in Eq. (3) as wave functions corresponding to a linear potential. Stokes' equation must be satisfied:

$$d^2\psi/dx^2=x\psi, \quad \text{with} \quad x=q_1(2MF/\hbar^2)^{\frac{1}{3}}, \qquad (4)$$

where q_1 is the displacement in the final state measured from the intersection of the linear potential and the vibrational energy level, M is the effective mass of the oscillator, and F is the slope of the linear potential. Solutions to Eq. (4) have been tabulated in convenient form.[6] A typical vibrational wave function ψ_{30} for the excited state is shown in Fig. 1. The absorption spectrum according to Eq. (3) was computed numerically at $T=0$. The result plotted on Fig. 2 is in excellent agreement with the semiclassical spectrum. It is concluded that the spectra obtained previously by the

[4] G. E. Uhlenbeck and L. S. Ornstein, Phys. Rev. **36**, 823 (1930), Note II; see also K. Husimi, Proc. Phys.-Math. Soc. Japan **22**, 264 (1940).

[5] P. D. Johnson and F. J. Studer, Phys. Rev. **82**, 976 (1951).

[6] "Tables of the modified Hankel functions of order one-third and of their derivatives" (Harvard University Press, Cambridge, 1945). The required solution to Eq. (4) which approaches zero for large positive x is, apart from normalization:

$$\psi(x)=\sqrt{3}R[h_1(-x)]-I[h_1(-x)]$$

in the notation of this reference. This function, with reversed sign, is plotted there on p. XXIII.

classical[1] and semiclassical[2] methods would be only slightly altered by the strictly quantum mechanical treatment according to Eq. (3).

IV. FRANCK-CONDON PRINCIPLE

The direct evaluation of the matrix elements for transitions between individual vibrational levels of the initial and final states provides new insight into the Franck-Condon principle. For absorption at $T=0$, one expects the most probable transitions to occur to levels in the excited state with vibrational quantum numbers near $f=41$, for which the classical turning point is at the equilibrium configuration for the ground state. It is clear from Fig. 1 that the probability of transition to levels with f much less than 41 will be small because ψ_i will overlap the exponential tail of ψ_f. On the other hand for f much greater than 41 ψ_i overlaps the periodic portion of ψ_f whose amplitude varies slowly; consequently, the probability of transition given by Eq. (3) will again be small because of effective cancellation arising from the rapid oscillations of ψ_f. In other words, the principal contribution to Eq. (3) results from configurations for the vibrational levels of the final state where the kinetic energy is comparable with the kinetic energy of the vibrational levels of the initial state. This is in accord with the Franck-Condon principle which states that the most probable electronic transitions leave momentum as well as position unchanged.

V. ACKNOWLEDGMENT

The authors are indebted to Miss J. Gillespie for the numerical calculation of the matrix elements.

PHYSICAL REVIEW VOLUME 84, NUMBER 6 DECEMBER 15, 1951

Nuclear Interactions of Cosmic Rays in a Silver Chloride Crystal*

FREDERICK C. BROWN† AND J. C. STREET
Harvard University, Cambridge, Massachusetts

(Received September 13, 1951)

A disk of silver chloride, cut from a large crystal grown by slowly cooling the melt, was operated as an ionization detector at sea level and at Climax, Colorado, elevation 11,200 feet. Calibration was achieved by testing the response of the crystal to single cosmic-ray particles ionizing near minimum. By means of a Geiger counter coincidence system stars produced in the crystal by ionizing particles (protons) were separated from those produced by non-ionizing particles. A pulse-height distribution is plotted for the larger pulses and is in approximate agreement with star data from photographic emulsions for energy releases in the crystal of greater than 80 Mev. Electron showers and slow protons which stop in the crystal are shown to contribute to the rates below this energy. An apparent absorption thickness in air of 114±5 g/cm² is obtained for the ionizing star-producing radiation between Climax and sea level. By assuming a geometrical cross section for interaction in the crystal, the intensity of energetic protons at Climax is estimated to be approximately 10 percent of the hard component.

I. INTRODUCTION

ARGUMENTS, such as those given by Rossi,[1] make it reasonable to assume that most nuclear disintegrations (stars) in the atmosphere are produced by the neutrons and protons in the cosmic radiation. The rate of star production has been shown to decrease approximately exponentially with depth in the lower atmosphere, and various observers have given absorption thicknesses for the star producing radiation from 125 to 150 g/cm².[2-7] A majority of low energy nuclear events (small stars) observed in photographic emulsions at moderate elevations is produced by non-ionizing radiation, that is, by neutrons. On the other hand, high energy nuclear events (larger stars containing thin prongs) vary somewhat more rapidly with atmospheric depth.[1,6,7] It is probably correct to identify these with penetrating showers. Such stars are more often produced by protons.[6] Direct information on the intensity and altitude variation of the nuclear interactions of protons is not very extensive. It should be noted that star production by pi-mesons may become important under rather thick layers of dense material.

In this paper are presented the results of a counting experiment designed to determine the rate of production of stars in a crystal of silver chloride by ionizing particles. A pulse-height distribution is given for the various events produced in the crystal. By making appropriate correlation assumptions, the distribution is compared with the star data from photographic emulsions.[6,8]

* Assisted by the joint program of the ONR and AEC.

† Now at the University of Washington, Seattle, Washington. Work performed in partial fulfillment of the requirements for the degree of Doctor of Philosophy at Harvard University.

[1] B. Rossi, Revs. Modern Phys. **20**, 537 (1948).

[2] E. P. George, Nature **162**, 333 (1948).

[3] Bernardini, Cortini, and Manfredini, Phys. Rev. **76**, 1792 (1949).

[4] N. H. Forester, Phys. Rev. **78**, 247 (1950).

[5] Lord, Schein, and Vidale, Phys. Rev. **76**, 171 (1949).

[6] Camerini, Coor, Davis, Fowler, Lock, Muirhead, and Tobin, Phil. Mag. **40**, 1073 (1949).

[7] See also the results of Bridge, Rossi, and Williams using thin-walled ionization chambers as reported in reference 1 and John Tinlot, Phys. Rev. **73**, 1476 (1948); Phys. Rev. **74**, 1197 (1948).

[8] Brown, Camerini, Fowler, Heitler, King, and Powell, Phil. Mag. **40**, 862 (1949).

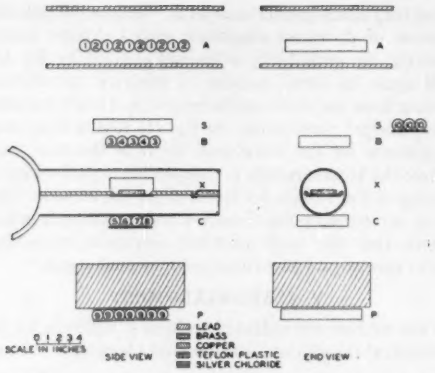

FIG. 1. Counter geometry showing side and end views of the crystal counter vacuum chamber.

From observations made at sea level and at an elevation of 11,200 feet (Climax, Colorado), an apparent absorption thickness in air is obtained for the high energy ionizing particles (protons) producing the interactions. Assuming a cross section for interaction in the crystal (157.5 g of silver chloride), the intensity of protons is estimated from the observed rate of star production.

In addition some information about the stars was obtained by observing penetrating particles below with a filter and auxiliary counter arrangement. A few delayed pulses believed to arise from μ-meson decay following a star were observed.

II. EXPERIMENTAL PROCEDURE

The silver chloride crystal has been previously used as a proportional device (a solid ionization chamber) by Voorhies and Street.[9] As described in this paper, the device can be calibrated by the passage of single minimum ionizing particles. It was also shown that this type of calibration can be used in deducing the energy loss in the crystal for more heavily ionizing particles.

Large single, or nearly single, crystals having the desired counting properties could not be obtained commercially. Consequently, crystals were grown by a technique similar to that first employed by Bridgman in 1925.[10] A crucible containing molten silver chloride was very slowly lowered through a temperature gradient into a region where the temperature was below the melting point. Various crucible materials were tried. Both Vycor glass coated with Aquadag, and platinum were found quite satisfactory. A disk 6 cm in diameter and 1 cm in thickness was cut from a boule grown in the platinum crucible. The crystal was heat treated and silver was developed out on the parallel surfaces, forming the electrodes.[11] For the experiment it was mounted in a vacuum chamber which contained a cooling system designed to minimize the amount of heavy material nearby.[12] Since the crystal counter had to be operated at low temperature for long periods of time, it was deemed necessary to have a large cooling reservoir. This was located away from the crystal and not in the solid angle subtended by the counter telescope. A 5-liter commercially available liquid air container was used for this purpose. The edges of the two copper spheres of this container are represented schematically at the left in Fig. 1. The crystal itself was situated near the center of the main vacuum chamber, a thin-walled ($\frac{1}{32}$-inch brass) tube 4 inches in diameter and 16 inches long. Cooling was accomplished by heat conduction through a copper shelf which fitted securely into a socket soldered to the inner sphere. In order to minimize heat leakage the other end of the shelf was supported by a Teflon rod which was held in place with a thin Nichrome support. Installation of the crystal was facilitated by having an opening through which the entire shelf could be inserted. In order to reduce radiation losses, the shelf was brightly polished, the interior of the vacuum chamber chrome plates, and a very thin radiation baffle put around the crystal and its electrical contacts. The entire space within the vacuum chamber, including that between the liquid air container spheres, was continuously pumped.

The counter arrangement was designed to detect nuclear disintegrations which were produced in the crystal by incident ionizing particles. The pulses from the Geiger counter trays A and B (see Fig. 1) and the crystal, X, were placed in triple coincidence ($A+B+X$), forming a counter telescope which detected ionizing particles incident on the crystal. A discriminator on the crystal output imposed the additional condition that the pulses from the crystal be greater than a predetermined size. Since the energy released in the crystal is proportional to pulse size, the discriminator permits the selection of events wherein the incident ionizing particle is associated with a large energy release in the crystal. Thus protons producing stars are recorded, but also protons simply stopping in the lower part of the crystal give fairly large pulses and are hard to separate from small stars. Also, an electronic shower associated with one or more electrons above would also be recorded. To minimize the number of counts resulting from such showers, a 1-cm lead plate was placed above tray A and another above tray B, and the circuit so arranged that if any of the Geiger tubes marked 1 in tray A (see Fig. 1) were discharged in coincidence with any of the Geiger tubes marked 2, the count was rejected. The Geiger tubes marked 3 and 4 in tray B operated in a similar manner. The assumption is that electronic mul-

[9] H.G. Voorhies and J. C. Street, Phys. Rev. **76**, 1100 (1949). For additional references on the silver chloride crystal counter see: P. J. van Heerden, thesis Utrecht (1945) or Physik **16**, 505 (1950), and R. Hofstadter, Nucleonics **4**, 2 (1949) and **4**, 29 (1949).

[10] P. W. Bridgman, Proc. Am. Acad. Arts Sci. **60**, 305 (1925).

[11] J. R. Haynes, Rev. Sci. Instr. **19**, 51 (1948).

[12] Silver chloride is an ionic conductor at room temperatures but operates satisfactorily as an ionization detector when cooled approximately to the temperature of liquid nitrogen.

tiplicity in the crystal will usually be associated with electronic multiplicity in trays A or B or both because of the proximity of the lead plates. In addition, a Geiger tube tray, S (Fig. 1), was placed outside the solid angle of the telescope. The 4-fold coincidences $A+B+X+S$ were recorded and interpreted as electronic showers from the side.

Additional information about the event occurring in the crystal was obtained by recording the number of Geiger tubes in tray C, below the crystal, which discharged in coincidence with $(A+B+X)$. This data yielded qualitative information about the number of secondary particles produced in the crystal by the incident primary.

A 10-cm lead absorber was placed beneath tray C and under this, a tray P. The discharge of any Geiger tube in tray P in coincidence with $A+B+X$ was recorded. The events $A+B+X+P$ indicated that at least one penetrating particle was associated with the large energy release in the crystal.

A block diagram of the circuits is shown in Fig. 2. The Geiger counter pulses were shaped so that the resolving times of the various coincidence circuits were about three microseconds. The output pulses from the crystal were fed through a preamplifier and a linear amplifier to a fast oscilloscope whose trace was photographed. Examples of crystal pulses obtained under similar conditions have been shown by Voorhies and Street.[9] Geiger counter and coincidence rates as well as the crystal counting rate were carefully monitored throughout all of the runs. Approximately 600 hours of operation were recorded at Cambridge, Massachusetts, elevation 25 feet above sea level. Approximately 200 hours of operation were recorded at Climax, Colorado, elevation 11,200 feet above sea level. The roofs and walls of the laboratory buildings at both sites were constructed of light materials and their effect on the cosmic ray intensities was neglected.

III. EXPERIMENTAL RESULTS

A. Crystal Response to Single Particles Ionizing Near Minimum

The crystal calibration was checked at regular intervals throughout the experiment by adjusting the amplitude discriminator to pass small pulses resulting from single particles traversing the crystal. Integral counting-rate curves of the type in Fig. 3 were taken. A characteristic region, the knee of the curve, was located and compared with the theoretical predictions of energy loss taking into account the fluctuation problem for fast particles.[13,14] In this manner, the pulse height in microvolts could be correlated with the energy-loss in Mev. In a general way this procedure seems satisfactory, and no doubt provides fairly good relative calibrations of the crystal. However, a difficulty becomes apparent when a flux curve of the type shown in Fig. 3 is examined more carefully in the region beyond the knee toward greater energy pulses. In this region, there are more pulses than can result from fluctuations alone. For example, in Fig. 3, the knee is at about 170 microvolts. If we consider the whole spectrum of sea level mesons, taking fluctuation into account.[15] the most probable pulse size, is about 200 microvolts, in reasonable agreement with the experimental curve. However, not more than 5 percent of the pulses are expected to be greater than 400 microvolts (twice the most probable value). The curve indicates more than 20 percent are greater. In the experiment of Whittemore and Street[15] this trouble did not appear. The present experiment differs, in that protection from small electronic showers was not as good and in that the crystal was run at low saturation. The latter would emphasize the effect of those regions in the crystal which are especially free from trapping centers. Such regions would produce pulses considerably larger than average.

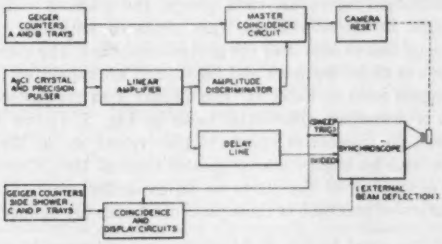

FIG. 2. A simplified block diagram of circuits. The precision pulser was used to calibrate and to check the stability of the linear amplifier and recording circuits.

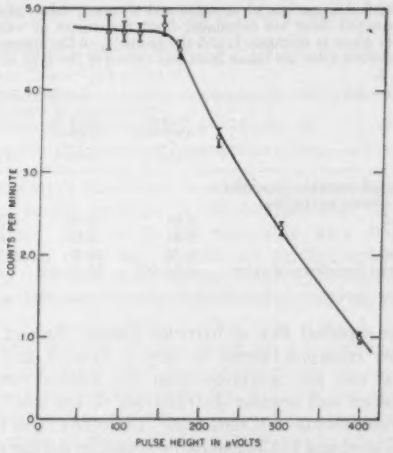

FIG. 3. A typical flux curve for cosmic rays at sea level, events ABX for low discriminator settings. Plotted are counts per minute against discriminator settings in microvolts.

[13] K. Symon, thesis, Harvard University (1948).
[14] L. Landau, J. Phys. (U.S.S.R.) VIII, No. 4, 201 (1944).
[15] W. L. Whittemore and J. C. Street, Phys. Rev. 76, 1786 (1949).

TABLE I. Comparison of expected and observed values of flux. The expected rates are calculated from the values of vertical intensity given in reference 1, and the geometry of the apparatus. The observed rates are taken from flux curves of the type shown in Fig. 3.

	Flux at Cambridge F_{el} (min^{-1})	Flux at Climax F_{el} (min^{-1})	F_{el}/F_{el}
Calculated from the geometry and known intensities:			
Hard	4.85	9.95	2.05
Soft	1.46	9.65	6.60
Total	6.30	19.6	3.10
Observed experimental rates:	4.8±0.2	11.0±0.5	2.29

The expected flux of particles passing through the counter telescope formed by tray A, tray B, and the crystal can be calculated from the known vertical intensities and angular distributions of the hard and soft components of cosmic rays.[1] These flux rates both at sea level and at Climax are presented in the top rows of Table I. The experimental rates, obtained by extrapolating the integral flux curve to zero pulse height are also given (see Fig. 3). It should be noted that the observed altitude dependence agrees more closely with that calculated for the hard component. At sea level, the two 1-cm lead plates in the counter telescope should eliminate more than half of the soft component by absorption. The shower protecting anticoincidence circuit also strongly reduces the rate of this component. Taking these effects into account, the expected rate should be about 5 per minute. Since the experimental value of 4.8±0.2 agrees favorably with this estimated rate, it may be assumed that the crystal was detecting nearly all of the particles passing through it.[16]

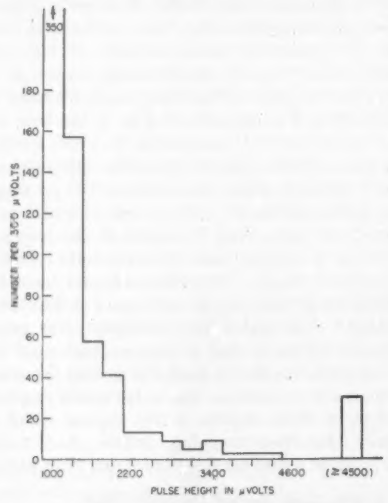

FIG. 4. A typical pulse-height group at Climax for all pulses above 850 microvolts, corresponding to about 43 Mev of energy loss in the crystal.

B. Large Pulses and Their Interpretation

After calibration, the discriminator was raised to a level corresponding to roughly 50 Mev of released energy (seven times that lost by a single particle ionizing at minimum). All pulses $(A+B+X)$ for a given discriminator setting were photographed and measured. The lower limit of the discriminator setting was large enough to eliminate pulses arising from mesons passing through the crystal or stopping as a consequence of normal ionization. Similarly, most proton pulses of normal ionization were eliminated.

Over long periods of time the sensitivity of the crystal was found to vary. After about ten days of continuous operation at Climax, a calibration run would show a decrease of about ten percent in pulse height for a given energy loss. Such an effect was attributed to a polarization slowly induced in the crystal by the applied field and continuous exposure to cosmic rays.

TABLE II. Complete $(A+B+X)$ coincidence data combined and listed in integral form with pulse sizes expressed in Mev dissipated in the crystal.

Pulse size in Mev dissipated	Climax			Sea level		
	No. of counts of equal or greater size	Hours	Rate hr^{-1}	No. of counts of equal or greater size	Hours	Rate hr^{-1}
400	21	169.1	0.124	...	...	...
300	45	202.1	0.221	8	560	0.014
200	102	236.2	0.432	10	560	0.018
100	314	236.2	1.33	30	560	0.0536
80	504	236.2	2.13	53	560	0.0947
60	1016	236.2	4.30	138	560	0.246
40	652	67.2	9.71	403	560	0.720

The crystal was depolarized by warming to room temperature with the collecting field off and then recooling. As would be expected, the polarization was observed to set in more slowly at sea level than at Climax.

The data were separated into groups of the type shown in Fig. 4 where the calibration of the crystal was constant to within ten percent for each group but was different from group to group. Using the appropriate calibration figure for each group, the scale of pulse height in microvolts was then replaced with one of energy loss in Mev and the groups combined. The complete data for sea level and for Climax are tabulated in integral form in Table II. The Climax data are plotted on a smoothed differential basis in Fig. 5. Curve A gives the number of counts in the crystal per 20 Mev per hour for energy release greater than 40 Mev. Curve B is the tail of the curve on an expanded scale. The statistical precision of these plots can be readily deduced

[16] The actual fraction of the soft component detected by the apparatus can be estimated from the increase in rates with elevation. A simple calculation from the data of Table I gives $\frac{1}{3}$ for this fraction.

from the number of counts listed in Table II and to avoid confusion is not shown in Fig. 5. The average rate between 100 and 200 Mev is uncertain to within about 7 percent. We shall show later that only the data above 80 Mev may be interpreted as due solely to star production in the crystal.

The counter telescope defines an angle from the vertical of roughly 20°. From the angular distribution of fast star-producing particles, as given by the Bristol group,[8] we estimate that our telescope selects a fraction 0.48 of these particles. Our crystal weighs 157.5 g. Therefore, to convert the rates above 80 Mev (Table II) to the number per gram per hour produced by particles incident at all angles, it is necessary to apply a factor of $1/(0.48\times157.5)=0.013$ to the tabulated values.

We have tried to make a comparison of our observations with the very different sort of data taken from photographic emulsions.[8] The intensities for the Bristol

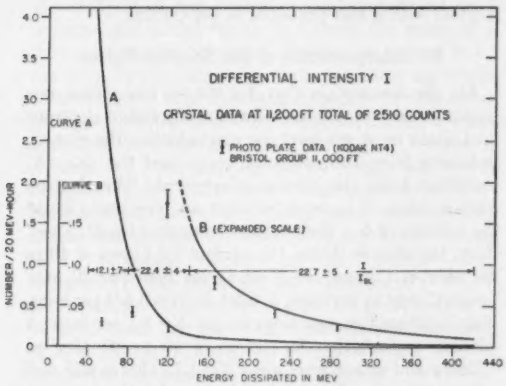

FIG. 5. Crystal data at Climax for $(A+B+X)$ coincidence events plotted on a differential basis. The ratios I/I_{sl} are the factors by which the rates in the indicated regions have to be reduced to fit the sea level data.

"ρ-stars," have been converted to counts per hour in the crystal, taking account of the solid angle subtended by the counter telescope and the angular distribution of star-producing particles. In addition, by using Table IV in reference 8 and range-energy curves for silver chloride, a correction was made for the average energy carried out of the crystal by escaping particles. The resulting conversion from number of prongs to Mev dissipated in the crystal is given in Table III. The final transformed intensities are plotted with statistical errors in Fig. 5. The two points below 100 Mev are plotted in the scale of curve A, the other four on the expanded scale of curve B. Above 80 Mev the agreement is fair. For smaller pulses, the crystal rate is considerably larger. Even for the larger pulses the emulsion points are a little low but this is not significant, considering the roughness of the conversion procedure. For example, the composition of the emulsion is different

TABLE III. Calculated conversion relations—emulsion to crystal data.

Size of "ρ-star" in number of heavy prongs	2	4	6	8	10	12	14
Estimated average energy dissipated in crystal in Mev	25	55	80	125	175	225	290

from that of the crystal. In addition it seems likely that some events produced in the chamber walls, or other adjacent portions of the apparatus were detected. Although these two effects can readily explain the slight difference above 80 Mev, they cannot explain the large difference between the emulsion and the crystal data for small pulses. It should be stressed that in making this comparison we have not adjusted any arbitrary factor, but have transformed the emulsion data on an absolute basis. The fact that the absolute intensities do agree reasonably well and the fact that the shape of the crystal and emulsion curves are the same above 80 Mev provide evidence for the assumption that in this energy range our arrangement is detecting mainly stars of the type observed in photographic emulsions.

Occasionally a star produced in the crystal will not be counted because a particle is projected upward into the anticoincidence arrangement of trays A and B (see Sec. II). However, such events should be rare because a small solid angle is subtended by alternate tubes in these trays and because the particles are absorbed by the material between these counters and the crystal. Air shower particles accompanying a nuclear particle which produced a star in the crystal might also trip this anticoincidence circuit. That both these occurrences are infrequent is born out by the relatively small frequency (1.3 percent) with which a count in the side shower tray, S, was registered in coincidence with a star in the crystal.

A comparison of the rates at sea level and at Climax is made in Table IV. The errors stated are the standard deviations calculated from the number of counts involved. It is estimated that the effect of the uncertainty in the calibration of the crystal for the various runs is considerably less than the statistical variation due to the small number of counts. Above 80 Mev, the increase with elevation is consistent with the assumption that mainly the effects of the nuclear component of the cosmic radiation were detected. Below 80 Mev, the

TABLE IV. Counting rates at sea level and at elevation 11,200 feet.

Range of energy loss in Mev	40–60	60–80	80–140	140 and greater
(I_{sl}) counts hour^{-1} at sea level	0.474	0.152	0.062	0.032
(I)counts hour^{-1} at elevation 11,200 feet	5.41	2.17	1.38	0.75
I/I_{sl}	11.5±0.9	14.3±1.7	22.4±4.0	22.7±5.0

smaller increase with elevation can be interpreted as the result of a partial contribution from the electronic component. For all counts above 80 Mev, the increase in rate with altitude is $I/I_{sl}=22.5\pm3.0$. Assuming exponential absorption of the star producing radiation in the 355 g/cm² of air between Climax and Cambridge the absorption thickness corresponding to the above factor is:

$$L_{air}=114\pm5 \text{ g/cm}^2.$$

C. Auxiliary Data, Including Observations with the *C* and *P* Counter Systems

At least one tube in the *C* tray beneath the crystal was triggered for 50 percent of the counts above 40 Mev. Two or more counters were triggered for 10 percent of the counts, indicating that in these cases at least two particles were able to get out of the crystal and penetrate the $\frac{3}{32}$-inch brass walls. When the shower protecting anticoincidence circuit associated with trays *A* and *B* was disconnected the counting rate data taken at Climax for energy releases of 40 Mev or greater increased about four times. Nearly every count which normally would have triggered this anticoincidence circuit showed a multiple count in tray *C*. Double counts in the *C* tray, then, were a fairly sensitive indication of electron showers as well as of multiple particles from stars.

At Climax a particle was detected in the *P* tray below the 10 cm of lead under the crystal for about 10 percent of the counts with 50 to 180 Mev energy-loss. For pulses larger than 180 Mev the *P* tray was triggered 27 percent of the time. One could argue that such *P* counts result from a μ-meson which has produced a large shower in the crystal or in the lead above, through knock-on or other processes. However, the expected rate of such events can be estimated and shown to be quite small. (See Appendix.) In addition, some *P* counts were registered at sea level at a rate (26 counts in 406 hours) very roughly 1/14 that at Climax. A short run was made with circuits which registered how many counters in the *P* tray fired. Among 200 events above 40 Mev only 21 showed a count below the 10 cm of lead. In only one of these 21 cases did more than one counter in the *P*-tray fire. It appears that showers under the lead are much less frequent than single particles. A simple interpretation of these *P* events is that a high energy proton produces an interaction in the crystal and then continues on with sufficient energy to penetrate the 113 g/cm² of lead (an event similar to that shown in Plate VI, reference 8).

The effect of additional lead absorbers placed above the crystal chamber was investigated qualitatively at Climax. A lead absorber 1.3 cm thick placed directly over the chamber produced less than ten percent change in the rate. For a short run of 24 hours at Climax, 12.7 cm of lead was inserted in the counter telescope between trays *A* and *B*. Forty-two counts from 50 to 90 Mev were recorded at a rate 25 percent of that without the lead. Only 16 counts above 90 Mev were recorded, indicating a rate roughly 40 percent of the rate without the lead. This leads to a lead absorption thickness of 170 ± 60 g/cm². The stronger absorption of the counts 50 to 90 Mev is in agreement with the assumption that in this range the rates are partly due to electron showers.

It should be mentioned that a few oscilloscope traces were recorded in which a second crystal pulse followed the main crystal pulse, delayed by a few microseconds. These amplified and shaped pulses were three microseconds long so we could readily resolve delays greater than four microseconds. There were three such cases occurring in 1300 counts at Climax. For these same 1300 counts at least ten events were recorded superimposed on the crystal pulse itself, with delays of from one to four microseconds. The pulse height and delay of these few counts were all consistent with a μ^+-meson β^+-decay process with the parent π^+-meson originating in connection with a star produced in the crystal.

D. Interpretation of the Smaller Pulses

On the assumption that, for the smaller pulses, our apparatus detects the same fraction of incident electrons at Climax as at sea level, we can calculate the rate, *S*, resulting from the soft component and the rate, *N*, resulting from the nuclear component. The electron rate is taken to increase between sea level and Climax by a factor of 6.6, the nuclear component by 22. Then, from the data in Table IV, we find for pulses of 40 to 60 Mev at Climax, $S+N=5.41$ per hour per 20 Mev interval, and at sea level, $S/6.6+N/22=0.474$ per hour. Solving these two equations we get $N=3.3$ per hour. A similar computation for pulses of 60 to 80 Mev at Climax and at sea level yield $N=1.7$. This is still well above the rate (0.4 per hour) given by the emulsion data for stars in this energy range (see Fig. 5). A part of the discrepancy can be accounted for in terms of single protons of moderate energies incident from above and stopping in or just below the crystal. Using range-energy curves and taking account of angular effects, a calculation shows that protons incident on the top lead plate in the momentum range $5\text{–}6\times10^8$ ev/c contribute pulses of 40 to 60 Mev in the crystal. Using the data of Miller *et al.*[17] a calculation applied to the present experiment indicates a rate of 1.3 per hour for such events. After subtracting this proton contribution from the above determined rate of 3.3 per hour for *N*, the remainder is still high in comparison with emulsion data (2.0 per hour compared with 0.3 per hour). It is not clear, without further investigation, whether the discrepancy arises from errors in estimating the electron and single-proton contributions, or whether other events, which contribute in this region of pulse size, have been overlooked.

[17] Miller, Henderson, Potter, Todd, and Wotring, Phys. Rev. **79**, 459 (1950).

E. Estimate of Proton Intensity

Assuming a cross section for the production of nuclear interactions in the crystal, the vertical intensity of the star-producing protons can be estimated. It is necessary to use the angle distribution of incident protons given by Brown *et al.* (reference 8, Fig. 4, page 867). From this we deduce that the vertical intensity is 1.16 times the average intensity for rays in the 0-to-20 degree angle covered by our counter telescope. The solid angle subtended is 0.47 sterad. The number of events recorded in the crystal per hour, a quantity which we call R, would be given by

$$R=(0.47\times 3600/1.16)A\sigma TI_v.$$

Here I_v is the vertical intensity (cm^{-2} sec^{-1} sterad^{-1}), σ is the cross section for collision (of the type observed) measured in cm^2/g, T is the thickness of the crystal in g/cm^2, and A is the area of the crystal (28.5 cm^2). To obtain σT, we calculated it separately for the silver and the chloride in the crystal, using geometrical cross sections, and added them. At Climax the value of R from our data for all pulses 100 Mev or greater is 1.3 per hour. In this range there is a reasonable agreement with emulsion data. For smaller pulses we may either extrapolate down to 40-Mev dissipation along a curve indicated from emulsion data (see Fig. 5), obtaining R_1(total)=2.7 per hour, or use our rates corrected as described in Sec. III-D above obtaining R_3(total)=5.3 per hour. For lack of a better criterion we arbitrarily choose the average of these, $R=4$ per hour. Solving for I_v, we obtain 1.6×10^{-3} cm^{-2} sec^{-1} sterad^{-1}. This represents 10 percent of the hard component at 11,200 feet elevation (atmospheric depth 675 g/cm^2). It is to be pointed out that the result is uncertain in the choice of R, as indicated above, and as to how well σT can be represented by geometrical cross sections.

We thank Dr. George Nonnemaker for valuable aid in the preparation of the manuscript, Mr. Richard Milburn for making some of the calculations, and Professor Kenneth Greisen of Cornell for his constructive criticism of the paper in preparation. In addition the authors acknowledge the many services rendered by the various members of the shops and offices of the physics laboratories at Harvard University. Living accommodations at Climax were made available by the Climax Molybdenum Company and many courtesies were extended by its general manager, Mr. C. J. Abrams.

APPENDIX

We seek an upper limit to the probability that a meson of an energy belonging to the observed sea level cosmic-ray spectrum will produce an electron cascade large enough to be recorded as a P event. To be specific, we estimate the chance of production of an electron cascade of more than 7 ionizing particles formed in 2 cm of Pb. From Heitler,[18] we deduce that such showers require initiating electrons or photons of energies greater than 500 Mev or so. We assume as a rough approximation that such electrons or photons are produced by mesons in the first centimeter of lead, since the second centimeter is needed for effective shower growth. The processes involved are as follows:

(a) Electrons emerging as knock-ons from the direct collision of incident mesons.

(b) Photons appearing as the bremsstrahlung of the incident mesons in the fields of heavy lead nuclei.

(c) Direct pair production in the fields of lead nuclei. We consider these processes in succession.

In each case we assume that the incident mesons have momenta belonging to the spectrum[19]

$$S(P)=AP^{-3.3}.$$

The specific exponent chosen is not critical, in view of the other more serious approximations made.

(a) Electronic knock-ons: The basic cross section used is that given by Janossy[20] for collisions of spin-½ mesons with electrons. To produce a 500-Mev electron by collision, momentum and energy conservation require an incident meson of at least 2000 Mev. To simplify calculation, however, it was assumed that any amount of momentum could be transferred, up to the incident momentum p. The collision cross section was thus integrated over electron momenta from 500 Mev/c to p. The result was weighted by the meson spectrum $S(p)$, above, and integrated over meson momenta from 2000 Mev/c to infinity. This procedure reduces the calculation to a series of elementary integrations, and will give an upper bound to the frequency of such knock-on processes. By this method one obtains $f_k=1.2\times 10^{-4}$ as the probability that a cosmic-ray meson will produce in 1 cm of lead a knock-on of greater than 500-Mev energy.

(b) Bremsstrahlung: We use the formulas of Heitler,[21] adapted to incident particles with 200-electron masses. The extreme relativistic approximation was applied to find the probability of incident cosmic-ray mesons forming photons of energies greater than 500 Mev in one cm of lead. This probability is calculated in the same manner as that for knock-on electrons, and is found to be $f_b=4.3\times 10^{-4}$, for an unscreened nucleus, and $=3.3\times 10^{-4}$, assuming complete Thomas-Fermi screening. The correct value is probably closer to the second of these.

(c) Direct pair production: In this case we use the formulas of Hayakawa and Tomonaga.[22] For ready calculation from their equations it is convenient to carry the integration over meson momenta only up to 6×10^4 Mev/c. For a spectrum $S(p)\alpha p^{-3}$, only one meson in 10^4 has a momentum above this. The probability that a pair of 500-Mev total energy is formed is then $f_p=6.4\times 10^{-7}$ when $S(p)=Ap^{-3.3}$.

This is smaller than the probability for bremsstrahlung near an unscreened nucleus by about $\alpha=1/137$, as is to be expected, since direct pair production is a higher order process.

In conclusion, we note that an upper limit to the probability of production of such large cascades by cosmic-ray mesons is about 5×10^{-4}, even assuming unscreened nuclei in the bremsstrahlung process. Actually the best estimate for the probability is about 2×10^{-4}. Thus at sea level, where about 300 mesons per hour traverse the equipment, some 6×10^{-2} seven-particle showers would be expected in a similar time. As noted in Sec. III-C the anticoincidence arrangement eliminates at least three-quarters of these showers and some of them would spread by scattering enough for several of the particles to miss the crystal. Therefore, the expected rate of such events at sea level is about 10^{-2} per hour and at Climax approximately twice this. That these rates are indeed negligible is shown by Table II. They are roughly only 1 percent of the rate at sea level and 0.2 percent at Climax, for dissipated energies greater than 40 Mev.

[18] W. Heitler, *Quantum Theory of Radiation* (Oxford University Press, London, 1944), second edition, pp. 237–239.

[19] L. Janossy, *Cosmic Rays* (Oxford-Clarendon Press, England, 1948), p. 171.

[20] See reference 19, p. 130.

[21] See reference 18, pp. 168–170.

[22] S. Hayakawa and S. Tomonaga, Prog. Theor. Phys. 4, 287 (1949).

Observations on Some High Energy Cosmic-Ray Collisions in Photographic Emulsions

E. Pickup and L. Voyvodic
Physics Division, National Research Council, Ottawa, Canada
(Received September 4, 1951)

A brief account is given of some high energy disintegrations initiated in photographic emulsions by primary cosmic-ray particles at about 90,000 feet above sea level. In particular, six events which show only relativistic or near relativistic fragments and a typical forward cone of shower particles are described in detail. The angular distribution of the shower particles is, in some of these cases, consistent with them, being due to the multiple production of mesons in a single interaction between an incoming nucleon and a hydrogen nucleus, or a nucleon on the edge of a heavier nucleus, according to the mechanism of Fermi's recent theory. One of these events has thus been interpreted as a collision between an incoming lithium nucleus with an energy of about 2×10^{12} ev per nucleon and a hydrogen nucleus in the emulsion.

I. INTRODUCTION

THE interactions of cosmic-ray particles with nuclei are interpreted in terms of primary collisions between individual nucleons. Owing to the great density of nuclear matter these primary interactions may be followed by secondary collision processes, after which any residual nucleus is left in an excited state and evaporation fragments may be emitted. Electromagnetic radiation could be emitted by bremsstrahlung or other processes, but there is no definite evidence for this in cosmic-ray disintegrations if we exclude the neutral pi-meson decay radiation. It is also known[1] that aggregates of nucleons, too energetic to be explained as evaporation products, are emitted occasionally in cosmic-ray disintegrations, although the mechanism for this is somewhat obscure at present.

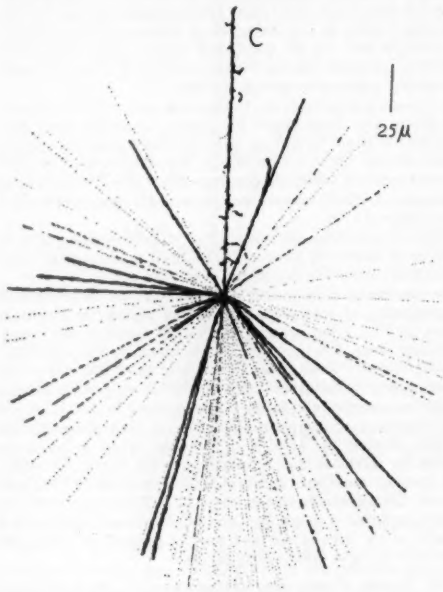

FIG. 1. 82-pronged star with primary carbon nucleus.

In the individual collisions between nucleons, neutral and charged pi-mesons are created depending on the energy available and the closeness of the collision. If the collisions are sufficiently energetic ($\gtrsim$several Bev) considerations following Yukawa's theory[2] indicate the possibility of the production of more than one meson in single interaction (multiple production), and the most complex disintegrations would then contain showers of mesons produced multiply in a series of collisions (pluromultiple production). These plural collisions may be subsequent collisions of the primary and knock-on nucleons, and further interactions of the initially produced mesons themselves with nucleons, with possible multiple meson production here, also. The collision of an incoming nucleon or heavier nucleus with a target nucleus may range from a central to a glancing type of collision, so that the interactions will be quite complex in general.

If the energy involved in a single collision is extremely high the situation may be further complicated by the production of nucleon-antinucleon pairs as recently postulated by Fermi.[3] Furthermore, the possible existence of mesons heavier than pi-mesons is still an outstanding cosmic-ray problem, although if such mesons exist, it would appear from their apparent scarcity, that they are either created rarely compared with pi-mesons or they are extremely short-lived. In the latter case they could play an important part in nuclear interactions, although they could not then be identified with the *V*-particles of cosmic-rays.

One of the more interesting problems is to show if pi-mesons are, in fact, produced multiply in single nucleonic interactions, and, if so, what laws they obey. A direct experiment, using hydrogen as a target nucleus, presents serious difficulties. In a photographic emulsion there is an admixture of hydrogen and heavier nuclei, and, occasionally, one would expect to observe a colli-

[1] S. O. C. Sorensen, Phil. Mag. **42**, 188 (1951); see also Fig. 3, present paper.

[2] R. Peierls, Reports on Progress in Physics (London) **6**, 78 (1939).

[3] E. Fermi, Prog. Theor. Phys. **5**, 570 (1951); referred to as Fermi *I*.

sion between an incoming proton and a hydrogen nucleus or a nucleon on the edge of a heavy nucleus, with the residual nucleus left relatively unexcited, or, conversely, between a nucleon in an incoming heavy nucleus and a hydrogen nucleus in the emulsion or a nucleon on the edge of a heavier nucleus. In the latter case the residue of the incoming nucleus may continue on its original path relatively undisturbed.

The main purpose of this paper is to describe in detail a few events which are believed to be examples of these rarer types of collision processes, and to compare the angular distributions of the minimum ionization tracks produced (assumed to be pi-mesons) with those predicted by Fermi's theory[3,4] of multiple meson production.

II. EXAMPLES OF COLLISION PROCESSES IN PHOTOGRAPHIC EMULSIONS

Before proceeding to discuss the special events, a few examples are given here of some of the "more" complex types of disintegrations. They were found in Ilford G5 emulsions exposed to cosmic radiation by means of free balloon flights at about 90,000 feet. More general information on the statistics of events will be given in a subsequent publication. The illustrations are from tracings made in a projection microscope. Different types of cosmic-ray disintegrations have also been discussed by various authors.[5–14] In particular, Bradt, and Peters[14] have shown that heavy primary nuclei are sometimes degraded into component nuclei in collisions, the general direction of motion being maintained.

Figure 1: This shows a central collision of an incoming carbon nucleus identified by delta-ray counting with a silver or bromine nucleus in the emulsion, giving a star with 82 charged fragments. There is a wide angle shower of about 35 particles with approximately minimum ionization, including 4 in the backward hemisphere, and from charge conservation in the collision at least 28 charged particles must have been created. If we assume that these are pi-mesons, then most of the shower particles must be charged pi-mesons. The wide angle shower undoubtedly results in part from plural collisions and the absence of any narrow cone is an indication that the carbon nucleus was not extremely energetic.

Figure 2: An α-particle makes a central collision with a silver or bromine nucleus giving a star with 59 charged fragments, including a fairly wide angle shower of 28, approximately minimum ionization particles. On the assumption that the target nucleus was silver, at least 9 of these were created in the collision (pi-mesons). The α-particle was about one-cm long in the emulsion, and multiple scattering measurements made on it indicate that the energy was greater than 65 Bev.

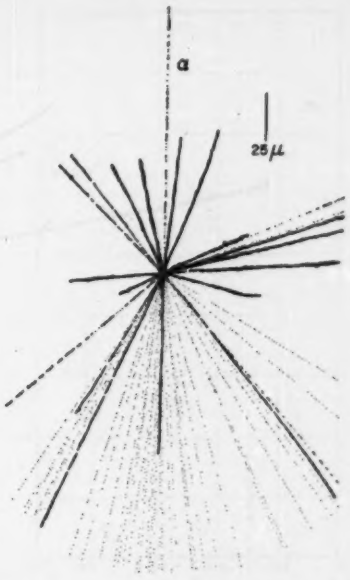

FIG. 2. 59-pronged star with primary α-particle.

Figure 3: A collision between an incident light nucleus and a silver or bromine nucleus gives a star with 60 charged fragments. The charge of the light nucleus, measured by delta-ray counting was 7 ± 1, and is thus probably nitrogen. The incident nucleus was approximately in line with the center of a wide cone of about 17 shower particles. One of the heavily ionizing particles ejected sideways was a Li^8 (or B^8) nucleus with an energy $\simeq$65 Mev, giving the characteristic "hammer" track, together with the disintegration electron. On the assumption that the target nucleus was silver and a nitrogen nucleus was incident, conservation of charge requires that at least 7 charged particles (pi-mesons) were created in the collision. This is probably an event of considerably lower energy than that of Fig. 1.

Figure 4: An incident, singly-charged particle makes a collision in which only two of the usual heavy evaporation tracks are produced, together with a somewhat asymmetric, fairly narrow cone of about 20 shower particles. One of the shower particles produces a fairly energetic secondary star. It is likely that the shower is partly the result of one or two nucleonic collisions with multiple meson production. The collision may be a

[4] E. Fermi, Phys. Rev. **81**, 863 (1951); referred to as Fermi *II*.
[5] LePrince-Ringuet, Bousser, Hoang Tchang Fong, Jauneou, and Morellet, Phys. Rev. **76**, 1278 (1949).
[6] J. J. Lord and M. Schein, Phys. Rev. **77**, 19 (1950).
[7] Brown, Camerini, Fowler, Heitler, King, and Powell, Phil. Mag. **40**, 862 (1949).
[8] Camerini, Coor, Davies, Fowler, Lock, Muirhead, and Tobin, Phil. Mag. **40**, 1073 (1949).
[9] Salant, Hornbostel, Fisk, and Smith, Phys. Rev. **79**, 184 (1950).
[10] L. S. Osborne, Phys. Rev. **81**, 239 (1951).
[11] Hoang Tchang Fong, Ann. Phys. **5**, 537 (1950).
[12] P. Freier and E. P. Ney, Phys. Rev. **77**, 337 (1950).
[13] Bradt, Kaplon, and Peters, Helv. Phys. Acta **23**, 24 (1950).
[14] H. L. Bradt and B. Peters, Phys. Rev. **77**, 54 (1950); **80**, 943 (1950).

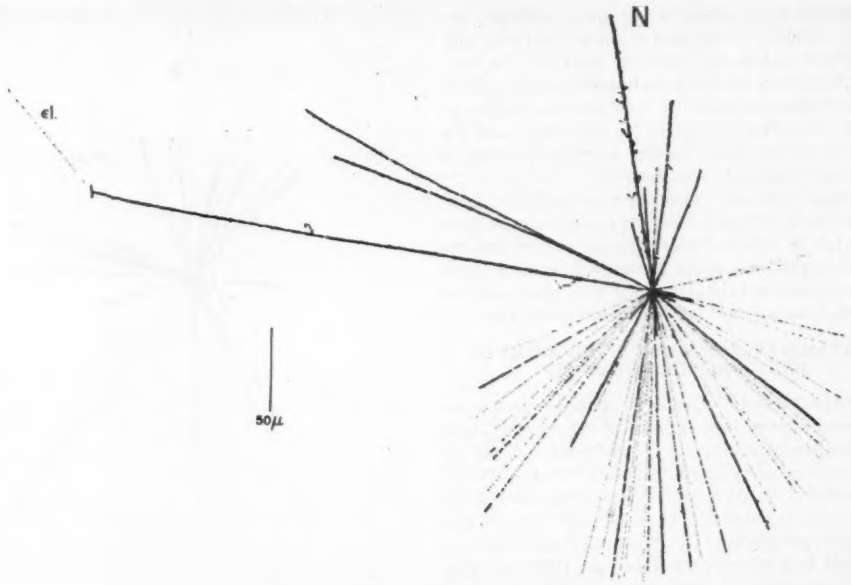

FIG. 3. 60-pronged star with primary nitrogen nucleus.

glancing collision with a heavy nucleus or a fairly complete break-up of a light nucleus in the emulsion with some meson production.

III. THEORY OF MESON PRODUCTION

While Heitler and Janossy[15] have presented a case for explaining most of the general features of meson showers in terms of single meson production in successive collisions (pure plural production), there would seem to be difficulties in attempting to explain the details of some of the showers by this picture. Furthermore, there is theoretical reason to expect multiple meson production if the collisions are sufficiently energetic. Heisenberg,[16] and Lewis, Oppenheimer, and Wouthuyen[17] have put forward different theories of multiple production, but, in their present form, both theories indicate a greater multiplicity than appears to be observed in practice in narrow shower cones.

Recently Fermi[3,4] presented a theory which predicts a lower multiplicity. Nucleons are considered to interact by virtue of surrounding pion (pi-meson) fields of fixed lateral dimensions $R \sim \hbar/\mu c$ (μ = the pion rest mass, and R is independent of energy). In a collision, thermodynamical equilibrium is assumed to be attained very rapidly throughout the colliding volume, and mesons may materialize with a certain energy distribution, the process being considered analogous to the emission of black body radiation in the collision of ultra-relativistic nucleons. Owing to a Lorentz contraction in the direction of motion, the pion fields will tend to behave as flat discs, and a considerable amount of angular momentum will be involved in off-centered collisions.

The average number of mesons created in such a very high energy collision is a function of the energy and of the collision impact parameter, r. The mesons are assumed to carry off any angular momentum created, and this gives rise to a preferential emission in backward and forward directions in the c.m. system. In the case of centered collisions, where no angular momentum is involved, the distribution will be isotropic. On converting to the laboratory system the net result for an off-centered collision is, on the average, a peaked forward cone of very high energy mesons, together with a diffuse tail or cone containing an equal number of mesons with lower energy.

If the energy is sufficiently high ($\gtrsim 5\times 10^{12}$ ev), Fermi suggests that the production of nucleon-antinucleon pairs may compete favorably with meson creation, and the number of all charged particles will be slightly greater than if mesons alone were created. Also, the creation of any heavy pi-mesons may be important at such energies. However, these possibilities are neglected in describing the events below. In any case they would not change the general conclusions.

For purposes of comparison with observed angular distributions, the theory in Fermi *II*[4] may conveniently

[15] W. Heitler and L. Janossy, Helv. Phys. Acta **23**, 417 (1950).
[16] W. Heisenberg, Z. Physik **126**, 569 (1949); Nature **164**, 65 (1949).
[17] Lewis, Oppenheimer, and Wouthuysen, Phys. Rev. **73**, 127 (1948).

be treated as follows: The number of mesons created is given by $N=C_1f(\rho)$, where

$$f(\rho)=(1+\rho^2)/\rho^3\ln(1+\rho)/(1-\rho)-2/\rho^2.$$

ρ is a parameter which depends on the angular momentum coefficient and the temperature attained in the equilibrium, but we have used r as the variable in the graphs below, since it has a more direct physical meaning. The impact parameter r is given by

$$r/R=3/2(f_1(\rho)/f(\rho)),$$

where

$$f_1(\rho)=2/\rho^3+(4/3\rho)/(1-\rho^2)-((1+\rho^2/3)/\rho^4)\ln(1+\rho)/(1-\rho)$$

and

$$f_2(\rho)=(1/\rho)\ln((1+\rho)/(1-\rho))+2/(1-\rho^2).$$

FIG. 4. 27-pronged star with primary proton.

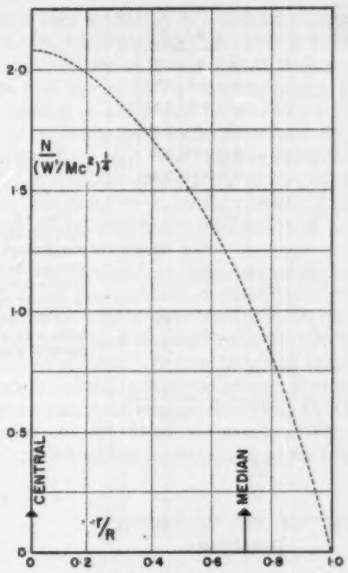

FIG. 5. Curve showing the variation of $N/(W'/Mc^2)^{\frac{1}{2}}$ with impact parameter r. N = number of mesons; W' = total energy in laboratory system.

The equation for N can also be written in the form $N/(W'/Mc^2)^{\frac{1}{2}}=C_2f(\rho)/(f_2(\rho))^{\frac{1}{2}}$, where C_2 is a constant, W' is the energy of the colliding nucleon in the laboratory system, and Mc^2 is the nucleonic rest mass energy. If there is only one kind of meson possible we calculate that $C_2=2.50$. If three kinds of mesons are possible, i.e., negative, positive, and neutral pi-mesons, C_2 will be increased by a statistical weighting factor $3^{\frac{1}{2}}$, and in this case $C_2=3.29$. Assuming equal probability for the three kinds of pi-mesons, the number of charged pi-mesons will then be given by

$$N/(W'/Mc^2)^{\frac{1}{2}}=2.19(3)(f(\rho)/(f_2(\rho)))^{\frac{1}{2}}.^{18}$$

Figure 5 shows a plot of $N/(W'/Mc^2)^{\frac{1}{2}}$ *versus* r/R for this latter formula.

The number of all charged mesons per radian at polar angle θ in the c.m. system can be expressed as

$$dN/d\theta=C_1\sin\theta f_4(\rho\cos\theta)=(N/f(\rho))\sin\theta f_4(\rho\cos\theta),$$

where $f_4(x)=2/(x^3(1-x^2))-(1/x^3)\ln(1+x)/(1-x)$. In Fig. 6 $(1/N)(dN/d\theta)$ is plotted against θ for several values of r/R.

Thus if N is known by observation and a valued assumed for r/R, Fig. 1 gives W' and Fig. 6 gives the

[18] For a median collision ($\rho\simeq0.96$; $r\simeq0.71$), $N=1.10(W'/Mc^2)^{\frac{1}{2}}$. When $\rho=0$, $N/(W'/Mc^2)^{\frac{1}{2}}=2.19(3)\times0.943=2.07$ which is the same as the formula for the case with no angular momentum deducible, from Fermi *I*,[3] paragraph 6. With the angular momentum correction 0.51 this gives $N/(W'/Mc^2)^{\frac{1}{2}}\simeq1.06$, which is the formula given by Fermi for charged pi-mesons when no nucleon-antinucleon pairs are possible.

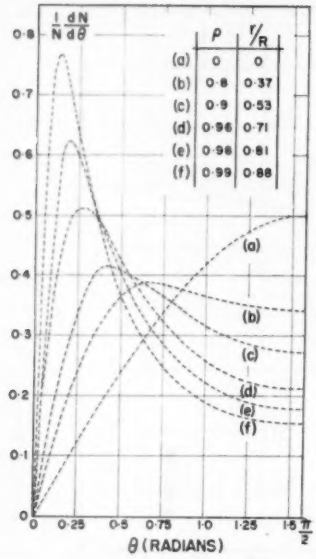

FIG. 6. Curves showing the angular distribution of mesons in the c.m. system for several values of impact parameter r. The distribution from 0 to π is symmetrical about $\pi/2$.

angular distribution $dN/d\theta$ in the c.m. system. The corresponding distribution in the laboratory system may be obtained by means of the following relativistic transformations, where the primed variables refer to the laboratory system:

$$\left(\frac{dN}{d\theta}\right)^1 = \bar{\gamma}\frac{dN/d\theta(\cos\theta+v'/v)^2}{\cos^2\theta'[1+(v'/v)\cos\theta]} \doteq \bar{\gamma}dN/d\theta\frac{(\cos\theta+1)}{\cos^2\theta'},$$

$$\tan\theta^1 = \sin\theta/\bar{\gamma}(\cos\theta+v'/v) \doteq 1/\bar{\gamma}(\tan\theta/2),$$

($\bar{\gamma}$ = energy in rest mass units of one nucleon in the c.m. system, v = meson velocity and θ = polar angle relative to incident direction), $\bar{\gamma}^2=(\gamma+1)/2$ or $\bar{\gamma}\doteq(\gamma/2)^{\frac{1}{2}}$, where $\gamma=1/[1-(v'/c)^2]^{\frac{1}{2}}\doteq W'/Mc^2$.

It should be noted that the result for very high energies is essentially independent of the meson energy spectrum, and will only be in serious error for a few mesons projected almost vertically backwards in the c.m. system. Also, in the above and in what follows, the nucleon-nucleon collisions are assumed to be essentially inelastic.

TABLE I. Details of the observed events.

Event	N	Polar angle, θ' (degrees)						
A	6	2.5	3.5	8.3	31	55 ($\lesssim$m)	70 (>m)	
B	7	1.4	3.0	3.8	7.0	35	47 (>m)	126
C	12	1.7 5.5	1.7 6.4	2.0 8.6	2.4 38 (1.5m)	2.8 41	4.7	5.3
D	13	0.6 20	2.0 21 (>m)	4.8 24	7.7 32	8.7 85	1.0 148 (>m)	12.8
E	8	0.24 29.2	0.28 ($\alpha\doteq 0$)	0.80	0.83	6.3	7.0	9.8
F	3	3.8	4.1	6.0	(α's;	$\doteq 0$	1.8	2.3)

IV. COMPARISON OF SPECIAL EVENTS WITH THEORY

Lord, Fainberg, and Schein[19] have described an event for which Fermi's theory gives a ready explanation in terms of multiple meson production in a median collision between an incoming proton ($W'=3\times10^{13}$ ev) and a nucleon on the edge of a nucleus in the emulsion. They were able to make some energy measurements by multiple scattering, which seem to support the general validity of the above picture. Camerini *et al.*[8] have also shown a photograph of an event which may be of this general type.

It should be noted here that many of the minimum ionization particles with which we are concerned are so energetic that, while in suitable cases it will be possible to measure their energy or set lower limits, it is impossible by present techniques to distinguish between protons and mesons. Consequently, in what follows we have assumed that all incoming particles of minimum ionization are protons, and that the forward shower particles are comprised mainly of pi-mesons.[20] The latter assumption was supported in the case of Lord, Fainberg, and Schein by the observation that pairs of minimum ionization particles (presumably electrons, and resulting from neutral pi-meson decay radiation) originated inside the inner shower cone. In our events below the numbers of tracks involved, and their lengths in the emulsion were such that, assuming approximately equal numbers of neutral, positive, and negative pi-mesons, we would have expected to observe about one electron pair for all the events, so the fact that we did not observe any is not statistically meaningful.

Unfortunately, because of limited track lengths in the emulsion and to distortion in some cases, we have not been able to make many useful energy measurements, and comparison with theory is made on the basis of numbers of shower particles and their angular distributions.

Details of the events are given in Table I. Events A, B, C, and D[21] were formed in a flight at about 85,000 feet in G5 emulsion of 250 microns thickness. Events E and F were formed in flights at over 90,000 feet in G5 emulsions of thicknesses 400 and 600 microns respectively.

Events A, B, C, and D: The events are illustrated in Figs. 7 and 8. In each of these four cases, the incoming particle has minimum ionization, and one or two of the oblique shower particles have ionization greater than

[19] Lord, Fainberg, and Schein, Phys. Rev. **80**, 970 (1951).

[20] The work of Camerini, Fowler, Lock, and Muirhead, Phil. Mag. **41**, 413 (1950), has indicated that the majority of shower particles with energies $\gtrsim$1 Bev are pi-mesons. These authors have also shown that fast pi-mesons may cause stars. However, since such mesons themselves must be produced in disintegrations in the upper atmosphere, it seems reasonable to ascribe incident singly charged particles, in the more energetic events, as protons.

[21] These events were found in 46 cc of emulsion containing ~450 stars with $\geqslant$5 shower particles. However, much of this emulsion was searched under conditions in which the special events may have been missed, and thus the four out of 450 stars probably represents a minimum for the frequency of these events.

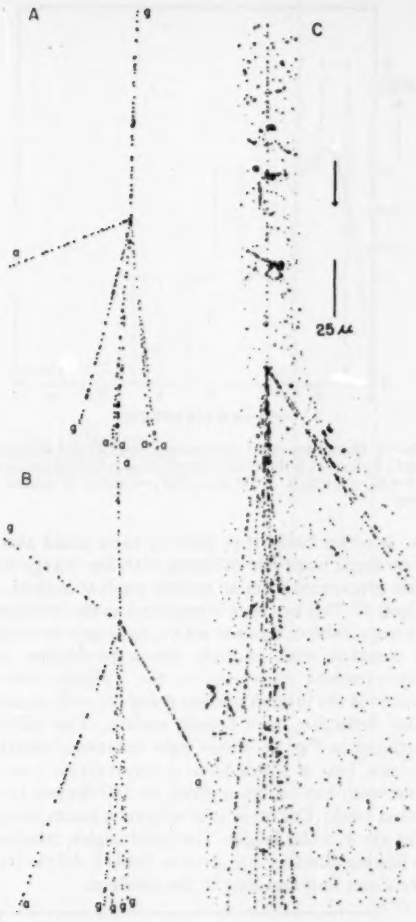

FIG. 7. Microprojections of events *A*, *B*, and *C*.

minimum (~1.5 to 2 times; see Table I). *B* and *C* have a short spur at the origin (~one micron long), which could be a recoil track resulting from a residual nucleus. Owing to the fairly large grain size in our emulsion, and the possibility of chance coincidence of several grains, it is difficult to be sure of these spurs, especially in case *A*, where the spur is shorter.

The numbers of tracks after collision were 6, 7, 12, and 13, respectively, so that, as we have pointed out previously,[22] from considerations of charge conservation (and assuming that the colliding particles remain as entities with enough kinetic energy, if charged, to give a visible track after the collision) the target nucleon in *B* and *D* could not have been a hydrogen nucleus, but must have been a nucleon in a heavier nucleus in the emulsion. On this basis also the events of Lord, Fainberg, and Schein and of Camerini *et al.* must have been collisions with nuclei heavier than hydrogen. Furthermore, although *A* and *C* can be p-hydrogen collisions according to the charge argument, we have noted that *C* has a possible, very short, nuclear recoil. The fact that most of these few cases cannot be simple hydrogen collisions (assuming the incoming particle to be a proton) may be reasonable on considerations of purely geometrical cross sections.

On the assumption that these events do represent multiple meson production in nucleonic interactions, we have plotted the angular distributions in the laboratory system and compared these with angular distributions calculated from Fermi's theory, assuming in each case a median or central type of nucleon-nucleon collision, and a given number of mesons, thus fixing both angular distribution and W'. Using the results of Fig. 6 relativistic transformations from the c.m. to the laboratory

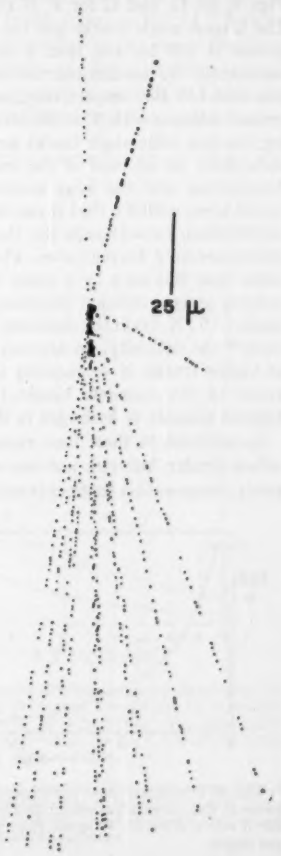

FIG. 8. Microprojections of event *D*.

[22] E. Pickup and L. Voyvodic, Phys. Rev. **82**, 265 (1951).

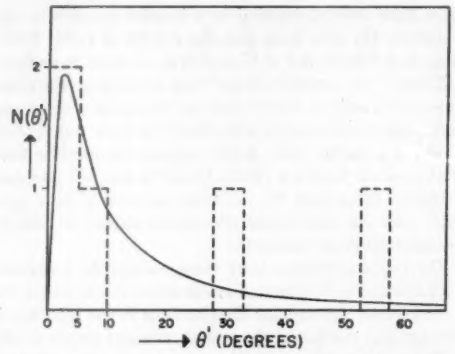

FIG. 9. Histogram shows experimental angular distribution for event A. Full curve is theoretical distribution in laboratory system for $N=5$, $r/R=0.37$, $W'\simeq 80$ Bev. $N(\theta')$ = number of mesons per degree.

system were made. The distributions are shown in Figs. 9, 10, 11, and 12 for A, B, C, and D, respectively. The largest angle tracks are not shown in the histograms. It will be seen that A and B are fairly well-represented by median-central collisions with $W'\simeq 80$ Bev and 145 Bev respectively, and $N=5$ and C by a central collision with $W'\simeq 600$ Bev and $N=10$ (excluding the two wide angle tracks here). D presents more difficulties, on account of the relatively wide angular distribution and the large number of tracks, and it would seem unlikely that it can be fitted to any single distribution, even though the theoretical distributions shown are only average ones. Thus we are led to conclude that this may be a more complicated event involving several collision processes, probably in a light nucleus (C, N, O) in the emulsion. We have noted previously[22] the difficulty, on account of the small number of visible tracks, of attempting to explain A and B in terms of the complete breakup of carbon, the next lightest element to hydrogen in the emulsion.

In addition to these four events, we have observed others similar, but with just one or two of the usual low energy evaporation fragments emitted in the disintegration. It seems likely that some of these could also be due to single nucleonic collisions with low energy fragments evaporated from an excited residual nucleus.

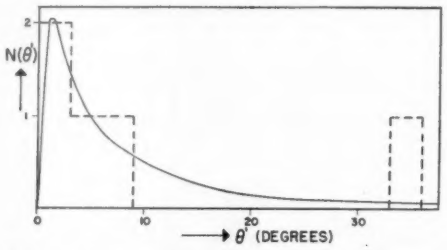

FIG. 10. Histogram shows experimental angular distribution for event B. Full curve is theoretical distribution in laboratory system for $N=5$, $r/R=0.53$, $W'\simeq 145$ Bev. $N(\theta')$ = number of mesons per degree.

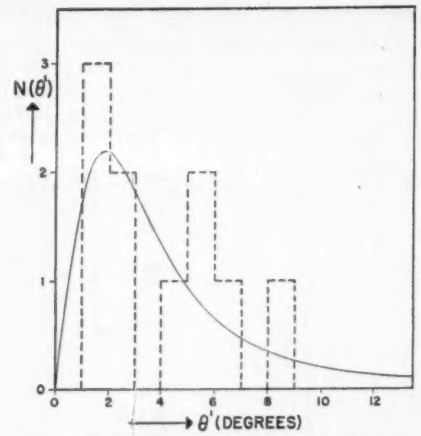

FIG. 11. Histogram shows experimental angular distribution for event C. Full curve is theoretical distribution in laboratory system for $N=10$, $r/R=0$, $W'\simeq 600$ Bev. $N(\theta')$ = number of mesons per degree.

Event E: This has been interpreted as the collision of a primary lithium nucleus with a hydrogen nucleus in the emulsion with multiple meson production in a nucleon-nucleon encounter in the collision, the remainder of the lithium nucleus going on, with no measurable deflection, as a helium nucleus. The collision, illustrated in Fig. 13, shows eight minimum ionization particles, four of which lie in a very narrow cone, together with the helium nucleus, at 180 degrees to the lithium track. The other four minimum ionization particles are at wider angles. The polar angles, relative to the lithium direction, are given in Table I. All the tracks were about four mm long in the emulsion.

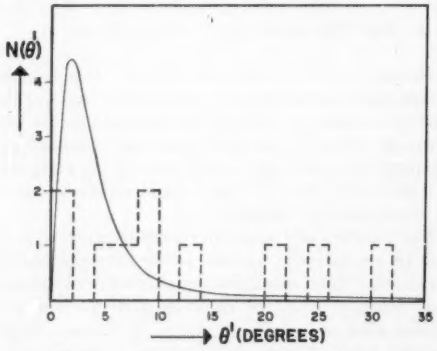

FIG. 12. Histogram shows experimental angular distribution for event D. Full curve is theoretical distribution in laboratory system for $N=10$, $r/R=0$, $W'\simeq 600$ Bev. $N(\theta')$ = number of mesons per two degrees.

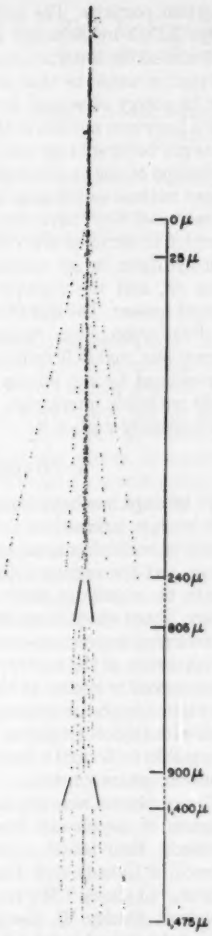

FIG. 13. Microprojection of event *E* (collision of lithium nucleus).

The grain density for the track identified as due to helium was 74±3 grains per 100 microns, while grain density for the minimum ionization tracks was 19±2 grains per 100 microns (being low in this particular batch of emulsion). This gives an ionization of almost four times minimum for the helium nucleus. Also the absolute number of delta-rays along this track (~0.9 δ-rays per 100 microns) was approximately as expected for a relativistic helium nucleus. Delta-ray counting was made along the primary track. The mean ratio of delta-rays for this track compared with the helium track was 2.5±0.5, whereas that expected for a primary relativistic nucleus with three units of charge is 2.25. Thus the incoming nucleus was identified as lithium.

The event is therefore tentatively described as follows:

$$Li_3^{7(6)}+H_1^1=He_2^{4(6)}+2p_1^1(n_0')+\Sigma \text{ (pi-mesons)}.$$

Conservation of mass units and charge, and the fact that there were eight minimum ionization tracks fix the number of charged mesons, N, on this picture as $6\leqslant N\leqslant 8$. While, on the basis of charge, we cannot definitely rule out the possibility that this event is really due to a collision with a carbon nucleus resulting in the complete break-up of carbon, rather than a hydrogen collision, the completely relativistic nature of the event and the small number of tracks appear to make this possibility unlikely.

Assuming the multiple production of seven charged mesons and a median nucleon-hydrogen collision ($r\simeq 0.71R$), Fermi's theory gives $W'\simeq 2\times 10^{12}$ ev. The observed angular distribution is compared graphically in Fig. 14 with that calculated for the above energy for a median collision. It will be seen that the agreement is quite reasonable considering the small number of tracks involved, and thus we conclude that the incoming nucleus is lithium with an energy of about 2×10^{12} ev per nucleon. For purposes of comparison the theoretical curve for seven charged mesons for a centered collision ($r=0$; $W'\simeq 150$ Bev) is also shown in Fig. 14.[23] Scattering measurements made on the two innermost minimum ionization tracks, relative to the α-particle, indicate that their energy was greater than 10 Bev. The tracks were not sufficiently long for more precise measurements.

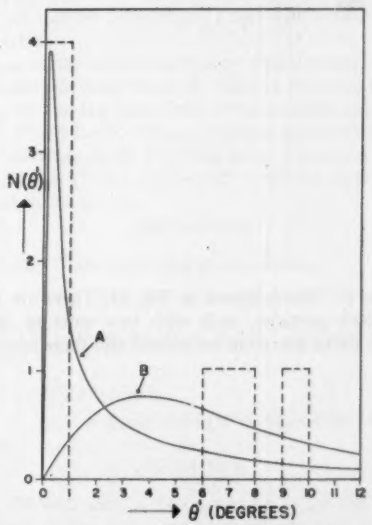

FIG. 14. Histogram shows experimental angular distribution for event *E*. Full curve *A* is theoretical distribution in laboratory system for $N=7$, $r/R=0.71$, $W'\simeq 2\times 10^{12}$ ev. For comparison curve *B* shows theoretical distribution for $N=7$, $r/R=0$, $W'\simeq 150$ Bev. $N(\theta')$ = number of mesons per degree.

[23] It may be noted that an isotropic distribution (regardless of theory) fitting the main forward cone of this event would give a much smaller probability for the more diffuse tracks than would Fermi's theory for an off-centered collision.

FIG. 15. Microprojection showing event *F* (collision of oxygen nucleus).

Event F: This is shown in Fig. 15. There are three relativistic particles, each with two units of charge (≐four times minimum ionization) and three minimum ionization particles. The primary was identified as of charge 7.5 ± 1 by delta-ray counting (using the delta-ray count on the α-particles as a criterion). The simplest explanation would be that an incoming oxygen nucleus with an energy of several Bev per nucleon has collided with a hydrogen nucleus in the emulsion, one α-particle of oxygen being split up into nucleons with the possible production of one or two mesons, and the residue of the oxygen nucleus splitting up into three α-particles.

Freier and Ney[12] have discussed an event, which they interpret in terms of the collision of a carbon nucleus with hydrogen in an emulsion, with a boron nucleus going on, and the multiple production of about 10 charged mesons. The spread of their experimental angular distribution, even though the picture is only an average one, makes it seem unlikely that the event can be explained by the present picture on the basis of a single nucleonic interaction, although two interactions could possibly explain it.

V. CONCLUSIONS

An attempt has been made to explain several special high energy interactions in terms of Fermi's recent theory of multiple meson production, and it has been shown that the angular distributions for some of these events fit reasonably well with those given by the theory. Those which do not fit so well could be explained by assuming more complicated collision processes. Our interpretation of the events must, however, be regarded as somewhat tentative at this stage. The special collisions are comparatively rare, and it is hoped that further work with thicker emulsions will yield events which are susceptible to accurate energy, as well as angular distribution, measurements.

The emulsions were exposed through a collaborative program of cosmic-ray investigations by the Bartol Research Foundation and the National Research Council of Canada with the cooperation of the ONR project, "Skyhook." We are also indebted to Barbara Woodruff, Shirley W. Young, and Beverley Mear for preliminary searching, to B. Bigham (Queen's University) for some calculations and measurements, and to D. Rushton for the drawings and photomicrographs.

A Deduction of the High Energy Spectrum of Cosmic-Ray Primary Nucleons from the Observed Muon Spectrum*

URI HABER-SCHAIM†
Institute for Nuclear Studies, University of Chicago, Chicago, Illinois
(Received August 31, 1951)

Fermi's theory of pion production is extended to treat collisions of nucleons with air nuclei. The energy distribution of the created pions and their daughter muons is approximately calculated, and is applied to correlate the observed muon spectrum in the energy range 10–100 Bev with the primary nucleon spectrum. The results and limitations of this procedure are discussed.

I. INTRODUCTION

IN two recent papers,[1,2] Fermi suggested a new theory for the production of pions in nucleon-nucleon collisions at very high energies. As one seldom observes high energy nuclear collisions, or stars, which can be interpreted as nucleon-nucleon collisions,[3–5] it was found worthwhile to try to extend the theory to nucleon-nucleus collisions and thereby obtain a correlation between the muon energy spectrum (as a result of $\pi\rightarrow\mu$ decay) and the primary nucleon spectrum of the cosmic radiation. In what follows primary protons in the energy range 100–1200 Mc^2,[6] giving rise mainly to muons of energy 10–100 Mc^2, are considered. There are several advantages of applying the Fermi theory in this region: (1) The energy degradation in one nucleon-nucleon collision is very large, so that only the first collision needs to be counted unless the second collision occurs inside the same nucleus. In other words, there are too few primaries of such high energy that the secondaries will contribute appreciably to the flux. (2) At these high energies most particles coming out of a nucleon-nucleon collision (and at least all the energetic ones) are collimated in rather narrow cones. This simplifies the treatment of the nucleon-nucleus collision because all the particles inside the cone will collide essentially with only one nucleon at a time. (3) The spectrum of muons (resulting from pion decay) may be taken from experiments made at sea level since both μ decay in flight and energy loss by ionization may be neglected. (4) In high energy collisions, where both nucleons and pions are extremely relativistic in the center-of-mass system, there will be equipartition of energy which also simplifies the treatment of nucleon-nucleus collisions.

An attempt is made to calculate the quantity which determines the relation between the observed muon spectrum and the primary proton spectrum. This quantity determines how many muons of energy between E' and $E'+dE'$[7] are produced in a nucleon-nucleus collision where the energy of the primary proton is W'. It turns out, however, that it is more convenient to express this number as a function of the energy available in the c.m. system of the primary proton and one nucleon in the nucleus. Let us denote this quantity by $R(W, E')$. Then the differential energy spectrum $g(E')$ of muons at sea level, and the primary proton spectrum, are related to each other by the following equation:

$$\int_{W_{\min}}^{\infty} f(W)dW R(W, E')=g(E'), \qquad (1)$$

where $f(W)$ is the number of primary protons which have an energy between $W/2$ and $\frac{1}{2}(W+dW)$ in the c.m. system.

$W_{\min}$ is the minimum energy which is required to produce a muon of energy E'. One can of course replace $W_{\min}$ by 0 at the lower limit of the integral and define $R(W, E')\equiv 0$ for $W<W_{\min}$. The main task of this paper is to calculate $R(W, E')$. This done, a solution of the integral Eq. (1) for $g(E')=BE'^{-r}$ will be obtained by the substitution

$$f(W)=AW^{-s}. \qquad (2)$$

W and W' are connected by the relation,

$$W=(2W'+1)^{\frac{1}{2}}\approx(2W)^{\frac{1}{2}}.$$

Hence the primary spectrum in the laboratory system will be

$$f(W')=f(W)(dW/dW')$$
$$=A(2W')^{-(s/2)}(W'^{-\frac{1}{2}}/\sqrt{2})=A'W'^{-s'}, \qquad (3)$$

where

$$s'=(s+1)/2.$$

In the next section two experiments for the determination of the muon spectrum at sea level are discussed. In Sec. III a correction for the loss of pions by collision is introduced. This is necessary at the high energies under consideration because there is an appreciable probability that the pions will collide with air nuclei before having a chance to decay into muons. In

* Supported in part by the joint program of the ONR and AEC.
† Now at the Isotope Department, Weizmann Institute of Science, Rehovot, Israel.
[1] E. Fermi, Prog. Theor. Phys. **5**, 570 (1950) quoted as *A*.
[2] E. Fermi, Phys. Rev. **81**, 683 (1951) quoted as *B*.
[3] Lord, Fainberg, and Schein, Phys. Rev. **80**, 970 (1950).
[4] Camerini, Fowler, Lock, and Muirhead, Phil. Mag. **41**, 413 (1950).
[5] E. Pickup and L. Voyvodic, Phys. Rev. **82**, 265 (1951).
[6] All energies will be expressed in Mc^2 where M is the nucleon mass.
[7] Primed quantities refer to laboratory system and unprimed quantities to c.m. system.

TABLE I. The fraction of charged pions decaying into muons.

E'	$c(E')$
100	0.514
80	0.632
50	0.715
20	0.773

Sec. IV the energy spectrum of pions (and their daughter muons) created in a nucleon-nucleon collision is presented. A way of treating the nucleon-nucleus collision is suggested in Sec. V. Finally, in Sec. VI, the results obtained are stated and the limitations of the present treatment are discussed.

II. THE MUON SPECTRUM

Measurements of the muon spectrum at sea level in the range 10–80 Mc^2 were made by several authors giving quite different results. Ehmert[8] measured the number of muons which passed through a counter telescope as a function of depth under water. Assuming that the rate of energy loss by ionization is independent of the energy of the muon, and that this is the only mechanism by which a muon can be stopped in the water, he deduced a differential spectrum of the form $B_1E'^{-r_1}$, with $r_1=2.9$. The vertical flux of particles of energy $E'>10\ Mc^2$ is given by Rossi,[9] as $I_v=9.5\times10^{-4}$ sec^{-1} cm^{-2} sterad^{-1}. This gives immediately the coefficient $B_1=0.142$.

Another experiment was performed by Glaser, Hamermesh, and Safonov.[10] These authors measured the spectrum of charged cosmic-ray particles about 800 feet above sea level. At this altitude practically all fast particles may be considered to be muons. The apparatus consisted of a magnetic spectrograph using two counter-controlled cloud chambers with a large electromagnet between them. A total of 127 particles of energy of 10 Bev and above was measured and the differential spectrum in the region 10–80 Bev was found to be also of the form E'^{-r_1} but with $r_1=2.2$. No attempt was made in this experiment to determine the total flux. This is again taken from Rossi, and the value $B_1=1.8\times10^{-2}$ is obtained.

III. CORRECTION FOR COLLISIONS OF PIONS IN THE AIR

At high energies the lifetime of the pions is sufficiently increased so that loss of pions resulting from collisions in air has to be considered. We shall assume that the mean-free path for collision in air is the same for nucleons and pions. Then the number of muons $d\mu$ resulting from the decay of $d\pi$ pions produced in an air layer of thickness dp at atmospheric depth p (measured in g cm^{-2}) is

$$d\mu=[\lambda_c/(\lambda_c+\lambda_d)]d\pi=[(\tfrac{2}{3}nN(P))/(\lambda_c+\lambda_d)]dp, \quad (4)$$

where λ_c and λ_d are the mean-free paths for collision and decay respectively, n is the number of pions produced in the collision and $N(p)$ is the number of primaries. The quantity λ_c is a constant when expressed in g cm^{-2} but λ_d depends on the atmospheric depth and on the energy of the pion. The fraction of charged pions which decays into muons $c(E')$ is obtained from the above equation by a straightforward calculation. The results are given in Table I, taking $\tau=2.6\times10^{-8}$ sec for the proper mean life of the charged pion. This correction function can be approximately represented by aE'^{-m} with $a=1.23$; $m=0.155$. Hence, if there were no loss of pions due to collisions, the muon spectrum would be

$$(B_1E'^{-r_1}/aE'^{-m})=BE'^{-\gamma}.$$

It is this quantity which will be set equal to $g(E')$ in (1).

IV. THE NUCLEON-NUCLEON COLLISION

In (A) the following expressions for the multiplicity was found:

$$n=1.34(W-2)^{\frac{1}{4}}/W^{\frac{1}{4}}. \quad (5)$$

This formula was found under the assumption that the collision is completely inelastic, i.e., that the total energy of the pions created is $W-2$. If we include the two nucleons in the equilibrium they will retain some kinetic energy and the energy available for pion production, and with it the average number of pions will somewhat decrease On the other hand, a correction for the conservation of angular momentum was included in (5) which holds only at very high energies but is too large for smaller energies. Taking both of these factors into account, we found that at the energy range under consideration (100–1000 Mc^2) they nearly cancel, and only at low energies Eq. (5) breaks down entirely. (A complete graph for the multiplicity was calculated and may be published separately.) So in all the following calculations Eq. (5) will be used, with the understanding that both the angular distribution and the incomplete inelasticity cancel as indicated.

In the c.m. system the particles coming out of the collision obey a certain energy and angular distribution. The most important factor determining the energy of a particle in the laboratory system is the angle at which it was emitted in the c.m. system with respect to the direction of the primary, not the amount of energy by which it deviated from the average energy in the c.m. system. Therefore each particle will be assumed to have an energy in the c.m. system of

$$E_\pi=W/(n+2). \quad (6)$$

At the energies under consideration the pions (and the nucleons to a good approximation) can be treated as extremely relativistic. Then

$$E_\pi'=\gamma E_\pi(1+\eta), \quad (7)$$

where $\eta=\cos\theta$, θ being the angle between the primary

[8] A. Ehmert, Z. Phys. **106**, 751 (1937). See also J. Clay, Revs. Modern Phys. **11**, 128 (1939).
[9] B. Rossi, Revs. Modern Phys. **20**, 57 (1948).
[10] Glaser, Hamermesh, and Safonov, Phys. Rev. **80**, 625 (1950).

direction and that of the escaping pion in the c.m. system, and

$$\gamma=1/(1-\beta^2)^{\frac{1}{2}}=W/2. \quad (8)$$

The velocity of the c.m. as measured from the laboratory β, (in c units) has been put equal to one. Equation (7) then gives as a correlation between the angular distribution in the c.m. system, $f_4(0.96\eta)$ given in (B) and the energy distribution in the laboratory system. Denoting the number of pions in the energy range E_π', $E_\pi'+dE_\pi'$ by $\rho(E_\pi')dE_\pi'$, we have:

$$\rho(E_\pi')dE_\pi'=\text{const}nf_4(0.96\eta)(d\eta/dE_\pi')dE_\pi'$$

$$=\text{const.}\frac{n}{\gamma E_\pi}f_4\left(0.96\left[\frac{E_\pi'}{\gamma E_\pi}-1\right]\right)dE_\pi', \quad (9)$$

$$f_4(x)=\frac{2}{x^2(1-x^2)}-\frac{1}{x^2}\ln\left(\frac{1+x}{1-x}\right).$$

The constant in (9) is obtained by integrating over E_π' and has the value 0.159.

The exact dependence of $n/\gamma E_\pi$ and γE_π on W is quite complicated as seen from Eqs. (5) and (6). In the region $12<W<70<$ this can be replaced by the following expressions with an accuracy of 2 percent:

$$n/\gamma E_\pi=4.12/W,$$
$$\gamma E_\pi=W^{\frac{1}{2}}/3.24. \quad (10)$$

Further, the energy E' of the muons is on the average smaller than their parent pions by a factor of 0.81. Taking all this into account we find for the energy distribution of the muons (which is obviously dependent also on W):

$$\rho(W, E')=\frac{0.54}{W}f_4\left(0.96\left[\frac{3.98E'}{W^{\frac{1}{2}}}-1\right]\right). \quad (11)$$

V. THE NUCLEON-NUCLEUS COLLISION

In treating this problem we neglect the motion of the nucleons inside the nucleus and adopt a static model. We assume an "air" nucleus consisting of 15 nucleons which are arranged in three layers in the following manner: four nucleons in the top layer, seven in the middle layer, and again four in the last one. This gives the nucleus a more or less spherical shape and also implies that a fast incoming nucleon cannot collide with more than three nucleons in succession. Taking the geometrical cross section for the nucleon-nucleon collision, it is found that these layers have a transparency of 0.37 and the probabilities for having a one, two, or three-layer collision are found to be $b=0.45$, $b_1=0.15$, $b_2=0.40$, respectively.

Let us look into the two-layer collision in some detail. The two nucleons and the pions produced in the first collision are strongly collimated in the forward direction; the angular distribution in the c.m. system favors the forward (and backward) direction; the transformation to the laboratory system causes the particles already in the forward half to be squeezed into a very small angle around the forward direction and simultaneously spreads all the rest of the particles. It is evident that practically all the energy is carried away by the particles in the narrow cone. As they hardly separate until they reach the second layer, it is assumed that all the particles in the core pass through one nucleon in the second layer. Because of the partial transparency only 63 percent of the particles in the core will, on the average, collid with the nucleon in the second layer.

The energy available in this collision in the laboratory system is given by

$$W_1'=0.63\delta(n+2)\alpha\gamma E_\pi, \quad (12)$$

where E is given by (6) and α is the ratio between the average energy in the core and the average energy γE_π of all the particles in the laboratory system, and δ is the percentage of particles in the core. The energy W_1 in the new c.m. system of the impinging composite "particle" and a nucleon of the second layer is given by

$$W_1\approx(2W_1')^{\frac{1}{2}}\equiv h_1W. \quad (12')$$

The degradation factor, h_1, is slowly varying with W as shown in Table II. The ratio of the number of pions in the core passing through the second layer without colliding and the total number of pions produced, O_1, is also slowly varying. The energy distribution for the pions produced in a two-layer collision can therefore be written in the form,

$$\rho_1(W, E')=\rho(W_1, E')+\phi_1(W, E')$$
$$=\rho(h_1W, E')+\phi_1(W, E'). \quad (13)$$

The function $\phi(W, E')$ corresponds to the particles left over from the first collision. For these we neglect the spread in energy by replacing f_4 by a δ-function

$$\phi_1(W, E')=(5.1/\alpha W)O_1\delta([3.98E'/\alpha W^{\frac{1}{2}}]-1). \quad (14)$$

Similarly we find for the three-layer collision

$$\rho_2(W, E')=\rho(h_2W, E')+\phi_{21}(W, E')+\phi_{22}(W, E'), \quad (13')$$

where ϕ_{21}, ϕ_{22} correspond to the left-over particles from the first and second collisions, respectively, and are given by

$$\phi_{21}(W, E')=(5.1/\alpha W)O_{21}\delta([3.98E'/\alpha W^{\frac{1}{2}}]-1),$$
$$\phi_{22}(W, E')=(5.1/\alpha h_1W)O_{22}\delta([3.98E'/\alpha h_1^{\frac{1}{2}}W^{\frac{1}{2}}]-1).$$

All the quantities used here are given in Table II.

The angle limiting the central core was taken equal

TABLE II. The various parameters as functions of W.

W	W'	η	δ in %	h_1	h_2	α	O_1	O_{21}	O_{22}
20	200	5.5	54	0.730	0.700	1.67	0.18	0.068	0.14
30	400	7.00	62.5	0.747	0.720	1.50	0.20	0.073	0.16
40	800	8.15	68.7	0.770	0.746	1.39	0.21	0.078	0.18
50	1230	9.10	73.7	0.790	0.778	1.34	0.22	0.082	0.19

TABLE III. Comparison of results with experiments.

W'	$F_G(W')$	$F_E(W')$	Hilberry	Stinchcomb
60	4.40×10^{-4}	6.0×10^{-4}	5.1×10^{-4}	4.10^{-3}
100	2.60×10^{-4}	2.8×10^{-4}	2.06×10^{-4}	

to 7°. In this region the angular distribution already flattens out, and hence the result is not sensitive to reasonable changes of that angle. The particles outside this core are assumed to collide with different nucleons, producing some additional pions of much lower energy escaping at large angles from the primary direction and disrupting the nucleus, thus giving rise to the usual pattern of stars as observed in photographic emulsions.

The function $R(W, E')$ which was introduced in (1) can now be written out explicitly

$$R(W,E')=b\rho(W,E')+b_1\rho_1(W,E')+b_2\rho_2(W,E') \quad (15)$$

Inserting this expression for $R(W, E')$ into (1) we obtain a sum of integrals. Let us look at the first one:

$$\int_{W_{\min}}^{\infty} f(W)\frac{dW}{W}f_4\left(0.96\left[\frac{3.98E'}{W^{\frac{1}{3}}}-1\right]\right).$$

For $W=W_{\min}$ the bracket inside the argument of f_4 becomes equal to one. By substituting

$$(3.98E'/W^{\frac{1}{3}})-1=u, \quad dW/W=-\tfrac{3}{3}du/(u+1),$$

the integral becomes

$$\int_{-1}^{+1} f\left(\left[\frac{u+1}{3.98E'}\right]^{-3}\right)\frac{du}{u+1}f_4(0.96u).$$

If this integral alone were to be set equal to BE'^{-r} then one would obtain an immediate solution for f by the use of (2). This gives

$$E'^{-1s}\int_{-1}^{+1}(u+1)^{1s-1}f(0.96u)du\sim E'^{-r},$$

and therefore

$$s=\tfrac{3}{2}r \quad (16)$$

It is easily recognized that if we use constant values for h_1, h_2, α, etc., Eq. (2) may be applied for the whole expression. This will be done and the error introduced will be discussed later. E' will then appear only in the form E'^{-1S}.

VI. RESULTS AND DISCUSSION

Taking for averages over the appropriate energies, $h_1=0.76$, $h_2=0.74$, $\alpha=1.44$, $O_1=0.2$, $O_{21}=0.075$, $O_{22}=0.17$, and making use of (1), (13′), (14′), (15), and (16), we obtain for the differential spectrum of the primaries

$$f_G(W')=0.030\times W'^{-2.03}$$

on the basis of the muon spectrum of Glaser *et al.*, and

$$f_E(W')=0.57\times W'^{-2.56}$$

on the basis of Ehmert's muon spectrum. The integrated spectrum (the total vertical flux) is given by

$$F_G(W')=0.029W'^{-1.03}$$

and

$$F_E(W')=0.37W'^{-1.56},$$

respectively. These results should be trusted only in the region $100<W'<1500\ Mc^2$.

It is interesting to note that although the two resulting integral spectra are quite different, their values at $W'=100$ are practically equal. The exponent in F_G is nearly the same as the one found by Winkler,[11] and Schein and Vidale[12] in the energy range $1<W'<15\ Mc^2$. The coefficient, however, is smaller than that found at low energies by a factor of ten. This contradiction is hard to reconcile unless one is willing to assume that the primary spectrum behaves in a very strange way between 15 and 100 Mc^2. The result obtained from Ehmert's muon spectrum seems therefore more plausible.

There are no direct measurements of the primary spectrum available in the energy band 100–1500 Mc^2. Comparison can be made with results deduced from electronic showers.

Hilberry[13] found for the integrated primary spectrum $H(W')=0.665\times W'^{-1.75}$ which agrees fairly well with our results. Another value for the primary flux also obtained from showers by Stinchcomb[14] at $W'=60$ is again about ten times larger than our value. A comparison is given in Table III.

Attention should be drawn to the effect of the approximations made and to the sensitivity of the results to changes in the theory itself.

One observes immediately that if the dependence of h_1, h_2, O_1, etc., on W is taken into account, the substitution (2) would yield a spectrum for the muons of the form,

$$\sum B_iE'^{-r_i},$$

where the r_i are slightly different from each other. This in itself is not objectionable because one can easily represent the experimental curve with such an expression.

Another question of interest is whether the correlation of the muon spectrum with the primary spectrum could be used to discriminate between the various theories of pion production.

One of the characteristics of the Fermi theory is the dependence of the average number of pions produced as the function of energy $n\sim W^{\frac{1}{4}}$. Let us see what the form of the primary spectrum will be if we replace $\frac{1}{4}$ by k where $0<k<1$. We have

$$n, n+2\sim W^k; \quad \gamma\sim W; \quad E_\pi\sim W^{1-k};$$

therefore

$$n/\gamma E_\pi\sim W^{-2(1-k)}; \quad 1/\gamma E_\pi\sim W^{-(2-k)};$$

[11] J. R. Winkler *et al.*, Phys. Rev. **79**, 656 (1950).
[12] Private communication by Professor M. Schein.
[13] N. Hilberry, Phys. Rev. **60**, 1 (1941).
[14] T. G. Stinchcomb, Phys. Rev. **80**, 479 (1950).

from which follows the general relation between s and r:

$$s=k(2-r)+2r-1;$$

for $r=2$ we get

$$s=3 \text{ independent of } k.$$

Only if r is quite different from 2 will it be possible to decide which k gives the best results.[15]

[15] Compare Lewis, Oppenheimer, and Wouthuysen, Phys. Rev. 73, 127 (1948). There $k=\frac{1}{2}$.

VII. ACKNOWLEDGMENT

It is a pleasure to express my gratitude to Professor E. Fermi, who suggested this problem, for his frequent advice and encouragement, and to Professor M. Schein for very stimulating discussions of the experimental problems involved in this work. I would like to express my appreciation to my colleague, Art Rosenfeld, for the reading of the manuscript and for valuable criticism. Thanks are also due to the Hebrew Technical Institute in New York for a grant in aid.

PHYSICAL REVIEW VOLUME 84, NUMBER 6 DECEMBER 15, 1951

A NaI (Tl) Scintillation Spectrometer Study of Proton Gamma-Ray Coincidences

ROBERT C. ALLEN,* JOHN E. MAY, AND WALDO RALL
Sloane Physics Laboratory, Yale University,† New Haven, Connecticut
(Received September 10, 1951)

A proton gamma-ray coincidence study of the $Al^{27}(\alpha,p)Si^{30}$ reaction has been made using a NaI(Tl) scintillation spectrometer. The decay scheme of the excited states of Si^{30} has been established and the energies of the gamma-rays have been measured. The decay of the third excited state was found to be a double cascade process: from the third to the second to the ground state, and from the third to the first to the ground state. The gamma-ray energies in the former process were determined to be 1.28 ± 0.06 Mev and 3.66 ± 0.15 Mev. The energies of both the gamma-rays in the latter transition were found to be between 2.2 and 2.7 Mev. Measurements on the second excited state showed that the decay was direct to the ground state, the energy of the gamma-rays being 3.63 ± 0.15 Mev. The gamma-ray energy from the first excited state was established to be 2.32 ± 0.05 Mev.

I. INTRODUCTION

EXCITED states of nuclei arising from nuclear reactions have been studied primarily by energy measurements of the product particles and by energy measurements of the gamma-rays from the residual nucleus. With the precision now achieved by several research groups, the energies of the levels may be coupled with the gamma-ray energies to suggest a decay scheme.

A coincidence method, in which the gamma-rays associated with a specific level are investigated, can give information as to the precise mode of decay of an excited state. Benson[1] established the existence of coincidences between gamma-rays and protons in the reaction $Al^{27}(\alpha,p)Si^{30}$. Landon[2] extended the technique to include energy measurements of the gamma-rays by absorption methods using a scintillation detector. From his measurements Landon was able to give a probable decay scheme for the excited states of Si^{30}. A NaI(Tl) scintillation spectrometer which provides high efficiency, large solid angle, good resolving time, and fair energy resolution appears well suited to this type of problem. The work described in this paper concerns the application of a NaI(Tl) gamma-ray counter to the energy measurement of the gamma-rays emitted in coincidence with the protons from the reaction $Al^{27}(\alpha,p)Si^{30}$. The reaction was produced with 7.8 Mev cyclotron alpha-particles.

II. Si^{30} ENERGY LEVELS

The low energy levels of Si^{30} as determined from the $Al^{27}(\alpha,p)Si^{30}$ reaction[1,2] lie at approximately 0, 2.4, 3.7, and 5.0 Mev. These agree fairly well with those found from the $Si^{29}(d,p)Si^{30}$ reactions,[3,4] except that Van Patter and his colleagues[5] find that there may be two levels around 3.7 Mev, namely at 3.52 and 3.79 Mev. The assignment of both of these levels to Si^{30}, they point out, is not yet definite, since a study of relative intensities from separated isotope targets did not give conclusive results on these levels. No indication of this

TABLE I. Breakdown of coincidence counts.

Si^{30} excited state	Coincidences	Observed / Accidental	Protons per coincidence	Coincidences per hour
First	3241	16	230	130
Second	8901	18	225	130
Third	20,666	16	145	700

* Part of a dissertation presented to the Faculty of the Graduate School of Yale University, in partial fulfillment of the requirements for the degree of Doctor of Philosophy.
† Assisted by the joint program of the ONR and AEC.
[1] B. B. Benson, Phys. Rev. 73, 7 (1948).
[2] H. H. Landon, Phys. Rev. 83, 1081 (1951).
[3] R. F. Humphreys and H. T. Motz, Phys. Rev. 80, 595 (1950).
[4] Van Patter, Sperduto, and Enge, Phys. Rev. 83, 212(A) (1951).
[5] Private communication from D. M. Van Patter.

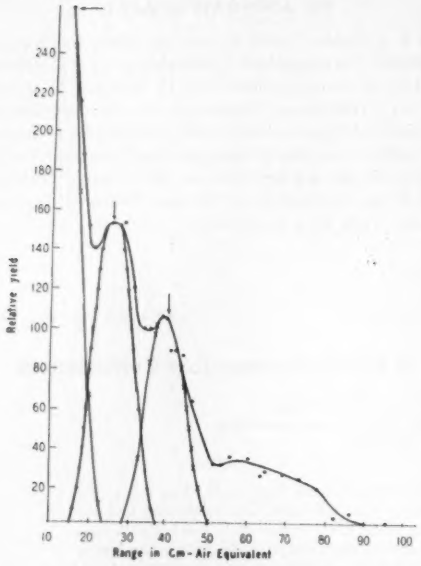

FIG. 1. Proton spectrum—$Al^{27}(\alpha,p)Si^{30}$.

doublet level was found in our work; however, neither the resolution of the proton groups nor the gamma-rays is such that we can rule out such a doublet, especially if the yield from one is low.

The proton spectrum used for the proton-gamma coincidence experiment is shown in Fig. 1, resolution being sacrified to gain solid angle. The protons were detected with a proportional counter and their range measured by absorption in aluminum. The protons corresponding to the first, second, and third excited states were selected by setting the absorption at 39.7, 25.3, and 14.4 cm air equivalent, respectively.

III. EXPERIMENTAL ARRANGEMENT

The arrangement of the bombardment chamber, aluminum target, proton proportional counter, and NaI(Tl) crystal gamma-ray counter is shown in Fig. 2. A block diagram of the circuit is shown in Fig. 3. The

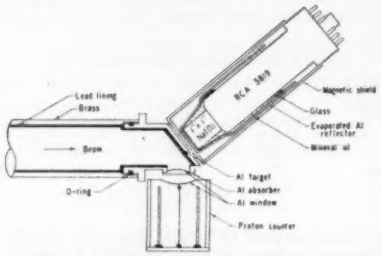

FIG. 2. Diagram of proton and gamma-ray counters.

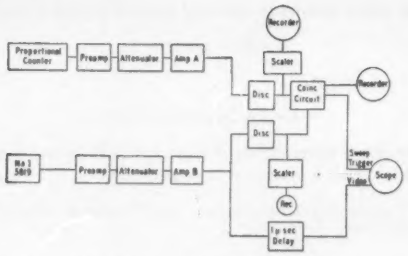

FIG. 3. Block diagram of apparatus.

proton and gamma-ray pulses were amplified, fed to a discriminator and coincidence circuit and to scalers and recorders. The gamma-ray pulses were also fed through a delay line to the y-axis amplifier of a synchroscope. The coincidence output was recorded and also used to trigger the sweep and intensifier gate of the synchroscope. In this way only the gamma-ray pulses in coincidence with a proton were displayed on the face of the cathode-ray tube. The individual pulses were photographed on continuously moving film, using a modified 16-mm movie camera with an f:2.5 lens.

Two types of calibration were made periodically throughout each run. Energy calibrations were made by taking time exposures[6] of the pulse distribution from the 1.28-Mev Na^{22} gamma-ray. A typical exposure is shown in Fig. 4. The top two bands correspond to the photoelectric and Compton processes of the 1.28-Mev gamma-ray, while the lower two are associated with Na^{22} positron annihilation radiation.

Square pulses of one microsecond duration and of

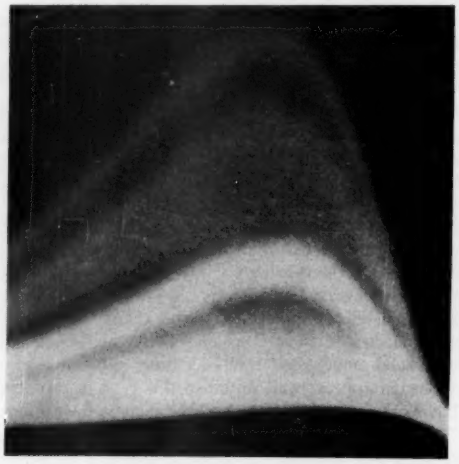

FIG. 4. Photographic distribution of Na^{22}.

[6] R. Hofstadter and J. A. McIntyre, Phys. Rev. **80**, 631 (1950).

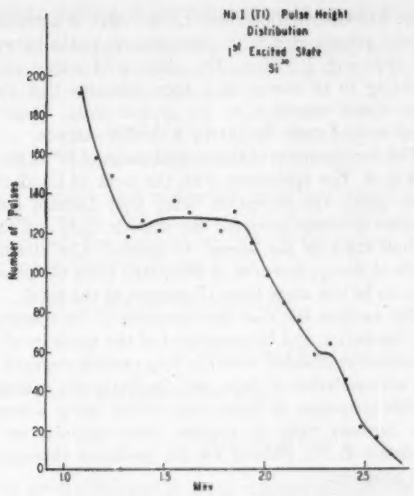

FIG. 5. Pulse-height distribution. First excited state—Si^{30}.

variable pulse height were introduced into the amplifier system and photographed to provide a frequent check on the stability of the electronic equipment.

IV. PULSE-HEIGHT DISTRIBUTIONS

Table I lists for each excited state the total number of coincidences, the ratio of observed to accidental coincidences, the number of protons required per coincidence, and the number of coincidences per hour. The low coincidence counting rates were required in order to maintain a high observed to accidental coincidence ratio.

For the analysis of the pulse-height data, the film was projected on a ruled screen and the height of each pulse was recorded. The resultant pulse-height distributions are shown in Figs. 5–7. Figure 5 gives the pulse height distribution of the gamma-rays from the first excited state of Si^{30}. The photoelectric and Compton peaks are apparent and establish an energy of 2.32 ± 0.05 Mev in excellent agreement with the value of the energy level.

For the second excited state the number of protons per coincidence was the same as that for the first excited state. This is definite evidence that the transition is direct to ground. Figure 6, however, shows the presence of two gamma-rays. The peak near 2.3 Mev and the broad distribution from 1.5 Mev to 2.0 Mev are attributed to photoelectric and Compton effects associated with gamma-rays from the first excited

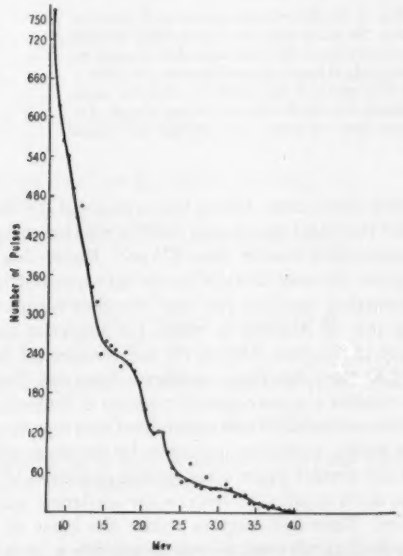

FIG. 6. Pulse-height distribution. Second excited state—Si^{30}.

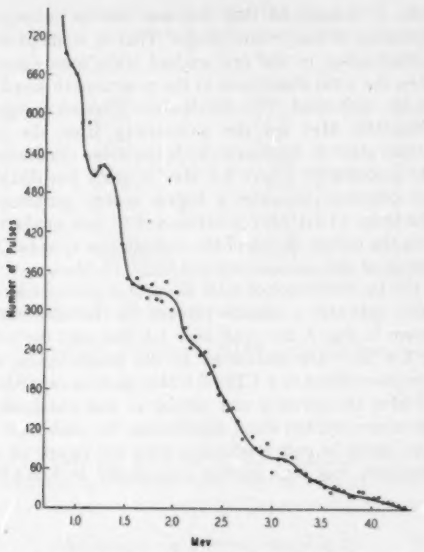

FIG. 7. Pulse-height distribution. Third excited state—Si^{30}.

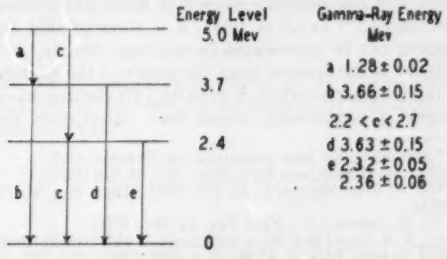

FIG. 8. Decay scheme of Si^{30}.

state. It is believed that this was due to inadequate separation of the proton groups. That is, some protons corresponding to the first excited state were counted when the total absorption in the proton path was 25.3 cm air equivalent. This distribution gives an energy of 2.36±0.06 Mev for the gamma-ray from the first excited state in agreement with the value cited above. The distribution above 2.5 Mev is much less distinct, but definitely indicates a higher energy gamma-ray. The bulge at 3.1 Mev is attributed to pair production with the escape of one of the annihilation quanta. The energy of this gamma-ray is 3.63±0.15 Mev.

For the third excited state the proton per coincidence value indicates a cascade process. In the distribution shown in Fig. 7, the peak near 1.3 Mev and the bulge at 1.0 Mev are attributed to the photoelectric and Compton effects of a 1.28±0.6 Mev gamma-ray. Above 2.7 Mev the curve is very similar to that obtained for the second excited state. Attributing the peak near 3.1 Mev again to pair production with the escape of one quantum, this high energy gamma-ray is 3.66±0.15 Mev. The distribution from 1.5–2.7 Mev is attributed to two gamma-rays with photoelectric peaks between 2.2 Mev and 2.7 Mev. The absence of pulses corresponding to an energy of 5 Mev indicates that there is no direct transition to the ground state. Thus the third excited state decays by a double cascade.

The decay scheme of the excited states of Si^{30} is shown in Fig. 8. The agreement with the work of Landon[3] is quite good, the exception being that Landon found positive evidence only for the cascade from the third excited state to the second to ground. The alternate mode of decay, however, is estimated from the present data to be not more than 15 percent of the total.

The authors feel that improvement of the spectrometer resolution and improvement of the stability of the electronic equipment over the long periods required for the accumulation of data, will facilitate the extension of this technique to more complicated decay schemes. The authors wish to express their appreciation to Professor E. C. Pollard for his guidance throughout this program.

PHYSICAL REVIEW VOLUME 84, NUMBER 6 DECEMBER 15, 1951

Elastic Scattering of Electrons*

HERMAN FESHBACH
Department of Physics and Laboratory for Nuclear Science and Engineering, Massachusetts Institute of Technology, Cambridge, Massachusetts

(Received September 13, 1951)

This paper considers the effect of the finite size of the nucleus on the electrostatic scattering of electrons whose energy greatly exceeds their rest mass. It is shown that the phase shift for a given total electron angular momentum j, is independent of their orbital angular momentum l; that the phase shift depends on the parameter R describing the extension of the nuclear charge only through the combination pR where p is the electron momentum. If the additional assumption $pR \ll 1$ is made, it may be shown that the phase shift η_0 for $j=\frac{1}{2}$ electron is independent of the model describing the distribution of nuclear charge. For models for which the potential is finite at the origin, η_0 depends upon the model only through the volume integral of the potential over the nucleus.

1. INTRODUCTION

THE effect of the finite size of the atomic nucleus on the scattering of high energy (~20 Mev) electrons has been recently demonstrated experimentally[1] and has been the subject of several theoretical discussions.[2–5] In all of these, it is assumed that the nucleus can be represented by a charge density, $\rho(r)$, where r is the distance from the center of the nucleus, an approximation which is valid only for electron wavelengths λ considerably larger than interparticle distances in the nucleus. Taking this to be about $\frac{1}{2}(e^2/mc^2)$, we find that these theories are valid for electron energies E considerably smaller than 274 mc^2. Under this assumption, the most accurate results have been obtained by numerical analysis; the most complete calculation being that of Acheson in which the scattering for a variety of elements ($13 \leq z \leq 79$) and energies (15 Mev $\leq E \leq 30$ Mev) has been considered. Rose and Parzen also consider the more general problem of formulating suitable methods for these calculations, deriving, among other results, variational principles for the phase shifts.

In the present paper some general properties of the phase shifts required to describe the scattering, will be derived. These will help to reduce the labor of the numerical calculations as well as provide a basis for interpreting the experimental results.

* Assisted by the joint program of the ONR and AEC.
[1] Lyman, Hanson, and Scott, Phys. Rev. **84**, 626 (1951).
[2] M. E. Rose, Phys. Rev. **73**, 279 (1948); Phys. Rev. **82**, 389 (1951).
[3] L. K. Acheson, Jr., Phys. Rev. **82**, 488 (1951).
[4] L. R. B. Elton, Proc. Phys. Soc. (London) **A63**, 1115–24 (1950).
[5] G. Parzen, Phys. Rev. **80**, 261 (1950); Phys. Rev. **82**, 355 (1950).

2. DIRAC RADIAL EQUATIONS IN THE LIMIT $E \gg mc^2$

(a) Upon separating out the angular and spin dependence in the well-known manner, one obtains a pair of coupled differential equations:

$$\begin{aligned} df_l/d\rho + kf_l/\rho + (\epsilon - 1 - U)G_l = 0, \\ dG_l/d\rho - kG_l/\rho - (\epsilon + 1 - U)f_l = 0, \end{aligned} \tag{1}$$

where we have used relativistic units $r = (\hbar/mc)\rho$ and $E = \epsilon mc^2$, while U is the potential of the electron in units of mc^2. The constant $k = \pm(j+\frac{1}{2})$ for $j = l \pm \frac{1}{2}$. The asymptotic forms of G_l and f_l are

$$\begin{aligned} G_l &\xrightarrow[p\rho \to \infty]{} (\epsilon+1)^{\frac{1}{2}} \cos[p\rho + (\alpha\epsilon/p)\ln 2p\rho \\ &\qquad - (l+1)\pi/2 + \eta_{l,-(l+1)}], \\ f_l &\xrightarrow[p\rho \to \infty]{} (\epsilon-1)^{\frac{1}{2}} \sin[p\rho + (\alpha\epsilon/p)\ln 2p\rho \\ &\qquad - (l+1)\pi/2 + \eta_{l,-(l+1)}], \end{aligned} \tag{2}$$

where $\alpha = (ze^2/\hbar c)$ and p is the electron momentum in relativistic units. The phase shift η_l appropriate for $k = j+\frac{1}{2}$, and $\eta_{-(l+1)}$ for $k = -(j+\frac{1}{2})$ is made up of two parts:

$$\eta_l = \eta_l^{(c)} + \eta_l'. \tag{3}$$

Here $\eta_l^{(c)}$ is the phase shift which would appear if the nucleus could be represented as a point charge, while η_l' is the deviation from the coulomb phase shift arising from the finite size of the nucleus.

We now make the approximation $\epsilon \gg 1$ in Eq. (1) and obtain

$$\begin{aligned} &\frac{df_l}{d\rho} + \frac{l+1}{\rho} f_l + (\epsilon - U)G_l = 0 \\ &\qquad\qquad k = (j+\tfrac{1}{2}), \quad j = (l+\tfrac{1}{2}), \\ &\frac{dG_l}{d\rho} - \frac{l+1}{\rho} G_l - (\epsilon - U)f_l = 0 \end{aligned} \tag{4}$$

while for $k = -(j+\frac{1}{2})$, $j = l' - \frac{1}{2}$, $l' = l+1$,

$$\begin{aligned} &\frac{df_{l+1}}{d\rho} - \frac{l+1}{\rho} f_{l+1} + (\epsilon - U)G_{l+1} = 0, \\ &\frac{dG_{l+1}}{d\rho} + \frac{l+1}{\rho} G_{l+1} - (\epsilon - U)f_{l+1} = 0. \end{aligned}$$

Comparing these two sets of equations we see that

$$f_{l+1} = -G_l, \quad G_{l+1} = f_l, \tag{5}$$

connecting the two sets of solutions for a given j arising from the two possible values of l, $j \pm \frac{1}{2}$.

Thus

$$G_{l+1} \xrightarrow[\epsilon \gg 1]{p\rho \to \infty} -\epsilon^{\frac{1}{2}} \sin[p\rho + (\alpha\epsilon/p)\ln 2p\rho - (l+1)(\tfrac{1}{2}\pi) + \eta_l].$$

TABLE I. Comparison of η_l' and $\eta'_{-(l+1)}$.

l	η_l'	$\eta'_{-(l+1)}$	Author
0	-0.196	-0.195	E
1	-0.002	-0.001	E
0	-0.271	-0.268	E
1	-0.004	-0.004	E
0	-0.5339	-0.5307	P
1	$0.2064-\pi$	$0.2091-\pi$	P
2	$0.2507-\pi$	$0.2572-\pi$	P
3	$0.0678-\pi$	$0.0711-\pi$	P
4	$0.0115-\pi$	$0.0124-\pi$	P
5	$0.0013-\pi$	$0.0015-\pi$	P
6	$0.0001-\pi$	$0.0001-\pi$	P

Comparing with (2) for $k = -(j+\frac{1}{2})$:

$$G_{l+1} \xrightarrow[\epsilon \gg 1]{p\rho \to \infty} \epsilon^{\frac{1}{2}} \cos[p\rho + (\alpha\epsilon/p)\ln 2p\rho - \tfrac{1}{2}(l+2)\pi + \eta_{-(l+2)}]$$

we obtain

$$\eta_l = \eta_{-(l+2)}. \tag{6}$$

Since we have not specified U, Eq. (6) should hold for the coulomb law of force. This may be verified directly since $\eta_l^{(c)}$ is known analytically. The error in that case is

$$\exp i[\eta_{-(l+2)} - \eta_l] \xrightarrow[\alpha \ll 1]{} 1 - i\alpha/\epsilon(l+1) \tag{7}$$

indicating that in the energy range under consideration, and for the largest z, the error is of the order of 1 percent. Identifying then $\eta_l^{(c)}$ and $\eta_{-(l+2)}^{(c)}$ we have

$$\eta_l' = \eta'_{-(l+2)}. \tag{8}$$

The accuracy with which this relation holds may be seen from the following table available from exact numerical calculations performed by Elton and Parzen for Au at 40 mc^2 and Pb at 100 Mev, respectively. The error $\eta_l' - \eta'_{-(l+2)}$ compared to one is of the order of 1 percent. The validity of Eq. (8) and Eq. (10) below was first noted by Acheson for the special models he considered.

(b) Suppose that the potential of the electron in the field of the nucleus is

$$U(\rho) = -(\alpha/\rho)[1 - q(\rho/R)], \tag{9}$$

where R is a parameter measuring the nuclear radius and $q(x)$ is a function which approaches zero very rapidly once $x > 1$. We shall then show that the dependence of the phase shift η_l upon the energy ϵ and the radius R occurs only in the dimensionless combination ϵR, i.e.,

$$\eta_l = \eta_l(\epsilon R; \alpha). \tag{10}$$

This result immediately follows if the approximate equations (4) are rewritten in terms of the independent variable $y = \epsilon\rho$

$$\frac{df_l}{dy} + \frac{l+1}{y} f_l + \left\{1 + \frac{\alpha}{y}\left[1 - q\left(\frac{y}{\epsilon R}\right)\right]\right\} G_l = 0, \tag{11a}$$

$$\frac{dG_l}{dy} - \frac{l+1}{y} G_l - \left\{1 + \frac{\alpha}{y}\left[1 - q\left(\frac{y}{\epsilon R}\right)\right]\right\} f_l = 0. \tag{11b}$$

We see that the only explicit dependence of these equations on ϵ and R occurs only through the combination ϵR proving Eq. (10). The main importance of this result lies in the connection it gives between the dependence of η_l on the energy and on the nuclear radius.

3. SCATTERING IN THE LONG WAVELENGTH LIMIT

It will now be shown that the phase shift $\eta_0(\simeq\eta_{-2})$ depends only upon the volume integral I, of the perturbing potential $(\alpha/\rho)q(\rho/R)$. In other words, the values of η_0 obtained for two different models with radii R_1 and R_2 will be equal if the ratio between their radii (R_1/R_2) is adjusted so that I is the same for both models. This result holds as long as $\epsilon R\ll 1$. We shall derive the value of the ratio (R_2/R_1) and shall illustrate with Acheson's results for the homogeneous and shell models. The functions q, q_h, and q_s for these models

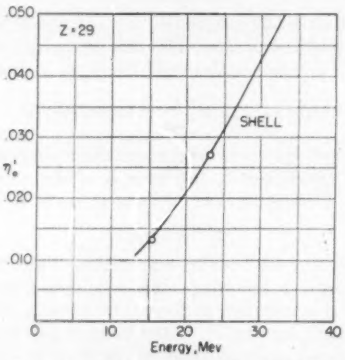

FIG. 1. Comparison of phase shifts η_0' for the shell and for the homogeneous models. The solid line gives Acheson's results for the shell model, the radius, R_s obtained from $(1.5\times10^{-13}\text{ cm})A^{\frac{1}{3}}$. The circles are computed from Acheson's curves for the homogeneous model employing however a radius R_h equal to $(10/6)^{\frac{1}{2}}R_s$.

with radii R_h and R_s, respectively, are as follows:

$$q_h(\rho/R_h)=\begin{cases}1-\frac{3}{2}(\rho/R_h)+\frac{1}{2}(\rho/R_h)^3 & \rho\leqslant R_h \text{ (homogeneous}\\ 0 & \rho\geqslant R_h \text{ model)}\end{cases}$$
$$q_s(\rho/R_s)=\begin{cases}1-(\rho/R_s) & \rho\leqslant R_s\\ 0 & \rho\geqslant R_s\end{cases}\text{(shell model).} \tag{12}$$

The derivation will be based upon a variational principle for $\cot\eta_l$ in order to take advantage of its stationary character. This variational principle may be obtained from the method discussed by Schwinger[6] with only some slight modifications arising from the characteristic differences between the Dirac and the Schroedinger equation which he discussed. The variation of the following integral is zero:

$$\int_0^\infty [G_l(df/d\rho)+(k/\rho)f_lG_l+\tfrac{1}{2}(\epsilon-1-U)G_l^2$$
$$+\tfrac{1}{2}(\epsilon+1-U)f_l^2]d\rho-\lim_{\delta\to0}\Big\{\int_\delta^\infty[\mathbf{G}_l(d\mathbf{f}_l/d\rho)$$
$$+(k/\rho)\mathbf{f}_l\mathbf{G}_l+\tfrac{1}{2}(\epsilon-1+(\alpha/\rho))\mathbf{G}_l^2$$
$$+\tfrac{1}{2}(\epsilon+1+(\alpha/\rho))\mathbf{f}_l^2]d\rho-(\epsilon+1/(\epsilon-1)^{\frac{1}{2}}$$
$$\times\tan\Phi_I\Big[1+\frac{2p\delta}{(2s-1)(\sin2\Phi_I)}\Big]\mathbf{f}_l^2(\delta)\Big\}$$
$$=(\epsilon+1)/(\epsilon-1)^{\frac{1}{2}}(N_k/M_k)(\cos(\Phi_R-\Phi_I)/\cos^2\Phi_I)$$
$$\times(\cos(\eta_l'-\zeta_l)/\sin\eta_l')\lim_{\delta\to0}(2\rho\delta)^{2s}\mathbf{f}_l^2(\delta). \tag{13}$$

The symbols will be defined below. The integrand is to be varied with respect to G_l, f_l, $\mathbf{G}_l$, and $\mathbf{f}_l$ subject to the boundary conditions:

$$G(0)=f(0)=0,\quad G_l\xrightarrow[p\rho\to\infty]{}\mathbf{G}_l;\quad f_l\xrightarrow[p\rho\to\infty]{}\mathbf{f}_l. \tag{14}$$

$\mathbf{G}_l$ and $\mathbf{f}_l$ satisfy the Dirac equation (1) for $U=-(\alpha/\rho)$, i.e., for a point nucleus and are therefore taken to be that linear combination of the exact coulomb wave functions which have the asymptotic dependence of G_l and f_l as given in Eq. (2). Therefore:

$$\mathbf{G}_l=(\epsilon+1)^{\frac{1}{2}}\sec\zeta_l[\cos(\eta_l'-\zeta_l)\Gamma_R-\sin\eta_l'\Gamma_I],$$
$$\mathbf{f}_l=(\epsilon-1)^{\frac{1}{2}}\sec\zeta_l[\cos(\eta_l'-\zeta_l)\chi_R-\sin\eta_l'\chi_I], \tag{15}$$

where

$$\Gamma_R+i\chi_R=N_ke^{i\Phi_R}e^{-ip\rho}(2p\rho)^s$$
$$\times{}_1F_1[s+(i\alpha\epsilon/p);\,2s+1;\,2ip\rho],$$
$$\Gamma_I+i\chi_I=M_ke^{i(\Phi_I-\frac{1}{2}\pi)}e^{-ip\rho}(2p\rho)^{-s}$$
$$\times{}_1F_1[-s+(i\alpha\epsilon/p);\,-2s+1;\,2ip\rho],$$
$$s=(k^2-\alpha^2)^{\frac{1}{2}},$$
$$\Gamma_R\to\cos[p\rho+(\alpha\epsilon/p)\ln2p\rho-\pi(l+1)/2+\eta_l^{(c)}],$$
$$\Gamma_I\to\sin[p\rho+(\alpha\epsilon/\rho)\ln2p\rho-\pi(l+1)/2+\eta_l^{(c)}+\zeta_l], \tag{16}$$
$$\exp(2i\eta_l^{(c)})=(-)^{l+1}e^{-\pi i\alpha}\frac{k+(i\alpha/p)}{s-(i\alpha\epsilon/p)}\frac{\Gamma(s+1-i\alpha\epsilon/p)}{\Gamma(s+1+i\alpha\epsilon/p)},$$
$$e^{2i\Phi_R}=[k-(i\alpha/p)]/[s+(i\alpha\epsilon/p)];$$
$$e^{2i\Phi_I}=[k-(i\alpha/p)]/[s-(i\alpha\epsilon/p)],$$
$$e^{2i\zeta_l}=e^{2\pi i\alpha}\sin\pi(s-i\alpha\epsilon/p)/\sin\pi(s+i\alpha\epsilon/p),$$
$$N_k=|\Gamma(s+1+i\alpha\epsilon/p)|/\Gamma(2s+1)e^{\frac{1}{2}\pi\alpha\epsilon/p},$$
$$M_k=\left|\frac{\pi(s+i\alpha\epsilon/p)}{\sin\pi(s+i\alpha\epsilon/p)\Gamma(1+s+i\alpha\epsilon/p)}\right|\frac{e^{\frac{1}{2}\pi\alpha\epsilon/p}}{\Gamma(1-2s)}.$$

[6] J. Schwinger, Phys. Rev. **78**, 135 (1950).

The necessity for the limiting process at the origin as included in variational principle (13) arises from the singular behavior of the irregular solution $(\Gamma_l+i\chi_l)$ at that point.

We may now ask under what circumstances will two models give the same phase shift at a given electron energy. Employing the exact wave functions associated with one of the models as a trial wave function in Eq. (13) for the wave function associated with the other model, we immediately find that the requirement for equality of phase shifts is:

$$\int_0^\infty q_1(\rho)[f_l^2+G_l^2]d\rho/\rho=\int_0^\infty q_2(\rho)[f_l^2+G_l^2]d\rho/\rho. \quad (17)$$

This result as well as the one below may of course be obtained from a perturbation analysis based directly on the differential Eqs. (1). The slope of the $\cot\eta_l'$ curve as a function of ϵ may be obtained in the high energy limit, $\epsilon\gg1$, by taking the energy derivative of Eq. (13). However, it is more convenient to make use of the fact that $\cot\eta_l'$ is a function of ϵR so that

$$\partial(\cot\eta_l')/\partial\epsilon=(R/\epsilon)\partial(\cot\eta_l')/\partial R.$$

Hence in the high energy limit $\epsilon\gg1$,

$$\left|\frac{[\Gamma(1+s+i\alpha)]^2\sin\pi(s+i\alpha)}{\pi(s+i\alpha)}\right|\frac{\Gamma(1-2s)}{\Gamma(2s+1)}\frac{\cos2\Phi_R}{\cos^2\Phi_R}$$

$$\times\lim_{\delta\to0}(2\rho\delta)^{2s}\mathbf{f}^2(\delta)\frac{\partial}{\partial\epsilon}\cot\eta_l'$$

$$=-\frac{R}{2\epsilon}\int_0^\infty\frac{\partial U}{\partial R}(f_l^2+G_l^2)d\rho, \quad (18)$$

where we must choose the normalization of $\mathbf{f}$ so that $(2\rho\delta)^{2s}\mathbf{f}^2(\delta)$ is independent of ρ. The derivative $\partial U/\partial R$ may be expressed in terms of q as follows:

$$\partial U/\partial R=(\alpha/\rho)\partial q(\rho/R)/\partial R. \quad (19)$$

For the energy slopes of $\cot\eta_l'$ to be model-independent, it is necessary that

$$R\int_0^\infty\partial q(\rho/R)/\partial R(f_l^2+G_l^2)d\rho/\rho \quad (20)$$

be the same for each model, where again we have employed as trial function the exact wave function associated with one of the models. By an integration by parts it is possible to transform expression (20) to

$$\int_0^\infty q_1(d/d\rho)(f_l^2+G_l^2)d\rho. \quad (21)$$

Comparing Eq. (21) with Eq. (17), we see that the conditions that $\cot\eta_l'$ and its energy slope be model-independent in the sense defined above are consistent

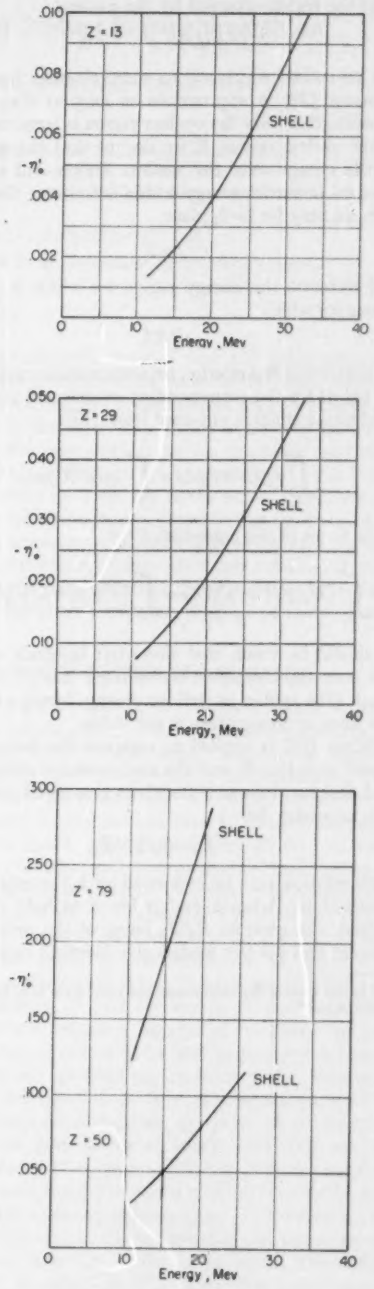

FIG. 2. Shell model phase shift for (a)—Al; (b)—Cu; and (c)—Ag and Au.

if, in the region occupied by the nucleus,

$$(f_l^2+G_l^2)\sim\rho^l, \quad l\neq 0. \tag{22}$$

For potentials which are no more singular than $(1/\rho)$ behavior (22) is appropriate as long as the electron wavelength within the nuclear region is large compared to the nuclear radius. If we assume that the spreading of the charge over the nuclear region will result in electron potential energy which is finite at the origin, then we may for $l=0$, place

$$l=2 \tag{23}$$

and estimate the energy region for which it is valid[7] as one for which

$$\epsilon R\ll 1. \tag{24}$$

In that event the relation between nuclear radii R_1 and R_2 for which the corresponding models will yield identical phase shifts is obtained from (17):

$$\int_0^\infty q_1(\rho/R_1)\rho d\rho=\int_0^\infty q_2(\rho/R_2)\rho d\rho, \tag{25}$$

or in terms of the potentials $U(\rho)$

$$I=\int_0^\infty [U_1(\rho)+\alpha/\rho]\rho^2 d\rho=\int_0^\infty [U_2(\rho)+\alpha/\rho]\rho^2 d\rho. \tag{26}$$

It should be noted that these last integrals appear if the Born approximation is evaluated near 0°. However, result (26) applies as well for energy domains in which the Born approximation is not valid.

When (25) is applied to compare the homogeneous model of radius R_h and the shell model of radius R_s we find that for these two models to give equal phase shift it is necessary for

$$R_s=(6/10)^{\frac{1}{2}}R_h. \tag{27}$$

This relation may be compared with the exact results obtained by Acheson and is found to hold very well indeed, the error in R_s/R_h being of the order of one percent and the two models give identical $\cot\eta_0'$ curves over a wide range in ϵR. This is shown for the case exhibiting the poorest agreement in Fig. 1. For all other cases, i.e., for elements Al, Ag, and Au, the two curves overlap completely, the energy range involved lying between 18 and 40 Mev. It should be emphasized that the phase-shift involved could not be predicted correctly from the Born approximation. Rather the results indicate that one may go from one model to another by an appropriate perturbation calculation.

Assuming the validity of Eq. (27), it becomes possible to extend Acheson's curves by combining the results for the two models. These are shown in Fig. 2, the product ϵR being appropriate for the shell model if R_s is taken as $(1.5\times 10^{-13}\text{ cm})A^{\frac{1}{3}}$, where A is the mass number. One may obtain the values of η_0' for other values of the radius by suitably charging the energy ϵ. It may be found for other models by relating the associated radius to the radius of the shell model through Eq. (25).

Perhaps the most important consequence of the results of this section lie in its implication for the interpretation of the experimental results. The energy dependence and magnitude of these results as summarized by the phase shift η_0' may be employed to determine one nuclear parameter, I, the volume integral of the perturbing potential. Any model may be made to conform to this value of I by the appropriate choice of a value for the nuclear radius R. Therefore, only when information on the value of the nuclear radius is available from other experiments, may electron scattering be employed to choose between nuclear models. Comparisons between nuclei should be made in terms of the values of (I/α) determined from experiment. Variations in this quantity may be interpreted either by an appropriate change of nuclear radius or nuclear model. Either interpretation would be particularly significant if the nuclei are isotopes.†

I am greatly indebted to Mr. Kerson Huang for his verification of the calculations reported in this paper.

[7] In the case of the shell model the error term is of the order of $(\epsilon+\alpha/R_s)^2R_s^2$.

† *Notes added in proof:*—(a) The evaluation by the Born approximation of the effect of finite nuclear size in the scattering of electrons by nuclei was first performed by E. Guth, Sitzungber. Akad. der Wiss. in Wien, November 22, 1934.

(b) Equations (5) and (17) are implicitly contained in the papers of M. E. Rose, reference 2.

Electron Capture and Loss Cross Sections for Protons Passing through Air

H. KANNER
Department of Physics and Institute for Nuclear Studies, University of Chicago, Chicago, Illinois
(Received August 31, 1951)

Measurements have been made of the electron-loss cross section σ_1 and the electron-capture cross section σ_c for hydrogen beams in air. σ_1 varied from 24.4×10^{-17} cm² at 40.8 kv to 13.6×10^{-17} cm² at 325 kv. σ_c varied from 20.8×10^{-17} cm² at 31.4 kv to 2.7×10^{-17} cm² at 122 kv. In the ranges quoted, the cross sections were well represented by the formulas,

$$\sigma_1=(24.54-0.866E/E_0)\times10^{-17}\text{ cm}^2,\quad \sigma_c=[41.1\exp(-0.562E/E_0)]\times10^{-17}\text{ cm}^2,$$

where $E_0=24.8$ kv, the energy of a proton having the velocity $e^2/\hbar$. By extrapolation of the data, σ_1 was found to equal σ_c at energy E_0.

I. INTRODUCTION

A KNOWLEDGE of the cross sections for electron capture and loss by light ions is a valuable aid to the understanding of the energy loss of these particles in matter, particularly at the low energy end of their range where charge exchanges are numerous. This is true for two reasons: (1) The rate of energy loss by ionization is dependent on the average charge of the particle, a quantity directly determined by the ratio of the capture and loss cross sections; and (2) a capture event followed by a loss event is equivalent to a simple ionizing encounter, and must in itself produce at least as great an energy loss as the latter.

The earlier work on this subject was performed using low energy canal rays,[1–5] or high-energy alpha particles from radioactive sources.[6–8] Recent measurements on proton beams of energies from 20 to 400 kv have been made by Hall,[9] who determined the ratio of the capture and loss cross sections in several metals; Montague,[10] who measured the loss cross section in hydrogen gas; and Ribe,[11] who measured both the capture cross section and the ratio of the capture and loss cross sections in hydrogen. The present work concerns itself with the capture and loss cross sections for protons in air, using essentially the methods and arrangement of apparatus of Montague and Ribe.

The procedure was to direct a proton beam at a thin nitrocellulose window. As a result of charge exchange processes in the window, the emergent beam contained a component of neutral hydrogen atoms as well as protons. A uniform magnetic field in the region beyond the window separated the charged and neutral components, each eventually entering a detecting device. When controlled pressures of air were admitted to the region between the window and the detectors, consequent electron exchanges between the beam particles and air atoms caused a diminution, with increasing air pressure, in the observed intensity at the two detectors. Making the assumption, to be examined critically below, that any change of charge suffered by a beam particle alters its trajectory to the extent that it can no longer enter its respective detector, the dependence of observed intensity on pressure is given by $\exp(-N\sigma d)$, where N is the number of gas atoms per cubic centimeter, d is the total path length in the gas-containing region, and σ is the cross section for the process under observation.

II. DESCRIPTION OF APPARATUS

The initial proton beam was produced by the University of Chicago 400-kv Cockroft-Walton accelerator (kevatron) described elsehwere.[12] A selecting magnet separated the proton beam from the molecular ions. The protons then passed through a collimating assembly consisting of two circular apertures 1.58 mm in diameter and 86 cm apart. After passing through an insulated wire gauze for monitoring purposes, the beam impinged on a nitrocellulose "zapon" window, which was aluminized to prevent its retaining an electrostatic charge.

It should be mentioned at this point that in the low energy work (<80 kv) the molecular ion beam was used. On striking the window, the ions would break up, yielding protons of half the energy of the ions. This procedure was necessary because of the failure of the kevatron to produce a well-focused beam at low voltages.

The window provided the entrance to the deflection chamber, described more fully in previous papers,[10,11] which was situated between the poles of an electromagnet, the pole pieces of which were 12.7 cm in diameter and 3.17 cm apart. The two detectors used in the work were located as follows: (1) diametrically opposite to the window, corresponding to no deflection of the initial beam; and (2) in a position corresponding to a 60 degree deflection of the initial beam. These will henceforth be called the 0° and 60° positions, respec-

[1] E. Ruchardt, Ann. Physik **71**, 377 (1923).
[2] A. Ruttenauer, Z. Physik **4**, 267 (1921).
[3] H. Bartels, Ann. Physik **6**, 957 (1930).
[4] H. Bartels, Ann. Physik **13**, 373 (1932).
[5] P. Rudnick, Phys. Rev. **38**, 1342 (1931).
[6] E. Rutherford, Phil. Mag. **47**, 277 (1924).
[7] P. Kapitza, Proc. Roy. Soc. (London) **106**, 602 (1924).
[8] G. H. Henderson, Proc. Roy. Soc. (London) **114**, 241 (1927).
[9] T. Hall, Phys. Rev. **79**, 504 (1950).
[10] J. H. Montague, Phys. Rev. **81**, 1026 (1951).
[11] F. L. Ribe, Phys. Rev. **84**, 1217 (1951).
[12] Allison, del Rosario, Hinton, and Wilcox, Phys. Rev. **71**, 139 (1947).

tively. The detectors themselves were of two kinds. One was simply a faraday cage behind an entrance slit; the other, which will henceforth be called the "Montague detector," consisted of a plate of beryllium-copper at a slight inclination to the beam and maintained at a negative potential of 67½ volts relative to ground. The entrance slits of both detectors, as well as the Zapon window, were tangent to the cylinder defined by the magnet poles.

Since the faraday cage was always kept within 0.2 volt of ground potential and was in the stray field of the magnet, any secondary electrons emitted from its walls were unable to escape. As a consequence, the faraday cage had zero response to neutral particles. The Montague detector, on the other hand, was specifically designed to collect the secondary electrons emitted from the beryllium-copper plate. By virtue of the near parallelism of the electric and magnetic fields, the sensitivity of the Montague detector was found to be independent of the magnetic field strength, and, within the limits of experimental error, was the same for neutral and charged particles. (The term "sensitivity" as used above and elsewhere in this paper shall be taken to mean the charge collected by a detector per particle entering it.)

The currents from the monitor and the detector in use were amplified by direct-current amplifiers,[13] and finally read as galvanometer deflections. In the usual procedure, a 100 megohm input grid resistor was used for the monitor current and a 1000 megohm one for the detector current. The amplifier gains could be conveniently varied by means of 1000K decade resistor boxes in series with the galvanometers.

A generating fluxmeter, whose armature projected into a can sealed in the chamber wall, served to provide readings of the relative magnetic field strength. This instrument was too inaccurate to be used for quantitative measurements; its principal use was to indicate when zero field had been attained after multiple reversals of the magnet current. By always following the procedure of first zeroing the magnet and then adjusting the magnet current in the direction of increasing current, a one-to-one relationship between magnet current and field strength was maintained.

The air used in the measurements was freed of CO_2 and moisture by passing it through a 3-ft-long drying tube containing, in one-foot sections, KOH pellets, "Dryerite," and finally glass beads dusted with P_2O_5. The air was admitted via this tube to a one-liter storage bulb at rates not exceeding 0.014 cm³ per minute. From the storage bulb the air could be admitted to the electron-exchange chamber by means of a needle valve, a method which gave adequate control since the pressure in the storage bulb was usually held at about 0.1 mm. The chamber pressures were measured with a McLeod gauge. During the measurements at "zero" pressure, the chamber was directly opened to a vacuum system, with a resulting chamber pressure that was always less than 10^{-4} mm.

[13] The circuit is given on the data sheet for the Raytheon CK5697/CK570 electrometer triode, published by the Raytheon Mfg. Co., Newton, Mass.

III. EXPERIMNETAL PROCEDURE

A. Cross-Section Measurement

All data were taken by simultaneous readings of the detector and monitor galvanometers. For brevity, the ratio of the detector and monitor galvanometer deflections will henceforth be termed *r*, the detector response. To minimize the effects of amplifier drift, the zero readings of these galvanometers were frequently taken, as will be described below. This was simply accomplished by turning off the current to the selecting magnet, so that no beam could enter the apparatus. In normal operation, the faraday cage was at the 60° position and the Montague detector at the 0° position. Both had their entrance slits set to about 1 mm.

The energy of the beam after penetrating the window was measured by taking a profile of the 60° detector response as a function of magnet current, the previously-mentioned precautions of first zeroing the magnet and then only increasing the magnet current being observed. During this energy measurement, the chamber would be open to the vacuum system. The zero readings of the two galvanometers were taken immediately before and after the profile readings. If the two sets of zero readings differed due to drift, a linear interpolation was used to obtain an assumed zero for each profile point.

A measurement of a capture or loss cross section would now be made, much of the procedure being common to both. In the case of the capture measurement, the faraday cage was used at the 60° position. The magnet was carefully zeroed and then set exactly to the field corresponding to the peak of the previously-obtained profile. For the loss measurements, the Montague detector was used at the 0° position and the magnet would usually be set approximately to the peaking field to obtain the standard radius of curvature of 11 cm for protons, but in some of the runs the magnet current was adjusted to obtain smaller radii of curvature.

The following procedure was used for either cross section: The desired pressure of air was admitted to the chamber, the McLeod gauge was read, and zero readings of the galvanometers were taken. Immediately following the last step, the selecting magnet current was rapidly adjusted to aim the kevatron beam at the window, and a minimum of three simultaneous detector *versus* monitor readings were taken. The chamber was now opened to the vacuum system after first trapping the gas in the McLeod gauge bulb for a second pressure reading. As soon as the chamber was fully pumped out, as indicated by an ionization gauge in the vacuum system, three or more detector and monitor readings were again taken, after which the selecting magnet

would be turned off and a second set of zero readings taken. The time required for pumping out was never over 20 seconds. This process, at a given beam energy, was repeated using from three to six pressure values.

B. Magnet Calibration

The magnet was calibrated by taking profiles of magnet current against 60° detector response at known beam energies with the Zapon window removed. The profiles were sufficiently sharp under these conditions (broadening due to scattering at the window eliminated) that it was necessary only to peak the detector galvanometer by eye. The beam energies were computed from the measured current drains through a permanent resistor stack leading from the kevatron ion source to ground. The values of this resistance, as a function of the current drain, had been determined by various earlier workers in this laboratory, using a cylindrical electrostatic analyzer[14] as the primary device for measuring the beam energy. The values of the stack resistance so obtained have always been reproducible to an accuracy of 1 percent.

IV. ANALYSIS OF DATA

In subtracting the zero readings to obtain the galvanometer deflections, the zeros first taken were subtracted from the pressure readings, and those obtained last were subtracted from the vacuum readings. The ratios of detector to monitor deflections under pressure and vacuum respectively were averaged to obtain $r(p)$ and $r(0)$.

The attenuation ratio, $\rho(p)$, is defined as $r(p)/r(0)$.

$$\rho(p)=\exp(-N\sigma d)=\exp(-1.930\times10^{19}pd\sigma/T), \quad (1)$$

where N is the number of gas atoms per cubic centimeter, σ is the capture or loss cross section per air atom, d is the effective path length of the particles, p is the gas pressure in mm of mercury, and T is the absolute temperature. From Eq. (1), we obtain

$$\log_{10}\rho=-0.8384\times10^{19}d\sigma p/T. \quad (2)$$

By finding the slope of the best possible straight line fitted to the experimental values of $\log_{10}\rho(p)$ *vs* p, subject to the condition that the line pass through the origin, we obtain the value of $-0.8384\times10^{19}\sigma d/T$. A least squares determination of these slopes was made, assuming that no error resided in the pressure measurements, and that the experimental values of ρ were subject to a constant probable error. Under these assumptions the probable errors in $\log\rho$ would be proportional to $1/\rho$, with the consequence that the point $(\log\rho_i, p_i)$ had to be given a weight proportional to ρ_i^2 in making the least squares fit. The formula for the slope, s, is then

$$S=\sum\rho_i^2p_i\log\rho_i/\sum\rho_i^2p_i^2, \quad (3)$$

and the probable error, Δ, in s is given by

$$\Delta=0.675\left\{\frac{\sum\rho_i^2(\log\rho_i)^2-s\sum\rho_i^2p_i\log\rho_i}{(n-1)\sum\rho_i^2p_i^2}\right\}^{\frac{1}{2}}, \quad (4)$$

where n is the number of points taken.[15]

The values of d, of course, depended on the detector used and its position. For the loss cross section, using the Montague detector at the 0° position, d was the distance from the window to the entrance slit: 12.70 cm. For the capture cross section, using the faraday cage at the 60° position, d was taken to be the length of the circular path from the window to the mouth of the faraday cage 0.5 cm behind the entrance slit, a total distance of 12.02 cm.

A typical semilogarithmic plot of $\rho(p)$ *vs* p and the best-fitting straight line to the data is given in Fig. 1.

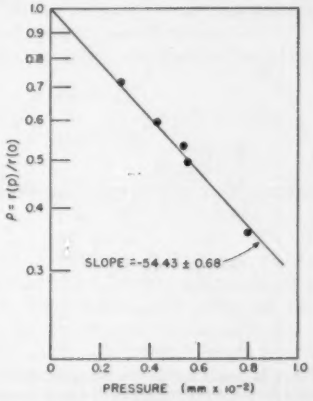

FIG. 1. Attenuation curve for a 221-kv hydrogen beam at the 0° detector.

V. SECONDARY EFFECTS

A. Effect of Gas on Detectors

Both the Montague detector and faraday cage suffered an increase in sensitivity with increasing air pressure. In the case of the Montague detector, which had a potential of 67½ volts between plates 0.32 cm apart, this effect might be ascribed to the collection of ions produced in the gas by the beam particles. The pressure dependence of the faraday cage sensitivity is not very well understood. A tentative explanation may be that, on the average, the electrons and positive ions produced a short distance in front of the faraday cage have a component of momentum in the direction toward the cage, but the exceedingly small radius of curvature of the electrons in the magnetic field present prevents their being collected.

[14] Allison, Frankel, Hall, Montague, Morrish, and Warshaw, Rev. Sci. Instr. **20**, 735 (1949).

[15] See D. Brunt, *The Combination of Observations* (Cambridge University Press, London, 1931), Chapter VI, for the theory of the probable errors of constants determined by least squares.

A measurement of the attenuation ratio with the Montague detector in the 0° position and with no magnetic field present provided a direct determination of the gas effect for this detector. The presence of gas in the chamber under conditions of no field affected the beam in two respects: (1) The ratio of charged to neutral particles entering the detector and (2) the fraction of the beam lost by simple scattering in the gas both depended on the pressure. Since the scattering cross section is strongly energy dependent, it was established that scattering effects were negligible by demonstrating that there was no reproducible dependence of the gas effect on beam energy. If the assumption that the Montague detector had equal sensitivity to charged and neutral particles is correct, the effect of gas pressure on the charge distribution of the beam does not influence this measurement. A verification of this assumption was made by repeating the gas effect

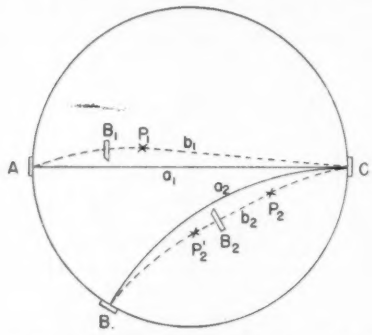

FIG. 2. Effect of scattering at the entrance window. Dotted curves depict orbits of scattered particles which would enter the detectors in the absence of baffles. A: 0° detector. B: 60° detector. C: entrance window.

measurements with a heavily aluminized zapon foil (0.1 mg/cm²) immediately in front of the detector slit. This foil was sufficiently thick that the charge distribution of the beam after penetration was independent of that of the impinging beam. No appreciable change in gas effect due to the introduction of this foil was observed.

The effect of gas on the faraday cage was measured by following the routine of a normal capture cross section measurement at such high energies ($\gtrsim$350 kv) that the capture cross section itself was negligible. The attenuation ratios for both gas effects were, of course, greater than unity.

The data for the gas effects were treated as if they were to be considered the equivalent of negative cross sections. That is, the best slopes were found for lines through the origin representing the experimental values of $\log\rho(\phi)$, the slopes in this case being positive. From the slopes, equivalent negative cross sections per gas atom were deduced. The magnitude of this cross section, for the detector used, was added to the capture or loss cross section to correct for the gas effect. The values accepted were 0.54×10^{-17} cm² for the Montague detector and 0.40×10^{-17} cm² for the faraday cage, the former at the 0° and the latter at the 60° positions.

As a verification of the methods, two capture cross sections were measured, using the Montague detector instead of the faraday cage at the 60° position. Recalling that the slope of the line depicting $\log\rho$ *vs* ϕ is divided by a factor proportional to the path length to obtain a cross section, the previously obtained gas effect cross section for the Montague detector had to be multiplied by 12.70/11.52, the ratio of the path lengths from window to detector slit in the two positions, to make it apply to the 60° position.

B. Effect of Scattering at the Window

Scattering of the incident beam by the window can cause a spurious measurement of the cross sections by processes illustrated in Fig. 2. The symbols a_1 and a_2 are the normal paths of neutral atoms and protons from the window to their respective detectors. The symbol b_1 is the path of a neutral particle which has suffered scattering in the window. If the particle loses its electron at the point P_1, it will eventually enter the 0° detector. Thus, there will be a contribution of particles to the detector, increasing with gas pressure, and therefore leading to a reduced value of the loss cross section. Similarly, b_2 represents the orbit of a scattered proton, which captures an electron at point P_2 and loses it again at P_2', these two events taking place at points such that it finally enters the 60° detector. Since this detector, the faraday cage, is sensitive only to charged particles, an electron loss process must be the final event in order that a spurious charge be detected.

Baffles B_1 and B_2 were placed in the chamber to interrupt orbits of the type just discussed. They were so placed as to miss grazing the unscattered beam by about a millimeter. Therefore, they did not completely eliminate all such orbits, leaving a residual effect that became serious only in measurements of σ_1 below 60 kv. This was evidenced by an apparent increase in the measured σ_1 with magnetic field, for the probability that a loss event can cause a scattered particle to enter the detector decreases with the radius of curvature of protons in the chamber. The experimental procedure, used in the energy range in which a dependence on magnetic field was noted, was to repeat the σ_1 measurements at increasing fields until the value of the cross section saturated. Values of σ_1 at approximately constant beam energy and varying radii of curvature are given in Table I to illustrate this saturation.[16]

No such test could be applied to the capture cross section, since the magnetic field had to be maintained at the value that would bring the unscattered proton beam to the 60° detector. However, in the case of the

[16] See Fig. 6 in reference 10 above for a graphical demonstration of this saturation.

capture cross section measurement, this effect was overshadowed by the effect of similar multiple charge exchanges in the nonscattered beam. This latter effect and the correction thereto are discussed below. No separate correction for the portion of the scattered beam not eliminated by baffle B_2 was deemed necessary.

C. Effect of Finite Detector Slit

A further correction to the loss cross section was necessitated by the failure of the Montague detector to discriminate between neutral and charged particles. If a neutral particle loses its electron when sufficiently close to the detector slit, it may still enter the detector despite the deflection caused by the magnetic field. The limiting distance from the slit for such an event is dependent on the magnetic field strength and the transverse position of the particle in the beam. By averaging this distance over the breadth of the beam, Montague[10] derived the approximate relationship,

$$b=\tfrac{2}{3}(2Rw)^{\frac{1}{2}}, \tag{5}$$

where b is the average distance in front of the slit for detection despite electron loss, R is the radius of curvature of a proton in the magnetic field present, and w is the slit width. Thus the effective path length from window to detector is reduced to $d-b$. The correction factor to be applied to the loss cross section is

$$1+(2/3d)(2Rw)^{\frac{1}{2}}=1+0.0237\,R^{\frac{1}{2}}, \tag{6}$$

an eight percent correction for the 11-cm radius of curvature usually used.

D. Correction of δ_c for the Effect of Multiple Charge Exchanges

At energy values at which $\sigma_1>3\sigma_c$, a departure from linearity was observed in the plots of $\log\rho$ against pressure, the departure being in the direction of too low values for $|\log\rho|$. This was ascribed to the effect of multiple processes of the following type: A proton captures an electron, travels in a straight line a distance δ, loses the electron again, and continues in a circular orbit equivalent to the initial one displaced a vector distance δ. If δ is less than a limiting value dependent on the position of the proton at the time of the capture, the ultimate orbit will still terminate within the detector entrance slit.

An approximate quantitative treatment of this effect has been attempted. The coordinates used are illustrated in Fig. 3. The letter x is the arc length along the bent beam, measured from the window; y is the transverse coordinate, measured from the outer periphery of the beam arc; and θ is the angular coordinate about the center of curvature of the beam, measured from the detector slit. The shaded area represents the portion of the beam that would normally enter the detector slit. The total beam has a somewhat greater width, equal to that of the collimating apertures. Only half of this excess width, shown as the nonshaded area in the figure, is pertinent to the treatment at hand.

TABLE I. Saturation of loss cross section with decreasing radius of curvature.

Beam energy E (kv)	Loss cross section σ_1 ($cm^2\times10^{-17}$)	Radius of curvature R (cm)
34.3	16.45±0.36	11.0
41.4	20.35±0.14	5.84
40.8	23.28±0.47	3.88
41.4	22.21±0.63	3.30

If a proton becomes neutral at a point (x, y) with $y<w$, the slit width, it will still enter the detector provided it loses the electron again before it has travelled a distance greater than $y/\sin\theta$. Particles in the region $y>w$, normally never entering the detector, will be detected if, after capturing an electron, they travel a distance between $(y-w)/\sin\theta$ and $y/\sin\theta$ before they lose it again.

We can then write the differential equation,

$$dn=nN\sigma_c dx\left\{\int_{0.107}^{0.136}\frac{dy}{0.107}\left[e^{-(y-0.107)N\sigma_1/\sin\theta}-e^{-yN\sigma_1/\sin\theta}\right]-\int_0^{0.107}\frac{dy}{0.107}e^{-yN\sigma_1/\sin\theta}\right\}, \tag{7}$$

where the slit width, w, is 0.107 cm; the total beam width considered is 0.136 cm; n is the flux of protons at position x; N is the number of gas atoms per cm^3; and σ_c and σ_1 are the electron capture and loss cross sections, respectively. The total arc length from window to slit is 11.52 cm and the radius of curvature of the beam is 11.0 cm. Hence θ will equal $(1/11)(11.52-x)$ radians.

For small values of θ, the above formulation becomes inaccurate. From Eq. (5) above, the average distance in front of the slit from which particles will enter the detector regardless of their charge state is 1.02 cm. Moreover, the mouth of the faraday cage was 0.5 cm behind the slit. Hence Eq. (7) was integrated to $x=10.5$ cm, and the flux entering the cage was obtained by multiplying the flux at 10.5 cm by the factor

$$[\sigma_c e^{-1.52N(\sigma_c+\sigma_1)}+\sigma_1]/(\sigma_c+\sigma_1).$$

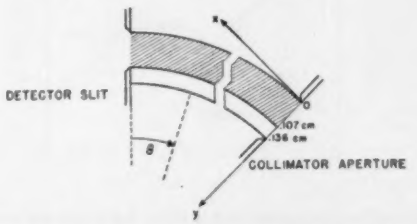

FIG. 3. The coordinates used in discussing the correction for multiple charge exchanges.

TABLE II. Result of numerical evaluation of $\int_0^{10.5} I(N\sigma_l, x)dx$ as a function of $N\sigma_l$.

$N\sigma_l$ (cm^{-1})	$\int_0^{10.5} I dx$
0.1	0.1100
0.2	0.2152
0.3	0.3160
0.4	0.4128
0.5	0.5053
0.6	0.5943
0.7	0.6797
0.8	0.7617
0.9	0.8404
1.0	0.9160
1.1	0.9889

Then the attenuation ratio, ρ, will be given by

$$\log_{10}\rho_1=\frac{-0.4343\sigma_e}{0.107\sigma_l}\int_0^{10.5} I(N\sigma_l, x)dx + \log_{10}\left\{\frac{\sigma_e e^{-1.52N(\sigma_e+\sigma_l)}+\sigma_l}{\sigma_e+\sigma_l}\right\}, \quad (8)$$

where

$$I\equiv \sin\theta e^{-0.029N\sigma_l/\sin\theta}[1-e^{-0.107N\sigma_l/\sin\theta}]. \quad (9)$$

The integration over x has been carried out numerically for a number of values of $N\sigma_l$, and the results listed in Table II. Figure 4 illustrates σ_l/σ_e times the predominant first term of Eq. (8) plotted against $N\sigma_l$, as compared to the line

$$(\sigma_l/\sigma_e)\log_{10}\rho(10.5\text{ cm})=-0.4343N\sigma_l\times 10.5,$$

where $\rho(10.5$ cm$)$ would be the attenuation ratio at $x=10.5$ cm, were multiple processes not present. The pressure is to be considered the varying parameter in $N\sigma_l$.

This derivation of the attenuation ratio clearly overestimates the effect of multiple processes, since it ignores the fact that a particle which has suffered a double charge exchange, and yet is in an orbit that will enter the detector, will also suffer a displacement of its orbit toward lower y-values. Loss from the beam following a subsequent capture process will then be more probable.

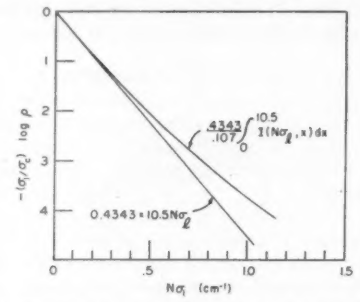

FIG. 4. The predominant term in $(\sigma_l/\sigma_e)\log\rho$ after consideration of the effect of multiple charge exchanges. The straight line represents the expected value of $(\sigma_l/\sigma_e)\log\rho$ in the absence of this effect.

An alternate treatment, which will underestimate the multiple process effect, is carried out by assuming a flux at x of strength $\exp(-N\sigma_e x)$ and considering the flux increment due to double processes as a perturbation. Then the contribution from double processes in dx at x will be given by

$$N\sigma_e dx\exp(-N\sigma_e x)[1-(1/0.107N\sigma_l)I(N\sigma_l, x)].$$

This contribution is assumed to decay by the factor $\exp[-N\sigma_e(10.5-x)]$, leaving a net contribution at $x=10.5$ cm of

$$N\sigma_e dx\exp(-10.5N\sigma_e)[1-(1/0.107N\sigma_l)I(N\sigma_l, x)].$$

Integrating this contribution over x, adding it to the unperturbed flux, and multiplying by the factor for the attenuation in the final 1.52 cm of the path, we have

$$\rho_2=e^{-10.5N\sigma_e}\left\{(1+10.5N\sigma_e) - \frac{\sigma_e}{0.107\sigma_l}\int_0^{10.5} I(N\sigma_l, x)dx\right\}\frac{\sigma_e e^{-1.52N(\sigma_e+\sigma_l)}+\sigma_l}{\sigma_e+\sigma_l}. \quad (10)$$

It can be easily shown that

$$\log_{10}\rho_2-\log_{10}\rho_1<0.2172\left[10.5N\sigma_e - (\sigma_e/0.107\sigma_l)\int_0^{10.5} I(N\sigma_l, x)dx\right]^2. \quad (11)$$

That Eq. (10) underestimates the multiple process effect is shown by the fact that the double process contribution taken is too small, since the true flux is greater than $\exp(-N\sigma_e x)$. Furthermore this contribution then decays less than $\exp[-N\sigma_e(10.5-x)]$, since it can undergo further double processes without being lost to the detector.

Defining $\log\bar{\rho}$ as the arithmetic mean of $\log\rho_1$ and $\log\rho_2$, and f as $12.02\times 0.4343N\sigma_e/(-\log\bar{\rho})$, we can correct the observed values of $\log\rho$ by multiplication by f. Table III lists $-\log\rho_1$, $-\log\rho_2$, $12.02\times 0.4343N\sigma_e$, and f *vs* $N\sigma_l$ for a typical case, in which $\sigma_e=3.24\times 10^{-17}$ cm^2 and $\sigma_l=21\times 10^{-17}$ cm^2. Figure 5 illustrates a typical set of capture points before and after this correction.

As can be seen from the illustration, this correction becomes significant only at pressures such that $N\sigma_l>0.2$ cm^{-1}. Hence, the departure from linearity was only noticed when $\sigma_e<13\times 10^{-17}$ cm^2, for only then were relatively high pressures ($p>10^{-2}$ mm) admitted to the chamber. Furthermore, the effect did not show up in Ribe's work, for the loss cross section in hydrogen is a factor of four smaller, and the highest pressure he used was 7×10^{-2} mm (limit of the McLeod gauge). Hence his highest value of $N\sigma_l$ was only 0.18 cm^{-1}.

E. Effect of Formation of H^- Ions

The possibility of the formation of negative hydrogen ions raises the question of whether the measured loss cross section is not in part the cross section for capture of an electron by a neutral hydrogen atom, a process which would also contribute to the attenuation of a neutral beam. While a complete answer cannot now be given to this question, a measurement has been made which leads to some estimate of the possibilities. The ratio of negative ions to protons leaving the window was found by Ribe[11] to be 0.026 at 35 kv, and less than 0.001 at 90 kv. This value was obtained by comparing the galvanometer deflections from the faraday cage at 60° for the two components, the magnetic field being reversed to bring the negative ions to the detector. If it is assumed that the window was of a thickness yielding charge equilibrium, the ratio of negative ions

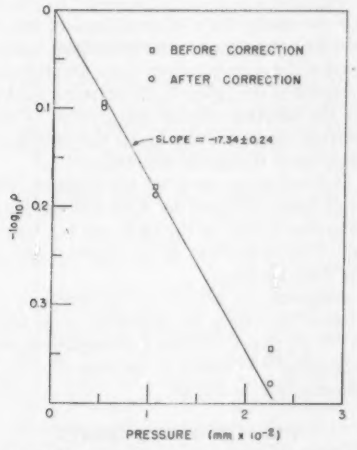

FIG. 5. Attenuation curve for a 93-kv proton beam at the 60° detector before and after correction for multiple charge exchanges.

to protons equals $\sigma_c\sigma_c^*/\sigma_l\sigma_l^*$, where σ_c and σ_l are defined as before, σ_c^* is the cross section for electron capture by a neutral atom, and σ_l^* is the cross section for electron loss by a negative ion. Then, at 35 kv

$$\sigma_c^*=0.026\sigma_l\sigma_l^*/\sigma_c>0.026\sigma_l^2/\sigma_c, \qquad (12)$$

since σ_l^* is certainly greater than σ_l. Assuming the same σ_l and σ_c for the window material as for air, this leads to $\sigma_c^*>0.77\times10^{-17}$ cm² at 35 kv, which is to be compared to an extrapolated value for σ_l of 23.5×10^{-17} cm². A crude upper limit to σ_c^* may be set by assuming that the collision radius for electron loss by an H^- ion is not greater than the sum of the radii of an H^- ion and an air atom. In a compilation by Wherry[17] of

[17] E. T. Wherry, Am. Mineral. 14, 54 (1929). The tabulation given is based on a set of wave-mechanical values computed by Pauling (J. Am. Chem. Soc. 49, 765, 1927), and values computed by V. M. Goldschmidt *et al.* on the basis of empirical assumptions (Geochemische Verteilungsgesetze der Elemente: VII. "Die Gesetze der Krystallochemie"; Skrifter Norske Videnskaps-Akad. Oslo. I. Mat.-Natur. Kl., No. 2, 1926). Pauling's value is used for H^-, and Goldschmidt's for N and O.

TABLE III. Dependence of $\log_{10}\rho_1$, $\log_{10}\rho_2$, $(0.4343)(12.02)N\sigma_c$, and f on $N\sigma_l$ for the case $\sigma_c=3.24\times10^{-17}$ cm², $\sigma_l=21\times10^{-17}$ cm². The parameter $N\sigma_l$ equals $13.72p$, where p is the pressure in mm of mercury.

$N\sigma_l$	$-\log_{10}\rho_1$	$-\log_{10}\rho_2$	$0.4343\times12.02N\sigma_c$	f
0.1	0.0684	0.0683	0.0706	1.032
0.2	0.1324	0.1324	0.1412	1.066
0.3	0.1927	0.1927	0.2118	1.100
0.4	0.2496	0.2497	0.2824	1.132
0.5	0.3034	0.3034	0.3530	1.166
0.6	0.3550	0.3547	0.4236	1.199
0.7	0.4042	0.4038	0.4942	1.231
0.8	0.4521	0.4512	0.5648	1.262
0.9	0.4987	0.4969	0.6354	1.294
1.0	0.5444	0.5413	0.7060	1.324
1.1	0.5901	0.5850	0.7766	1.353

accepted values of atomic radii, 0.71×10^{-8} cm and 0.60×10^{-8} cm are given for the neutral nitrogen and oxygen atoms, respectively; and 2.08×10^{-8} cm is given for the negative hydrogen ion. Using the value for nitrogen, an upper limit of 24.4×10^{-16} cm² is obtained for σ_l^*, leading to upper limits for σ_c^* of 8×10^{-17} cm² at 35 kv and 1×10^{-17} cm² at 90 kv.

VI. RESULTS

The final values of σ_l and σ_c are listed in Table IV and also plotted in Fig. 6. The two points labelled "*M*" on the σ_c curve were taken with the Montague detector at the 60° position. In the energy range shown, σ_l and σ_c are well represented by the following empirical formulas:

$$\sigma_l=(24.54-0.866E/E_0)\times10^{-17}\text{ cm}^2, \qquad (13)$$

$$\sigma_c=[41.1\exp(-0.562E/E_0)]\times10^{-17}\text{ cm}^2, \qquad (14)$$

where $E_0=24.8$ kv, the kinetic energy of a proton

TABLE IV. The electron capture and loss cross sections for hydrogen beams passing through air.

Beam energy E (kv)	Electron-loss cross section per atom σ_l (cm²×10⁻¹⁷)	Beam energy E (kv)	Electron-capture cross section per atom σ_c (cm²×10⁻¹⁷)
40.8	24.37±0.47	31.4	20.80±0.37
41.4	23.17±0.63	38.2	17.65±0.21
67.0	22.22±0.06	40.6	15.97±0.46
105	20.84±0.25	43.0	15.64±0.30
107	21.00±0.30	49.4	13.39±0.36
117	20.63±0.11	55.7	11.59±0.23
142	19.76±0.10	56.6	11.51±0.22
156	18.88±0.06	58.1	10.07±0.14
193	17.35±0.35	63.0	9.74±0.21
221	16.74±0.19	65.6	9.26±0.19
252	14.42±0.72	73	6.80±0.29
280	14.53±0.30	77	7.06±0.18
325	13.58±0.25	93	5.52±0.07
...	...	114	3.38±0.04
...	...	117	2.72±0.07
...	...	122	2.70±0.04

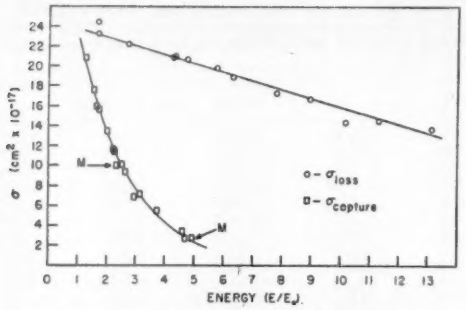

FIG. 6. Electron capture and loss cross sections as functions of ion energy for hydrogen beams in air. $E_0=24.8$ kv, the kinetic energy of a proton moving with the Bohr velocity.

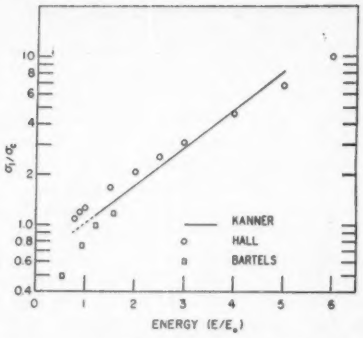

FIG. 7. The ratio of loss to capture cross sections as a function of ion energy. The solid curve is a plot of σ_l/σ_c as given by Eqs. (13) and (14). Bartels' points are for hydrogen beams in air, and Hall's points for hydrogen beams in the metals Be and Ag.

moving with velocity $v_0=e^2/\hbar$. σ_l/σ_c as given by Eqs. (13) and (14) is plotted in Fig. 7, which also shows the values obtained by Bartels[3] for air and by Hall[9] for metals. Both the capture and loss cross sections decrease considerably less steeply with increasing energy than has been predicted theoretically by Bohr,[18] who gives a dependence proportional to E^{-1} for the loss cross section, and proportional to E^{-3} for the capture cross section. Since both of Bohr's formulas require $v\gg v_0$, (say $v\sim 6v_0$) this disagreement in the energy range of the present investigation is not surprising.

VII. DISCUSSION OF ERRORS

The uncertainties listed in Table IV as accompanying the cross sections are derived purely from the scattering of the $\rho(p)$ values about the chosen straight line by application of Eq. (4). They therefore take into account random errors during a measurement, such as those originating in faulty instrument reading, amplifier drift, and beam inhomogeneity.

The accuracy of the energy measurements is greater for the capture cross section than for the loss cross section, a fortunate circumstance in view of the steeper energy dependence of the former. The system of collimator, magnetic field, and 60° detector slit acted as a magnetic spectrometer, so that the outstanding uncertainty in the energy for a σ_c measurement was due to the probable 1 percent error in the magnet calibration. In the case of the σ_l measurements, the additional uncertainty because of straggling in the entrance window and ripple in the kevatron voltage was present. Of the two, the 3 percent ripple overshadowed the contribution of the straggling to the energy uncertainty.

The McLeod gauge used for the pressure measurements had been calibrated by Ribe and the author by measuring the volume of the bulb and the bore of the capillary. This calibration is considered to be correct to better than 1 percent.

The measured gas effects on the detectors are believed correct to within an equivalent cross section of 0.2×10^{-17} cm², thus introducing maximum errors in the cross sections of 1.5 percent in the value of σ_l at 325 kv and 8 percent in σ_c at 125 kv.

[18] N. Bohr, Kgl. Danske Videnskab. Selskab. Mat.-fys. Medd. (1948), Equations 4.2.8 and 4.3.5.

VIII. ACKNOWLEDGMENTS

The author wishes to express his gratitude to Dr. S. K. Allison for suggesting the problem and extending the facilities of his laboratory. Thanks are also due Dr. F. L. Ribe, Mr. D. S. Bushnell, and Mrs. L. C. Kanner for their aid in taking the many data. Finally, the author wishes to thank Mr. H. Casson and Mr. J. Alexander for their valuable participation in discussions of the correction for multiple charge exchanges.

The Thick Target Yield of the Reaction $C^{12}(p, \gamma)N^{13}(\beta^+)C^{13}$*

JOHN D. SEAGRAVE
Kellogg Radiation Laboratory, California Institute of Technology, Pasadena, California
(Received September 10, 1951)

The yield of N^{13} from a thick carbon target bombarded with protons of energy up to 2.5 Mev has been studied by detecting annihilation quanta with a scintillation crystal. Resonances at 0.45 and 1.70 Mev are confirmed, and independent values are obtained for their relative and absolute intensities.

INTRODUCTION

THE thick target yield of the reaction $C^{12}(p, \gamma)N^{13}$ exhibits two resonances in the range $0<E_p<2$ Mev, at 0.45 Mev,[1] and at 1.70 Mev.[2] The ratio of maximum thick target yields is reported by Van Patter[2] as $Y(1.70)/Y(0.45)=1.3\pm0.2$, and the absolute yield of the lower resonance is reported by Fowler and Lauritsen[3] as $7.3\times10^{-10}\gamma/p$ (at $E_p=1.00$ Mev).

EXPERIMENTAL METHOD

The present investigation was undertaken to obtain a more precise value of the ratio of yields and an independent value for the absolute yield, and to check with a thick target the position and width of the 1.70-Mev resonance.

As in Van Patter's work, the (p, γ) yield was investigated indirectly, by measuring the $N^{13}(\beta^+)C^{13}$ activity built up in the target. Measurements of absolute yields of beta-particles are subject to uncertainties arising from self-absorption and back-scattering effects. These difficulties were avoided in the work reported here by detecting instead the annihilation quanta associated with absorption of the positrons. Satisfactory counting rates were obtained by taking advantage of the high sensitivity of a NaI scintillation counter to annihilation quanta. Absolute yields were computed from measurements on a Na^{22} positron source of known strength.

The targets comprised a series of identical discs machined (dry) from a block of Acheson graphite. They were mounted in quick-change probe, which permitted easy insertion into and removal from the target chamber of an electrostatic accelerator. The target assembly could be rotated to one side and the proton beam accurately aligned on a quartz window. After bombardment, the activated carbon targets were removed from the vacuum system and placed in a standard position on the aluminum light shield directly over a NaI crystal and photomultiplier. The targets were covered with a recessed block of aluminum so the positrons ($E_{max}=1.2$ Mev) were annihilated in the immediate vicinity of the target. Loss of N^{13} by diffusion out of the graphite was considered negligible at the moderate temperatures developed in the targets, as no build-up of activity was detected by a shielded Geiger counter placed in the exhaust line of the target pumping system.

N^{13} has a half-life of 10.1 minutes, and a corresponding decay constant $\lambda=1.142\times10^{-3}$ sec^{-1}. If the target is bombarded for a time t_b with a proton current i, the activity is allowed to decay for a time t_d, and is then counted for a time t_c by a counter whose effective efficiency is $f=2\epsilon_{0.51}\Omega$, then

$$\text{counts recorded}=\text{yield}\times f\times i\lambda^{-1}(1-e^{-\lambda t_b})\times e^{-\lambda t_d}(1-e^{-\lambda t_c}). \quad (1)$$

For $\lambda t_b \ll 1$, the bombardment factor can be expanded in a rapidly convergent series, and (it_b) set equal to the total charge q collected by the integrator, so that the bombardment factor becomes

$$i\lambda^{-1}(1-e^{-\lambda t_b})=q[1-\tfrac{1}{2}(\lambda t_b)+\tfrac{1}{6}(\lambda t_b)^2+\cdots]. \quad (2)$$

In this application, the effect of rapid current fluctuations is smoothed out. Throughout this experiment, t_b did not exceed a few minutes, and the approximation made in obtaining the above equations was generally negligible. For an example of the quantities involved, bombarding at 1.00 Mev, collecting 222 microcoulombs in 200 sec, followed by a delay of 90 sec, and a counting period of 240 sec led to about 15,000 counts, about $\frac{1}{3}$ of

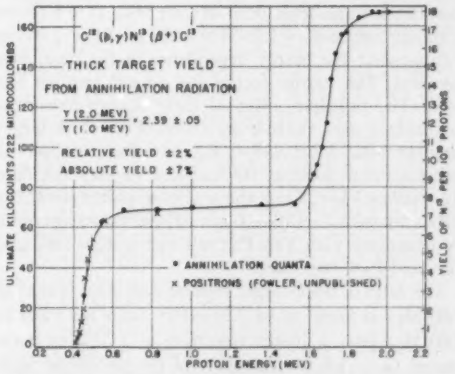

FIG. 1. Thick target excitation function for the reaction $C^{12}(p, \gamma)N^{13}(\beta^+)C^{13}$. The positron data for the shape of the lower resonance was supplied by Dr. W. A. Fowler (see reference 1, Fig. 1).

* This work was supported by the joint program of the AEC and ONR.

[1] Fowler, Lauritsen, and Lauritsen, Revs. Modern Phys. **20**, 236 (1948).
[2] D. M. Van Patter, Phys. Rev. **76**, 1264(L) (1949).
[3] W. A. Fowler and C. C. Lauritsen, Phys. Rev. **76**, 314 (1949).

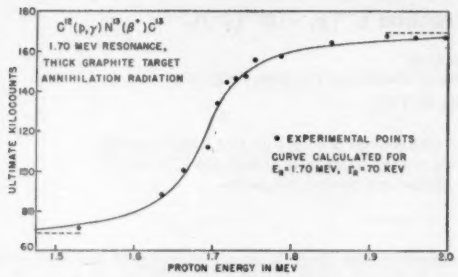

FIG. 2. Detail of the 1.70-Mev resonance. The curve is the integral of a single-level Breit-Wigner dispersion formula, taking into account the barrier for p-wave protons and other energy-dependent terms, assuming that $E_R=1.70$ Mev and $\Gamma_R=70$ kev.

the "ultimate" value obtained using Eqs. (1) and (2). and giving less than 1 percent random counting error,

THICK TARGET EXCITATION CURVE

The excitation function for the reaction was determined between 0.45 and 2.2 Mev with a single-channel differential pulse analyzer straddling the annihilation photopeak, and simultaneously with a discriminator set just below the peak. The integral data, corrected as outlined above, is shown in Fig. 1, and is believed to give the relative excitation function to within ± 2 percent. The 0.45-Mev and 1.70-Mev resonances are exhibited, and no other resonances of intensity >2 percent that of the 0.45-Mev resonance appear below 2.1 Mev, or >15 percent between 2.1 and 2.5 Mev. In the upper region, irregularities in the operation of the Van de Graaff accelerator increased the error of using Eq. (2), and bombardment corrections could not be made with certainty. In particular, a possible weak resonance near 2.3 Mev could not be confirmed.

The 1.70-Mev resonance is shown in more detail in Fig. 2. The curve shown is based on a numerical integration of the single-level Breit-Wigner resonance formula with parameters $E_R=1.70$ Mev and $\Gamma_R=70$ kev, taking into account the energy dependence of the quantities involved. The barrier factor[4] for p-wave protons was used. The principal effect of these energy-dependent factors is to shift the half-maximum of the thick-target yield to some 5 kev below E_R, so from the observed half-maximum point at 1693 ± 5 kev we may calculate $E_R=1698\pm5$ kev. From the scatter of points about the curve, we take $\Gamma_R=70\pm10$ kev. These values are quite in agreement with Van Patter's values $E_R=1697\pm12$ kev, and $\Gamma_R=74\pm9$ kev.

The ratio of thick-target yield at 2.00 Mev to that at 1.00 Mev is found to be 2.39 ± 0.05. Since the yield at 2.00 Mev from a 70-kev resonance at 1.70 Mev is expected to be 4.5 percent short of the maximum yield (indicated by dotted lines in Fig. 2), we conclude that the total yield of the upper resonance is 1.45 ± 0.03 times that of the lower resonance (at 1.00 Mev), a result which is within the probable error given by Van Patter.

ABSOLUTE YIELD

The effective efficiency f was determined by comparison of the counting rate in the annihilation channel with that from a Na^{22} source of known strength placed in the standard position. A weak source of Na^{22} was prepared, and compared on a Geiger-tube "bench" with a "standard" Na^{22} source determined by T. Lauritsen in a β-spectrometer as 3.53×10^6 disintegrations/second (±5 percent) on 27 February, 1951. This value itself was determined by comparison of the 1.3-Mev Na^{22} line with a standard Co^{60} source. Allowing for a 3 percent decay (2.6-year half-life) since the time of determination, the weak source was found to have a strength of 3.0×10^4 disint/sec (±5.5 percent). This gave the efficiency $f=5.0$ percent. Two separate comparisons were made of the radiation in the annihilation channel from N^{13} at $E_p=1.00$ Mev and that from the Na^{22} source, and a systematic error due to radiation scattered into the annihilation channel from the 1.3-Mev line was found from the complete integral and differential bias curves to amount to 10 ± 1 percent. The yield of $C^{12}(p,\gamma)N^{13}$ was then computed as 7.7×10^{-10} N^{13}/proton (±10 percent) for normal carbon at $E_p=1.00$ Mev, which is in agreement with a value 7.3×10^{-10} previously reported.[3] Averaging these two independent measurements, we conclude that the yield is $7.5\pm0.5\times10^{-10}$ N^{13}/proton.

DISCUSSION

Investigators at Wisconsin[5] have studied elastic scattering of protons by carbon up to 4 Mev, and find in addition to the 0.45-Mev resonance a pronounced anomaly near 1.7 Mev which has been interpreted[6] as indicating the existence of two closely spaced levels, with $J=\frac{3}{2}$ and $5/2$, respectively. The observation of only one resonance for gamma-radiation is consistent with this hypothesis, since the intensity of radiation from a $J=5/2$ level either to the ground state (presumably $J=\frac{1}{2}$) or to the 2.4-Mev level may be expected to be at least an order of magnitude weaker than radiation from a $J=\frac{3}{2}$ level to the ground state. However, a marked discrepancy does exist between the width found for the radiating level and those proposed by Jackson and Galonsky,[6] who have fitted the (p,p) data with a 45-kev $P_{\frac{1}{2}}$ level at approximately the position of the (p,γ) resonance, and a $D_{\frac{3}{2}}$ level also about 45 kev wide, some 50 kev higher. From the thick target data alone, it is not possible to exclude a small contribution from a second resonance, since within certain limits, the data

[4] R. F. Christy and R. Latter, Revs. Modern Phys. **20**, 185 (1948).

[5] G. Goldhaber and R. M. Williamson, Phys. Rev. **82**, 495 (1951).

[6] We are indebted to H. L. Jackson and A. I. Galonsky for making available to us their paper in advance of publication [Phys. Rev. **84**, 401 (1951)].

may be "fitted" by superposition of two resonances, making appropriate adjustment of widths, positions, and intensities. If the widths and positions are constrained to the values suggested by Jackson and Galonsky, the upper resonance would have to show a gamma intensity not less than half as strong as the lower. Were this the case, both resonances should appear in thin target data. Van Patter has obtained a curve[7] for positrons with a 10-kev target, and gamma-ray curves have been obtained at this laboratory for several targets with thicknesses between 16 and 50 kev. All of these curves point to a single radiating resonance. If there are two which radiate, they are separated by less than 20 kev, and at least one of them has a width greater than 60 kev. It may be remarked that radiation from a weak, narrow resonance above 1.76 Mev might have been obscured by the strong radiation due to C^{13} which appears at that energy[8] but no evidence appeared in the positron data.

[7] D. M. Van Patter, M.I.T. Progress report (October 1, 1949), p. 32.

[8] Seagrave, Day, and Perry, Phys. Rev. 81, 661(A) (1951).

PHYSICAL REVIEW VOLUME 84, NUMBER 6 DECEMBER 15, 1951

The Scattering of Slow Electrons by Atoms

DAVID LAYZER*
Observatory of the University of Michigan, Ann Arbor, Michigan†
(Received June 21, 1951)

A new approximation is proposed for calculating cross sections for the scattering of slow electrons by atoms. Although the proposed approximation embodies the essential feature of Born's approximation it is compatible with the exclusion principle for electrons, and yields nonvanishing cross sections for the excitation by electron impact of intersystem transitions in normal-coupling atoms. Unlike Oppenheimer's approximation it yields unambiguous results when approximate atomic wave functions are used in the calculation of excitation cross sections, provided that these wave functions belong to a single hermitian operator that differs from the exact hamiltonian only through a term in the potential energy.

1. INTRODUCTION

MANY astrophysical and geophysical problems require for their solution accurate estimates of cross sections for the excitation of atoms by collision with slow electrons. Unfortunately, the simplest and most successful of the approximation methods available for calculating scattering cross sections, that of Born,[1] is least reliable in the low-energy domain. There are two reasons: (a) Born's approximation is a first approximation in the sense of the perturbation theory. Hence the smaller the perturbation suffered by an incident electron in exciting a particular atomic transition, the more accurately should Born's approximation predict the corresponding cross section. But the cross section itself is a measure of the perturbation. Since scattering cross sections increase with decreasing impact energy (except in the immediate neighborhood of the threshold energy), Born's approximation should deteriorate with decreasing impact energy. (b) Born's approximation is based, in part, on the simplifying assumption that the colliding electron is distinguishable from the atomic electrons. But the effects on scattering cross sections of the exchange interaction between the colliding electron and the atomic electrons, which are thereby neglected. are known to be significant in the low-energy domain,

Of particular importance in astrophysical and geophysical applications is the excitation by electron impact of optically forbidden transitions. Since, in general, cross sections for this type of excitation are intrinsically small, it seems likely that for these transitions the principal source of inaccuracy in the cross sections calculated on Born's approximation is the neglect of exchange, not the neglect of second- and higher-order perturbation effects. If this view is correct, a first approximation compatible with the Pauli exclusion principle would suffice for the calculation of many cross sections of astrophysical and geophysical importance that cannot be accurately calculated on Born's approximation. In any event it would constitute a reasonable point of departure for further refinements.

An approximation resembling that of Born but compatible with the exclusion principle was proposed by Oppenheimer in 1928,[2] and has since served as the basis for many calculations. Recently, however, Bates, Fundaminsky, Leech, and Massey[3] have presented convincing evidence that Oppenheimer's approximation is actually far less reliable than Born's. Among their results are the following:

(a) Where a comparison is possible, cross sections calculated on Born's approximation are found to agree far better with experiment than those calculated on

* National Research Council Postdoctoral Fellow, 1950–1951.
† Now Department of Astronomy, University of California, Berkeley, California.

[1] M. Born, Z. Physik 37, 863 (1926).

[2] J. R. Oppenheimer, Phys. Rev. 32, 361 (1928).

[3] Bates, Fundaminsky, Leech, and Massey, Trans. Roy. Soc. (London) 243, 117 (1950).

Oppenheimer's approximation, which "generally leads to gross errors at low energies." (b) Calculations based on Oppenheimer's approximation frequently violate the conservation theorem of Mott and of Bohr, Peierls, and Placzek, which sets an upper bound on theoretical cross sections, (c) Oppenheimer's approximation involves a serious "prior-post discrepancy": there are two equally justifiable ways of applying the approximation, which frequently lead to very different results when approximate (rather than exact) atomic wave functions are used in the calculation.

Bates, Fundaminsky, and Massey[4] have exhibited in detail and intercompared the specific sources of error in the Born and Oppenheimer approximations. They find several important differences.

We shall here adopt an approach that differs from and complements that of Bates, Fundaminsky, and Massey. It is based on the remark that Born's approximation can hardly owe its success to the incorrect assumption that the colliding electron is distinguishable from the atomic electrons; the essential features of the approximation must be independent of this assumption. We shall therefore attempt to combine these features with the assumption that the colliding electron is indistinguishable from the atomic electrons. The result will be a set of requirements that must be fulfilled by any approximation that retains those features of Born's approximation that are compatible with the exclusion principle and is itself compatible with it. After showing that Oppenheimer's approximation fails to satisfy these requirements we shall exhibit an approximation that does.

2. MODIFICATION OF BORN'S APPROXIMATION

In the following we shall rely as much as possible upon Dirac's treatment of the scattering problem,[5] which is so general that only relatively minor changes are required to make it consistent with the exclusion principle and with the circumstance that the unperturbed colliding electron must ordinarily be described by a coulomb (rather than a plane) wave.

Let $H(A, B)$ denote the hamiltonian for a system made up of A electrons and an infinitely massive nucleus of charge Be located at the origin. The system we wish to consider is characterized by the hamiltonian $H(N+1, Z)$. To save writing we set[6]

$$\begin{aligned} &H(N+1, Z)=H, \quad H(N, Z)=H_o, \\ &H(1, Z-N)=W, \quad V_i=H-H_o^i-W_i. \end{aligned} \tag{1}$$

With neglect of spin-dependent terms

$$W=p^2/2m-(Z-N)e^2/r, \tag{2}$$

and

$$V_i=\sum_{j(\neq i)} e^2(1/r_{ij}-1/r_i). \tag{3}$$

It follows from Eq. (3) that

$$r_iV_i\sim 0. \tag{4}$$

By virtue of Eq. (4) the eigenvalue equation

$$(\langle \mathbf{X}|H|H'\rangle\equiv)H_{op}\langle \mathbf{X}|H'\rangle=H'\langle \mathbf{X}|H'\rangle \tag{5}$$

has a solution with the asymptotic form,

$$\begin{aligned} \langle \mathbf{X}|H'\rangle\sim\delta_i\{&\psi_a(\mathbf{x}_i, \mathbf{k}^0)\cdot|s_i^0\rangle\langle \mathbf{X}^i|\alpha^0\rangle \\ &+\sum_{\alpha'\sigma'}\psi_b(\mathbf{x}_i, \mathbf{k}')\cdot|s_i'\rangle\langle \mathbf{X}^i|\alpha'\rangle\}. \end{aligned} \tag{6}$$

Here $\langle \mathbf{X}^i|\alpha\rangle$ is an eigenrepresentative of H_o^i in which the numerical order of the N electron suffixes $1, 2, \cdots, i-1, i+1, \cdots, N+1$ is taken as standard; $\delta_i=+1$ or -1 according as $N-i$ is odd or even; and $|s_i\rangle$ is a spin ket for the colliding electron. Thus the right-hand side of (6) is antisymmetrical. The wave functions

$$\psi_b(\mathbf{x}, \mathbf{k})=u(\vartheta\varphi\alpha)r^{-1}\exp[ikr+i\gamma\log kr], \tag{7}$$

and

$$\left.\begin{aligned} \psi_a(\mathbf{x}, \mathbf{k})=&\exp[i\mathbf{k}\cdot\mathbf{x}-i\gamma\log(kr-\mathbf{k}\cdot\mathbf{x})] \\ &-f(k\Theta)r^{-1}\exp[ikr+i\gamma\log kr] \\ f(k\Theta)=&\exp[i\gamma\log(1-\cos\Theta)+2i\eta_0] \\ &\cdot(\gamma/2k)\operatorname{cosec}^2(\Theta/2) \end{aligned}\right\} \tag{8}$$

are asymptotic solutions of the wave equation

$$W_{op}\langle \mathbf{x}|W\rangle=W\langle \mathbf{x}|W\rangle,$$

or

$$(\nabla^2+k^2+2k\gamma/r)\langle \mathbf{x}|W\rangle=0, \tag{9}$$

belonging to the eigenvalues

$$W=H'-H_o(\alpha).[7] \tag{10}$$

As usual

$$\mathbf{x}\equiv(r\vartheta\varphi), \tag{11}$$

and we have set

$$\begin{aligned} &k^2=2m\hbar^{-2}W; \quad \gamma=(Z-N)me^2/\hbar^2k; \\ &\mathbf{k}\cdot\mathbf{x}=kr\cos\Theta; \quad \exp[2i\eta_0]=\Gamma(1-i\gamma)/\Gamma(1+i\gamma). \end{aligned} \tag{12}$$

[4] Bates, Fundaminsky, and Massey, Trans. Roy. Soc. (London) **243**, 93 (1950).

[5] P. A. M. Dirac, *The Principles of Quantum Mechanics* (Oxford University Press, London, 1947), third edition, Secs. 48–50. We have followed Dirac's notation where possible. The complex conjugate of a quantity ψ is here denoted by ψ^* instead of by $\bar{\psi}$.

[6] In order to avoid the repetition of certain qualifying phrases we shall adhere to the following conventions. (a) When the variable suffix i appears as a subscript it labels dynamical variables that refer to the colliding electron; when it appears as a superscript it indicates the omission of these variables. Thus $\mathbf{x}_i$ denotes the set of cartesian coordinates of the colliding electron, $\mathbf{X}^i$ the set of $3N$ cartesian coordinates of the electrons, and $\mathbf{X}$ the set of $3(N+1)$ cartesian coordinates of all the electrons in the system. (b) All statements and relations in which the suffix i occurs will be understood to hold for all values of i $(=1, 2, \cdots, N+1)$. (c) The word 'asymptotic' and the symbol '$\sim$' will be understood to imply that the statement or relation in question holds approximately when $r_i\gg r_j$ (all $j\neq i$), and exactly in the limit $r_i=\infty$.

[7] N. F. Mott and H. S. W. Massey, *The Theory of Atomic Collisions* (Oxford University Press, London, 1949), second edition, p. 136.

According to the statistical interpretation described by Dirac,[5] the right-hand side of (6) represents a collection of electrons moving in the field of a point charge $(Z-N)\epsilon$ located at the origin, together with a collection of atoms, each of which is located at the origin and is in a definite stationary state. There is a one-to-one correspondence between the electrons and the atoms: the incoming electrons are all associated with atoms in the state α^0, and constitute a coulomb wave characterized by the momentum vector $\hbar\mathbf{k}^0$; the outgoing electrons are associated with atoms in the states α' (including α^0), and each state α' corresponds to a definite radial coulomb wave. Thus far the physical interpretation is the same as on Born's approximation. But now in contrast with the picture underlying Born's approximation each colliding electron is distinguished from the electrons in the corresponding atom only by its being much more distant from the origin than they are—not by the suffix i, which is variable.

The scattering coefficient is

$$\left.\begin{array}{ll}(k'/k^0)\cdot|u(\vartheta\varphi\alpha')|^2 & (\alpha'\neq\alpha^0)\\ |f(k^0\Theta)+u(\vartheta\varphi\alpha^0)|^2 & (\alpha'=\alpha^0)\end{array}\right\}. \tag{13}$$

In order to calculate the amplitudes $u(\vartheta\varphi\alpha)$ we make use of the first-order perturbation theory.[5]

The hamiltonian E for the unperturbed system has the asymptotic form,

$$E\sim H_s{}^iW_i\equiv E_i. \tag{14}$$

Accordingly,

$$E'=H_s(\alpha')+W'=H'. \tag{15}$$

In the unperturbed system only incident and Rutherford-scattered electrons are present at great distances from the origin. Hence the eigenrepresentatives of E, which we denote by $\langle\mathbf{X}|\beta(\alpha\mathbf{k})\rangle$, must have the asymptotic form,

$$\langle\mathbf{X}|\beta(\alpha\mathbf{k})\rangle\sim\delta_i\hbar^{-\frac{1}{2}}\psi_a(\mathbf{x}_i,\mathbf{k})\cdot|s_i\rangle\langle\mathbf{X}^i|\alpha\rangle. \tag{16}$$

On Born's approximation the asymptotic relations (14) and (16) are replaced by equations, the suffix i being assigned a fixed value. Since, however, in Dirac's solution with the p-representation[5] of the equation,

$$(H'-E)|1\rangle=\hbar^{\frac{1}{2}}V|\beta(\alpha^0\mathbf{k}^0)\rangle, \tag{17}$$

where

$$V\equiv H-E, \tag{18}$$

and (in the present case)

$$\langle\mathbf{X}|1\rangle\sim\delta_i\sum\psi_b(\mathbf{x}_i,\mathbf{k}')\cdot|s_i'\rangle\langle\mathbf{X}^i|\alpha'\rangle, \tag{19}$$

the representatives $\langle\mathbf{X}|\beta\rangle$ and $\langle\mathbf{X}|1\rangle$ occur only in asymptotic form, this solution can be applied with only minor changes to the problem at hand. Thus, for example, to find the mixed representative $\langle\mathbf{x}_i\alpha'|1\rangle$ multiply (19) by $\langle\alpha'|\mathbf{X}^i\rangle$ and integrate over all values of ϑ_j, φ_j (all $j\neq i$) and over a range $0\leq r_j\leq D$ (all $j\neq i$), where $r_i\gg D\gg d$, an atomic dimension. Then

$$\langle\mathbf{x}_i\alpha'|1\rangle\sim\delta_i\psi_b(\mathbf{x}_i,\mathbf{k}')\cdot|s_i'\rangle. \tag{20}$$

It turns out that the form of Dirac's final result is preserved: The scattering coefficient is

$$\left.\begin{array}{ll}4\pi^2m^2\hbar^2(k'/k^0) & \\ \quad\times|\langle\beta^*(\alpha'\mathbf{k}')|V|\beta(\alpha^0\mathbf{k}^0)\rangle|^2 & (\alpha'\neq\alpha^0)\\ |f(\Theta k^0)-2\pi mh\exp[i\gamma^0\log 2] & \\ \quad\cdot\langle\beta^*(\alpha^0\mathbf{k}')|V|\beta(\alpha^0\mathbf{k}^0)\rangle|^2 & (\alpha'=\alpha^0)\end{array}\right\}, \tag{21}$$

where

$$\langle\mathbf{X}|\beta^*(\alpha\mathbf{k})\rangle\sim\delta_i\hbar^{-\frac{1}{2}}\psi_a{}^*(\mathbf{x}_i,-\mathbf{k})\cdot|s_i\rangle\langle\mathbf{X}^i|\alpha\rangle. \tag{22}$$

It may be mentioned explicitly that Dirac's solution of (17) with the x-representation, and *a fortiori* the solutions used by Bates, Fundaminsky, and Massey[4] and by Mott and Massey,[7] are not sufficiently general to allow the derivation of (21) with only the information provided by (14), (15), and (16).

3. OPPENHEIMER'S APPROXIMATION

Bates, Fundaminsky, and Massey remark (in effect) that Oppenheimer's formula for the inelastic-scattering coefficient is a special case of Dirac's general formula (21) with

$$\langle\mathbf{X}|\beta(\alpha\mathbf{k})\rangle=\hbar^{-\frac{1}{2}}\sum_{j=1}^{N+1}\delta_j\psi(\mathbf{x}_j,\mathbf{k})\cdot|s_j\rangle\langle\mathbf{X}^j|\alpha\rangle, \tag{23}$$

and E defined by

$$E\psi(\mathbf{x}_i,\mathbf{k})\cdot|s_i\rangle\langle\mathbf{X}^i|\alpha\rangle = (N+1)^{-1}E_i\psi(\mathbf{x}_i,\mathbf{k})\cdot|s_i\rangle\langle\mathbf{X}^i|\alpha\rangle, \tag{24}$$

where

$$\psi(\mathbf{x},\mathbf{k})=e^{\pi\gamma/2}\Gamma(1-i\gamma) \times\exp[ikr\cos\Theta]\,{}_1F_1(i\gamma;1;ikr(1-\cos\Theta)), \tag{25}$$

is the exact solution of (9) whose asymptotic form is $\psi_a(\mathbf{x},\mathbf{k})$.[8]

Now we have just seen that the $\langle\mathbf{X}|\beta(\alpha\mathbf{k})\rangle$ must be eigenrepresentatives of E and that E itself must satisfy (14). But (23) and (24) are obviously not compatible with either of these requirements. In fact the definition (24) of E is not even self-consistent. For it implies that the representatives $\psi(\mathbf{x}_i,\mathbf{k})\cdot|s_i\rangle\langle\mathbf{X}^i|\alpha\rangle$, which constitute a complete orthonormal set and are the eigenrepresentatives of $E_i(=H_s{}^i+W_i)$, are also eigenrepresentatives of E, and that $E'=E_i'/(N+1)$. It therefore follows from (24) that $E=E_i/(N+1)$ for all values of i, which is impossible.

Thus Oppenheimer's approximation is certainly not a generalization of Born's approximation, in the re-

[8] See reference 7, Chap. III.

stricted sense of the preceding section. This fact provides, perhaps, the simplest explanation of the great disparity in quality between the results that have been obtained from the two approximations.

4. THE DETERMINATION OF E

If in Eqs. (1)–(22) we replace the variable suffix i by the fixed suffix $N+1$ and drop conventions (a) and (b),[8] we obtain a new set of Eqs. (1b)–(22b) that are valid on the assumption that the colliding electron is distinguishable from the atomic electrons. We shall now construct a particular approximation that is compatible with the exclusion principle by carrying this parallelism a step further.

Written out explicitly, the relations (14b) and (16b), (14) and (16) are as follows:

$$\left.\begin{aligned} E&=H_a^{N+1}+W_{N+1} \qquad (14b)\\ \langle \mathbf{X}|\beta(\alpha\mathbf{k})\rangle&=h^{-\frac{1}{2}}\psi_a(\mathbf{x}_{N+1},\mathbf{k})|s_{N+1}\rangle\langle \mathbf{X}^{N+1}|\alpha\rangle \qquad (16b)\end{aligned}\right\} r_{N+1}\gg r_j \quad (\text{all } j\neq N+1),$$

$$\left.\begin{aligned} E&=H_a^{i}+W_i \qquad (14)\\ \langle \mathbf{X}|\beta(\alpha\mathbf{k})\rangle&=\delta_{is}h^{-\frac{1}{2}}\psi_a(\mathbf{x}_i,\mathbf{k})\cdot|s_i\rangle\langle \mathbf{X}^{i}|\alpha\rangle \qquad (16)\end{aligned}\right\} r_i\gg r_j \quad (\text{all } j\neq i) \quad i=1,2,\cdots,N+1.$$

We get Born's approximation itself by extending the domain of definition of E and its eigenrepresentatives:

$$E=H_a^{N+1}+W_{N+1}, \qquad (26b)$$

$$\langle \mathbf{X}|\beta(\alpha\mathbf{k})\rangle=h^{-\frac{1}{2}}\psi(\mathbf{x}_{N+1},\mathbf{k})\langle \mathbf{X}^{N+1}|\alpha\rangle. \qquad (27b)$$

Making the corresponding changes in (14) and (16) we get[9]

$$\left.\begin{aligned} E&=H_a^{i}+W_i \qquad (26)\\ \langle \mathbf{X}|\beta(\alpha\mathbf{k})\rangle&=\delta_{is}h^{-\frac{1}{2}}\psi(\mathbf{x}_i,\mathbf{k})\langle \mathbf{X}^{i}|\alpha\rangle \qquad (27)\end{aligned}\right\} r_i>r_j \text{ (all } j\neq i).$$

According to the definitions (26) and (27), in the unperturbed system the electron most distant from the nucleus is identified with the colliding electron, and there is no interaction between the colliding electron and the atomic electrons.

The definitions (26) and (27) are incomplete in that E and its eigenrepresentatives are not yet defined at those points in the $3(N+1)$-dimensional configuration space for which $r_i=r_j\geq r_k$ (all $k\neq i, j$). Such points correspond to configurations in which two or more electrons are equally distant from the nucleus and more distant from it than any of the other electrons. Since in the unperturbed system the probability density of the colliding electron is independent ($Z=N$) or nearly independent ($Z\neq N$) of position, we shall assume that when $r_i=r_j>r_k$ (all $k\neq i, j$) the electrons i and j share equally the status of colliding electron:

$$\langle \mathbf{X}|\beta(\alpha\mathbf{k})\rangle=2^{-\frac{1}{2}}h^{-\frac{1}{2}}\{\delta_{is}\psi(\mathbf{x}_i,\mathbf{k})\cdot|s_i\rangle\langle \mathbf{X}^{i}|\alpha\rangle$$
$$+\delta_{js}\psi(\mathbf{x}_j,\mathbf{k})\cdot|s_j\rangle\langle \mathbf{X}^{j}|\alpha\rangle\} \ (r_i=r_j>r_k, \text{all } k\neq i,j). \qquad (28)$$

The definition (27) must be completed in such a way that the representatives defined by (26) and (28) are actually eigenrepresentatives of E. It follows from (26) and (27) that

$$E=H_a^{i}+W^{i}-V_{kij} \quad r_i\geq r_j>r_k \text{ (all } k\neq i,j), \qquad (29)$$

and hence

$$V=V_i+V_{kij} \quad r_i\geq r_j>r_k \text{ (all } k\neq i,j), \qquad (30)$$

where V_{kij} vanishes except for $r_i=r_j$. Since only the part of V_{kij} that is proportional to $\delta(r_i-r_j)$ contributes to the matrix element $\langle\beta^*|V_{kij}|\beta\rangle$, this operator is sufficiently well determined by the requirement

$$|\langle \mathbf{X}|E|\beta\rangle|_{r_i=r_j>r_k}<\infty \quad (\text{all}''k\neq i,j), \qquad (31)$$

or, with neglect of terms that do not give rise to infinities,

$$\left|\left\{-\frac{\hbar^2}{2m}\left(\frac{\partial^2}{\partial r_i^2}+\frac{2}{r_i}\frac{\partial}{\partial r_i}+\frac{\partial^2}{\partial r_j^2}+\frac{2}{r_j}\frac{\partial}{\partial r_j}\right)\right.\right.$$
$$\left.\left.-V_{kij}\right\}\langle \mathbf{X}|\beta\rangle\right|_{r_i=r_j>r_k}<\infty \quad (\text{all } k\neq i,j). \qquad (32)$$

Now if a function $f(x)$ is discontinuous at the point $x=a$, then[10]

$$\frac{\partial}{\partial x}f(x)\bigg|_{x=a}=\delta(x-a)\Delta_{xa}f(x), \qquad (33)$$

where, by definition,

$$\Delta_{xa}f(x)=f(a+0)-f(a-0). \qquad (34)$$

With the help of (33) and (34) one finds that

$$\left(\frac{\partial^2}{\partial r_i^2}+\frac{2}{r_i}\frac{\partial}{\partial r_i}+\frac{\partial^2}{\partial r_j^2}+\frac{2}{r_j}\frac{\partial}{\partial r_j}\right)\langle \mathbf{X}|\beta\rangle\bigg|_{r_i=r_j>r_k}$$
$$=\delta(r_i-r_j)\Delta_{r_ir_j}\left(\frac{\partial}{\partial r_i}-\frac{\partial}{\partial r_j}\right)\langle \mathbf{X}|\beta\rangle. \qquad (35)$$

Hence, by (32) and (35),

$$V_{kij}=-\frac{\hbar^2}{2m}\delta(r_i-r_j)\Delta_{r_ir_j}\left(\frac{\partial}{\partial r_i}-\frac{\partial}{\partial r_j}\right). \qquad (36)$$

[8] In the following the suffixes i and j are variable in the sense of footnote 6(b), and distinct.

[10] See reference 5, Sec. 15.

Finally, since the operators V_{ijk}, etc., defined analogously to V_{ij}, contribute nothing to the matrix element $\langle\beta^*|V|\beta\rangle$ they may be entirely neglected, and we may set

$$V=\sum_{q(\neq i)}\epsilon^2(1/r_{iq}-1/r_i)+V_{ij}$$
$$r_i\geqslant r_j\geqslant r_k \quad \text{(all } k=i,j\text{)}. \quad (37)$$

Thus, on the proposed approximation the scattering coefficients (21) are to be calculated with the help of Eqs. (27), (28), (36), and (37).

5. PURE EXCHANGE EFFECTS

The excitation by electron impact of intersystem transitions in normal-coupling atoms, which is the chief mechanism for the excitation of some of the strongest auroral and nebular spectral lines, is a pure exchange effect. The matrix element $\langle\beta^*(\alpha'\mathbf{k}')|V|\beta(\alpha^0\mathbf{k}^0)\rangle$ reduces in this case to $\langle\beta^*(\alpha'\mathbf{k}')|V_s|\beta(\alpha^0\mathbf{k}^0)\rangle$. A straightforward calculation, here omitted for the sake of brevity, shows that

(a) In general $\langle\beta^*(\alpha'\mathbf{k}')|V_s|\beta(\alpha^0\mathbf{k}^0)\rangle\neq 0$.

(b) An l-wave incident on a two-electron atom characterized by the quantum numbers l_a, l_b can excite an intersystem transition either to a state characterized by l, l_b, the scattered wave being an l_a-wave, or to a state characterized by l, l_a, the scattered wave being an l_b-wave.

(c) If the incident electron beam is unpolarized, each of the three transitions ${}^1L_L\rightarrow{}^3L'_{J'}$ $(J'=L', L'\pm 1)$ is equally probable.

Since every stationary state of a many-electron atom can be regarded as a superposition of states in which a given pair of electrons are in definite two-electron states characterized by the quantum numbers l_a, l_b, these results can immediately be extended to atoms with more than two electrons.

6. THE PRIOR-POST DISCREPANCY

It is apparent from (27) that the eigenrepresentatives $\langle\mathbf{X}|\beta(\alpha\mathbf{k})\rangle$ are not mutually orthogonal. It follows that E, and hence V, are not hermitian operators. Nevertheless

$$\langle\beta^*(\alpha'\mathbf{k}')|V|\beta(\alpha^0\mathbf{k}^0)\rangle=\langle\beta(\alpha^0\mathbf{k}^0)|V|\beta^*(\alpha'\mathbf{k}')\rangle^*. \quad (38)$$

For, since H is hermitian,

$$\langle\beta^*(\alpha'\mathbf{k}')|(H-E)|\beta(\alpha^0\mathbf{k}^0)\rangle=\langle\beta(\alpha^0\mathbf{k}^0)|H|\beta^*(\alpha'\mathbf{k}')\rangle^*$$
$$-E'\langle\beta(\alpha^0\mathbf{k}^0)|\beta^*(\alpha'\mathbf{k}')\rangle^*$$
$$=\langle\beta(\alpha^0\mathbf{k}^0)|(H-E)|\beta^*(\alpha'\mathbf{k}')\rangle^*.$$

Now in practice one must ordinarily use approximate atomic wave functions in the calculation of scattering coefficients. Suppose then that $\langle\mathbf{X}^i|\alpha^0\rangle$ and $\langle\alpha'|\mathbf{X}^i\rangle$ are eigenrepresentatives not of $H_s{}^i$ but of $H_s{}^i+h^i$, where h^i is a multiplicative hermitian operator (in the x-representation). Then

$$\langle\beta^*(\alpha'\mathbf{k}')|V|\beta(\alpha^0\mathbf{k}^0)\rangle$$
$$=\langle\beta^*(\alpha'\mathbf{k}')|\{H+h-(E+h)\}|\beta(\alpha^0\mathbf{k}^0)\rangle$$
$$=\langle\beta(\alpha^0\mathbf{k}^0)|(H+h)|\beta^*(\alpha'\mathbf{k}')\rangle^*$$
$$-E'\langle\beta(\alpha^0\mathbf{k}^0)|\beta^*(\alpha'\mathbf{k}')\rangle^*$$
$$=\langle\beta(\alpha^0\mathbf{k}^0)|(H-E)|\beta^*(\alpha'\mathbf{k}')\rangle^*,$$

where

$$h=h^i \quad r_i>r_j \quad \text{(all } j\neq i\text{)}.$$

Thus (38) continues to hold, and the approximation is unambiguous provided only that the approximate atomic wave functions are eigenfunctions of a single hermitian operator that differs from the exact Hamiltonian only by a term in the potential energy.

In contrast, Oppenheimer's approximation involves a "prior-post discrepancy" whenever approximate atomic wave functions are used, except under very special circumstances.[4] This discrepancy arises not from the non-orthogonality of the representatives (23) but from the circumstance that Oppenheimer's V is not defined in a self-consistent way.

7. CONCLUSION

The approximation here proposed provides an unambiguous method for calculating scattering cross sections inclusive of exchange effects, predicts nonvanishing cross sections for the excitation of intersystem transitions in normal-coupling atoms, and is intimately related to Born's approximation. A quantitative check on the approximation must, however, await the results of numerical calculations, some of which are being planned.

Wave Functions in Momentum Space*

E. E. SALPETER
Newman Laboratory of Nuclear Studies, Cornell University, Ithaca, New York
(Received August 24, 1951)

The integral equation, satisfied by the momentum-space wave function $\phi(p)$ for a nonrelativistic two-body problem with a phenomenological central interaction potential, is solved by means of an iteration method. A general prescription is given for finding suitable trial wave functions, which depend on some adjustable parameters. Reasonable values for these parameters are found by iteration of the wave function for particularly convenient values of the momentum. Successive iterations, giving better approximations $\phi_n(p)$ for $\phi(p)$, are carried out in a form suitable for numerical work. Besides $\phi_n(p)$, approximations are obtained for (a) the binding energy for certain bound states and (b) the phase shifts for scattering problems. For scattering at fairly low energies reasonable approximations are obtained with the same method both for weak and for fairly strong potentials.

Extensions of the method are discussed for (a) two-body problems including tensor forces, (b) simple three-body problems, and (c) a relativistic equation for the two-body problem.

I. INTRODUCTION

IN a number of current problems in nuclear physics the momentum distribution of nucleons in nuclei is of importance. For instance, the production cross sections of fast deuterons by the bombardment of nuclei by fast neutrons[1] depend critically on the momentum distribution of the protons in the nucleus. Similarly, the way in which the energy and momentum distribution of a π-meson and a nucleon produced by photon bombardment of hydrogen differs from that for bombardment of other nuclei again depends on the momentum distribution of the nucleons in such a nucleus. It therefore may be of some practical use to develop further the methods for finding wave functions in momentum space directly for a particle in a bound state in a fixed potential. For some problems involving the escape of slow nucleons from a nucleus it may also be of use to find the wave functions in momentum space for a particle of positive energy in the field of a fixed potential.

Approximation methods have been developed previously[2,3] for solving the wave equation in momentum space for a particle in a central potential. These methods are very powerful in cases where the necessary calculations can be carried out analytically, but are not very suitable in cases where numerical methods have to be used. The momentum-space wave function for a nonrelativistic particle in a fixed potential satisfies a well-known integral equation. It is the main aim of the present paper to show that a rapidly converging iteration method can also be found in many cases where the application of a variation method, like that used by Svartholm, is unsuitable. A general prescription for finding a reasonably good initial trial wave function for potentials with a finite range is given and the method is presented in a form suitable for numerical work.

* Work supported in part by the ONR.
[1] G. F. Chew and M. L. Goldberger, Phys. Rev. **77**, 470 (1950).
[2] N. Svartholm, thesis, Lund (1945).
[3] M. Levy, Proc. Roy. Soc. (London) **A204**, 145 (1950).

II. GROUND STATE IN A CENTRAL POTENTIAL

Consider a bound state of energy E for a nonrelativistic particle of mass M in a fixed potential $U(\mathbf{r})$. We put

$$\hbar=c=1; \quad \gamma^2=-2ME. \tag{1}$$

The Schrödinger equation in ordinary space,

$$[(-\nabla^2/2M)+U(\mathbf{r})]\psi(\mathbf{r})=E\psi(\mathbf{r}), \tag{2}$$

transforms into an integral equation in momentum space:

$$(p^2+\gamma^2)\phi(\mathbf{p})=-2M\int d^{(3)}p' V(\mathbf{p}-\mathbf{p}')\phi(\mathbf{p}'). \tag{3}$$

There $[(2\pi)^{\frac{1}{2}}V(\mathbf{p})]$ and $\phi(\mathbf{p})$ are the p-space potential and wave function respectively; i.e., they are the three-dimensional fourier transforms of $U(\mathbf{r})$ and $\psi(\mathbf{r})$, respectively.

We restrict ourselves in this section to the special case of a spherically symmetric potential of finite "range" μ^{-1}. The p-space potential is then some spherically symmetric function $V(p;\mu)$ which, in most cases of interest here, is some monotonically decreasing function of p, decreasing fairly slowly for $p\lesssim\mu$ and decreasing rapidly for $p\gg\mu$ (usually a simple function of $[p^2+\gamma^2]$). Instead of calculating E for a fixed potential strength, we assume the binding energy E to be known (which is the case for the deuteron) and that the potential is

$$V(p)=\lambda V_0(p;\mu), \tag{4}$$

where $V_0(p;\mu)$ is a given function. We then have to solve Eq. (3) for the eigenvalue λ and for $\phi(\mathbf{p})$. We restrict ourselves further to the spherically symmetrical ground state wave function $\phi(p)$, which corresponds to a configuration-space wave function $\psi(r)$ with no nodes.

We wish to solve Eq. (3) by an iteration method; i.e., we assume some initial spherically symmetrical trial wave function $\phi_0(p)$; substitute this on the right-hand side of Eq. (3) and thus obtain a better approximation to the wave function, $\phi_1(p)$. On substituting $\phi_1(p)$ on the right-hand side of Eq. (3), a better approxi-

TABLE I. Trial wave functions $\psi_0(r)$ and $\phi_0(p)$ for some potential shapes $U_0(r)$ and $V_0(p)$, in configuration and momentum space, respectively, for a ground state of energy $(-\gamma^2/2M)$.

Shape	$U_0(r)$	$V_0(p)$	$\psi_0(r)$	$\phi_0(p)$
Yukawa	$e^{-\mu r}/\mu r$	$[2\pi^{\frac{1}{2}}\mu(\mu^2+p^2)]^{-1}$	$r^{-1}[e^{-\gamma r}-e^{-\alpha\mu r}]$	$(2/\pi)^{\frac{1}{2}}(a^2\mu^2-\gamma^2)/(p^2+\gamma^2)(a^2\mu^2+p^2)$
Exponential	$e^{-\mu r}$	$\mu[\pi^2(\mu^2+p^2)^2]^{-1}$	$r^{-1}[e^{-\gamma r}-e^{-\alpha\mu r}]-(a^2\mu^2-\gamma^2)e^{-\alpha\mu r}/2a\mu$	$(2/\pi)^{\frac{1}{2}}(a^2\mu^2-\gamma^2)^2/(p^2+\gamma^2)(a^2\mu^2+p^2)^2$
Gaussian[a]	$e^{-\mu^2r^2}$	$[2\pi^{\frac{1}{2}}\mu]^{-3}e^{-p^2/4\mu^2}$	$f(r)r^{-1}[e^{-\gamma r}-\exp[-\mu^2r^2-(2\mu^2+\gamma^2)^{\frac{1}{2}}r]]$	$e^{-p^2/4a^2\mu^2}/(p^2+\gamma^2)$

[a] $f(r)$ is a slowly varying function of r. See reference 2. For large values of p the iterations for the Gaussian potential converge very slowly and the correct asymptotic behavior $\phi_0(p)$ is somewhat different from that of $\phi_0(p)$.

mation still, $\phi_2(p)$, is obtained, etc. It will be more convenient to use, instead of the $\phi_n(p)$ themselves,

$$\Phi_n(p)=\lambda^{-n}\phi(p),$$

which are then defined by the equation,

$$(p^2+\gamma^2)\Phi_{n+1}(\mathbf{p})=-2M\int d^{(3)}p' V_0(\mathbf{p}-\mathbf{p}';\mu)\Phi_n(\mathbf{p}'). \quad (5)$$

No general discussion of the convergence, and hence of the range of validity, of this iteration procedure will be given in this paper, but in each particular application the convergence can be investigated fairly easily.

The first step then is to find a general prescription for a good initial wave function $\phi_0(p)$. For the case of a monotonically decreasing potential $V_0(p,\mu)$ the correct wave function will be a monotonic function, decreasing with increasing values of (p/μ) more rapidly than $V_0(p;\mu)$. If we took as $\phi_0(p)$ a three-dimensional delta-function, we would obtain a $\Phi_1(p)$ which is proportional to $(p^2+\gamma^2)^{-1}V_0(p;\mu)$. Such arguments suggest that we try an initial wave function of similar form, but with an extra dimensionless parameter a which can be adjusted to make agreement even better. Our prescription for $\phi_0(p)$ is then

$$\phi_0(p)=(p^2+\gamma^2)^{-1}V_0(p/a;\mu). \quad (6)$$

In Table I we give the form of $\phi_0(p)$ for the special cases of a potential of Yukawa, exponential, and gaussian shape, respectively, as well as the form of the potential both in momentum space, $V_0(p)$, and in coordinate space, $U_0(r)$. The fourier transforms of $\phi_0(p)$ can be calculated in most of these cases and give a rough, but usually simple, approximation $\psi_0(r)$ to the wave function in coordinate space. For the Yukawa potential $\psi_0(r)$ has the form of the well known wave function for a Hulthén potential. For the exponential potential $\psi_0(r)$ is also a simple function and is given in Table I. For the gaussian potential $\psi_0(r)$ is a rather complicated function (see Svartholm),[2] but a simple function which approximates $\psi_0(r)$ is given in Table I.

In many cases it is impossible, or at least too tedious, to carry out the integral in Eq. (5), with n equal to zero, analytically for all values of p. In these cases the conventional variation method for finding the "best value" for the parameter a is not very suitable. Usually, however, the integral can be carried out much more easily (usually analytically and certainly numerically) for special values of p, like $p=0$, $p\ll\mu$, $p=a\mu$, $p\gg\mu$. A simple method for finding reasonable values for a is to find $\Phi_1(p)$ for some of these special values p_1, p_2, etc., and define a by means of the equation,

$$\Phi_1(p_1)/\Phi_1(p_2)=\phi_0(p_1)/\phi_0(p_2). \quad (7)$$

Since both ϕ_0 and Φ_1 are in general monotonically decreasing our criterion (7) means that we are using a value of a which makes the rapidity of the decrease of $\Phi_1(p)$ with p roughly the same as that of $\phi_0(p)$.

Having fixed the $\phi_0(p)$ to be used by means of Eqs. (6) and (7), we have to carry out the integrals (5) to obtain the successive approximations $\Phi_n(p)$. If no analytic formula can be found for $\Phi_n(p)$ for a particular value of n, it is most convenient to calculate $\Phi_n(p)$ numerically for a number of values of p between zero and infinity and from this to determine, for these values of p, a function $a_n(p)$ defined by the relation,

$$\phi_n(p)=(p^2+\gamma^2)^{-1}V_0[p/a_n(p);\mu]. \quad (8)$$

Whereas $\Phi_n(p)$ is a fairly rapidly varying function, tending towards zero for large p, $a_n(p)$ is a very slowly varying function and takes on finite values of equal orders of magnitude for both large and small values of p. This makes it possible to interpolate fairly accurately for $a_n(p)$ after it has been determined for only a few values of p. This interpolation furnishes a good approximation to $\Phi_n(p)$ to be substituted in Eq. (5), $\Phi_{n+1}(p)$ is then calculated for a few values of p, and so on.

As mentioned before, if $\Phi_n(p)$ is known, it is usually easier to calculate $\Phi_{n+1}(0)$ than Φ_{n+1} for other values of p. We therefore define an approximation to the eigenvalue λ of (3) by means of

$$\lambda_{n+1}=\Phi_n(0)/\Phi_{n+1}(0). \quad (9)$$

The approximations λ_n do not necessarily (unlike the approximations of Svartholm[2]) form a monotonically decreasing series, but they are much easier to calculate and approximate λ very closely for even quite low values of n.

As a very simple (and somewhat fortunate) example, consider the case of a Yukawa potential for which the binding energy of the ground state is known to be zero, $\gamma=0$. Equation (7) for p_1, p_2 equal to 0 and ∞, respectively, gives a as the solution of

$$a+1=a^2; \quad a\approx 1.62. \quad (10)$$

A similar calculation for $p_1=0$, $p_2\ll\mu$ gives a value for

a of 1.37. Taking a mean of these values, $a=1.50$, Eqs. (5) and (9) give then $\lambda_1 \approx 1.67$ after a very simple integration. In this case $\Phi_1(p)$ can be calculated analytically, and $a_1(p)$ varies from $a_1(0)=1.39$ to $a_1(\infty)=1.58$. Then λ_2 can be calculated, its value being 1.6823. The values of $a_1(p)$ are then accurate to within about 1 percent and λ_2 to within 1 in 10,000.

Approximations to $\phi(p)$ for the case of a Yukawa, exponential, and gaussian potential are being calculated by Mr. J. Goldstein for values of γ/μ corresponding to the experimental values for the triplet effective range for the n-p system and for the binding energy of the deuteron. These calculations are carried as far as $\Phi_2(p)$ and λ_3 and will be reported on in a later paper.

The integral equation (3) holds also for the states of higher angular momentum. For a central potential $V(p)$ the wave function $\phi(\mathbf{p})$ takes the general form,

$$\phi_{l,m}(\mathbf{p})=\phi_l(p)Y_{l,m}(\theta,\phi), \tag{11}$$

where $Y_{l,m}(\theta,\phi)$ is a spherical surface harmonic in p-space. Using the spherical harmonics addition theorem one can derive from Eq. (3) the equation,[4]

$$(p^2+\gamma^2)\phi_l(p)=-4\pi M\int_0^\infty dp'p'^2V_l(p;p')\phi_l(p'),$$
$$V_l(p;p')\equiv\int_{-1}^{1}dxV[(p^2+p'^2-2pp'x)^{\frac{1}{2}}]P_l(x). \tag{12}$$

For l bigger than zero $V_l(p;p')$ is no longer a monotonically decreasing function of p, $V_l(0;p')$ being zero, but will usually not change sign. For the lowest energy state, for a given value of l, $\phi_l(p)$ will have no nodes and an iteration method could be used to solve (12). A reasonable initial wave function $\phi_{l,0}(p)$ could be used of the form,

$$\phi_{l,0}(p)=(p^2+\gamma^2)^{-1}V_l(p/a;\mu). \tag{13}$$

Such an iteration method will probably still converge fairly rapidly even for moderately large values of l, but probably not as rapidly as for $l=0$. The method described in this section is not suitable without modification for the higher states for which the wave function has nodes

III. SCATTERING IN A CENTRAL POTENTIAL

Consider the problem of the scattering of a nonrelativistic particle of definite energy E by a fixed central potential. If the wavelength of the particle is not too small compared with the range μ^{-1} of the potential, a partial wave analysis is a convenient method for solving the problem. Usually one attempts to solve the Schrödinger differential equation for $\psi_l(r)$, the radial wave function in configuration space for each particular angular momentum l, and the asymptotic phases η_l then determine the scattering cross section completely.

[4] Equation (12) is derived in Appendix 1.

A method of partial waves can also be applied in momentum space. The wave function $\phi_l(\mathbf{p})$ in momentum space for a particular value of l is of the form (11) with m equal to zero. For a scattering problem $\phi_l(p)$ satisfies an equation which is similar to Eq. (12); except that (a) γ^2 is replaced by $(-k^2)$, where

$$k=(2ME)^{\frac{1}{2}}$$

and (b) that the left-hand side contains an additional term proportional to $\delta(p-k)$ whose coefficient determines the phase η_l. For a monotonically decreasing potential $V(p)$ of sufficiently low strength, so that at most one bound state for a particular value of l is possible, and for sufficiently small energy ($k \lesssim \mu$), it seems likely that the methods described in the last section can be applied to obtain successive approximations to $\phi_l(p)$ and η_l, which converge fairly rapidly. This method might be particularly useful for some scattering problems for very low energy where S-scattering is predominant and where the momentum distribution for a fixed wave-number k (obtained automatically with this method) is of interest. We shall restrict ourselves in this section to the case of l equal to zero and shall omit the subscript l.

The asymptotic expression for the wave function in configuration space for $l=0$, $\psi(r)$, is then proportional to

$$\psi^{as}(r)=\sin(kr+\eta)/r\sin\eta, \tag{14}$$

where η is the S-phase which determines the S-wave scattering cross section. If $\psi(r)$ is normalized so that Eq. (14) is its asymptotic expression, then

$$\rho(E,E)=2\int_0^\infty dr r^2\{|\psi^{as}(r)|^2-|\psi(r)|^2\} \tag{15}$$

is finite and is equal to the effective range as defined by Blatt and Jackson[5] and by Bethe.[6] The fourier transform of $\psi^{as}(r)$ is

$$\phi^{as}(p)=(2/\pi)^{\frac{1}{2}}\beta^{-1}\{\delta(p-k)+\beta/(p^2-k^2)\},$$
$$\beta\equiv(2/\pi)k\tan\eta, \tag{16}$$

where $\delta(p-k)$ is a Dirac delta-function.[7] Since $\rho(E,E)$ is merely a multiple of the difference of the normalization integrals of the two configuration space wave functions, it can also be written as

$$\rho(E,E)=2\int_0^\infty dp p^2\{|\phi^{as}(p)|^2-|\phi(p)|^2\} \tag{17}$$

if $\phi(p)$ is normalized to be the fourier transform of $\psi(r)$. For the integral (17) to be finite, $\phi(p)$ and $\phi^{as}(p)$ must be identically equal for $p\to k$.

The wave function $\phi(p)$ satisfies an integral equation,

[5] J. M. Blatt and J. D. Jackson, Phys. Rev. **76**, 18 (1949).
[6] H. A. Bethe, Phys. Rev. **76**, 38 (1949).
[7] A derivation of Eq. (16) and some discussion is given in Appendix 2.

equivalent to Eq. (3),

$$(p^2-k^2)\{\phi(\mathbf{p})+c\delta(p-k)\}$$
$$=-2M\int d^{(3)}p'V(\mathbf{p}-\mathbf{p}')\phi(\mathbf{p}'), \quad (18)$$

where the constant c is as yet undetermined. We are interested only in the case $k\lesssim\mu$, for which the integral occurring on the right-hand side of Eq. (18) will be of fairly similar form to that occurring in Eq. (3), and an initial trial wave function analogous to Eq. (6) for $p\neq k$ should again be a good starting point. In the present case, however, we must choose $\phi(p)$ so that it is proportional to Eq. (16) for $p\to k$. We therefore take an initial wave function proportional to

$$\phi_0(p)=\{(p^2-k^2)^{-1}+\delta(p-k)/\beta_1\}V_0(p/a;\mu) \quad (19)$$

with β_1 left unspecified.

In the present problem both the total energy E and the strength of the potential are given. The unknown parameter to be determined by the iteration method is the constant β, of the same dimensions as the wave number k, which determines η and hence the S-wave scattering cross section. We define successive approximations to $\phi(p)$ by means of

$$\phi_n(\mathbf{p})=-\{(p^2-k^2)^{-1}+\delta(p-k)/\beta_{n+1}\}$$
$$\times\int d^{(3)}p'V(\mathbf{p}-\mathbf{p}')\phi_{n-1}(\mathbf{p}'), \quad (20)$$

starting with $n=1$. The integral in Eq. (20) is first evaluated with β_n in the expression for $\phi_{n-1}(p')$ left unspecified. Then β_n is determined by requiring that

$$\phi_n(p_0)=\phi_{n-1}(p_0) \quad (21)$$

for some suitably chosen fixed value, p_0, of $p\neq k$ (e.g., zero or a value differing from k by an infinitesimally small amount). The values β_n are then successive approximations to the parameter β which determines the phase shift. Before this iteration process can be carried out, a reasonable value for the parameter a must be found. This is again done by using Eq. (7). Equation (21) with $n=0$ and Eq. (7) both contain a and β_1 as unknowns, and these two equations have to be solved simultaneously. Since the exact choice of a is not very important, an approximate solution of these two simultaneous equations is sufficient.

One nice feature of this method is that it converges fairly rapidly both for a very weak potential and for one strong enough to allow one (but no more) bound state. For a potential, for instance, strong enough to introduce a phase-shift near $\pi/2$ (resonance) the values obtained for β_n will be very large compared with k; the term involving the delta-function in the integrand of Eq. (20) will be unimportant, and the iteration will proceed in close analogy to that for bound states.

For a very weak potential, on the other hand, Eqs. (20) and (21) with $n=1$ will yield a value of β_1 much smaller than k and the term involving the delta-function in the integrand of Eq. (21) will be much more important than the term involving $(p^2-k^2)^{-1}$. Complete omission of this term involving $(p^2-k^2)^{-1}$ in the expression for $\phi_0(p')$ in Eq. (21) would be equivalent to first-order Born approximation. With p_0 differing from k by an infinitesimally small amount, and making this omission, Eqs. (20) and (21) yield an approximation to β_1 which is quite independent of the value used for a:

$$\beta_1^{(B)}=-16\pi Mk^2\int_0^1 dyyV(2ky). \quad (22)$$

Since $\beta_1\ll k$, Eq. (16) gives

$$\eta^{(B)}\approx\tan\eta^{(B)}=-8\pi^2Mk\int_0^1 dyyV(2ky). \quad (23)$$

A simple calculation shows that this expression is identical with the usual first-order Born approximation to η:

$$\eta^{(B)}=-2Mk^{-1}\int_0^\infty dr\sin^2(kr)U(r). \quad (24)$$

More generally, an expression independent of the choice of a and equivalent to the nth Born approximation could be derived from the nth iteration of the present method by the omission of certain terms. If, however, the iterations are carried out as described above without any omissions, then even β_1, obtained after one single iteration, contains (at least approximately) corrections proportional to higher powers of the potential, in addition to the linear term $\beta_1^{(B)}$. In fact, as discussed in the last paragraph, β_1 remains a fairly good approximation even for a fairly strong potential for which the Born approximation breaks down completely.

IV. OTHER APPLICATIONS

(A) Tensor Forces

The method discussed in the preceding two sections for the evaluation of momentum-space wave functions for a two-particle system can be extended to the case of an interaction potential which contains a tensor-force term in addition to the spherically symmetrical central-potential term. A potential in configuration-space of the form,

$$U_c(r)+gU_T(r)S_{12}(\theta_r) \quad (25)$$

corresponds to a momentum-space potential of form,

$$V_c(p)+gV_T(p)S_{12}(\theta_p), \quad (26)$$

where

$$S_{12}(\theta_r)=3[(\boldsymbol{\sigma}_1\cdot\mathbf{r})(\boldsymbol{\sigma}_2\cdot\mathbf{r})/r^2]-(\boldsymbol{\sigma}_1\cdot\boldsymbol{\sigma}_2) \quad (27)$$

and $V_T(p)$ is proportional to

$$\int d^{(3)}rU_T(r)e^{i\mathbf{p}\cdot\mathbf{r}}P_2(\cos\theta_r). \quad (28)$$

For most of the commonly used simple forms of $U_T(r)$ the function $V_T(p)$ is usually fairly complicated. There are, however, a few types of tensor-potentials for which both $U_T(r)$ and $V_T(p)$ are fairly simple functions. For problems where calculations have to be carried out both in configuration and in momentum space it might be useful to employ such potentials. For instance,

$$V_T(p)=p^2/(p^2+\mu^2)^2 \tag{29}$$

corresponds to a $U_T(r)$ proportional to

$$(r^{-1}+\mu)e^{-\mu r}. \tag{30}$$

A consideration of momentum-space potentials leads to a more direct understanding of the well-known fact that, for very low energies, a tensor potential of form $U_T(r)$ is much less important than a central potential of the same form, $U_c(r)=U_T(r)$. Note, for instance, that $V_T(p)$ of the form (29) is proportional to p^2 for small momenta p, whereas the momentum-space potential $V_c(p)$ corresponding to a central potential $U_c(r)$ of form (30) is not.

The momentum-space wave function for the neutron-proton triplet system, for instance, with an interaction potential given by Eq. (26) is of the form,

$$\phi_c(p)\chi_m{}^3+\phi_T(p)\sum_{m'=-1}^{1}a_{m,m'}Y_{2,m'}(\theta,\phi)\chi_{-m'}{}^3 \tag{31}$$

where $\chi_m{}^3$ denotes one of the triplet spin-wave functions. The Schrödinger equation in momentum space can then be reduced to two coupled integral equations involving the two functions $\phi_c(p)$ and $\phi_T(p)$. For the case of the ground state of the deuteron, where the percentage of D-state is known to be small, an iteration method analogous to that described in Sec. II should be applicable. As initial trial wave functions one might take, in this case,

$$\begin{aligned}\phi_c(p)&=(p^2+\gamma^2)^{-1}V_c(p/a);\\ \phi_T(p)&=(p^2+\gamma^2)^{-1}GV_T(p/b),\end{aligned} \tag{32}$$

where there are now three parameters, a, b, and G, to be determined (instead of one, a, as in Sec. I).

(B) Three-Body Problem

The problem of the ground states of H^3 and He^3, using only central potentials, has already been treated by Svartholm[2] using a variation-iteration procedure in momentum-space. The momentum space wave function is here a function of two momentum variables $\mathbf{p}_1$ and $\mathbf{p}_2$. As Svartholm[2] has already pointed out it is convenient to employ as an initial wave function $\phi_0(\mathbf{p}_1,\mathbf{p}_2)$ a function of $(p_1{}^2+p_2{}^2+\mathbf{p}_1\cdot\mathbf{p}_2)$ only. As a starting point, either for a variation-iteration method as used by Svartholm or for an iteration method as described in this paper, more rapid convergence is obtained when an initial function of form,

$$\phi_0(\mathbf{p}_1,\mathbf{p}_2)=(p_1{}^2+p_2{}^2+\mathbf{p}_1\cdot\mathbf{p}_2+\gamma^2)^{-1}\times V_0[(p_1{}^2+p_2{}^2+\mathbf{p}_1\cdot\mathbf{p}_2)/a;\mu] \tag{33}$$

is used than with the functions previously used by Svartholm.[2]

(C) Relativistic Two-Body Equation

In the following paper[8] an integral equation is derived, from a relativistic treatment of the two-body problem, for a wave function $\psi(\mathbf{p},\epsilon)$, which is a function of a momentum variable p and an energy variable ϵ. This integral equation is of the form,

$$F(p,\epsilon)\psi(\mathbf{p},\epsilon)=-\lambda\int\int d^{(3)}p'd\epsilon V_0(\mathbf{p}-\mathbf{p}',\epsilon-\epsilon';\mu)\psi(p',\epsilon'). \tag{34}$$

By analogy with Eqs. (3) and (6) an initial trial wave function of the form,

$$\psi_0(p,\epsilon)=F^{-1}(p,\epsilon)V_0(p/a,\epsilon/b;\mu) \tag{35}$$

can be used. Reasonable values for the two parameters a and b can then be found by means of the equation (analogous to Eq. (7)),

$$\psi_1(p_1,\epsilon_1)/\psi_1(p_2,\epsilon_2)=\psi_0(p_1,\epsilon_1)/\psi_0(p_2,\epsilon_2) \tag{36}$$

for suitably chosen combinations of the values p_1, ϵ_1 and p_2, ϵ_2.

The author wishes to thank Mr. J. S. Goldstein for some assistance with this work and the ONR for support of part of the work.

APPENDIX I. DERIVATION OF EQ. (12)

We shall first derive a general property of spherical harmonics, Eq. (A4). Let

$$Y_{l,m}(\boldsymbol{\Theta})=P_l{}^{|m|}(x)e^{im\phi},$$

where $\boldsymbol{\Theta}$ denotes the unit vector (θ,ϕ) and $x=\cos\theta$. From the spherical harmonics addition theorem for $P_l(\cos|\boldsymbol{\Theta}-\boldsymbol{\Theta}_0|)$ and from the normalization integrals for the associated Legendre polynomials[9] it follows that

$$\int_{-1}^{1}dx'\int_0^{2\pi}d\phi' Y_{l,m}(\boldsymbol{\Theta}')P_l(\cos|\boldsymbol{\Theta}'-\boldsymbol{\Theta}|)=(4\pi/2l+1)Y_{l,m}(\boldsymbol{\Theta}). \tag{A1}$$

We can expand $Y_{l,m}(\boldsymbol{\Theta}+\boldsymbol{\Theta}_0)$ in terms of $Y_{l,m'}(\boldsymbol{\Theta})$,

$$Y_{l,m}(\boldsymbol{\Theta}+\boldsymbol{\Theta}_0)=\sum_{m'=-l}^{l}a_{m'}(\boldsymbol{\Theta}_0)Y_{l,m'}(\boldsymbol{\Theta}). \tag{A2}$$

[8] E. E. Salpeter and H. A. Bethe, Phys. Rev. 84, 1232 (1951).
[9] E. Jahnke and F. Emde, *Tables of Functions* (Dover Publications, New York, 1945), pp. 115 and 116.

Multiplying Eq. (A2) by $P_l(x)$ and integrating over x and ϕ, we obtain, after changing the variable of integration from Θ to $\Theta'\equiv(\Theta+\Theta_0)$ and using Eq. (A1),

$$a_0(\Theta_0)=Y_{l,m}(\Theta_0). \tag{A3}$$

If $f(\theta)$ is an arbitrary function of θ, not depending on ϕ, it follows from the above equations and from the orthogonality property of the spherical harmonics that

$$\int_{-1}^{1}dx\int_0^{2\pi}d\phi Y_{l,m}(\Theta+\Theta_0)f(\theta) =2\pi Y_{l,m}(\Theta_0)\int_{-1}^{1}dxP_l(x)f(\theta). \tag{A4}$$

Consider Eq. (3) for $\phi_{l,m}(\mathbf{p})$ of the form (11) with $\mathbf{p}$ parallel to the unit vector Θ_0. Let Θ now denote spherical polar coordinates with the vector Θ_0 taken as axis. Equation (3) then becomes

$$\begin{aligned}(p^2+\gamma^2)\phi_l(p)Y_{l,m}(\Theta_0)&\\ =-2M\int_0^\infty dp'p'^2\phi_l(p')\int_{-1}^{1}dx\int_0^{2\pi}d\phi&\\ \times V[(p^2+p'^2-2pp'x)^{\frac{1}{2}}]Y_{l,m}(\Theta+\Theta_0).&\end{aligned} \tag{A5}$$

Using Eq. (A4), we may reduce Eq. (A5) (after dropping the suffix zero) to Eq. (12) of the text.

APPENDIX II. DERIVATION OF EQ. (16)

We first note that, for an arbitrary analytic function $f(y)$,

$$\begin{aligned}&\operatorname*{Lim}_{\epsilon\to0}\int_{-\infty}^{\infty}dyf(y)\int_0^\infty dxe^{-\epsilon x}\cos(yx)=\pi f(0),\\ &\operatorname*{Lim}_{\epsilon\to0}\int_{-\infty}^{\infty}dyf(y)\int_0^\infty dxe^{-\epsilon x}\sin(yx)\\ &\qquad=\mathcal{P}\left\{\int_0^\infty dyf(y)/y\right\},\end{aligned} \tag{A6}$$

where $\mathcal{P}$ denotes the principal part. The Dirac delta-function $\delta(y)$ can be defined by means of its property

$$\int_{-\infty}^{\infty}dyf(y)\delta(y-a)=f(a). \tag{A7}$$

We therefore have the relations,

$$\begin{aligned}&\operatorname*{Lim}_{\epsilon\to0}\int_0^\infty dxe^{-\epsilon x}\cos(yx)=\pi\delta(y),\\ &\operatorname*{Lim}_{\epsilon\to0}\int_0^\infty dxe^{-\epsilon x}\sin(yx)=(1/y),\end{aligned} \tag{A8}$$

where it is to be understood that the principal part has to be taken of any integral in which this term $(1/y)$ occurs.

To obtain the fourier transform $\phi^{as}(\mathbf{p})$ of the wave function $\psi^{as}(\mathbf{r})$, Eq. (14), we first make the fourier integral definite by adding a convergence factor $e^{-\epsilon r}$ and then proceed to the limit of ϵ tending to zero.

$$\begin{aligned}\phi^{as}(p)&=(2\pi)^{-\frac{1}{2}}\operatorname*{Lim}_{\epsilon\to0}\int_0^\infty drr^2e^{-\epsilon r}\int_{-1}^{1}dx\\ &\quad\times\int_0^{2\pi}d\phi e^{ipr\alpha}\sin(kr+\eta)/r\sin\eta\\ &=(2\pi)^{-\frac{1}{2}}(p\sin\eta)^{-1}\operatorname*{Lim}_{\epsilon\to0}\int_0^\infty dre^{-\epsilon r}\\ &\quad\times\{\sin\eta[\sin(pr+kr)+\sin(pr-kr)]\\ &\quad+\cos\eta[\cos(pr-kr)-\cos(pr+kr)]\}.\end{aligned} \tag{A9}$$

Remembering that both p and k are positive, so that $\delta(p+k)$ can be replaced by zero, and using Eqs. (A8), we then have

$$\begin{aligned}\phi^{as}(\mathbf{p})=(\pi/2)^{\frac{1}{2}}\cot\eta\{&p^{-1}\delta(p-k)\\ &+(2/\pi)\tan\eta/(p^2-k^2)\}.\end{aligned} \tag{A10}$$

Since, from Eq. (A7), we have

$$(p-k)\delta(p-k)=0, \tag{A11}$$

the factor p^{-1} in Eq. (A10) can be replaced by k^{-1}, and Eq. (A10) then reduces to Eq. (16) of the text.

It also follows from Eq. (A11) that the coefficient c of the delta-function in the integral equation (18) is completely arbitrary. Hence, $\phi(k)$ cannot be determined from Eq. (18) alone, but is determined from the condition $\phi(k)=\phi^{as}(k)$. It should be noted that, throughout Sec. III of this paper, the principal part has to be taken of any integral over p in which the term $(p^2-k^2)^{-1}$ occurs.

A Relativistic Equation for Bound-State Problems

E. E. SALPETER AND H. A. BETHE
Newman Laboratory of Nuclear Studies, Cornell University, Ithaca, New York
(Received August 24, 1951)

The relativistic S-matrix formalism of Feynman is applied to the bound-state problem for two interacting Fermi-Dirac particles. The bound state is described by a wave function depending on separate times for each of the two particles. Two alternative integral equations for this wave function are derived with kernels in the form of an expansion in powers of g^2, the dimensionless coupling constant for the interaction. Each term in these expansions gives Lorentz-invariant equations. The validity and physical significance of these equations is discussed. In extreme nonrelativistic approximation and to lowest order in g^2 they reduce to the appropriate Schrödinger equation.

One of these integral equations is applied to the deuteron ground state using scalar mesons of mass μ with scalar coupling. For neutral mesons the Lorentz-invariant interaction is transformed into the sum of the instantaneous Yukawa interaction and a retarded correction term. The value obtained for g^2 differs only by a fraction proportional to $(\mu/M)^2$ from that obtained by using a phenomenological Yukawa potential. For a purely charged meson theory a correction term is obtained by a direct solution of the relativistic integral equation using only the first term in the expansion of the kernel. This correction is due to the fact that a nucleon can emit, or absorb, positive and negative mesons only alternately. The constant g^2 is increased by a fraction of $1.1(\mu/M)$ or 15 percent.

I. INTRODUCTION

VARIOUS mathematical formalisms, all equivalent physically, for a relativistic treatment of scattering problems for two or more particles have been developed in the last few years by Dyson, Feynman, Schwinger, and Tomonaga. It is the aim of this paper to present an extension of the Feynman formalism[1] to bound-state problems involving several particles. Throughout this paper we shall deal only with two Fermi-Dirac particles interacting with each other by means of an arbitrary (electrodynamic or mesonic) interaction in the absence of any external forces, particles, or quanta. The extension of the method to more complex bound states should, in principle, be straightforward, although the computational work might well become prohibitive.

For a scattering problem involving two such particles, the Feynman formalism consists essentially of giving a prescription for the amplitude function (or kernel) $K(3,4;1,2)$, representing the probability amplitude for the one particle to proceed from time and place $x_{\mu 1}$ to $x_{\mu 3}$, while the other particle proceeds from time and place $x_{\mu 2}$ to $x_{\mu 4}$. This meaning of the amplitude function suggests that we should describe a state of the system by a wave function $\psi(x_{\mu 1}, x_{\mu 2})$ with 16 spinor components, depending on a separate time for each of the particles as well as on the spatial coordinates of the two particles. Such an approach bears some similarity to the many-times formalism of Dirac, Fock, and Podolski[2] and of Bloch.[3] In a purely formal way $\psi(3,4)$ can be calculated, by the help of $K(3,4;1,2)$ and prescriptions given in FI and II, if $\psi(1,2)$ is known. $K(3,4;1,2)$ is defined in terms of a doubly infinite series, but a relatively simple integral equation can be derived for it. From this an integral equation can be derived for $\psi(3,4)$ with an inhomogeneous term depending on $\psi(1,2)$. $K(3,4;1,2)$ also obeys a differential-integral equation from which a homogeneous differential-integral equation can be derived for $\psi(3,4)$ which does not contain any boundary conditions for t_1 and t_2 explicitly.

These equations are derived in Sec. II and their validity discussed in Sec. III. These equations are applied to the deuteron ground state using a scalar meson theory with scalar interaction in Secs. IV and V.

II. DERIVATION OF THE EQUATIONS

Throughout this paper we shall use, wherever possible, the notation of FI and FII and shall put $\hbar=c=1$. We first give a formal derivation of two equations for the wave function $\psi(1,2)$ and the amplitude function $K(3,4;1,2)$ based on the expression given in FII for $K(3,4;1,2)$ and postpone a discussion of the validity of these equations till the following section.

Consider two Fermi-Dirac particles of masses m_a and m_b, respectively (electrons or nucleons), capable of interacting with each other through "the virtual emission and absorption of quanta" (photons or mesons). Let $G(1,2)$ be the interaction function corresponding to a simple exchange of one quantum written in its lorentz invariant form (proportional to a dimensionless coupling constant g^2). For the case of electrodynamics we have

$$G(1,2)=e^2\gamma_\mu{}^a\gamma_\mu{}^b\delta_+(s_{12}{}^2). \tag{1}$$

For scalar mesons with scalar coupling $G(1,2)$ is the relativistic generalization of the Yukawa potential, etc. (for further details see Sec. 10 of FII). We now define reducible and irreducible graphs in a manner similar to that used by Dyson;[4] i.e., we call a graph reducible if it can be split into two simpler graphs by drawing a line which cuts no quantum lines at all and each of the two particle lines only once. The remaining irreducible graphs can be ordered according to the power of the

[1] R. P. Feynman, Phys. Rev. **76**, 749 (1949), hereafter referred to as FI, and R. P. Feynman, Phys. Rev. **76**, 769 (1949), hereafter referred to as FII.
[2] Dirac, Fock, and Podolski, Physik. Z. d. Sowjetunion **2**, 468 (1932).
[3] F. Bloch, Physik. Z. d. Sowjetunion **5**, 301 (1934).
[4] F. J. Dyson, Phys. Rev. **75**, 486 and 1736 (1949).

coupling constant g^2 occurring in the expression we ascribe to the graph, this power being half the number of particle vertices in the graph. For the first power of g^2 we have only one graph, labeled 1 in Fig. 1, to which corresponds the expression $G(1,2)$. We define two more quantities G' and $G^{(1)}$

$$G(1,2)=\Gamma_{a\tau}\Gamma_{b\tau}G'(1,2),$$
$$G^{(1)}(1,2;3,4)=G(1,2)\delta^{(4)}(1,3)\delta^{(4)}(2,4), \quad (2)$$

where $\delta^{(4)}(1,3)$ is the four-dimensional delta-function

$$\prod_{\mu=1}^{4}\delta(x_{\mu 1}-x_{\mu 3})$$

and Γ_a, a "vertex part," is an operator made up of Dirac matrices operating on particle a only, while Γ_b operates only on particle b. The index τ represents summation over different operator components (4 for electrodynamics; 1, 4 or 16 for simple meson theories, etc.); $G'(1,2)$, the "quantum propagator," is a function of $(x_{\mu 1}-x_{\mu 3})$ not containing any Dirac operators. To the other irreducible graphs we ascribe mathematical expressions $G^{(n)}(1,2;3,4)$. The expressions corresponding to the three graphs $2A$, $2B$, and $2C$, shown in Fig. 1, are

$$G^{(2A)}(1,2;3,4)=-i\Gamma_{a\sigma}\Gamma_{b\tau}K_{+a}(3,1)K_{+b}(4,2)\times\Gamma_{a\tau}\Gamma_{b\sigma}G'(1,4)G'(2,3), \quad (3a)$$

$$G^{(2B)}(1,2;3,4)=-i\int d\tau_5\delta^{(4)}(2,4)\times\Gamma_{a\sigma}K_{+a}(3,5)\Gamma_{a\tau}K_{+a}(5,1)\times\Gamma_{a\sigma}\Gamma_{b\tau}G'(1,3)G'(2,5), \quad (3b)$$

$$G^{(2C)}(1,2;3,4)=-i\int d\tau_5\delta^{(4)}(2,4)\times\Gamma_{a\sigma}K_{+a}(3,5)\Gamma_{a\sigma}K_{+a}(5,1)\times\Gamma_{a\tau}\Gamma_{b\tau}G'(3,5)G'(1,2), \quad (3c)$$

where $K_{+a}(1,3)$ is the amplitude function for the propagation of particle a as a free particle. The expressions corresponding to graphs $2C$ and $2D$, self-energy and mass-renormalization terms respectively, must be taken together with that for $2B$. As an example of more complicated graphs we choose $3A$:

$$G^{(3A)}(1,2;3,4)=-\int\int d\tau_5 d\tau_6\Gamma_{a\sigma}K_{+a}(3,5)\times\Gamma_{a\tau}K_{+a}(5,1)\Gamma_{a\rho}\Gamma_{b\rho}K_{+b}(4,6)\times\Gamma_{b\sigma}K_{+b}(6,2)\Gamma_{b\tau}G'(3,6)\times G'(5,2)G'(1,4). \quad (4)$$

The prescription for the general term $G^{(n)}(1,2;3,4)$ should be obvious from these few examples. It should be noted that, no matter how complicated the diagram (n), $G^{(n)}$ depends explicitly only on the four variables $x_{\mu 1}$, $x_{\mu 2}$, $x_{\mu 3}$, $x_{\mu 4}$.

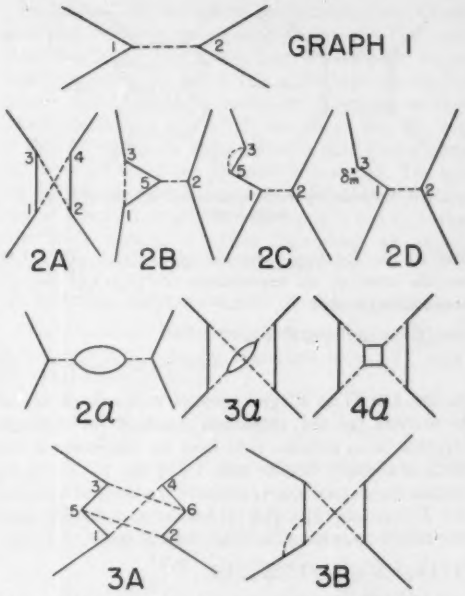

FIG. 1. Irreducible graphs of various orders. Solid lines denote Fermi-Dirac particles, broken lines denote quanta.

The expression given in FII for the amplitude function $K(3,4;1,2)$ consists of a doubly infinite sum of terms, one corresponding to each of the possible reducible or irreducible graphs, plus the term $K_{+a}(3,1)K_{+b}(4,2)$ corresponding to the propagation of both particles without the exchange of any quanta. For an irreducible graph (n) we have a term

$$K^{(n)}(3,4;1,2)=-i\int\int\int\int d\tau_5 d\tau_6 d\tau_7 d\tau_8\times K_{+a}(3,5)K_{+b}(4,6)G^{(n)}(5,6;7,8)\times K_{+a}(7,1)K_{+b}(8,2). \quad (5)$$

For a reducible graph which can be split up into two irreducible graphs, (n) and (m), respectively, we have a term

$$K^{(n,m)}(3,4;1,2)=-i\int\int\int\int d\tau_5 d\tau_6 d\tau_7 d\tau_8\times K_{+a}(3,5)K_{+b}(4,6)G^{(n)}(5,6;7,8)\times K^{(m)}(7,8;1,2). \quad (6)$$

For a graph reducible into 3 irreducible graphs we have

$$K^{(n,m,k)}(3,4;1,2)=-i\int\int\int\int d\tau_5 d\tau_6 d\tau_7 d\tau_8\times K_{+a}(3,5)K_{+b}(4,6)G^{(n)}(5,6;7,8)\times K^{(m,k)}(7,8;1,2), \quad (7)$$

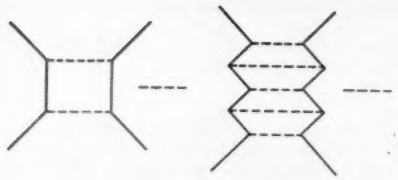

FIG. 2. Reducible graphs whose effect is included in the single term $G^{(1)}$.

and so on, for any reducible graph. Let $\bar{G}(1,2;3,4)$ be the sum of all expressions $G^{(n)}(1,2;3,4)$ for all *irreducible* graphs:

$$\bar{G}=\{G^{(1)}+G^{(2A)}+G^{(2B)}+G^{(2C)}+G^{(2D)}+G^{(2\alpha)}+G^{(3A)}+\cdots\}. \quad (8)$$

In Sec. 3 of FI an integral equation with a simple kernel is derived for the amplitude function for a single electron in an external field from an expression in the form of a singly infinite sum. Using Eq. (5) to (8) we obtain, by an analogous argument, an integral equation for $K(3,4;1,2)$ from the expression as a double sum, the kernel containing the singly infinite sum $\bar{G}(1,2;3,4)$:

$$K(3,4;1,2)-K_{+a}(3,1)K_{+b}(4,2)=i\int\int\int\int d\tau_5 d\tau_6 d\tau_7 d\tau_8 K_{+a}(3,5)K_{+b}(4,6)\times\bar{G}(5,6;7,8)K(7,8;1,2). \quad (9)$$

The expression (8) for $\bar{G}(1,2;3,4)$ consists of an expansion in powers of the coupling constant. Each term in this expansion can, in principle, be calculated, but no closed expression for $\bar{G}(1,2;3,4)$ has as yet been found; and hence the method described in this paper is not immediately applicable to bound-state problems for which the coupling constant is large. For problems for which the coupling constant is reasonably small, there is, however, considerable simplification to be gained from a treatment involving the function $\bar{G}$ over a method involving summation over all reducible graphs. If, for instance, in Eq. (9) $\bar{G}$ is replaced by merely the first term in its expansion $G^{(1)}$, this is equivalent to an inclusion of an infinite number of reducible "ladder-type" graphs, examples of which are given in Fig. 2, in addition to the irreducible graph 1 in the double-sum expression for $K(3,4;1,2)$. This means that some graphs of higher power in g^2 are included automatically in such an approximation, while others are not. The value of this for the case of small g^2 can perhaps be made plausible by means of the following physical arguments. In a bound state the particles interact with each other for an infinite (or at least very long) time. If g^2 is very small, the probability for "finding one virtual quantum in the field" is small and the probability for "finding two virtual quanta simultaneously" is much smaller still. Although the probability for the exchange of a quantum during a small time interval is fairly small, during the infinite time of existence of the bound state an indefinite number of quanta may be exchanged *successively*. It is just such processes that the ladder-type graphs deal with. On the other hand, all graphs omitted in such an approximate treatment, except for self energy and mass renormalization graphs, involve "crossed quantum lines" (for example, graph $2A$ or $3A$) or Lamb-shift-type terms (for example, $2B$). Such graphs refer to processes in which two or more quanta are "in the field simultaneously," which are indeed unimportant if the coupling constant is small. If $\bar{G}$ is thus replaced by $G^{(1)}$ in Eq. (9), this integral equation reduces, with the help of Eq. (2), to a simpler equation involving $G(1,2)$.

If one wants to include the higher terms in the expansion of $\bar{G}$, further simplification can be obtained by modifying the $\Gamma_{a\tau}$, G', etc., along lines outlined by Dyson.[4] Thus, by modifying G', graph 2α (vacuum polarization term) could be automatically included in the expression for graph 1. Graph 3α is then included in graph $2A$, etc. Similarly, a modification of $\Gamma_{a\tau}$ and $\Gamma_{b\sigma}$ would include graph $2B$ (Lamb shift type) in 1 and graph $3B$ in $2A$, etc. A modification in $G^{(2A)}$ would include graphs containing parts like graph 4α in graphs containing parts like graph $2A$ and so on.

We can, again in a purely formal way, write down an equation for the propagation of the wave function $\psi(1,2)$ in terms of $K(3,4;1,2)$ according to the prescriptions of FI and FII (see FI, Eq. (18)).

$$\psi(3,4)=\int\int K(3,4;1,2)N^a(1)N^b(2)\times\psi(1,2)d^3V_1 d^3V_2, \quad (10)$$

where, for any four-vector A_μ,

$$A^a\equiv A_\mu\gamma_{\mu a}.$$

In the $x_{\mu 1}$-space the integration is carried out over a closed 3-dimensional surface in space-time completely enclosing the point $x_{\mu 3}$. The essential parts of this surface are two spacelike surfaces, i.e., all of three-dimensional space at two times $t_1<t_3$ and $t_1'>t_3$. N_μ is the inward drawn normal to the surface. For the time t_1 only the components of $\psi(1,2)$ corresponding to positive energy of particle a occur, for t_1' only those for negative energy. The prescription for $x_{2\mu}$ and particle b is analogous.

Let $\phi_{1,2}(3,4)$ denote the expression obtained for $\psi(3,4)$ from Eq. (10) by replacing $K(3,4;1,2)$ by $K_{+a}(3,1)K_{+b}(4,2)$. Then $\phi_{1,2}(3,4)$ is a wave function which varies with t_3 and t_4 like the wave function for two free particles and is equal to $\psi(1,2)$ for $t_3=t_1$ and $t_4=t_2$. Substituting Eq. (9) into Eq. (10), we obtain an inhomogeneous integral equation for $\psi(3,4)$:

$$\psi(3,4)=\phi_{1,2}(3,4)-i\int\int\int\int d\tau_5 d\tau_6 d\tau_7 d\tau_8\times K_{+a}(3,5)K_{+b}(4,6)\bar{G}(5,6;7,8)\psi(7,8). \quad (11)$$

It will be convenient to separate the motion of the center of mass from the relative motion. This is made slightly difficult by the fact that in relativity theory the coordinate of the center of mass cannot be defined. However, the total *momentum*, which is the momentum of the center-of-mass motion, can be defined. One can then select some coordinate, more or less arbitrarily, to represent the absolute position, in time and space, of the system, and use apart from this only relative coordinates. Let us denote the "absolute" coordinate by X_μ; it may be for instance the position of particle a itself, or a linear combination

$$X_\mu = \alpha x_{\mu 1} + (1-\alpha) x_{\mu 2} \tag{12}$$

with α any arbitrary constant. Let the relative coordinate be denoted by

$$x_\mu = x_{\mu 1} - x_{\mu 2}. \tag{12a}$$

Primed quantities, x_μ', X_μ', etc., denote the equivalent expressions with 1 and 2 replaced by 3 and 4. If the interaction function $G(1,2)$ does not depend on any external factors, it will be a function $G(x_\mu)$ of x_μ only. $\bar{G}(1,2;3,4)$ will then be a differential-operator function of the relative space-time coordinates x_μ and x_μ' and of the difference of the two "absolute" coordinates $(X_\mu - X_\mu')$, but not of X_μ itself. In this case we can look for solutions for our wave function which have the special form,

$$\psi(1,2) = \exp(iK_\mu X_\mu)\psi(x_\mu), \tag{13}$$

where K_μ is an arbitrary constant four-dimensional vector. Such a wave function represents an eigenstate of the operator P_μ of the total momentum and hence a stationary state with total energy K_4. The condition for this state being a bound state is then

$$K^2 \equiv K_\mu K_\mu < (m_a + m_b)^2. \tag{14}$$

An arbitrary solution of Eq. (11) may be analyzed into fourier components of the form (13). If we select a fourier component satisfying the energy condition (14), then for this component the term $\phi_{1,2}(3,4)$ in Eq. (11) cannot contribute because it represents a free state of the two particles and hence the bound-state condition (14) cannot be true for it. For a bound state, we therefore obtain Eq. (11) without the inhomogeneous term,

$$\psi(3,4) = -i \int\int\int\int d\tau_5 d\tau_6 d\tau_7 d\tau_8 K_{+a}(3,5) \times K_{+b}(4,6)\bar{G}(5,6;7,8)\psi(7,8). \tag{11a}$$

Precisely this equation has been derived rigorously from quantum field theory by Gell-Mann and Low.[5] Its relevance also to states of "positive" energy can perhaps be made plausible from the fact that, in any stationary state, there will be an infinite number of scatterings, so that any free-particle function like $\phi_{1,2}(3,4)$, which may "initially" have been present, will be destroyed "in the course of time."

[5] M. Gell-Mann and F. Low, Phys. Rev. **84**, 350 (1951).

In contrast to the rigorous derivations of Gell-Mann and Low, we have merely derived Eqs. (9), (11), and (11a) in a purely formal way from Eq. (10) and Feynman's expression for $K(3,4;1,2)$ in the form of a doubly infinite sum. Gell-Mann and Low[5] have shown that this expression for $K(3,4;1,2)$, and hence Eq. (9), can be derived rigorously from quantum field theory even for times for which the interaction is acting. The use of Eq. (10), however, is *not* correct unless the interaction can be neglected at and between times t_1 and t_2. If the interaction remains constant throughout all times, Eq. (11a), and not Eq. (11), is then correct.

III. FURTHER DEVELOPMENT OF THE EQUATION*

It is convenient to introduce momentum variables. If $\chi(p_3, p_4)$ is the fourier transform of $\psi(3,4)$, then Eq. (11a) transforms into

$$\chi(p_3, p_4) = i \int\int dp_7 dp_8 [\not{p}_3^a - m_a]^{-1} [\not{p}_4^b - m_b]^{-1} \times \bar{G}(p_3, p_4; p_7, p_8)\chi(p_7, p_8), \tag{15}$$

where

$$\bar{G}(p_3, p_4; p_7, p_8) = (2\pi)^{-8} \int\int\int\int d\tau_5 d\tau_6 d\tau_7 d\tau_8 \times \exp\{i[p_3 x_5 + p_4 x_6 - p_7 x_7 - p_8 x_8]\} \times \bar{G}(5,6;7,8).$$

The symbols p_3, etc., denote four-vectors, $p_3 x_5$ four-dimensional scalar products, and each of the integrals in Eq. (15) goes over four-dimensional momentum space. The superscript a in $\not{p}_3^a$ means that the Dirac γ-operators for particle a must be inserted.

Next, we may introduce total and relative momenta. Defining coordinates as in (12), (12a), we have for the conjugate momenta

$$\left.\begin{aligned} P_\mu &\equiv i\partial x_\mu = i\partial x_{\mu 1} + i\partial x_{\mu 2} \\ p_\mu &\equiv i\partial x_\mu = i(1-\alpha)\partial x_{\mu 1} - i\alpha\partial x_{\mu 2}. \end{aligned}\right\} \tag{12b}$$

Of these, P_μ is obviously the total momentum and is uniquely defined, whereas the definition of the relative momentum can be changed by changing α, which amounts to the addition of an arbitrary multiple of the total momentum. To facilitate the transition to the nonrelativistic limit, it is convenient to make the special choice

$$\alpha = m_a/(m_a + m_b) \tag{12c}$$

then in the nonrelativistic limit (12) goes over into the normal definition of the center of mass. All the calculations in this section, however, are independent of this choice.

With the change of variable in (12) to (12c), Eq. (15) reduces to

$$\psi(p_\mu) = i \int d^4p' \mathfrak{S}^{-1} \bar{G}(p, p'; K)\psi(p_\mu'), \tag{16}$$

* These equations are summarized in the Appendix.

where

$$\bar{G}(p,p';K)=(2\pi)^{-4}\int\int\int d\tau_x d\tau_{x'} d\tau_{X-X'} \times\exp\{i[K(X-X')+px-p'x']\} \times G(x,x';X-X')$$

and

$$\mathfrak{F}=[(m_a/m_a+m_b)\boldsymbol{K}^a+\boldsymbol{p}^a-m_a] \times[(m_b/m_a+m_b)\boldsymbol{K}^b-\boldsymbol{p}^b-m_b]$$

Equation (16) is an integral equation for the momentum-space wave function $\psi(p_\mu)$ which depends on only four variables, namely, the components of the relative momentum of the two interacting particles. It differs from the ordinary Schrödinger momentum wave function by the appearance of the "relative energy" $\epsilon\equiv p_4$ as a fourth independent variable. $\bar{G}(p,p';K)$ is the generalized interaction function in four-dimensional momentum space.

It is tempting to simplify Eq. (16) (or Eq. (15)) by multiplying it by the operator $\mathfrak{F}$, since it does not depend on the variables of integration p', P'. Equation (16) then leads to

$$\mathfrak{F}\psi(p_\mu)=i\int d^4p'\bar{G}(p,p';K)\psi(p_\mu'). \tag{17}$$

From Eq. (17) we can derive the equivalent equation in coordinate space:

$$\mathfrak{F}\psi(x_\mu)=i\int d\tau_{x'}\bar{G}(x,x';K)\psi(x_\mu'), \tag{18}$$

where

$$\bar{G}(x,x';K)=\int d\tau_{X'}\exp[iK(X-X')]\bar{G}(x,x';X-X')$$

and $\boldsymbol{p}^a$ is now considered as the differential operator $i\boldsymbol{\nabla}^a\equiv i\gamma_{\mu a}\partial_{x_\mu}$. As $\psi(p_\mu)$ depends on the "relative energy" p_4, so $\psi(x_\mu)$ in Eq. (18) depends not only on three relative distance variables $\mathbf{x}$ but also on $t\equiv x_4$, the "relative time" variable. Equation (18) is still manifestly lorentz-invariant and is to be considered as an eigenvalue equation in a four-dimensional space with K^2 as eigenvalue, the binding energy being $[m_a+m_b-|K|]$.

An integral-differential equation, similar to Eq. (18), can be obtained, without going to the center-of-mass system and without using Eq. (13), by applying to Eq. (11) *or* Eq. (11a) the operator $(i\boldsymbol{\nabla}_3{}^a-m_a)(i\boldsymbol{\nabla}_4{}^b-m_b)$. This yields

$$(i\boldsymbol{\nabla}_3{}^a-m_a)(i\boldsymbol{\nabla}_4{}^b-m_b)\psi(3,4) =i\int\int d\tau_5 d\tau_6\bar{G}(3,4;5,6)\psi(5,6). \tag{19}$$

Equation (19) is the analog in our problem of the Dirac equation for a Fermi-Dirac particle in an external field. As discussed in FI, to obtain results equivalent to Dirac's hole theory both masses m_a and m_b in Eq. (19) (and in Eqs. (17), (18)) must be considered to contain an infinitesimal negative imaginary part.

If the coupling constant g^2 is small, we should obtain a reasonable approximation by replacing $\bar{G}(1,2;3,4)$ by $G^{(1)}(1,2;3,4)$. This substitution simplifies Eqs. (11), (11a), (15), (16), (17), (18), and (19) considerably, owing to the presence of the delta-functions in Eq. (2). In this approximation, Eq. (17) reduces to

$$\mathfrak{F}\psi(p_\mu)=(2\pi)^{-2}i\int d^4kG(k_\mu)\psi(p_\mu+k_\mu), \tag{17a}$$

where $G(k_\mu)$, the interaction function in momentum space, is the *four*-dimensional fourier transform of $G(1,2)$. Similarly, Eqs. (18) and (19) reduce to ordinary differential equations,

$$\mathfrak{F}\psi(x_\mu)=iG(x_\mu)\psi(x_\mu) \tag{18a}$$

and

$$(i\boldsymbol{\nabla}_1{}^a-m_a)(i\boldsymbol{\nabla}_2{}^b-m_b)\psi(1,2)=iG(1,2)\psi(1,2). \tag{19a}$$

Whereas any solution of Eq. (11a) also satisfies Eq. (19), the inverse is not necessarily true, since Eq. (19) is derived from Eq. (11) or Eq. (11a) by the application of two differential operators. The solutions of Eq. (11a) (or of the equivalent equations (15) and (16)) corresponding to a fixed value of the total energy determine uniquely stationary states of the system. In practice, however, it may be more convenient to solve Eq. (19) (or the equivalent (17) and (18)) than Eq. (11a). Since Eq. (19) is a necessary but not sufficient condition, only those solutions of Eq. (19) will be physically acceptable which can be shown to satisfy Eq. (11a). It would be more satisfactory from a practical point of view to have some criteria of "good behavior" of the wave function $\psi(1,2)$ which would determine directly which of the solutions of Eq. (19) correspond to physical states, without any reference to Eq. (11a). No completely satisfactory set of such criteria has as yet been found, but the following discussion of a purely fictitious adiabatic variation of the coupling constant g^2 may be useful in a search for such criteria and for an understanding of the physical significance of the wave-function $\psi(1,2)$.

Let T be the time coordinate X_4 of the center of mass in the coordinate system in which it is at rest. Let us assume that $G(1,2)$ is not absolutely invariant, but that the coupling constant g^2 is an extremely slowly (adiabatically) varying function of T, $g^2(T)$ such that, for very large positive and negative values of T, $g^2(T)$ is arbitrarily small, while for $-T_0<T<T_0$, $g^2(T)$ is practically constant and has its correct physical value $g_0{}^2$. Let us assume we have found a set of solutions of the eigenvalue equation (18), one solution for every value of g^2 between zero and $g_0{}^2$ such that both K^2 and $\psi(x_\mu)$ are "smooth continuous" functions of g^2. In the limit of extremely slow variation of $g^2(T)$ the wave

function is given by the adiabatic approximation

$$\psi(x_\mu;\ \mathbf{X},\ T)=\exp\left\{i\mathbf{K}\cdot\mathbf{X}+i\int_{-\infty}^{T}dT'K_4[g^2(T')]\right\}\times\psi[x_\mu;\ g^2(T)]. \quad (20)$$

For the solution $\psi(x_\mu;\ \mathbf{X},\ T)$ to be physically acceptable, $\psi[x_\mu;\ g^2(T)]$ for $g^2(\pm\infty)=0$ must then be a wave function describing two free Fermi-Dirac particles of masses m_a and m_b, respectively. If a particular set of solutions of Eq. (18) satisfies this "boundary condition," it automatically satisfies Eq. (11).†

The bound states we have discussed so far reduce, when the coupling constant is adiabatically reduced to zero, to a state in which only two particles and no other particle pairs or quanta are present. When the interaction is "on" $\psi(1,2)$ only represents the partial probability amplitude for the presence of only two particles. But it should then, in principle, be possible to express the partial probability amplitudes for the presence of any number of additional particle pairs and quanta uniquely in terms of $\psi(1,2)$ and $K^2(g^2)$. These expressions then contain expansions in positive powers of g^2 and reduce to zero in the limit of g^2 tending to zero. More complicated types of bound states may also exist. For instance there can be a bound state of two particles, plus an extra quantum. (For large enough values of g^2, the quantum itself may perhaps also be bound to the two particles.) The fundamental wave function for such a bound state would be of form $\psi(1,2;\ q_\mu)$, where q_μ denotes the coordinates of the quantum, and would satisfy a more complicated equation analogous to (11a). The probability amplitudes for the presence of two particles and no quanta, or of two quanta, etc., would then be expressible in terms of $\psi(1,2;\ q_\mu)$ and g^2 and would tend to zero as g^2 does.

In the nonrelativistic limit and for the case of small coupling constant, the formalism of this paper leads exactly to the ordinary nonrelativistic Schrödinger equation for a bound state for two particles. An example of this, and of the way Eq. (19) may be solved in practice, is given in the next section.

IV. SCALAR MESONS. EXTREME NONRELATIVISTIC LIMIT

We consider the problem of the deuteron ground state with scalar meson theory with scalar coupling. We shall solve only the approximate equation (19a), obtained from Eq. (19) by replacing $\bar{G}$ by the first term in its expansion, $G^{(1)}$. It is most convenient to use the equivalent equation in relative-momentum space, Eq. (17a). This becomes

$$(\tfrac{1}{2}K^a+p^a-M)(\tfrac{1}{2}K^b-p^b-M)\psi(p_\mu)=-g^2(4\pi^3i)^{-1}\int d^4k[k_\nu^2-\mu^2]^{-1}\psi(p_\mu+k_\mu), \quad (21)$$

where we have used the relativistic generalization of the Yukawa potential,

$$G(k_\mu)=g^2[\pi(k_\nu^2-\mu^2)]^{-1}. \quad (22)$$

M and μ are the nucleon and meson mass, respectively, each including an infinitesimal negative imaginary part, and g^2 is the dimensionless coupling constant equivalent to the fine structure constant in quantum electrodynamics. Without loss of generality, we can choose the coordinate system in which the center of mass is at rest. The first three components of K_μ are then zero and K_4 is the eigenvalue of Eq. (21).

The range of nuclear forces is large compared with the Compton wavelength of a nucleon, and hence the meson mass μ is small compared with the nucleon mass M. Furthermore, the binding energy of the deuteron is smaller than μ^2/M. Under these circumstances, a nonrelativistic calculation for the deuteron problem shows that the coupling constant g^2 is of the order of magnitude of μ/M and hence small compared with unity. It is further found that the momentum distribution in the deuteron falls off rapidly for momenta greater than μ; i.e., the "velocities" in the deuteron are of the order of magnitude of g^2 and hence small. Such a nonrelativistic solution should then be a good approximation and should be identical with the extreme nonrelativistic limit of our Eq. (21).

The wave function $\psi(p_\mu)$, or $\psi(x_\mu)$, is a 16-component spinor, the 16 components referring to the two possible spin directions and two signs of the energy for each of the particles. In analogy with the usual treatment of the nonrelativistic limit of the ordinary Dirac equation, we wish to carry out a reduction to the "large components" of Eq. (19a) or Eq. (21); i.e., we want an approximate equation involving only the spinor components referring to both particles in positive energy states. Various methods, analogous to various methods used for the Dirac equation,[6] are possible for such a reduction. One way is to transfer the term involving G to the left-hand side in the differential equation (19a) and to multiply this equation to the left by the operator $[(p_1^a+m_a)(p_2^b+m_b)-iG]$ which gives the equation,

$$\{(p_1^2-m_a^2)(p_2^2-m_b^2)-i[G,\ (p_1^a p_2^b+m_a m_b)]_+ +i[G,\ (p_1^a m_b+p_2^b m_a)]_--G^2\}\psi(1,2)=0, \quad (23)$$

where $p_1^a=i\gamma_{\mu a}\partial_{x_{\mu 1}}$ and Eq. (23) is considered as an ordinary differential equation in configuration space. A similar equation can be obtained from Eq. (21). We expand in powers of (p/M) and g^2 (which are of the same order of magnitude) and retain only the first two nonvanishing powers in this expansion (p^4 and p^6/M, respectively). The spatial components of γ_μ are of the order of (p/M). From Eq. (24), about to be derived,

† It would then seem that this criterion of good behavior would be sufficient; but it is not unambiguous, since the adiabatic variation of the wave function is not well-defined for the value of $g^2(T)$ which just gives a bound state of zero binding energy.

[6] H. A. Bethe, *Handbuch der Physik* (Verlag. Julius Springer, Berlin, 1933), Vol. 24/1, p. 304. H. A. Kramers, *Hand-u. Jahrbuch der chemischen Physik* (Akad. Verlag., Leipzig, 1938), Vol. 1, p. 295.

it follows that G is of the order of p^4/M^2. Hence,‡ the third and fourth terms in Eq. (23) contribute only terms of order p^6/M^2 or higher. Let $E\equiv(2M-K_4)$ be the binding energy, $\epsilon\equiv p_4$ the "relative energy" variable, and $\mathbf{p}\equiv\mathbf{p}_a=-\mathbf{p}_b$ the three-dimensional relative momentum. Equation (23) then reduces to the following approximate equation for the "large components," in the relative energy-momentum space, which does not contain any Dirac- (or spin-) operators at all:

$$(\tfrac{1}{2}E+\epsilon+p^2/2M)(\tfrac{1}{2}E-\epsilon+p^2/2M)\psi(\mathbf{p},\epsilon)$$
$$=-(g^2/2\pi i)\int\int d^3k d\omega[2\pi^2(k^2-\omega^2+\mu^2)]^{-1}$$
$$\times\psi(\mathbf{p}+\mathbf{k},\epsilon+\omega). \quad (24)$$

Since in Eq. (21) M (but not p_4) contains an infinitesimal negative imaginary part, $\frac{1}{2}E$ in both factors of Eq. (24) also contains a negative imaginary part.

An iteration method for solving Eq. (24) will be described in the next section. However, if the relative-energy term ω^2 is omitted in the denominator on the right-hand side, we shall now show that this equation reduces exactly to the ordinary Schrödinger equation for two nonrelativistic particles. This omission of ω^2 is equivalent to replacing the lorentz-invariant, and hence retarded, Yukawa interaction by an interaction which is instantaneous in the center of mass system. We change the variable of integration from ω to $(\omega+\epsilon)$ and define

$$\phi(\mathbf{p})=\int_{-\infty}^{\infty}d\epsilon'\psi(\mathbf{p},\epsilon'). \quad (25)$$

The right-hand side of the modified Eq. (24) does not contain ϵ now, and on the left-hand side ψ is multiplied by a simple number (not operator). We can then write the modified Eq. (24) in the form,

$$\psi(\mathbf{p},\epsilon)=-g^2\{[(E/2)+(p^2/2M)+\epsilon]$$
$$\times[(E/2)+(p^2/2M)-\epsilon]2\pi i\}^{-1}$$
$$\times\int d^3k\phi(\mathbf{p}+\mathbf{k})[2\pi^2(k^2+\mu^2)]^{-1}. \quad (26)$$

The first two factors in Eq. (26) are now the only ones depending on ϵ, and they are easily integrated over ϵ, using the fact that E contains a small negative imaginary part. This yields a simple equation for $\phi(\mathbf{p})$:

$$(E+p^2/M)\phi(\mathbf{p})$$
$$=-g^2\int d^3k\phi(\mathbf{p}+\mathbf{k})[2\pi^2(k^2+\mu^2)]^{-1}. \quad (27)$$

Equation (27) is identical with the Schrödinger equation in momentum space for two nonrelativistic nucleons interacting by means of a static central Yukawa potential.

The relative motion of the two nucleons could be described by a "mixed" wave function $\psi(\mathbf{p},t)$, instead of by $\psi(x_\mu)$ or $\psi(p_\mu)$, obtained by taking the fourier transform of $\psi(\mathbf{x},t)$ only for the three space coordinates but not for the relative time t. The function $\phi(\mathbf{p})$, which is the conventional momentum-space wave function, is then seen to be, except for a multiplicative constant, $\psi(\mathbf{p},t)$ for the special value $t=0$, i.e., for equal times for the two particles. The general expression for $\psi(\mathbf{p},t)$ can be obtained from Eqs. (26) and (27), and the total wave function is proportional to $\phi(\mathbf{p})$ times

$$\left.\begin{aligned}&\exp\{iET+i(\tfrac{1}{2}E+p^2/2M)t\}\\&\quad=\exp\{i(E+p^2/2M)t_1-i(p^2/2M)t_2\}\quad\text{for}\quad t<0,\\&\exp\{iET-i(\tfrac{1}{2}E+p^2/2M)t\}\\&\quad=\exp\{i(E+p^2/2M)t_2-i(p^2/2M)t_1\}\quad\text{for}\quad t>0.\end{aligned}\right\} \quad (28)$$

This wave function (28) can be said to correspond to propagation into the "future" as free waves (frequency $p^2/2M$) and into the "past" in a more complicated "bound" manner.

V. EXACT SOLUTION OF NONRELATIVISTIC EQUATION

The solutions of Eq. (24) differ from those of the approximation to it, Eq. (26), by terms of the relative order of magnitude of g^2. It was found that a straightforward application of a perturbation expansion in powers of g^2, starting with a sclution of Eq. (26) as zero-order wave function, leads to wrong results even for a very small value of g^2. This is due to the fact that one of the integrands occurring in the solution of Eq. (24) has a pole for a value of ϵ for which the solution of Eq. (26) is a very poor approximation. However, in the preceding paper[7] a method was described for solving integral equations of a type similar to that of Eq. (24) by an iteration method which does not involve any expansion in powers of g^2.

Such an iteration method has been applied previously[8] to the solution of Eq. (27) for the ground state of the deuteron with an initial trial wave function of the form,

$$\phi_0(\mathbf{p})=[(E+p^2/M)(p^2a^{-2}+\mu^2)]^{-1}, \quad (29)$$

where a is a dimensionless parameter. By analogy with the prescriptions of the preceding paper[7] we assume an initial trial wave function for the ground-state solution of Eq. (24) in the form,

$$\psi_0(\mathbf{p},\epsilon)=[(\tfrac{1}{2}E+p^2/2M)^2-\epsilon^2]^{-1}$$
$$\times(p^2a^{-2}-\epsilon^2b^{-2}+\mu^2)^{-1}, \quad (30)$$

where a and b are dimensionless coefficients which have to be determined and where E and μ are considered to have infinitesimal negative imaginary parts. For values of ϵ small compared with μ, the function ψ_0 differs little

‡ This demonstration involves some algebra.

[7] E. E. Salpeter, Phys. Rev. **84**, 1226 (1951).
[8] J. S. Goldstein and E. E. Salpeter (to be published).

from the equivalent solution of Eq. (26). The first factor of Eq. (30) suggests that $\psi(\mathbf{p}, \epsilon)$ will be of interest mainly for values of $|\epsilon|$ of the order of magnitude of (μ^2/M), which is indeed much less than μ. The expression (30) for ψ_0 is then substituted for in ψ the integral on the right-hand side of Eq. (24), which yields a better approximation to $\psi(\mathbf{p}, \epsilon)$, i.e., the first iterated function $\psi_1(\mathbf{p}, \epsilon)$:

$$\psi_1(\mathbf{p}, \epsilon) = -g^2[(\tfrac{1}{2}E + p^2/2M)^2 - \epsilon^2]^{-1} \times \int\int d^3k d\omega \psi_0(\mathbf{p}+\mathbf{k}; \epsilon+\omega) \times [4\pi^3 i(k^2 - \omega^2 + \mu^2)]^{-1}. \quad (31)$$

In principle this iteration procedure could be repeated any number of times.

Since the binding energy of the deuteron is known, we shall consider E as given and g^2 as the eigenvalue of Eq. (24). We then find successive approximations g_1^2, g_2^2, etc., to g^2 by requiring that

$$\psi_{n+1}(0,0) = \psi_n(0,0). \quad (32)$$

For convenience in calculation it is useful to define two functions $a_n(p)$ and $b_n(p, \epsilon)$ by

$$\psi_n(\mathbf{p}, \epsilon) = [(\tfrac{1}{2}E + p^2/2M) - \epsilon^2]^{-1} \times \{p^2 a_n^{-2}(p) - \epsilon^2 b_n^{-2}(p, \epsilon) + \mu^2\}^{-1}. \quad (33)$$

The advantage of these two functions a_n and b_n is that they vary *slowly* with p and ϵ. We then determine "reasonable" values for a and b by requiring, for some conveniently chosen values of p and ϵ, that

$$\psi_1(p, 0)/\psi_1(0, 0) = \psi_0(p, 0)/\psi_0(0, 0), \text{ i.e., } a_1(p) = a; \quad (34)$$

$$\psi_1(p, \epsilon)/\psi_1(p, 0) = \psi_0(p, \epsilon)/\psi_0(p, 0), \text{ i.e., } b_1(p, \epsilon) = b. \quad (35)$$

For a more detailed discussion of the method used see the preceding paper.[7]

A meson mass μ of $275m_e$ agrees fairly well both with the mass of the charged π-meson[9] and with calculations[10] on the triplet effective range of the neutron-proton force. We therefore take a value of 0.150 for μ/M. For the ratio $(EM)^{\frac{1}{2}}/\mu$ we take a value of 0.32, which agrees fairly well with a deuteron binding energy E of 2.226 Mev and the above value for the meson mass. We determine the value to be used for a by applying condition (34) for $p = a$. For the extreme nonrelativistic equation[4] (26) a similar choice[8] gives a value for a of approximately 1.85; and the three-dimensional equations equivalent to Eqs. (31) and (32) with $n=0$ give a value for g_1^2 of $2.39(\mu/M)$. This value of g_1^2 differs from the exact value of g^2 for Eq. (26) by only a fraction of one percent.[8]

Estimates for b for the four-dimensional equation (24) can be obtained easily from Eqs. (31) and (35) for the four cases of p and ϵ very small or very large compared with μ, estimates for a from Eqs. (31) and (34). These calculations for a and b could in principle be carried out for any value of (μ/M), but would be rather involved, since Eqs. (34) and (35) are coupled equations for the two unknowns a and b. In order to simplify the computations, an expansion in powers of (μ/M) was employed and only the first two terms in this expansion retained. Equation (35) involves, to this approximation, only the value 1.85 and not a itself and, for $p \ll \mu$ and $\epsilon \ll \mu$ gave $b = 1.31$; for $p \ll \mu$ and $\epsilon \gg \mu$, $b = 1.93$; for $p \gg \mu$ and any value for ϵ, $b = 1.85$. For the following calculations a somewhat arbitrary value of $b = 1.6$ was used. Equation (34) with $p = a$ was then solved for a, the solution involving a short numerical integration. With the values thus obtained for a and b, Eqs. (31) and (32), with $n=0$, give a value for g_1^2:

$$\left.\begin{aligned} a &= 1.85(1 - 0.5_8\mu/M), \quad b = 1.6; \\ g_1^2 &= 2.39(\mu/M)(1 + 0.9_8\mu/M). \end{aligned}\right\} \quad (36)$$

The integrals occurring in Eq. (31) cannot be carried out analytically for general p and ϵ, but the numerical work involved in evaluating $\psi_1(p, \epsilon)$ for any particular pair of values for p and ϵ is not very lengthy. The function $a_1(p)$ is real for all values of p; $b_1(p, \epsilon)$ is real for $\epsilon < \mu$ but is, in general, complex for $\epsilon > \mu$. The function $a_1(p)$ and the absolute value of $b_1(p, \epsilon)$ are slowly varying functions and, in the whole range $0 < p$, $\epsilon < M$, do not vary by more than about 50 percent. Hence, if required, $\psi_1(p, \epsilon)$, $a_1(p)$, and $b_1(p, \epsilon)$ could be evaluated for a few values each of p and ϵ and an interpolation method used on $a_1(p)$ and $b_1(p, \epsilon)$ for intermediate values of p and ϵ. A better approximation g_2^2 to the coupling constant for Eq. (24) could then be obtained after one more double integration, using Eq. (31) with $n=1$. However, g_1^2 is probably not in error by very much more than one or two percent. Since in the derivation of Eq. (24), terms of relative order of magnitude of $(\mu/M)^2 > 0.01$ have in any case been omitted, an evaluation of g_2^2 was not considered worth while.

The mixed wave function corresponding to $\psi_0(\mathbf{p}, \epsilon)$ is

$$\frac{\exp(iET)}{[b^2(p^2a^{-2} + \mu^2) - (E/2 + p^2/2M)^2]} \times \left\{ \frac{\exp[\pm i(\tfrac{1}{2}E + p^2/2M)t]}{(\tfrac{1}{2}E + p^2/2M)} - \frac{\exp[\pm ib(p^2a^{-2} + \mu^2)^{\frac{1}{2}}t]}{b(p^2a^{-2} + \mu^2)^{\frac{1}{2}}} \right\}, \quad (37)$$

where the + sign holds for $t < 0$ and the − sign for $t > 0$. The first term of (37) is of the same form as Eq. (28); the second term gives a contribution to the wave function which does *not* correspond to the propagation into the "future" as free waves and is connected with the fact that a retarded interaction is used. The two different denominators occurring in the first and second

[9] Smith, Barkas, Bishop, Bradner, and Gardner, Phys. Rev. 78, 86(A) (1950).
[10] E. E. Salpeter, Phys. Rev. 82, 60 (1951).

terms of (37) are of the order of magnitude of (μ^2/M) and μ, respectively. Thus, the absolute value of the second term is smaller than that of the first by a factor of the order of (μ/M).

Expression (36) for g_1^2 shows that appreciably different results are obtained if the relativistic retarded interaction function $(k^2-\omega^2+\mu^2)^{-1}$ is used instead of the instantaneous function $(k^2+\mu^2)^{-1}$. We can get a better insight into the significance of these differences by deriving an approximate equation involving a three-dimensional wave function from Eq. (24). We again define $\phi_n(\mathbf{p})$ by means of

$$\phi_n(\mathbf{p})=\int_{-\infty}^{\infty} d\epsilon' \psi_n(\mathbf{p},\epsilon').$$

In Eq. (24), unlike in Eq. (26), ϵ and ω cannot be eliminated unless the dependence of $\psi(\mathbf{p},\epsilon)$ on ϵ is known. But if the expression (30) is substituted into Eq. (31), then the integration over ω can be carried out. The ensuing expression for $\psi_1(\mathbf{p},\epsilon)$ can then be integrated over ϵ giving an expression for $\phi_1(\mathbf{p})$ not involving ϵ or ω. Finally, the integrand in this expression can be expressed in terms of $\phi_0(\mathbf{p})$. Neglecting terms of order of magnitude $(\mu/M)^2$ compared with unity, this expression becomes

$$(E+p^2/M)\phi_1(\mathbf{p})=-g^2\int d^3k[2\pi^2(k^2+\mu^2)]^{-1} \times\{1+F(\mathbf{p},\mathbf{k})\}\phi_0(\mathbf{p}+\mathbf{k}) \quad (38)$$

$$F(\mathbf{p},\mathbf{k})\equiv -\frac{E+(p^2+|\mathbf{p}+\mathbf{k}|^2)/2M}{(k^2+\mu^2)^{\frac{1}{2}}} +\frac{\frac{1}{2}E+|\mathbf{p}+\mathbf{k}|^2/2M}{b(p^2a^{-2}+\mu^2)^{\frac{1}{2}}+(k^2+\mu^2)^{\frac{1}{2}}}. \quad (39)$$

Equation (38) is identical with the equation for the iterated function $\phi_1(\mathbf{p})$ obtained from Eqs. (26) and (27), except for the presence of the additional term involving $F(\mathbf{p},\mathbf{k})$. Thus, the difference between the retarded and instantaneous interaction functions can, to first order in (μ/M), be included in an equation for the orthodox three-dimensional wave function $\phi(\mathbf{p})$ by adding an extra interaction function to $(k^2+\mu^2)^{-1}$. This additional term depends on $\mathbf{p}$ as well as on $\mathbf{k}$ and represents therefore a velocity-dependent potential. For $p,\ k,\lesssim\mu$, $F(\mathbf{p},\mathbf{k})$ is of the order of magnitude of (μ/M).

An approximation to g^2, somewhat more accurate than g_1^2, can also be obtained from Eq. (38). If we again consider (μ/M) small and expand in powers of it, $F(\mathbf{p},\mathbf{k})$ is small compared with unity throughout the whole range over which the integrand of Eq. (38) is appreciable. We can therefore use first-order perturbation theory, taking the ground-state solution of Eq. (27) as the unperturbed wave function and considering $(k^2+\mu^2)^{-1}F(\mathbf{p},\mathbf{k})$ as the perturbation potential. It should be noted that an attempt to use perturbation theory directly in Eq. (24) would be equivalent to an unjustified omission of the second half of expression (39) for $F(\mathbf{p},\mathbf{k})$. Using the expression (29) as an approximation to the unperturbed wave function the first order perturbation treatment for Eq. (38) was carried out. After some rather tedious numerical and analytical integrations we found, keeping the deuteron binding energy constant,

$$g^2=2.39(\mu/M)(1+1.0_7\mu/M). \quad (40)$$

The expression (40) represents only the first two terms in an expansion in powers of (μ/M). The coefficient 1.0_7 of the second term in Eq. (40) should be accurate to better than ten percent and agrees, as well as can be expected, with the equivalent coefficient in the less accurate expression (36) for g_1^2.

VI. DISCUSSION

We have found in Eq. (40) that the value of g^2 required to obtain the correct binding energy of the deuteron in relativistic theory differs from the non-relativistic value by an amount of relative order μ/M. This is of the same order as the coupling constant g^2, and as the "average" value of p/M in the deuteron ground state. Thus we get a correction of relative order v/c where v is the "average" nucleon velocity, in contrast to the well-known result in the theory of the hydrogen atom that relativistic effects (fine structure) are of relative order $(v/c)^2\approx(e^2/\hbar c)^2$.

This surprising result is not due to a mistake because, in the derivation of Eq. (24) from the Lorentz-invariant Eq. (21), only errors of the relative order (p/M^2) or smaller were made. Indeed, we shall prove that the result (40) is correct, neglecting terms of relative order $(\mu/M)^2$, if only *charged mesons can be emitted and absorbed* by nucleons. On the other hand, for *neutral* mesons, and also for electromagnetic interaction as in the hydrogen atom, our result in the last section must be corrected.

Indeed, Eq. (21), the basis of our calculations in the last section, differs from the complete Eq. (19) by the replacement of the full interaction $\bar{G}$ by the one-meson interaction $G^{(1)}$. But for a neutral field theory all other contributions $G^{(n)}$ also have to be included, and in particular the graphs $2A-2D$ of Fig. 1 will give contributions containing only one power of g^2 more than the "main" term $G^{(1)}$ which alone was included in (21). It must therefore be expected that these terms will give corrections to (40) of the order $g^2\approx\mu/M$, i.e., of the same order by which (40) differs from the nonrelativistic result. In charged meson theory, the graphs $2A-2D$ do *not* contribute as will be shown below.

From the example of the hydrogen fine structure, it should be expected that the contribution from the "two-meson graphs" $2A-2D$ not only is of the same order as the relativistic correction in (40) but actually cancels this correction exactly, leaving only corrections of the relative order $(\mu/M)^2$ to the nonrelativistic result.

Indeed, the *usual* derivation of Eq. (27) from field theory, by separation of a "static" interaction, seems to neglect only terms of relative order $(p/M)^2$. This has been confirmed by a detailed relativistic analysis of the problem by Dancoff.[11] We must therefore show that our theory also gives the nonrelativistic result to order $(\mu/M)^2$. This could of course be done by explicitly calculating the contributions of graphs $2A-2D$ and showing that they compensate exactly the relativistic correction term in (40), but this would be both tedious and unconvincing. Instead, we shall use a transformation of the theory which will give the result directly and will in addition be useful for the practical application of the theory to neutral fields.

Such a transformation is somewhat analogous to that described in Sec. 8 of FII for the elimination of the longitudinal field in quantum electrodynamics. Feynman showed that the formal incorporation of a certain interaction function, which depends explicitly on the energy change of the interacting particle, into the matrix elements for any arbitrary process undergone by a particle (initially and finally in a free state) does not affect the total amplitude function for any such physical process. For the case of electrodynamics the addition of these terms to the two longitudinal components of the retarded electrodynamic interaction results exactly in an instantaneous coulomb interaction. We shall now show that the formal incorporation of a slightly different interaction function does not affect the total amplitude function, for any physical processes involving neutral scalar mesons. The addition of this interaction to the retarded scalar meson interaction (22) results in the sum of an instantaneous Yukawa interaction and a more complicated, but smaller, retarded interaction.

Consider the probability amplitude function for any arbitrary graph for two Fermi-Dirac particles, initially and finally in a free state, interacting N times by means of arbitrary interactions with "vertex parts" Γ. For the special case of scalar meson interactions with scalar couplings Γ, defined in Eq. (2), is unity. Consider an additional interaction, involving an energy-momentum change of q_μ, with a velocity-dependent vertex-part Λ:

$$\Lambda=(\not{p}-M)\gamma_4-\gamma_4(\not{\pi}-M)=(\mathbf{p}+\boldsymbol{\pi})\cdot\boldsymbol{\gamma}\gamma_4-\omega \quad (41)$$

where p_μ and $\pi_\mu\equiv(p_\mu+q_\mu)$ are the energy-momentum vectors before and after the interaction respectively; ω is the energy change q_4 and $\mathbf{p}$, $\boldsymbol{\pi}$ the three-dimensional momenta. This interaction function is similar to the one used in FII except that γ_4 is replaced by unity.

We next modify the above mentioned arbitrary graph involving N Γ-interactions by including one additional interaction involving a vertex part Λ either before the first Γ-interaction of particle a or between the first and second, etc., the corresponding vertex parts for particle b being left arbitrary. We now sum the amplitude functions corresponding to these $(N+1)$ modified graphs, following the procedure explained in FII. The contribution to this sum of the first term in expression (41) for Λ acting between the nth and the $(n+1)$st Γ-interaction, plus that of the second term of Eq. (41) between the $(n-1)$th and nth Γ-interaction, contains the following factors:

$$\begin{aligned}&\cdots(\not{p}_{n-1}-M)^{-1}\Gamma_n(\not{p}_n-M)^{-1}\\&\qquad\times[(\not{p}_n-M)\gamma_4](\not{\pi}_n-M)^{-1}\cdots,\\&-\cdots(\not{p}_{n-1}-M)^{-1}[\gamma_4(\not{\pi}_{n-1}-M)]\\&\qquad\times(\not{\pi}_{n-1}-M)^{-1}\Gamma_n(\not{\pi}_n-M)^{-1}\cdots.\end{aligned} \quad (42)$$

The first term of Eq. (41) acting before the first Γ-interaction, and the second term acting after the last Γ-interaction, give no contribution, since particle a is initially and finally in a free state. The sum of the amplitude functions for these $(N+1)$ modified graphs is then equivalent to the sum for N modified graphs, in each of which one of the N Γ-interactions is replaced by a combined interaction with vertex part Λ'[a]:

$$\Lambda'=\Gamma\gamma_4-\gamma_4\Gamma. \quad (43)$$

If each Γ is unity, then Λ' is zero and the introduction of the Λ-interactions does not affect the total amplitude function. The Λ used in FII (γ_4 replaced by unity) led to a Λ' equal to zero for any Γ.

In the center-of-mass system ($p_{a\mu}=-p_{b\mu}\equiv p_\mu$) we define an interaction between particles a and b involving an energy-momentum transfer $q_\mu=(\mathbf{k},\omega)$, with a velocity-dependent interaction function $L(p_\mu;\mathbf{k},\omega)$:

$$\begin{aligned}L=g^2&[4\pi^2(k^2-\omega^2+\mu^2)(k^2+\mu^2)]^{-1}\\&\times\{\Lambda^a(\Lambda^b-2\omega)+(\Lambda^a+2\omega)\Lambda^b\}.\end{aligned} \quad (44)$$

We can write the Lorentz-invariant retarded scalar meson interaction function $G(\mathbf{k},\omega)$, expression (22), as $\{[G-L]+L\}$. Using Eq. (44) and the second expression in Eq. (41), we find

$$\begin{aligned}G-L=&\frac{g^2}{2\pi^2(k^2+\mu^2)}\\&\times\left\{1-\frac{(\mathbf{p}+\boldsymbol{\pi})\cdot\boldsymbol{\gamma}^a\gamma_4{}^a(\mathbf{p}+\boldsymbol{\pi})\cdot\boldsymbol{\gamma}^b\gamma_4{}^b}{(k^2-\omega^2+\mu^2)}\right\}.\end{aligned} \quad (45)$$

The first of the two terms of expression (45) is exactly the *instantaneous* Yukawa interaction function and, when substituted for G, leads to Eq. (27) and not to Eq. (24). The second term in Eq. (45) represents a velocity- (and spin-) dependent interaction and, since p, k, and $|\boldsymbol{\gamma}M|$ are all of the order of magnitude of μ, is smaller than the first term by a factor of order $(\mu/M)^2$. Since Γ for the scalar meson interaction is unity, it follows from Eq. (43) that the additional interaction function $+L$ does not contribute to the

[11] S. M. Dancoff, Phys. Rev. **78**, 382 (1950).

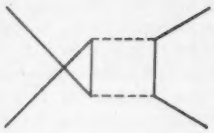

FIG. 3. Graph for a process involving virtual pair creation and annihilation which is included in graph 2A.

total amplitude function for any interaction between the two particles.

The "crossed" graph 2A might be considered to represent the "presence of two mesons in flight simultaneously." The first part of Eq. (45) represents an instantaneous exchange of mesons, and one might expect that such an interaction should not contribute anything to the term $G^{(2A)}$ corresponding to graph 2A. In reality its contribution to $G^{(2A)}$ is not exactly zero, since processes involving intermediate states of negative energy (represented in Fig. 3) are included in graph 2A, but is smaller than the expression $G^{(2A)}$ for the retarded interaction function (22) by a factor of order $(\mu/M)^2$. The second term of Eq. (45) is itself small, and its contribution to $G^{(2A)}$ is still smaller by a factor of order (μ/M); the total sum of expressions $[G^{(2B)}+G^{(2C)}+G^{(2D)}]$ should be of the same order of magnitude as this contribution. We have therefore shown that replacing $\bar{G}$ by the instantaneous Yukawa interaction function $g^2/2\pi^2(k^2+\mu^2)$ only introduces errors of relative order of magnitude $(\mu/M)^2$, the leading correction term being given by the second term of Eq. (45).

However, for a purely *charged* scalar meson theory the position is radically different if we assume that a nucleon cannot change into a double charged or negatively charged proton by the emission or absorption of charged mesons and if we assume no coupling with neutral mesons at all. In this case a nucleon can emit (or absorb) positive and negative mesons only alternately, and the crossed graph 2A and Lamb shift graph 2B are completely forbidden by charge conservation. Since the nucleons in the deuteron are not free, the self-energy and mass-renormalization graphs 2C and 2D together may contribute nonvanishing terms; but these, as well as the terms due to more complicated graphs, are of a smaller order of magnitude than $G^{(2A)}$ with a retarded scalar interaction function. Therefore, Eq. (24) and the approximate solution derived for it in the last section give correctly the first two terms in an expansion in powers of (μ/M) for *charged* scalar mesons (in the absence of multiply charged nucleon states). It should be noted that the transformation carried out above for neutral mesons is based on the condition that a Λ-interaction can be introduced into any graph at *any* point. If we are restricted to charged mesons, and neutrons and protons only, this condition cannot be fulfilled (because of charge conservation) and the above transformation cannot be carried out.

For a purely charged scalar theory the coupling constant g^2 required for the interaction is then larger by approximately $1.1(\mu/M)$, or 15 percent, than for a purely neutral theory. For a Serber mixture of charged and neutral mesons (giving no force in p-states) the increase is only one quarter of this amount; for a Kemmer charge-symmetric mixture there is a decrease of very roughly four times this amount. It should be emphasized that calculations on a scalar meson theory were carried out in this paper merely to illustrate the methods developed and not because of any belief in this theory being correct physically.

The equations described in this paper are being applied to an investigation of the relativistic corrections to the fine structure and hyperfine structure of hydrogen. No way has as yet been found to apply this equation to problems in which the coupling constant is not small, e.g., the deuteron with pseudo-scalar mesons. Given any *phenomenological* interaction potential, however, one can always find a relativistically invariant generalization of it. This Lorentz-invariant interaction function could then be substituted in Eq. (14) or Eq. (19); and a relativistic, but purely phenomenological, equation for bound states for two particles is then obtained. An investigation of the theory of Fermi and Yang,[12] using such an equation, is planned.

The authors wish to thank Professor R. P. Feynman and several of their colleagues at the Princeton Institute for Advanced Study and elsewhere for stimulating discussions and Dr. M. Gell-Mann and Dr. F. Low for communicating their results to us prior to publication.

APPENDIX. SUMMARY OF EQUATIONS DERIVED IN SECS. II AND III

The amplitude function $K(3,4;1,2)$ is defined uniquely by the inhomogeneous integral equation (9). This definition is exactly equivalent to that given by Feynman in the form of a double infinite series. Equation (9) leads to Eq. (11) or (11a) for the wave function in coordinate space, $\psi(1,2)$. Equation (11) is obtained if the interaction is "on" only for a finite time, Eq. (11a) if the interaction is constant throughout all time. Equation (11) contains a boundary condition in the form of an inhomogeneous term $\phi_{1,2}(3,4)$ and therefore has only one solution. Equation (11a) is a homogeneous integral-differential equation and has an infinite number of solutions, each one corresponding to a "physically acceptable state." The fourier transform of Eq. (11a) is Eq. (15), an equation for the momentum-space wave function $\chi(p_1, p_2)$.

For the case of an interaction constant throughout all time, we may look for special solutions for our wave function satisfying the condition (13). These solutions correspond to states with a definite total momentum and total energy. For these states, Eq. (11a) reduces to a more special equation (which is not given explicitly in the text) and Eq. (15) to the special equation (16).

By applying certain operators to Eqs. (11a) or (11) we obtain Eq. (19) and an equivalent equation (not given explicitly) can be derived from Eq. (15). By applying equivalent operators to Eq. (16) and its counterpart in coordinate space, we obtain Eqs. (17) and (18), respectively. These four derived equations are more convenient for practical solutions, but are only necessary and not sufficient conditions. If the expression $\bar{G}$ is replaced by the first term in its expansion, $G^{(1)}$, Eqs. (17), (18), and (19) reduce to the approximate Eqs. (17a), (18a), and (19a), respectively.

[12] E. Fermi and C. N. Yang, Phys. Rev. 76, 1739 (1949).

Letters to the Editor

PUBLICATION of brief reports of important discoveries in physics may be secured by addressing them to this department. The closing date for this department is five weeks prior to the date of issue. No proof will be sent to the authors. The Board of Editors does not hold itself responsible for the opinions expressed by the correspondents. Communications should not exceed 600 words in length.

The Lifetime of the μ^+-Meson

W. E. Bell* and E. P. Hincks
Atomic Energy Project, National Research Council of Canada, Chalk River, Ontario, Canada
(Received November 5, 1951)

AN experiment is in progress to determine the probabilities of nuclear capture of μ^--mesons stopped in elements of low atomic number. The apparatus, which accepts the normal sea level mixture of positive and negative mesons, measures the distribution of delays between the stopping of mesons and the emission of decay electrons. The composite decay curve, so obtained, is then analyzed for positive and negative meson decay components. It was first necessary to determine accurately the μ^+-meson lifetime by stopping the mesons in iron, whose atomic number is sufficiently large that no μ^--decays are recorded,[1] and this result is reported here since it is believed to be more accurate than previously published values.

Three trays of GM counters, *A*, *B*, *C* (Fig. 1), are used. The meson absorber, bars of pure iron filling a volume 50 cm×47 cm

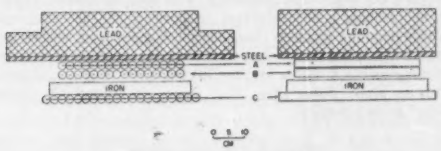

FIG. 1. Experimental arrangement. All counters are 1-inch diameter with 0.7-mm brass walls; those in tray *B* feed individual pulse-shaping amplifiers. Above *A* is a 5½-inch thick lead shield for soft radiation, while the only material immediately below the counters is a steel frame supporting them 4½ feet above the floor.

×3.8 cm, is placed in the 5-cm gap between trays *B* and *C*. Electronic circuits record the distribution of delays between mesons stopping [anticoincidences $(AB-C)$] and decay electrons [single counts in *B* or *C*] with ten nearly contiguous coincidence channels, each ~1 μsec wide. The first channel has a preselected initial delay. An automatic calibration of all channel delay limits is made daily, using two artificial pulses generated by an accurate "interval marker."[2] Each channel limit determination has a maximum random error of ±0.005 μsec; systematic error is believed to be <0.3 percent.

Runs were made for four different conditions as summarized in Table I. The differential decay curve, shown in Fig. 2, combines the results of runs 1 and 2. Corrections were made for dead-time losses, for drifts of the channel positions, for prompt events delayed by counter lags, for inequality of channel widths, and for chance coincidences; only the last two were of appreciable importance. The number of chance delayed coincidences was computed from the prompt coincidence rates and verified by the results of runs 2, 3, and 4. Run 3 showed, in addition to chance counts, a background of decays with an intensity one-sixth that resulting from the iron absorber. Since these are caused by mesons stopping mainly in the brass counter walls and in the steel framework, and since they showed a lifetime not statistically different from that obtained from run 1, no correction was made

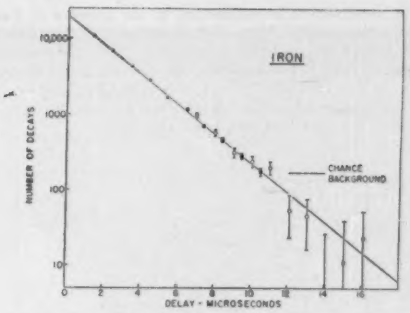

FIG. 2. Semilogarithmic plot of the number of decays recorded in each channel (after corrections) at the delay corresponding to the midpoint of the channel. The solid circles indicate the data of run 1, and the open circles, the data of run 2 normalized to the same number of stopped mesons. Standard deviations are indicated.

for them. A least squares fit to the data plotted in Fig. 2 gives a mean life $\tau=2.22\pm0.02$ (standard deviation) μsec for the μ^+-meson. The corresponding half-life is 1.54 μsec. The best previous

TABLE I. Description of the four runs.

Run	Iron absorber	Initial delay (μsec)	Total hours	Approximate total number of delayed counts recorded: μ-decays (10 channels)	Chance (10 channels)	Counter lags (all in first channel)
1	In	0.8	398.2	29100	1690	500
2	In	6.4	105.6	640	440	0
3	Out	0.8	249.0	3030	1110	330
4	Out	6.4	43.7	40	180	6

measurements by Nereson and Rossi[3] ($\tau=2.15\pm0.07$ μsec), by Ticho[4] ($\tau=2.11\pm0.10$ μsec), and by Conversi and Piccioni[5] ($\tau=2.33\pm0.15$ μsec), are all in agreement with our value.

* Now with Newmont Exploration, Ltd., Jerome, Arizona.
[1] Conversi, Pancini, and Piccioni, Phys. Rev. 71, 209 (1947); T. Sigurgeirsson and K. A. Yamakawa, Revs. Modern Phys. 21, 124 (1949).
[2] W. E. Bell and E. P. Hincks (to be published).
[3] N. Nereson and B. Rossi, Phys. Rev. 64, 199 (1943).
[4] H. K. Ticho, Phys. Rev. 74, 1337 (1948).
[5] M. Conversi and O. Piccioni, Phys. Rev. 70, 859 (1946).

The Radioactive Decay of Ca^{41}

F. Brown, G. C. Hanna, and L. Yaffe
Atomic Energy Project, National Research Council of Canada, Chalk River, Ontario
(Received October 26, 1951)

THE measurements of Richards, Smith, and Browne[1] on the threshold of the reaction $K^{41}(p,n)Ca^{41}$ show that 0.44±0.02 Mev is available for the decay of Ca^{41} by *K*-capture to K^{41}.

As a result of their studies of the neutron capture γ-ray spectrum of calcium, Kinsey, Bartholomew, and Walker[2] have proposed a cross section of about 0.35 barn for the reaction $Ca^{40}(n,\gamma)Ca^{41}$.

Calcium oxide samples were irradiated with slow neutrons for varying lengths of time. After extensive chemical purification the calcium sources were examined in an attempt to detect the characteristic *K* x-rays of potassium (K_α—3.31 kev) produced by *K*-capture in Ca^{41}. A proportional counter with a thin polystyrene window (1.5 mg/cm²) was used. The counter was filled with a mixture of argon and methane. The x-ray energy was measured by comparison with the *K* x-rays of copper (K_α—8.05 kev).

This measurement is complicated by the presence of β-rays, which arise mainly from Ca^{45} produced by the reaction $Ca^{44}(n, \gamma)Ca^{45}$. These β-rays were excluded from the counter by a magnetic field, but in traversing the calcium source they produced the characteristic K x-rays of calcium (K_α—3.69 kev). In our early experiments these were so intense that the expected potassium K x-rays were completely masked.

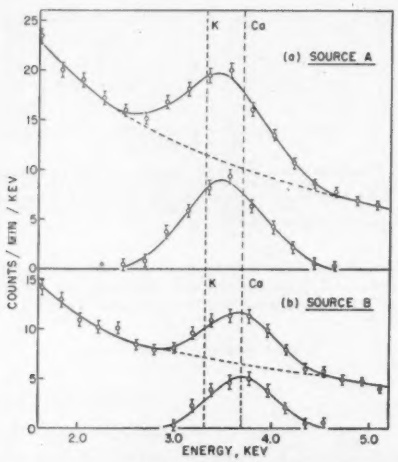

FIG. 1. Typical curves obtained using no absorber. The counter was filled with argon plus methane. The x-ray peaks are shown with and without subtraction of the interpolated background. The dotted lines show the expected positions of potassium and calcium K x-rays.

A sample[3] of calcium depleted 200-fold in mass 44 was irradiated in the NRX heavy water reactor for 6 weeks. From this a source (A) of calcium oxalate (0.4 mg Ca) having an area of 1.1 cm² was prepared. For comparison another source (B) was prepared using the same weight of unirradiated calcium oxalate plus a tracer amount of heavily irradiated ordinary calcium, sufficient to give source B the same Ca^{45} β-activity as source A.

Sources A and B should produce the same calcium x-ray activity. In addition A will give potassium x-rays if Ca^{41} is present in a detectable amount; B will not since its Ca^{41} content is negligible. Figure 1 shows that source B gives pure calcium x-rays, and A a mixture.

The shape of a single x-ray peak was accurately determined in subsidiary experiments, using a large source of irradiated ordinary calcium, and the expected positions of calcium and potassium x-rays are known. These data enable a complex peak to be analyzed into its two components. Several runs were made on each source and the peaks analyzed. The mean values of the potassium and calcium x-ray counting rates thus obtained are given in Table I. The agreement between the calcium x-ray counting rates of the two sources provides a check on the analysis.

TABLE I. No absorber.

Source	Total rate cpm	Potassium rate cpm	Calcium rate cpm
A	8.8 ±0.4	5.3 ±0.5	3.5 ±0.5
B	4.5 ±0.4	0.3 ±0.5	4.2 ±0.5

A further check was made by comparing the two sources through a "critical" absorber consisting of 3 mg/cm² of potassium metal sealed between polystyrene foils. This will attenuate potassium and calcium x-rays by factors of about 2.5 and 12, respectively.[4] A magnetic field prevented the Ca^{45} β-rays from striking the potassium.

Typical curves are shown in Fig. 2 and the mean value of all results in Table II. The analyses of the peaks into two components

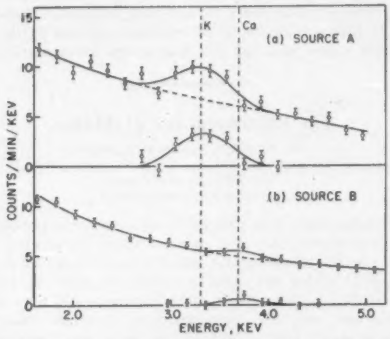

FIG. 2. Typical curves obtained with a potassium critical absorber and argon plus methane filling.

are rather inaccurate, but the counting rates are in satisfactory agreement with those calculated from Table I knowing the effect of the absorber.

A counter filled with argon and covered with a potassium absorber will have a peak in its response to x-rays whose energy lies between the argon and potassium K absorption limits. Thus, if bremsstrahlung is an important constituent of the background in this region, a spurious "potassium" K x-ray peak will be generated. We have shown that this effect is negligible here by examining source A with a krypton-filled counter. Further, source B with an argon filling (Fig. 2(b)) shows no appreciable "potassium" x-ray intensity.

TABLE II. Potassium absorber.

Source	Total rate cpm Calc	Total rate cpm Obs	Potassium rate cpm Calc	Potassium rate cpm Obs	Calcium rate cpm Calc	Calcium rate cpm Obs
A	2.4 ±0.5	2.4 ±0.3	2.1 ±0.4	2.4 ±0.5	0.3 ±0.1	0 ±0.5
B	0.4 ±0.1	0.55 ±0.25	0	0 ±0.2	0.4 ±0.1	0.55 ±0.3

Assuming the fluorescence yield of potassium is 0.1, the half-life of Ca^{41} for K-capture is calculated from the foregoing data to be $1.2 \pm 0.4 \times 10^5$ years.

This disagrees markedly with the value of the "order of several months" recently obtained by Sailor and Floyd.[5] Surprisingly, these authors report no activity attributable to calcium x-rays.

Assuming the transition to be $f_{7/2} \rightarrow d_{3/2}$, Elliott[6] has suggested a half-life of 1.5×10^4 years, with upper and lower limits of 6×10^4 and 4×10^3 years. Our value is outside these limits, but errors in the assumed values of the (n, γ) cross section of Ca^{40} and the $K^{41}-Ca^{41}$ mass difference may be responsible.

A full report on this work is now in preparation.

[1] Richards, Smith, and Browne, Phys. Rev. **80**, 524 (1950).
[2] Kinsey, Bartholomew, and Walker (to be published).
[3] We wish to express our appreciation to Dr. D. B. Langmuir, USAEC Liaison Officer at Chalk River, who obtained this sample for us from the Isotope Division at Oak Ridge.
[4] These figures include a small effect due to a change in geometry. The former figure is calculated, the latter measured using a large source of irradiated ordinary Ca. The calculation of calcium K x-ray attenuation, which gives a higher figure, is too sensitive to possible non-uniformity of foil thickness to be reliable.
[5] V. L. Sailor and J. J. Floyd, Phys. Rev. **82**, 960 (1951).
[6] L. G. Elliott, private communication.

"Slow Beats" in F^{19} Nuclear Spin Echoes*

E. B. McNeil, C. P. Slichter, and H. S. Gutowsky
University of Illinois, Urbana, Illinois
(Received October 31, 1951)

HAHN has reported[1] a modulation, or "slow beat," in the proton spin echo envelope of ethanol. Steady state observations[2] of the F^{19} nuclear magnetic resonance in BrF_5 and IF_5 revealed a complex line structure which has been associated[3] with an interaction among the F^{19} nuclei, via a coupling with the nuclear magnetic shielding fields.[4] We have found that the F^{19} spin echoes in these compounds exhibit slow beats.[5] Herein are presented the results and an analysis, which show that the slow beats originate from the interaction responsible for the steady state multiplets.

The F^{19} steady state resonance[2] in BrF_5 and IF_5 consists of two groups of lines, the centers of which are separated by a chemical shift $\delta\Omega$. The components in each group are separated equally by an amount $\delta\omega$. Typical echo envelopes for BrF_5 are shown in Figs. 1 and 2. Each echo[1] occurs at 2τ, where τ is the time between the two rf pulses. There are two slow beat "frequencies" in the envelope. The difference in τ between successive maxima of the rapid variation satisfies the equation $\Delta\tau=2\pi/\delta\Omega$. The slower variation satisfies the relation $\Delta\tau=2\pi/\delta\omega$. Steady state experiments show that $\delta\Omega$ is proportional to applied magnetic field[4] and that $\delta\omega$ is independent of field.[5] The echo envelopes were observed at two different applied fields, and the "frequencies" satisfied the above equations.

Figures 3(a) and 3(b) show individual echoes. It is seen that they are similar to echoes obtained from samples containing two noninteracting nuclei whose Larmor frequencies differ by a chemical shift,[1] except for an asymmetry in our echoes. Qualitatively, the echo shape is similar to that obtained by multiplying a symmetrical echo by a function having the general shape of the echo envelope. Thus echoes of maximum or minimum height are symmetrical.

Simple interference among magnetic moments precessing at the different frequencies known from steady state experiments does not explain the observed slow beat amplitudes. It has been pointed out elsewhere[3] in connection with steady state experiments that there are good grounds for assuming two nuclei of spin $\mathbf{I}_1$ and $\mathbf{I}_2$ are coupled by an interaction of the form $\mathbf{I}_1\cdot\mathbf{I}_2$. Hahn and Maxwell have predicted[6] the echo envelope for a system of two spins on the assumption that there is a chemical shift between their Larmor frequencies and such a dot product coupling between the spins. Subsequently we have made calculations using the following

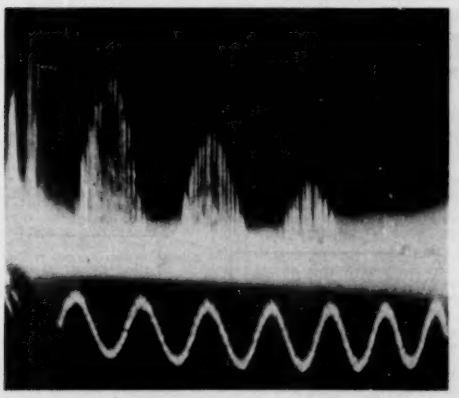

FIG. 1. The F^{19} echo envelope in BrF_5 at 30 Mc showing two modulation "frequencies." The envelope is obtained by multiple exposures; 60 cps timing below.

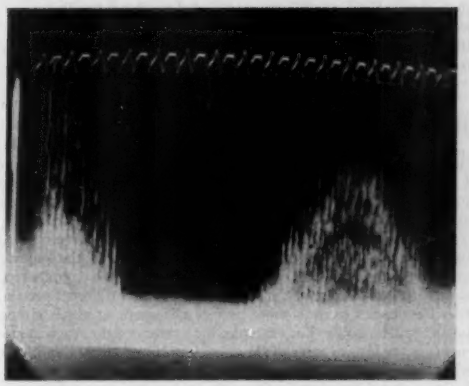

FIG. 2. First two groups of Fig. 1 on faster sweep to show the details better. Each of the sharp peaks is composed of several individual echoes.

Hamiltonian

$$H=\hbar\Omega I_{1z}+\hbar(\Omega+\delta\Omega)I_{2z}+\hbar\delta\omega I_{1z}I_{2z},$$

where Ω is the Larmor frequency of nucleus number one, and I_{1z} and I_{2z} are the components of spin of the two nuclei along the static applied field. Since in practice $\delta\Omega\gg\delta\omega$, this Hamiltonian is a close approximation to that obtained with dot product coupling, and may be considered as the Hamiltonian for a first-order per-

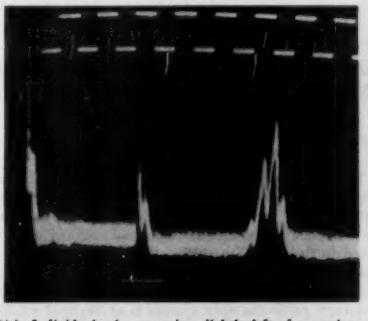

FIG. 3(a). Individual echo occurring slightly left of a maximum in the faster variation in Figs. 1 and 2. The distortion tends to follow the envelope shape.

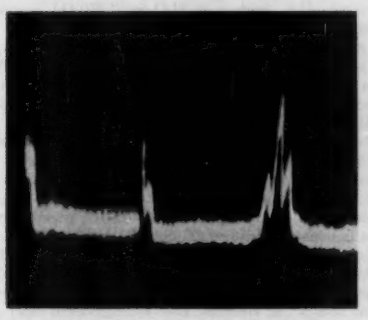

FIG. 3(b). Individual echo occurring slightly right of same maximum.

turbation calculation. We have carried through such calculations for $\omega_1 t_w = \pi/2$ in Hahn's notation[1] (spins turned through $\pi/2$ by the radiofrequency pulses) and $\omega_1 \gg \delta\Omega$, $\delta\omega$. We find the echo envelope is proportional to

$$|1+\cos\delta\omega\tau+(1-\cos\delta\omega\tau)\cos\delta\Omega\tau|.$$

This agrees with the results of Hahn and Maxwell.[6]

In addition, our calculation explains the echo asymmetries in the following manner. We consider separately the two spin groups 1 and 2 whose Larmor frequencies are chemically shifted relative to one another. At time $t=2\tau$ there is a resultant magnetization of group 1 and of group 2. The echo amplitude and asymmetry result from the following: (a) The length of the magnetization vectors is a function of τ. (b) The relative spatial orientation of the vectors at $t=2\tau$ depends on τ. Feature (b) accounts for the asymmetry, since if the vectors are not in phase at $t=2\tau$, their different precession frequencies cause a more perfect alignment at times either before or after $t=2\tau$. For example, the vectors might reach alignment on the leading edge of the echo, but not on the trailing edge with the result that the leading edge would be stronger than the trailing edge. The analysis shows that when $\delta\Omega\tau = n\pi$, where n is an integer, the vectors are in phase at $t=2\tau$, and the echo is symmetrical. This result is in agreement with the experimental facts mentioned earlier since these values of τ are the ones for which the envelope has a maximum or a minimum.

* Supported by the ONR.

[1] E. L. Hahn, Phys. Rev. **80**, 58 (1950).
[2] H. S. Gutowsky and C. J. Hoffman, J. Chem. Phys. (to be published.)
[3] Gutowsky, McCall, and Slichter, Phys. Rev. **84**, 589 (1951).
[4] W. C. Dickinson, Phys. Rev. **81**, 717 (1951); W. G. Proctor and F. C. Yu, Phys. Rev. **81**, 20 (1951).
[5] In a letter to HSG, E. L. Hahn stated he had found proton slow beats only in compounds having a fine structure in chemically shifted lines.
[6] E. L. Hahn and D. E. Maxwell, Phys. Rev. **84**, 1246 (1951). We are indebted to Dr. Hahn for sending us a copy of their letter in advance of publication.

Chemical Shift and Field Independent Frequency Modulation of the Spin Echo Envelope*

E. L. Hahn† and D. E. Maxwell
Stanford University, Stanford, California
(Received October 31, 1951)

FURTHER investigation of the echo envelope modulation effect[1] has been carried out and related to measurements made by slow passage nuclear resonance methods.[2,3] According to the echo method, two short, intent pulses of radiofrequency power are applied to the spin ensemble at the nuclear resonance condition, and are separated by time interval τ. The echo appears with a given maximum amplitude at time 2τ. At the onset of the first radiofrequency pulse the spin system is at thermal equilibrium. For each setting of τ the maximum of the echo signal is measured and plotted as a function of increasing τ. If the spin ensemble consists of magnetic moments located in equivalent chemical environments [i.e., protons in H_2O or $(CH_3)_2O$], a monotonic decay in the echo envelope is obtained.

The envelope modulation effect is observed in molecules in which nuclear magnetic dipoles have neighboring nuclear dipoles in nonequivalent chemical environments. Examples are dichloroacetaldehyde ($CHCl_2CHO$), 1-fluoro-1,2,2 trichloro-ethane ($CFClH-CCl_2H$), and ethyl alcohol (C_2H_5OH), where H and F^{19} are the resonant nuclei concerned. In general these molecules may fall into either of two classes which contain resonant nuclear moments in the following arrangements: A resonant nucleus (or chemically equivalent nuclei) may have one or more neighboring dipole nuclei which are (1) identical with the resonant one, but chemically nonequivalent, or (2) not identical.

In molecules such as $CHCl_2CHO$, C_2H_5OH,[1] and $CCl_3(CHCl)_2CCl_3$, two distinct modulation frequencies appear on the echo envelope: (1) One frequency corresponds to the difference in chemical shift,[4,5] δ, between two nonequivalent spin groups, which is measured by the slow passage method as a frequency difference between peaks of resonance signals.[2,3] (2) A second frequency, J, appears which is generally smaller than the frequency due to the chemical shift. This frequency is observed to be independent of the dc magnetic field H_0. In cases where it can be resolved[6] by the slow passage method[3,7] it is measured by the splitting of resonance lines belonging to equivalent spin groups.

If either of these frequencies is zero the modulation is absent. Many molecules exist (i.e., CH_3COOH) which have a chemical shift between nonequivalent nuclei as measured by the slow passage method. This shift, however, does not always appear on the echo envelope, but will only appear in those molecules in which these nuclei are sufficiently close neighbors. For these molecules the frequency J becomes finite, which in turn makes possible the appearance of the chemical shift on the echo envelope. For the special case involving two nonequivalent nuclei in CCl_2HCHO[8,9] these properties and the shape of the echo envelope can be predicted if the empirical Hamiltonian operator

$$\mathcal{H} = -\hbar[\gamma\sigma_{1z}(H_0+h_1)+\gamma\sigma_{2z}(H_0+h_2) + J(\sigma_{1x}\sigma_{2x}+\sigma_{1y}\sigma_{2y}+\sigma_{1z}\sigma_{2z})] \quad (1)$$

is chosen to describe the system. h_1 and h_2 are the absolute chemical shifts in gauss of the nuclei 1 and 2, respectively, and $\gamma(h_1-h_2)=\delta$. γ is the gyromagnetic ratio and σ_1, σ_2 are Pauli spin operators. The eigenvalues and the splitting which results in the stationary state are shown by the Zeeman level diagram in Fig. 1. The top and bottom levels are pure triplet states and each of the two closely spaced levels is a linear combination of singlet and triplet states. For $\delta \to 0$ the mixed state with the energy eigenvalue $J+(4J^2+\delta^2/4)^{\frac{1}{2}}$ now becomes a pure singlet state. The J splitting therefore disappears because transitions to and from the pure singlet state are forbidden. This supports the fact in the case of two equivalent nuclei that no J splitting is observed.[2,3,10]

The time-dependent population coefficients of each state have been evaluated under the initial conditions imposed by the application of two radiofrequency pulses. Each pulse at H_1 gauss maximum amplitude lasts for t_w seconds, where $t_w \ll \tau$ and $1/t_w$, $\gamma H_1 (=\omega_1) \gg \gamma\Delta H$, δ, J. ΔH is the magnitude of the external field inhomogeneity over the sample. For the case $\delta \gg J$ the expression for the observed echo amplitude (excluding damping due to relaxation) is given by

$$V = M_0|\sin^3(\omega_1 t_w/2)\sin(\omega_1 t_w)\cos(4J\tau)\sin^2(\delta\tau/2) - \cos(\omega_1 t_w)\cos^2(\delta\tau/2)+\tfrac{1}{2}\sin^2\omega_1 t_w \cos^2(\delta\tau/2)|, \quad (2)$$

where M_0 is the macroscopic magnetic moment. For $\omega_1 t_w = \pi/2$ the observed plot of the envelope due to protons in CCl_2HCHO is given in Fig. 2. The plot agrees with (2) within experimental error when normalized to unity in order to correct for damping due to T_2 (total relaxation time) and molecular diffusion.[1] A generalized form of the Hamiltonian operator (1) containing terms with more than two spin operators is now being used to calculate the shape of the echo envelope. The results thus obtained will be

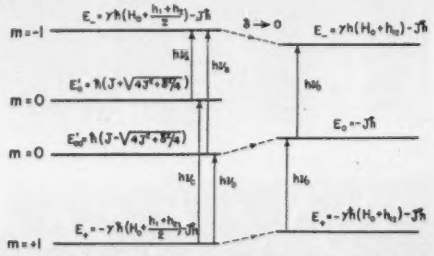

FIG. 1. Zeeman energy level diagram for a nonequivalent two spin system (for each spin, $I=\frac{1}{2}$). For $\delta \to 0$ the magnitude of $h_{12}=h_1=h_2$ chosen is arbitrary. For $\delta \sim J$ the intensities of the transitions indicated are determined by the particular transition probabilities between the given states as well as by their statistical weights. For δ finite, two pairs of resonance lines results where $h(\nu_C-\nu_B)=h(\nu_D-\nu_A)=4J\hbar$ is the separation between lines in each pair, and $h(\nu_B-\nu_A)=h(\nu_C-\nu_D)=2\hbar(4J^2+\delta^2/4)^{\frac{1}{2}}$.

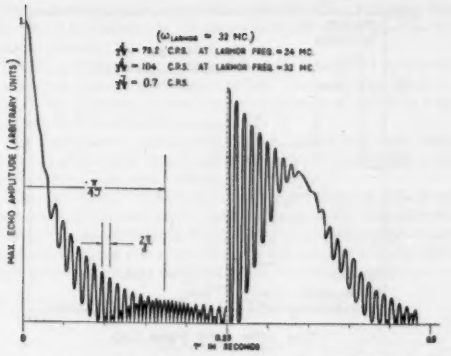
(ω LARMOR = 32 MC)
1/T = 79.2 C.P.S. AT LARMOR FREQ. = 24 MC.
1/T = 104 C.P.S. AT LARMOR FREQ. = 32 MC.
1/T = 0.7 C.P.S.
MAX. ECHO AMPLITUDE (ARBITRARY UNITS)
τ IN SECONDS

FIG. 2. Echo envelope plot for protons in dichloroacetaldehyde. The break in the plot at $\tau=0.25$ sec indicates continuation of the plot in the region of small echo amplitude, but multiplied by a factor in order to make the plot readable.

compared with experiment. Apart from explaining the shape of the echo envelope, its consistency with observations made by the slow passage method also remains to be established.

We are not prepared, at present, to propose a detailed mechanism which can explain the observed effects.[11] It is well known that the direct nuclear dipole-dipole coupling averages out completely due to the rapid and random rotations of a molecule in a liquid.[12] We wish to point out, however, that any anisotropy effects would prevent a complete averaging out of this coupling, and, for reasons of rotational invariance, could indeed be expected to lead to a Hamiltonian of the form (1).[13]

The authors are grateful to Professor F. Bloch for his valuable advice and suggestions. The authors are grateful to Gutowsky, McCall, and Slichter[5] for sending them a copy of their letter in advance of publication to which was later added (while in press) the suggestion, arrived at independently, that the J splitting depends on the interaction $\sigma_1 \cdot \sigma_2$. One of us (E. L. H.) wishes to thank the National Research Council for Fellowship support during the course of this research.

* This research supported in part by the ONR. See accompanying letter on independent work by McNeil, Slichter, and Gutowsky.
† National ResearchCouncil Post doctoral Fellow.
[1] E. L. Hahn, Phys. Rev. **80**, 580 (1950).
[2] Arnold, Dharmatti, and Packard, J. Chem. Phys. **19**, 507 (1951).
[3] H. S. Gutowsky and D. W. McCall, Phys. Rev. **82**, 748 (1951); Gutowsky, McCall, and Slichter, Phys. Rev. **84**, 589 (1951).
[4] W. G. Proctor and F. C. Yu, Phys. Rev. **77**, 717 (1950).
[5] W. C. Dickinson, Phys. Rev. **77**, 736 (1950).
[6] For long relaxation times the echo method has the advantage of being able to resolve frequencies of the order of 1 cps even though the external field inhomogeneity over the sample produces a spread in Larmor frequencies much greater than this.
[7] J. T. Arnold and M. E. Packard, Phys. Rev. **83**, 210 (1951).
[8] The rapid transfer between possible structural isomers of $CHCl_2CHO$ causes an averaging into two definite chemical shifts, one for each proton. This will result when the lifetimes in each isomeric state (obtained from known chemical potential barriers) are much shorter than the period associated with the observed frequency difference between chemical shifts (104 cps at a Larmor frequency of 32 Mc).
[9] Because of electric quadrupole broadening, the magnetic moments of the Cl^{35}, Cl^{37} nuclei are assumed to be ineffective because their quantum states have lifetimes short compared to the relaxation time of the protons and $1/J$.
[10] In references 3 it is observed that the J splitting depends upon the statistical weights of possible orientations of nonequivalent neighbors and the magnitude of their magnet moments.
[11] The operator (1) is formally obtained if one considers that two nonequivalent protons mutually exchange positions in the molecule by quantum mechanical exchange. Because of mass considerations, the exchange hypothesis is excluded since F^{19} nuclei are observed to exhibit the J splitting as well as protons.
[12] Bloembergen, Pound, and Purcell, Phys. Rev. **73**, 679 (1948).
[13] As a possible source of anisotropy we have considered that caused by the electron configuration. Gutowsky, McCall, and Slichter have also suggested that a coupling takes place via the electrons (see reference 3). This would be similar to the pseudo-quadrupole effect for a single nucleus, discussed by H. M. Foley, Phys. Rev. **72**, 504 (1947). This effect is also related, in its origin, to Ramsey's proposal [N. F. Ramsey, Phys. Rev. **78**, 699 (1950)] for explaining chemical shifts. It seems, however, difficult to reconcile the orders of magnitude of J to be thus expected with the experimental values.

$\pi^- - p$ Scattering Observed in a Diffusion Cloud Chamber*

R. P. SHUTT, E. C. FOWLER, D. H. MILLER, A. M. THORNDIKE, AND W. B. FOWLER
Brookhaven National Laboratory, Upton, New York
(Received October 25, 1951)

SCATTERING of 60-Mev negative pions has been observed in a diffusion cloud chamber similar to one previously mentioned,[1] operated in a pion beam at the Columbia University Nevis cyclotron.† The diffusion chamber shown in Fig. 1 was operated with 21 atmos of hydrogen and methanol vapor filling, bottom temperature −65°C and top +20°C. The track-sensitive layer was about 6 cm deep, starting at the bottom. The cyclotron ion source was pulsed every 4 to 6 sec so as to produce about 20 tracks which were photographed stereoscopically. Between pulses a clearing potential of about 1000V was applied while tracks settled out and vapor was replenished.

5600 pictures taken during the first day's operation have been examined. Since the pion beam contains some electrons and μ-mesons,[2] the pion path length was estimated from the fact that 642 $\pi-\mu$ decays in flight were observed with projected $\pi-\mu$ angles $>4°$ in one view. A correction of 30 percent must be applied to obtain the total number of $\pi-\mu$ decays of all angles. From the pion lifetime of 0.029 μsec,[3] pion energy, and hydrogen density, one can calculate that there is one $\pi-\mu$ decay per 2.0 g/cm^2 of hydrogen traversed, so that the total path length observed is 1670 g/cm^2.

From the angles, densities of ionization, ranges, and lack of multiple scattering of the tracks involved, $\pi^- - p$ scattering events can be identified with fair certainty. Among beam tracks scatterings of a few degrees that could be identified as electron-electron collisions were fairly numerous, but only three cases have been observed which can be considered to be $\pi^- - p$ scatterings, of which one is doubtful. The three events are very similar in appearance to the one shown in Fig. 2. The angles, measured from the incident pion direction, are: pion 54° and recoil proton 57° in the first case (Fig. 2); pion 70° and proton 44° in the second; pion leaves illuminated region and proton 35° in the third. It is not likely that scattering events were missed in scanning because the heavily ionizing recoil proton makes them more obvious than $\pi-\mu$ decays, and independent repeated scanning indicated an efficiency for observing $\pi-\mu$ decays of about 80 percent.

These data give a cross section of 3 millibarns for the scattering of 60-Mev negative pions by hydrogen, with a large statistical uncertainty. Chedester *et al.* have given a value of 13 millibarns

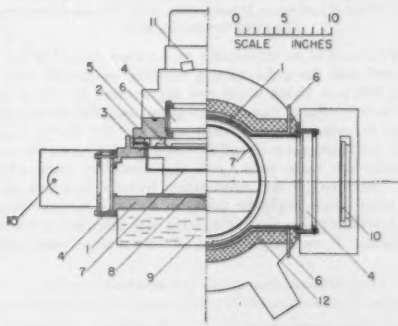

FIG. 1. Diagram of a high pressure diffusion chamber: chamber vessel (1), bottom plate and top flange cold-rolled steel, side walls $\frac{1}{2}$-in. stainless steel, velvet lined; top plate (2), cold-rolled steel; Bakelite ring (3), for thermal insulation; windows (4), inside $\frac{1}{2}$-in. "Allite" to withstand alcohol, outside "Plexiglas"; two concentric alcohol troughs (5), $\frac{1}{16}$-in. copper in thermal contact with (2); heater wires (6); sweeping field wires (7); black "Cararra" glass plate (8); dry ice—alcohol pan (9); light sources (10); stereoscopic camera (11); thermal insulation (12).

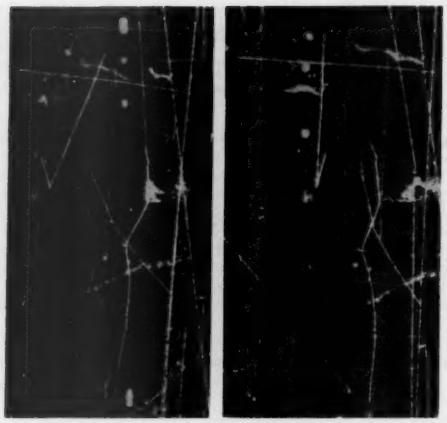

FIG. 2. Photograph of $\pi^- - p$ scattering. Event could be electron-proton scattering, but electron intensity is relatively small and Coulomb scattering through a large angle is extremely improbable.

for negative pions of 85 Mev.[3] The difference may be due to the difference in energy, or possibly to "charge exchange" scattering which would be missed in our experiment, or simply to our poor statistics. Our result agrees with a value of 2 to 4 mb calculated by Bethe and Wilson.[4]

We are indebted to the Nevis cyclotron staff for the opportunity to operate there and for the generous cooperation of members of the staff and operating crew. Many members at this laboratory contributed to this work, especially H. Marshak, R. Walker, and V. P. Kenney who have scanned many of the pictures.

* Work performed at the Brookhaven National Laboratory, Upton, New York, under the auspices of the AEC.
† Supported jointly by the ONR and AEC

[1] Miller, Fowler, and Shutt, Rev. Sci. Instr. **22**, 280 (1951).
[2] Lederman, Booth, Byfield, and Kessler, Phys. Rev. **83**, 685 (1951).
[3] Chedester, Isaacs, Sachs, and Steinberger, Phys. Rev. **82**, 958 (1951).
[4] H. A. Bethe and R. R. Wilson, Phys. Rev. **83**, 690 (1951).

Satellite Pulses from Photomultipliers*

T. N. K. GODFREY, F. B. HARRISON, AND J. W. KEUFFEL
Palmer Physical Laboratory, Princeton University, Princeton, New Jersey
(Received October 22, 1951)

IN the course of an experiment on μ-meson decay,[1] it was observed that the pulse from a scintillation counter was frequently followed within about one microsecond by one or more pulses, usually smaller than the first pulse, and that the frequency of these secondary pulses greatly exceeded the known rate of random noise pulses. Let us call the pulse which triggers the counting device the main pulse, and the secondary ones satellite pulses. The object of the investigation reported here was to find information which might be useful in devising methods of preventing satellite pulses from interfering with scintillation counting experiments. Three specific items of information were sought:

TABLE I. Comparison of noise and scintillation satellites.

Type of main pulse	Scintillation	Noise
Number of main pulses	140	129
Gross number of satellites	154	144
Estimated number of satellites due to random noise	30	10
Net number of satellites	124	134
Number of satellites per main pulse	0.89 ± 0.08	1.04 ± 0.09

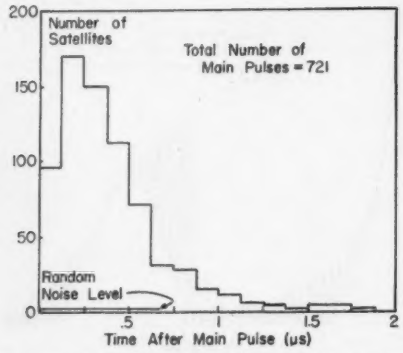

FIG. 1. Time distribution of satellites following scintillation pulses. The number of pulses shown in the first $\frac{1}{4}$-μsec channel is unreliable because there the presence of the main pulse made the search for small pulses difficult.

the source of the satellites, their distribution in time after the main pulse, and how their frequency of occurrence depends on the voltage applied to the photomultiplier.

In order to determine whether the satellites originate in the scintillator or in the photomultiplier, we took first a group of oscilloscope pictures in which the main pulse was known to be a scintillation pulse, and secondly, a group of pictures in which the main pulse was a noise pulse. The pulses from a 1P21 photomultiplier looking into a cell with a terphenyltoluene solution were sent through distributed amplifiers, and displayed on an oscilloscope trace. Scintillations in the solution were detected by using coincidences with an auxiliary photomultiplier to trigger the oscilloscope. When noise pulses were being studied, the cell was removed, and the oscilloscope was triggered directly by the photomultiplier pulses. The traces were photographed, and then searched for satellites, the smallest pulse accepted being 1/30 of the minimum main pulse size. To make sure that the effect studied did not arise in the amplifier or oscilloscope, we verified that fast artificial pulses did not give satellites. In addition, satellites were observed with setups involving several different amplifiers and oscilloscopes. Twelve photomultipliers, including both 1P21's and 5819's, were examined, and all showed satellites.

Table I gives the results of the analysis of the two groups of pictures taken to determine the source of the sattelites. The photomultiplier was run at 1100 volts. The errors quoted are statistical. The distributions in time of the satellites after the main pulses were similar in the two cases. After 1.5 μsec the curves were essentially flat; so the random noise rate in Table I was computed by counting the number of pulses on the last 4 μsec of the trace.

The fact that there are the same number of satellites per main pulse, within the statistical error, whether the main pulse comes

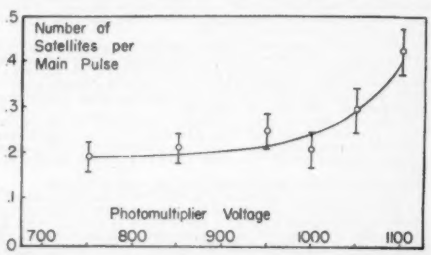

FIG. 2. Variation of satellite rate with photomultiplier voltage. The ordinate gives the number of satellites per trace greater than 1/15 of the minimum main pulse size.

from a scintillation or from photomultiplier noise, indicates that the satellites originate in the photomultiplier rather than in the counter solution.

The time distribution of the satellites was measured in another group of pictures of scintillation pulses. The results are given in Fig. 1. The variation of the rate of occurrence of satellites with photomultiplier voltage is shown in Fig. 2.

The time delays of the satellites are consistent with their being due to single positive ions, produced by the electrons of the main pulse, drifting back and striking an electrode.

In an experiment in which one records more than one pulse from the same scintillation counter—for instance, in the measurement of the π^+ meson lifetime—it will be necessary to take into account the multiple pulses due to satellites, which will give a background much greater than that calculated from the random noise rate.

* Supported by the joint program of the ONR and AEC.
[1] Harrison, Keuffel, and Reynolds, Phys. Rev. 83, 680 (1951).

An Energy Level in Li^6

WILLIAM M. HARRIS*
University of Rochester, Rochester, New York
(Received October 30, 1951)

PRIOR to the work reported herein and the concomitant investigation of Gove and Harvey,[1] there had been no conclusive evidence for the position of an energy level in Li^6.[2] Bjerge and Broström proposed a level at 3.7 Mev from the beta-decay of He^6,[3] and Pollard and Margenau deduced a level at 2.4 Mev from the resonance yield in the recoil deuterons when 2.6-Mev alpha-particles were scattered in deuterium.[4,5]

A level has been determined at 2.12 ± 0.05 Mev (Fig. 1) by using a single-focusing 180° magnetic spectrograph in conjunction with the 7-Mev proton beam of the Rochester 26″ cyclotron to measure the energy spectrum of protons scattered from an enriched target. The target was prepared from a sample of LiF, enriched in Li^6,[6] by evaporating the LiF onto a thin film of polystyrene. By bombarding through such a target (i.e., so that the spectrograph slit accepts scattered particles which have emerged from the "back" face of the target), the angles between the target plane, incident beam, and emergent beam can be so chosen as to permit a first-order correction for energy loss in the target.

The low mass of the Li^6 target nucleus created a difficult problem: In a given scattering experiment the energy carried away by the recoiling target nucleus is a function of the scattering angle, and the variation of the scattering angle over the aperture of the spectrograph introduces, for light nuclei, so large a change in the recoil energy as to interfere seriously with the conditions of 180° focusing. It was found, however, that the position of a line on which focus is restored can be computed in terms of the parameters of the experiment.

Eastman NTA plates were used for detection. Background was materially reduced by having the microscopist accept only those tracks whose orientation in the emulsion satisfied stringent criteria.

* Assisted in part by a grant from the Research Corporation of America. Now at Brookhaven National Laboratory, Upton, New York.
[1] H. E. Gove and J. A. Harvey, Phys. Rev. 82, 658 (1951).
[2] Browne, *et al.* [Phys. Rev. 83, 179 (1951)] announce a level at 2.19 Mev from the reaction $Be^9(p,\alpha)Li^{6*}$.
[3] T. Bjerge and K. J. Broström, Nature 135, 400 (1936).
[4] E. Pollard and H. Margenau, Phys. Rev. 47, 571 (1935).
[5] E. Pollard and H. Margenau, Phys. Rev. 47, 833 (1935).
[6] Obtained from the Stable Isotopes Division of Oak Ridge.

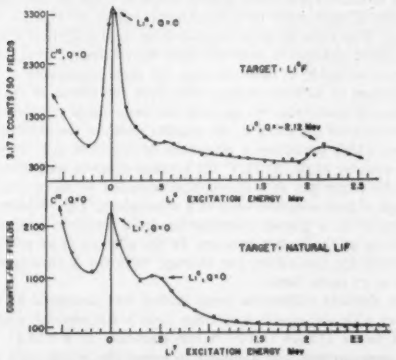

FIG. 1. Comparison of excitation curves obtained by proton scattering in which the targets were lithium fluoride enriched in Li^6, and natural lithium fluoride. The intensities have been normalized to correspond to the same bombarding flux per atom of lithium.

Shot Noise in Germanium Single Crystals*

G. B. HERZOG† AND A. VAN DER ZIEL
Department of Electrical Engineering, University of Minnesota, Minneapolis, Minnesota
(Received October 29, 1951)

THE excess noise of thin single-crystal Germanium filaments has been measured over the frequency range 1–1600 kc by connecting the filaments to the input of a sensitive selective amplifier and measuring the noise ratio n of the filament.[1] The filaments were of the type used by Montgomery and Shockley in their noise measurements at lower frequencies.[2] They consisted of N-type material, but the excess noise was found to be caused by the generation of holes at the surface of the filament. The lifetime of the holes was of the order of 10^{-4} sec. At lower frequencies the noise ratio could be represented by a formula:[2]

$$n=1+AI^2/f, \tag{1}$$

where I is the dc current and A a constant.

The noise of one of the filaments measured by us showed important deviations from (1) at higher frequencies; we found that the experimental values of n could be very well represented over a wide frequency range by a formula of the type (Fig. 1):

$$n=1+AI^2/f+BI^2/[1+(f/f_0)^2]. \tag{2}$$

At a filament current of 3 ma we found

$$AI^2=9.3\times10^6; \quad BI^2=54 \quad \text{and} \quad f_0=1.5\times10^5 \text{ cycles/sec};$$

f_0 was practically independent of the dc current.

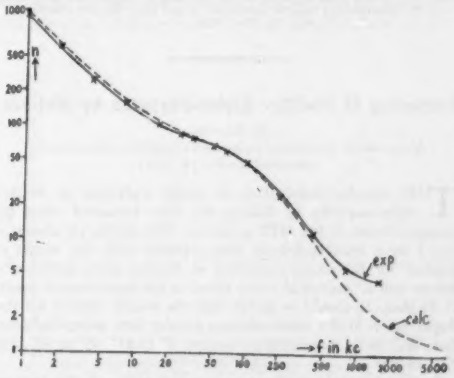

FIG. 1. Noise ratio n as a function of frequency for a current I of 3 ma. Crosses and full-drawn line: experimental results; dotted line: formula (2) with $AI^2=9.3\times10^6$; $BI^2=54$; $f_0=1.5\times10^5$ cycles/sec.

It was checked very carefully that this effect was real. We showed that it was not caused by noise generated in the end contacts of the filament, nor by a fault in the amplifier. We also showed that it was not caused by the input circuit of the amplifier nor by the presence of barriers in the Ge-filament; the input circuit incorporating the filament behaved as a simple RC circuit with frequency-independent values of R and C for the whole frequency range.

According to the theory[3] the shot effect in semiconductors resulting from carriers of charge $\pm e$, having an average lifetime τ_0 and a drift time τ and giving a contribution I_e to the dc current, is

$$\langle i^2\rangle_{hf}=2eI_d(\tau_0/\tau)\Delta f/[1+\tfrac{1}{3}(\omega\tau_0)^2] \quad (3)$$

if $\tau_0\ll\tau$. As $1/\tau$ is proportional to I_e, $\langle i^2\rangle_{hf}$ is actually proportional to I_d^2.

The third term in (2) can thus be interpreted as a shot effect term. The value $f_0=1.5\times10^5$ cycles/sec corresponds to a lifetime τ_0 of the carriers of 2×10^{-6} sec. As this is comparable to the lifetime of the holes in the filament reported by Montgomery and Shockley,[3] the third term in (2) can be interpreted as resulting from the shot effect of the holes.

N-type Ge-filaments should also show a shot effect of the electrons; this requires the addition of a term of the type

$$CI^2/[1+(f/f_1)^2] \quad (4)$$

to (2). $f_1\gg f_0$, as the time constant τ_1 involved in this process (representing the average time between the liberation of an electron from a donor atom and its subsequent temporary capture by an ionized donor) is much smaller than τ_0. Our measurements above 500 kc seem to indicate that such an effect exists but they do not extend to sufficiently high frequencies to establish this with certainty.

The relative importance of the terms $BI^2/[1+(f/f_0)^2]$, $CI^2/[1+(f/f_1)^2]$ and AI^2/f depends upon many factors such as the time constants τ_0 and τ_1, the conductivity of the material, the treatment of the surface of the filament, etc. For that reason it should not be expected that the noise of all Ge-filaments will show the same pronounced deviations from the $1/f$-law as reported here. In fact we found for another filament that the measurements were not accurate enough to detect deviations from the $1/f$-law.

* Supported by the Non-medical Research Fund of the University of Minnesota and by a Minneapolis-Honeywell Scholarship to one of us (G. B. H.). The Ge-single crystals were donated by the Bell Telephone Laboratories through the courtesy of Dr. H. C. Montgomery.

† Now at Radio Corporation of America Laboratories, Princeton, New Jersey.

[1] By excess noise we mean the noise generated by the flow of dc current which is over and above the thermal noise. The noise ratio n of a device is defined as: n = total available noise power of the device/available noise power of equivalent circuit at room temperature. $n=1$ if there is no excess noise; $(n-1)$ is a good measure for the amount of excess noise generated.

[2] H. C. Montgomery and W. Shockley, Phys. Rev. **78**, 646 (1950).

[3] A. van der Ziel, Physica **16**, 359 (1950).

Scattering of 30-Mev Alpha-Particles by Helium*

E. GRAVES†
Massachusetts Institute of Technology, Cambridge, Massachusetts
(Received October 26, 1951)

THE angular distribution of elastic scattering of 30-Mev alpha-particles by helium has been measured using the emergent beam of the MIT cyclotron. The results are shown in Fig. 1 on a semilogarithmic plot, together with the results of Mather[1] for the elastic scattering of 20-Mev alpha-particles by helium and a theoretical curve fitted to the experimental results at 30-Mev. It should be noted that the results plotted for this single region in the center-of-mass system were assembled from three regions in the laboratory system: 0° to 45°, 45° to 90°, and 270° to 360°.

Scattered alpha-particles were detected with a double proportional counter, which could be rotated within a 2-foot-diameter scattering chamber filled with helium at 1 or ½ atmosphere.[2] The outputs of the two shallow counters, located back to back, were placed in time coincidence to reduce background.

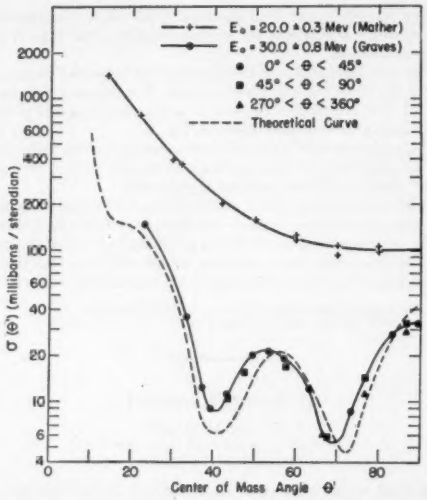
E₀ = 20.0 ± 0.3 Mev (Mather)
E₀ = 30.0 ± 0.8 Mev (Graves)
0° < Θ < 45°
45° < Θ < 90°
270° < Θ < 360°
Theoretical Curve
σ (Θ') (millibarns / steradian)
Center of Mass Angle Θ'

FIG. 1. The angular distribution of alpha-particles elastically scattered from helium, shown in the center-of-mass system on a semilogarithmic plot: at 20 Mev, according to the earlier work of K. B. Mather, and at 30 Mev, according to the present work, with a theoretical curve for scattering at 30 Mev based on three phase shifts: $\epsilon_0=-85.5°$, $\epsilon_2=+45.5°$, and $\epsilon_4=+35.5°$.

Intensities were measured using both differential and integral energy spectra, which were obtained by range analysis with a remotely controlled aluminum foil changer mounted in front of the counters. Differential spectra were obtained by "peaking" with a low level discriminator in the circuitry for the output of the second counter. The intensity was taken as proportional to the height of the integral "step" or to the area under the differential curve, with a correction for background when present. Alternate measurements at a normalization angle permitted correction for drifts in over-all counting efficiency. The measured intensity was multiplied by the factor $\sin\theta$ to correct for the change in scattering volume in the gaseous target with detector angle θ and by the factor $g(\theta)=\frac{1}{2}\cos\theta$ to convert laboratory intensity to center-of-mass intensity.

The estimated root-mean-square probable error for the relative intensity at each angle of measurement, except $\theta=11.6°$, is ±15 percent. This error includes contributions from statistical fluctuations, from changes in over-all counting efficiency, from an inaccuracy of ±0.5° in detector angle for each measurement, from fluctuations in incident energy, and from the effects of multiple small-angle scattering. No attempt has been made to correct the distribution for the effect of the angular width of the detector slit system, which permitted a maximum deviation of ±2° from the mean counter angle. At 11.6° the average of seven measurements with the target gas at 1 atmosphere exceeded by 40 percent the average of four measurements at ½ atmosphere. This difference is attributed to a greater contribution from multiple small-angle scattering at the higher pressure. In the absence of an adequate correction for this effect, the average value for ½ atmosphere is given as an upper limit.

The absolute differential cross section was measured by comparison with the elastic scattering from a 6.6 mg/cm² gold foil target to be $(2.8\pm0.7)\times10^{-26}$ cm²/steradian at $\theta'=83.2°$. The gold cross section was assumed to equal the Rutherford cross section, since earlier work by H. E. Gove at MIT revealed that the elastic scattering of 28-Mev alpha-particles from gold obeys the inverse $\sin^4(\theta/2)$ relationship back to $\theta=50°$.

A brief investigation revealed no evidence of an excited state in He^4 up to 14 Mev.

An expansion in partial waves, involving the 0th-, 2nd-, and 4th-order phase shifts due to nuclear scattering, has been fitted to the experimental data by the method of Wheeler.[3] We computed the ratio R of the experimental cross section to the Mott cross section[4] (center-of-mass system):

$$\sigma_{\text{Mott}}=(z^2e^2/mv^2)^2(\csc^4\theta+\sec^4\theta+2\Phi\csc^2\theta\sec^2\theta),$$

where $\Phi=\cos[(z^2e^2/\hbar v)\tan^2\theta]$. The partial wave expansion for this ratio is[4]

$$R(\theta)=|1+(ihv/z^2e^2)\sin^2\theta\exp[i(\hbar v/z^2e^2)\ln\sin^2\theta]$$
$$\Sigma_l\exp[2i(\zeta_l-\zeta_0)][\exp(2i\kappa_l)-1](2l+1)P_l(\cos2\theta)|^2,$$

in which the Coulomb component of the phase shift is

$$\zeta_l=\arg\Gamma[l+1+i(\hbar v/z^2e^2)],$$

and the nuclear components κ_l of the phase shifts are to be determined. $P_2(\cos2\theta)$ and $P_4(\cos2\theta)$ have zeros at three angles between 0° and 45°. A graphical solution in the complex plane yielded eight sets of values of κ_0, κ_2, and κ_4 consistent with the experimental values of R at these three angles. Only one of these sets gave substantial agreement with the experimental values of R at 20° and 45°:

$$\kappa_0=-85.5°,\quad \kappa_2=+45.5°,\quad \kappa_4=+35.5°.$$

The theoretical curve in Fig. 1 has been computed using this set of κ values and the expressions above for σ_{Mott} and R.

The writer is indebted to Dr. M. Stanley Livingston, Dr. Martin Deutsch, Dr. Henry Primakoff, and Dr. H. E. Gove for their invaluable advice and assistance in this research.

* Assisted by the joint program of the AEC and ONR.
† Major, U. S. Army, now stationed at SHAPE, APO 55, c/o Postmaster, New York, New York.

[1] K. B. Mather, Phys. Rev. **82**, 126 (1951).
[2] See Boyer, Gove, Harvey, Deutsch, and Livingston, Rev. Sci. Instr. **22**, 310 (1951) for a thorough description of the instrumentation of the emergent beam of the MIT cyclotron.
[3] J. A. Wheeler, Phys. Rev. **59**, 16 (1941).
[4] N. F. Mott and H. S. W. Massey, *The Theory of Atomic Collisions* (Oxford University Press, London, 1949), second edition.

Removal of Space Charge in Cadmium Sulfide Crystals and Their Conduction Properties under Electron Bombardment

R. Ramanna* and Ved Prakash Duggal
Tata Institute of Fundamental Research, Bombay, India
(Received September 21, 1951)

SINGLE crystals of cadmium sulfide were grown here by the method used by Frerichs.[1] These crystals were 2.5 cm long and 0.2 cm wide, with a thickness between 0.002 cm and 0.008 cm.

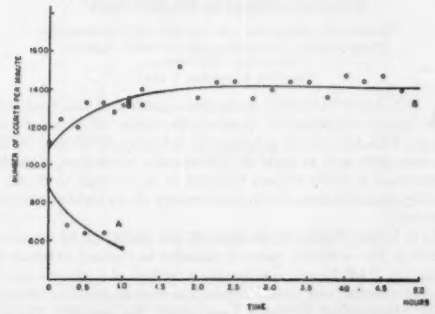

FIG. 1. Counting rate *versus* time. A. Crystal before heating. B. Crystal after heating for one minute.

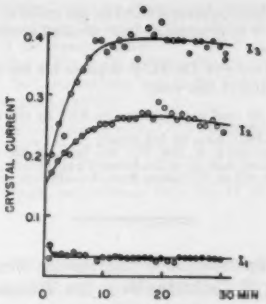

FIG. 2. Crystal current *versus* time. Electron energy 20 kev. Voltage across crystal 306 v. Incident current $I_3>I_2>I_1$.

A conventional arrangement was used for the detection of Po−α-particles by these crystals. The amplifier was similar to that described by Jordan and Bell.[2]

The space-charge formation in these crystals was studied, and it was found that the counting rate decreased rapidly with time, the effect being greater at lower fields across the crystal. In order to eliminate this effect the crystal was heated for one minute by means of a hot wire. It was found that for the first half hour the counting rate increased and then remained constant for about five hours. This method was tried for several crystals and found reliable. Figure 1 shows the counting rate before and after heating. This method of eliminating space charge by heating the crystal seems very successful in CdS because of its strong absorption in the infrared region. Corresponding effects have been observed in diamond when irradiated by violet and red light by Willardson and Danielson[3] and by heat by Pearlstein and Sutton.[4]

The conduction properties of CdS crystals under electron bombardment were also studied. The electrons were produced from an electron-gun and accelerated by a dc generator producing 100 kv. The amplification factor (current through the crystal/incident current) was found to be of the order of 10^3, and this remained constant for several hours. It seems that an equilibrium is reached between the electrons trapped and the reemission of these electrons resulting from the heating effect of the bombarding electrons. As shown in Fig. 2, the crystal current is steadier at smaller values of the incident current. The crystal currents for various energies of the incident electrons are shown in Fig. 3. The increase in the current is not linear, and this may possibly be because of the fact that at lower incident energies the surface effects play an important part.

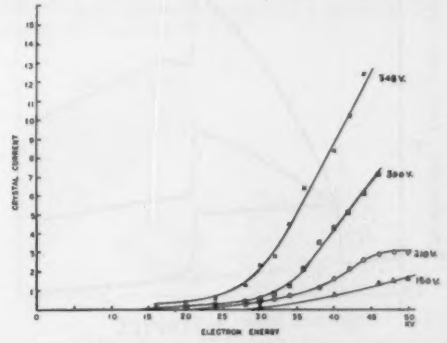

FIG. 3. Crystal current *versus* electron energy at various voltages across crystal.

A study of the temperature effect on the mobility of the conduction electrons is in progress and the detailed results will be published elsewhere.

Our thanks are due Dr. H. J. Bhabha for his encouragement during the course of this work.

* Member of the Staff appointed for the AEC by the Tata Institute of Fundamental Research.

[1] R. Frerichs, Phys. Rev. **72**, 594 (1947).
[2] W. H. Jordan and P. R. Bell, Rev. Sci. Instr. **18**, 703 (1947).
[3] R. K. Willardson and G. C. Danielson, Phys. Rev. **77**, 300 (1950).
[4] E. Pearlstein and R. B. Sutton, Phys. Rev. **79**, 217 (1950).

Spectral Dependence of Thermionic Emission from (Ba−Sr)O Cathodes over the Visible Region

TADATOSI HIBI AND KAZUO ISHIKAWA
Research Institute for Scientific Measurements, Tôhoku University, Sendai, Japan
(Received July 23, 1951)

As already reported,[1] the trapping energy of an electron in an isolated impurity center, according to the aggregation theory, seems to be higher than 1.32 ev. Expecting the appearance of some thermionic emission peaks, by analogy with the production of various color centers in alkali halides, we observed the spectral dependence of thermionic emission from oxide cathodes illuminated by light of the visible region.

In order to obtain monochromatic light various filters were used, but the wavelength region was limited to within 435–635 mμ owing to the kinds of filters available. Five commercial diodes "KX-142" were used as specimens and a 750-watt incandescent lamp as a light source. Since the variation of thermionic emission caused by the illumination was still small, the original emission was compensated, and only the effect of the light was measured with a microammeter. This observation was carried out repeating the checks on a standard in order to avoid irregularity of results because of changes in the physical conditions. The temperature of the oxide-coated cathodes was about 800°K.

Figure 1 is a typical example of the curves of variation of thermionic emission *versus* time. From this figure it is found that the thermionic emission rapidly increases for a short time and then slowly approaches the maximum emission current. The increase of emission current for a few seconds after the light illumination may be attributed to the external photoelectric effect. The thermionic emission peaks appear at about 460 mμ, 500 mμ, and 570 mμ, as is seen in Fig. 2. The amount of variation was different in five specimens, and the peak at 460 mμ did not appear in one of them. This peak always appeared, however, in each of the other four, with an experimental error of less than 2 percent in the wavelength. Though it is not yet known why the intensities of the peaks differ with every specimen, it is very important that the thermionic emission peaks exist at the definite wavelengths.

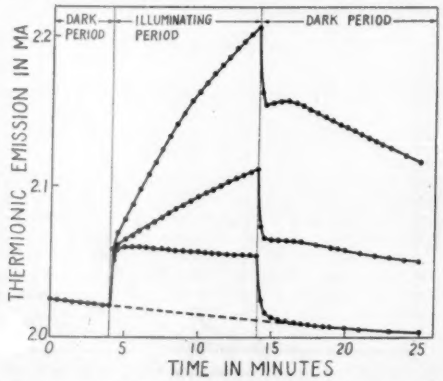

FIG. 1. A typical example of the curves giving the variation of thermionic emission as a result of the light illumination *versus* time.

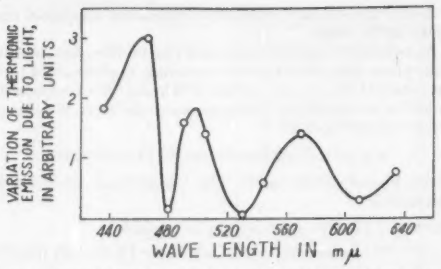

FIG. 2. Spectral dependence of the variation of thermionic emission.

The optical absorption, photoconductivity or photoelectric emission of single crystals or vaporization films of BaO or SrO were observed by Tyler,[2] Sproull,[3] and Dickey[4] in the ultraviolet region, and they found the photoelectric threshold value and one absorption peak in this region. Therefore, the result obtained here is very important in confirming experimentally the existence of several trapping levels (donators) between the filled band and the conduction band of oxide cathodes.

In this case it is necessary to call attention to the results of Stout,[5] who observed the luminescence of BaO produced by an electron bombardment of 3-kev energy over the 250–860-mμ range. According to his results, activated oxide shows an intense band at 410 mμ which is not obtained from inactive oxide, and, on the contrary, inactive oxide shows an intense band at 460 mμ which appears only faintly in the active sample. For an activated cathode, therefore, the appearance of a peak of thermionic emission at 410 mμ may also be expected. On the other hand, it may be expected from the aggregation theory that several peaks of the thermionic emission appear in the infrared region. In order to ascertain these facts, further accurate measurements are in progress.

[1] T. Hibi and K. Ishikawa, Phys. Rev. **83**, 659 (1951).
[2] W. W. Tyler, Phys. Rev. **76**, 179, 1887 (1949).
[3] R. L. Sproull, Phys. Rev. **78**, 630 (1950).
[4] J. E. Dickey and E. A. Taft, Phys. Rev. **80**, 308 (1950).
[5] V. L. Stout, Phys. Rev. **77**, 744 (1950).

Absence of a Detectable Diurnal Variation in the Frequency of Heavy Primaries and Nuclear Disintegrations at 80,000 Feet*

GORDON W. MCCLURE AND MARTIN A. POMERANTZ
Bartol Research Foundation of the Franklin Institute, Swarthmore, Pennsylvania
(Received November 1, 1951)

A BALLOON-BORNE ionization chamber of the type previously employed to measure the variation of burst frequency with altitude at geomagnetic latitudes 52°N[1] and 69°N[2] has been sent aloft at night at Minneapolis, Minnesota, with the cooperation of ONR Project Skyhook in an attempt to detect a possible diurnal fluctuation in the intensity of the burst-producing radiation.

As in former flights, the instrument was calibrated by means of a built-in Po−α source, and was adjusted to respond to bursts of ionization $\geq$1.0 Po−α. Our standard method of burst-telemetering and recording was used. Altitude data were supplied by General Mills Aeronautical Research Laboratory. To maintain the internal temperature at a safe level during the night, the gondola

was wrapped in a 3-inch layer of cellulose padding and was heated electrically by storage batteries.

According to preflight plans, the instrument was to reach about 80,000 feet shortly after sundown and remain near that level until the following afternoon. Had this performance been realized, data from the Minnesota flight alone would have sufficed to establish the magnitude of the diurnal effect. Actually, the balloon altitude dropped rather rapidly after midnight and did not increase again at daybreak; consequently, it was necessary to compare the night counting rates at Minneapolis (geomag. lat. 55°N) with the day rates recorded at Swarthmore (geomag. lat. 52°N). The necessity of relying on the data from a single night flight is not regarded as a serious source of error, since variations in the data obtained from different instruments in numerous flights at Swarthmore and Ft. Churchill have been within the statistical uncertainties.

The latitude effect between Swarthmore and Minneapolis for this type of instrument is regarded as negligible in the light of previous measurements which have established that the daytime burst rates are the same at 52°N and 69°N at all altitudes up to 100,000 feet.

The altitudes and burst rates recorded during the night flight are plotted in Fig. 1. The dashed curve represents the counting rates averaged from four daytime flights at corresponding altitudes. The night counting rates are in excellent agreement with the day rates at all altitudes attained between sunset and sunrise. If a diurnal variation in the burst rate exists at all, its magnitude does not exceed the combined statistical and systematic uncertainties which are estimated as ±5 percent.

According to a previous analysis[1] of the daytime results, 37 percent of the bursts at 80,000 feet are caused by primary heavy nuclei of charge $Z \geq 8$ and the remainder by nuclear disintegrations occurring in the chamber walls. Excluding the possibility that the intensities of the heavy nuclei and of the star-producing radiation vary from night to day in opposite senses (an increase in one being partially compensated by a decrease in the other), it is concluded that the heavy nucleus intensity does not change by more than ±13 percent, nor the frequency of stars by more than ±9 percent from night to day.

Photographic emulsion results[2] have indicated that the diurnal variation in the frequency of stars at balloon altitudes is smaller than 5 percent. On the other hand, the available emulsion data concerning heavy nuclei[3-6] seem to show a nighttime drop in intensity of 50 to 70 percent below the daytime value for nuclei with $Z \geq 10$.

If the emulsion evidence is correct on both points, the ion chamber rates should have been 18 to 26 percent lower during the night, at 80,000 feet. Such an effect is not observed and indeed lies considerably outside the range of the systematic and statistical uncertainties in the present results.

We are grateful to Mr. A. T. Bauman for the arrangement and supervision of the balloon flight, and to the National Geographic Society for continued support.

* Assisted by the joint program of the ONR and AEC.

[1] G. W. McClure and M. A. Pomerantz, Phys. Rev. 79, 911 (1950).
[2] Results to be published.
[3] J. J. Lord and M. Schein, Phys. Rev. 78, 484 (1950).
[4] J. J. Lord and M. Schein, Phys. Rev. 80, 304 (1950).
[5] Freier, Ney, Naugle, and Anderson, Phys. Rev. 79, 206 (1950).

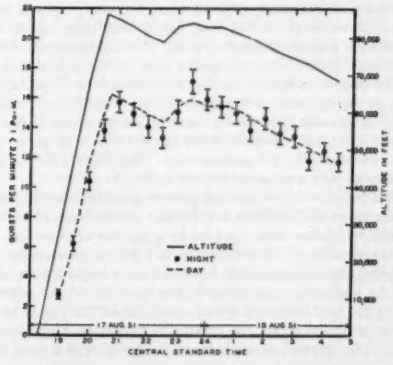

FIG. 1. Altitude *vs* time curve (solid line) for night flight at geomagnetic latitude 55°N and counting rates (solid circles) obtained with ionization chamber biased to record bursts ≥ 1 Po $-\alpha$. Counting rates averaged from four daytime flights (dashed curve) at corresponding altitudes show no significant deviations from night rates.

Isolation of Radioactive C^{11} Formed by the Interaction of π^- Mesons on Oxygen and Nitrogen*

A. TURKEVICH AND J. B. NIDAY
Institute for Nuclear Studies, University of Chicago, Chicago, Illinois
(Received November 2, 1951)

PHOTOGRAPHIC plate studies[1] on nuclear stars produced by mesons imply that the residual nucleus left after the evaporation of neutrons and protons should often be radioactive. The 145-Mev π^- meson beam at the University of Chicago synchrocyclotron has been found to be sufficiently intense and free from other high energy particles to detect this expected production of radioactivity. The reactions leading to the formation of $C^{11}(\beta^+, 20.5\text{ m})$ that have been observed are

$$O^{16}(\pi^-; p, 4n)C^{11} \text{ and/or } O^{16}(\pi^-; 5n)N^{11} \xrightarrow{\beta^+} C^{11}$$

and

$$N^{14}(\pi^-; 3n)C^{11}.$$

The experimental arrangment is indicated in Fig. 1. Negative π-mesons are produced in the synchrocyclotron by the bombardment of an internal target with 450-Mev protons. The trajectories of the mesons produced in a forward direction are such as to bring them out of the vacuum chamber through a thin Lucite window. A channel through the six-foot iron shield of the cyclotron accepts only those mesons that have energies in the range of 140–150 Mev. After emerging from the shield they are bent through 45° by the analyzing magnet *A*. The intensity of the meson beam is measured by counting coincidences in two large liquid scintillation counters *B* and *C*. At least 98 percent of the coincidences disappear if the analyzing magnet field is changed appreciably from the correct value for 145-Mev π^- mesons.

The magnetic analysis establishes the sign and momentum of the charged particles. That the particles have the proper mass was established by a measurement of their range in aluminum and carbon[2] and by the measurement of their velocity using a Čerenkov detector.[3] Analysis of the range curve established the constitution of the beam as being 94±4 percent π^- mesons, 6±4 percent μ^- mesons, and <1 percent electrons.[3]

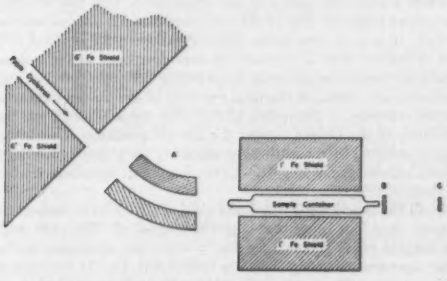

FIG. 1. Experimental arrangements for the irradiation of samples with π^- mesons.

TABLE I. Yields of C^{11} from π^- interaction with H_2O and NH_4NO_3 solutions.

Initial activity of C^{11} (counts/min)[a]	Saturation activity of C^{11} at 1-watt level (dis/min)[b]	Saturation activity of C^{11} at 1-watt level with analyzing magnet off (dis/min)	Net activity of C^{11} resulting from mesons (dis/min)	Meson intensity at 1-watt level (mesons/min)[c]	Yield of C^{11} per meson (percent)
Experiments with H_2O					
26	127	27	100	4500	2.3
46	159	5	155	9350	1.6
63	123	5	118	9250	1.3
53	162	14	148	6950	2.1
46	171	14	157	7100	2.2
				Average = 1.9 ± 0.4	
Experiments with 11M NH_4NO_3 solutions					
70	236	41	195	6500	3.0
58	296	41	255	5600	4.6
44	264	41	223	5650	4.0
57	268	9	259	9300	2.8
86	268	9	259	10000	2.6
57	459	36	423	9100	4.6
66	332	36	296	9450	3.1
34	355	36	318	8400	3.8
64	220	9	211	6750	3.1
123	285	9	276	6950	4.0
				Average = 3.6 ± 0.6	

[a] This represents the activity in counts/min (background subtracted) about ½ hr after a 40-min irradiation.
[b] Activity of C^{11} expressed in disintegrations per minute immediately after an infinite irradiation corrected for chemical yield. Customary irradiations were for about forty minutes at a level of 4 to 12 watts, and the usual chemical yield was 60 percent. The counting efficiency was 22 percent.
[c] This represents the meson intensity with the analyzing magnetic field set at the correct value for 145-Mev π^-. The meson intensity with the magnet off was less than two percent of this value.

The samples to be irradiated were placed between the analyzing magnet A and the first crystal counter B. They consisted of 4 liters of acidified water or saturated NH_4NO_3 solution (pH~3.5) in gas-tight glass vessels of about 4-inch diameter. The solutions also contained about 15 mg of CO_2 added as $NaHCO_3$, and in the last experiments, some CO. The path length for the mesons in the samples was in all cases appreciably greater than the range. About one-third of the mesons of this energy can be expected to undergo nuclear interactions before being slowed down; the remainder react after losing their kinetic energy.

After irradiation the radiocarbon in the chemical forms of CO and CO_2 was swept out of the sample with an inert gas, passed over hot CuO to oxidize the CO to CO_2, and then absorbed in 100 ml of dilute NaOH solution. Calcium carbonate was precipitated from the solution and the precipitate was mounted and counted with an end-window Geiger tube.[4] It was established that the radioactivity produced decayed with the expected half-life of 20.5 minutes and that the radiations had the proper absorption characteristics for C^{11}. Postponing the addition of the few milligrams of the carbon carrier until after the irradiation did not decrease the yield.

Table I gives the results of our experiments with and without the proper magnetic field in the analyzing magnet. The saturation activity in a given irradiation (disintegrations per minute of C^{11}) was calculated from a record of the heat developed in the meson-producing target (usual levels of operation were between four and twelve watts), from the chemical recovery of the C^{11} (as measured by the recovery of the added CO or CO_2 carrier), and from the efficiency of the Geiger counter for the C^{11} positrons. This latter was established by measuring the efficiency for a sample having a known number of disintegrations per minute and radiations similar to those of C^{11}.

In all the experiments listed, the yield of C^{11} with the magnet on is more than four times that with the magnet off. The yield with the magnet off is presumably due to stray fast neutrons. In the later experiments (using the extra iron shield, Fig. 1) the ratio is nine or greater. The results indicate that C^{11} is the product of about two percent of the interactions of the mesons with O^{16}. Since the experiments measure only that C^{11} that ends up in the chemical forms of CO or CO_2, the true yield may be a little higher.

The yield of C^{11} with the NH_4NO_3 solutions appears to be significantly higher. Although chemical effects in the NH_4NO_3 solution leading to a larger fraction of the radioactive carbon as CO and CO_2 cannot be completely ruled out, the results are explicable by postulating a fourfold higher yield of C^{11} from N^{14} than from O^{16}.

This work was made possible by the advice and equipment of Professor H. L. Anderson and by the cooperation of Mr. Ronald Martin.

* This research has been supported in part by a grant from the AEC.
[1] W. B. Chesterton and L. J. B. Goldfarb, Phys. Rev. **78**, 683 (1950).
[2] H. L. Anderson (private communication).
[3] John Marshall (private communication).
[4] The very low activity samples were usually measured with a Geiger tube shielded by iron and lead and anticoincidence counters such that the background was 2.3 counts/min. The authors gratefully acknowledge the use of this equipment of the Argonne National Laboratory.

Electric Forming of n-Germanium Transistors Using Donor-Alloy Contacts

R. L. LONGINI
Electronics and Nuclear Physics Department, Westinghouse Research Laboratories, East Pittsburgh, Pennsylvania
(Received November 2, 1951)

STELMAK[1] shows that the presence of phosphorus (a donor material) in the collector probe is important for good collector formation in n-type germanium. He suggests that this is caused by the superficial diffusion of phosphorus into the germanium.

The process of diffusion into the germanium most probably involves the more rapid diffusion of lattice vacancies. These vacancies, in their random motion, permit diffusion of the impurity, but simultaneously themselves diffuse into the germanium. Furthermore, they must precede the impurity in this diffusion process. The maximum density of vacancies and impurities is, however, determined by the temperature for the former and the saturation solution for the latter (which may be temperature dependent). However, the density of impurity diffused into the germanium adjacent to the surface (the saturation density of impurity) is not dependent on the lattice-vacancy density, which merely determines the diffusion rate.[2]

It is proposed here that this combination of lattice vacancies and impurities can give rise to a $p-n$ hook[3] region near the probe, and that the process of electrical forming may consist of producing such a region.

Assuming a lattice-vacancy mechanism of diffusion of impurities, it follows that there will be a high density of impurities near the probe which drops off rapidly with distance from the probe. The density of vacancies, depending on the energy of the pulse, will be high at the probe but dropping off much less rapidly with distance than does the impurity content. For a proper pulse energy the vacancy density near the probe may be much less than the impurity density. Adjacent to the probe there is in all probability an n-type region because of high donor impurity density, whereas slightly farther out there is certainly an excess of vacancies and therefore a p-type region. Still farther out the bulk germanium n-type characteristic will predominate. Thus there will be a $p-n$ hook surrounding a properly formed collector.

Such a region will give rise to a current amplification (α) greater than the value of 2.5 which is expected[4] on the basis of mobility alone and which has been reported by a number of observers.

An examination of the possibilities in a p-type germanium transistor show that no equivalent hook (an $n-p$ hook) is possible, as again the vacancies must precede the impurity of the collector. An acceptor type impurity would merely make the region around the collector more p-type, as would the vacancies. Thus electrons would not be trapped as are holes in the p region of a $p-n$ hook.

[1] J. P. Stelmak, Phys. Rev. **83**, 165 (1951).
[2] R. M. Barrer, *Diffusion in and Through Solids* (University Press, Cambridge, England, 1941).
[3] Shockley, Sparks, and Teal, Phys. Rev. **85**, 151 (1951).
[4] L. P. Hunter, Phys. Rev. **77**, 558 (1950).

Low Temperature Polymorphic Transformation in WO_3

B. T. Matthias and Elizabeth A. Wood
Bell Telephone Laboratories, Murray Hill, New Jersey
(Received October 24, 1951)

TUNGSTEN trioxide has been described as having a triclinic structure of corner-linked WO_6 octahedra at room temperature[1] and a tetragonal structure at 740°C.[2] We have found a polymorphic transformation near −50°C below which the symmetry is again higher. The temperature of the transition varies widely with small variations in the composition of the crystals. The transformation has been repeatedly observed with the polarizing microscope and confirmed by x-ray diffraction photographs, both Laue type and powder.

Kehl, Hay, and Wahl find that the structure of the high temperature tetragonal form is that suggested by Kittel for an antiferroelectric crystal.[3] When WO_3 is placed in an alternating electric field at −198°C, a hysteresis loop is observed, indicating that it is ferroelectric at this temperature.[4] An x-ray diffraction pattern taken by Matthias[5] near this temperature is closely similar to that taken at −60°C and the structure is probably the same.

These observations suggest that WO_3 has a high temperature, antiferroelectric tetragonal form and a low temperature, ferroelectric form. The form at intermediate temperatures[1] may or may not be ferroelectric.[6]

[1] Haakon Bräkken, Z. Krist. **78**, 484 (1931).
[2] Kehl, Hay, and Wahl, Phys. Rev. **82**, 774 (1951).
[3] Private communication, to be published soon in J. Appl. Phys.
[4] B. T. Matthias, Phys. Rev. **76**, 430 (1949).
[5] At the University of Chicago, Chicago, Illinois.
[6] Sawada, Ando, and Nomura, Phys. Rev. **82**, 952 (1951).

"Anomalous" $\pi-\mu$ Decay*

H. Primakoff
Washington University, St. Louis, Missouri
(Received October 26, 1951)

THE process of $\pi-\mu$ decay of a slow π-meson $\pi\to\mu+\nu$, involving as it does the sudden creation of a rapidly moving charged particle (the μ-meson with velocity $\approx(3/10)c$), is necessarily accompanied by the simultaneous production of a spectrum of "soft" photons.[1] Such soft photons have been theoretically predicted[2] and experimentally observed[3] in the analogous situation of nuclear β-decay, while Feer[4] and Schiff[5] have given theoretical discussions of the expected soft photon intensity accompanying, respectively, the β-decay of a μ-meson[6] and the creation of a π-meson in a nucleon-nucleon collision. In the present note we wish to report the theoretically expected result for the soft photon intensity produced in $\pi-\mu$ decay; we find that occasionally—probability per decay $\approx 10^{-2}$ to 10^{-4}—the soft photon spectrum accompanying the emitted μ-meson carries away so much energy that the μ-meson appears with an "anomalously" small energy, and therefore an anomalously short range in, for example, a photographic emulsion.

More specifically, application of the energy and momentum conservation laws to the $\pi-\mu$ decay with accompanying soft photon emission gives, to a rough but sufficient approximation,

$$E_\mu = E_\mu^{(0)}(1-\epsilon/\epsilon_{\max}). \tag{1}$$

In Eq. (1) E_μ is the kinetic energy of the emitted μ-meson, and $E_\mu^{(0)}=(m_\pi-m_\mu)^2/2m_\pi=4.15$ Mev is the maximum value of this kinetic energy; ϵ is the total energy carried off by the soft photon spectrum accompanying the μ-meson, and $\epsilon_{\max}=\frac{1}{2}(m_\pi-m_\mu)=17.1$ Mev is the maximum value of this total energy; m_π, m_μ are the π-meson and μ-meson rest energies; the angular distribution of the soft photons relative to the μ-meson velocity direction has been taken, as is true to lowest order in 1/137, as following the $\sin^2$ law. Further, the probability that any particular $\pi-\mu$ decay is accompanied by a soft photon spectrum carrying off a total energy between ϵ and $\epsilon+d\epsilon$ is[7]

$$P(\epsilon)d\epsilon = A(\epsilon/\epsilon_{\max})^4 d\epsilon/\epsilon;\ \int_0^\infty P(\epsilon)d\epsilon = 1 \tag{2}$$

with

$$A\approx(2/3\pi)(1/137)(2E_\mu^{(0)}/m_\mu).$$

Equation (2) yields, as a numerical example, a probability of 1/5000 for emission of a soft photon spectrum with total energy between $\frac{1}{4}\epsilon_{\max}$ and $\frac{3}{4}\epsilon_{\max}$; this corresponds, from Eq. (1), to a μ-meson energy E_μ between $\frac{1}{2}E_\mu^{(0)}$ and $\frac{1}{4}E_\mu^{(0)}$, i.e., to a μ-meson range R between $(5/6)^{1.7}$ and $(1/4)^{1.7}$ times the "normal" range,[8] or to 450 microns $\geqq R\geqq 60$ microns. Experimentally, first Smith, and then Gross, working in Sagane's group at Berkeley have found several "anomalously" short tracks in an examination of some 1000 $\pi-\mu$ decays,[9] Branson, Seifert, and Havens[10] report one such anomalously short μ-meson track, with length less than 450 microns (235 microns), in a study of 1500 $\pi-\mu$ decays, while Fry[11] finds four μ-meson tracks which can be definitely considered as anomalously short (260, 258, 185, 120 microns) in 3018 decays. The longer two of Fry's four anomalous tracks can conceivably be interpreted as originating in $\pi-\mu$ decay in flight with backward emission of the μ in the π's rest frame; in the case of his two shorter tracks, however, such an assumption leads to calculated π-meson velocities and so to estimated grain densities which do not correspond to observation.[11]

The above discussion makes it obvious that much more experimental $\pi-\mu$ decay data are necessary before any agreement or disagreement with the present theory can be considered as at all statistically significant; if a disagreement is eventually indicated, as, for example, would be the case if a greater prevalence of anomalously short tracks were found than is predicted by Eqs. (2) and (1), other possibilities of interpretation of a majority of the short tracks will have to be entertained. One such, already suggested by Fry,[11] involves the assumption of a relatively rare alternative mode of decay of the π-meson; another interpretation would postulate the possession by the μ-meson of a relatively improbable (more or less catastrophic) energy loss mechanism operating in addition to the usual atomic excitation and ionization. The implied μ-meson nucleus interaction cross section, assuming this last explanation, would, however, be too large by many orders of magnitude to reconcile with the otherwise known properties of the μ-meson.

We wish to thank Dr. R. W. Williams and Dr. W. B. Cheston for helpful discussion of the possible interpretation of the anomalously short tracks.

* Assisted by the joint program of the ONR and AEC.
[1] See the discussion of the basic theory of soft photons in F. Bloch and A. Nordsieck, Phys. Rev. **52**, 54 (1937), and in W. Pauli and M. Fierz, Nuovo cimento **15**, 167 (1938). An application to soft photon emission in hard photon radiation processes is given in H. Primakoff and F. Villars, Phys. Rev. **83**, 686 (1951).
[2] J. K. Knipp and G. E. Uhlenbeck, Physica **3**, 425 (1936); F. Bloch, Phys. Rev. **50**, 272 (1936); C. S. W. Chang and D. Falkoff, Phys. Rev. **76**, 365 (1949).
[3] L. Madansky and F. Rasetti, Phys. Rev. **83**, 187 (1951) and earlier references there given; T. B. Novey, Phys. Rev. **84**, 145 (1951).
[4] D. Feer, Phys. Rev. **75**, 931 (1949).
[5] L. I. Schiff, Phys. Rev. **76**, 89 (1949).
[6] Feer (reference 4) assumes however a two-particle decay scheme: $\mu\to e+\nu$.
[7] Equation (2) is obtained by a field theoretic extension to the case where a (nonrelativistic) charged particle is created or destroyed, of the argument required to obtain the probability of soft photon emission in the case of an atomic electron transition with emission or absorption of a hard photon. The expressions for the soft photon emission probabilities are actually essentially identical in the two cases, as may be seen by comparing Eq. (2) with Eqs. (1), (2) of the last reference of footnote 1. It may also be remarked that the general argument of the references of footnote 1 may be used to show that, in the overwhelming majority of individual instances of emission (e.g., during $\pi-\mu$ decay) of a soft photon spectrum carrying a total energy between ϵ and $\epsilon+d\epsilon$, this spectrum consists of a single fairly energetic soft photon with energy $\eta\approx\epsilon$, and of an associated indefinite (infinite) number of very soft photons with total energy $\epsilon-\eta\ll\epsilon$.
[8] The "normal" $\pi-\mu$ decay μ-meson range in C2 emulsions is about 600 microns; in these emulsions, $R=\text{const}(E_\mu)^{1.7}$. See C. F. Powell, Reports on Progress in Physics, **13**, 350 (1950).
[9] Private communication.
[10] Bramson, Seifert, and Havens, Bull. Am. Phys. Soc. **26**, No. 6, 23 (1951).
[11] W. C. Fry, Phys. Rev. **83**, 1268 (1951).

The Solution of the Janossy G-Equation

H. MESSEL
Department of Mathematical Physics, University of Adelaide, Adelaide, Australia
AND
G. W. GARDNER
National Research Council of Canada, Chalk River, Ontario
(Received October 29, 1951)

JANOSSY[1] in a recent paper gave the following equation describing the development of a nucleon cascade in homogeneous nuclear matter,

$$\Phi(\epsilon, n_1, n_2; x)=\int_0^x \exp[-(x-\theta)]d\theta \times \sum_{\substack{n_1'+n_1''=n_1\\ n_2'+n_2''=n_2}} \int_0^\infty \int_0^\infty \Phi(\epsilon/\epsilon_1, n_1', n_2'; \theta)\Phi(\epsilon/\epsilon_2, n_1'', n_2''; \theta) \times w(\epsilon_1, \epsilon_2)d\epsilon_1 d\epsilon_2, \quad (1)$$

where $\Phi(\epsilon, n_1, n_2; x)$ expresses the probability of finding n_1 nucleons with energies $>\epsilon E_0$ and n_2 nucleons with energies $<\epsilon E_0$ at a depth x in homogeneous nuclear matter as a result of a single primary nucleon of energy E_0. The cross section for nucleon-nucleon collisions is given by $w(\epsilon_1, \epsilon_2)d\epsilon_1 d\epsilon_2$. The difficulty of solving Eq. (1) directly led Janossy to introduce a generating function defined by

$$G(\epsilon, U; x)=\Sigma_N U^N \Phi(\epsilon, N; x), \quad (2)$$

in which U is written for u_1 and u_2; N for $n_1; n_2$ and U^N for $u_1^{n_1}, u_2^{n_2}$. Equation (1) was then transformed into

$$\frac{\partial}{\partial x}G(\epsilon, U; x)+G(\epsilon, U; x) =\int_0^\infty \int_0^\infty G(\epsilon/\epsilon_1, U; x)G(\epsilon/\epsilon_2, U; x)w(\epsilon_1, \epsilon_2)d\epsilon_1 d\epsilon_2 \quad (3)$$

with the initial condition

$$G(\epsilon, u_1, u_2; 0)=\begin{cases} u_1 & \text{for } \epsilon<1 \\ u_2 & \text{for } \epsilon>1. \end{cases} \quad (4)$$

We have been able to develop methods whereby the solution of Eq. (1) may be obtained without resorting to the G equation. We find

$$\Phi(\epsilon, n_1, n_2; x)=2^{n-1}f_n(x)/n!(n-1)! \times \int_0^\epsilon \cdots \int_0^\epsilon \int_\epsilon^1 \cdots \int_\epsilon^1 L_n\Lambda_n(s_1, \cdots, s_n)ds_1 \cdots ds_n \quad (5)$$

with $n_1+n_2=n$ and

$$f_n(x)=e^{-x}(1-e^{-x})^{n-1}. \quad (6)$$

L_n is the n-fold inverse Mellin transform operator expressed by

$$L_n=\frac{1}{(2\pi i)^n}\int_{s_1'-i\infty}^{s_1'+i\infty} \cdots \int_{s_n'-i\infty}^{s_n'+i\infty} \epsilon_1^{-(s_1+1)} \cdots \epsilon^{-(s_n+1)}ds_1 \cdots ds_n \quad (7)$$

and

$$\Lambda_n(s_1, \cdots, s_n)=\sum_{a\neq b}{}^1 W(s_a, s_b) \sum_{a\neq b\neq c\neq d}{}^2 W(s_c, s_d) \cdots \times \sum_{a\neq b\neq \cdots \neq y\neq z}{}^{n-1} W(s_y, s_z) \quad (8)$$

with

$$W(s_1, s_2)=\int_0^\infty \int_0^\infty \epsilon_1^{s_1}\epsilon_2^{s_2}w(\epsilon_1, \epsilon_2)d\epsilon_1 d\epsilon_2. \quad (9)$$

The superscripts beside each summation refer to the order in which the summations are carried out. The first summation yields W functions for all possible combinations of the n variables s_i, $i=1, \cdots, n$ taken two at a time. The second summation then gives W functions for all possible combinations of the $n-1$ variables $s_a+s_b, s_1', \cdots, s_{n-2}'$ taken two at a time; similarly the third summation gives W functions for all possible combinations of the $n-2$ variables, $s_a+s_d, s_1', \cdots, s_{n-3}'$ taken two at a time, and so on for the remainder of the summations.

The solution of the G equation (3), is now immediately given by Eqs. (2) and (5).

We have been successful in solving the complete fluctuation problem in nucleon cascade theory, and the results with details shall be presented in a subsequent publication. The methods developed are moreover directly applicable to the similar problem in electron-photon cascade theory. We shall present, shortly, solutions for the distribution functions and Janossy G-equations in this instance as well.

[1] L. Janossy, Proc. Phys. Soc. (London) **A63**, 241 (1949).

Electrostatic Fields in Close-Packed Crystals

L. LORNE CAMPBELL,* JOSEPH M. KELLER, AND ERNEST KOENIGSBERG
Department of Physics and Institute for Atomic Research, Iowa State College, Ames, Iowa
(Received November 2, 1951)

THE splitting of free atomic or ionic energy levels by the electrostatic fields within a crystal is believed to play an important part in various phenomena (specific heat, magnetic susceptibility, etc.) in solids. In his original work on crystalline fields, Bethe[1] pointed out the usefulness of expanding the potentials in spherical harmonics. He also showed that for a crystal with cubic (point) symmetry, no spherical harmonics occur of degree less than 4. Bethe estimated the magnitude of the different terms for an ionic crystal by using Madelung's[2] method to expand the potential, and by calculating appropriate derivatives at the atomic positions.

We have been interested in electrostatic fields of metals in hexagonal close-packed and cubic-face centered crystals. In hexagonal crystals, spherical harmonics occur of degree 2 and 3, as well as higher degrees. In order to determine the magnitudes of spherical harmonics up to the 4th degree, we have approximated a metal as a collection of positive point charges of magnitude q at the ion sites, superimposed on a uniform negative charge of density ρ. For such a model, Madelung's method of calculating the potential cannot be used.

We choose the origin at the position of an ion. Then for a sufficiently large crystal the potential at small distances can be represented in spherical coordinates as

$$V=q/r-(2\pi/3)\rho r^2+\Sigma_{l,m}A_{lm}r^lY_l^m(\vartheta, \varphi), \quad (1)$$

where the Y_l^m are surface spherical harmonics. The sum in Eq. (1) contains contributions from all the ions except that at the origin. It is possible to express the coefficients A_{lm} as

$$A_{lm}=[4\pi/(2l+1)]q\Sigma R^{-(l+1)}Y_l^m(\Theta, \Phi), \quad (2)$$

where R, Θ, Φ are coordinates of one of the ions, and the sum is taken over all ions (except the one at the origin).

Equation (2) provides a suitable method of calculating the coefficients for $l\geq 4$. The factor $R^{-(l+1)}$ makes the contributions of successive neighbors fall off in a sufficiently rapid way. For $l=2$ and 3, we used Ewald's[3] method of calculating the potential near the origin, and took appropriate derivatives.

For a hexagonal close-packed crystal with lattice parameters b perpendicular to the hexagonal axis, and c along the axis, we consider ions at $(x, y, z)=(0, 0, 0)$ and $(0, b/\sqrt{3}, c/2)$ in the unit cell. Writing the potential near the origin in the form,

$$V=q/r+(8\pi/3\sqrt{3})q\rho^2/b^2c+k_1(2z^2-x^2-y^2)+k_2(y^3-3x^2y) +k_3[8z^4-24z^2(x^2+y^2)+3(x^2+y^2)^2]+\ldots, \quad (3)$$

we find for the "ideal" ratio of lattice parameters, $c/b=(8/3)^{\frac{1}{2}}$,

$$k_1=(0.001692\pm 0.000004)q/b^3, \quad k_2=(0.43780\pm 0.00002)q/b^4, \quad k_3=(0.1134\pm 0.0014)q/b^5. \quad (4)$$

Other spherical harmonics of degree 4 and less do not occur in Eq. (3) because of crystal symmetry.

We have also calculated derivatives of k_1 and k_2 with respect to the lattice parameter c. For $c/b=(8/3)^{\frac{1}{2}}$, we find

$$dk_1/dc=(-1.10721\pm0.00006)q/b^4, \quad (5)$$
$$dk_2/dc=(-1.60363\pm0.00010)q/b^5.$$

For a face-centered cubic crystal of cubic lattice parameter a, the potential takes the form,

$$V=q/r+(8\pi/3)qr^3/a^3 +k_4[x^4+y^4+z^4-3(x^2y^2+x^2z^2+y^2z^2)]+\ldots, \quad (6)$$

where coordinate axes are chosen parallel to cube edges, and

$$k_4=(-7.653\pm0.035)q/a^5. \quad (7)$$

The arrangement of ions in a hexagonal close-packed crystal with ideal ratio of c/b is very similar to that in a face-centered cubic crystal. For the case $a=\sqrt{2}b$, the ions in each crystal have 12 nearest neighbors, with the same spacing, and almost the same arrangement. Nevertheless, not only does the hexagonal potential have extra terms, but even the 4th degree harmonics in the two cases differ in both form and magnitude.

In assuming a uniform distribution of conduction electrons, the model we have used neglects screening by these electrons. This screening is likely to be different for the different harmonics or multipoles.

* Now at the Department of Applied Mathematics, University of Toronto, Toronto, Canada.

[1] H. A. Bethe, Ann. Physik **3**, 133 (1929).

[2] M. Born and M. Goeppert-Mayer, *Handbuch der Physik* (Springer, Berlin, Germany, 1933), Vol. XXIV, Part 2, p. 709.

[3] M. Born and M. Goeppert-Mayer, *Handbuch der Physik* (Springer, Berlin, Germany, 1933), Vol. XXIV, Part 2, p. 710.

Photoconductivity of Trapped Electrons in KBr Crystals at Room Temperature

J. J. Oberly
Crystal Branch, Metallurgy Division, Naval Research Laboratory, Washington, D. C.

(Received October 26, 1951)

THE room temperature photoconductivity of all the stable color center absorption bands attributed to electrons trapped at lattice defects has been reported briefly for KCl[1] and for KBr.[2] The quantitative data for KBr generally verified the initial findings with KCl and allowed a comparison of the product ηw—quantum yield times electron range—for the various bands. This note will discuss the KBr results in more detail. The crystals were colored by x-rays from a Machlett AEG-50A tube having a tungsten target and beryllium window and were polarized by 500 volts dc while continuous records of photocurrent *vs* wavelength were made.

Soft x-rays produce the F-absorption band and a much weaker M-absorption band, both of which are photoconductive. After a very short x-irradiation, when the M-band is too weak to be observed, a peak is found in the photoresponse (photocurrent/incident energy) at the M-band wavelength which is 500 times weaker than the F-peak. Further x-irradiation strengthens both absorption bands and their photoresponse until the condition shown in Fig. 1 is obtained. The splitting of the F-peak can be attributed to the inhomogeneous distribution of F-centers produced by soft x-rays. Since F-centers are good electron traps, the range being inversely proportional to F-center concentration, they make the photoresponse smaller at the center of the band where the monochromatic light is absorbed in a high concentration of F-centers near the entrance surface. Unstable centers (F'), which have a lifetime of the order of a second, form and decay during the measurement, raising the photoresponse nonuniformly. This is evident in the difference between the two curves obtained by sweeping in opposite directions through the spectral region.

Illuminating the crystal with F-light (F-bleach) weakens the F-band and also affects the M-band and forms the R-, N-, and

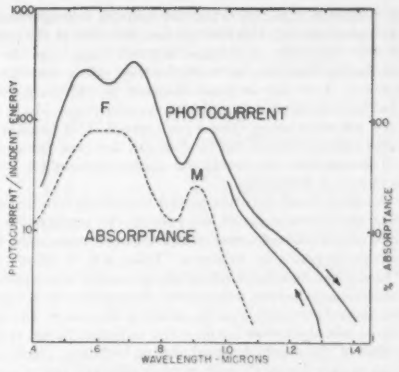

FIG. 1. Photoresponse and absorptance of F- and M-centers in KBr after long exposure to soft x-rays.

L-bands (R_1 and R_2 are not usually resolved in KBr at room temperature; L designates the short wavelength companion of the F-band). It is found that F photoresponse is not proportional to absorptance during F-bleach. This is shown in Fig. 2(a) for a crystal x-rayed through $\frac{1}{16}$-inch aluminum to produce a more homogeneous distribution of F-centers. The rate of weakening during bleaching is much greater in F photoresponse than in F absorptance, and a decrease in the rate of weakening during bleaching is evident in both. This greater effect on photoresponse

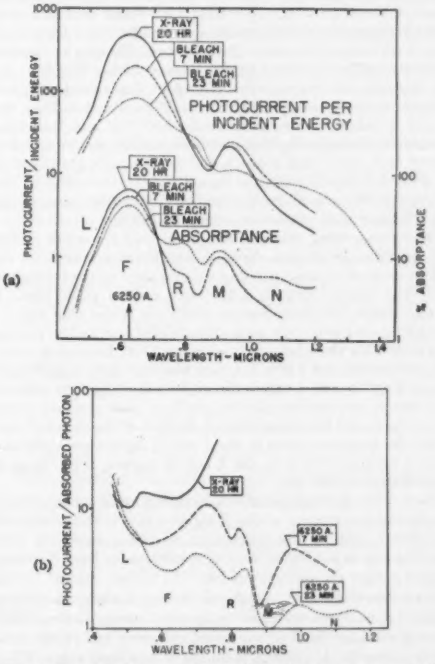

FIG. 2. Trapped electron centers in KBr after long exposure to hard x-rays and subsequent F-bleach: (a) photoresponse and absorptance; (b) product of quantum yield and electron range (ηw) in arbitrary units.

is also evident in Fig. 2(b) where the ordinate is proportional to the ratio photocurrent absorbed photon and thus to the product ηw. If the destruction of F-center electron traps were the only process during bleaching, ηw would increase rather than decrease as observed. A similar decrease observed in additively colored KCl has been attributed to colloidal electron traps[3] which, however, are not expected in these x-ray crystals. It is possible that the other centers formed during F-bleach are even better traps than F-centers, but this would not readily account for the decrease in rate of weakening.

On the other hand, both the greater weakening rate for photoresponse and the decrease in the rate can be explained by the existence of two kinds of centers which together produce the F-absorption as suggested by Przibram.[4] These will be called "soft" and "hard," the bleachable-photoconductive and the nonbleachable-nonphotoconductive, respectively. X-rays form both with the relative amounts depending on the nature of the x-rays. The superposition of two absorption bands is also indicated by the familiar small shift of the absorption peak during bleaching which is not apparent in this figure. Petroff[5] recently reported that F-centers in additively colored KCl transform into M-centers by way of an intermediate stage (B-centers) whose absorption coincides with the F-band, but no such genetic relationship is yet apparent between soft and hard centers. The changing stability of the F-band during bleaching has recently been attributed to a changing capture cross section of V-centers for the electrons freed from F-centers,[6] the stability increasing with decreasing cross section. However, such a mechanism would produce an increase in ηw during bleaching, rather than the observed decrease, since the decreasing cross section would allow the range of the electron to increase.

The photoconductivity of the other color center bands is also shown in Figs. 2(a) and 2(b). The well-known increase and decrease of the M-band during F-bleach is evident in Fig. 2(a) in both photoresponse and absorptance, the height above the general curve level being significant in the latter case. The greater decrease in photoresponse compared to absorptance during F-bleach, and the occurrence of the same effect during M-bleach (with M-light), indicate the existence of soft and hard M-centers also. Thus, the F- and M-bands are similar in having both soft and hard components; their similarity is also evident in their greater stability to heat than the R- and N-bands and in their rapid growth while the R- and N-bands disappear during a short x-irradiation. The L-, R-, and N-bands all have corresponding photoresponse peaks which become more prominent during F-bleach.

The corresponding values of the product ηw are shown in Fig. 2(b). If the range w were the same for electrons freed from the various types of centers, each curve would show relative quantum yield. The minima located at the band centers would result if for any reason the photoresponse peaks are flatter than the absorptance peaks or if some more efficient photoconductive process is present over the whole spectral range. The R'-band is broad and photoconductive but it has been observed only in additively colored KCl.[7] In the L-region the product is not greatly affected by F-bleach, but elsewhere it changes by a fairly constant factor during the second bleaching interval. In both of the bleached conditions the quantum yields in the F and R regions are equal and about 3 times the yields in the R and N regions, if the range is assumed constant for all.

When F-bleach is continued still further, a minimum appears in the photoresponse curve at the F region which is then similar to the curve in Fig. 1. The appearance of such a minimum after bleaching can be attributed only to absorption by hard F-centers remaining after the soft centers near the surface entered by the light are bleached away. As shown in Fig. 3 where the photocurrent has not been corrected to an equal energy basis, further F-bleach weakens the F photocurrent still more and at the same time weakens the M and builds up the N to a fixed value. While these changes take place, the R photocurrent remains constant. This unusual stability of photoconductivity is even more evident

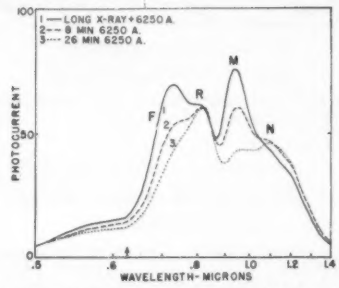

FIG. 3. Effect of further F-bleach on photoconductivity of the trapped electron centers in KBr.

during irradiation with R-light for several hours; the R photo current changes very little, while F and M photocurrent o- either side weaken considerably.

The writer wishes to express his appreciation to Elias Burstein for the suggestion of this problem and for his continued interest in the work.

[1] J. J. Oberly and E. Burstein, Phys. Rev. **79**, 217 (1950).
[2] J. J. Oberly, Phys. Rev. **83**, 228 (1951).
[3] G. Glaser, Gött. Nachr., Fachgruppe II, **3**, 31 (1937).
[4] K. Przibram, Z. Physik **68**, 403 (1931).
[5] St. Petroff, Z. Physik **127**, 443 (1950).
[6] Casler, Pringsheim, and Yuster, J. Chem. Phys. **18**, 887 (1950).
[7] A. B. Scott and L. P. Bupp, Phys. Rev. **79**, 341 (1950).

Equivalence of the S-Matrix in Different Representations

L. M. YANG
University of Edinburgh, Edinburgh, Scotland
(Received October 5, 1951)

SINCE the first formulation of the S-matrix[1] in the interaction representation, the corresponding S-matrix in the Heisenberg representation has been defined by Yang and Feldman,[2] and shown to be equivalent to the S-matrix of Dyson. It will be pointed out in this note that the equivalence of the S-matrix in different representations can be directly inferred to hold generally from kinematical considerations without having to go through explicit transformation for each particular set of fields. For this purpose one observes that a matrix element of the type $\langle\chi(\sigma)|F(\sigma)|\Psi(\sigma)\rangle$, where $\Psi(\sigma)$, $\chi(\sigma)$ are two state vectors of the system referring to the same space-like surface σ and $F(\sigma)$ any dynamical variable of the system, corresponds to a measurement on the surface σ; its value for the same σ is therefore independent of the representation used. For convenience we assume that the surface corresponds to $t=$constant and that the interaction is turned on and off at t_i and t_f, respectively. (In the limit one can have $t_i\to-\infty$ and $t_f\to+\infty$.) In particular, when $t=t_f$ we have

$$\langle\chi_I(t_f,t_i)|F_I(t_f,t_i)|\Psi_I(t_f,t_i)\rangle=\langle\chi_H(t_f)|F_H(t_f,t_i)|\Psi_H(t_f)\rangle,$$

where the subscripts I and H indicate operators and state vectors in the interaction and Heisenberg representation, respectively. To go from the Heisenberg to the interaction representations, one uses the unitary operator $S(t,t_i)$ defined by

$$i\hbar(\partial/\partial t)S(t,t_i)=V_I(t)S(t,t_i),\quad S(t_i,t_i)=1,$$

where $V_I(t)$ is the interaction energy in the interaction representation. Thus for any time t between t_i and t_f we have

$$|\Psi_I(t,t_i)\rangle=S(t,t_i)|\Psi_H(t)\rangle,$$
$$F_H(t,t_i)=S^\dagger(t,t_i)F_I(t,t_i)S(t,t_i).$$

For $t=t_f$, $S(t_f, t_i)$ is in the limit $t_i \to -\infty$, $t_f \to \infty$ the S-matrix of Dyson, and for $F_H(t_f, t_i)$ one has

$$F_H(t_f, t_i) = S^\dagger(t_f, t_i) F_I(t_f, t_i) S(t_f, t_i). \quad (1)$$

Now $F_H(t_f, t_i)$ is the outgoing operator $F_H{}^{\text{out}}$, and $F_I(t_f, t_i)$, which moves in the Hilbert space like a free field operator, differs from $F_I(t_i, t_i)$ only by a constant phase factor. But at t_i we have

$$F_I(t_i, t_i) = F_H(t_i, t_i) = F_H{}^{\text{in}}.$$

Thus we have shown that, apart from an unimportant constant phase factor, Eq. (1) is just the definition of the S-matrix in the Heisenberg representation

$$F_H{}^{\text{out}} = S^\dagger F_H{}^{\text{in}} S,$$

where F_H stands for any of the field operators.

One can of course define the S-matrix in the Schroedinger representation. In a recent paper, Wu[3] has obtained an S-matrix identical with Dyson's by starting from the Schroedinger representation and using conventional perturbation theory. But he is essentially working in the interaction representation after the general wave amplitude is expanded in terms of the time-dependent energy eigenfunctions of the unperturbed Hamiltonian.

[1] F. J. Dyson, Phys. Rev. **75**, 486 (1949); **75**, 1736 (1949).
[2] C. N. Yang and D. Feldman, Phys. Rev. **79**, 972 (1950).
[3] Shi-Shu Wu, Phys. Rev. **83**, 730 (1951).

Principle of Detailed Balance

F. COESTER
State University of Iowa, Iowa City, Iowa
(Received October 8, 1951)

ACCORDING to Hamilton and Peng[1] the principle of detailed balance cannot be expected to hold in quantum theory when perturbation theory is not applicable. In the concrete case which they discuss, the principle holds, however, if averages over the spin variables are taken. Heitler[1] conjectures that this is true, in general. The purpose of this note is to show that the principle of detailed balance holds rigorously in a form slightly different from that implied by Heitler, Hamilton, and Peng, and to give a proof for Heitler's conjecture.

The principle of detailed balance may be stated as follows: *The transition probabilities for a certain process and its inverse are always equal.* This statement needs, however, to be supplemented by a definition of the inverse of a given transition. Hamilton and Peng consider the transition $B \to A$ to be the inverse of the transition $A \to B$. Detailed balance would then imply symmetry properties of the S-matrix which cannot be expected to hold in general. On the other hand detailed balance becomes a simple consequence of the invariance of the interaction under time reversal if we adopt the following definition: *The inverse of a given transition is obtained by reversal of the time.*

The operation of time reversal in quantum mechanics has been investigated by Wigner.[2] Generalizing slightly Wigner's results, we note the relation,

$$K\Psi(p, s, t) = U\Psi^*(-p, -s, -t). \quad (1)$$

K denotes the operator of time reversal, p stands for the momenta of all the particles present, and s for their spin variables. The star indicates the complex conjugate. U is a unitary operator which operates on the spin variables only. For one particle with spin $\frac{1}{2}$ we have $U=\sigma_2$, and for one particle with spin 1 we have $U=-1$, if the usual representation of the spin matrices

$$\sigma_2 = \begin{pmatrix} 0 & -i \\ i & 0 \end{pmatrix}$$

is assumed. In the most general case we need only form the appropriate product of one-particle operators. From these remarks it can be seen that U is also Hermitian and that

$$(UHU)^* = UH^*U \quad (2)$$

for any operator H which does not change the number of Fermions by an odd number. The interaction Hamiltonian and consequently the S-matrix have this property. The invariance under time reversal of the Hamiltonian in the interaction representation can be stated in the equation,

$$(p', s'|H(t)|p, s) = (p', s'|KH(t)K^{-1}|p, s) = (-p', -s'|UH(-t)U|-p, -s)^*. \quad (3)$$

Since H is Hermitian and U unitary, there follows

$$(p', s'|H(t)|p, s) = (-p, -s|UH(-t)U|-p', -s'). \quad (4)$$

In order to exploit the relation (4) for the proof of the principle of detailed balance, we write the S-matrix in the form,

$$S = 1 + \sum_{n=1}^{\infty} (-i)^n \int dt_n \ldots \int dt_1 \theta(t_n, t_{n-1}) \ldots \theta(t_2, t_1) H(t_n) \ldots H(t_1), \quad (5)$$

where

$$\theta(t_2, t_1) = \begin{cases} 1 & \text{if } t_2 > t_1 \\ 0 & \text{if } t_2 < t_1, \end{cases}$$

and hence

$$\theta(t_2, t_1) = \theta(-t_1, -t_2). \quad (6)$$

From (4) follows

$$(p', s'|H(t_n) \ldots H(t_1)|p, s) = (-p, -s|UH(-t_1) \ldots H(-t_n)U|-p', -s'), \quad (7)$$

and hence with (5) and (6)

$$(p', s'|S|p, s) = (-p, -s|USU|-p', -s') = \pm(-p, -s|S|-p', -s'). \quad (8)$$

The last step follows from the representation for U described above and the fact that S does not change the number of Fermions by an odd number.

From Eq. (8) follows immediately that the transition probabilities for the transition $p, s \to p', s'$ and $-p', -s' \to -p, -s$ are equal. This proves the general validity of the principle of detailed balance provided the interaction is invariant under time reversal and an appropriate definition for the inverse of a transition is adopted.

Moreover, upon summation over the spin variables one finds

$$\Sigma_s \Sigma_{s'} |(-p, -s|S|-p', -s')|^2 = \Sigma_s \Sigma_{s'} |(p, s|S|p', s')|^2. \quad (9)$$

This follows from the invariance of the transition probability under reflection of the coordinate axes. Combining (8) and (9) we find

$$\Sigma_s \Sigma_{s'} |(p, s|S|p', s')|^2 = \Sigma_s \Sigma_{s'} |(p', s'|S|p, s)|^2. \quad (10)$$

This completes the proof of Heitler's conjecture.

I am indebted to Dr. J. M. Jauch for clarifying discussions on the subject of time reversal.

[1] J. Hamilton and H. W. Peng, Proc. Roy. Ir. Acad. **A49**, 197 (1944). See also W. Heitler, *Quantum Theory of Radiation* (Oxford University Press, London, 1944) second edition, p. 252.
[2] E. P. Wigner, Göttinger Nachr. 546 (1932).

Perturbation Theory and Configuration Space Methods in Field Theory*

S. SCHWEBER
Palmer Physical Laboratory, Princeton University, Princeton, New Jersey
(Received October 24, 1951)

WE have investigated the configuration space treatment of relativistic field theories, both in coordinate and momentum space, with the aim of treating problems of interacting fields.

One of the problems being analyzed is the two-body problem in the neutral scalar and pseudoscalar meson theory. This has been previously investigated by Tamm[1] and by Dancoff,[2] who, how-

ever, neglected the influence of pair formation, and more recently by Jean,[3] using methods similar to those developed independently by us.[4]

We would like to point out that, within this framework, bound state problems can be treated in a manner which yields in a natural fashion a somewhat better perturbation calculus than the usual one. The method consists in retaining only a limited number of particle-wave functions in configuration space, and thus can only be formulated in a configuration space treatment of field theory. The method is applicable in either coordinate or momentum space. We shall, however, work in momentum space since one then deals with algebraic rather than differential equations.

Consider first the one-body problem in scalar or pseudoscalar meson theory. We restrict ourselves to a Fock configuration space wave function which includes all the effects caused by the presence of a single meson and a single pair. Thus

$$\Phi^{(1\text{ particle})}=\left\{\begin{matrix} f^{(1,0;0)}(p^{(1)}s^{(1)}) \\ f^{(1,0;1)}(p^{(1)}s^{(1)};\ k^{(1)}) \\ f^{(2,1;1)}(p^{(1)}s^{(1)},\ p^{(2)}s^{(2)};\ q^{(1)}t^{(1)};\ k^{(1)}) \end{matrix}\right\} \tag{1}$$

where $p^{(1)}s^{(1)}\cdots$ are the momentum and spin coordinates of the nucleons, $q^{(1)}t^{(1)}\cdots$ those of the antinucleons and $k^{(1)}\cdots$ those of the mesons. The superscript $(l, m; n)$ on the particle-wave functions refers to the eigenvalue of the number operator for the nucleons, antinucleons, and mesons, respectively. In the Schroedinger representation the equation of motion of the system is given by

$$\left\{P_0^{(0)}+\int d^3x\mathcal{H}(x)+H_0\right\}\Phi=E\Phi \tag{2}$$
$$(\hbar=c=1),$$

where $P_0^{(0)}$ is the fourth component of the energy-momentum vector of the free field. $\mathcal{H}(x)$ is the interaction energy given by

$$\mathcal{H}(x)=\tfrac{1}{2}g[\bar{\psi}(x)\mathcal{O},\psi(x)]\phi(x)+\tfrac{1}{2}\delta\kappa[\bar{\psi}(x),\psi(x)], \tag{3}$$

where g is the coupling constant, $\delta\kappa$ an infinite constant designed to cancel the divergent self energy, $\psi(x)$ and $\phi(x)$ the usual nucleon and meson operators, respectively,

$$\mathcal{O}=i\gamma_5 \quad \text{for pseudoscalar mesons}$$
$$=1 \quad \text{for scalar mesons.}$$

The infinite constant H_0 defines the zero level of energy of the interacting fields. The equations of motion for the individual wave functions can easily be written down using methods analogous to those of Fock,[5] care being taken that phase factors are included so that all operators obey the proper commutation rules. One then readily finds that $f^{(1,0;0)}(p^{(1)}s^{(1)})$ satisfies the equation,

$$(P_0^{(1)}-E)f^{(1,0;0)}(p^{(1)}s^{(1)})=0, \tag{4}$$

if $\delta\kappa$ in Eq. (3) is equal to[6]

$$\delta\kappa=\pm\kappa g^2[(3/2\pi)\log(1/\gamma\omega_0)+\text{finite terms}], \tag{5}$$
$$\kappa=\text{nucleon mass}.$$

An infinite term [proportional to $\delta(0)$] is canceled by the H_0 term. The latter [$\delta(0)$] term corresponds to the shift in the zero level of energy as a result of the interaction and implies nothing of physical interest. The minus sign in Eq. (5) occurs in the scalar meson theory, whereas the plus sign occurs in pseudoscalar meson theory.

This whole procedure in configuration space is made relativistically invariant using the momentum space integration techniques of Umezawa and Kawabe.[7]

To the same approximation the two-particle wave function is taken to be

$$\Phi=\left\{\begin{matrix} f^{(2,0;0)}(p^{(1)}s^{(1)},\ p^{(2)}s^{(2)}) \\ f^{(2,0;1)}(p^{(1)}s^{(1)}p^{(2)}s^{(2)}k^{(1)}) \\ f^{(2,1;1)}(p^{(1)}s^{(1)}p^{(2)}s^{(2)}p^{(3)}s^{(3)};\ q^{(1)}t^{(1)};\ k^{(1)}) \end{matrix}\right\}. \tag{6}$$

Carrying out the same operations as before, one obtains for the $f^{(2,0;0)}$ an equation which after the $f^{(2,0;1)}$ and $f^{(2,1;1)}$ have been eliminated has the following structure:

$$(P_0^{(1)}+P_0^{(2)}-E)f^{(2,0;0)}(p_1s^{(1)}p_2s^{(2)}) \tag{7}$$

= Møller interaction terms + self-energy terms for nucleon 1 and 2, for system in state characterized by energy eigenvalue E + a term corresponding to shift of zero energy level [$\propto\delta(0)$] + terms proportional to $\delta\kappa$ corresponding to the self energy + H_0 term. The term corresponding to the shift of zero level of energy [$\propto\delta(0)$] is again cancelled by the H_0 term. We note that the self energy terms encountered are of the form,

$\Delta E^{(SE)}$(particle 1)

$$\sim\frac{g^2}{[2(2\pi)^3]^2}\int\frac{d^3k}{\epsilon(k)}\sum_{j=1,2}\bar{u}_s{}^{(1)}(p^{(1)})\mathcal{O}\left(\frac{\gamma_\mu(p^{(1)}-k)_\mu-\kappa}{2\omega(p^{(1)}-k)}\right)\mathcal{O}u_j(p^{(1)})$$
$$\times\frac{1}{\Delta E+\omega(p^{(1)})-\omega(p^{(1)}-k)-\epsilon(k)}f^{(2,0;0)}(p^{(1)}j;\ p^{(2)}s^{(2)}) \tag{8}$$

+ a similar term arising from pair production.

Here

$$\omega(p)=[p^2+\kappa^2]^{\frac{1}{2}}=p_0 \quad (\kappa=\text{nucleon mass})$$
$$\epsilon(k)=[k^2+\mu^2]^{\frac{1}{2}} \quad (\mu=\text{meson mass})$$

and

$$\Delta E=E-\omega(p^{(1)})-\omega(p^{(2)}). \tag{9}$$

Using the algebraic identity

$$\frac{1}{\Delta E+\Omega(p^{(1)},k)}=\frac{1}{\Omega(p^{(1)},k)}-\frac{1}{\Omega(p^{(1)},k)}\,\frac{\Delta E}{\Delta E+\Omega(p^{(1)},k)} \tag{10}$$

with $\Omega(p^{(1)},k)=\omega(p^{(1)})-\omega(p^{(1)}-k)-\epsilon(k)$, we recognize that the first term gives rise to the universal self mass (i.e., independent of the state of motion) of the nucleons and thus is canceled by the $\delta\kappa$ terms. The second term in Eq. (10), the difference between the self energy of a free and a bound nucleon, corresponds to a part of the Lamb shift. In the present perturbation calculus a contribution to the Lamb shift thus already appears in a "second-order" calculation. It is therefore seen that the present approximation method does not correspond to a power series expansion in $g^2/\hbar c$ and thus may be of value in situations where power series expansions in the coupling constant are not applicable.

Calculations of the deuteron energy levels using this formalism are now in progress. A detailed paper presenting the relativistic configuration space methods and the relevant renormalization program will appear shortly in collaboration with Professor Wightman.

The author wishes to express his sincerest gratitude to Professor A. Wightman for his valuable advice.

[3] M. Jean, Compt. rend. 233, 573 (1951).
[4] S. Schweber and A. Wightman (to be published).
[5] V. Fock, Z. Physik 75, 622 (1932).
[6] P. T. Matthews, Phys. Rev. 76, 1657 (1949).
[7] Umezawa and Kawabe, Prog. Theor. Phys. 4, 420, 461 (1949).

Influence of the Chemical State on the Lifetime of an Isomer*

KENNETH T. BAINBRIDGE† AND M. GOLDHABER, *Department of Physics*, AND ELIZABETH WILSON, *Department of Chemistry*, *Brookhaven National Laboratory, Upton, New York*

(Received October 26, 1951)

A TRANSITION from a nuclear isomeric state may occur by internal conversion or by gamma-ray emission. The observed decay constant, λ, is related to the decay constant for gamma-ray emission alone, λ_γ, by the relation $\lambda=\lambda_\gamma(1+\alpha)$, where the conversion coefficient α equals the ratio of the number of electrons to the number of gamma-rays emitted per second.

As the internal conversion coefficient is influenced by the "electronic environment" of an isomer, one might expect changes in the decay constant when this environment is altered. This

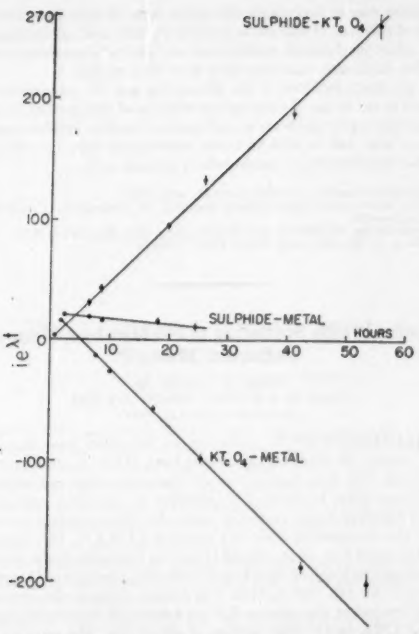

FIG. 1. $ie^{\lambda t}=i_0-\Delta\lambda I_0 t$ (divisions) plotted against t. The statistical errors of each point are shown. The lines indicate the least-squares fit to the points. $I_0=15030$ divisions for sources sulfide-$KTcO_4$, 12350 for sulfide-metal, 13270 for $KTcO_4$-metal. The initial time points, $t=0$, for each curve are 0.75, 2.45, and 1.83 hours, respectively.

influence can best be tested by using an isomer in different chemical states which has a highly converted low energy isomeric transition.

We have carried out a series of experiments with Tc^{99m} (6 hours), an isomer with a 2-kev highly converted isomeric transition followed promptly by a 140-kev partially converted gamma-ray[1,2] which can be conveniently measured. We find that the decay constant of the 2-kev isomeric transition does assume different values which are dependent on the chemical state of the element.

When long-lived Tc^{99} is used as a carrier, λ for Tc^{99m} in $KTcO_4$, as the dry salt, is $1+0.0030\pm0.00010$ times greater than λ for Tc^{99m} electrolytically deposited on copper.[3] In another experiment the same value, within the expressed error, was found for $KTcO_4$ in basic aqueous solution.

The experimental data for the dry salt $KTcO_4$ and the sulfide[3] (Tc_2S_7) compared with electrolytically deposited Tc^{99m} are shown in Fig. 1. λ for Tc^{99m} as the sulfide is $1+0.00031\pm0.00012$ times greater than λ for Tc^{99m} electrolytically deposited on copper. The radiations from the long-lived Tc^{99} carrier, $\sim$25 micrograms for an individual source, have a negligible effect on these measurements.

The measurements were made by the balance method introduced by Rutherford[4] in which two identical ionization chambers housing the sources under comparison are connected to collect ions of opposite sign. Thus the difference current produced by two closely matched sources is small and can be measured with a precision[4-7] approaching that defined by the statistics of the number of separate ionization events which have occurred during an observation.[4,8] The difference current is $i=i_0e^{-\lambda t}-I_0\Delta\lambda te^{-\lambda t}$ at any time t, where i_0 is the initial unbalance current, I_0 is the initial intensity of the stronger source whose transition constant is λ, and $\lambda-\Delta\lambda$ is the transition constant of the other source.

The observed effect is discussed theoretically by Slater in an accompanying letter.

We are indebted to Mr. M. McKeown for checking the purity of the sources with a NaI scintillation spectrometer, to Dr. G. Friedlander for advice on some chemical aspects of this work, to the Brookhaven Reactor Group for irradiations, to Miss Jean Snover for help in the computations, and to the Isotopes Division of the AEC for the long-lived Tc carrier material. The ionization chambers were constructed under ONR contract with Harvard University.

* Research carried out under contract with the AEC.
† On leave from Harvard University, Cambridge, Massachusetts.
[1] Medicus, Maeder, and Schneider, Helv. Phys. Acta 22, 603 (1950).
[2] Mihelich, Goldhaber, and Wilson, Phys. Rev. 82, 972 (1951).
[3] Motta, Larsen, and Boyd, quoted by A. C. Wahl and N. A. Bonner, *Radioactivity Applied to Chemistry* (John Wiley and Sons, Inc., New York, 1951).
[4] E. Rutherford, Wien. Ber. 120, 303 (1911).
[5] M. Curie, J. phys. radium 2, 405 (1924).
[6] C. Wiegand, MDDC 1098 (1947).
[7] Boucher, Daudel, Daudel, Muxart, and Rogozinski, J. phys. radium 10, 201 (1949).
[8] E. Segrè and C. Wiegand, Phys. Rev. 75, 39 (1949); 81, 284 (1951).

The Effect of Chemical Combination on the Internal Conversion in Tc*

J. C. SLATER†
Brookhaven National Laboratory, Upton, New York
(Received October 26, 1951)

BAINBRIDGE, Goldhaber, and Wilson[1] have shown experimentally that the probability of a certain internal conversion in Tc^{99m} depends on the state of chemical combination. In this conversion, the nucleus loses about 2 kev of energy, undergoing an electric octopole transition of $\Delta l=3$. This energy is only enough to remove an M or N electron from the Tc atom, and since these electrons lie toward the outside of the atom, it was thought that their wave functions might be appreciably affected by chemical combination, with consequent appreciable effect on the conversion probability. In the reference just cited, it was found in fact that there is such an effect, of the order of three-tenths of a percent, and that furthermore, $KTcO_4$ has a somewhat greater conversion probability than Tc metal. It is the purpose of this note to show that this is not unreasonable theoretically.

In the first place, a very rough calculation has been made of the relative contributions of the various electronic shells to the internal conversion probability. The matrix component which has to be computed is the integral of the product of the wave function of the bound electron in the Tc atom or crystal, the wave function of an electron in the continuum with an energy 2 kev greater than the bound electron, and a quantity representing the potential of the nuclear octopole. Since the electromagnetic wavelength of a gamma-ray of 2 kev is about 6A, and the distances concerned in the integral are a rather small fraction of an angstrom, we are justified in representing this potential electrostatically, so that it is given by a spherical harmonic of $l=3$, times $1/r^4$. The integral then involves a product of three spherical harmonics, one from each wave function and one from the potential. Such integrals are zero unless certain relations exist between the l values, resulting in selection principles, which in the present case result in possible transitions from the bound s states to an f state in the continuum, from a bound p state to a d state in the continuum, and from a bound d state to a p state in the continuum. The functions of angles are easily computed, and the matrix component, whose square is proportional to the transition probability, reduces to an integral over r, of the product of the radial wave functions of bound and continuum states, times $1/r^4$, times the volume elements r^2dr.

To compute these radial integrals, a very rough numerical integration for both the bound and continuum wave functions has been made, using as a potential the Fermi-Thomas potential for Tc, corrected for exchange. The integrand in each case proves to start for small r's proportionally to r (the singularity in the

TABLE I. Contribution of electron shells to transition probabilities.

Electron	Transition probability	Ionization potential, ev
$3p$	0.60	430
$3d$	0.27	260
$4p$	0.10	45
$4d$	0.03	7
	Sum 1.00	

quantity $1/r^4$ being canceled by positive powers arising from the wave functions), to rise to a maximum, and to become negligibly small for values of r greater than about 0.2A, so that the effect depends on the behavior of the wave function for small values of r. The required integrals have been computed numerically. For transitions from the bound s wave functions to the continuum, the probabilities prove to be negligibly small, for a rather trivial reason: the integrand is partly positive, partly negative in the range of integration on account of the innermost node of the s functions, and the contributions almost cancel. For the transitions from the p and d electrons, in the free atom, the relative contributions to the internal conversion, as computed, are given in Table I. These values are to be regarded as very rough approximations, on account of the very crude numerical integration which has so far been used to approximate the wave functions. In Table I we give also very rough approximations to the ionization potentials of the various shells, obtained by interpolation between known x-ray term values.

In the metal or in $KTcO_4$, as contrasted to the free atom, these probabilities will be affected only as the charge density of the various electronic shells is altered at distances less than 0.2A, which alone contribute to the transition probabilities. A rough estimate indicates that the $3p$ and $3d$ electrons will not be affected to a significant extent. The $4p$ shell, which certainly does not contribute to binding, will be somewhat squeezed, and very rough estimates indicate that it might increase its charge density in the required region by a few percent of its total density, giving an increase of probability of a few tenths of a percent over all. The change in the $4d$ shell is less easy to estimate. These electrons doubtless take part in the binding, both in the metal and the $KTcO_4$. In the metal, they are certainly somewhat squeezed as compared with the free atom. In the $KTcO_4$, an ionic picture, regarding the $(TcO_4)^-$ ion as being made up of $Tc^{+7}(O^-)_4$, would lead to a large removal of $4d$ electrons from the neighborhood of the Tc, piling them up around the oxygens. No one, however, supposes that this really happens, and the writer suspects that the actual density of valence electrons near the Tc atom is not very different in $KTcO_4$ from what it is in the free atom or the metal. In other words, it is uncertain whether the contribution 0.03 of the $4d$ electrons in the free atom would be increased or decreased in the crystals. These considerations, in other words, lead to the order of magnitude of a fraction of a percent for the total change, as has been observed, probably arising mostly from the $4p$ wave functions.

As to why the probability of internal conversion is greater in $KTcO_4$ than in the metal, the most straightforward explanation seems to be that the Tc atom is squeezed more in the $KTcO_4$. The Tc—Tc distance in the metal is about 2.7A.[3] The distance has not been measured in $KTcO_4$, but an interpolation between similar tetrahedral ions indicates a probable distance from Tc to O of about 1.7A. Discussion of the sizes of the atoms shows that this indicates a much greater squeezing in the $KTcO_4$, on account of the close distance of approach of the O atoms. This effect would probably be felt on the $4p$ electrons as well as on the $4d$'s; the effect would also be strong on the $5s$'s, but would not appear in the internal conversion probability on account of the small contribution of these electrons.

Of course, it is to be realized that the wave functions of the valence electrons surrounding the Tc, in the ion $(TcO_4)^-$, will be quite different from what they are in the isolated atom, and work is under way to investigate the actual form of wave functions in ions of this sort. It will not be possible to make real calculations of the effect of chemical combination on internal conversion probability until such wave functions have been studied.

I am much indebted to Dr. Bainbridge and Dr. Goldhaber for pointing out to me the interesting relations of this problem to the electronic wave functions in molecules and solids. Similar experiments may well be able to throw considerable light on the electronic distributions in compounds of various sorts.

* Research carried out under contract with AEC.
† On leave from Massachusetts Institute of Technology, Cambridge, Massachusetts.
[1] Bainbridge, Goldhaber, and Wilson, Phys. Rev. **84**, 1260 (1951).
[2] R. C. L. Mooney, Acta Cryst. **1**, 161 (1948).

Proton-Proton Scattering at 240 Mev by a Magnetic Deflection Method*

OSCAR A. TOWLER, JR.
University of Rochester, Rochester, New York
(Received October 22, 1951)

PROTON–PROTON scattering at 240 Mev has been observed for eight angles ranging from 171.3° to 108.1° center of mass. The cross section has the previously observed isotropic behavior down to about 15° (referring to the more commonly used supplementary scattering angle for the conjugate proton) and then increases sharply by a factor of 3.5 at 8.7°. This increase at the small c.m. angle, caused in part by Coulomb effects, has the same general trend observed by Chamberlain, Segrè, and Wiegand[1] at 11.3° for 345-Mev protons. The average value of the cross section (excluding the value at 8.7°) is 4.66 ± 0.39 mb/sterad., based on a $C^{12}(p, pn)C^{11}$ cross section of 49 ± 3 mb. The error in the average value includes the statistical error, the 6 percent error in the C^{11} cross section, a 4 percent error in the beta-counter calibration, and other estimated errors.

The apparatus has been described briefly before.[2] The detectors were photographic plates placed in the tank of the Rochester cyclotron near the lower pole tip. The protons scattered by protons in a hydrocarbon $(CH_2)_n$ target arrive at a given position on a plate in a nearly collimated group which corresponds to a well-defined angle of proton-proton scattering, while the protons scattered by the carbon nucleons arrive uncollimated. The angles at which the protons entered the plates were measured with a protractor eyepiece attached to a microscope. Entrance angle distributions were obtained for both hydrocarbon and carbon targets of suitable thicknesses, the incident beam being monitored by the C^{11} activity induced in each target. The number of protons scattered by protons was determined by subtracting the carbon target distribution from the hydrocarbon target distribution. As a result of energy loss in the thinnest carbon targets that could be used, thin polystyrene $(CH)_n$ targets were used to check the distribution of protons scattered by the carbon nucleons in the polyethylene $(CH_2)_n$ targets for the laboratory angles 83.1° and 85.4°.

The center-of-mass cross sections obtained are presented in Table I and Fig. 1. The indicated errors are the statistical errors in the number of tracks in the proton-proton peak and carbon background.

TABLE I. Experimental differential scattering cross section.

$\pi-\theta_{c.m.}$	$d\sigma/d\Omega$, mb/sterad.
71.9°	4.33 ± 0.22
45.2°	4.81 ± 0.25
36.6°	4.90 ± 0.28
28.3°	4.43 ± 0.21
27.2°	4.38 ± 0.38
18.6°	4.59 ± 0.31
13.0°	5.16 ± 0.39
8.7°	$15.8\ \pm1.6$

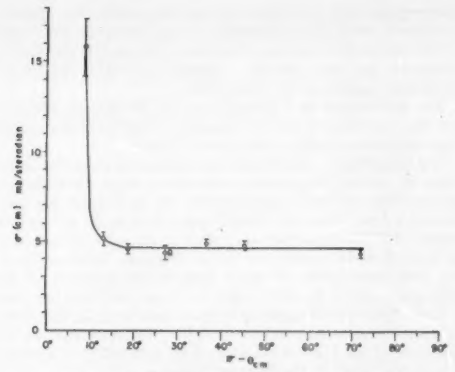

FIG. 1. Differential cross section for proton-proton scattering at 240 Mev.

These results agree with those of Oxley and Schamberger[3] of this laboratory, who obtain an average cross section of 4.97±0.42 mb/sterad from 27.5° to 90° cm. The relative error in both of these experiments is 0.22 mb/sterad, since the errors in the C^{11} cross section and the beta-counter calibration are mutual. The combined value of the two experiments gives 4.81±0.38 mb/sterad for the isotropic part of the cross section.

These measurements are about 30 percent higher than those published by Chamberlain *et al.*[1] The cause of this discrepancy is not clear at the present time.

Details of this experiment will be published at a later date. I wish to thank Professor C. L. Oxley for many suggestions during the course of this work.

* Assisted by the joint program of the ONR and AEC.
[1] Chamberlain, Segre, and Wiegand, Phys. Rev. **83**, 923 (1951).
[3] O. A. Towler, Jr., and C. L. Oxley, Phys. Rev. **78**, 326 (1950).
[2] C. L. Oxley and R. D. Schamberger, Phys. Rev. (to be published).

Thermodynamic Functions on the Generalized Fermi-Thomas Theory

MALCOLM K. BRACHMAN
Argonne National Laboratory, Chicago, Illinois
(Received July 30, 1951)

RECENTLY, equations of state of the elements[1] based on the generalized Fermi-Thomas theory have been developed. It has been shown[2] that exchange effects may be neglected for high temperatures, and they will not be considered here. In the past, the pressure has been obtained by calculating the rate of flow of momentum through the surface of the atom, which is assumed to be a sphere of radius a. It is also possible to find the pressure from the free energy or the logarithm of the partition function.[3] The purpose of this note is to show that the pressure calculated from the free energy using the generalized Fermi-Thomas model for arbitrary temperatures agrees with that found by mechanical considerations based on the same model, and, in addition, one obtains expressions for the entropy and the specific heat.

Our model leads to the kinetic energy density[4]

$$E_K(r)=(4\pi/h^3)(2m)^{3/2}\beta^{-5/2}I_{3/2}[\eta+\beta eV(r)], \tag{1a}$$

and the electron number density

$$\rho(r)=(4\pi/h^3)(2m)^{3/2}\beta^{-3/2}I_{1/2}[\eta+\beta eV(r)], \tag{1b}$$

where $V(r)$ is the total potential, V_N+V_e, and $\beta=(kT)^{-1}$. Here V_N is the nuclear potential Ze/r, and $-V_e$ satisfies Poisson's equation with the charge density $e\rho(r)=\rho_e$. The boundary conditions are the vanishing of the total potential and the electric field at the surface of the atom. The volume integral of (1a) is the kinetic energy E_{kin} and that of (1b) is Z, the nuclear charge. The potential energy E_{pot} is

$$E_{\text{pot}}=-\tfrac{1}{2}\int_0^a \rho_e V_e d\tau-\int_0^a \rho_e V_N d\tau=E_{e,e}+E_{e,N}, \tag{2}$$

where $d\tau$ is $4\pi r^2 dr$. By mathematical manipulation, one finds the virial theorem

$$E_{\text{kin}}=\tfrac{3}{2}pv-\tfrac{1}{2}E_{\text{pot}}. \tag{3}$$

The difference between our calculation and previous ones is that the pressure is obtained by macroscopic rather than microscopic considerations.

The pressure p and the entropy S are found from the free energy $F=E_{\text{tot}}-TS$, where T is the absolute temperature, by means of the thermodynamic relations,

$$p=-(\partial F/\partial v)_T, \tag{4a}$$

$$S=-(\partial F/\partial T)_v. \tag{4b}$$

The basis of our work is the Gibbs-Helmholtz equation in the form,

$$E_{\text{tot}}=(\partial/\partial\beta)[\beta F], \tag{5}$$

of which we obtain the indefinite integral. This is done by integrating the various terms of E_{tot} by parts and using the relations between the derivatives of $E_K(r)$ and ρ_e obtained by differentiating (1a) with respect to a, β, and r, including the cross derivatives. Employing Green's theorem, one finds

$$F=-\tfrac{2}{3}E_{\text{kin}}-E_{e,e}+ZkT\eta. \tag{6}$$

From the relations (4a) and (4b) it follows that

$$p=\tfrac{2}{3}E_K(a), \tag{7a}$$

$$S=T^{-1}\{(5/3)E_{\text{kin}}+2E_{e,e}+E_{e,N}\}-Zk\eta. \tag{7b}$$

The first of these is the value obtained from mechanical considerations. Consideration of the Fermi factor shows that there is a maximum value of the momentum, $p_m(r)$, given by

$$P_m^2(r)/2m=eV(r)+\eta kT, \tag{8}$$

in the sense that in the limit as T tends to zero the Fermi factor is one for $p<p_m(r)$ and is zero for $p>p_m(r)$. Integrating Eq. (8), which is the same as the last equation of Sec. IV of reference 1, over the phase space at absolute zero yields

$$(5/3)E_{\text{kin}}=-2E_{e,e}-E_{e,e}+ZkT\eta. \tag{9}$$

This shows that $\lim_{T\to 0} S=0$, as it should.

The specific heat at constant volume, C_v, given by the relation,

$$C_v=-\beta(\partial S/\partial\beta)_v, \tag{10}$$

may be expressed in the form,

$$\frac{4}{3}TC_v=\frac{5}{2}pv+\frac{7}{6}E_{e,e}+\frac{1}{6}E_{e,N}-Z\left\{\frac{\partial\eta}{\partial\beta}+e\beta\frac{\partial V_e(0)}{\partial\beta}\right\}+T\left(\frac{\partial p}{\partial T}\right)_v. \tag{11}$$

This may be shown to agree with that given in reference 1 as T tends to zero. The expression derived in reference 1 is based upon relationships valid at $T=0$, whereas our relations are valid at an arbitrary temperature.

[1] Feynman, Metropolis, and Teller, Phys. Rev. **75**, 1561 (1949).
[2] H. Jensen, Z. Physik **111**, 373 (1938).
[3] Marshak, Morse, and York, Astrophys. J. **111**, 214 (1950).
[4] The notation is the same as that of reference 1, except that our $\rho=-\rho_e$ of it.

The Near Infrared Spectrum of Lightning*

W. PETRIE AND R. SMALL
Physics Department, University of Saskatchewan, Saskatoon, Saskatchewan, Canada
(Received October 25, 1951)

ON September 18, 1951, a spectrum of lightning in the wavelength range 7100–9100 angstroms was secured on an Eastman spectroscopic plate type 1*N*. The instrument used was one

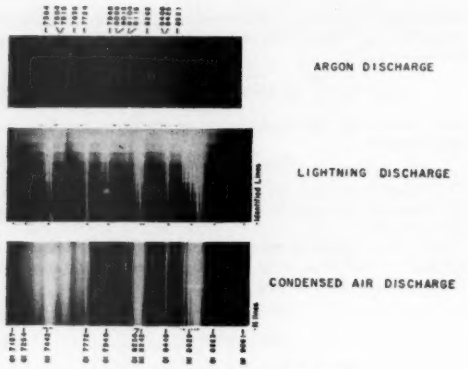

FIG. 1. The infrared spectrum of lightning.

of our auroral spectrographs, the optics of which consist of a mirror collimator, a plane grating, and an $f0.8$ flat field Schmidt camera. The linear dispersion of the instrument is approximately 85 angstroms/mm in the first-order spectrum. The spectrum recorded is the result of many flashes from a storm which lasted about one hour.

Figure 1 shows the lightning spectrum (a step-slit was used) and for comparison the spectra of argon and a condensed discharge through air. The latter spectra were produced by a grating instrument which has a dispersion of approximately twice that of the auroral spectrograph, and hence by varying the magnification, it has been possible to match reasonably well similar wavelength regions on the three prints.

The wavelengths and identifications of the spectral features, and the excitation potentials of the upper energy levels from which these radiations originate, are given in Table I.

It is interesting to note the complete absence of molecular radiations; all the spectral features are atomic in origin. Furthermore, all radiations are from neutral atoms. The same result has been found by José.[1] The most intense argon lines in the wavelength region 7300–8500 angstroms are present in the lightning spectrum as they are in the spectrum of the air discharge. This is evidently the first identification of argon lines in the spectrum of the atmosphere above the earth's surface. A portion of the low level C I multiplet $^3P^0-{}^3P$ appears to be a feature of the spectrum. It is our intention to compute excitation temperatures from the intensities of the N I and O I lines; these data will yield information on the energy in the lightning discharge.

TABLE I. Wavelengths of infrared lightning spectral features.

Wavelength	Identification	Excitation potential
7157	O I $^1D^0-{}^1D$	14.40
7217	...	...
7254	O I $^5P-{}^5S^0$	12.64
7267	...	...
7280	...	...
7384	A I	...
7424	N I $^4P-{}^4S^0$	11.94
7442		
7468		
7504	A I	13.42
7515	A I	...
7550	...	...
7724	A I	13.10
7761	...	...
7772	O I $^3S^0-{}^3P$	10.69
7862	...	...
7891	A I	...
7901	...	...
7918	...	...
7948	O I $^1D^0-{}^1F$	14.04
8005	A I	13.11
8015	A I	13.04
8104	A I	13.10
8115	A I	13.02
8185	N I $^4P-{}^4P^0$	11.79
8188		
8210		
8216	N I $^4P-{}^4P^0$	11.79
8223		
8242		
8265	A I	13.27
8408	A I	13.24
8425	A I	13.24
8446	O I $^3S^0-{}^3P$	10.94
8521	A I	13.23
8568	N I $^2P-{}^2P^0$	12.07
8594		
8629		
8656		
8680	N I $^4P-{}^4D^0$	11.70
8683		
8686		
8703		
8712		
8719		
8729		
8747		
8820	O I $^1D^0-{}^1F$	14.07
9041	...	...
9061	N I $^2S^0-{}^2P$	12.91
	C I $^3P^0-{}^3P$	8.81
9078	C I $^3P^0-{}^3P$	8.81

* This work was supported by the Geophysics Research Division, Air Force, Cambridge Research Center of the U. S. Air Force.

[1] P. D. José, J. Geophys. Research **55**, 39 (1950).

The Binding Energy of Four Neutrons in U^{239} and the Disintegration Energies of U^{239} and Np^{239}

J. R. HUIZENGA, L. B. MAGNUSSON, M. S. FREEDMAN, AND F. WAGNER, JR.
Argonne National Laboratory, Chicago, Illinois
(Received November 2, 1951)

FROM the recent measurements of the binding energy of a neutron in U^{239}, U^{238}, Th^{232}, and Th^{230} and the alpha-energies of U^{235}, U^{236}, and U^{237}, it is possible to calculate the binding energy[1-4] of four neutrons in U^{239}. The alpha-energy of U^{237} is estimated from alpha-systematics.[5] This value can also be derived from the following cycle.

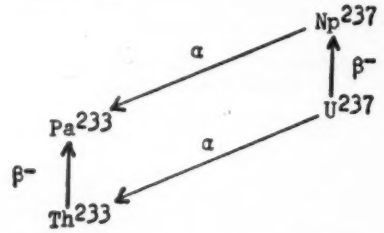

Recent measurements on the total decay energy of Th^{232} [6,7] and U^{237} [7] give a calculated α-energy for U^{237} in agreement with systematics.

The binding energy of a neutron in U^{237} and U^{236} is calculated from the following cycles. The binding energy

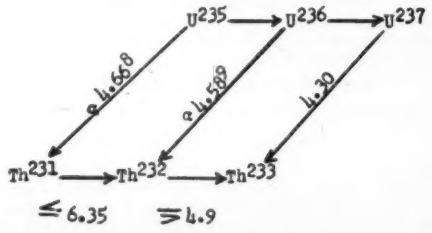

of four neutrons in U^{239} is found to be 22.21 Mev by summing the binding energies of one neutron in U^{239} ($\gtrsim$4.63), U^{238} ($\lesssim$5.97), U^{237} ($\gtrsim$5.18), and U^{236} ($\lesssim$6.43).

The sum of the disintegration energies of U^{239} and Np^{239} can be calculated from the following cycle with the aforenamed data and the α-disintegration energy of Pu^{239}.

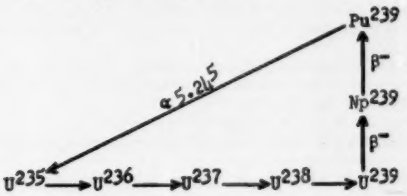

$E_{\beta\beta}$ = [Mass ($4n$'s) − Mass (He^4)] − E_α (Pu^{239}) − binding energy of $4n$'s in U^{239}

= 29.79[10] − 5.24 − 22.21

$E_{\beta\beta}$ = 2.34 Mev.

Slätis[11] has proposed a decay scheme for U^{239} of total disintegration energy 2.06 Mev, including a 2.06-Mev beta in 3 percent abundance and 0.9-Mev and 0.073-Mev gammas in cascade with a 1.12-Mev beta. For Np^{239} he reports a beta-component of 1.181 Mev in 1 percent abundance leading to the ground state of Pu^{239}, together with betas of 0.678, 0.406, and 0.288 Mev, and suggests a decay scheme including 7 observed gammas. Thus a double decay energy $E_{\beta\beta}$ of 3.24 Mev follows.

The apparent discrepancy with the aforementioned calculation led us to reexamine the beta-spectra of U^{239} and Np^{239}. By employing a very active sample of U^{239} prepared by neutron irradiation of depleted U^{238} and radiochemically separated from fission products, in our double lens spectrometer we establish an upper limit of 0.02 percent on the abundance of a 2-Mev beta. A thinner sample was used to measure the main beta for which we find an energy of 1.22 Mev. On a scintillation spectrometer we observe only the prominent *ca* 0.075-Mev gamma; the 0.9-Mev gamma, if present, has a relative intensity of less than 1 percent. Thus the spectrum appears to be simple, with a total disintegration energy of 1.295 Mev.

The beta- and gamma-spectra of Np^{239} have recently been carefully examined by Graham and Bell[12] who by spectrometer coincidence techniques show that the 705-kev beta has no gammas in sequence, and by Tomlinson *et al.*,[13] who find, in a high resolution spectrometer, betas of 0.715, 0.654, 0.44, and 0.33 Mev, and 88 conversion lines assigned to 11 gammas. We examined a very intense sample of Np^{239} for hard betas and report a maximum relative abundance of 0.01 percent for betas of greater than 0.72 Mev. A second spectrum on a thin sample (<0.1 mg/cm²) disclosed 45 conversion lines above 10 kev and four beta-components, in essentially complete agreement with the results of reference 13. Thus the beta of 0.715 Mev is probably correctly assigned to the ground state transition,[13] and the double beta-decay energy is then 2.01 Mev. This value is 0.33 Mev less than the value calculated with the aid of the binding energy of four neutrons in U^{239}. Some of this discrepancy may be caused by the uncertainty in the mass difference of four neutrons and helium. There is also some possibility of a weak γ (*ca* 0.05 Mev) in cascade with the Pu^{239} alpha-particle.[5] Since the experimental disintegration energies of Np^{239} and U^{239} are probably more accurate than the experimental binding energies, the binding energy of four neutrons in U^{239} may be too small by about 0.3 Mev.

TABLE I. Neutron binding energies

Isotope	Neutron binding energy (Mev) measured by (d, p)	(γ, n)	Neutron binding energy (Mev)[d]
92^{238}	...	5.97 ±0.1[b]	≤5.97
92^{239}	4.63 ±0.15[a]	...	≥4.63
90^{238}	...	6.35 ±0.1[c]	≤6.35
90^{239}	4.9 ±0.2[a]	...	≥4.9

[a] See reference 1. [b] See reference 2. [c] See reference 3. [d] See reference 4

[1] J. A. Harvey, Phys. Rev. **81**, 353 (1951).
[2] Huizenga, Magnusson, Fields, Studier, and Duffield, Phys. Rev. **82**, 561 (1951).
[3] Magnusson, Huizenga, Fields, Studier, and Duffield, Phys. Rev. **84**, 166 (1951).
[4] Huizenga, Magnusson, Simpson, and Winslow, Phys. Rev. **79**, 908 (1950).
[5] Perlman, Ghiorso, and Seaborg, Phys. Rev. **77**, 26 (1950).
[6] Bunker, Langer, and Moffat, Phys. Rev. **80**, 468 (1950).
[7] Freedman, Wagner, Engelkemeir, and Huizenga, Preliminary values, private communication.
[8] A. Ghiorso, Phys. Rev. **82**, 979 (1951).
[9] Jaffey, Diamond, Hirsch, and Mech, Phys. Rev. **84**, 785 (1951).
[10] Tollestrup, Fowler, and Lauritsen, Phys. Rev. **78**, 372 (1950).
[11] H. Slätis, Arkiv Mat. Astron. Fys. **35A**, No. 3, (1948).
[12] R. L. Graham and R. E. Bell, Phys. Rev. **83**, 222 (1951).
[13] Tomlinson, Fulbright, and Howland, Phys. Rev. **83**, 223 (1951).

Author Index to Volume 84

References with (A) are to abstracts of papers presented at meetings of the American Physical Society, and those with (T) designate title only. References with (L) are to Letters to the Editor.

Adair, R. K. (see Bockelman, C. K.)—69
—— (see Johnson, C. H.)—775
Aeppli, H., H. Albers-Schönberg, A. S. Bishop, H. Frauenfelder, and E. Heer. Determination of the magnetic moment of an excited nuclear level Cd^{111}, 247 kev)—370(L)
Agnew, H. M., W. T. Leland, H. V. Argo, R. W. Crews, A. H. Hemmendinger, W. E. Scott, and R. F. Taschek. Measurement of the cross section for the reaction $T+T \rightarrow He^4+2n+11.4$ Mev—862(L)
Ahearn, A. J. Effect of inhomogeneities on the electrical properties of diamond—798
Albers-Schönberg, H. (see Aeppli, H.)—370(L)
Alburger, D. E. (see Friedlander, G.)—231
Alder, Kurt. Angular correlation in magnetic fields—369(L)
Alers, P. B., J. W. McWhirter, and C. F. Squire. Eddy currents and supercurrents in rotating metal spheres at liquid helium temperatures—104
—— **and R. T. Webber.** Anomalous magnetoresistance of bismuth at low temperatures—863(L)
Allen, Robert C., John E. May, and Waldo Rall. NaI(Tl) scintillation spectrometer study of proton γ-ray coincidences—1203
Allis, W. P., Sanborn C. Brown, and Edgar Everhart. Electron density distribution in a high frequency discharge in the presence of plasma resonance—519
Allred, J. C. Differential cross section of the reaction $He^3(d,p)He^4$ at 10.2-Mev bombarding energy and search for excited state in He^4—695
Alpher, Ralph A. and Robert C. Herman. Neutron-capture theory of element formation in an expanding universe—60
—— **and Robert C. Herman.** Primeval lead isotopic abundances and the age of the earth's crust—1111
Al-Salam, Sue Gray. Meson-induced fission—254
Anderson, G. W. and J. E. Naugle. Search for a diurnal variation in the rate of star formation—864(L)
—— (see Freier, P. S.)—322
Ando, Rinjiro (see Sawada, Shozo)—1054(L)
Andrews, C. L. Diffraction pattern of electromagnetic waves near apertures—1077(A)
Andrews, F. A., R. T. Webber, and D. A. Spohr. Thermal conductivities of pure metals at low temperatures. I. Aluminum—994
Apker, L., E. Taft, and J. Dickey. Photoelectric emission and energy structure of BaO—508
Arfken, G. B., L. C. Biedenharn, and M. E. Rose. Isotropy in nuclear gamma-radiation—89
Argo, H. V. (see Agnew, H. M.)—862(L)
Axel, Peter (see Bowe, J. C.)—939
—— (see Mann, Lloyd G.)—221

Backus, John and Norman E. Huston. Energies of positive ions in a cold-cathode discharge in a magnetic field—1074(A)
Baggett, L. M. and S. J. Bame, Jr. Gamma-ray spectrum from the deuteron bombardment of C^{13}—154
—— (see Bame, S. J., Jr.)—891
Bainbridge, Kenneth T., M. Goldhaber, and Elizabeth Wilson. Influence of the chemical state on the lifetime of an isomer —1260(L)
Balasubrahmanyam, V. K. (see Rao, A. S.)—364(L)
Baldinger, E., P. Huber, and W. G. Proctor. Scattering of fast neutrons from O^{16}—1058(L)
Baldwin, H. W. (see Simpson, J. A.)—332
Ball, George A. Computation of two-dimensional laminar flames—614(A)
Bame, S. J., Jr., and L. M. Baggett. Internal pair spectrum from $B^{10}+d$—891
—— (see Baggett, L. M.)—154(L)
Bandel, Herman W. Point-to-plane corona in dry air—92
Banks, E. (see Brown, B. W.)—609(L)
Baranger, Michel. Relativistic corrections to the Lamb shift —866(L)
Barbiere, Domenick. Energy distribution, drift velocity, and temperature of slow electrons in helium and argom—653
Bardeen, J. (see Hall, Harry H.)—129
Barker, D. B. (see Huibregtse, E. J.)—142
Barnes, John W. and Arthur J. Freedman. Some new isotopes of antimony and tin—365(L)
Barrett, Paul H. Absorption of extensive showers in water—339
Barrett, Robert E. and Robert T. Beyer. Anomalous effect in the ultrasonic absorption of an electrolytic solution—1060(L)
Barschall, H. H. (see Bockelman, C. K.)—69
Bartell, F. O. and Sheldon Softky. Excitation functions for deuterons and protons on Mg—463
Bashkin, S. and H. T. Richards. Proton bombardment of the lithium isotopes—1124
Batzel, Roger E., Daniel R. Miller, and Glenn T. Seaborg. High-energy spallation products of copper—671
Bauer, E. Dissociation of hydrogen molecules by vibrational excitation and three-body recombination coefficient—315
Beck, F. J., J. S. Kouvelites, and L. W. McKeehan. Magnetostrictive vibration of prolate spheroids. Analysis and experimental results—957
Becker, R. A. (see Brown, H. N.)—292
Belinfante, Frederik J. Energy density tensor in gauge-independent quantum electrodynamics—648
—— New covariant auxiliary condition for quantum electrodynamics—644
—— Phenomenological theory of the Lamb shift and of anomalous magnetic moments—949
—— Variational principle for gauge-independent electrodynamics—546
—— **and John S. Lomont.** Gauge-independent quantum electrodynamics—541
Beling, J. K., B. T. Feld, and I. Halpern. $\alpha-\gamma$ angular correlation in the decay of radiothorium—155(L)
Bell, R. E. (see Graham, R. L.)—380(L)
Bell, W. E. and E. P. Hincks. Lifetime of the μ^+-meson—1243(L)
Bendel, W. L. (see Brown, H. N.)—292
Bergmann, Peter G. Generalized statistical mechanics—1026
—— (see Heller, Jack)—665
Berlin, T. H. (see Madansky, L.)—596(L)
Bernardini, G. and F. Lèvy. Capture and scattering of π^+-mesons—610(L)
Bernstein, Ira B. and T. Holstein. Electron distribution functions in combined dc space charge and ac fields—1074(A)
Bershader, Daniel and Boyd Cary. Interferometric studies of two-dimensional turbulent jet mixing at $M1.7$—612(A)
Bethe, H. A. (see Heidmann, J.)—274
—— (see Salpeter, E. E.)—1232
Beyer, Robert T. (see Barrett, Robert E.)—1060(L)
Bhattacharya, P. C. Penetrating showers in copper—1052(L)
Biedenharn, L. C. (see Arfken, G. B.)—89
Biltz, M. Temperature dependence of the spectral sensitivity of photographic emulsions—1078(A)
Biondi, Manfred A. Attachment of thermal electrons in oxygen—1072(A)
Birks, J. B. Specific fluorescence of anthracene and other organic materials—364(L)
Bishop, A. S. (see Aeppli, H.)—370(L)